
Chapter 8

SINGLE-VARIABLE PROBLEMS IN TWO DIMENSIONS

8.1 INTRODUCTION

Finite element analysis of two-dimensional problems involves the same basic steps as those described for one-dimensional problems in Chapters 3–6. The analysis is somewhat complicated by the fact that two-dimensional problems are described by partial differential equations over geometrically complex regions. The boundary Γ of a two-dimensional domain Ω is, in general, a curve. Therefore, finite elements are simple two-dimensional geometric shapes that allow approximations of a given two-dimensional domain as well as the solution over it. Thus, in two-dimensional problems we not only seek an approximate solution to a given problem on a domain, but we also approximate the domain by a suitable finite element mesh. Consequently, we will have approximation errors due to the approximation of the solution as well as discretization errors due to the approximation of the domain in the finite element analysis of two-dimensional problems. The finite element mesh (discretization) consists of simple two-dimensional elements, such as triangles, rectangles, and/or quadrilaterals, that allow unique derivation of the interpolation functions. The elements are connected to each other at nodal points on the boundaries of the elements. The ability to represent domains with irregular geometries by a collection of finite elements makes the method a valuable practical tool for the solution of boundary, initial, and eigenvalue problems arising in various fields of engineering.

The objective of this chapter is to extend the basic steps discussed earlier for one-dimensional problems to two-dimensional boundary value problems involving a single dependent variable. Once again, we describe the basic steps of the finite element analysis with a model second-order partial differential equation governing a single variable. This equation arises in a number of fields including electrostatics, heat transfer, fluid mechanics, and solid mechanics (see Table 8.1.1).

Table 8.1.1 Some examples of the Poisson equation

Field of application	$-\nabla \cdot (k \nabla u) = f$ in Ω			
	Primary variable u	Material constant k	Source variable f	Secondary variables $q, \frac{\partial u}{\partial x}, \frac{\partial u}{\partial y}$
	Natural boundary condition: $k \frac{\partial u}{\partial n} + \beta(u - u_\infty) = q$ on Γ_q			
Essential boundary condition: $u = \hat{u}$ on Γ_u				
Heat transfer	Temperature T	Conductivity k	Heat source g	Heat flow due to conduction $k \frac{\partial T}{\partial n}$ convection $h(T - T_\infty)$
Irrational flow of an ideal fluid	Stream function ψ	Density ρ	Mass production σ	Velocities $\frac{\partial \psi}{\partial x} = -v$ $\frac{\partial \psi}{\partial y} = u$
	Velocity potential ϕ	Density ρ	Mass production σ	$\frac{\partial \phi}{\partial x} = u$ $\frac{\partial \phi}{\partial y} = v$
Groundwater flow	Piezometric head ϕ	Permeability K	Recharge f (pumping, $-f$)	Seepage $q = k \frac{\partial \phi}{\partial n}$ Velocities $u = -k \frac{\partial \phi}{\partial x}$ $v = -k \frac{\partial \phi}{\partial y}$
Torsion of cylindrical members	Stress function Ψ	$k = 1$ $G =$ shear modulus	$f = 2$ $\theta =$ angle of twist per unit length	$G \theta \frac{\partial \Psi}{\partial x} = -\sigma_{yz}$ $G \theta \frac{\partial \Psi}{\partial y} = \sigma_{xz}$
Electrostatics	Scalar potential ϕ	Dielectric constant ϵ	Charge density ρ	Displacement flux density D_n
Magnetostatics	Magnetic potential ϕ	Permeability μ	Charge density ρ	Magnetic flux density B_n
Membranes	Transverse deflection u	Tension in membrane T	Transversely distributed load	Normal force q

8.2 BOUNDARY VALUE PROBLEMS

8.2.1 The Model Equation

Consider the problem of finding the solution $u(x, y)$ of the second-order partial differential equation

$$-\frac{\partial}{\partial x} \left(a_{11} \frac{\partial u}{\partial x} + a_{12} \frac{\partial u}{\partial y} \right) - \frac{\partial}{\partial y} \left(a_{21} \frac{\partial u}{\partial x} + a_{22} \frac{\partial u}{\partial y} \right) + a_{00}u - f = 0 \quad (8.2.1)$$

for given data a_{ij} ($i, j = 1, 2$), a_{00} and f , and specified boundary conditions. The form of the boundary conditions will be apparent from the weak formulation. As a special case, we

can obtain the Poisson equation from (8.2.1) by setting $a_{11} = a_{22} = k(x, y)$ and $a_{12} = a_{21} = a_{00} = 0$:

$$-\nabla \cdot (k \nabla u) = f(x, y) \quad \text{in } \Omega \quad (8.2.2)$$

where ∇ is the gradient operator. If $\hat{\mathbf{i}}$ and $\hat{\mathbf{j}}$ denote the unit vectors directed along the x and y axes, respectively, the gradient operator can be expressed as (see Sec. 2.2.3)

$$\nabla = \hat{\mathbf{i}} \frac{\partial}{\partial x} + \hat{\mathbf{j}} \frac{\partial}{\partial y}$$

and (8.2.2) in the Cartesian coordinate system takes the form

$$-\frac{\partial}{\partial x} \left(k \frac{\partial u}{\partial x} \right) - \frac{\partial}{\partial y} \left(k \frac{\partial u}{\partial y} \right) = f(x, y) \quad (8.2.3)$$

In the following, we shall develop the finite element model of (8.2.1). The major steps are as follows:

1. Discretization of the domain into a set of finite elements.
2. Weak (or weighted-integral) formulation of the governing differential equation.
3. Derivation of finite element interpolation functions.
4. Development of the finite element model using the weak form.
5. Assembly of finite elements to obtain the global system of algebraic equations.
6. Imposition of boundary conditions.
7. Solution of equations.
8. Postcomputation of solution and quantities of interest.

Steps 6 and 7 remain unchanged from one-dimensional finite element analysis because at the end of Step 5 we have a set of algebraic equations whose form is independent of the dimension of the domain or nature of the problem. In the following sections, we discuss each step in detail.

8.2.2 Finite Element Discretization

In two dimensions there is more than one simple geometric shape that can be used as a finite element (see Fig. 8.2.1). As we shall see shortly, the interpolation functions depend not only on the number of nodes in the element and the number of unknowns per node, but also on the shape of the element. The shape of the element must be such that its geometry is uniquely defined by a set of points, which serve as the element nodes in the development of the interpolation functions. As will be discussed later in this section, a triangle is the simplest geometric shape, followed by a rectangle.

The representation of a given region by a set of elements (i.e., discretization or *mesh generation*) is an important step in finite element analysis. The choice of element type, number of elements, and density of elements depends on the geometry of the domain, the problem to be analyzed, and the degree of accuracy desired. Of course, there are no specific formulae to obtain this information. In general, the analyst is guided by his or her technical background, insight into the physics of the problem being modeled

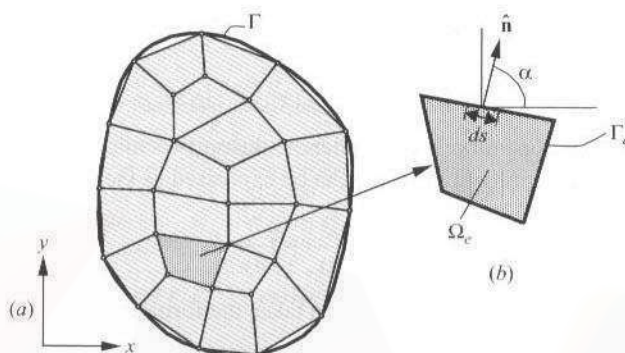


Figure 8.2.1 Finite element discretization of an irregular domain: (a) discretization of a domain by quadrilateral elements; and (b) a typical quadrilateral element Ω_e (with the unit normal \hat{n} on the boundary Γ_e of the element).

(e.g., a qualitative understanding of the solution), and experience with finite element modeling. The general rules of mesh generation for finite element formulations include:

1. The elements that are selected should characterize the governing equations of the problem.
2. The number, shape, and type (i.e., linear or quadratic) of elements should be such that the geometry of the domain is represented as accurately as desired.
3. The density of elements should be such that regions of large gradients of the solution are adequately modeled (i.e., use more elements or higher-order elements in regions of large gradients).
4. Mesh refinements should vary gradually from high-density regions to low-density regions. If *transition elements* are used, they should be used away from critical regions (i.e., regions of large gradients). Transition elements are those that connect lower-order elements to higher-order elements (e.g., linear to quadratic).

8.2.3 Weak Form

In the development of the weak form we need only consider a typical element. We assume that Ω_e is a typical element, whether triangular or quadrilateral, of the finite element mesh, and we develop the finite element model of (8.2.1) over Ω_e . Various two-dimensional elements will be discussed in the sequel.

Following the three-step procedure presented in Chapters 2 and 3, we develop the weak form of (8.2.1) over the typical element Ω_e . The first step is to multiply (8.2.1) with a weight function w , which is assumed to be differentiable once with respect to x and y , and then integrate the equation over the element domain Ω_e :

$$0 = \int_{\Omega_e} w \left[-\frac{\partial}{\partial x}(F_1) - \frac{\partial}{\partial y}(F_2) + a_{00}u - f \right] dx dy \quad (8.2.4a)$$

where

$$F_1 = a_{11} \frac{\partial u}{\partial x} + a_{12} \frac{\partial u}{\partial y}, \quad F_2 = a_{21} \frac{\partial u}{\partial x} + a_{22} \frac{\partial u}{\partial y} \quad (8.2.4b)$$

In the second step we distribute the differentiation among u and w equally. To achieve this, we integrate the first two terms in (8.2.4a) by parts. First, we note the identities

$$\frac{\partial}{\partial x}(w F_1) = \frac{\partial w}{\partial x} F_1 + w \frac{\partial F_1}{\partial x} \quad \text{or} \quad -w \frac{\partial F_1}{\partial x} = \frac{\partial w}{\partial x} F_1 - \frac{\partial}{\partial x}(w F_1) \quad (8.2.5a)$$

$$\frac{\partial}{\partial y}(w F_2) = \frac{\partial w}{\partial y} F_2 + w \frac{\partial F_2}{\partial y} \quad \text{or} \quad -w \frac{\partial F_2}{\partial y} = \frac{\partial w}{\partial y} F_2 - \frac{\partial}{\partial y}(w F_2) \quad (8.2.5b)$$

Next, we use the component form of the gradient (or divergence) theorem

$$\int_{\Omega_e} \frac{\partial}{\partial x}(w F_1) dx dy = \oint_{\Gamma_e} w F_1 n_x ds \quad (8.2.6a)$$

$$\int_{\Omega_e} \frac{\partial}{\partial y}(w F_2) dx dy = \oint_{\Gamma_e} w F_2 n_y ds \quad (8.2.6b)$$

where n_x and n_y are the components (i.e., the direction cosines) of the unit normal vector

$$\hat{\mathbf{n}} = n_x \hat{\mathbf{i}} + n_y \hat{\mathbf{j}} = \cos \alpha \hat{\mathbf{i}} + \sin \alpha \hat{\mathbf{j}} \quad (8.2.7)$$

on the boundary Γ_e , and ds is the length of an infinitesimal line element along the boundary (see Fig. 8.2.1b). Using (8.2.5a), (8.2.5b), (8.2.6a), and (8.2.6b) in (8.2.4a), we obtain

$$0 = \int_{\Omega_e} \left[\frac{\partial w}{\partial x} \left(a_{11} \frac{\partial u}{\partial x} + a_{12} \frac{\partial u}{\partial y} \right) + \frac{\partial w}{\partial y} \left(a_{21} \frac{\partial u}{\partial x} + a_{22} \frac{\partial u}{\partial y} \right) + a_{00} w u - w f \right] dx dy \\ - \oint_{\Gamma_e} w \left[n_x \left(a_{11} \frac{\partial u}{\partial x} + a_{12} \frac{\partial u}{\partial y} \right) + n_y \left(a_{21} \frac{\partial u}{\partial x} + a_{22} \frac{\partial u}{\partial y} \right) \right] ds \quad (8.2.8)$$

From an inspection of the boundary integral in (8.2.8), we note that the specification of u constitutes the essential boundary condition, and hence u is the primary variable. The specification of the coefficient of the weight function in the boundary expression

$$q_n \equiv n_x \left(a_{11} \frac{\partial u}{\partial x} + a_{12} \frac{\partial u}{\partial y} \right) + n_y \left(a_{21} \frac{\partial u}{\partial x} + a_{22} \frac{\partial u}{\partial y} \right) \quad (8.2.9)$$

constitutes the natural boundary condition; thus, q_n is the secondary variable of the formulation. The function $q_n = q_n(s)$ denotes the projection of the vector $\mathbf{a} \cdot \nabla u$ along the unit normal $\hat{\mathbf{n}}$. By definition, q_n is taken positive outward from the surface as we move counterclockwise along the boundary Γ_e . In most problems, the secondary variable q_n is of physical interest. For example, in the case of heat transfer through an anisotropic medium, a_{ij} are the conductivities of the medium, and q_n is the negative of the heat flux (because of the Fourier heat conduction law) normal to the boundary of the element.

The third and last step of the formulation is to use the definition (8.2.9) in (8.2.8) and write the weak form of (8.2.1) as

$$0 = \int_{\Omega_e} \left[\frac{\partial w}{\partial x} \left(a_{11} \frac{\partial u}{\partial x} + a_{12} \frac{\partial u}{\partial y} \right) + \frac{\partial w}{\partial y} \left(a_{21} \frac{\partial u}{\partial x} + a_{22} \frac{\partial u}{\partial y} \right) + a_{00} w u - w f \right] dx dy \\ - \oint_{\Gamma_e} w q_n ds \quad (8.2.10)$$

or,

$$B^e(w, u) = l^e(w) \quad (8.2.11a)$$

where the bilinear form $B^e(\cdot, \cdot)$ and linear form $l^e(\cdot)$ are

$$B^e(w, u) = \int_{\Omega_e} \left[\frac{\partial w}{\partial x} \left(a_{11} \frac{\partial u}{\partial x} + a_{12} \frac{\partial u}{\partial y} \right) + \frac{\partial w}{\partial y} \left(a_{21} \frac{\partial u}{\partial x} + a_{22} \frac{\partial u}{\partial y} \right) + a_{00} w u \right] dx dy \quad (8.2.11b)$$

$$l^e(w) = \int_{\Omega_e} w f dx dy + \oint_{\Gamma_e} w q_n ds$$

The weak form (or *weighted integral statement*) in (8.2.10) or (8.2.11a) and (8.2.11b) is the basis of the finite element model of (8.2.1).

Whenever $B^e(w, u)$ is symmetric in its arguments w and u [i.e., $B^e(w, u) = B^e(u, w)$], the quadratic functional associated with the variational problem (8.2.11a) can be obtained from [see Eq. (2.4.19)]

$$I^e(w) = \frac{1}{2} B^e(w, w) - l^e(w) \quad (8.2.12a)$$

The bilinear form in (8.2.11b) is symmetric if and only if $a_{12} = a_{21}$. Then the functional is given by

$$\begin{aligned} I^e(w) &= \frac{1}{2} \int_{\Omega_e} \left[a_{11} \left(\frac{\partial u}{\partial x} \right)^2 + 2a_{12} \frac{\partial u}{\partial x} \frac{\partial u}{\partial y} + a_{22} \left(\frac{\partial u}{\partial y} \right)^2 + a_{00} u^2 \right] dx dy \\ &\quad + \int_{\Omega_e} u f dx dy + \oint_{\Gamma_e} u q_n ds \end{aligned} \quad (8.2.12b)$$

Vector Form of the Variational Problem

It is common, especially in structural mechanics literature, to express finite element formulations in vector notation (i.e., in terms of matrices). While the vector/matrix notation is concise, it is not as transparent as the explicit form that has been used throughout the book. However, for the sake of completeness, the vector form of the variational (or weak) problem (8.2.11a) and (8.2.11b) is presented here. We shall use bold face letters for matrices of different order, including the 1×1 matrix and row and column matrices.

We begin with Eq. (8.2.11a), which can be written as

$$B^e(\mathbf{w}, \mathbf{u}) = l^e(\mathbf{w}) \quad (8.2.13)$$

where, in the present case, \mathbf{w} is simply w and \mathbf{u} is u . Next, we express $B^e(\cdot, \cdot)$ and $l^e(\cdot)$ in matrix form. Let

$$\mathbf{C} = \begin{bmatrix} a_{11} & a_{12} & 0 \\ a_{21} & a_{22} & 0 \\ 0 & 0 & a_{00} \end{bmatrix}, \quad \mathbf{D} = \begin{Bmatrix} \frac{\partial}{\partial x} \\ \frac{\partial}{\partial y} \\ 1 \end{Bmatrix} \quad (8.2.14)$$

Then B^e and l^e of (8.2.11b) can be expressed as

$$B^e(w, u) = \int_{\Omega_e} \left\{ \begin{array}{c} \frac{\partial w}{\partial x} \\ \frac{\partial w}{\partial y} \\ w \end{array} \right\}^T \begin{bmatrix} a_{11} & a_{12} & 0 \\ a_{21} & a_{22} & 0 \\ 0 & 0 & a_{00} \end{bmatrix} \begin{bmatrix} \frac{\partial u}{\partial x} \\ \frac{\partial u}{\partial y} \\ u \end{bmatrix} dx dy \quad (8.2.15a)$$

$$l^e(w) = \int_{\Omega_e} \{w\}^T \{f\} dx dy + \oint_{\Gamma_e} \{w\}^T \{q_n\} ds$$

or, simply

$$B^e(\mathbf{w}, \mathbf{u}) = \int_{\Omega_e} (\mathbf{D}\mathbf{w})^T \mathbf{C} \mathbf{D}\mathbf{u} dx dy, \quad l^e(\mathbf{w}) = \int_{\Omega_e} \mathbf{w}^T \mathbf{f} dx dy + \int_{\Gamma_e} \mathbf{w}^T \mathbf{q} ds \quad (8.2.15b)$$

8.2.4 Finite Element Model

The weak form in (8.2.10) requires that the approximation chosen for u should be at least linear in both x and y so that there are no terms in (8.2.10) that are identically zero. Since the primary variable is simply the function itself, the Lagrange family of interpolation functions is admissible.

Suppose that u is approximated over a typical finite element Ω_e by the expression

$$u(x, y) \approx u_h^e(x, y) = \sum_{j=1}^n u_j^e \psi_j^e(x, y) \quad \text{or} \quad u_h^e(x, y) = (\Psi^e)^T \mathbf{u}^e \quad (8.2.16a)$$

where \mathbf{u}^e and Ψ^e are $n \times 1$ vectors

$$\mathbf{u}^e = \{u_1^e \ u_2^e \ u_3^e \ \dots \ u_n^e\}^T, \quad \Psi^e = \{\psi_1^e \ \psi_2^e \ \psi_3^e \ \dots \ \psi_n^e\}^T \quad (8.2.16b)$$

and u_j^e is the value of u_h^e at the j th node (x_j, y_j) of the element and ψ_j^e are the Lagrange interpolation functions, with the property

$$\psi_i^e(x_j, y_j) = \delta_{ij} \quad (i, j = 1, 2, \dots, n) \quad (8.2.17)$$

In deriving the finite element equations in algebraic terms, we need not know the shape of the element Ω_e or the form of ψ_i^e . The specific form of ψ_i^e will be developed for triangular and rectangular geometries of the element Ω_e in Section 8.2.5, and higher-order interpolation functions will be presented in Chapter 9.

Substituting the finite element approximation (8.2.16a) for u into the weak form (8.2.10) or (8.2.13), we obtain

$$0 = \int_{\Omega_e} \left[\frac{\partial w}{\partial x} \left(a_{11} \sum_{j=1}^n u_j^e \frac{\partial \psi_j^e}{\partial x} + a_{12} \sum_{j=1}^n u_j^e \frac{\partial \psi_j^e}{\partial y} \right) + \frac{\partial w}{\partial y} \left(a_{21} \sum_{j=1}^n u_j^e \frac{\partial \psi_j^e}{\partial x} + a_{22} \sum_{j=1}^n u_j^e \frac{\partial \psi_j^e}{\partial y} \right) + a_{00} w \sum_{j=1}^n u_j^e \psi_j^e - wf \right] dx dy - \oint_{\Gamma_e} w q_n ds \quad (8.2.18a)$$

or

$$0 = \int_{\Omega_e} (\mathbf{D}\mathbf{w})^T \mathbf{C} \mathbf{D}(\Psi^T \mathbf{u}^e) dx dy - \int_{\Omega_e} \mathbf{w}^T \mathbf{f} dx dy - \oint_{\Gamma_e} \mathbf{w}^T \mathbf{q} ds \quad (8.2.18b)$$

This equation must hold for every admissible choice of weight function w . Since we need n independent algebraic equations to solve for the n unknowns, $u_1^e, u_2^e, \dots, u_n^e$, we choose n linearly independent functions for w : $w = \psi_1^e, \psi_2^e, \dots, \psi_n^e$ (or, $\mathbf{w} = \{\psi_1^e \ \psi_2^e \ \dots \ \psi_n^e\} = \Psi^T$). This particular choice of weight function is a natural one when the weight function is viewed as a virtual variation of the dependent unknown (i.e., $w = \delta u \approx \sum_{i=1}^n \delta u_i \psi_i$), and the resulting finite element model is known as the *weak-form finite element model* or *Ritz finite element model*. For each choice of w we obtain an algebraic relation among $(u_1^e, u_2^e, \dots, u_n^e)$. We label the algebraic equation resulting from substitution of ψ_i^e for w into (8.2.18a) as the first algebraic equation, that resulting from $w = \psi_2^e$ as the second equation, and so on. Thus, the i th algebraic equation is obtained by substituting $w = \psi_i^e$ into (8.2.18a):

$$0 = \sum_{j=1}^n \left\{ \int_{\Omega_e} \left[\frac{\partial \psi_i^e}{\partial x} \left(a_{11} \frac{\partial \psi_j^e}{\partial x} + a_{12} \frac{\partial \psi_j^e}{\partial y} \right) + \frac{\partial \psi_i^e}{\partial y} \left(a_{21} \frac{\partial \psi_j^e}{\partial x} + a_{22} \frac{\partial \psi_j^e}{\partial y} \right) \right. \right. \\ \left. \left. + a_{00} \psi_i^e \psi_j^e \right] dx dy \right\} u_j - \int_{\Omega_e} f \psi_i^e dx dy - \oint_{\Gamma_e} \psi_i^e q_n ds$$

or

$$\sum_{j=1}^n K_{ij}^e u_j^e = f_i^e + Q_i^e \quad (i = 1, 2, \dots, n) \quad (8.2.19a)$$

where

$$K_{ij}^e = \int_{\Omega_e} \left[\frac{\partial \psi_i^e}{\partial x} \left(a_{11} \frac{\partial \psi_j^e}{\partial x} + a_{12} \frac{\partial \psi_j^e}{\partial y} \right) + \frac{\partial \psi_i^e}{\partial y} \left(a_{21} \frac{\partial \psi_j^e}{\partial x} + a_{22} \frac{\partial \psi_j^e}{\partial y} \right) \right. \\ \left. + a_{00} \psi_i^e \psi_j^e \right] dx dy \quad (8.2.19b)$$

$$f_i^e = \int_{\Omega_e} f \psi_i^e dx dy, \quad Q_i^e = \oint_{\Gamma_e} q_n \psi_i^e ds$$

In matrix notation, (8.2.19a) takes the form

$$[\mathbf{K}^e]\{\mathbf{u}^e\} = \{f^e\} + \{Q^e\} \quad \text{or} \quad \mathbf{K}^e \mathbf{u}^e = \mathbf{f}^e + \mathbf{Q}^e \quad (8.2.20a)$$

where [see Eq. (8.2.18b)]

$$\mathbf{K}^e = \int_{\Omega_e} \mathbf{B}^T \mathbf{C} \mathbf{B} dx dy, \quad \mathbf{f}^e = \int_{\Omega_e} \Psi \mathbf{f} ds, \quad \mathbf{Q}^e = \int_{\Gamma_e} \Psi \mathbf{q} ds \quad (8.2.20b)$$

$$\mathbf{B} = \mathbf{D} \Psi^T = \begin{bmatrix} \psi_{1,x}^e & \psi_{2,x}^e & \dots & \psi_{n,x}^e \\ \psi_{1,y}^e & \psi_{2,y}^e & \dots & \psi_{n,y}^e \\ \psi_1^e & \psi_2^e & \dots & \psi_n^e \end{bmatrix}$$

Note that $K_{ij}^e = K_{ji}^e$ (i.e., $[\mathbf{K}^e]$ is a symmetric matrix of order $n \times n$) only when $a_{12} = a_{21}$. Equations (8.2.20a) and (8.2.20b) represents the finite element model of (8.2.1). This completes the finite element model development. Before we discuss assembly of element equations, it is informative to consider the derivation of the interpolations ψ_i^e for certain basic elements and the evaluation of the element matrices in Eqs. (8.2.19b).

8.2.5 Derivation of Interpolation Functions

The finite element approximation $u_h^e(x, y)$ over an element Ω_e must satisfy the following conditions in order for the approximate solution to converge to the true solution:

- $1.$ u_h^e must be continuous as required in the weak form of the problem (i.e., all terms in the weak form are represented as nonzero values).
- $2.$ The polynomials used to represent u_h^e must be complete (i.e., all terms, beginning with a constant term up to the highest-order used in the polynomial, should be included in u_h^e).
- $3.$ All terms in the polynomial should be linearly independent.

The number of linearly independent terms in the representation of u_h^e dictates the shape and number of degrees of freedom of the element. Next, we discuss some of the basic polynomials and associated elements for the model problem with a single degree of freedom per node.

Triangular Element

An examination of the weak form (8.2.10) and the finite element matrices in (8.2.19b) shows that ψ_i^e should be at least linear functions of x and y . The complete linear polynomial in x and y in Ω_e is of the form

$$u_h^e(x, y) = c_1^e + c_2^e x + c_3^e y \quad (8.2.21)$$

where c_i^e are constants. The set $\{1, x, y\}$ is linearly independent and complete. Equation (8.2.21) defines a unique plane for fixed c_i^e . Thus, if $u(x, y)$ is a curved surface, $u_h^e(x, y)$ approximates the surface by a plane. In particular, $u_h^e(x, y)$ is uniquely defined on a triangle by the three values of $u_h^e(x, y)$ at the vertices of the triangle (see Fig. 8.2.2). Let us denote

$$u_h^e(x_1, y_1) = u_1^e, \quad u_h^e(x_2, y_2) = u_2^e, \quad u_h^e(x_3, y_3) = u_3^e \quad (8.2.22)$$

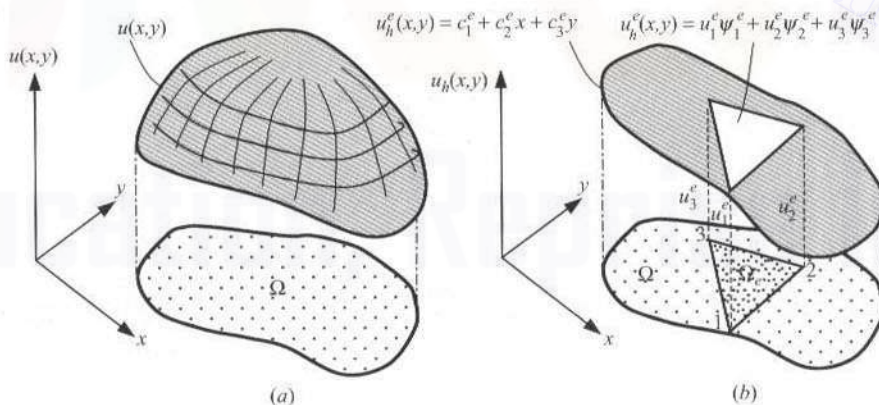


Figure 8.2.2 Approximation of a curved surface over a triangle.

where (x_i, y_i) denote the coordinates of the i th vertex of the triangle. Note that the triangle is uniquely defined by the three pairs of coordinates (x_i, y_i) .

The three constants c_i^e ($i = 1, 2, 3$) in (8.2.21) can be expressed in terms of three nodal values u_i^e ($i = 1, 2, 3$). Thus, the polynomial (8.2.21) is associated with a triangular element and there are three nodes identified, namely, the vertices of the triangle. Equations in (8.2.22) have the explicit form

$$u_1 \equiv u_h(x_1, y_1) = c_1 + c_2 x_1 + c_3 y_1$$

$$u_2 \equiv u_h(x_2, y_2) = c_1 + c_2 x_2 + c_3 y_2$$

$$u_3 \equiv u_h(x_3, y_3) = c_1 + c_2 x_3 + c_3 y_3$$

where the element label e is omitted for simplicity. Throughout the following discussion, this format will be followed. In matrix form, we have

$$\begin{Bmatrix} u_1 \\ u_2 \\ u_3 \end{Bmatrix} = \begin{bmatrix} 1 & x_1 & y_1 \\ 1 & x_2 & y_2 \\ 1 & x_3 & y_3 \end{bmatrix} \begin{Bmatrix} c_1 \\ c_2 \\ c_3 \end{Bmatrix} \text{ or } \mathbf{u} = \mathbf{A}\mathbf{c} \quad (8.2.23)$$

Solution of (8.2.23) for c_i ($i = 1, 2, 3$) requires the inversion of the coefficient matrix \mathbf{A} in (8.2.23). The inverse ceases to exist whenever any two rows or columns are the same. Two rows or columns of the coefficient matrix in (8.2.23) will be the same only when all three nodes lie on the same line. Thus, in theory, as long as the three vertices of the triangle are distinct and do not lie on a line, the coefficient matrix is invertible. However, in actual computations, if any two of the three nodes are *very close* to the third node or the three nodes are almost on the same line, the coefficient matrix can be *nearly singular* and numerically noninvertible. Hence, we should avoid elements with narrow geometries (see Fig. 8.2.3) in finite element meshes.

Inverting the coefficient matrix in (8.2.23), we obtain

$$[A]^{-1} = \frac{1}{2A} \begin{bmatrix} \alpha_1 & \alpha_2 & \alpha_3 \\ \beta_1 & \beta_2 & \beta_3 \\ \gamma_1 & \gamma_2 & \gamma_3 \end{bmatrix}, \quad 2A = \alpha_1 + \alpha_2 + \alpha_3$$

where $2A$ is the determinant of the matrix \mathbf{A} , A being the area of the triangle whose three vertices are at (x_i, y_i) ($i = 1, 2, 3$). Solving for c_i in terms of u_i (i.e., $\{c\} = [A]^{-1}\{u\}$),

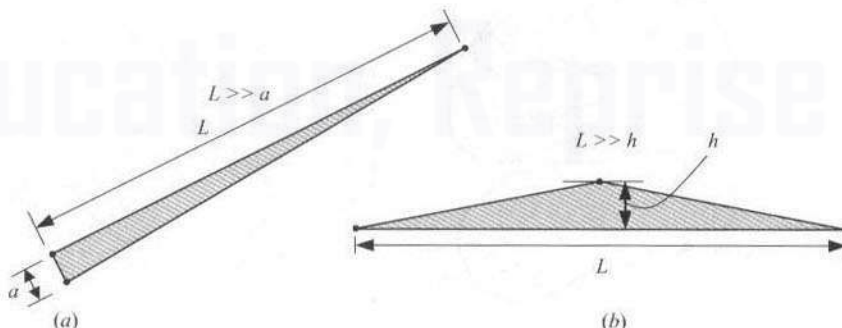


Figure 8.2.3 Triangular geometries that should be avoided in finite element meshes.

we obtain

$$\begin{aligned} c_1 &= \frac{1}{2A}(\alpha_1 u_1 + \alpha_2 u_2 + \alpha_3 u_3) \\ c_2 &= \frac{1}{2A}(\beta_1 u_1 + \beta_2 u_2 + \beta_3 u_3) \\ c_3 &= \frac{1}{2A}(\gamma_1 u_1 + \gamma_2 u_2 + \gamma_3 u_3) \end{aligned} \quad (8.2.24a)$$

where α_i , β_i , and γ_i are constants that depend only on the global coordinates of element nodes (x_i, y_i)

$$\left. \begin{array}{l} \alpha_i = x_j y_k - x_k y_j \\ \beta_i = y_j - y_k \\ \gamma_i = -(x_j - x_k) \end{array} \right\} (i \neq j \neq k; i, j, \text{ and } k \text{ permute in a natural order}) \quad (8.2.24b)$$

Substituting for c_i from (8.2.24a) into (8.2.21), we obtain

$$\begin{aligned} u_h^e(x, y) &= \frac{1}{2A}[(u_1\alpha_1 + u_2\alpha_2 + u_3\alpha_3) + (u_1\beta_1 + u_2\beta_2 + u_3\beta_3)x \\ &\quad + (\gamma_1 u_1 + \gamma_2 u_2 + \gamma_3 u_3)y] \\ &= \sum_{i=1}^3 u_i^e \psi_i^e(x, y) \end{aligned} \quad (8.2.25a)$$

where ψ_i^e are the linear interpolation functions for the triangular element

$$\psi_i^e = \frac{1}{2A_e}(\alpha_i^e + \beta_i^e x + \gamma_i^e y) \quad (i = 1, 2, 3) \quad (8.2.25b)$$

and α_i^e , β_i^e , and γ_i^e are the constants defined in (8.2.24b). The linear interpolation functions ψ_i^e are shown in Fig. 8.2.4.

The interpolation functions ψ_i^e have the properties

$$\psi_i^e(x_j^e, y_j^e) = \delta_{ij} \quad (i, j = 1, 2, 3) \quad (8.2.26a)$$

$$\sum_{i=1}^3 \psi_i^e = 1, \quad \sum_{i=1}^3 \frac{\partial \psi_i^e}{\partial x} = 0, \quad \sum_{i=1}^3 \frac{\partial \psi_i^e}{\partial y} = 0 \quad (8.2.26b)$$

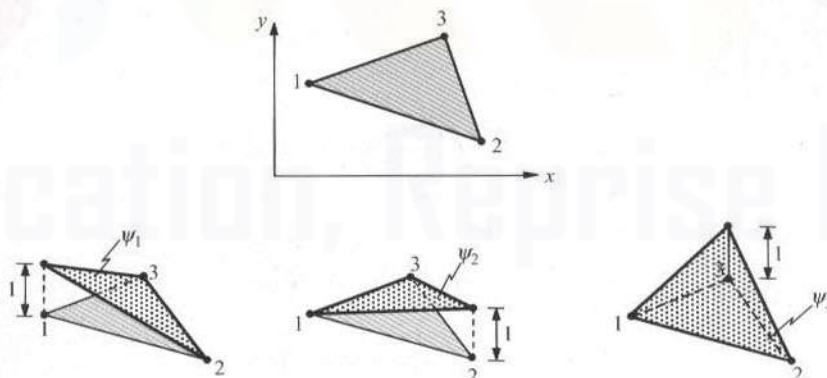


Figure 8.2.4 Interpolation functions for the three-node triangle.

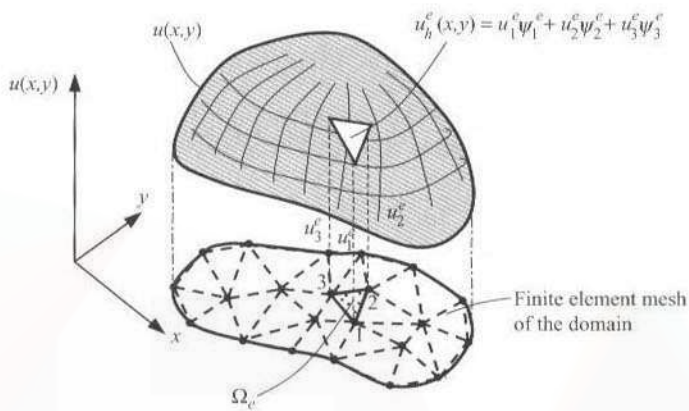


Figure 8.2.5 Representation of a continuous function $u(x, y)$ by linear interpolation functions of three-node triangular elements.

Note that (8.2.24a) determines a plane surface passing through u_1 , u_2 , and u_3 . Hence, use of the linear interpolation functions ψ_i^e of a triangle will result in the approximation of the curved surface $u(x, y)$ by a planar function $u_h^e = \sum_{i=1}^3 u_i^e \psi_i^e$ as shown in Fig. 8.2.5. We consider an example of computing ψ_i^e .

Example 8.2.1

Consider the triangular element shown in Fig. 8.2.6. Let

$$u_h(x, y) = c_1 + c_2x + c_3y = [1 \ x \ y] \begin{Bmatrix} c_1 \\ c_2 \\ c_3 \end{Bmatrix}$$

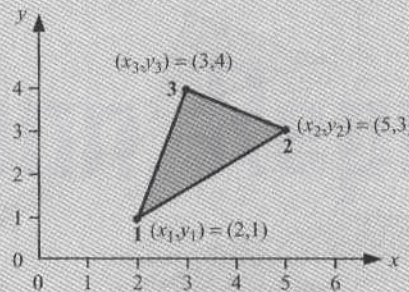


Figure 8.2.6 The triangular element of Example 8.2.1.

Evaluating this polynomial at nodes 1, 2, and 3, we obtain the equations

$$\begin{Bmatrix} u_1 \\ u_2 \\ u_3 \end{Bmatrix} = \begin{bmatrix} 1 & 2 & 1 \\ 1 & 5 & 3 \\ 1 & 3 & 4 \end{bmatrix} \begin{Bmatrix} c_1 \\ c_2 \\ c_3 \end{Bmatrix}, \quad \begin{Bmatrix} c_1 \\ c_2 \\ c_3 \end{Bmatrix} = [A]^{-1} \begin{Bmatrix} u_1 \\ u_2 \\ u_3 \end{Bmatrix}$$

where

$$[A]^{-1} = \begin{bmatrix} 1 & 2 & 1 \\ 1 & 5 & 3 \\ 1 & 3 & 4 \end{bmatrix}^{-1} = \frac{1}{7} \begin{bmatrix} 11 & -5 & 1 \\ -1 & 3 & -2 \\ -2 & -1 & 3 \end{bmatrix}$$

Substituting the last expression into u_h , we obtain

$$\begin{aligned} u_h(x, y) &= \{1 - x - y\} [A]^{-1} \begin{Bmatrix} u_1 \\ u_2 \\ u_3 \end{Bmatrix} = \frac{1}{7} \{11 - x - 2y, -5 + 3x - y, 1 - 2x + 3y\} \begin{Bmatrix} u_1 \\ u_2 \\ u_3 \end{Bmatrix} \\ &\equiv \{\psi_1^e \quad \psi_2^e \quad \psi_3^e\} \begin{Bmatrix} u_1 \\ u_2 \\ u_3 \end{Bmatrix} = \sum_{i=1}^3 \psi_i^e u_i^e \end{aligned}$$

where

$$\psi_1^e = \frac{1}{7}(11 - x - 2y), \quad \psi_2^e = \frac{1}{7}(-5 + 3x - y), \quad \psi_3^e = \frac{1}{7}(1 - 2x + 3y)$$

Alternatively, from definitions (8.2.24b), we have

$$\alpha_1 = 5 \times 4 - 3 \times 3 = 11, \quad \alpha_2 = 3 \times 1 - 2 \times 4 = -5, \quad \alpha_3 = 2 \times 3 - 5 \times 1 = 1$$

$$\beta_1 = 3 - 4 = -1, \quad \beta_2 = 4 - 1 = 3, \quad \beta_3 = 1 - 3 = -2$$

$$\gamma_1 = -(5 - 3) = -2, \quad \gamma_2 = -(3 - 2) = -1, \quad \gamma_3 = -(2 - 5) = 3$$

$$2A = \alpha_1 + \alpha_2 + \alpha_3 = 7$$

The interpolation functions are

$$\psi_1^e = \frac{1}{7}(11 - x - 2y), \quad \psi_2^e = \frac{1}{7}(-5 + 3x - y), \quad \psi_3^e = \frac{1}{7}(1 - 2x + 3y)$$

which are the same as those obtained earlier.

Linear Rectangular Element

Next, consider the complete polynomial

$$u_h^e(x, y) = c_1^e + c_2^e x + c_3^e y + c_4^e xy \quad (8.2.27)$$

which contains four linearly independent terms and is linear in x and y , with a bilinear term in x and y . This polynomial requires an element with four nodes. There are two possible geometric shapes: a triangle with the fourth node at the center (or centroid) of the triangle or

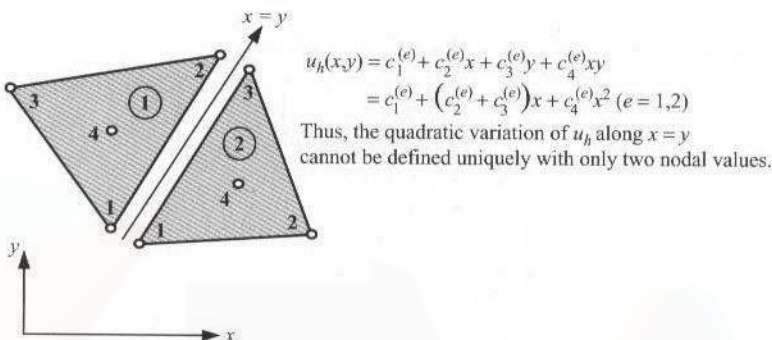


Figure 8.2.7 Incompatible four-node triangular elements.

a rectangle with the nodes at the vertices. A triangle with a fourth node at the center does not provide a single-valued variation of u at interelement boundaries, resulting in *incompatible* variation of u at interelement boundaries and is therefore not admissible (see Fig. 8.2.7). The linear rectangular element is a compatible element because on any side u_h^e varies only linearly and there are two nodes to uniquely define it.

Here we consider an approximation of the form (8.2.27) and use a rectangular element with sides a and b [see Fig. 8.2.8(a)]. For the sake of convenience, we choose a local coordinate system (\bar{x}, \bar{y}) to derive the interpolation functions. We assume that (the element label is omitted)

$$u_h(\bar{x}, \bar{y}) = c_1 + c_2\bar{x} + c_3\bar{y} + c_4\bar{x}\bar{y} \quad (8.2.28)$$

and require

$$\begin{aligned} u_1 &= u_h(0, 0) = c_1 \\ u_2 &= u_h(a, 0) = c_1 + c_2a \\ u_3 &= u_h(a, b) = c_1 + c_2a + c_3b + c_4ab \\ u_4 &= u_h(0, b) = c_1 + c_3b \end{aligned} \quad (8.2.29)$$

Solving for c_i ($i = 1, \dots, 4$), we obtain

$$\begin{aligned} c_1 &= u_1, & c_2 &= \frac{u_2 - u_1}{a} \\ c_3 &= \frac{u_4 - u_1}{b}, & c_4 &= \frac{u_3 - u_4 + u_1 - u_2}{ab} \end{aligned} \quad (8.2.30)$$

Substituting (8.2.30) into (8.2.28), we obtain

$$\begin{aligned} u_h(\bar{x}, \bar{y}) &= u_1 \left(1 - \frac{\bar{x}}{a} - \frac{\bar{y}}{b} + \frac{\bar{x}\bar{y}}{ab} \right) + u_2 \left(\frac{\bar{x}}{a} - \frac{\bar{x}\bar{y}}{ab} \right) + u_3 \frac{\bar{x}\bar{y}}{ab} + u_4 \left(\frac{\bar{y}}{b} - \frac{\bar{x}\bar{y}}{ab} \right) \\ &= u_1^e \psi_1^e + u_2^e \psi_2^e + u_3^e \psi_3^e + u_4^e \psi_4^e = \sum_{i=1}^4 u_i^e \psi_i^e \end{aligned} \quad (8.2.31)$$

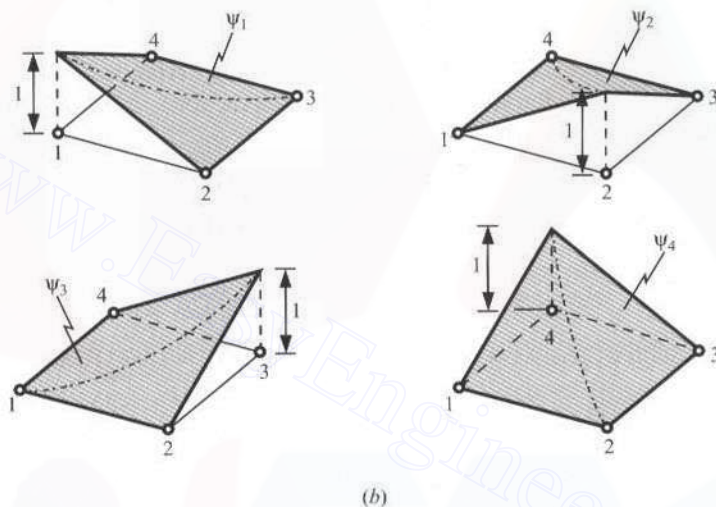
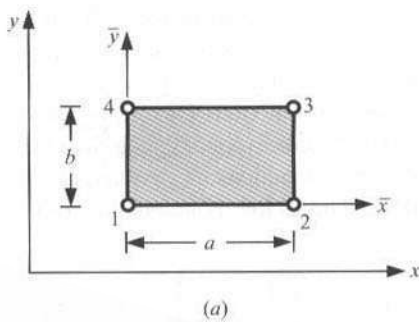


Figure 8.2.8 Linear rectangular element and its interpolation functions.

where

$$\begin{aligned}\psi_1^e &= \left(1 - \frac{\bar{x}}{a}\right) \left(1 - \frac{\bar{y}}{b}\right), & \psi_2^e &= \frac{\bar{x}}{a} \left(1 - \frac{\bar{y}}{b}\right) \\ \psi_3^e &= \frac{\bar{x}}{a} \frac{\bar{y}}{b}, & \psi_4^e &= \left(1 - \frac{\bar{x}}{a}\right) \frac{\bar{y}}{b}\end{aligned}\quad (8.2.32a)$$

or, in concise form,

$$\psi_i^e(\bar{x}, \bar{y}) = (-1)^{i+1} \left(1 - \frac{\bar{x} + \bar{x}_i}{a}\right) \left(1 - \frac{\bar{y} + \bar{y}_i}{b}\right) \quad (8.2.32b)$$

where (\bar{x}_i, \bar{y}_i) are the (\bar{x}, \bar{y}) coordinates of node i . The interpolation functions are shown in Fig. 8.2.8(b). Once again, we have

$$\psi_i^e(\bar{x}_j, \bar{y}_j) = \delta_{ij} \quad (i, j = 1, \dots, 4), \quad \sum_{i=1}^4 \psi_i^e = 1 \quad (8.2.33)$$

The procedure given above for the construction of the interpolation functions involves the inversion of an $n \times n$ matrix, where n is the number of nodes in the element. When n is large, the inversion becomes very tedious.

Alternatively, the interpolation functions for rectangular element can also be obtained by taking the tensor product of the corresponding one-dimensional interpolation functions. To obtain the linear interpolation functions of a rectangular element, we take the “tensor product” of the one-dimensional linear interpolation functions (3.2.19) associated with sides 1–2 and 1–3:

$$\begin{Bmatrix} 1 - \frac{\bar{x}}{a} \\ \frac{\bar{x}}{a} \end{Bmatrix} \begin{Bmatrix} 1 - \frac{\bar{y}}{b} \\ \frac{\bar{y}}{b} \end{Bmatrix}^T = \begin{bmatrix} \psi_1 & \psi_4 \\ \psi_2 & \psi_3 \end{bmatrix} \quad (8.2.34)$$

The alternative procedure that makes use of the interpolation properties (8.2.33) can also be used. Here we illustrate the alternative procedure for the four-node rectangular element. Equation (8.2.26a) requires that

$$\psi_1^e(\bar{x}_i, \bar{y}_i) = 0 \quad (i = 2, 3, 4), \quad \psi_1^e(\bar{x}_1, \bar{y}_1) = 1$$

That is, ψ_1^e is identically zero on lines $\bar{x} = a$ and $\bar{y} = b$. Hence, $\psi_1^e(\bar{x}, \bar{y})$ must be of the form

$$\psi_1^e(\bar{x}, \bar{y}) = c_1(a - \bar{x})(b - \bar{y}) \quad \text{for any } c_1 \neq 0$$

Using the condition $\psi_1^e(\bar{x}_1, \bar{y}_1) = \psi_1^e(0, 0) = 1$, we obtain $c_1 = 1/ab$. Hence,

$$\psi_1^e(\bar{x}, \bar{y}) = \frac{1}{ab}(a - \bar{x})(b - \bar{y}) = \left(1 - \frac{\bar{x}}{a}\right)\left(1 - \frac{\bar{y}}{b}\right)$$

Likewise, we can obtain the remaining three interpolation functions.

Quadratic Elements

A quadratic triangular element must have three nodes per side in order to define a unique quadratic variation along that side. Thus, there are a total of six nodes in a quadratic triangular element [see Fig. 8.2.9(a)]. A six-term complete polynomial that includes both x and y is

$$u_h^e(x, y) = c_1 + c_2x + c_3y + c_4xy + c_5x^2 + c_6y^2 \quad (8.2.35)$$

The constants may be expressed in terms of the six nodal values by the procedure outlined for the three-node triangular element and four-node rectangular element. However, in practice the interpolation functions of higher-order elements are derived using the alternative procedure (i.e., use the interpolation properties).

Similarly, a quadratic rectangular element has three nodes per side, resulting in an eight-node rectangular element [see Fig. 8.2.9(b)]. The eight-term polynomial is

$$u_h^e(x, y) = c_1 + c_2x + c_3y + c_4xy + c_5x^2 + c_6y^2 + c_7xy^2 + c_8yx^2 \quad (8.2.36)$$

The interpolation functions of this element cannot be generated by the tensor product of one-dimensional quadratic functions (3.2.27). Indeed, the two-dimensional interpolation functions associated with the tensor product of one-dimensional quadratic functions correspond to the nine-node rectangular element [see Fig. 8.2.9(c)]. The nine-term polynomial

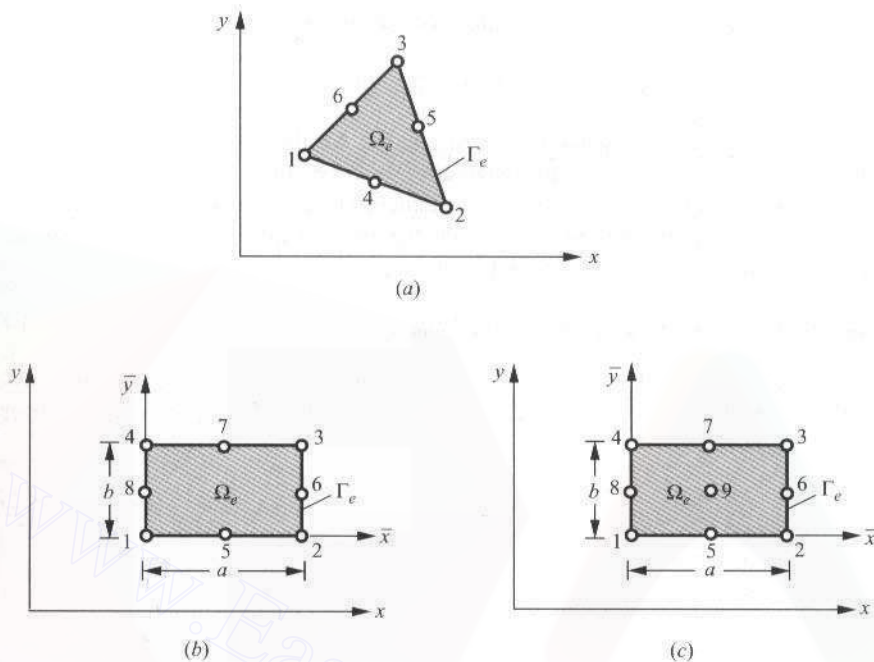


Figure 8.2.9 (a) Quadratic triangular element. (b) Eight-node quadratic rectangular element. (c) Nine-node quadratic rectangular element.

is given by

$$u_h^e(x, y) = c_1 + c_2x + c_3y + c_4xy + c_5x^2 + c_6y^2 + c_7xy^2 + c_8yx^2 + c_9x^2y^2 \quad (8.2.37)$$

Additional discussion on the derivation of element interpolation functions is presented in Chapter 9.

8.2.6 Evaluation of Element Matrices and Vectors

The exact evaluation of the element matrices $[K^e]$ and $\{f^e\}$ in (8.2.19b) is, in general, not easy. In general, they are evaluated using numerical integration techniques described in Section 9.3. However, when a_{ij} , a_{00} , and f are elementwise constant, it is possible to evaluate the integrals exactly over the linear triangular and rectangular elements discussed in the previous section. The boundary integral in $\{Q^e\}$ of (8.2.19b) can be evaluated whenever q_n is known. For an interior element (i.e., an element that does not have any of its sides on the boundary of the problem), the contribution from the boundary integral cancels with similar contributions from adjoining elements of the mesh (analogous to the Q_i^e in the one-dimensional problems). A more detailed discussion is given below.

For the sake of brevity, we rewrite $[K^e]$ in (8.2.19b) as the sum of five basic matrices $[S^{\alpha\beta}]$ ($\alpha, \beta = 0, 1, 2$)

$$[K^e] = a_{00}[S^{00}] + a_{11}[S^{11}] + a_{12}[S^{12}] + a_{21}[S^{12}]^T + a_{22}[S^{22}] \quad (8.2.38)$$

where $[\cdot]^T$ denotes the transpose of the enclosed matrix, and

$$S_{ij}^{\alpha\beta} = \int_{\Omega_e} \psi_{i,\alpha} \psi_{j,\beta} dx dy \quad (8.2.39)$$

with $\psi_{i,\alpha} \equiv \partial \psi_i / \partial x_\alpha$, $x_1 = x$, and $x_2 = y$; $\psi_{i,0} = \psi_i$. All the matrices in (8.2.38) and interpolation functions in (8.2.39) are understood to be defined over an element, i.e., all expressions and quantities should have the element label e , but these are omitted in the interest of brevity. We now proceed to compute the matrices in (8.2.39) and (8.2.19b) using the linear interpolation functions derived in the previous section.

Element Matrices of a Linear Triangular Element

First, we note that integrals of polynomials over arbitrary shaped triangular domains can be evaluated exactly. To this end, let I_{mn} denote the integral of the expression $x^m y^n$ over an arbitrary triangle Δ

$$I_{mn} \equiv \int_{\Delta} x^m y^n dx dy \quad (8.2.40)$$

Then, it can be shown that

$$\begin{aligned} I_{00} &= \int_{\Delta} x^0 y^0 dx dy = \int_{\Delta} 1 \cdot dx dy = A \quad \text{area of the triangle} \\ I_{10} &= \int_{\Delta} x^1 y^0 dx dy = \int_{\Delta} x dx dy = A \hat{x}, \quad \hat{x} = \frac{1}{3} \sum_{i=1}^3 x_i \\ I_{01} &= \int_{\Delta} x^0 y^1 dx dy = \int_{\Delta} y dx dy = A \hat{y}, \quad \hat{y} = \frac{1}{3} \sum_{i=1}^3 y_i \\ I_{11} &= \int_{\Delta} xy dx dy = \frac{A}{12} \left(\sum_{i=1}^3 x_i y_i + 9 \hat{x} \hat{y} \right) \\ I_{20} &= \int_{\Delta} x^2 dx dy = \frac{A}{12} \left(\sum_{i=1}^3 x_i^2 + 9 \hat{x}^2 \right) \\ I_{02} &= \int_{\Delta} y^2 dx dy = \frac{A}{12} \left(\sum_{i=1}^3 y_i^2 + 9 \hat{y}^2 \right) \end{aligned} \quad (8.2.41)$$

where (x_i, y_i) are the coordinates of the vertices of the triangle. We can use the above results to evaluate integrals defined over triangular elements.

Next, we evaluate $[K^e]$ and $\{f^e\}$ for linear triangular element under the assumption that a_{ij} and f are elementwise constant. Also, note that (see Problem 8.1)

$$\sum_{i=1}^3 \alpha_i^e = 2A_e, \quad \sum_{i=1}^3 \beta_i^e = 0, \quad \sum_{i=1}^3 \gamma_i^e = 0 \quad (8.2.42a)$$

$$\alpha_i^e + \beta_i^e \hat{x}_e + \gamma_i^e \hat{y}_e = \frac{2}{3} A_e \quad (8.2.42b)$$

$$\frac{\partial \psi_i}{\partial x} = \frac{\beta_i^e}{2A_e}, \quad \frac{\partial \psi_i}{\partial y} = \frac{\gamma_i^e}{2A_e} \quad (8.2.43)$$

we obtain

$$\begin{aligned} S_{ij}^{11} &= \frac{1}{4A} \beta_i \beta_j, \quad S_{ij}^{12} = \frac{1}{4A} \beta_i \gamma_j, \quad S_{ij}^{22} = \frac{1}{4A} \gamma_i \gamma_j \\ S_{ij}^{00} &= \frac{1}{4A} \left\{ [\alpha_i \alpha_j + (\alpha_i \beta_j + \alpha_j \beta_i) \hat{x} + (\alpha_i \gamma_j + \alpha_j \gamma_i) \hat{y}] \right. \\ &\quad \left. + \frac{1}{A} [I_{20} \beta_i \beta_j + I_{11} (\gamma_i \beta_j + \gamma_j \beta_i) + I_{02} \gamma_i \gamma_j] \right\} \end{aligned} \quad (8.2.44)$$

In view of the identity (8.2.42b) and for an elementwise constant value of $f = f_e$, we have

$$\begin{aligned} f_i^e &= \int_{\Delta_e} f_e \psi_i^e(x, y) dx dy = \frac{f_e}{2A_e} \int_{\Delta_e} (\alpha_i^e + \beta_i^e x + \gamma_i^e y) dx dy \\ &= \frac{f_e}{2A_e} (\alpha_i^e I_{00} + \beta_i^e I_{10} + \gamma_i^e I_{01}) \\ &= \frac{f_e}{2A_e} (\alpha_i^e A_e + \beta_i^e A_e \hat{x}_e + \gamma_i^e A_e \hat{y}_e) \\ &= \frac{1}{2} f_e (\alpha_i^e + \beta_i^e \hat{x}_e + \gamma_i^e \hat{y}_e) = \frac{1}{3} f_e A_e \end{aligned} \quad (8.2.45)$$

The result in (8.2.45) should be obvious because for a constant source f_e the total magnitude of the source (say, heat) on the element is equal to $f_e A_e$, which is then distributed equally among the three nodes, giving a nodal value of $f_e A_e / 3$.

Once the coordinates of the element nodes are known, we can compute α_i^e , β_i^e , and γ_i^e from (8.2.24b) and substitute into (8.2.44) to obtain the element matrices, which in turn can be used in (8.2.38) to obtain the element matrix $[K^e]$. In particular, when a_{12} , a_{21} , and a_{00} are zero and a_{11} and a_{22} are elementwise constant, Eq. (8.2.1) becomes

$$-\left(a_{11} \frac{\partial^2 u}{\partial x^2} + a_{22} \frac{\partial^2 u}{\partial y^2} \right) - f = 0 \text{ in } \Omega_e \quad (8.2.46)$$

and the associated element coefficient matrix for a linear triangular element is

$$K_{ij}^e = \frac{1}{4A_e} (a_{11}^e \beta_i^e \beta_j^e + a_{22}^e \gamma_i^e \gamma_j^e) \quad (8.2.47)$$

Example 8.2.2

Consider the right-angle triangle shown in Fig. 8.2.10(a). We wish to determine the element coefficient matrix $[K^e]$ of (8.2.47) and source vector $\{f^e\}$ associated with the Poisson equation (8.2.46). We note that the element calculations do not depend on the global coordinate system (x, y) . Therefore, we choose the local coordinate system (\hat{x}, \hat{y}) to compute A , α , β , and γ for

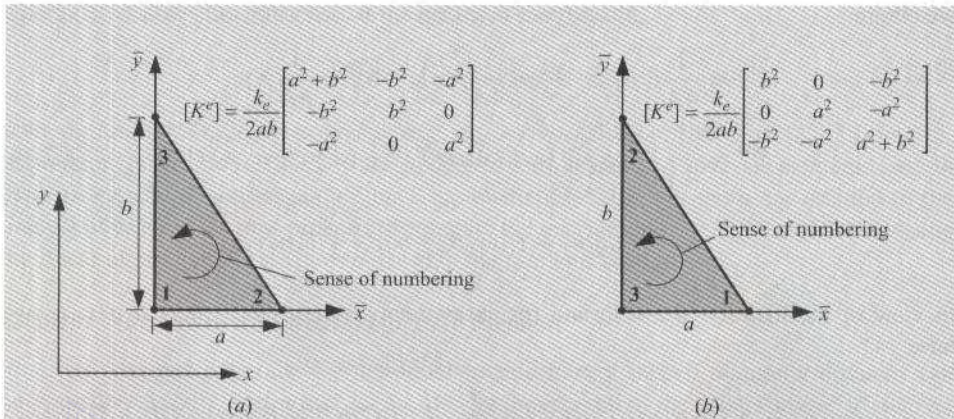


Figure 8.2.10 The right-angle linear triangular element of Example 8.2.2.

the element. We have

$$2A = ab, \quad \alpha_1 = ab, \quad \alpha_2 = 0, \quad \alpha_3 = 0, \quad \beta_1 = -b, \quad \beta_2 = b, \quad \beta_3 = 0, \quad \gamma_1 = -a, \quad \gamma_2 = 0, \quad \gamma_3 = a$$

$$\psi_1 = 1 - \frac{\bar{x}}{a} - \frac{\bar{y}}{b}, \quad \psi_2 = \frac{\bar{x}}{a}, \quad \psi_3 = \frac{\bar{y}}{b}$$

and

$$[K^e] = \frac{a_{11}^e}{2ab} \begin{bmatrix} b^2 & -b^2 & 0 \\ -b^2 & b^2 & 0 \\ 0 & 0 & 0 \end{bmatrix} + \frac{a_{22}^e}{2ab} \begin{bmatrix} a^2 & 0 & -a^2 \\ 0 & 0 & 0 \\ -a^2 & 0 & a^2 \end{bmatrix}, \quad \{f^e\} = \frac{f_e ab}{6} \begin{Bmatrix} 1 \\ 1 \\ 1 \end{Bmatrix} \quad (8.2.48)$$

If $a_{11}^e = a_{22}^e = k_e$, for the numbering system shown in Fig. 8.2.10(a), we have

$$[K^e] = \frac{k_e}{2ab} \begin{bmatrix} b^2 + a^2 & -b^2 & -a^2 \\ -b^2 & b^2 & 0 \\ -a^2 & 0 & a^2 \end{bmatrix}, \quad \{f^e\} = \frac{f_e ab}{6} \begin{Bmatrix} 1 \\ 1 \\ 1 \end{Bmatrix} \quad (8.2.49)$$

In addition, if $a = b$, we have

$$[K^e] = \frac{k_e}{2} \begin{bmatrix} 2 & -1 & -1 \\ -1 & 1 & 0 \\ -1 & 0 & 1 \end{bmatrix}, \quad \{f^e\} = \frac{f_e a^2}{6} \begin{Bmatrix} 1 \\ 1 \\ 1 \end{Bmatrix} \quad (8.2.50)$$

We note that contents of $[K^e]$ depend, even for the same geometry, on the node numbering scheme, as shown in Figs. 8.2.10(a) and 8.2.10(b). For the same element, if the node numbering is changed, the element coefficients will change accordingly. For example, if we renumber the element nodes of the element in Fig. 8.2.10(a) to be those in Fig. 8.2.10(b), then $[K^e]$ for the element in Fig. 8.2.10(b) is obtained from (8.2.49) [which corresponds to the element numbering in Fig. 8.2.10(a)] by moving rows and columns 1 \rightarrow 3, 3 \rightarrow 2, and 2 \rightarrow 1 (if the first row and column are moved after the third row and column, the last two

(moves are automatic):

$$\frac{k_e}{2ab} \begin{bmatrix} b^2 + a^2 & -b^2 & -a^2 \\ -b^2 & b^2 & 0 \\ -a^2 & 0 & a^2 \end{bmatrix} \rightarrow \frac{k_e}{2ab} \begin{bmatrix} -b^2 & -a^2 & b^2 + a^2 \\ b^2 & 0 & -b^2 \\ 0 & a^2 & -a^2 \end{bmatrix} \rightarrow \frac{k_e}{2ab} \begin{bmatrix} b^2 & 0 & -b^2 \\ 0 & a^2 & -a^2 \\ -b^2 & -a^2 & b^2 + a^2 \end{bmatrix}$$

In addition, all elements with the same geometry and node numbering, irrespective of their orientation (i.e., rigid body rotation about an axis perpendicular to the plane of the element), have the same coefficient matrix. Elements with the same coefficient matrix are listed in Fig. 8.2.11. For uniformity, we fix the sign convention and use counterclockwise numbering scheme for the element nodes.

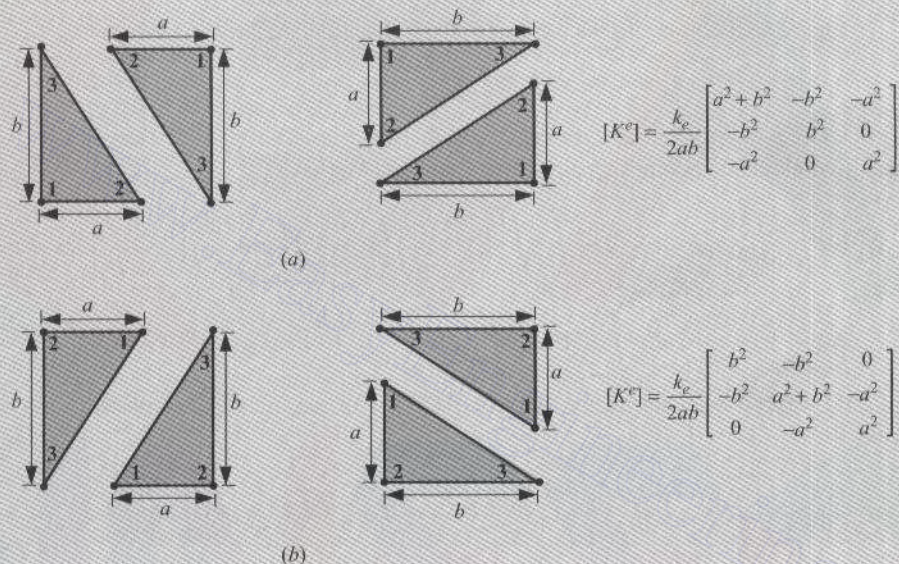


Figure 8.2.11 Coefficient matrices associated with Eq. (8.2.46) with $a_{11}^e = a_{22}^e = k_e$ for two different element node numbers of linear right-angle triangular elements.

Element Matrices of a Linear Rectangular Element

When the data a_{ij} ($i, j = 0, 1, 2$) and f of the problem is not a function of x and y , we can use the interpolation functions in (8.2.32a), expressed in the local coordinates (\bar{x}, \bar{y}) that are mere translation of (x, y) (see Fig. 8.2.12), to compute the element coefficients $S_{ij}^{\alpha\beta}$ ($\alpha, \beta = 1, 2$) of Eq. (8.2.39). For example, we have

$$S_{ij}^{00} = \int_{\Omega_e} \psi_i(x, y) \psi_j(x, y) dx dy = \int_0^a \int_0^b \psi_i \psi_j d\bar{x} d\bar{y}$$

where a and b are the lengths along the \bar{x} and \bar{y} axes of the element. Since the integration with respect to \bar{x} and \bar{y} can be carried out independent of each other, integration over a

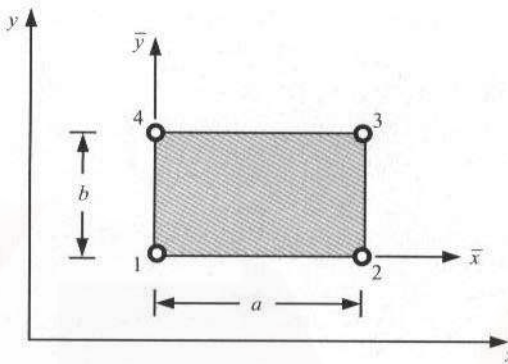


Figure 8.2.12 A rectangular element with the global and local coordinate systems.

rectangular element becomes a pair of line integrals. We have

$$\begin{aligned} S_{11}^{00} &= \int_0^a \int_0^b \psi_1 \psi_1 d\bar{x} d\bar{y} = \int_0^a \int_0^b \left(1 - \frac{\bar{x}}{a}\right) \left(1 - \frac{\bar{y}}{b}\right) \left(1 - \frac{\bar{x}}{a}\right) \left(1 - \frac{\bar{y}}{b}\right) d\bar{x} d\bar{y} \\ &= \int_0^a \left(1 - \frac{\bar{x}}{a}\right)^2 d\bar{x} \int_0^b \left(1 - \frac{\bar{y}}{b}\right)^2 d\bar{y} = \frac{ab}{3} \frac{ab}{3} = \frac{ab}{9} \end{aligned}$$

Similarly, we can evaluate all the matrices $[S^{\alpha\beta}]$ with the aid of the following integral identities:

$$\begin{aligned} \int_0^a \left(1 - \frac{s}{a}\right) ds &= \frac{a}{2}, \quad \int_0^a \frac{s}{a} ds = \frac{a}{2} \\ \int_0^a \left(1 - \frac{s}{a}\right)^2 ds &= \frac{a}{3}, \quad \int_0^a \frac{s}{a} \left(1 - \frac{s}{a}\right) ds = \frac{a}{6}, \quad \int_0^a \left(\frac{s}{a}\right)^2 ds = \frac{a}{3} \end{aligned} \quad (8.2.51)$$

In summary, the element matrices $[S^{\alpha\beta}]$ for a rectangular element are

$$[S^{11}] = \frac{b}{6a} \begin{bmatrix} 2 & -2 & -1 & 1 \\ -2 & 2 & 1 & -1 \\ -1 & 1 & 2 & -2 \\ 1 & -1 & -2 & 2 \end{bmatrix}, \quad [S^{12}] = \frac{1}{4} \begin{bmatrix} 1 & 1 & -1 & -1 \\ -1 & -1 & 1 & 1 \\ -1 & -1 & 1 & 1 \\ 1 & 1 & -1 & -1 \end{bmatrix} \quad (8.2.52)$$

$$[S^{22}] = \frac{a}{6b} \begin{bmatrix} 2 & 1 & -1 & -2 \\ 1 & 2 & -2 & -1 \\ -1 & -2 & 2 & 1 \\ -2 & -1 & 1 & 2 \end{bmatrix}, \quad [S^{00}] = \frac{ab}{36} \begin{bmatrix} 4 & 2 & 1 & 2 \\ 2 & 4 & 2 & 1 \\ 1 & 2 & 4 & 2 \\ 2 & 1 & 2 & 4 \end{bmatrix}$$

$$\{f\} = \frac{1}{4} f_e ab \{1 \ 1 \ 1 \ 1\}^T$$

Example 8.2.3

Here, we wish to determine the element coefficient matrix $[K^e]$ associated with the Poisson equation (8.2.46) over a linear rectangular element. We have

$$[K^e] = a_{11}^e [S^{11}] + a_{22}^e [S^{22}]$$

or

$$[K^e] = \frac{a_{11}^e b}{6a} \begin{bmatrix} 2 & -2 & -1 & 1 \\ -2 & 2 & 1 & -1 \\ -1 & 1 & 2 & -2 \\ 1 & -1 & -2 & 2 \end{bmatrix} + \frac{a_{22}^e a}{6b} \begin{bmatrix} 2 & 1 & -1 & -2 \\ 1 & 2 & -2 & -1 \\ -1 & -2 & 2 & 1 \\ -2 & -1 & 1 & 2 \end{bmatrix} \quad (8.2.53)$$

Note that the coefficient matrix is a function of both element aspect ratios a/b and b/a . Therefore, elements with very large aspect ratios should not be used as they will result in an ill-conditioned matrix (i.e., very large numbers are added to very small numbers), where either $[S^{11}]$ or $[S^{22}]$ will dominate the element matrix.

For $a_{11}^e = a_{22}^e = k_e$, the element coefficient matrix becomes

$$[K^e] = \frac{k_e}{6ab} \begin{bmatrix} 2(a^2 + b^2) & a^2 - 2b^2 & -(a^2 + b^2) & b^2 - 2a^2 \\ a^2 - 2b^2 & 2(a^2 + b^2) & b^2 - 2a^2 & -(a^2 + b^2) \\ -(a^2 + b^2) & b^2 - 2a^2 & 2(a^2 + b^2) & a^2 - 2b^2 \\ b^2 - 2a^2 & -(a^2 + b^2) & a^2 - 2b^2 & 2(a^2 + b^2) \end{bmatrix} \quad (8.2.54)$$

When the element aspect ratio is $a/b = 1$, the coefficient matrix in Eq. (8.2.54) becomes

$$[K^e] = \frac{k_e}{6} \begin{bmatrix} 4 & -1 & -2 & -1 \\ -1 & 4 & -1 & -2 \\ -2 & -1 & 4 & -1 \\ -1 & -2 & -1 & 4 \end{bmatrix} \quad (8.2.55)$$

Evaluation of Boundary Integrals

Here, we consider the evaluation of boundary integrals of the type [see Eq. (8.2.19b)]

$$Q_i^e = \oint_{\Gamma_e} q_n^e \psi_i^e(s) ds \quad (8.2.56)$$

where q_n^e is a known function of the distance s along the boundary Γ_e . It is not necessary to compute such integrals when a portion of Γ_e does not coincide with the boundary Γ of the total domain Ω [see Fig. 8.2.13(a)]. On portions of Γ_e that are in the interior of the domain Ω , q_n^e on side (i, j) of element Ω_e cancels with q_n^f on side (p, q) of element Ω_f when sides (i, j) of element Ω_e and (p, q) of element Ω_f are the same (i.e., at the interface of elements Ω_e and Ω_f). This can be viewed as the equilibrium of the internal "flux" [see Fig. 8.2.13(b)]. When Γ_e falls on the boundary of the domain Ω , q_n is either known as a function of s [see Fig. 8.2.13(c)] or to be determined in the postcomputation. The primary variable must be specified on the portion of the boundary where q_n is not specified.

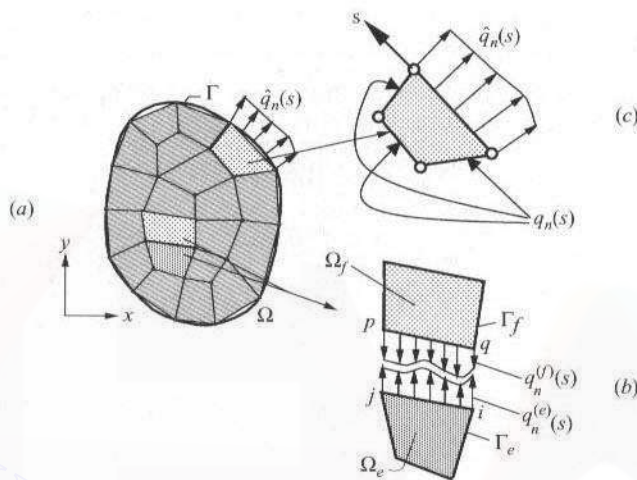


Figure 8.2.13 (a) Finite element discretization. (b) Equilibrium of fluxes at element interfaces. (c) Computation of forces on the boundary of the total domain.

The boundary Γ_e of a two-dimensional element consist of line segments, which can be viewed as one-dimensional elements. Thus, the evaluation of the boundary integrals on two-dimensional problems amounts to evaluating line integrals. It should not be surprising that when two-dimensional interpolation functions are evaluated on the boundary of an element, we obtain the corresponding one-dimensional interpolation functions.

For example, consider a linear triangular element shown in Fig. 8.2.14. The linear interpolation functions for this element are given by (8.2.25b). Now let us choose a coordinate system (s, t) with its origin at node 1 and the coordinate s parallel to the side connecting nodes 1 and 2. The two coordinate systems (x, y) and (s, t) are related as follows:

$$x = a_1 + b_1 s + c_1 t$$

$$y = a_2 + b_2 s + c_2 t$$

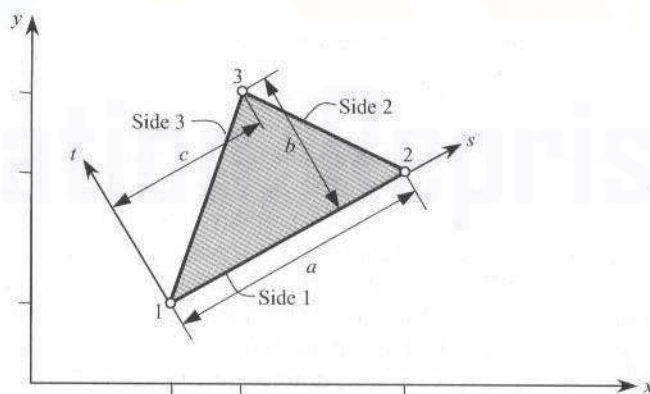


Figure 8.2.14 The linear triangular element in the global (x, y) and local (s, t) coordinate systems.

The constants a_1, b_1, c_1, a_2, b_2 , and c_2 can be determined with the following conditions:

$$\text{when } s = 0, t = 0, \quad x = x_1, \quad y = y_1$$

$$\text{when } s = a, t = 0, \quad x = x_2, \quad y = y_2$$

$$\text{when } s = c, t = b, \quad x = x_3, \quad y = y_3$$

We obtain

$$\begin{aligned} x(s, t) &= x_1 + (x_2 - x_1) \frac{s}{a} + \left[\left(\frac{c}{a} - 1 \right) x_1 - \frac{c}{a} x_2 + x_3 \right] \frac{t}{b} \\ y(s, t) &= y_1 + (y_2 - y_1) \frac{s}{a} + \left[\left(\frac{c}{a} - 1 \right) y_1 - \frac{c}{a} y_2 + y_3 \right] \frac{t}{b} \end{aligned} \quad (8.2.57)$$

Equations (8.2.57) allow us to express $\psi_i(x, y)$ as $\psi_i(s, t)$, which can be evaluated on the side connecting nodes 1 and 2 by setting $t = 0$ in $\psi_i(s, t)$:

$$\psi_i(s) \equiv \psi_i(s, 0) = \psi_i(x(s, 0), y(s, 0))$$

$$x(s) = x_1 + (x_2 - x_1) \frac{s}{a}, \quad y(s) = y_1 + (y_2 - y_1) \frac{s}{a}$$

For instance, we have

$$\begin{aligned} \psi_1(s) &= \frac{1}{2A} \left\{ \alpha_1 + \beta_1 \left[\left(1 - \frac{s}{a} \right) x_1 + \frac{s}{a} x_2 \right] + \gamma_1 \left[\left(1 - \frac{s}{a} \right) y_1 + \frac{s}{a} y_2 \right] \right\} \\ &= \frac{1}{2A} (\alpha_1 + \alpha_2 + \alpha_3) \left(1 - \frac{s}{a} \right) = 1 - \frac{s}{a} \end{aligned}$$

where the definitions of α_1, β_1 , and γ_1 are used to rewrite the entire expression. Similarly, we have

$$\psi_2(s) = \frac{s}{a}, \quad \psi_3(s) = 0$$

where $a = h_{12}$ is the length of side 1–2. We note that $\psi_1(s)$ and $\psi_2(s)$ are precisely the linear, one-dimensional, interpolation functions associated with the line element connecting nodes 1 and 2.

Similarly, when $\psi_i(x, y)$ are evaluated on side 3–1 of the element, we obtain

$$\psi_1(s) = \frac{s}{h_{13}}, \quad \psi_2 = 0, \quad \psi_3(s) = 1 - \frac{s}{h_{13}}$$

where the s coordinate is taken along the side 3–1, with origin at node 3, and h_{13} is the length of side 1–3. Thus, evaluation of Q_i^e involves the use of appropriate one-dimensional interpolation functions and the known variation of q_n on the boundary.

In general, the integral (8.2.56) over the boundary of a linear triangular element can be expressed as

$$\begin{aligned} Q_i^e &= \int_{1-2} \psi_i(s) q_n(s) ds + \int_{2-3} \psi_i(s) q_n(s) ds + \int_{3-1} \psi_i(s) q_n(s) ds \\ &\equiv Q_{i1}^e + Q_{i2}^e + Q_{i3}^e \end{aligned} \quad (8.2.58a)$$

where \int_{i-j} denotes integral over the line connecting node i to node j , the s coordinate is taken from node i to node j , with the origin at node i (see Fig. 8.2.15), and Q_{ij}^e is defined

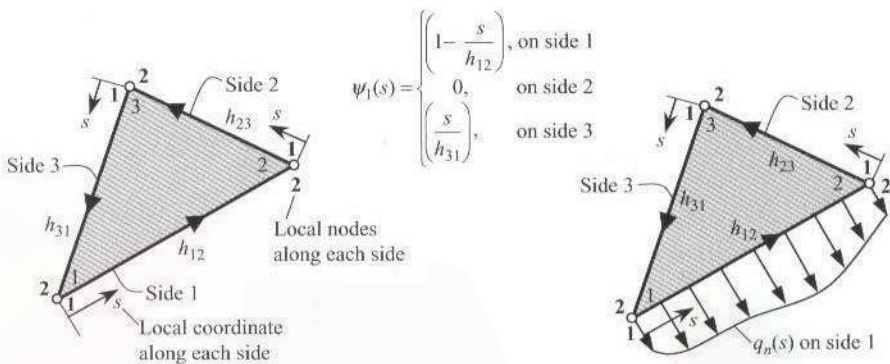


Figure 8.2.15 Computation of the boundary integral (8.2.56) over a linear triangular element.

to be the contribution of q_n on side J of element Ω_e to Q_i^e :

$$Q_{iJ}^e = \int_{\text{side } J} \psi_i q_n \, ds \quad (8.2.58b)$$

where i refers to the i th node of the element and J refers to the J th side of the element. For example, we have

$$Q_1^e = \oint_{\Gamma_e} q_n \psi_1(s) \, ds = \int_{1-2} (q_n)_{1-2} \psi_1 \, ds + 0 + \int_{3-1} (q_n)_{3-1} \psi_1 \, ds$$

The contribution from side 2–3 is zero because ψ_1 is zero on side 2–3 of a triangular element. For a rectangular element, Q_1^e has four parts but only contributions from sides 1–2 and 3–1 are nonzero because ψ_1 is zero on sides 2–3 and 3–4.

Example 8.2.4

We wish to evaluate the boundary integral Q_i^e in (8.2.56) for the four cases of $q(s)$ and finite element meshes shown in Fig. 8.2.16. For each case we must use the $q(s)$ and the interpolation functions associated with the type of boundary element (i.e., linear or quadratic). On element sides on which q_n is not shown, assume that it is zero.

Case 1. $q(s) = q_0 = \text{constant}$, linear element. Clearly, q_0 will contribute to the nodal values at element nodes 1 and 2. The contribution to node 3 is zero ($Q_3^e = 0$) as there is no specified flux on sides 2–3 and 3–1. We have

$$Q_1^e = \oint_{\Gamma_e} q_n(s) \psi_1(s) \, ds = \int_0^{h_{12}} q_0 (\psi_1)_{1-2} \, ds + \int_0^{h_{31}} (0) (\psi_1)_{3-1} \, ds = Q_{11}^e = \frac{1}{2} q_0 h_{12}$$

$$Q_2^e = \oint_{\Gamma_e} q_n(s) \psi_2(s) \, ds = \int_0^{h_{12}} q_0 (\psi_2)_{1-2} \, ds + \int_0^{h_{23}} (0) (\psi_2)_{2-3} \, ds = Q_{21}^e = \frac{1}{2} q_0 h_{12}$$

where

$$(\psi_1)_{1-2} = 1 - \frac{s}{h_{12}}, \quad (\psi_2)_{1-2} = \frac{s}{h_{12}}$$

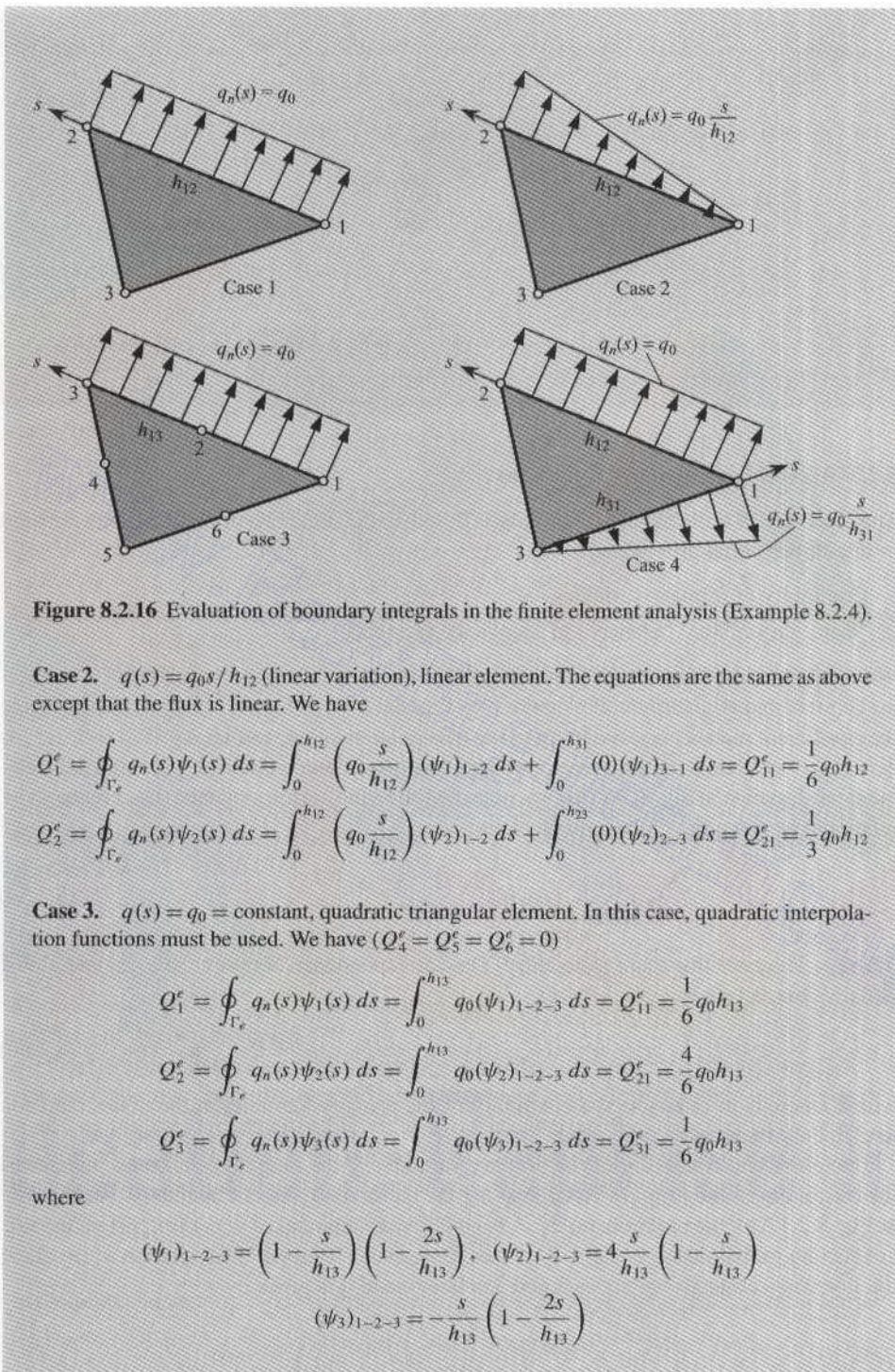


Figure 8.2.16 Evaluation of boundary integrals in the finite element analysis (Example 8.2.4).

Case 2. $q(s) = q_0 s / h_{12}$ (linear variation), linear element. The equations are the same as above except that the flux is linear. We have

$$Q_1^e = \oint_{\Gamma_e} q_n(s) \psi_1(s) ds = \int_0^{h_{12}} \left(q_0 \frac{s}{h_{12}} \right) (\psi_1)_{1-2} ds + \int_0^{h_{31}} (0)(\psi_1)_{3-1} ds = Q_{11}^e = \frac{1}{6} q_0 h_{12}$$

$$Q_2^e = \oint_{\Gamma_e} q_n(s) \psi_2(s) ds = \int_0^{h_{12}} \left(q_0 \frac{s}{h_{12}} \right) (\psi_2)_{1-2} ds + \int_0^{h_{23}} (0)(\psi_2)_{2-3} ds = Q_{21}^e = \frac{1}{3} q_0 h_{12}$$

Case 3. $q(s) = q_0 = \text{constant}$, quadratic triangular element. In this case, quadratic interpolation functions must be used. We have ($Q_4^e = Q_5^e = Q_6^e = 0$)

$$Q_1^e = \oint_{\Gamma_e} q_n(s) \psi_1(s) ds = \int_0^{h_{13}} q_0 (\psi_1)_{1-2-3} ds = Q_{11}^e = \frac{1}{6} q_0 h_{13}$$

$$Q_2^e = \oint_{\Gamma_e} q_n(s) \psi_2(s) ds = \int_0^{h_{13}} q_0 (\psi_2)_{1-2-3} ds = Q_{21}^e = \frac{4}{6} q_0 h_{13}$$

$$Q_3^e = \oint_{\Gamma_e} q_n(s) \psi_3(s) ds = \int_0^{h_{13}} q_0 (\psi_3)_{1-2-3} ds = Q_{31}^e = \frac{1}{6} q_0 h_{13}$$

where

$$(\psi_1)_{1-2-3} = \left(1 - \frac{s}{h_{13}} \right) \left(1 - \frac{2s}{h_{13}} \right), \quad (\psi_2)_{1-2-3} = 4 \frac{s}{h_{13}} \left(1 - \frac{s}{h_{13}} \right)$$

$$(\psi_3)_{1-2-3} = -\frac{s}{h_{13}} \left(1 - \frac{2s}{h_{13}} \right)$$

Case 4. Two sides have nonzero $q(s)$, as shown in Fig. 8.2.16, on a linear element. In this case, all three nodes will have nonzero contributions. We have

$$\begin{aligned} Q_1^e &= \oint_{\Gamma_e} q_e(s) \psi_1(s) ds = \int_0^{h_{12}} q_0(\psi_1)_{1-2} ds + \int_0^{h_{31}} \left(q_0 \frac{s}{h_{31}} \right) (\psi_1)_{3-1} ds \\ &= Q_{11}^e + Q_{13}^e = q_0 \left(\frac{h_{12}}{2} + \frac{h_{31}}{3} \right) \\ Q_2^e &= \oint_{\Gamma_e} q_e(s) \psi_2(s) ds = \int_0^{h_{12}} q_0(\psi_2)_{1-2} ds + \int_0^{h_{31}} \left(q_0 \frac{s}{h_{31}} \right) (0) ds = Q_{21}^e = \frac{1}{2} q_0 h_{12} \\ Q_3^e &= \oint_{\Gamma_e} q_e(s) \psi_3(s) ds = \int_0^{h_{12}} q_0(0) ds + \int_0^{h_{31}} \left(q_0 \frac{s}{h_{31}} \right) (\psi_3)_{3-1} ds = Q_{33}^e = \frac{1}{6} q_0 h_{31} \end{aligned}$$

8.2.7 Assembly of Element Equations

The assembly of finite element equations is based on the same two principles that were used in one-dimensional problems:

1. Continuity of primary variables
2. “Equilibrium” (or “balance”) of secondary variables

We illustrate the procedure by considering a finite element mesh consisting of a triangular element and a quadrilateral element [see Fig. 8.2.17(a)]. Let K_{ij}^1 ($i, j = 1, 2, 3$) denote the coefficient matrix corresponding to the triangular element, and let K_{ij}^2 ($i, j = 1, \dots, 4$) denote the coefficient matrix corresponding to the quadrilateral element. From the finite element mesh shown in Fig. 8.2.17(a), we note the following correspondence (i.e., connectivity relations) between the global and element nodes:

$$[B] = \begin{bmatrix} 1 & 2 & 3 & \times \\ 2 & 4 & 5 & 3 \end{bmatrix} \quad (8.2.59)$$

where \times indicates that there is no entry. The correspondence between the local and global nodal values is [see Fig. 8.2.17(a)]

$$u_1^1 = U_1, \quad u_2^1 = u_1^2 = U_2, \quad u_3^1 = u_4^2 = U_3, \quad u_2^2 = U_4, \quad u_3^2 = U_5 \quad (8.2.60)$$

which amounts to imposing the continuity of the primary variables at the nodes common to elements 1 and 2.

Note that the continuity of the primary variables at the interelement nodes guarantees the continuity of the primary variable along the entire interelement boundary. For the case in Fig. 8.2.17(a), the requirement $u_2^1 = u_1^2$ and $u_3^1 = u_4^2$ guarantees $u_h^1(s) = u_h^2(s)$ on the side connecting global nodes 2 and 3. This can be shown as follows. The solution $u_h^1(s)$ along the line connecting global nodes 2 and 3 is linear, and it is given by

$$u_h^1(s) = u_2^1 \left(1 - \frac{s}{h} \right) + u_3^1 \frac{s}{h}$$

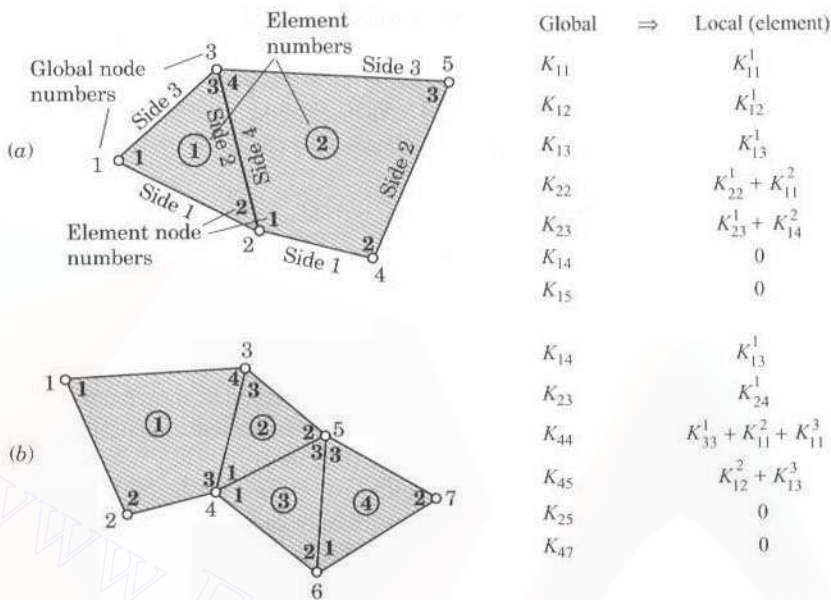


Figure 8.2.17 Assembly of finite element coefficient matrices using the correspondence between global and element nodes (one unknown per node): (a) assembly of two elements; and (b) assembly of several elements. Single primary degree of freedom per node is assumed.

where s is the local coordinate with its origin at global node 2 and h is the length of the side 2–3 (or side 2). Similarly, the finite element solution along the same line but from element 2 is

$$u_h^2(s) = u_1^2 \left(1 - \frac{s}{h}\right) + u_4^2 \frac{s}{h}$$

Since $u_1^2 = u_2^1$ and $u_4^2 = u_3^1$, it follows that $u_h^1(s) = u_h^2(s)$ for every value of s along the interface of the two elements.

Next we use the balance of secondary variables. At the interface between the two elements, the flux from the two elements should be equal in magnitude and opposite in sign. For the two elements in Fig. 8.2.17(a), the interface is along the side connecting global nodes 2 and 3. Hence, the internal flux q_n^1 on side 2–3 of element 1 should balance the flux q_n^2 on side 4–1 of element 2 (recall the sign convention on q_n^e):

$$(q_n^1)_{2-3} = (q_n^2)_{4-1} \text{ or } (q_n^1)_{2-3} = (-q_n^2)_{1-4} \quad (8.2.61)$$

In the finite element method we impose the above relation in a weighted integral sense:

$$\int_{h_{23}^1} q_n^1 \psi_2^1 ds = - \int_{h_{14}^2} q_n^2 \psi_1^2 ds, \quad \int_{h_{23}^1} q_n^1 \psi_3^1 ds = - \int_{h_{14}^2} q_n^2 \psi_4^2 ds \quad (8.2.62a)$$

where h_{pq}^e denotes length of the side connecting node p to node q of element Ω_e . The above equations can be written in the form,

$$\int_{h_{23}^1} q_n^1 \psi_2^1 ds + \int_{h_{14}^2} q_n^2 \psi_1^2 ds = 0, \quad \int_{h_{23}^1} q_n^1 \psi_3^1 ds + \int_{h_{14}^2} q_n^2 \psi_4^2 ds = 0 \quad (8.2.62b)$$

or

$$Q_{22}^1 + Q_{14}^2 = 0, \quad Q_{32}^1 + Q_{44}^2 = 0 \quad (8.2.62c)$$

where Q_{iJ}^e denotes the part of Q_i^e that comes from side J of element e :

$$Q_{iJ}^e = \int_{\text{side } J} q_n^e \psi_i^e ds$$

The sides of triangular and quadrilateral elements are numbered as shown in Fig. 8.2.17(a). These balance relations must be imposed in assembling the element equations. We note that Q_{iJ}^e is only a portion of Q_i^e [see Eqs. (8.2.56) and (8.2.58b)].

The element equations of the two-element mesh shown in Fig. 8.2.17(a) are written first. For the model problem at hand, there is only one primary degree of freedom (NDF = 1) per node. For the triangular element, the element equations are of the form

$$\begin{aligned} K_{11}^1 u_1^1 + K_{12}^1 u_2^1 + K_{13}^1 u_3^1 &= f_1^1 + Q_1^1 \\ K_{21}^1 u_1^1 + K_{22}^1 u_2^1 + K_{23}^1 u_3^1 &= f_2^1 + Q_2^1 \\ K_{31}^1 u_1^1 + K_{32}^1 u_2^1 + K_{33}^1 u_3^1 &= f_3^1 + Q_3^1 \end{aligned} \quad (8.2.63a)$$

For the quadrilateral element, the element equations are given by

$$\begin{aligned} K_{11}^2 u_1^2 + K_{12}^2 u_2^2 + K_{13}^2 u_3^2 + K_{14}^2 u_4^2 &= f_1^2 + Q_1^2 \\ K_{21}^2 u_1^2 + K_{22}^2 u_2^2 + K_{23}^2 u_3^2 + K_{24}^2 u_4^2 &= f_2^2 + Q_2^2 \\ K_{31}^2 u_1^2 + K_{32}^2 u_2^2 + K_{33}^2 u_3^2 + K_{34}^2 u_4^2 &= f_3^2 + Q_3^2 \\ K_{41}^2 u_1^2 + K_{42}^2 u_2^2 + K_{43}^2 u_3^2 + K_{44}^2 u_4^2 &= f_4^2 + Q_4^2 \end{aligned} \quad (8.2.63b)$$

In order to impose the balance of secondary variables in (8.2.62c), it is required that we add the second equation of element 1 to the first equation of element 2, and also add the third equation of element 1 to the fourth equation of element 2:

$$\begin{aligned} (K_{21}^1 u_1^1 + K_{22}^1 u_2^1 + K_{23}^1 u_3^1) + (K_{11}^2 u_1^2 + K_{12}^2 u_2^2 + K_{13}^2 u_3^2 + K_{14}^2 u_4^2) \\ = (f_2^1 + Q_2^1) + (f_1^2 + Q_1^2) \\ (K_{31}^1 u_1^1 + K_{32}^1 u_2^1 + K_{33}^1 u_3^1) + (K_{41}^2 u_1^2 + K_{42}^2 u_2^2 + K_{43}^2 u_3^2 + K_{44}^2 u_4^2) \\ = (f_3^1 + Q_3^1) + (f_4^2 + Q_4^2) \end{aligned}$$

Using the global-variable notation in (8.2.60), we can rewrite the above equations as [which amounts to imposing continuity of the primary variables in (8.2.60)]:

$$\begin{aligned} K_{21}^1 U_1 + (K_{22}^1 + K_{11}^2) U_2 + (K_{23}^1 + K_{14}^2) U_3 + K_{12}^2 U_4 + K_{13}^2 U_5 \\ = f_2^1 + f_1^2 + (Q_2^1 + Q_1^2) \end{aligned}$$

$$\begin{aligned} K_{31}^1 U_1 + (K_{32}^1 + K_{41}^2) U_2 + (K_{33}^1 + K_{44}^2) U_3 + K_{42}^2 U_4 + K_{43}^2 U_5 \\ = f_3^1 + f_4^2 + (Q_3^1 + Q_4^2) \end{aligned}$$

Now we can impose the conditions in (8.2.62c) by setting appropriate portions of the expressions in parenthesis on the right-hand side of the above equations to zero:

$$\begin{aligned} Q_2^1 + Q_1^2 &= (Q_{21}^1 + Q_{22}^1 + Q_{23}^1) + (Q_{11}^2 + Q_{12}^2 + Q_{13}^2 + Q_{14}^2) \\ &= Q_{21}^1 + Q_{23}^1 + \underline{(Q_{22}^1 + Q_{14}^2)} + Q_{11}^2 + Q_{12}^2 + Q_{13}^2 \\ Q_3^1 + Q_4^2 &= (Q_{31}^1 + Q_{32}^1 + Q_{33}^1) + (Q_{41}^2 + Q_{42}^2 + Q_{43}^2 + Q_{44}^2) \\ &= Q_{31}^1 + Q_{33}^1 + \underline{(Q_{32}^1 + Q_{44}^2)} + Q_{41}^2 + Q_{42}^2 + Q_{43}^2 \end{aligned}$$

The underlined terms are zero by the balance requirement (8.2.62c). The remaining terms of each equation will be either known because q_n is known on the boundary or remain unknown because the primary variable is specified on the boundary.

In general, when several elements are connected, the assembly of the elements is carried out by putting element coefficients K_{ij}^e , f_i^e , and Q_i^e into proper locations of the global coefficient matrix and right-hand column vectors. This is done by means of the connectivity relations, i.e., correspondence of the local node number to the global node number. For example, if global node number 3 corresponds to node 3 of element 1 and node 4 of element 2, then we have

$$F_3 = F_3^1 + F_4^2 \equiv f_3^1 + f_4^2 + Q_3^1 + Q_4^2, \quad K_{33} = K_{33}^1 + K_{44}^2$$

If global node numbers 2 and 3 correspond, respectively, to nodes 2 and 3 of element 1 and nodes 1 and 4 of element 2, then global coefficients K_{22} , K_{23} , and K_{33} are given by

$$K_{22} = K_{22}^1 + K_{11}^2, \quad K_{23} = K_{23}^1 + K_{14}^2, \quad K_{33} = K_{33}^1 + K_{44}^2$$

Similarly, the source components of global nodes 2 and 3 are added:

$$F_2 = F_2^1 + F_1^2, \quad F_3 = F_3^1 + F_4^2$$

For the two-element mesh shown in Fig. 8.2.17(a), the assembled equations are given by

$$\left[\begin{array}{ccccc} K_{11}^1 & K_{12}^1 & K_{13}^1 & 0 & 0 \\ K_{21}^1 & K_{22}^1 + K_{11}^2 & K_{23}^1 + K_{14}^2 & K_{12}^2 & K_{13}^2 \\ K_{31}^1 & K_{32}^1 + K_{41}^2 & K_{33}^1 + K_{44}^2 & K_{42}^2 & K_{43}^2 \\ 0 & K_{21}^2 & K_{24}^2 & K_{22}^2 & K_{23}^2 \\ 0 & K_{31}^2 & K_{34}^2 & K_{32}^2 & K_{33}^2 \end{array} \right] \left[\begin{array}{c} U_1 \\ U_2 \\ U_3 \\ U_4 \\ U_5 \end{array} \right] = \left[\begin{array}{c} F_1^1 \\ F_2^1 + F_1^2 \\ F_3^1 + F_4^2 \\ F_2^2 \\ F_3^2 \end{array} \right] \quad (8.2.64)$$

The assembly procedure described above can be used to assemble elements of any shape and type. The procedure can be implemented in a computer, as described for one-dimensional problems, with the help of the array $[B]$ (program variable is NOD). For hand calculations, the readers are required to use the procedure described above. For example, consider the finite element mesh shown in Fig. 8.2.17(b). The location (4,4) of the global coefficient matrix contains $K_{33}^1 + K_{11}^2 + K_{11}^3$. The location 4 in the assembled column vector contains $F_3^1 + F_1^2 + F_1^3$. Locations (1,5), (1,6), (1,7), (2,5), (2,6), (2,7), (3,6), (3,7), and (4,7) of the

global matrix contain zeros because $K_{IJ} = 0$ when global nodes I and J do not correspond to nodes of the same element in the mesh.

This completes the first five steps in the finite element modeling of the model equation (8.2.1). The next two steps of the analysis, namely, the imposition of boundary conditions and solution of equations will remain the same as for one-dimensional problems. The postprocessing of the solution for two-dimensional problems is discussed next.

8.2.8 Postcomputations

The finite element solution at any point (x, y) in an element Ω_e is given by

$$u_h^e(x, y) = \sum_{j=1}^n u_j^e \psi_j^e(x, y) \quad (8.2.65)$$

and its derivatives are computed from (8.2.65) as

$$\frac{\partial u_h^e}{\partial x} = \sum_{j=1}^n u_j^e \frac{\partial \psi_j^e}{\partial x}, \quad \frac{\partial u_h^e}{\partial y} = \sum_{j=1}^n u_j^e \frac{\partial \psi_j^e}{\partial y} \quad (8.2.66)$$

Equations (8.2.65) and (8.2.66) can be used to compute the solution and its derivatives at any point (x, y) in the element. It is useful to generate, by the interpolation of (8.2.65), information needed to plot contours of u_h^e and its gradient.

The derivatives of u_h^e will not be continuous at interelement boundaries because continuity of the derivatives is not imposed during the assembly procedure. The weak form of the equations suggests that the primary variable is u , which is to be carried as the nodal variable. If additional variables, such as higher-order derivatives of the dependent unknown, are carried as nodal variables in the interest of making them continuous across interelement boundaries, the degree of interpolation (or order of the element) increases. In addition, the continuity of higher-order derivatives that are not identified as the primary variables may violate the physical principles of the problem. For example, making $\partial u / \partial x$ continuous will violate the requirement that $q_x (= a_{11} \partial u / \partial x)$ be continuous at the interface of two dissimilar materials because a_{11} is different for the two materials at the interface.

For the linear triangular element, the derivatives are constants within each element:

$$\begin{aligned} \psi_j^e &= \frac{1}{2A_e}(\alpha_j + \beta_j x + \gamma_j y), & \frac{\partial \psi_j^e}{\partial x} &= \frac{1}{2A_e}\beta_j, & \frac{\partial \psi_j^e}{\partial y} &= \frac{1}{2A_e}\gamma_j \\ \frac{\partial u_h^e}{\partial x} &= \sum_{j=1}^n \frac{u_j^e \beta_j}{2A_e}, & \frac{\partial u_h^e}{\partial y} &= \sum_{j=1}^n \frac{u_j^e \gamma_j}{2A_e} \end{aligned} \quad (8.2.67)$$

For linear rectangular elements, $\partial U^e / \partial \bar{x}$ is linear in \bar{y} and $\partial u_h^e / \partial \bar{y}$ is linear in \bar{x} [see (8.2.32b)]:

$$\begin{aligned} \frac{\partial \psi_j^e}{\partial \bar{x}} &= -\frac{1}{a} \left(1 - \frac{\bar{y} + \bar{y}_j}{b} \right), & \frac{\partial \psi_j^e}{\partial \bar{y}} &= -\frac{1}{b} \left(1 - \frac{\bar{x} + \bar{x}_j}{a} \right) \\ \frac{\partial u_h^e}{\partial \bar{x}} &= \frac{1}{a} \sum_{j=1}^n (-1)^{j+2} u_j^e \left(1 - \frac{\bar{y} + \bar{y}_j}{b} \right), & \frac{\partial u_h^e}{\partial \bar{y}} &= \frac{1}{b} \sum_{j=1}^n (-1)^{j+2} u_j^e \left(1 - \frac{\bar{x} + \bar{x}_j}{a} \right) \end{aligned} \quad (8.2.68)$$

where \bar{x} and \bar{y} are the local coordinates [see Fig. 8.2.8(a)]. Although $\partial u_h^e / \partial \bar{x}$ and $\partial u_h^e / \partial \bar{y}$ are linear functions of y and x , respectively, in each element, they are discontinuous at interelement boundaries. Consequently, quantities computed using derivatives of the finite element solution u_h^e are discontinuous at interelement boundaries. For example, if we compute $q_x^e = a_{11}^e \partial u_h^e / \partial x$ at a node shared by three different elements, three different values of q_x^e are expected. The difference between the three values will diminish as the mesh is refined. Some commercial finite element software give a single value of q_x at the node by averaging the values obtained from various elements connected at the node.

8.2.9 Axisymmetric Problems

In studying problems involving cylindrical geometries, it is convenient to use the cylindrical coordinate system (r, θ, z) to formulate the problem. If the geometry, boundary conditions, and loading (or source) of the problem are independent of the angular coordinate θ , the problem solution will also be independent of θ . Consequently, a three-dimensional problem is reduced to a two-dimensional one in (r, z) coordinates (see Fig. 3.4.1). Here we consider a model axisymmetric problem, develop its weak form, and formulate the finite element model.

Model Equation

Consider the partial differential equation,

$$-\frac{1}{r} \frac{\partial}{\partial r} \left(r \hat{a}_{11} \frac{\partial u}{\partial r} \right) - \frac{\partial}{\partial z} \left(\hat{a}_{22} \frac{\partial u}{\partial z} \right) + \hat{a}_{00} u = \hat{f}(r, z) \quad (8.2.69)$$

where \hat{a}_{00} , \hat{a}_{11} , \hat{a}_{22} , and \hat{f} are given functions of r and z . The equation arises in the study of heat transfer in cylindrical geometries, as well as in other fields of engineering and applied science. Our objective is to develop the finite element model of the equation based on the weak formulation of (8.2.69).

Weak Form

Following the three-step procedure, we write the weak form of (8.2.69):

$$\begin{aligned} \text{(i)} \quad 0 &= \int_{\Omega_e} w \left[-\frac{1}{r} \frac{\partial}{\partial r} \left(r \hat{a}_{11} \frac{\partial u}{\partial r} \right) - \frac{\partial}{\partial z} \left(\hat{a}_{22} \frac{\partial u}{\partial z} \right) + \hat{a}_{00} u - \hat{f} \right] r dr dz \\ \text{(ii)} \quad 0 &= \int_{\Omega_e} \left(\frac{\partial w}{\partial r} \hat{a}_{11} \frac{\partial u}{\partial r} + \frac{\partial w}{\partial z} \hat{a}_{22} \frac{\partial u}{\partial z} + w \hat{a}_{00} u - w \hat{f} \right) r dr dz \\ &\quad - \oint_{\Gamma_e} w \left(\hat{a}_{11} \frac{\partial u}{\partial r} n_r + \hat{a}_{22} \frac{\partial u}{\partial z} n_z \right) ds \\ \text{(iii)} \quad 0 &= \int_{\Omega_e} \left(\hat{a}_{11} \frac{\partial w}{\partial r} \frac{\partial u}{\partial r} + \hat{a}_{22} \frac{\partial w}{\partial z} \frac{\partial u}{\partial z} + \hat{a}_{00} w u - w \hat{f} \right) r dr dz - \oint_{\Gamma_e} w q_n ds \end{aligned} \quad (8.2.70)$$

where w is the weight function and q_n is the normal flux

$$q_n = \left(\hat{a}_{11} \frac{\partial u}{\partial r} n_r + \hat{a}_{22} \frac{\partial u}{\partial z} n_z \right) \quad (8.2.71)$$

Note that the weak form (8.2.70) does not differ significantly from that developed for model (8.2.1) when $a_{12} = a_{21} = 0$. The only difference is the presence of r in the integrand. Consequently, (8.2.70) can be obtained as a special case of (8.2.10) for $a_{00} = \hat{a}_{00}x$, $a_{11} = \hat{a}_{11}x$, $a_{22} = \hat{a}_{22}x$, and $f = \hat{f}x$; the coordinates r and z are treated like x and y , respectively.

Finite Element Model

Let us assume that $u(r, z)$ is approximated by the finite element interpolation u_h^e over the element Ω_e

$$u \approx u_h^e(r, z) = \sum_{j=1}^n u_j^e \psi_j^e(r, z) \quad (8.2.72)$$

The interpolation functions $\psi_j^e(r, z)$ are the same as those developed in (8.2.25a) and (8.2.32a) for linear triangular and rectangular elements, with $x = r$ and $y = z$. Substitution of (8.2.72) for u and ψ_i^e for w into the weak form gives the i th equation of the finite element model

$$\begin{aligned} 0 &= \sum_{j=1}^n \left[\int_{\Omega_e} \left(\hat{a}_{11} \frac{\partial \psi_i^e}{\partial r} \frac{\partial \psi_j^e}{\partial r} + \hat{a}_{22} \frac{\partial \psi_i^e}{\partial z} \frac{\partial \psi_j^e}{\partial z} + \hat{a}_{00} \psi_i^e \psi_j^e \right) r dr dz \right] u_j^e \\ &\quad - \int_{\Omega_e} \psi_i^e \hat{f} r dr dz - \oint_{\Gamma_e} \psi_i^e q_n ds \end{aligned} \quad (8.2.73)$$

or

$$0 = \sum_{j=1}^n K_{ij}^e u_j^e - f_i^e - Q_i^e \quad (8.2.74a)$$

where

$$\begin{aligned} K_{ij}^e &= \int_{\Omega_e} \left(\hat{a}_{11} \frac{\partial \psi_i^e}{\partial r} \frac{\partial \psi_j^e}{\partial r} + \hat{a}_{22} \frac{\partial \psi_i^e}{\partial z} \frac{\partial \psi_j^e}{\partial z} + a_{00} \psi_i^e \psi_j^e \right) r dr dz \\ f_i^e &= \int_{\Omega_e} \psi_i^e \hat{f} r dr dz, \quad Q_i^e = \oint_{\Gamma_e} \psi_i^e q_n ds \end{aligned} \quad (8.2.74b)$$

The evaluation of the integrals in K_{ij}^e and f_i^e for polynomial forms of \hat{a}_{ij} and \hat{f} is possible. However, we evaluate them numerically using the numerical integration methods discussed in Chapter 7 for one-dimensional cases (see Section 7.1.5) and reviewed in Chapter 9 for two-dimensional problems. This completes the development of finite element model of an axisymmetric problem.

8.3 A NUMERICAL EXAMPLE

The model equation in (8.2.1) arises in many fields of engineering and applied sciences, and some examples are given in Table 8.1.1. The application of the finite element model developed in Sections 8.2.2–8.2.8 to problems governed by the Poisson equations is discussed here. This example is designed to illustrate selection of the computational domain, choice of elements and mesh, assembly of element equations, imposition of boundary conditions,

and postprocessing. The physical background of the problem is not discussed here but Table 8.1.1 provides the background.

Example 8.3.1

Consider a problem described by the Poisson equation

$$-\nabla^2 u = f_0 \quad \text{or} \quad -\left(\frac{\partial^2 u}{\partial x^2} + \frac{\partial^2 u}{\partial y^2}\right) = f_0 \quad \text{in } \Omega \quad (8.3.1)$$

in a square region [see Fig. 8.3.1(a)]

$$\Omega = \{(x, y) : -A < x < A, -A < y < A\}$$

where $u(x, y)$ is the dependent unknown and f_0 is the uniformly distributed source. We shall consider the following boundary conditions for the problem:

$$u = 0 \quad \text{on the entire boundary } \Gamma \quad (8.3.2)$$

We wish to use the finite element method to determine $u(x, y)$ everywhere in Ω .

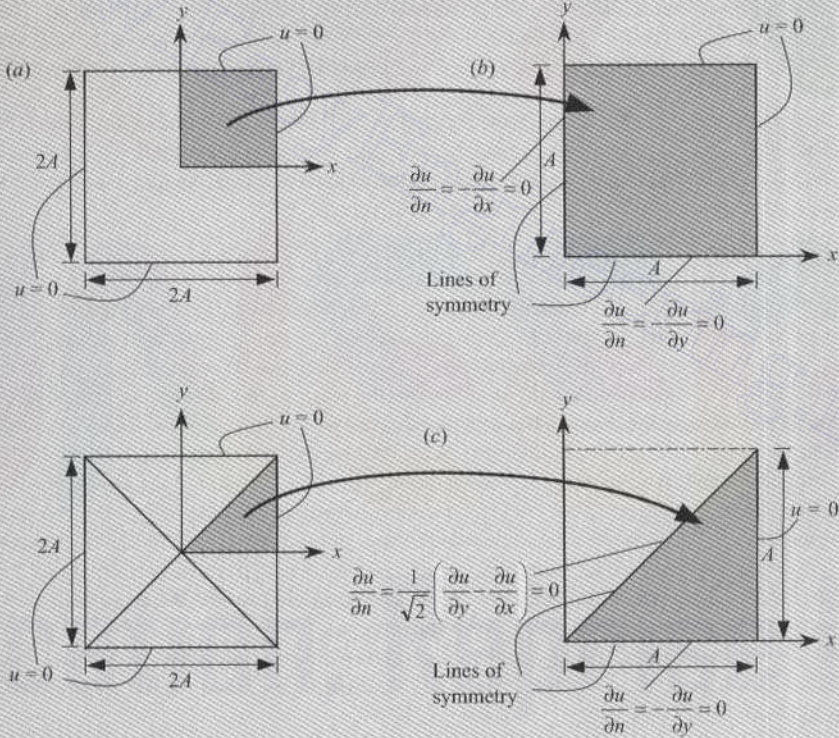


Figure 8.3.1 Finite element analysis of the Poisson equation in a square region: (a) Geometry of the actual domain with boundary conditions. (b) Computational domain based on biaxial symmetry. (c) Computational domain based on biaxial as well as diagonal symmetry.

Selection of the Computational Domain

When the given domain Ω exhibits solution symmetries, it is sufficient to solve the problem on a portion of Ω that provides the solution on the entire domain. A problem possesses symmetry of the solution about a line only when symmetry of the (a) geometry, (b) material properties, (c) source variation, and (d) boundary conditions exist about the line. Whenever a portion of the domain is modeled to exploit symmetries available in the problem, the lines of symmetries become a portion of the boundary of the computational domain. On lines of symmetry, the normal derivative of the solution (i.e., derivative of the solution with respect to the coordinate normal to the line of symmetry) is zero:

$$q_n = \frac{\partial u}{\partial n} = \frac{\partial u}{\partial x} n_x + \frac{\partial u}{\partial y} n_y = 0 \quad (8.3.2)$$

The problem at hand has the geometric symmetry about the $x = 0$ and $y = 0$ axes; since the coefficients describing the material behavior, a_{ij} , are either zero or unity, material symmetry about the $x = 0$ and $y = 0$ axes is automatically met. The symmetry of source variation is dictated by f . Since it is uniform, i.e., $f = f_0$, constant, the data is symmetric with respect to the $x = 0$ and $y = 0$ axes. Lastly, the boundary conditions are symmetric with respect to the $x = 0$ and $y = 0$ axes. Thus, the solution is symmetric about the $x = 0$ and $y = 0$ axes, and hence, a quadrant of the domain can be used as the computational domain [see Fig. 8.3.1(b)]. The solution is also symmetric about the diagonal lines, and an octant can be used as the computational domain [see Fig. 8.3.1(c)]. In the latter case, a mesh of only rectangular elements cannot be used.

While it is possible to mix triangular and rectangular elements to represent the computational domain as well as the solution, in much of this book we shall use only one type of element at a time. Two different finite element meshes for the triangular and rectangular computational domains are shown in Figs. 8.3.2 and 8.3.3, respectively.

Solution by Linear Triangular Elements

Due to the symmetry along the diagonal $x = y$, we model the triangular domain shown in Fig. 8.3.1(c). As a first choice we use a uniform mesh of four linear triangular elements, as shown in Fig. 8.3.2(a), to represent the domain (mesh T1), and then use the refined mesh (mesh T2) shown in Fig. 8.3.2(b) to compare the solutions. In the present case, there is no discretization error involved because the geometry is exactly represented.

The elements 1, 3, and 4 are identical in orientation as well as geometry. Element 2 is geometrically identical to element 1, except that it is oriented differently. If we number the local nodes of element 2 to match those of element 1, then all four elements have the same element matrices, and it is necessary to compute them only for element 1. When the element matrices are computed on a computer, such considerations are not taken into account. In solving the problem by hand, we use the similarity between a master element (element 1) and the other elements in the mesh to avoid unnecessary computations.

We consider element 1 as the typical element. The element is exactly the same as the one shown in Fig. 8.2.11(b). Hence, the element coefficient matrix and source vector are (the reader should independently verify this)

$$[K^1] = \frac{1}{2ab} \begin{bmatrix} b^2 & -b^2 & 0 \\ -b^2 & a^2 + b^2 & -a^2 \\ 0 & -a^2 & a^2 \end{bmatrix}, \quad [f^1] = \frac{f_0 ab}{6} \begin{Bmatrix} 1 \\ 1 \\ 1 \end{Bmatrix} \quad (8.3.4)$$

where in the present case $a = b = A/2 = 0.5$.

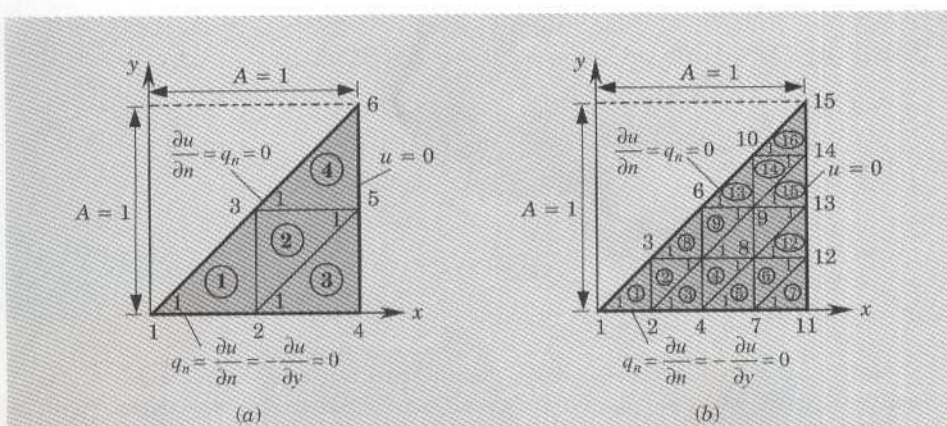


Figure 8.3.2 (a) Mesh T1 of triangular elements. (b) Mesh T2 of triangular elements.

The element matrix in (8.3.4) is valid for the Laplace operator $-\nabla^2$ on any right-angle triangle with sides a and b in which the right angle is at node 2, and the diagonal line of the triangle connects node 3 to node 1. Note that the off-diagonal coefficient associated with the nodes on the diagonal line is zero for a right-angled triangle.

In summary, for the mesh shown in Fig. 8.3.2(a), we have

$$[K^1] = [K^2] = [K^3] = [K^4], \quad \{f^1\} = \{f^2\} = \{f^3\} = \{f^4\}$$

with

$$[K^e] = \frac{1}{2} \begin{bmatrix} 1 & -1 & 0 \\ -1 & 2 & -1 \\ 0 & -1 & 1 \end{bmatrix}, \quad \{f^e\} = \frac{f_0}{24} \begin{Bmatrix} 1 \\ 1 \\ 1 \end{Bmatrix} \quad (8.3.5)$$

The assembled coefficient matrix for the finite element mesh is 6×6 , because there are six global nodes with one unknown per node. The assembled matrix can be obtained directly by using the correspondence between the global nodes and the local nodes, expressed through the connectivity matrix,

$$[B] = \begin{bmatrix} 1 & 2 & 3 \\ 5 & 3 & 2 \\ 2 & 4 & 5 \\ 3 & 5 & 6 \end{bmatrix} \quad (8.3.6)$$

A few representative global coefficients are given below in terms of the element coefficients.

$$\begin{aligned} K_{11} &= K_{11}^1 = \frac{1}{2}, \quad K_{12} = K_{12}^1 = -\frac{1}{2}, \quad K_{22} = K_{22}^1 + K_{33}^2 + K_{11}^3 = \frac{2}{2} + \frac{1}{2} + \frac{1}{2} \\ K_{13} &= K_{13}^1 = 0, \quad K_{14} = 0, \quad K_{15} = 0, \quad K_{16} = 0, \quad K_{23} = K_{23}^1 + K_{32}^2 = -\frac{1}{2} - \frac{1}{2} \\ K_{33} &= K_{33}^1 + K_{22}^2 + K_{11}^3 = \frac{1}{2} + \frac{2}{2} + \frac{1}{2}, \quad F_1 = F_1^1 = Q_1^1 + f_1^1 \\ F_2 &= (Q_2^1 + Q_3^2 + Q_1^3) + (f_2^1 + f_3^2 + f_1^3), \quad F_3 = (Q_3^1 + Q_2^2 + Q_1^3) + (f_3^1 + f_2^2 + f_1^3) \\ F_4 &= F_2^1 = Q_2^1 + f_2^1, \quad F_5 = (Q_1^2 + Q_3^3 + Q_2^4) + (f_1^2 + f_3^3 + f_2^4), \quad F_6 = F_3^4 = Q_3^4 + f_3^4 \end{aligned} \quad (8.3.7)$$

The assembled system of equations associated with mesh T1 are

$$\frac{1}{2} \begin{bmatrix} 1 & -1 & 0 & 0 & 0 & 0 \\ -1 & 4 & -2 & -1 & 0 & 0 \\ 0 & -2 & 4 & 0 & -2 & 0 \\ 0 & -1 & 0 & 2 & -1 & 0 \\ 0 & 0 & -2 & -1 & 4 & -1 \\ 0 & 0 & 0 & 0 & -1 & 1 \end{bmatrix} \begin{Bmatrix} U_1 \\ U_2 \\ U_3 \\ U_4 \\ U_5 \\ U_6 \end{Bmatrix} = \frac{f_0}{24} \begin{Bmatrix} 1 \\ 3 \\ 3 \\ 1 \\ 3 \\ 1 \end{Bmatrix} + \begin{Bmatrix} Q_1^1 \\ Q_2^1 + Q_3^2 + Q_1^3 \\ Q_3^1 + Q_2^2 + Q_1^4 \\ Q_2^3 \\ Q_1^2 + Q_3^3 + Q_2^4 \\ Q_3^4 \end{Bmatrix} \quad (8.3.8)$$

Note that at nodes 4 and 6, both u and q_n are specified (a type of singularity in the specified data). However, we shall give priority to the primary variable over the secondary variable. Thus, we assume that

$$U_4 = U_5 = U_6 = 0 \quad (8.3.9)$$

and Q_4 , Q_5 , and Q_6 , assumed to be unknown, are determined in the postcomputation. The specified secondary degrees of freedom are (all due to symmetry)

$$Q_1 = Q_1^1 = 0, \quad Q_2 = Q_2^1 + Q_3^2 + Q_1^3 = 0, \quad Q_3 = Q_3^1 + Q_2^2 + Q_1^4 = 0 \quad (8.3.10)$$

For example, consider the sum

$$\begin{aligned} Q_2^1 + Q_3^2 + Q_1^3 &= (Q_{21}^1 + Q_{22}^1) + (Q_{32}^2 + Q_{31}^2) + (Q_{11}^3 + Q_{13}^3) \\ &= Q_{21}^1 + (Q_{22}^1 + Q_{32}^2) + (Q_{31}^2 + Q_{13}^3) + Q_{11}^3 = 0 + 0 + 0 + 0 \end{aligned}$$

where Q_{21}^1 and Q_{11}^3 are zero because of $q_n = 0$ and $Q_{22}^1 + Q_{32}^2$ and $Q_{31}^2 + Q_{13}^3$ are zero because of the balance of fluxes between neighboring elements.

Since the only unknown primary variables for mesh T1 are U_1 , U_2 , and U_3 , the condensed equations for the primary unknowns can be obtained by deleting rows and columns 4, 5, and 6 from the system (8.3.8). In retrospect, it would have been sufficient to write the finite element equations associated with the global nodes 1, 2, and 3:

$$\begin{aligned} K_{11}U_1 + K_{12}U_2 + K_{13}U_3 &= F_1 \\ K_{21}U_1 + K_{22}U_2 + K_{23}U_3 + K_{24}U_4 + K_{25}U_5 &= F_2 \\ K_{31}U_1 + K_{32}U_2 + K_{33}U_3 + K_{35}U_5 + K_{36}U_6 &= F_3 \end{aligned}$$

Noting that $U_4 = U_5 = U_6 = 0$, we can write the above equations in terms of the element coefficients:

$$\begin{bmatrix} K_{11}^1 & K_{12}^1 & K_{13}^1 \\ K_{21}^1 & K_{22}^1 + K_{31}^2 + K_{11}^3 & K_{23}^1 + K_{32}^2 \\ K_{31}^1 & K_{32}^1 + K_{21}^2 & K_{33}^1 + K_{22}^2 + K_{11}^4 \end{bmatrix} \begin{Bmatrix} U_1 \\ U_2 \\ U_3 \end{Bmatrix} = \begin{Bmatrix} f_1^1 \\ f_2^1 + f_3^2 + f_1^3 \\ f_3^1 + f_2^2 + f_1^4 \end{Bmatrix} \quad (8.3.11)$$

The unknown secondary variables Q_4 , Q_5 , and Q_6 can be computed from the element equations

$$\begin{Bmatrix} Q_4 \\ Q_5 \\ Q_6 \end{Bmatrix} = - \begin{Bmatrix} f_2^3 \\ f_1^2 + f_3^2 + f_2^4 \\ f_3^4 \end{Bmatrix} + \begin{bmatrix} 0 & K_{21}^3 & 0 \\ 0 & K_{13}^2 + K_{31}^3 & K_{12}^2 + K_{21}^4 \\ 0 & 0 & K_{31}^4 \end{bmatrix} \begin{Bmatrix} U_1 \\ U_2 \\ U_3 \end{Bmatrix} \quad (8.3.12)$$

For example, we have

$$\begin{aligned} Q_4 = Q_2^3 &= Q_{21}^3 + Q_{22}^3 + Q_{23}^3 \\ &= \int_{1-2} q_n^3 \psi_2^3 dx + \int_{2-3} q_n^3 \psi_2^3 dy + \int_{3-1} q_n^3 \psi_2^3 ds \end{aligned} \quad (8.3.13a)$$

where

$$\begin{aligned} (q_n^3)_{1-2} &= \left(\frac{\partial u}{\partial x} n_x + \frac{\partial u}{\partial y} n_y \right)_{1-2} = 0 \quad (n_x = 0, \quad \frac{\partial u}{\partial y} = 0) \\ (q_n^3)_{2-3} &= \left(\frac{\partial u}{\partial x} n_x + \frac{\partial u}{\partial y} n_y \right)_{2-3} = \frac{\partial u}{\partial x} \quad (n_x = 1, \quad n_y = 0) \\ (\psi_2^3)_{2-3} &= 1 - \frac{y}{h_{23}}, \quad (\psi_2^3)_{3-1} = 0 \end{aligned} \quad (8.3.13b)$$

Thus, we have

$$Q_4 = Q_{22}^3 = \int_0^{h_{23}} \frac{\partial u}{\partial x} \left(1 - \frac{y}{h_{23}} \right) dy$$

where $\partial u / \partial x$ is calculated using $\partial u_h / \partial x$ from the finite element interpolation

$$\frac{\partial u_h}{\partial x} = \sum_{j=1}^3 u_j^3 \frac{\beta_j^3}{2A_3}$$

We obtain ($h_{23} = a = 0.5$, $\beta_1^3 = -a = -0.5$, $2A_3 = a^2 = 0.25$, $U_4 = U_5 = 0$),

$$Q_4 = \frac{h_{23}}{4A_3} \sum_{j=1}^3 u_j^3 \beta_j^3 = \frac{h_{23}}{4A_3} (\beta_1^3 U_2 + \beta_2^3 U_4 + \beta_3^3 U_5) = -0.5 U_2 \quad (8.3.14)$$

Using the numerical values of the coefficients K_{ij}^e and f_i^e , (with $f_0 = 1$), we write the condensed equations for U_1 , U_2 , and U_3 as

$$\begin{bmatrix} 0.5 & -0.5 & 0.0 \\ -0.5 & 2.0 & -1.0 \\ 0.0 & -1.0 & 2.0 \end{bmatrix} \begin{Bmatrix} U_1 \\ U_2 \\ U_3 \end{Bmatrix} = \frac{1}{24} \begin{Bmatrix} 1 \\ 3 \\ 3 \end{Bmatrix} \quad (8.3.15)$$

Solving (8.3.15) for U_i ($i = 1, 2, 3$), we obtain

$$\begin{Bmatrix} U_1 \\ U_2 \\ U_3 \end{Bmatrix} = \frac{1}{24} \begin{bmatrix} 3 & 1 & 0.5 \\ 1 & 1 & 0.5 \\ 0.5 & 0.5 & 0.75 \end{bmatrix} \begin{Bmatrix} 1 \\ 3 \\ 3 \end{Bmatrix} = \frac{1}{24} \begin{Bmatrix} 7.5 \\ 5.5 \\ 4.25 \end{Bmatrix} = \begin{Bmatrix} 0.31250 \\ 0.22917 \\ 0.17708 \end{Bmatrix} \quad (8.3.16)$$

and, from (8.3.12), we have

$$\begin{Bmatrix} Q_{22}^3 \\ Q_{32}^3 + Q_{22}^4 \\ Q_{32}^4 \end{Bmatrix} = -\frac{1}{24} \begin{Bmatrix} 1 \\ 3 \\ 1 \end{Bmatrix} + \begin{Bmatrix} 0 & -0.5 & 0 \\ 0 & 0 & -1 \\ 0 & 0 & 0 \end{Bmatrix} \begin{Bmatrix} U_1 \\ U_2 \\ U_3 \end{Bmatrix} = \begin{Bmatrix} -0.197917 \\ -0.302083 \\ -0.041667 \end{Bmatrix} \quad (8.3.17)$$

By interpolation, Q_4 is equal to $-0.5U_2$, and it differs from Q_{22}^3 computed from equilibrium by the amount f_2^3 ($= \frac{1}{24}$).

Solution by Linear Rectangular Elements

We use a 2×2 (2 elements in the x direction and 2 elements in the y direction) uniform mesh (mesh R1) of four linear rectangular elements [see Fig. 8.3.3(a)] to discretize a quadrant of the domain. The 4×4 mesh (mesh R2) [see Fig. 8.3.3(b)] will be used for comparison. Once again, no discretization error is introduced in the present case.

Since all the elements in the mesh are identical, we need to compute the element coefficient matrices for only one element, say element 1. The element coefficient matrix is available from Example 8.2.3 with $a = b$. We have

$$[K^e] = \frac{1}{6} \begin{bmatrix} 4 & -1 & -2 & -1 \\ -1 & 4 & -1 & -2 \\ -2 & -1 & 4 & -1 \\ -1 & -2 & -1 & 4 \end{bmatrix}, \quad \{f^e\} = \frac{f_0 a^2}{4} \begin{Bmatrix} 1 \\ 1 \\ 1 \\ 1 \end{Bmatrix} \quad (8.3.18)$$

The coefficient matrix of the condensed equations for the primary unknowns in mesh R1 can be directly assembled. There are four unknowns (at nodes 1, 2, 4, and 5). The finite element equations associated with the four unknowns are (noting that $U_3 = U_6 = U_7 = U_8 = U_9 = 0$)

$$\begin{aligned} K_{11}U_1 + K_{12}U_2 + K_{14}U_4 + K_{15}U_5 &= F_1 \\ K_{21}U_1 + K_{22}U_2 + K_{24}U_4 + K_{25}U_5 &= F_2 \\ K_{41}U_1 + K_{42}U_2 + K_{44}U_4 + K_{45}U_5 &= F_4 \\ K_{51}U_1 + K_{52}U_2 + K_{54}U_4 + K_{55}U_5 &= F_5 \end{aligned} \quad (8.3.19a)$$

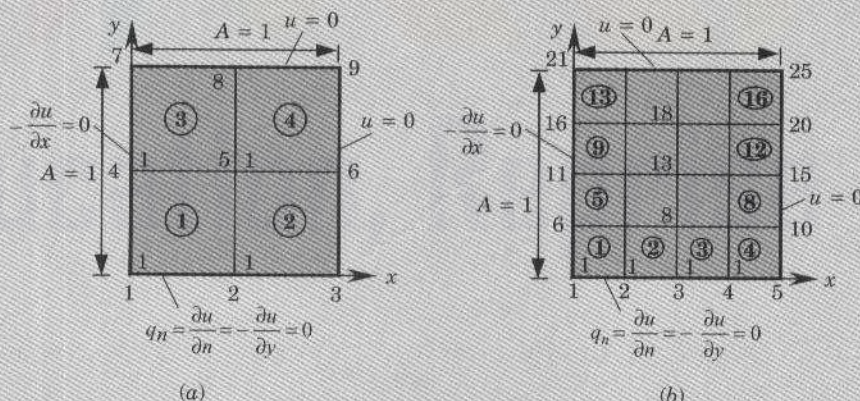


Figure 8.3.3 (a) Mesh R1 (2×2) of rectangular elements. (b) Mesh R2 (4×4) of rectangular elements.

where K_{ij} and F_i are the global coefficients, which can be written in terms of the element coefficients as

$$\begin{aligned} K_{11} &= K_{11}^1, \quad K_{12} = K_{12}^1, \quad K_{14} = K_{14}^1, \quad K_{15} = K_{13}^1 \\ K_{22} &= K_{22}^1 + K_{11}^2, \quad K_{24} = K_{24}^1, \quad K_{25} = K_{23}^1 + K_{14}^2 \\ K_{44} &= K_{44}^1 + K_{11}^3, \quad K_{45} = K_{43}^1 + K_{12}^3, \quad K_{55} = K_{33}^1 + K_{44}^2 + K_{11}^4 + K_{22}^3 \quad (8.3.19b) \\ F_1 &= f_1^1 + Q_1^1, \quad F_2 = f_2^1 + f_2^2 + Q_2^1 + Q_1^2, \quad F_4 = f_4^1 + f_4^3 + Q_4^1 + Q_1^3 \\ F_5 &= f_3^1 + f_4^2 + f_1^4 + f_2^3 + Q_3^1 + Q_4^2 + Q_1^4 + Q_2^3 \end{aligned}$$

The boundary conditions on the secondary variables are

$$Q_1^1 = 0, \quad Q_2^1 + Q_1^2 = 0, \quad Q_4^1 + Q_1^3 = 0 \quad (8.3.20a)$$

and the balance of secondary variables at global node 5 requires

$$Q_3^1 + Q_4^2 + Q_2^3 + Q_1^4 = 0 \quad (8.3.20b)$$

Thus, the condensed equations for the primary unknowns are (for $f_0 = 1$ and $a = 0.5$)

$$\frac{1}{6} \begin{bmatrix} 4 & -1 & -1 & -2 \\ -1 & 8 & -2 & -2 \\ -1 & -2 & 8 & -2 \\ -2 & -2 & -2 & 16 \end{bmatrix} \begin{Bmatrix} U_1 \\ U_2 \\ U_4 \\ U_5 \end{Bmatrix} = \frac{1}{16} \begin{Bmatrix} 1 \\ 2 \\ 2 \\ 4 \end{Bmatrix} \quad (8.3.21)$$

The solution of these equations is

$$U_1 = 0.31071, \quad U_2 = 0.24107, \quad U_4 = 0.24107, \quad U_5 = 0.19286 \quad (8.3.22)$$

The secondary variables $Q_3 = Q_7$, $Q_6 = Q_8$, and Q_9 at nodes 3 (7), 6 (8), and 9, respectively (by symmetry), can be computed from the equations ($Q_3 = Q_2^2$, $Q_6 = Q_3^2 + Q_2^4$, and $Q_9 = Q_3^4$)

$$\begin{Bmatrix} Q_3 \\ Q_6 \\ Q_9 \end{Bmatrix} = - \begin{Bmatrix} f_2^2 \\ f_5^2 + f_2^4 \\ f_3^4 \end{Bmatrix} + \begin{bmatrix} K_{31} & K_{32} & K_{34} & K_{35} \\ K_{61} & K_{62} & K_{64} & K_{65} \\ K_{91} & K_{92} & K_{94} & K_{95} \end{bmatrix} \begin{Bmatrix} U_1 \\ U_2 \\ U_4 \\ U_5 \end{Bmatrix} \quad (8.3.23a)$$

where

$$\begin{aligned} K_{31} &= 0, \quad K_{32} = K_{21}^2, \quad K_{34} = 0, \quad K_{35} = K_{24}^2 \\ K_{61} &= 0, \quad K_{62} = K_{31}^2, \quad K_{64} = 0, \quad K_{65} = K_{34}^2 + K_{21}^4 \\ K_{91} &= 0, \quad K_{92} = 0, \quad K_{94} = 0, \quad K_{95} = K_{31}^4 \end{aligned} \quad (8.3.23b)$$

Substituting the numerical values, we obtain

$$\begin{Bmatrix} Q_3 \\ Q_6 \\ Q_9 \end{Bmatrix} = - \frac{1}{16} \begin{Bmatrix} 1 \\ 2 \\ 1 \end{Bmatrix} + \frac{1}{6} \begin{bmatrix} 0 & -1 & 0 & -2 \\ 0 & -2 & 0 & -2 \\ 0 & 0 & 0 & -2 \end{bmatrix} \begin{Bmatrix} U_1 \\ U_2 \\ U_4 \\ U_5 \end{Bmatrix} = - \begin{Bmatrix} 0.16697 \\ 0.26964 \\ 0.12679 \end{Bmatrix} \quad (8.3.24)$$

Table 8.3.1 Comparison of the finite element solutions $u(0, y)$ with the series solution and the Ritz solution of (8.3.1).

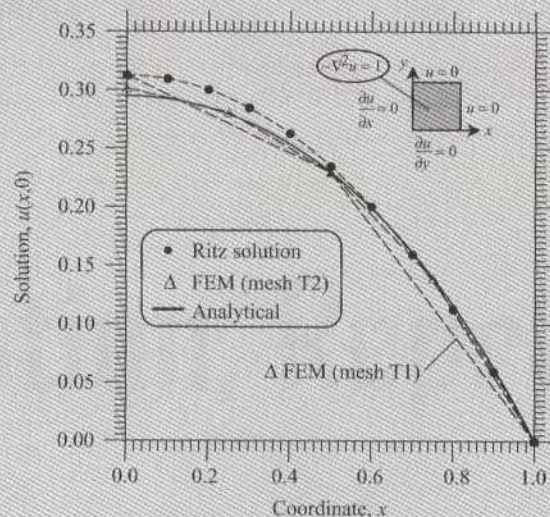
y	Triangular elem.		Rectangular elem.		Ritz solution (2.5.39)	Series solution (2.5.40)
	Mesh T1	Mesh T2	Mesh R1	Mesh R2		
0.00	0.3125	0.3013	0.3107	0.2984	0.3125	0.2947
0.25	0.2708 [†]	0.2805	0.2759	0.2824	0.2930	0.2789
0.50	0.2292	0.2292	0.2411	0.2322	0.2344	0.2293
0.75	0.1146 [†]	0.1393	0.1205 [†]	0.1414	0.1367	0.1397
1.00	0.0000	0.0000	0.0000	0.0000	0.0000	0.0000

[†]Interpolated values

The finite element solutions obtained by two different meshes of triangular elements and two different meshes of rectangular elements are compared in Table 8.3.1 with the 50-term series solution (at $x = 0$ for varying y) in (2.5.40) (set $k = 1$, $g_0 = f_0 = 1$) and the one-parameter Ritz solution in (2.5.39); see also Fig. 8.3.4. The finite element solution obtained by 16 triangular elements (in an octant) is the most accurate when compared to the series solution. The accuracy of the triangular element mesh is due to the large number of elements it has compared to the number of elements in the rectangular element mesh for the same size of the domain.

The solution u and components of flux (q_x, q_y) can be computed at any interior point of the domain. For a point (x, y) in element Ω_e , we have ($k = 1$)

$$u_h^e(x, y) = \sum_{j=1}^R u_j^e \psi_j^e(x, y) \quad (8.3.25a)$$

**Figure 8.3.4** Comparison of the finite element solution with the two-parameter Ritz solution and the analytical (series) solution.

$$q_y^e(x, y) = -k \frac{\partial u_h^e}{\partial y} = - \sum_{i=1}^n u_i^e \frac{\partial \psi_i^e}{\partial y}, \quad q_x^e(x, y) = -k \frac{\partial u_h^e}{\partial x} = - \sum_{i=1}^n u_i^e \frac{\partial \psi_i^e}{\partial x} \quad (8.3.25b)$$

The negative sign in the definition of fluxes is dictated by the physics of the problem. Here we interpreted the problem at hand to be one of heat transfer. Note that for a linear triangular element, q_x and q_y are constants over an entire element, whereas q_e is linear in y and q_y is linear in x for a linear rectangular element. For example, consider element 1 of mesh T1 of triangular elements

$$\begin{aligned} q_x^1(x, y) &= -\frac{k}{2A_1} \sum_{i=1}^3 u_i^1 \beta_i^1 = -2(U_2 - U_1) = 0.16667 \\ q_y^1(x, y) &= -\frac{k}{2A_1} \sum_{i=1}^3 u_i^1 \gamma_i^1 = -2(U_3 - U_2) = 0.10417 \end{aligned} \quad (8.3.26a)$$

Clearly, the gradients (and hence the components of flux) are constant. For element 1 of mesh R1 rectangular element (four elements) we have

$$\begin{aligned} q_x^1(x, y) &= -k \sum_{i=1}^4 u_i^1 \frac{\partial \psi_i^1}{\partial x} = 2U_1(1-2y) - 2U_2(1-2y) - 4yU_5 + 4yU_4 \\ q_x^1(0.25, 0.25) &= 0.11785 \\ q_y^1(x, y) &= -k \sum_{i=1}^4 u_i^1 \frac{\partial \psi_i^1}{\partial y} = 2U_1(1-2x) - 2U_2(1-2x) - 4xU_5 + 4xU_4 \\ q_y^1(0.25, 0.25) &= 0.11785 \end{aligned} \quad (8.3.26b)$$

Plots of q_x , obtained by mesh T1 (8 elements) and mesh T2 (16 elements) of linear triangular elements as a function of x (for $y = 0.0$) are shown in Fig. 8.3.5.

The computation of *isolines*, i.e., lines of constant u , for linear finite elements is straightforward. Suppose that we wish to find $u = u_0$ (constant) isoline. On a side of a linear triangle or rectangular element, the solution u varies according to the equation

$$u_h^e(s) = u_1^e + \frac{u_2^e - u_1^e}{h} s$$

where s is the local coordinate with its origin at node 1 of the side, (u_1^e, u_2^e) are the nodal values (see Fig. 8.3.6), and h is the length of the side. Then, if $u \equiv u_0$ lies on the line (i.e., $u_1^e < u_0 < u_2^e$ or $u_2^e < u_0 < u_1^e$), the point s_0 at which $U^e(s_0) = u_0$ is given by

$$s_0 = \frac{(u_0 - u_1^e)h}{(u_2^e - u_1^e)} \quad (8.3.27)$$

Similar equations apply for other sides of the element. Since the solution varies linearly between any two points of linear elements, the isoline is determined by joining two points on any two sides of the element for which (8.3.27) gives a positive value (and $s_0 < h$).

For quadratic elements, isolines are determined by finding three points s_i in the element at which $u_h^e(s_i) = u_0$ ($i = 1, 2$, and 3):

$$\frac{s_0}{h} = \frac{-b \pm \sqrt{b^2 - 4ac}}{2a} > 0 \quad (8.3.28a)$$

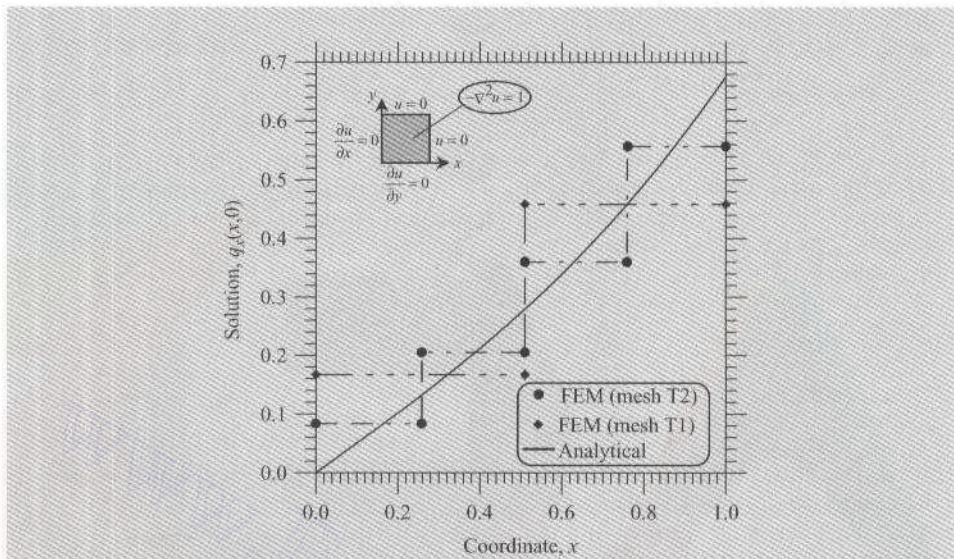


Figure 8.3.5 Comparison of the finite element solution with the analytical (series) solution of $q_x(x, 0)$.

where

$$c = u_1^e - u_0, \quad b = -3u_1^e + 4u_2^e - u_3^e, \quad a = 2(u_1^e - 2u_2^e + u_3^e) \quad (8.3.28b)$$

Equation (8.3.28a) is to be applied on any three lines in the element until three different values $h > s_0 > 0$ are found.

The problem considered here has several physical interpretations (see Table 8.1.1). The problem can be viewed as one of finding the temperature u in a unit square with uniform internal heat generation, where the sides $x = 0$ and $y = 0$ are insulated and the other two sides are subjected to zero temperature (see Section 8.5.1). Another interpretation of the equation is that it defines the torsion of a 2-inch-square cross-sectional cylindrical bar (see Section 8.5.3). In this case, u denotes the stress function Ψ , and the components of the gradient of the solution

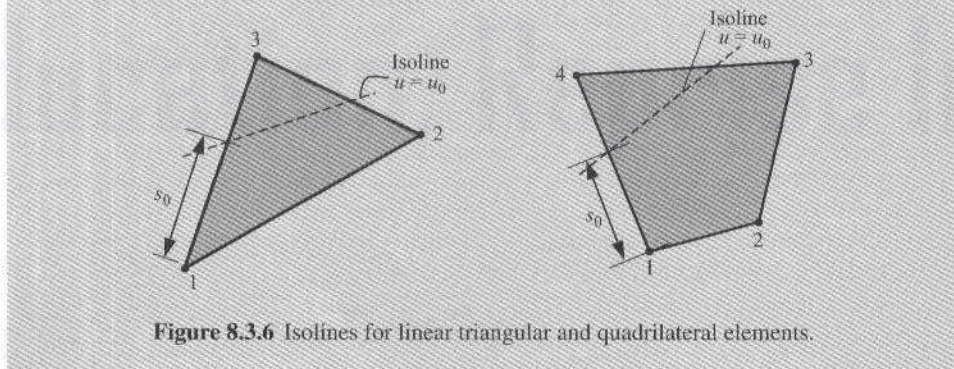


Figure 8.3.6 Isolines for linear triangular and quadrilateral elements.

are the stresses (which are of primary interest):

$$\sigma_{xz} = G\theta \frac{\partial \Psi}{\partial y}, \quad \sigma_{yz} = -G\theta \frac{\partial \Psi}{\partial x}$$

where G is the shear modulus and θ is the angle of twist per unit length of the bar.

A third interpretation of (8.3.1) is provided by groundwater (seepage) and potential flow problems. In this case, u denotes the piezometric head ϕ , stream function ψ , or velocity potential ϕ (see Section 8.5.2). The x and y components of the velocity for the groundwater flow are defined as

$$u_1 = -a_{11} \frac{\partial \phi}{\partial x}, \quad u_2 = -a_{22} \frac{\partial \phi}{\partial y}$$

where a_{11} and a_{22} are the permeabilities of the soil along the x and y directions, respectively. Examples of each of these field problems will be considered in Section 8.5.

8.4 SOME COMMENTS ON MESH GENERATION AND IMPOSITION OF BOUNDARY CONDITIONS

8.4.1 Discretization of a Domain

The representation of a given domain by a collection of finite elements requires engineering judgement on the part of the finite element practitioner. The number, type (e.g., linear or quadratic), shape (e.g., triangular or rectangular), and density (i.e., mesh refinement) of elements used in a given problem depend on a number of considerations. The first consideration is to discretize the domain as closely as possible with elements that are admissible. As we shall see later, we can use one set of elements for the approximation of a domain and another set for the solution. In discretizing a domain, consideration must be given to an accurate representation of the domain, point sources, distributed sources with discontinuities (i.e., sudden change in the intensity of the source), and material and geometric discontinuities, including a reentrant corner. The discretization should include, for example, nodes at point sources (so that the point source is accurately lumped at the node), reentrant corners, and element interfaces where abrupt changes in geometry and material properties occur.

A second consideration, which requires some engineering judgement, is to discretize the body or portions of the body into sufficiently small elements so that steep gradients of the solution are accurately calculated. The engineering judgement should come from both a qualitative understanding of the behavior of the solution and an estimate of the computational costs involved in the mesh refinement (i.e., reducing the size of the elements). For example, consider the inviscid flow around a cylinder in a channel. The flow entering the channel at the left goes around the cylinder and exits the channel at the right [see Fig. 8.4.1(a)]. Since the section at the cylinder is smaller than the inlet section, it is expected that the flow accelerates in the vicinity of the cylinder. On the other hand, the velocity field far from the cylinder (e.g., at the inlet) is essentially uniform. Such knowledge of the qualitative behavior of the flow allows us to employ a coarse mesh (i.e., elements that are relatively

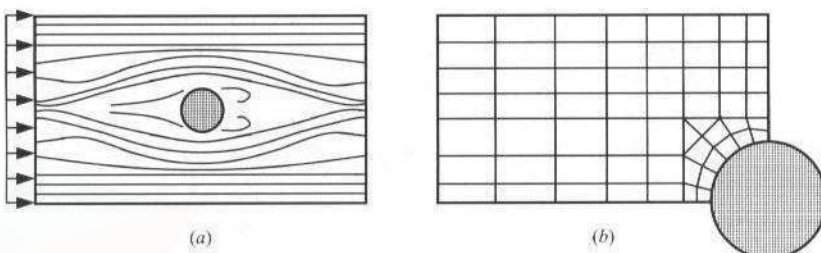


Figure 8.4.1 (a) Flow of an inviscid fluid around a cylinder (streamlines). (b) A typical mesh for a quadrant of the domain.

large in size) at sites sufficiently far from the cylinder, and a fine one at closer distances to the cylinder [see Fig. 8.4.1(b)]. Another reason for using a refined mesh near the cylinder is to accurately represent the curved boundary of the domain there. In general, a refined mesh is required in places where acute changes in geometry, boundary conditions, loading, material properties, or solution occur.

A mesh refinement should meet three conditions: (1) All the previous meshes should be contained in the current refined mesh; (2) every point in the body can be included within an arbitrarily small element at any stage of the mesh refinement; and (3) the same order of approximation for the solution should be retained through all stages of the refinement process. The last requirement eliminates comparison of two different approximations in two different meshes.

When a mesh is refined, care should be taken to avoid elements with very large aspect ratios (i.e., the ratio of one side of an element to the other) or small angles. Recall from the element matrices in Eqs. (8.2.48) and (8.2.53) that the coefficient matrices depend on the ratios of a to b and b to a , where a and b are the lengths of elements in the x and y directions, respectively. If the value of a/b or b/a is very large, the resulting coefficient matrices are ill-conditioned (i.e., numerically not invertible). Although the safe lower and upper limits on b/a are believed to be 0.1 and 10, respectively, the actual values are much more extreme and they depend on the nature of physical phenomenon being modeled. For example, in the inviscid flow problem discussed above, large aspect ratios are allowed at the entrance of the channel.

The words “coarse” and “fine” are relative. In any given problem, we begin with a finite element mesh that is believed to be adequate (based on experience and engineering judgement) to solve the problem at hand. Then, as a second choice, we select a mesh that consists of a larger number of elements (and includes the first one as a subset) to solve the problem once again. If there is a significant difference between the two solutions, we see the benefit of mesh refinement and further mesh refinement may be warranted. If the difference is negligibly small, further mesh refinements are not necessary. Such numerical experiments with mesh refinements are not always feasible in practice, mostly due to the computational costs involved.

In cases where computational cost is the prime concern, we must depend on our judgement concerning what is a reasonably good mesh, which is often dictated by the geometry and qualitative understanding of the variations of the solution and its gradient. Since most

practical problems are approximated in their engineering formulations, we should not be overly concerned with the numerical accuracy of the solution. A feel for the relative proportions and directions of various errors introduced into the analysis helps the finite element practitioner to make a decision on when to stop refining a mesh. In summary, engineering knowledge and experience with a given class of problems are essential to a suitable numerical study.

8.4.2 Generation of Finite Element Data

An important part of finite element modeling is the mesh generation, which involves numbering the nodes and elements, and the generation of nodal coordinates and the connectivity matrix. While the task of generating such data is not difficult, the type of the data has an effect on the computational efficiency as well as on accuracy. More specifically, the numbering of the nodes directly affects the bandwidth of the final assembled equations, which in turn increases the storage requirement and computational cost if equation solvers with the Gauss elimination procedure are used. The elements can be numbered arbitrarily because it has no effect on the half-bandwidth. In a general-purpose program with a preprocessor, options to minimize the bandwidth are included. The saving of computational cost due to a smaller bandwidth in the solution of equations can be substantial, especially in problems where a large number of nodes and degrees of freedom per node are involved. While element numbering does not affect the half-bandwidth, it may affect the computer time required to assemble the global coefficient matrix (usually, a very small percentage of the time required to solve the equations).

The accuracy of the finite element solution can also depend on the choice of the finite element mesh. For instance, if the mesh selected violates the symmetry present in the problem, the resulting solution will be less accurate than one obtained using a mesh that agrees with the physical symmetry present in the problem. Geometrically, a triangular element has fewer (or no) lines of symmetry when compared to a rectangular element, and therefore meshes of triangular elements should be used with care (e.g., select a mesh that does not contradict the mathematical symmetry present in the problem).

The effect of the finite element meshes shown in Fig. 8.4.2 on the solution of the Poisson equation in Example 8.3.1 is investigated. The finite element solutions obtained by the three meshes are compared with the series solution in Table 8.4.1. Clearly, the solution obtained using mesh 3 is less accurate. This is expected because mesh 3 is symmetric about the diagonal line connecting node 3 to node 7, whereas the mathematical symmetry is about the diagonal line connecting node 1 to node 9 (see Fig. 8.4.2). Mesh 1 is the most desirable of the three because it does not contradict the mathematical symmetry of the problem.

Next, the effect of mesh refinement with rectangular elements is investigated. Four different meshes of rectangular elements are shown in Fig. 8.4.3. Each of the meshes contains the previous mesh as a subset. The mesh shown in Fig. 8.4.3(c) is nonuniform; it is obtained by subdividing the first two rows and columns of elements of the mesh shown in Fig. 8.4.3(b). The finite element solutions obtained by these meshes are compared in Table 8.4.2. The numerical convergence of the finite element solution of the refined meshes to the series solution is apparent from the results presented.

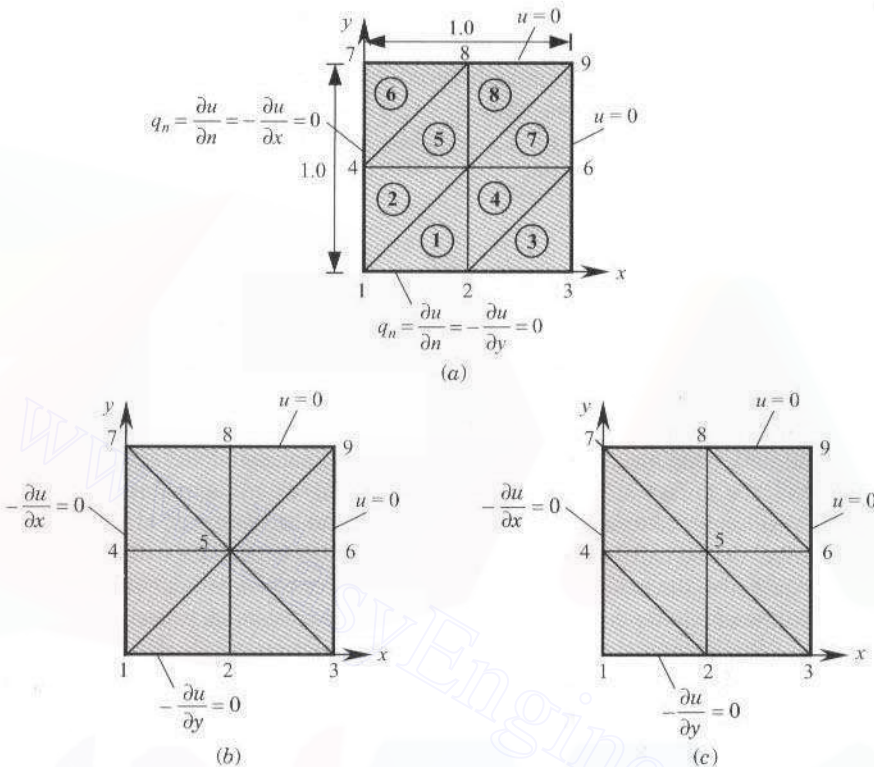


Figure 8.4.2 Various types of triangular-element meshes for the domain of Example 8.3.1: (a) mesh 1; (b) mesh 2; and (c) mesh 3.

8.4.3 Imposition of Boundary Conditions

In some problems of interest we encounter situations where at a point of the boundary both primary and secondary degrees of freedom are specified at the same point. Such points are called *singular points*. In this case we impose the boundary condition on the primary variable and let the secondary variable take its value (calculated in the postcomputation).

Table 8.4.1 Comparison of the finite element solutions obtained using various linear triangular-element meshes[†] with the series solution of the problem in Example 8.3.1.

Node	Finite element solution			Series solution
	Mesh 1	Mesh 2	Mesh 3	
1	0.31250	0.29167	0.25000	0.29469
2	0.22917	0.20833	0.20833	0.22934
3	0.22917	0.20833	0.20833	0.22934
4	0.17708	0.18750	0.16667	0.18114

[†]See Fig. 8.4.2 for the finite element meshes.

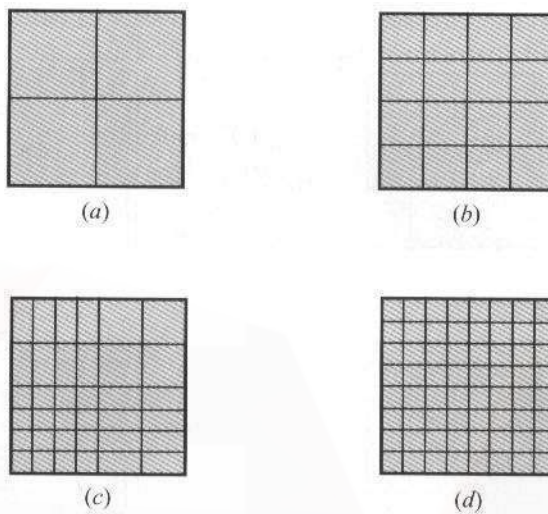


Figure 8.4.3 Mesh refinement; the meshes in (a), (b), and (d) are uniform; the mesh in (c) is nonuniform: (a) 2×2 mesh; (b) 4×4 mesh; (c) 6×6 mesh; and (d) 8×8 mesh.

This is because the boundary conditions on the primary variables are often maintained more strictly than those on the secondary variables. Of course, if the problem is such that the essential boundary conditions are a result of the natural boundary conditions, then we must impose the natural boundary conditions.

Another type of singularity we encounter in the solution of boundary value problems is the specification of two different values of a primary variable at the same point.

Table 8.4.2 Convergence of the finite element solution (with mesh refinement)[†] of the problem in Example 8.3.1.

Location		Finite element solution				Series solution
x	y	2×2	4×4	6×6	8×8	
0.000	0.0	0.31071	0.29839	0.29641	0.29560	0.29469
0.125	0.0	—	—	0.29248	0.29167	0.29077
0.250	0.0	—	0.28239	0.28055	0.27975	0.27888
0.375	0.0	—	—	0.26022	0.24943	0.25863
0.500	0.0	0.24107	0.23220	0.23081	0.23005	0.22934
0.625	0.0	—	—	—	0.19067	0.19009
0.750	0.0	—	0.14137	0.14064	0.14014	0.13973
0.875	0.0	—	—	—	0.07709	0.07687
0.125	0.125	—	—	0.28862	0.28781	0.28692
0.250	0.250	—	0.26752	0.26580	0.26498	0.26415
0.375	0.375	—	—	0.22960	0.22873	0.22799
0.500	0.50	0.19286	0.18381	0.18282	0.18179	0.18114
0.625	0.625	—	—	—	0.12813	0.12757
0.750	0.750	—	0.07506	0.07481	0.07332	0.07282
0.875	0.875	—	—	—	0.02561	0.02510

[†]See Fig. 8.4.3 for the finite element meshes.

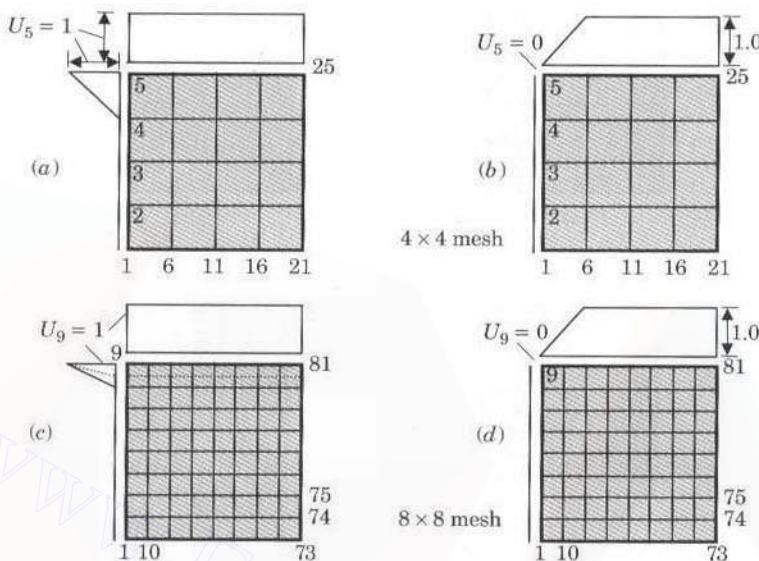


Figure 8.4.4 Effect of specifying two values of a primary variable at a node [node 5 in (a) and (b) and node 9 in (c) and (d)].

An example of such cases is provided by the problem in Fig. 8.4.4, where u is specified to be zero on the boundary defined by the line $x = 0$ and is specified to be unity on the boundary defined by the line $y = 1$. Consequently, at $x = 0$ and $y = 1$, u has two different values. The analyst must make a choice between the two values. In either case, the true boundary condition is replaced by an approximate condition. Often, the larger value is used to obtain a conservative design. The closeness of the approximate boundary condition to the true one depends on the size of the element containing the point (see Fig. 8.4.3). A mesh refinement in the vicinity of the singular point often yields an acceptable solution.

Additional comments on the choice of element geometry, meshes, and load-representation in finite element analysis are presented in Section 9.4.

8.5 APPLICATIONS

8.5.1 Conduction and Convection Heat Transfer

In Section 4.3, heat transfer (by conduction and convection) in one-dimensional (axial and radially symmetric) systems was considered. Here we consider heat transfer in two-dimensional plane and axisymmetric systems. The derivation of two-dimensional heat transfer equations in plane and axisymmetric geometries follows the same procedure as in one dimension but the heat transfer is in two directions. Details of such derivations can be found in textbooks on heat transfer [e.g., Holman (1986) and Özisik (1985)]. Here we record the governing equations for various cases, construct their finite element models, and present typical applications.

For heat conduction in plane or axisymmetric geometries, the finite element models developed in Sections 8.2 and 8.3 are immediately applicable with the following interpretation of the variables:

$$\begin{aligned}
 u &= T \equiv \text{temperature } (\text{°C}) \\
 q_n &\equiv \text{negative of heat flux } [\text{W}/(\text{m}^2 \cdot \text{°C})] \\
 a_{11}, a_{22} &\equiv \text{conductivities } [\text{W}/(\text{m} \cdot \text{°C})] \text{ of an orthotropic medium} \\
 &\quad \text{whose principal material axes coincide with the } (x, y) \text{ axes} \\
 f &\equiv \text{internal heat generation } (\text{W}/\text{m}^3) \\
 a_{00} &= 0
 \end{aligned} \tag{8.5.1}$$

For convection heat transfer, i.e., when heat is transferred from one medium to the surrounding medium (often, a fluid) by convection, the finite element model developed earlier requires some modification. The reason for this modification is that in two-dimensional problems, the convective boundary is a curve as opposed to a point in one-dimensional problems. Therefore, the contribution of the convection (or Newton's type) boundary condition to the coefficient matrix and source vector are to be computed by evaluating boundary integrals involving the interpolation functions of elements with convection boundaries. The model to be presented allows the computation of the additional contributions to the coefficient matrix and source vector whenever the element has the convection boundary condition.

Plane Systems

The governing equation for steady-state heat transfer in plane systems is a special case of (8.2.1) and is given by

$$-\frac{\partial}{\partial x} \left(k_x \frac{\partial T}{\partial x} \right) - \frac{\partial}{\partial y} \left(k_y \frac{\partial T}{\partial y} \right) = f(x, y) \tag{8.5.2}$$

where T is the temperature (in °C), k_x and k_y are the thermal conductivities [in $\text{W}/(\text{m} \cdot \text{°C})$] along the x and y directions, respectively, and f is the internal heat generation per unit volume (in W/m^3). For a convection boundary, the natural boundary condition is a balance of energy transfer across the boundary due to conduction *and/or* convection (i.e., Newton's law of cooling):

$$k_x \frac{\partial T}{\partial x} n_x + k_y \frac{\partial T}{\partial y} n_y + \beta(T - T_\infty) = \hat{q}_n \tag{8.5.3}$$

where β is the convective conductance (or the convective heat transfer coefficient) [in $\text{W}/(\text{m}^2 \cdot \text{°C})$], T_∞ is the (ambient) temperature of the surrounding fluid medium, and \hat{q}_n is the specified heat flux. The first term accounts for heat transfer by conduction, the second by convection, and the third accounts for the specified heat flux, if any. It is the presence of the term $\beta(T - T_\infty)$ that requires some modification of (8.2.10).

The weak form of (8.5.2) can be obtained from (8.2.8). The boundary integral should be modified to account for the convection heat transfer boundary condition in (8.5.3).

The coefficient of w , $k_x(\partial T / \partial x)n_x + k_y(\partial T / \partial y)n_y$, in the boundary integral is replaced with $q_n - \beta(T - T_\infty)$:

$$\begin{aligned} 0 &= \int_{\Omega_e} \left(k_x \frac{\partial w}{\partial x} \frac{\partial T}{\partial x} + k_y \frac{\partial w}{\partial y} \frac{\partial T}{\partial y} - wf \right) dx dy - \oint_{\Gamma_e} w \left(k_x \frac{\partial T}{\partial x} n_x + k_y \frac{\partial T}{\partial y} n_y \right) ds \\ &= \int_{\Omega_e} \left(k_x \frac{\partial w}{\partial x} \frac{\partial T}{\partial x} + k_y \frac{\partial w}{\partial y} \frac{\partial T}{\partial y} - wf \right) dx dy - \oint_{\Gamma_e} w [q_n - \beta(T - T_\infty)] ds \\ &= B(w, T) - l(T) \end{aligned} \quad (8.5.4a)$$

where w is the test function and $B(\cdot, \cdot)$ and $l(\cdot)$ are the bilinear and linear forms, respectively,

$$\begin{aligned} B(w, T) &= \int_{\Omega_e} \left(k_x \frac{\partial w}{\partial x} \frac{\partial T}{\partial x} + k_y \frac{\partial w}{\partial y} \frac{\partial T}{\partial y} \right) dx dy + \oint_{\Gamma_e} \beta w T ds \\ l(T) &= \int_{\Omega_e} wf dx dy + \oint_{\Gamma_e} \beta w T_\infty ds + \oint_{\Gamma_e} w \hat{q}_n ds \end{aligned} \quad (8.5.4b)$$

The finite element model of (8.5.4a) and (8.5.4b) is obtained by substituting the finite element approximation of the form,

$$T = \sum_{j=1}^n T_j^e \psi_j^e(x, y) \quad (8.5.5)$$

for T and ψ_i^e for w into (8.5.4a):

$$\sum_{j=1}^n (K_{ij}^e + H_{ij}^e) T_j^e = F_i^e + P_i^e \quad (8.5.6a)$$

where

$$\begin{aligned} K_{ij}^e &= \int_{\Omega_e} \left(k_x \frac{\partial \psi_i^e}{\partial x} \frac{\partial \psi_j^e}{\partial x} + k_y \frac{\partial \psi_i^e}{\partial y} \frac{\partial \psi_j^e}{\partial y} \right) dx dy \\ F_i^e &= \int_{\Omega_e} f \psi_i^e dx dy + \oint_{\Gamma_e} \hat{q}_n^e \psi_i^e ds \equiv f_i^e + Q_i^e \\ H_{ij}^e &= \beta^e \oint_{\Gamma_e} \psi_i^e \psi_j^e ds, \quad P_i^e = \beta^e \oint_{\Gamma_e} \psi_i^e T_\infty ds \end{aligned} \quad (8.5.6b)$$

Note that by setting the heat transfer coefficient β to zero, we obtain the heat conduction model that accounts for no convection.

The additional coefficients H_{ij}^e and P_i^e due to the convection boundary conditions can be computed by evaluating boundary integrals. These coefficients must be computed only for those elements and boundaries that are subjected to a convection boundary condition. The computation of the coefficients for the linear triangular and rectangular elements is presented in the following paragraphs. The coefficients H_{ij}^e and P_i^e for a linear triangular

element are defined by

$$\begin{aligned} H_{ij}^e &= \beta_{12}^e \int_0^{h_{12}^e} \psi_i^e \psi_j^e ds + \beta_{23}^e \int_0^{h_{23}^e} \psi_i^e \psi_j^e ds + \beta_{31}^e \int_0^{h_{31}^e} \psi_i^e \psi_j^e ds \\ P_i^e &= \beta_{12}^e T_{\infty}^{12} \int_0^{h_{12}^e} \psi_i^e ds + \beta_{23}^e T_{\infty}^{23} \int_0^{h_{23}^e} \psi_i^e ds + \beta_{31}^e T_{\infty}^{31} \int_0^{h_{31}^e} \psi_i^e ds \end{aligned} \quad (8.5.7)$$

where β_{ij}^e is the film coefficient (assumed to be constant) for the side connecting nodes i and j of element Ω_e , T_{∞}^{ij} is the ambient temperature on the side, and h_{ij}^e is the length of the side. For a rectangular element, expressions in (8.5.7) must be modified to account for four line integrals on four sides of the element.

Only those line integrals that have a convection boundary condition need to be evaluated. The boundary integrals are line integrals involving the interpolation functions. The local coordinate s is taken along the side, with its origin at the first node of the side (see Fig. 8.5.1). As noted earlier, the interpolation functions on any given side are the one-dimensional interpolation functions. Therefore, the evaluation of integrals is made easy. Indeed, the integrals

$$\int_0^{h_{ij}^e} \psi_i^e \psi_j^e ds, \quad \int_0^{h_{ij}^e} \psi_i^e ds$$

have been evaluated in Chapter 3 in connection with mass matrix coefficients and source vector coefficients for linear and quadratic elements. We summarize the results here.

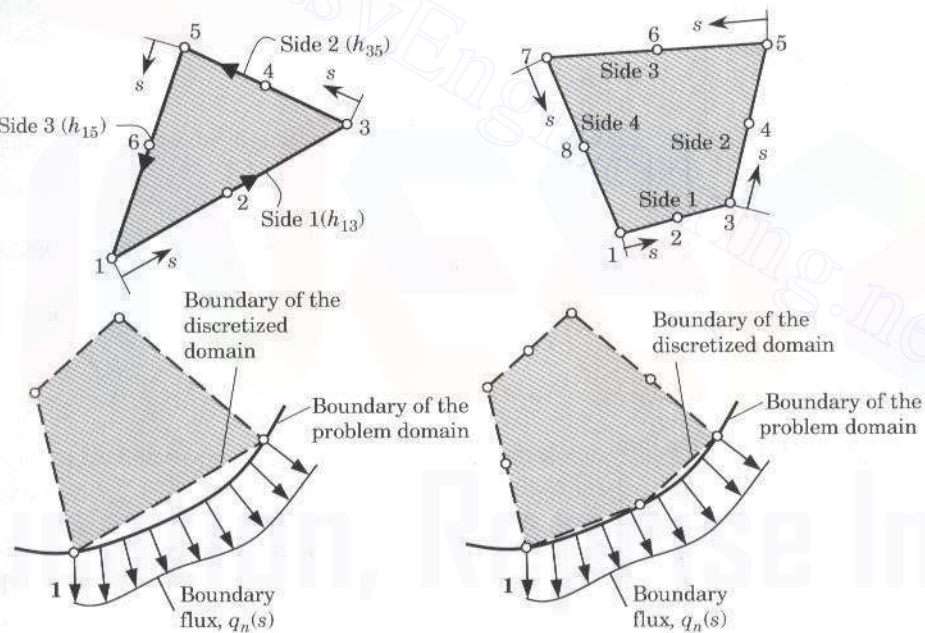


Figure 8.5.1 Triangular and quadrilateral elements, with node numbers and local coordinates for the evaluation of the boundary integrals. Also shown are the boundary approximation and flux representation using linear and quadratic elements.

Linear Triangular Element

The matrices $[H^e]$ and $\{P^e\}$ are given by

$$[H^e] = \frac{\beta_{12}^e h_{12}^e}{6} \begin{bmatrix} 2 & 1 & 0 \\ 1 & 2 & 0 \\ 0 & 0 & 0 \end{bmatrix} + \frac{\beta_{23}^e h_{23}^e}{6} \begin{bmatrix} 0 & 0 & 0 \\ 0 & 2 & 1 \\ 0 & 1 & 2 \end{bmatrix} + \frac{\beta_{31}^e h_{31}^e}{6} \begin{bmatrix} 2 & 0 & 1 \\ 0 & 0 & 0 \\ 1 & 0 & 2 \end{bmatrix} \quad (8.5.8a)$$

$$\{P^e\} = \frac{\beta_{12}^e T_\infty^{12} h_{12}^e}{2} \begin{Bmatrix} 1 \\ 1 \\ 0 \end{Bmatrix} + \frac{\beta_{23}^e T_\infty^{23} h_{23}^e}{2} \begin{Bmatrix} 0 \\ 1 \\ 1 \end{Bmatrix} + \frac{\beta_{31}^e T_\infty^{31} h_{31}^e}{2} \begin{Bmatrix} 1 \\ 0 \\ 1 \end{Bmatrix} \quad (8.5.8b)$$

Quadratic Triangular Element

$$[H^e] = \frac{\beta_{13}^e h_{13}^e}{30} \begin{bmatrix} 4 & 2 & -1 & 0 & 0 & 0 \\ 2 & 16 & 2 & 0 & 0 & 0 \\ -1 & 2 & 4 & 0 & 0 & 0 \\ 0 & 0 & 0 & 0 & 0 & 0 \\ 0 & 0 & 0 & 0 & 0 & 0 \\ 0 & 0 & 0 & 0 & 0 & 0 \end{bmatrix} + \frac{\beta_{35}^e h_{35}^e}{30} \begin{bmatrix} 0 & 0 & 0 & 0 & 0 & 0 \\ 0 & 0 & 0 & 0 & 0 & 0 \\ 0 & 0 & 4 & 2 & -1 & 0 \\ 0 & 0 & 2 & 16 & 2 & 0 \\ 0 & 0 & -1 & 2 & 4 & 0 \\ 0 & 0 & 0 & 0 & 0 & 0 \end{bmatrix} \\ + \frac{\beta_{51}^e h_{51}^e}{30} \begin{bmatrix} 4 & 0 & 0 & 0 & -1 & 2 \\ 0 & 0 & 0 & 0 & 0 & 0 \\ 0 & 0 & 0 & 0 & 0 & 0 \\ 0 & 0 & 0 & 0 & 0 & 0 \\ -1 & 0 & 0 & 0 & 4 & 2 \\ 2 & 0 & 0 & 0 & 2 & 16 \end{bmatrix} \quad (8.5.9a)$$

$$\{P^e\} = \frac{\beta_{13}^e T_\infty^{13} h_{13}^e}{6} \begin{Bmatrix} 1 \\ 4 \\ 1 \\ 0 \\ 0 \\ 0 \end{Bmatrix} + \frac{\beta_{35}^e T_\infty^{35} h_{35}^e}{6} \begin{Bmatrix} 0 \\ 0 \\ 1 \\ 4 \\ 1 \\ 0 \end{Bmatrix} + \frac{\beta_{51}^e T_\infty^{51} h_{51}^e}{6} \begin{Bmatrix} 1 \\ 0 \\ 0 \\ 0 \\ 1 \\ 4 \end{Bmatrix} \quad (8.5.9b)$$

Linear Rectangular Element

The matrix $[H^e]$ is of the form

$$[H^e] = \frac{\beta_{12}^e h_{12}^e}{6} \begin{bmatrix} 2 & 1 & 0 & 0 \\ 1 & 2 & 0 & 0 \\ 0 & 0 & 0 & 0 \\ 0 & 0 & 0 & 0 \end{bmatrix} + \frac{\beta_{23}^e h_{23}^e}{6} \begin{bmatrix} 0 & 0 & 0 & 0 \\ 0 & 2 & 1 & 0 \\ 0 & 1 & 2 & 0 \\ 0 & 0 & 0 & 0 \end{bmatrix} \\ + \frac{\beta_{34}^e h_{34}^e}{6} \begin{bmatrix} 0 & 0 & 0 & 0 \\ 0 & 0 & 0 & 0 \\ 0 & 0 & 2 & 1 \\ 0 & 0 & 1 & 2 \end{bmatrix} + \frac{\beta_{41}^e h_{41}^e}{6} \begin{bmatrix} 2 & 0 & 0 & 1 \\ 0 & 0 & 0 & 0 \\ 0 & 0 & 0 & 0 \\ 1 & 0 & 0 & 2 \end{bmatrix} \quad (8.5.10a)$$

and $\{P^e\}$ is given by

$$\{P^e\} = \frac{\beta_{12}^e T_\infty^{12} h_{12}^e}{2} \begin{Bmatrix} 1 \\ 1 \\ 0 \\ 0 \end{Bmatrix} + \frac{\beta_{23}^e T_\infty^{23} h_{23}^e}{2} \begin{Bmatrix} 0 \\ 1 \\ 1 \\ 0 \end{Bmatrix} + \frac{\beta_{34}^e T_\infty^{34} h_{34}^e}{2} \begin{Bmatrix} 0 \\ 0 \\ 1 \\ 1 \end{Bmatrix} + \frac{\beta_{41}^e T_\infty^{41} h_{41}^e}{2} \begin{Bmatrix} 1 \\ 0 \\ 0 \\ 1 \end{Bmatrix} \quad (8.5.10b)$$

Similar expressions hold for a quadratic rectangular element.

Axisymmetric Systems

For symmetric heat transfer about the z axis (i.e., independent of the circumferential coordinate), the governing equation is given by

$$-\left[\frac{1}{r} \frac{\partial}{\partial r} \left(r k_r \frac{\partial T}{\partial r} \right) + \frac{\partial}{\partial z} \left(k_z \frac{\partial T}{\partial z} \right) \right] = f(r, z) \quad (8.5.11)$$

where r is the radial coordinate and z is the axial coordinate. We define the flux vector (i.e., negative of heat flux) by

$$\mathbf{q} = \left(k_r \frac{\partial T}{\partial r} \hat{\mathbf{i}} + k_z \frac{\partial T}{\partial z} \hat{\mathbf{j}} \right)$$

and its normal component across the surface is

$$q_n = \left(k_r \frac{\partial T}{\partial r} n_r + k_z \frac{\partial T}{\partial z} n_z \right) \quad (8.5.12)$$

where n_r and n_z are the direction cosines of the unit normal $\hat{\mathbf{n}}$

$$\hat{\mathbf{n}} = n_r \hat{\mathbf{i}} + n_z \hat{\mathbf{j}}$$

The weak form of (8.5.11) is given by

$$\begin{aligned} 0 &= 2\pi \int_{\Omega_e} w \left\{ -\left[\frac{1}{r} \frac{\partial}{\partial r} \left(k_r r \frac{\partial T}{\partial r} \right) + \frac{\partial}{\partial z} \left(k_z \frac{\partial T}{\partial z} \right) \right] - f \right\} r dr dz \\ &= 2\pi \int_{\Omega_e} \left(k_r \frac{\partial w}{\partial r} \frac{\partial T}{\partial r} + k_z \frac{\partial w}{\partial z} \frac{\partial T}{\partial z} - wf \right) r dr dz - 2\pi \oint_{\Gamma_e} w q_n ds \end{aligned} \quad (8.5.13a)$$

where 2π is due to the integration with respect to the circumferential coordinate over $(0, 2\pi)$, and q_n is given by (8.5.12). The convection boundary condition is of the form

$$q_n + \beta(T - T_\infty) = \hat{q}_n \quad (8.5.13b)$$

Substituting for $q_n = -\beta(T - T_\infty) + \hat{q}_n$ into (8.5.13a), we obtain

$$\begin{aligned} 0 &= 2\pi \int_{\Omega_e} \left(k_r \frac{\partial w}{\partial r} \frac{\partial T}{\partial r} + k_z \frac{\partial w}{\partial z} \frac{\partial T}{\partial z} - wf \right) r dr dz \\ &\quad - 2\pi \oint_{\Gamma_e} w [-\beta(T - T_\infty) + \hat{q}_n] ds \end{aligned} \quad (8.5.14)$$

The finite element model of (8.5.11) with convective boundary condition (8.5.13b) is

$$[K^e + H^e]\{T^e\} = \{f^e\} + \{P^e\} + \{Q^e\} \quad (8.5.15a)$$

where

$$\begin{aligned} K_{ij}^e &= 2\pi \int_{\Omega_e} \left(k_r \frac{\partial \psi_i^e}{\partial r} \frac{\partial \psi_j^e}{\partial r} + k_z \frac{\partial \psi_i^e}{\partial z} \frac{\partial \psi_j^e}{\partial z} \right) r dr dz \\ H_{ij}^e &= 2\pi \oint_{\Gamma_e} \beta^e \psi_i^e \psi_j^e ds, \quad f_i^e = 2\pi \int_{\Omega_e} \psi_i^e f(r) r dr dz \quad (8.5.15b) \\ Q_i^e &= 2\pi \oint_{\Gamma_e} \hat{q}_n \psi_i^e ds, \quad P_i^e = 2\pi \oint_{\Gamma_e} \beta^e T_\infty^e \psi_i^e ds \end{aligned}$$

Evaluation of the integrals in $[K^e]$, $[H^e]$, $\{F^e\}$, and $\{P^e\}$ follows from the discussion of Section 8.2.6.

Clearly, the finite element models in (8.5.6a) and (8.5.15a) are valid for Newton's type (i.e., convective heat transfer) boundary conditions. Radiative heat transfer boundary conditions are nonlinear and therefore are not considered here. For problems with no convective boundary conditions, the convective contributions $[H^e]$ and $\{P^e\}$ to the element coefficients are omitted. In addition, the convective heat transfer contributions have to be included only for those elements whose sides fall on the problem boundary with convection heat transfer specified. For example, if side 2–3 of a linear triangular element Ω_e is on the boundary with convection boundary conditions, then the only contribution to $[H^e]$ and $\{P^e\}$ comes from the second integral of respective expressions in (8.5.7).

Example 8.5.1

Consider steady-state heat conduction in an isotropic rectangular region of dimensions $3a \times 2a$ [see Fig. 8.5.2(a)]. The origin of the x and y coordinates is taken at the lower left corner such that x is parallel to the side $3a$ and y is parallel to side $2a$. The boundaries $x = 0$ and $y = 0$ are insulated, the boundary $x = 3a$ is maintained at zero temperature, and the boundary $y = 2a$ is maintained at a temperature $T = T_0 \cos(\pi x/6a)$. We wish to determine the temperature distribution using the finite element method in the region and the heat required at boundary $x = 3a$ to maintain it at zero temperature.

To analyze the problem, first we note that the problem is governed by (8.5.2) with zero internal heat generation, $f = 0$, and no convection boundary conditions:

$$-k \nabla^2 T = 0 \quad (8.5.16)$$

Hence, the finite element model of the problem is given by

$$[K^e]\{T^e\} = \{Q^e\}$$

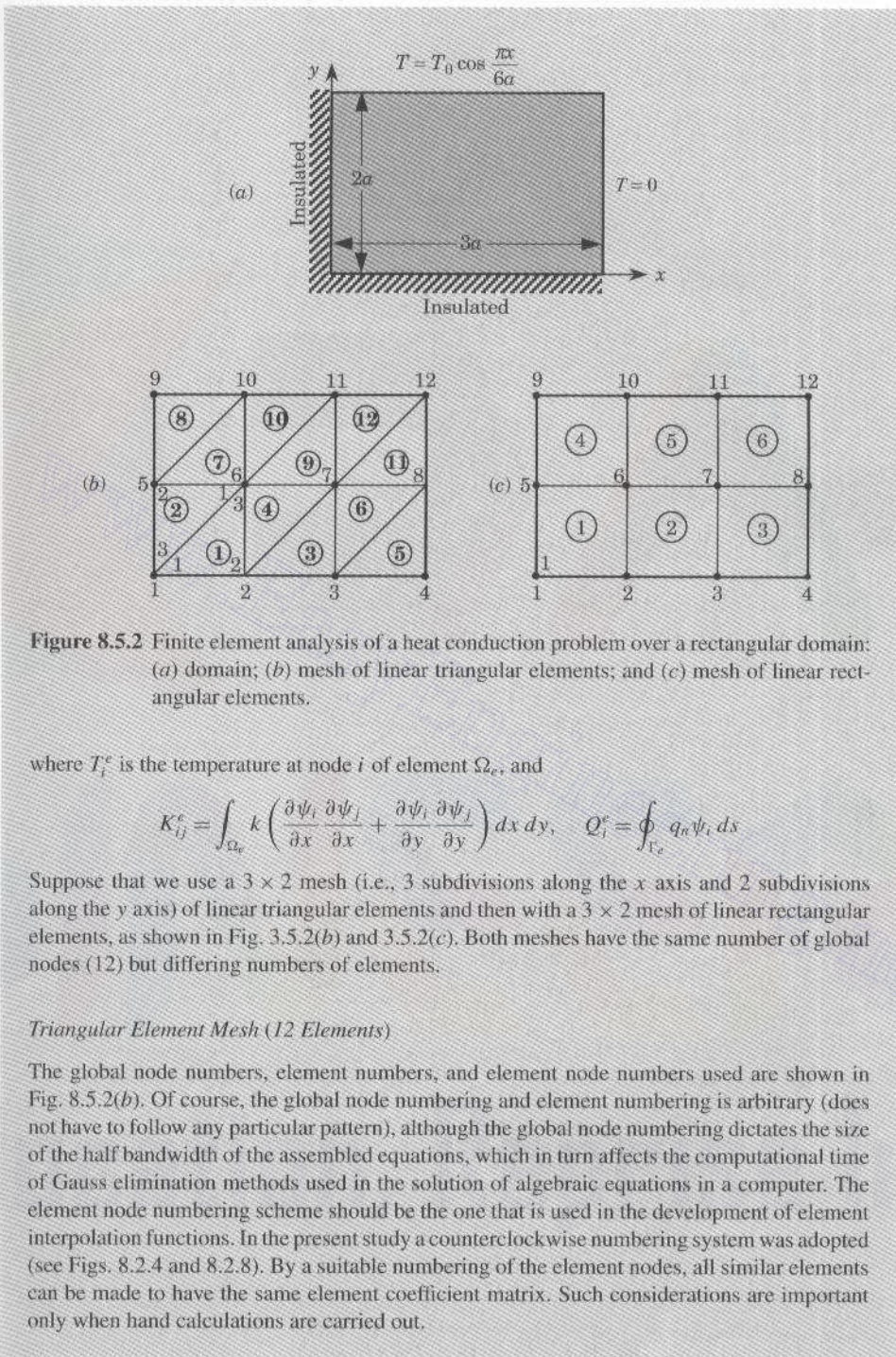


Figure 8.5.2 Finite element analysis of a heat conduction problem over a rectangular domain: (a) domain; (b) mesh of linear triangular elements; and (c) mesh of linear rectangular elements.

where T_i^e is the temperature at node i of element Ω_e , and

$$K_{ij}^e = \int_{\Omega_e} k \left(\frac{\partial \psi_i}{\partial x} \frac{\partial \psi_j}{\partial x} + \frac{\partial \psi_i}{\partial y} \frac{\partial \psi_j}{\partial y} \right) dx dy, \quad Q_i^e = \oint_{\Gamma_e} q_n \psi_i ds$$

Suppose that we use a 3×2 mesh (i.e., 3 subdivisions along the x axis and 2 subdivisions along the y axis) of linear triangular elements and then with a 3×2 mesh of linear rectangular elements, as shown in Fig. 3.5.2(b) and 3.5.2(c). Both meshes have the same number of global nodes (12) but differing numbers of elements.

Triangular Element Mesh (12 Elements)

The global node numbers, element numbers, and element node numbers used are shown in Fig. 8.5.2(b). Of course, the global node numbering and element numbering is arbitrary (does not have to follow any particular pattern), although the global node numbering dictates the size of the half bandwidth of the assembled equations, which in turn affects the computational time of Gauss elimination methods used in the solution of algebraic equations in a computer. The element node numbering scheme should be the one that is used in the development of element interpolation functions. In the present study a counterclockwise numbering system was adopted (see Figs. 8.2.4 and 8.2.8). By a suitable numbering of the element nodes, all similar elements can be made to have the same element coefficient matrix. Such considerations are important only when hand calculations are carried out.

For a typical element of the mesh of triangles in Fig. 8.5.2(b), the element coefficient matrix is given by [see Eqs. (8.3.4) and (8.3.5)],

$$[K^e] = \frac{k}{2} \begin{bmatrix} 1 & -1 & 0 \\ -1 & 2 & -1 \\ 0 & -1 & 1 \end{bmatrix} \quad (8.5.17)$$

where k is the conductivity of the medium. Note that the element matrix is independent of the size of the element, as long as the element is a right-angle triangle with its base equal to its height.

The assembly of the elements (in a computer) follows the logic discussed earlier. For example, we have

$$K_{11} = K_{11}^1 + K_{31}^2 = \frac{k}{2}(1+1), \quad K_{12} = K_{12}^1 = \frac{k}{2}(-1), \quad K_{13} = 0$$

$$K_{15} = K_{32}^2 = \frac{k}{2}(-1), \quad K_{16} = K_{13}^1 + K_{31}^2 = 0+0, \quad \text{etc.}$$

$$F_1 = Q_1^1 + Q_3^2, \quad F_6 = Q_3^1 + Q_1^2 + Q_2^4 + Q_2^7 + Q_1^9 + Q_3^{10}, \quad \text{etc.}$$

The boundary conditions require that (U_i denotes the temperature at global node i)

$$U_4 = U_8 = U_{12} = 0, \quad U_9 = T_0, \quad U_{10} = \frac{\sqrt{3}}{2}T_0, \quad U_{11} = \frac{T_0}{2} \quad (8.5.18)$$

$F_1 = F_2 = F_3 = F_5 = 0$ (zero heat flow due to insulated boundary)

and the balance of internal heat flow requires that

$$F_6 = F_7 = 0 \quad (8.5.19)$$

Thus, the unknown primary variables and secondary variables of the problem are:

$$\begin{array}{ccccccc} U_1, & U_2, & U_3, & U_5, & U_6, & U_7 \\ F_4, & F_8, & F_9, & F_{10}, & F_{11}, & F_{12} \end{array}$$

We first write the six finite element equations for the six unknown primary variables. These equations come from rows 1, 2, 3, 5, 6, and 7 (corresponding to the same global nodes):

$$\begin{aligned} K_{11}U_1 + K_{12}U_2 + \cdots + K_{1(12)}U_{12} &= F_1 = (Q_1^1 + Q_3^2) = 0 \\ K_{21}U_1 + K_{22}U_2 + \cdots + K_{2(12)}U_{12} &= F_2 = (Q_2^1 + Q_1^3 + Q_3^4) = 0 \\ &\vdots \\ K_{71}U_1 + K_{72}U_2 + \cdots + K_{7(12)}U_{12} &= F_7 = (Q_3^3 + Q_1^4 + Q_2^6 + Q_2^9 + Q_1^{11} + Q_3^{12}) = 0 \end{aligned} \quad (8.5.20)$$

Using the boundary conditions and the values of K_{IJ} , we obtain

$$\begin{aligned} k\left(U_1 - \frac{1}{2}U_2 - \frac{1}{2}U_5\right) &= 0 \\ k\left(-\frac{1}{2}U_1 + 2U_2 - \frac{1}{2}U_3 - U_6\right) &= 0 \\ k\left(-\frac{1}{2}U_3 + 2U_4 - U_7\right) &= 0 \\ k\left(-\frac{1}{2}U_1 + 2U_5 - U_6 - \frac{1}{2}U_9\right) &= 0 \quad (U_9 = T_0) \\ k(-U_2 - U_5 + 4U_6 - U_7 - U_{10}) &= 0 \quad \left(U_{10} = \frac{\sqrt{3}}{2}T_0\right) \\ k(-U_3 - U_6 + 4U_7 - U_{11}) &= 0 \quad \left(U_{11} = \frac{1}{2}T_0\right) \end{aligned}$$

In matrix form we have

$$k \begin{bmatrix} 2 & -1 & 0 & -1 & 0 & 0 \\ -1 & 4 & -1 & 0 & -2 & 0 \\ 0 & -1 & 4 & 0 & 0 & -2 \\ -1 & 0 & 0 & 4 & -2 & 0 \\ 0 & -2 & 0 & -2 & 8 & -2 \\ 0 & 0 & -2 & 0 & -2 & 8 \end{bmatrix} \begin{bmatrix} U_1 \\ U_2 \\ U_3 \\ U_5 \\ U_6 \\ U_7 \end{bmatrix} = \frac{k}{2} \begin{bmatrix} 0 \\ 0 \\ 0 \\ T_0 \\ \sqrt{3}T_0 \\ T_0 \end{bmatrix} \quad (8.5.21)$$

The solution of these equations is (in $^{\circ}\text{C}$)

$$\begin{aligned} U_1 &= 0.63627T_0, & U_2 &= 0.5510T_0, & U_3 &= 0.3181T_0 \\ U_5 &= 0.7214T_0, & U_6 &= 0.6248T_0, & U_7 &= 0.3607T_0 \end{aligned} \quad (8.5.22)$$

The exact solution of (8.5.16) for the boundary conditions shown in Fig. 8.5.2(a) is,

$$T(x, y) = T_0 \frac{\cosh(\pi y/6a) \cos(\pi x/6a)}{\cosh(\pi/3)} \quad (8.5.23)$$

Evaluating the exact solution at the nodes, we have (in $^{\circ}\text{C}$)

$$\begin{aligned} T_1 &= 0.6249T_0, & T_2 &= 0.5412T_0, & T_3 &= 0.3124T_0 \\ T_5 &= 0.7125T_0, & T_6 &= 0.6171T_0, & T_7 &= 0.3563T_0 \end{aligned} \quad (8.5.24)$$

The heat at node 4, for example, can be computed from the fourth finite element equation

$$\begin{aligned} F_4 = Q_2^5 &= K_{41}U_1 + K_{42}U_2 + K_{43}U_3 + K_{44}U_4 + K_{45}U_5 \\ &\quad + K_{46}U_6 + K_{47}U_7 + K_{48}U_8 + \dots \end{aligned} \quad (8.5.25)$$

Noting that $K_{41} = K_{42} = K_{45} = \dots = K_{4(12)} = 0$ and $U_4 = U_8 = 0$, we obtain

$$Q_2^5 = -\frac{1}{2}kU_3 = -0.1591kT_0 \text{ (in W)} \quad (8.5.26)$$

Rectangular Element Mesh (6 Elements)

For a 3×2 mesh of linear rectangular elements [see Fig. 8.5.2(c)], the element coefficient matrix is given by (8.2.55)

$$[K^e] = \frac{k}{6} \begin{bmatrix} 4 & -1 & -2 & -1 \\ -1 & 4 & -1 & -2 \\ -2 & -1 & 4 & -1 \\ -1 & -2 & -1 & 4 \end{bmatrix}, \quad \{f^e\} = \{0\} \quad (8.5.27)$$

The present mesh of rectangular elements is nodewise equivalent to the triangular element mesh considered in Fig. 8.5.2(b). Hence the boundary conditions in (8.5.18) and (8.5.19) are valid for the present case. The six finite element equations for the unknowns U_1, U_2, U_3, U_4, U_5 , and U_6 again have the same form as those in (8.5.20), with

$$\begin{aligned} K_{11} &= K_{11}^1, & K_{12} &= K_{12}^1, & K_{15} &= K_{14}^1 \\ K_{16} &= K_{13}^1, & K_{22} &= K_{22}^1 + K_{11}^2, & K_{23} &= K_{12}^2, & K_{25} &= K_{24}^1 \\ K_{26} &= K_{23}^1 + K_{14}^2, & K_{27} &= K_{13}^2, & \text{etc.} \\ F_1 &= Q_1^1, & F_2 &= Q_2^1 + Q_1^2, & F_3 &= Q_2^2 + Q_1^3, & F_4 &= Q_2^3, & \text{etc.} \end{aligned}$$

The equations for the unknown temperatures (i.e., condensed equations for the unknown primary variables) are

$$\frac{k}{6} \begin{bmatrix} 4 & -1 & 0 & -1 & -2 & 0 \\ -1 & 8 & -1 & -2 & -2 & -2 \\ 0 & -1 & 8 & 0 & -2 & -2 \\ -1 & -2 & 0 & 8 & -2 & 0 \\ -2 & -2 & -2 & -2 & 16 & -2 \\ 0 & -2 & -2 & 0 & -2 & 16 \end{bmatrix} \begin{Bmatrix} U_1 \\ U_2 \\ U_3 \\ U_5 \\ U_6 \\ U_7 \end{Bmatrix} = \frac{k}{6} \begin{Bmatrix} 0 \\ 0 \\ 0 \\ T_0 + \sqrt{3}T_0 \\ 2T_0 + \sqrt{3}T_0 + T_0 \\ \sqrt{3}T_0 + T_0 \end{Bmatrix} \quad (8.5.28)$$

Table 8.5.1 Comparison of the nodal temperatures $T(x, y)/T_0$, obtained using various finite element meshes¹ with the analytical solution (Example 8.5.1).

x	y	Triangles		Rectangles		Analytical solution
		3×2	6×4	3×2	6×4	
0.0	0.0	0.6362	0.6278	0.6128	0.6219	0.6249
0.5	0.0	—	0.6064	—	0.6007	0.6036
1.0	0.0	0.5510	0.5437	0.5307	0.5386	0.5412
1.5	0.0	—	0.4439	—	0.4398	0.4419
2.0	0.0	0.3181	0.3139	0.3064	0.3110	0.3124
2.5	0.0	—	0.1625	—	0.1610	0.1617
0.0	1.0	0.7214	0.7148	0.7030	0.7102	0.7125
0.5	1.0	—	0.6904	—	0.6860	0.6882
1.0	1.0	0.6248	0.6190	0.6088	0.6150	0.6171
1.5	1.0	—	0.5054	—	0.5022	0.5038
2.0	1.0	0.3607	0.3574	0.3515	0.3551	0.3563
2.5	1.0	—	0.1850	—	0.1838	0.1844

¹See Fig. 8.5.2 for the geometry and meshes.

The solution of these equations is (in $^{\circ}\text{C}$)

$$\begin{aligned} U_1 &= 0.6128T_0, & U_2 &= 0.5307T_0, & U_3 &= 0.3064T_0 \\ U_5 &= 0.7030T_0, & U_6 &= 0.6088T_0, & U_7 &= 0.3515T_0 \end{aligned} \quad (8.5.29)$$

The value of the heat at node 4 is given by

$$Q_2^3 = K_{43}U_3 + K_{47}U_7 = -\frac{k}{6}U_3 - \frac{2k}{6}U_7 = -0.1682kT_0 \text{ (in W)} \quad (8.5.30)$$

We note that the results obtained using the 3×2 mesh of rectangular elements is not as accurate as that obtained with the 3×2 mesh of triangular elements. This is due to the fact that there are only half as many elements in the former case when compared to the latter. Table 8.5.1 contains a comparison of the finite element solutions with the analytical solution (8.5.23) for two different meshes of linear triangular and rectangular elements.

Example 8.5.2

Consider heat transfer in a rectangular region of dimensions a by b , subjected to the boundary conditions shown in Fig. 8.5.3. We wish to write the finite element algebraic equations for the unknown nodal temperatures and heats. For illustrative purposes a 4×2 mesh of rectangular elements is chosen. We assume that the medium is orthotropic, with conductivities k_x and k_y in the x and y directions, respectively. No internal heat generation is assumed.

The heat transfer in the region is governed by the energy equation

$$-\frac{\partial}{\partial x} \left(k_x \frac{\partial T}{\partial x} \right) - \frac{\partial}{\partial y} \left(k_y \frac{\partial T}{\partial y} \right) = 0 \text{ in } \Omega$$

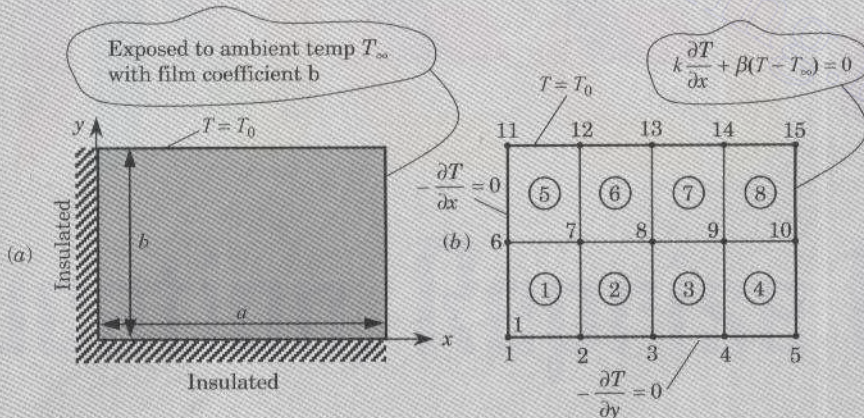


Figure 8.5.3 Domain and boundary conditions for convective heat transfer in a rectangular domain. A mesh of linear rectangular elements is also shown (Example 8.5.2).

The finite element model of the equation is given by

$$[K^e + H^e]\{T^e\} = \{Q^e\} + \{P^e\} \quad (\{f^e\} = \{0\}) \quad (8.5.31)$$

where T_i^e denotes the temperature at node i of element Ω_e , and

$$\begin{aligned} K_{ij}^e &= \int_{\Omega_e} \left(k_x \frac{\partial \psi_i}{\partial x} \frac{\partial \psi_j}{\partial x} + k_y \frac{\partial \psi_i}{\partial y} \frac{\partial \psi_j}{\partial y} \right) dx dy \\ H_{ij}^e &= \oint_{\Gamma_e} \beta^e \psi_i \psi_j ds \\ Q_j^e &= \oint_{\Gamma_e} q_n \psi_i ds, \quad P_i^e = \oint_{\Gamma_e} \beta^e T_\infty^e \psi_i ds \end{aligned} \quad (8.5.32)$$

We note that $[H^e]$ and $\{P^e\}$ must be calculated only for elements 4 and 8, which have convective boundaries.

The element matrices for the problem at hand are given by [see Eq. (8.2.53)]

$$\begin{aligned} [K^e] &= \frac{k_x \mu}{6} \begin{bmatrix} 2 & -2 & -1 & 1 \\ -2 & 2 & 1 & -1 \\ -1 & 1 & 2 & -2 \\ 1 & -1 & -2 & 2 \end{bmatrix} + \frac{k_y}{6\mu} \begin{bmatrix} 2 & 1 & -1 & -2 \\ 1 & 2 & -2 & -1 \\ -1 & -2 & 2 & 1 \\ -2 & -1 & 1 & 2 \end{bmatrix} \quad (e = 1, 2, \dots, 8) \\ [H^e] &= \frac{\beta_{23}^e h_{23}^e}{6} \begin{bmatrix} 0 & 0 & 0 & 0 \\ 0 & 2 & 1 & 0 \\ 0 & 1 & 2 & 0 \\ 0 & 0 & 0 & 0 \end{bmatrix}, \quad \{P^e\} = \frac{\beta_{23}^e T_\infty^{23} h_{23}^e}{2} \begin{Bmatrix} 0 \\ 1 \\ 1 \\ 0 \end{Bmatrix} \quad (\text{for } e = 4, 8) \end{aligned}$$

where μ is the aspect ratio

$$\mu = \frac{1}{2} b \sqrt{\frac{1}{4} a^2} = 2b/a$$

There are ten nodal temperatures that are to be determined, and heats at all nodes except nodes 1, 2, 3, 4 and 6 are to be computed. To illustrate the procedure, we write algebraic equations for only representative temperatures and heats.

Node 1 (for Temperatures)

$$K_{11}^1 U_1 + K_{12}^1 U_2 + K_{14}^1 U_6 + K_{13}^1 U_7 = Q_1^1 = 0$$

Node 2 (for Temperatures)

$$K_{21}^1 U_1 + (K_{22}^1 + K_{11}^2) U_2 + K_{12}^2 U_3 + K_{24}^1 U_6 + (K_{23}^1 + K_{14}^2) U_7 + K_{13}^2 U_8 = Q_2^1 + Q_1^2 = 0$$

Node 5 (for Temperatures)

$$K_{21}^4 U_4 + (K_{22}^4 + H_{22}^4) U_5 + K_{24}^4 U_9 + (K_{23}^4 + H_{23}^4) U_{10} = Q_2^4 + P_2^4 = P_2^4 \quad (\text{known})$$

Node 10 (for Temperatures)

$$K_{31}^4 U_4 + (K_{32}^4 + H_{32}^4) U_5 + (K_{34}^4 + K_{21}^8) U_9 + (K_{33}^4 + H_{33}^4 + K_{22}^8 + H_{22}^8) U_{10} + K_{24}^8 U_{14} \\ + (K_{23}^8 + H_{23}^8) U_{15} = (Q_3^4 + P_3^4) + (Q_2^8 + P_2^8) = P_3^4 + P_2^8 \text{ (known)}$$

Node 14 (for Heat Q_{14})

$$Q_{14} = Q_3^7 + Q_4^8 = K_{31}^7 U_8 + (K_{32}^7 + K_{41}^8) U_9 + K_{42}^8 U_{10} + K_{34}^7 U_{13} + (K_{33}^7 + K_{44}^8) U_{14} + K_{43}^8 U_{15}$$

From the boundary conditions, we know temperatures at nodes 11 through 15 (i.e., $U_{11}, U_{12}, \dots, U_{15}$ are known values). Substituting the values of K_{ij}^e , H_{ij}^e , and P_i^e , we obtain explicit form of the algebraic equations. For example, the algebraic equation corresponding to node 10 is

$$-\frac{1}{6} \left(k_x \mu + \frac{k_y}{\mu} \right) U_4 + \left[\frac{1}{6} \left(k_x \mu - \frac{2k_y}{\mu} \right) + \frac{1}{12} \beta b \right] U_5 \\ + \frac{1}{6} \left[\left(-2k_x \mu + \frac{2k_y}{\mu} \right) + \left(-2k_x \mu + \frac{k_y}{\mu} \right) \right] U_9 + \frac{2}{3} \left[\left(k_x \mu + \frac{k_y}{\mu} \right) + \frac{\beta b}{2} \right] U_{10} \\ + \frac{1}{6} \left(k_x \mu - \frac{2k_y}{\mu} \right) U_{14} + \frac{1}{6} \left[k_x \mu - \frac{2k_y}{\mu} + \frac{\beta b}{2} \right] U_{15} = \frac{1}{2} \beta b T_\infty$$

This completes the example.

Example 8.5.3

Consider heat transfer in a homogeneous, isotropic medium. The governing equation, in nondimensional form, is given by

$$-\nabla^2 u = f_0 \text{ in } \Omega$$

over the domain shown in Fig. 8.5.4.

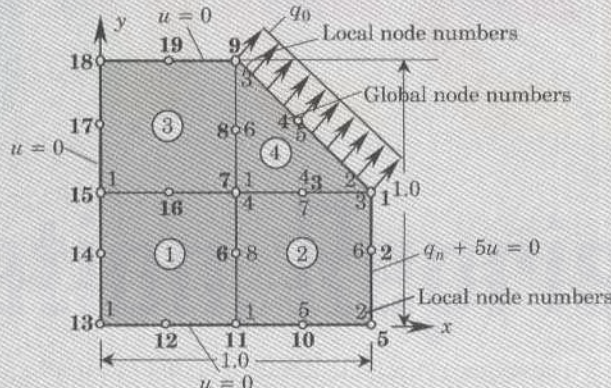


Figure 8.5.4 Domain with finite element mesh and boundary conditions for a heat transfer problem discussed in Example 8.5.3.

We wish to

- write the finite element equation associated with global node 1 in terms of element coefficients,
- compute the contribution of the flux q_0 to global nodes 1 and 4, and
- compute the contribution of the boundary condition $q_n + 5u = 0$ to the finite element equations.
- The finite element equation associated with global node 1 is

$$K_{11}U_1 + K_{12}U_2 + K_{13}U_3 + K_{14}U_4 + K_{16}U_6 + K_{17}U_7 + K_{18}U_8 = F_1$$

Writing the global coefficients in terms of the element coefficients, we obtain

$$\begin{aligned} & (K_{33}^{(2)} + K_{22}^{(4)} + H_{33}^{(2)} + H_{22}^{(4)})U_1 + (K_{36}^{(2)} + H_{36}^{(2)})U_2 + (K_{37}^{(2)} + K_{24}^{(4)})U_3 \\ & + K_{25}^{(4)}U_4 + K_{38}^{(2)}U_6 + (K_{34}^{(2)} + K_{21}^{(4)})U_7 + K_{26}^{(4)}U_8 = F_3^{(2)} + P_3^{(2)} + F_2^{(4)} \end{aligned}$$

Explicit form of H_{ij}^e ($P_i^e = 0$ because $u_\infty = 0$) will be given in Part (c).

- The contributions of uniform flux q_0 to global nodes 1, 4, and 9 are readily known from one-dimensional quadratic element [see Eq. (3.2.37b)]. It can be calculated as follows:

$$\begin{aligned} Q_2^4 &= \int_0^L q_0 \psi_2^4(s) ds = q_0 \int_0^L \left(1 - \frac{s}{L}\right) \left(1 - \frac{2s}{L}\right) ds \\ &= q_0 \int_0^L \left(1 - 3\frac{s}{L} + \frac{2s^2}{L^2}\right) ds = q_0 \left(L - 3\frac{L}{2} + \frac{2L}{3}\right) = \frac{q_0 L}{6} = Q_3^4 \end{aligned}$$

where $L = 1/\sqrt{2} = 0.7071$. Similarly, contribution to global node 4 is

$$\begin{aligned} Q_5^4 &= \int_0^L q_0 \psi_5^4(s) ds = q_0 \int_0^L 4\frac{s}{L} \left(1 - \frac{s}{L}\right) ds \\ &= 4q_0 \int_0^L \left(\frac{s}{L} - \frac{s^2}{L^2}\right) ds = 4q_0 \left(\frac{L}{2} - \frac{L}{3}\right) = \frac{4q_0 L}{6} \end{aligned}$$

- The contribution of the boundary condition $q_n + 5u = 0$ to the finite element equation associated with node 1 is

$$\begin{aligned} Q_3^2 &= \int_0^{0.5} q_n \psi_3^{(2)}(s) ds = -5 \int_0^{0.5} (u_2^{(2)} \psi_2^{(2)} + u_6^{(2)} \psi_6^{(2)} + u_3^{(2)} \psi_3^{(2)}) \psi_3^{(2)} ds \\ &= -5 \left(\frac{0.5}{30}\right) (4 \times U_1 + 2 \times U_2 - 1 \times U_5) = -\frac{1}{3}U_1 - \frac{1}{6}U_2 \end{aligned}$$

8.5.2 Fluid Mechanics

Here, we consider the equations governing potential flows of an ideal fluid. An *ideal fluid* is one that has zero viscosity and is incompressible. A fluid is said to be *incompressible* if the volume change is zero, (i.e., ρ is constant)

$$\nabla \cdot \mathbf{v} = 0 \quad (8.5.33)$$

where \mathbf{v} is the velocity vector. A fluid is termed *inviscid* if the viscosity is zero, $\mu = 0$. A flow with negligible angular velocity is called *irrotational* if

$$\nabla \times \mathbf{v} = 0 \quad (8.5.34)$$

The irrotational flow of an ideal fluid (i.e., $\rho = \text{constant}$ and $\mu = 0$) is called a *potential flow*.

For an ideal fluid, the continuity and the momentum equations can be written as [see Schlichting (1969)]

$$\nabla \cdot \mathbf{v} = 0 \quad (8.5.35a)$$

$$\frac{1}{2}\rho \nabla(\mathbf{v} \cdot \mathbf{v}) - \rho[\mathbf{v} \times (\nabla \times \mathbf{v})] = -\nabla \hat{P} \quad (8.5.35b)$$

where $\nabla \hat{P} = \nabla P - \mathbf{f}$. For irrotational flow the velocity field \mathbf{v} satisfies (8.5.34). For two-dimensional irrotational flows, these equations have the form

$$\frac{\partial v_x}{\partial x} + \frac{\partial v_y}{\partial y} = 0 \quad (8.5.35c)$$

$$\frac{1}{2}\rho(v_x^2 + v_y^2) + \hat{P} = \text{constant} \quad (8.5.35d)$$

$$\frac{\partial v_x}{\partial y} - \frac{\partial v_y}{\partial x} = 0 \quad (8.5.35e)$$

These three equations are used to determine v_x , v_y , and \hat{P} .

The problem of determining v_x , v_y , and \hat{P} is simplified by introducing a function $\psi(x, y)$ such that the continuity equation is identically satisfied:

$$v_x = \frac{\partial \psi}{\partial y}, \quad v_y = -\frac{\partial \psi}{\partial x} \quad (8.5.36)$$

Then the irrotational flow condition in terms of ψ takes the form,

$$\frac{\partial^2 \psi}{\partial y^2} + \frac{\partial^2 \psi}{\partial x^2} \equiv \nabla^2 \psi = 0 \quad (8.5.37)$$

Equation (8.5.37) is used to determine ψ ; then velocities v_x and v_y are determined from (8.5.36) and \hat{P} from (8.5.35d). The function ψ has the physical significance that lines of constant ψ are lines across which there is no flow, i.e., they are streamlines of the flow. Hence, $\psi(x, y)$ is called the *stream function*.

In the cylindrical coordinates, the continuity equation (8.5.35a) takes the form

$$\frac{\partial v_r}{\partial r} + \frac{1}{r} \frac{\partial v_\theta}{\partial \theta} = 0 \quad (8.5.38)$$

where v_r and v_θ are the radial and circumferential velocity components. The stream function $\psi(r, \theta)$ is defined as

$$v_r = \frac{1}{r} \frac{\partial \psi}{\partial \theta}, \quad v_\theta = -\frac{\partial \psi}{\partial r} \quad (8.5.39)$$

and (8.5.37) takes the form

$$\nabla^2 \psi \equiv \frac{\partial^2 \psi}{\partial r^2} + \frac{1}{r} \frac{\partial \psi}{\partial r} + \frac{1}{r^2} \frac{\partial^2 \psi}{\partial \theta^2} = 0 \quad (8.5.40)$$

There exists an alternative formulation of the potential flow equations (8.5.35a) and (8.5.35b). We can introduce a function $\phi(x, y)$, called the *velocity potential*, such that the condition of irrotational flow, Eq. (8.5.35e) is identically satisfied:

$$v_x = -\frac{\partial \phi}{\partial x}, \quad v_y = -\frac{\partial \phi}{\partial y} \quad (8.5.41)$$

Then the continuity equation (8.5.35c) takes the form,

$$-\nabla^2 \phi = 0 \quad (8.5.42)$$

Comparing (8.5.39) with (8.5.41), we note that

$$-\frac{\partial \phi}{\partial x} = \frac{\partial \psi}{\partial y}, \quad -\frac{\partial \phi}{\partial y} = -\frac{\partial \psi}{\partial x} \quad (8.5.43)$$

The velocity potential has the physical significance that lines of constant ϕ are lines along which there is no change in velocity. The equipotential lines and streamlines intersect at right angles.

Although both ψ and ϕ are governed by the Laplace equation, the boundary conditions on them are different in a flow problem, as should be evident by the definitions (8.5.39) and (8.5.41). In this section, we consider applications of the finite element method to potential flows, i.e., the solution of (8.5.36) and (8.5.43).

We consider two examples of fluid flow. The first one deals with a groundwater flow problem and the second with the flow around a cylindrical body. In discussing these problems, emphasis is placed on certain modeling aspects, data generation, and postprocessing of solutions. Evaluation of element matrices and assembly are amply illustrated in previous examples and will not be discussed as it takes substantial space to write the assembled equations even for the crude meshes used in these examples.

Example 8.5.4 (Groundwater Flow or Seepage)

The governing differential equation for a homogeneous (i.e., material properties do not vary with position) aquifer of unit depth, with flow in the xy plane, is given by

$$-\frac{\partial}{\partial x} \left(a_{11} \frac{\partial \phi}{\partial x} \right) - \frac{\partial}{\partial y} \left(a_{22} \frac{\partial \phi}{\partial y} \right) = f \text{ in } \Omega \quad (8.5.44)$$

where a_{11} and a_{22} are the coefficients of permeability (in $\text{m}^3/\text{day}/\text{m}^2$) along the x and y directions, respectively, ϕ is the piezometric head or velocity potential (in m), measured from a reference level (usually the bottom of the aquifer), and f is the rate of pumping (in $\text{m}^3/\text{day}/\text{m}^3$). We know from the previous discussions that the natural and essential boundary conditions associated with (8.5.44) are as follows:

Natural

$$a_{11} \frac{\partial \phi}{\partial x} n_x + a_{22} \frac{\partial \phi}{\partial y} n_y = \phi_n \quad \text{on } \Gamma_2 \quad (8.5.45)$$

Essential

$$\phi = \phi_0 \quad \text{on } \Gamma_1 \quad (8.5.46)$$

where Γ_1 and Γ_2 are the portions of the boundary Γ of Ω such that $\Gamma_1 + \Gamma_2 = \Gamma$.

Here we consider the following specific problem: Find the lines of constant potential ϕ (equipotential lines) in a $3000 \text{ m} \times 1500 \text{ m}$ rectangular aquifer Ω (see Fig. 8.5.5) bounded on the long sides by an impermeable material (i.e., $\partial\phi/\partial n = 0$) and on the short sides by a constant head of 200 m ($\phi_0 = 200 \text{ m}$). In the way of sources, suppose that a river is passing through the aquifer, infiltrating the aquifer at a rate of $q_0 = 0.24 \text{ m}^3/\text{day/m}$, and that two pumps are located at (830, 1000) and (600, 1900), pumping at a rate of $Q_1 = 1200 \text{ m}^3/\text{day}$ and $Q_2 = 2400 \text{ m}^3/\text{day}$, respectively.

A mesh of 64 triangular elements and 45 nodes is used to model the domain [see Fig. 8.5.6(a)]. The river forms the interelement boundary between elements (26, 28, 30, 32) and (33, 35, 37, 39). In the mesh selected, neither pump is located at a node. This is done intentionally for the purpose of illustrating the calculation of the generalized forces due to a point source within an element. If the pumps are located at a node, then the rate of pumping Q_0 is input as the specified secondary variable of the node. When a source (or sink) is located at a point other than a node, we must calculate its contribution to the nodes. Similarly, the source components due to the distributed line source (i.e., the river) should be computed.

First, consider the line source. We can view the river as a line source of constant intensity, $q_0 = 0.24 \text{ m}^3/\text{day/m}$. Since the length of the river is equally divided by nodes 21 through 25 (into four parts), we can compute the contribution of the infiltration of the river at each of the nodes 21 through 25 by evaluating the integrals [see Fig. 8.5.6(b)]:

$$\begin{aligned} \text{node 25: } & \int_0^h (0.24)\psi_1^1 \, ds \\ \text{node 24: } & \int_0^h (0.24)\psi_2^1 \, ds + \int_0^h (0.24)\psi_1^2 \, ds \end{aligned}$$

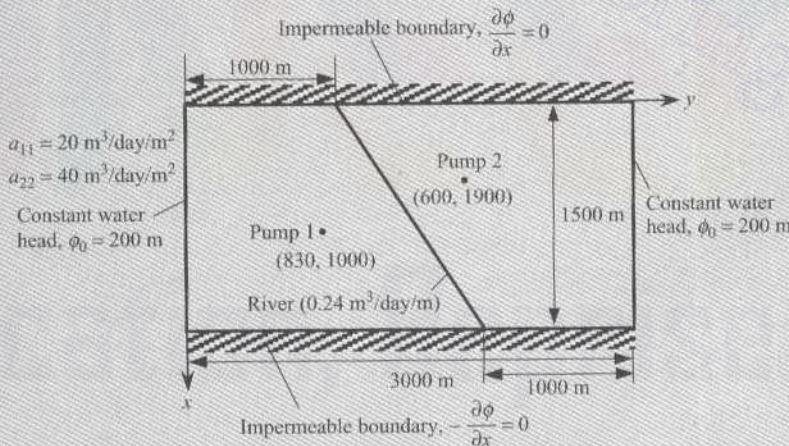


Figure 8.5.5 Geometry and boundary conditions for the groundwater flow problem of Example 8.5.4.

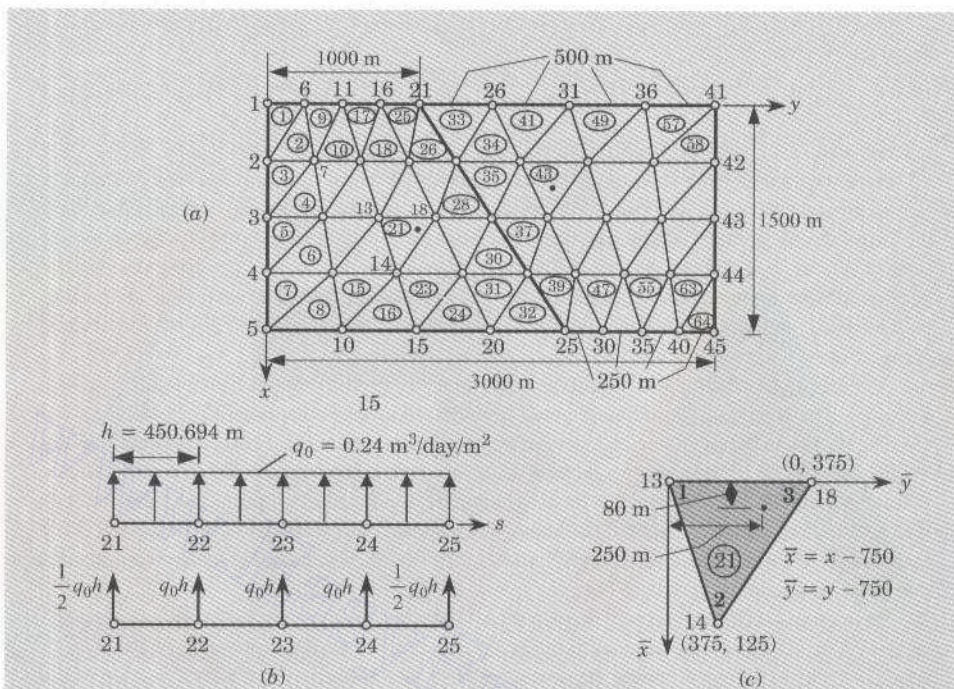


Figure 8.5.6 (a) Finite element mesh of triangular elements (45 nodes and 64 elements), (b) computation of global forces due to the infiltration of the river, and (c) computation of global forces for pump 1 located inside element 21 for the groundwater flow problem of Example 8.5.4.

$$\text{node 23: } \int_0^h (0.24)\psi_2^2 ds + \int_0^h (0.24)\psi_1^3 ds$$

$$\text{node 22: } \int_0^h (0.24)\psi_2^3 ds + \int_0^h (0.24)\psi_1^4 ds$$

$$\text{node 21: } \int_0^h (0.24)\psi_2^4 ds$$

For constant intensity q_0 and the linear interpolation functions $\psi_1^e(s) = 1 - s/h$ and $\psi_2^e(s) = s/h$, the contribution of these integrals is well known:

$$\int_0^h q_0 \psi_i^e ds = \frac{1}{2} q_0 h, \quad h = \frac{1}{4} [(1000)^2 + (1500)^2]^{\frac{1}{2}}, \quad q_0 = 0.24$$

Hence, we have

$$F_{21} = \frac{1}{2} q_0 h, \quad F_{22} = F_{23} = F_{24} = q_0 h, \quad F_{25} = q_0 h \frac{1}{2}$$

Next, we consider the contribution of the point sources. Since the point sources are located inside an element, we distribute the source to the nodes of the element by interpolation [see Fig. 8.5.6(c)]:

$$f_i^e = \int_{\Omega_e} Q_0 \delta(x - x_0, y - y_0) \psi_i^e(x, y) dx dy = Q_0 \psi_i^e(x_0, y_0)$$

For example, the source at pump 1 (located at $x_0 = 830$ m, $y_0 = 1000$ m) can be expressed as (pumping is considered to be a negative point source)

$$Q_1(x, y) = -1200 \delta(x - 830, y - 1000) \text{ or } Q_1(\bar{x}, \bar{y}) = -1200 \delta(\bar{x} - 80, \bar{y} - 250)$$

where $\delta(\cdot)$ is the Dirac delta function [see Eq. (3.3.3)]. The interpolation functions ψ_i^e for element 21 are [in terms of the local coordinates \bar{x} and \bar{y} ; see Fig. 8.5.6(c)]

$$\psi_i(\bar{x}, \bar{y}) = \frac{1}{2A} (\alpha_i + \beta_i \bar{x} + \gamma_i \bar{y}), \quad (i = 1, 2, 3)$$

$$2A = (375)^2, \quad \alpha_1 = (375)^2, \quad \alpha_2 = 0, \quad \alpha_3 = 0$$

$$\beta_1 = -250, \quad \beta_2 = 375, \quad \beta_3 = -125, \quad \gamma_1 = -375, \quad \gamma_2 = 0, \quad \gamma_3 = 375$$

Therefore, we have

$$\psi_1(80, 250) = 0.1911, \quad \psi_2(80, 250) = 0.5956, \quad \psi_3(80, 250) = 0.2133$$

Similar computations can be done for pump 2 (see Problem 8.8).

In summary, primary variables and nonzero secondary variables are:

$$U_1 = U_2 = U_3 = U_4 = U_5 = U_{41} = U_{42} = U_{43} = U_{44} = U_{45} = 200.0$$

$$F_{21} = 54.0833, \quad F_{22} = F_{23} = F_{24} = 108.1666, \quad F_{25} = 54.0833$$

$$F_{13} = -229.33, \quad F_{14} = -256.0, \quad F_{18} = -714.67, \quad F_{27} = -411.429$$

$$F_{28} = -1440.0, \quad F_{32} = -548.571$$

The secondary variables at nodes 6–12, 15–17, 19, 20, 26, 29–31, and 33–40 are zero. This completes the data generation for the problem.

The assembled equations are solved after imposing the specified boundary conditions for the values of ϕ at the nodes. The equipotential lines can be determined using (8.3.27). The lines of constant ϕ are shown in Fig. 8.5.7(a).

The velocity components are determined in the postcomputation using the definition (8.5.41)

$$v_x = -\frac{\partial \phi}{\partial x}, \quad v_y = -\frac{\partial \phi}{\partial y}$$

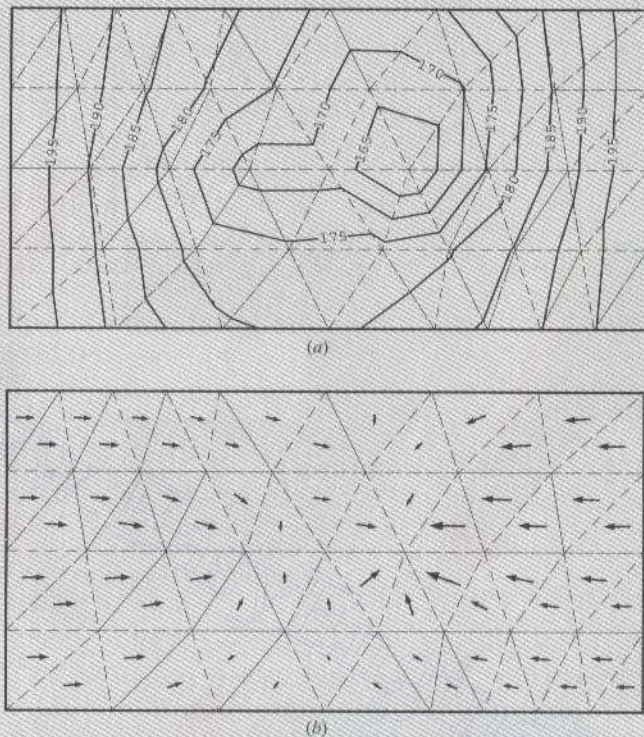


Figure 8.5.7 Plots of constant piezometric head and velocity vector for the groundwater flow:
(a) lines of constant ϕ ; and (b) plot of velocity vectors (Example 8.5.4).

and the velocity vector is given by

$$\mathbf{v} = v_x \hat{\mathbf{i}} + v_y \hat{\mathbf{j}}, \quad |\mathbf{v}| = \sqrt{v_x^2 + v_y^2}, \quad \theta = \tan^{-1} \frac{v_y}{v_x}$$

where θ is the angle, measured in counterclockwise direction, of the velocity vector form along the +ve x axis. The velocity vectors for the problem at hand are shown in Fig. 8.5.7(b). The greatest drawdown of water occurs at node 28, which has the largest portion of discharge from pump 2. This completes the discussion of the groundwater flow problem.

Next, we consider an example of irrotational flows of an ideal fluid (i.e., a nonviscous fluid). Examples of physical problems that can be approximated by such flows are provided by flow around bodies such as weirs, airfoils, buildings, and so on, and by flow of water through the earth and dams. Laplace equations (8.5.37) and (8.5.42) governing these flows are a special case of (8.2.1) and therefore, we can use the finite element equations developed earlier to model these problems.

Example 8.5.5 (Confined Flow around a Circular Cylinder)

The irrotational flow of an ideal fluid about a circular cylinder, placed with its axis perpendicular to the plane of the flow between two *long* horizontal walls (see Fig. 8.5.8) is to be analyzed using the finite element method. The equation governing the flow is given by

$$-\nabla^2 u = 0 \quad \text{in } \Omega$$

where u is either (a) the stream function or (b) the velocity potential. If u is the stream function ψ , the velocity components $\mathbf{v} = (v_x, v_y)$ of the flow field are given by

$$v_x = \frac{\partial \psi}{\partial y}, \quad v_y = -\frac{\partial \psi}{\partial x}$$

If u is the velocity potential, ϕ , the velocity components can be computed from

$$v_x = -\frac{\partial \phi}{\partial x}, \quad v_y = -\frac{\partial \phi}{\partial y}$$

In either case, the velocity field is not affected by a constant term in the solution u . We analyze the problem using both formulations. For both formulations, symmetry exists about the horizontal and vertical center lines, therefore, only a quadrant of the flow region is used as the computational domain. To determine the constant state of the solution, which does not affect the velocity field, we arbitrarily set the functions ψ and ϕ to zero (or a constant) on appropriate boundary lines.

Stream Function Formulation

The boundary conditions on the stream function ψ can be determined as follows. Streamlines have the property that flow perpendicular to a streamline is zero. Therefore, the fixed walls correspond to streamlines. Note that for inviscid flows, fluid does not stick to rigid walls. Due to the biaxial symmetry about the horizontal and vertical centerlines, only a quadrant (say, ABCDE in Fig. 8.5.9) of the domain need be used in the analysis. The fact that the velocity component perpendicular to the horizontal line of symmetry is equal to zero allows us to use that line as a streamline. Since the velocity field depends on the relative difference of two

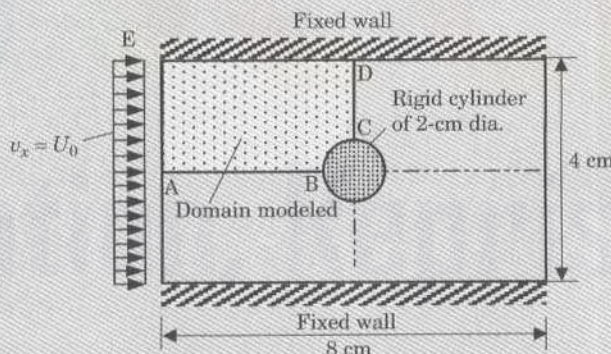


Figure 8.5.8 Domain and boundary conditions for the stream function and velocity potential formulations of irrotational flow about a cylinder (Example 8.5.5).

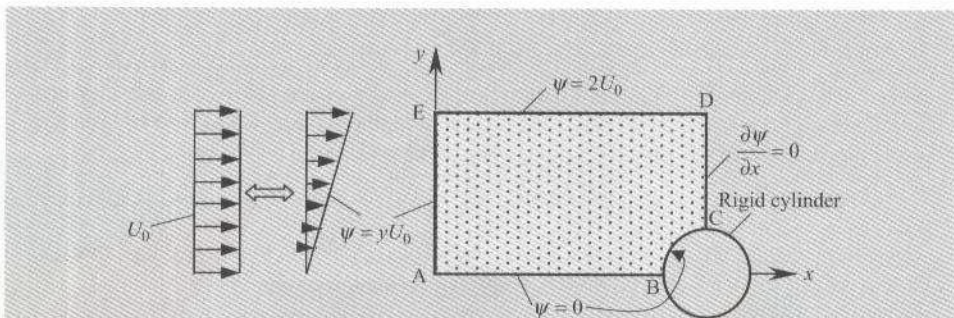


Figure 8.5.9 Computational domain and boundary conditions for the stream function formulation of inviscid flow around a cylinder (see Fig. 8.5.8).

streamlines, we take the value of the stream function that coincides with the horizontal axis of symmetry (i.e., on ABC) to be zero and then determine the value of ψ on the upper wall from the condition

$$\frac{\partial \psi}{\partial y} = U_0$$

where U_0 is the inlet horizontal velocity of the field. We determine the value of the stream function on the boundary $x = 0$ by integrating the above equation with respect to y

$$\int_0^y \frac{d\psi}{dy} dy = \int_0^y U_0 dy + \psi_A = U_0 y + 0 \quad (8.5.47)$$

because $\psi_A = 0$ by the previous discussion. This gives the boundary condition on AE. Since the line ED is a streamline and its value at point E is $2U_0$, it follows that $\psi = 2U_0$ on line ED. Lastly, on CD we assume the vertical velocity is zero (i.e., $v_y = 0$); hence, $\partial\psi/\partial x = 0$ on CD. The boundary conditions are shown on the computational domain in Fig. 8.5.9.

In selecting a mesh, we should note that the velocity field is uniform (i.e., streamlines are horizontal) at the inlet and that it takes a parabolic profile at the exit (along CD). Therefore, the mesh at the inlet should be uniform, and the mesh close to the cylinder should be relatively more refined to be able to model the curved boundary and capture the rapid change in ψ . Two coarse finite element meshes are used to discuss the boundary conditions, and results for refined meshes will be discussed subsequently. Mesh T1 consists of 32 triangular elements and mesh Q1 consists of 16 quadrilateral elements. Both meshes contain 25 nodes (see Fig. 8.5.10). The mesh with solid lines in Fig. 8.5.10 corresponds to mesh Q1, and the mesh with solid and dashed lines in Fig. 8.5.10 correspond to mesh T1. It should be noted that the discretization error is not zero for this case.

The specified primary degrees of freedom (i.e., nodal values of ψ) for mesh T1 and mesh Q1 are:

$$\begin{aligned} U_1 &= U_2 = \dots = U_6 = U_{12} = U_{18} = U_{24} = U_{30} = U_{36} = U_{42} = 0.0 \\ U_7 &= 1.333, \quad U_{13} = 0.667, \quad U_{19} = U_{25} = U_{31} = U_{37} = 2.0 \end{aligned} \quad (8.5.48)$$

There are no nonzero specified secondary variables; the secondary variables are specified to be zero at the nodes on line CD:

$$F_{38} = F_{39} = F_{40} = F_{41} = 0$$

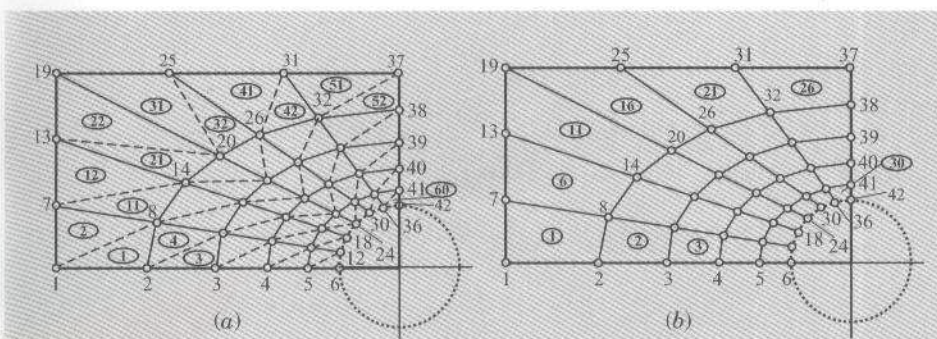


Figure 8.5.10 Meshes used for inviscid flow around a cylinder. (a) Mesh of linear triangles. (b) Mesh of linear quadrilaterals.

Although the secondary variable is specified to be zero at nodes 37 and 42, where the primary variable is also specified, we choose to impose the boundary conditions on the primary variable over the secondary variables.

Velocity Potential Formulation (PF)

The boundary conditions on the velocity potential ϕ can be derived as follows (see Fig. 8.5.11). The fact that $v_y = -\partial\phi/\partial y = 0$ (no penetration) on the upper wall as well as on the horizontal line of symmetry gives the boundary conditions there. Along AE the velocity $v_x = -\partial\phi/\partial x$ is specified to be U_0 . On the surface of the cylinder the normal velocity, $v_n = -\partial\phi/\partial n$, is zero. Thus, all boundary conditions, so far, are of the flux type. On the boundary CD we must know either ϕ or $\partial\phi/\partial n = \partial\phi/\partial x$. It is clear that $-\partial\phi/\partial x = v_x$ is not known on CD. Therefore, we assume that ϕ is known, and we set it equal to $\phi_0 = \text{constant}$. The constant ϕ_0 is arbitrary, and it does not contribute to the velocity field (because $-\partial\phi/\partial x = v_x$ and $-\partial\phi/\partial y = v_y$ are independent of the constant ϕ_0). It should be noted that determining the constant part in the solution for ϕ (i.e., eliminating the rigid body motion) requires knowledge of ϕ at one or more points of the mesh. We take $\phi = \phi_0 = 0$ on CD.

The mathematical boundary conditions of the problem must be translated into finite element data. The boundary conditions on the primary variables come from the boundary CD. We have

$$U_{37} = U_{38} = U_{39} = U_{40} = U_{41} = U_{42} = 0.0$$

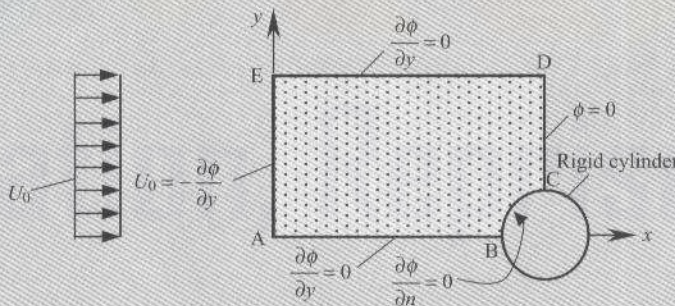


Figure 8.5.11 Computational domain and boundary conditions for the velocity potential formulation of inviscid flow around a cylinder (see Fig. 8.5.8).

The only nonzero boundary conditions on the secondary variables come from the boundary AE. There, we must evaluate the boundary integral

$$\int_{\Gamma_E} \frac{\partial \phi}{\partial n} \psi_i \, ds = U_0 \int_{AE} \psi_i(y) \, dy$$

for each node i on AE. We obtain ($h = 2/3 = 0.66667$)

$$Q_1 = U_0 \int_0^h \left(1 - \frac{\bar{y}}{h}\right) d\bar{y} = 0.33333U_0$$

$$Q_7 = U_0 \int_0^h \frac{\bar{y}}{h} d\bar{y} + U_0 \int_0^h \left(1 - \frac{\bar{y}}{h}\right) d\bar{y} = 0.66667U_0$$

$$Q_{13} = U_0 \int_0^h \frac{\bar{y}}{h} d\bar{y} + U_0 \int_0^h \left(1 - \frac{\bar{y}}{h}\right) d\bar{y} = 0.66667U_0$$

$$Q_{19} = U_0 \int_0^h \frac{\bar{y}}{h} d\bar{y} = \frac{hU_0}{2} = 0.33333U_0$$

Numerical Results

Table 8.5.2 contains the values of the stream function and its derivative ($\partial \psi / \partial y$) ($= v_x$) at selected points/elements of the meshes. The finite element program **FEM2D** (see Chapter 13 for details) is used in the analysis. The stream function values obtained with mesh T1 and mesh Q1 are very close to each other. Recall that the derivative $\partial \psi / \partial y$ is constant in a linear triangular element, whereas it varies linearly with x in a linear rectangular element. Therefore, mesh T1 and mesh Q1 results will not be the same. The velocities included in Table 8.5.2 correspond to elements closest to the symmetry line (i.e., $y = 0$ line) and surface of the cylinder.

The tangential velocity v_t on the cylinder surface can be computed from the relation,

$$v_t(\theta) = v_x \sin \theta + v_y \cos \theta = \frac{\partial \psi}{\partial y} \sin \theta - \frac{\partial \psi}{\partial x} \cos \theta \quad (8.5.49)$$

Contour plots of streamlines, velocity potential, and horizontal velocity $v_x = \partial \psi / \partial y$ obtained with mesh Q1 are shown in Fig. 8.5.12. Note that there is a difference between the

Table 8.5.2 Finite element results from the stream function formulation of inviscid flow around a cylinder (Example 8.5.5).

x	y	Stream function		Velocity $v_c = \partial \psi / \partial y$		Velocity $v_x = -\partial \phi / \partial x$	
		Mesh T1	Mesh Q1	Mesh T1	Mesh Q1	Mesh T1	Mesh Q1
1.3183	0.7354	0.7092	0.7095	0.9643(1) ^f	0.9852(1)	0.9922(1)	0.9989(1)
2.2705	0.5444	0.4372	0.4379	0.8032(3)	0.9005(2)	0.9371(3)	0.9408(2)
2.8564	0.4268	0.1667	0.1650	0.3906(5)	0.6432(3)	0.7047(5)	0.7018(3)
1.4112	1.4459	1.4241	1.4270	0.0000(7)	0.2679(4)	0.2999(7)	0.3197(4)
2.4305	1.0457	0.8730	0.8823	0.4469(15)	0.8746(8)	0.6469(15)	0.8364(8)
3.0577	0.7995	0.3357	0.3384	1.636(24)	1.586(12)	1.873(24)	1.453(12)
2.6931	1.5388	1.3758	1.4010	2.544(32)	2.4551(16)	2.163(32)	2.075(16)
3.1937	1.2057	0.7706	0.7980				
3.5018	1.0007	0.2520	0.2658				
4.0000	1.5714	1.2395	1.2065				
4.0000	1.2619	0.6191	0.5796				
4.0000	1.0714	0.1817	0.1588				

^fThe numbers in parentheses denote element number; the derivatives of ψ and ϕ are evaluated at the center of this element.

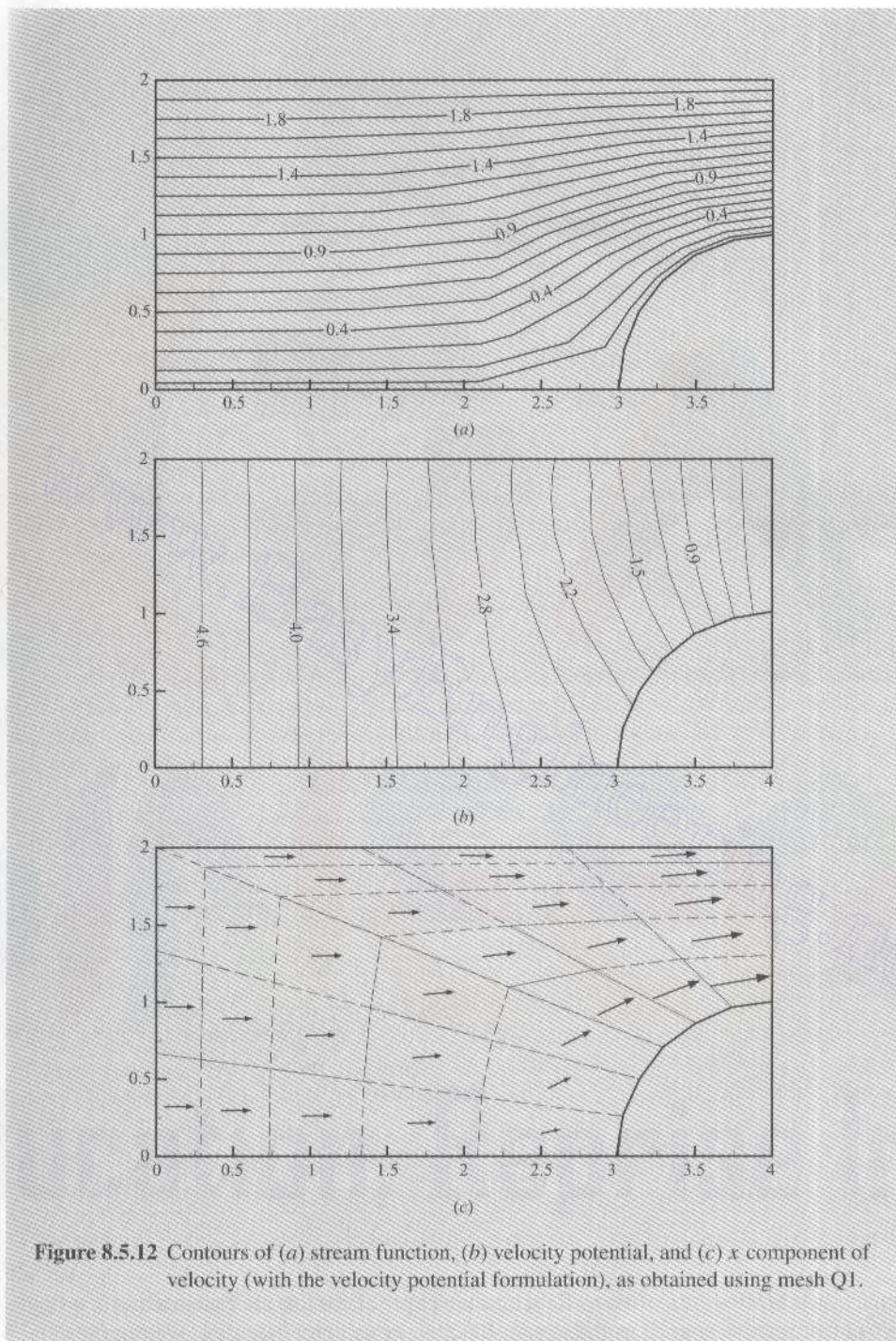


Figure 8.5.12 Contours of (a) stream function, (b) velocity potential, and (c) x component of velocity (with the velocity potential formulation), as obtained using mesh Q1.

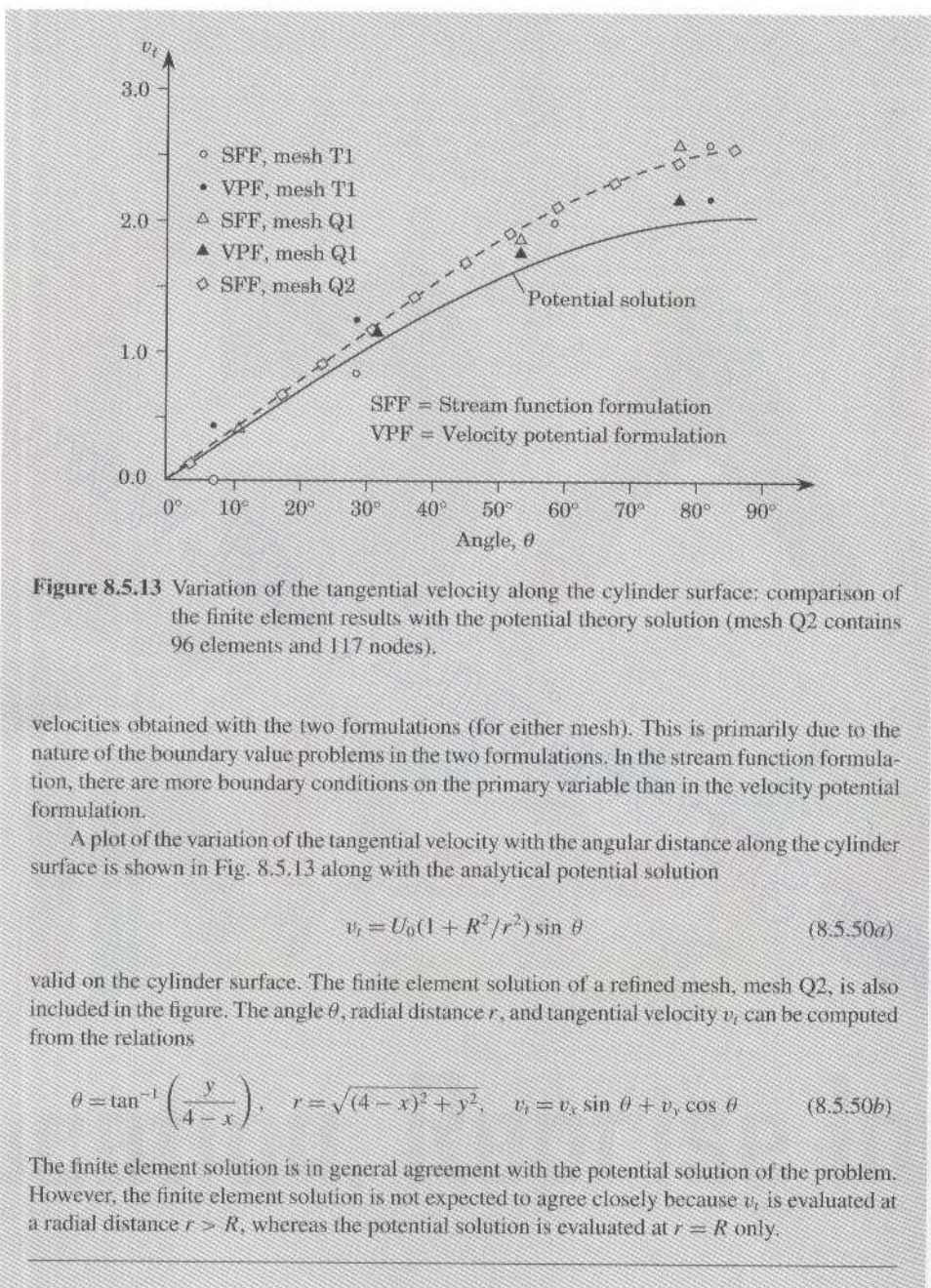


Figure 8.5.13 Variation of the tangential velocity along the cylinder surface: comparison of the finite element results with the potential theory solution (mesh Q2 contains 96 elements and 117 nodes).

velocities obtained with the two formulations (for either mesh). This is primarily due to the nature of the boundary value problems in the two formulations. In the stream function formulation, there are more boundary conditions on the primary variable than in the velocity potential formulation.

A plot of the variation of the tangential velocity with the angular distance along the cylinder surface is shown in Fig. 8.5.13 along with the analytical potential solution

$$v_t = U_0(1 + R^2/r^2) \sin \theta \quad (8.5.50a)$$

valid on the cylinder surface. The finite element solution of a refined mesh, mesh Q2, is also included in the figure. The angle θ , radial distance r , and tangential velocity v_t can be computed from the relations

$$\theta = \tan^{-1} \left(\frac{y}{4-x} \right), \quad r = \sqrt{(4-x)^2 + y^2}, \quad v_t = v_r \sin \theta + v_\theta \cos \theta \quad (8.5.50b)$$

The finite element solution is in general agreement with the potential solution of the problem. However, the finite element solution is not expected to agree closely because v_t is evaluated at a radial distance $r > R$, whereas the potential solution is evaluated at $r = R$ only.

This completes the section on fluid mechanics problems that are cast in terms of a single dependent unknown, such as the stream function or velocity potential. We return to fluid

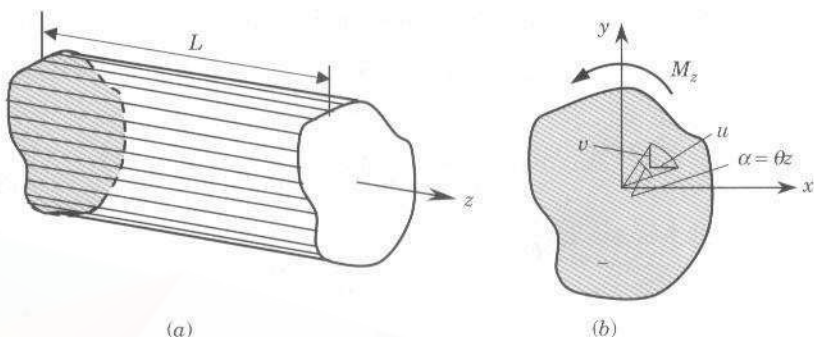


Figure 8.5.14 Torsion of cylindrical members: (a) a cylindrical member and (b) domain of analysis.

mechanics later in Chapter 10 to consider two-dimensional flows of viscous, incompressible fluids. The governing equations of such problems consist of several dependent variables and as many differential equations.

8.5.3 Solid Mechanics

In this section we consider two-dimensional boundary value problems of solid mechanics that are cast in terms of a single dependent unknown. These problems include torsion of cylindrical members and transverse deflection of membranes. This study is restricted to small deformations.

Torsion of Cylindrical Members

Consider a cylindrical bar (i.e., a long, uniform cross-sectional member), fixed at one end and twisted by a couple (i.e., torque) of magnitude M_z that is directed along the axis (z) of the bar, as shown in Fig. 8.5.14(a). We wish to determine the amount of twist and the associated stress field in the bar. To this end, we first derive the governing equations and then analyze the equation using the finite element method.

In general, a noncircular cross-sectional member subjected to torsional moment experiences warping at any section. We assume that all cross sections warp in the same way (which holds true for small twisting moments and deformation). This assumption allows us to assume that the displacements (u, v, w) along the coordinates (x, y, z) are of the form [see Fig. 8.5.14(b)]

$$u = -\theta zy, \quad v = \theta zx, \quad w = \theta \phi(x, y) \quad (8.5.51)$$

where $\phi(x, y)$ is a function to be determined and θ is the angle of twist per unit length of the bar.

The displacement field in (8.5.51) can be used to compute the strains, and stresses are computed using an assumed constitutive law. The stresses thus computed must satisfy the

three-dimensional equations of stress equilibrium in Eq. (2.3.52):

$$\begin{aligned}\frac{\partial \sigma_{xx}}{\partial x} + \frac{\partial \sigma_{xy}}{\partial y} + \frac{\partial \sigma_{xz}}{\partial z} &= 0 \\ \frac{\partial \sigma_{xy}}{\partial x} + \frac{\partial \sigma_{yy}}{\partial y} + \frac{\partial \sigma_{yz}}{\partial z} &= 0 \\ \frac{\partial \sigma_{xz}}{\partial x} + \frac{\partial \sigma_{yz}}{\partial y} + \frac{\partial \sigma_{zz}}{\partial z} &= 0\end{aligned}\quad (8.5.52)$$

and the stress boundary conditions on the lateral surface and at the end of the cylindrical bar. Calculation of strains and then stresses using the generalized Hooke's law gives the expressions,

$$\sigma_{xz} = G\theta \left(\frac{\partial \phi}{\partial x} - y \right), \quad \sigma_{yz} = G\theta \left(\frac{\partial \phi}{\partial y} + x \right) \quad (8.5.53)$$

and all other stresses are identically zero. Here G denotes the shear modulus of the material of the bar. Substitution of these stresses into (8.5.52) yields [the first two equations in (8.5.52) are identically satisfied and the third one leads to the following equation]:

$$\frac{\partial}{\partial x} \left(G\theta \frac{\partial \phi}{\partial x} \right) + \frac{\partial}{\partial y} \left(G\theta \frac{\partial \phi}{\partial y} \right) = 0 \quad (8.5.54)$$

throughout the cross section Ω of the cylinder. The boundary conditions on the lateral surfaces Γ require that $\sigma_{xz}n_x + \sigma_{yz}n_y = 0$:

$$\left(\frac{\partial \phi}{\partial x} - y \right) n_x + \left(\frac{\partial \phi}{\partial y} + x \right) n_y = 0 \Rightarrow \frac{\partial \phi}{\partial n} = yn_x - xn_y \quad (8.5.55)$$

Here (n_x, n_y) denote the direction cosines of the unit normal at a point on Γ .

In summary, the torsion of a cylindrical bar is governed by the equations (8.5.54) and (8.5.55). The function $\phi(x, y)$ is called the *torsion function* or *warping function*. Since the boundary condition in (8.5.55) is of the flux type, the function can be determined within an additive constant. The stresses in (8.5.53), however, are independent of this constant. The additive constant has the meaning of rigid body movement of the cylinder as a whole in the z -direction. For additional discussion of the topic the reader is referred to Timoshenko and Goodier (1970).

The Laplace equation (8.5.54) and the Neumann boundary condition (8.5.55) governing ϕ are not convenient in the analysis because of the nature and form of the boundary condition, especially for irregular cross-sectional members. The theory of analytic functions can be used to rewrite these equations in terms of the *stress function* $\Psi(x, y)$, which is related to the warping function $\phi(x, y)$ by the equations

$$\frac{\partial \Psi}{\partial x} = -\frac{\partial \phi}{\partial y} - x, \quad \frac{\partial \Psi}{\partial y} = \frac{\partial \phi}{\partial x} - y \quad (8.5.56)$$

Eliminating ϕ from (8.5.54) and (8.5.55) gives, respectively, the results

$$-\left(\frac{\partial^2 \Psi}{\partial x^2} + \frac{\partial^2 \Psi}{\partial y^2}\right) = 2 \quad (8.5.57)$$

$$\frac{\partial \Psi}{\partial y} n_x - \frac{\partial \Psi}{\partial x} n_y = 0 \quad (8.5.58)$$

The left side of (8.5.58) denotes the tangential derivative $d\Psi/ds$, and $d\Psi/ds = 0$ implies that

$$\Psi = \text{constant} \quad \text{on } \Gamma$$

Since the constant part of Ψ does not contribute to the stress field

$$\sigma_{xz} = G\theta \frac{\partial \Psi}{\partial y}, \quad \sigma_{yz} = -G\theta \frac{\partial \Psi}{\partial x} \quad (8.5.59)$$

we can take $\Psi = 0$ on the boundary.

In summary, the torsion problem can now be stated as one of determining the stress function Ψ such that

$$\begin{aligned} -\nabla^2 \Psi &= 2 && \text{in } \Omega \\ \Psi &= 0 && \text{on } \Gamma \end{aligned} \quad (8.5.60)$$

Once Ψ is determined, the stresses can be computed from (8.5.59) for a given angle of twist per unit length (θ) and shear modulus (G).

The finite element model of (8.5.60) follows immediately from that of Eq. (8.2.1):

$$[K^e]\{u^e\} = \{f^e\} + \{Q^e\} \quad (8.5.61a)$$

where u_i^e is the value of Ψ at the i th node of Ω_e and

$$\begin{aligned} K_{ij}^e &= \int_{\Omega_e} \left(\frac{\partial \psi_i}{\partial x} \frac{\partial \psi_j}{\partial x} + \frac{\partial \psi_i}{\partial y} \frac{\partial \psi_j}{\partial y} \right) dx dy \\ f_i^e &= \int_{\Omega_e} 2\psi_i dx dy \quad Q_i^e = \oint_{\Gamma_e} \frac{\partial \Psi}{\partial n} \psi_i ds \end{aligned} \quad (8.5.61b)$$

Example 8.5.6 (Torsion of a Square Cross-Sectional Bar)

Here we consider torsion of a square ($a \times a$) cross-section bar. Note that the problem is antisymmetric as far as the loading and stress distribution are concerned; however, the stress function, being a scalar function governed by the Poisson equation (8.5.60), is symmetric about the x and y axes as well as the diagonal lines. When using rectangular elements, one quadrant of the bar cross section can be used in the finite element analysis. The biaxial symmetry about the x and y axes requires imposition of the following boundary conditions on Ψ (see Example 8.3.1):

$$\frac{\partial \Psi}{\partial x} = 0 \quad \text{on the line } x = 0, \quad \frac{\partial \Psi}{\partial y} = 0 \quad \text{on the line } y = 0$$

In addition, on the actual boundary we have the condition $\Psi = 0$ on lines $x = a$ and $y = b = a$.

Table 8.5.3 Convergence of the finite element solutions for Ψ using linear and quadratic rectangular elements (four-node and nine-node elements) in Example 8.5.6.

x	y	Linear elements			Quadratic elements [†]		
		2 × 2	4 × 4	8 × 8	1 × 1	2 × 2	4 × 4
0.0000	0.0000	0.15536	0.14920	0.14780	0.14744	0.14730	0.14734
0.0625	0.0000	—	—	0.14583	—	—	0.14538
0.1250	0.0000	—	0.14120	0.13987	—	0.13941	0.13944
0.1875	0.0000	—	—	0.12972	—	—	0.12931
0.2500	0.0000	0.12054	0.11610	0.11502	0.11378	0.11463	0.11467
0.3125	0.0000	—	—	0.09534	—	—	0.09505
0.3750	0.0000	—	0.07069	0.07007	—	0.069873	0.06986
0.4375	0.0000	—	—	0.03854	—	—	0.03844
0.1250	0.2500	—	0.11031	0.10925	—	0.10887	0.10890
0.2500	0.2500	0.09643	0.09191	0.09090	0.09095	0.09056	0.09057
0.3750	0.2500	—	0.05729	0.05660	—	0.05626	0.05636

[†]The 4×4 mesh of nine-node quadratic elements gives a solution that coincides with the analytical solution to five significant decimal places.

The results of a convergence study are summarized in Tables 8.5.3 and 8.5.4. The analytical solution of the problem is given by [see (2.5.40)]

$$\Psi(x, y) = \frac{a^2}{4} - x^2 - \frac{8a^2}{\pi^3} \sum_{n=0}^{\infty} \frac{(-1)^n}{(2n+1)^3} \frac{\cosh k_n y \cos k_n x}{\cosh(k_n b/2)} \quad (8.5.62a)$$

$$\sigma_{xz} = -\frac{8aG\theta}{\pi^2} \sum_{n=0}^{\infty} \frac{(-1)^n}{(2n+1)^2} \frac{\sinh k_n y \cos k_n x}{\cosh(k_n b/2)} \quad (8.5.62b)$$

$$\sigma_{yz} = G\theta \left[2x - \frac{8a}{\pi^2} \sum_{n=0}^{\infty} \frac{(-1)^n}{(2n+1)^2} \frac{\cosh k_n y \sin k_n x}{\cosh(k_n b/2)} \right] \quad (8.5.62c)$$

Table 8.5.4 Comparison of finite element solutions for the shear stress $\bar{\sigma}_{yz}(x, y)$ [$= -\bar{\sigma}_{zy}(y, x)$], computed using various meshes, with the analytical solution (Example 8.5.6).

x	y	Mesh			Analytical solution
		2 × 2	4 × 4	8 × 8	
0.03125	0.03125	—	—	0.0312	0.0312
0.09375	0.03125	—	—	0.0946	0.0946
0.15625	0.03125	—	—	0.1612	0.1611
0.21875	0.03125	—	—	0.2332	0.2331
0.28125	0.03125	—	—	0.03127	0.3124
0.34375	0.03125	—	—	0.4015	0.4011
0.40625	0.03125	—	—	0.5013	0.5008
0.46875	0.03125	—	—	0.6135	0.6128
0.06250	0.0625	—	0.06175	—	0.0618
0.1875	0.0625	—	0.1942	—	0.1939
0.3125	0.0625	—	0.3529	—	0.3516
0.4375	0.0625	—	0.5528	—	0.5504
0.1250	0.1250	0.1179	—	—	0.1193
0.3750	0.1250	0.4339	—	—	0.4272

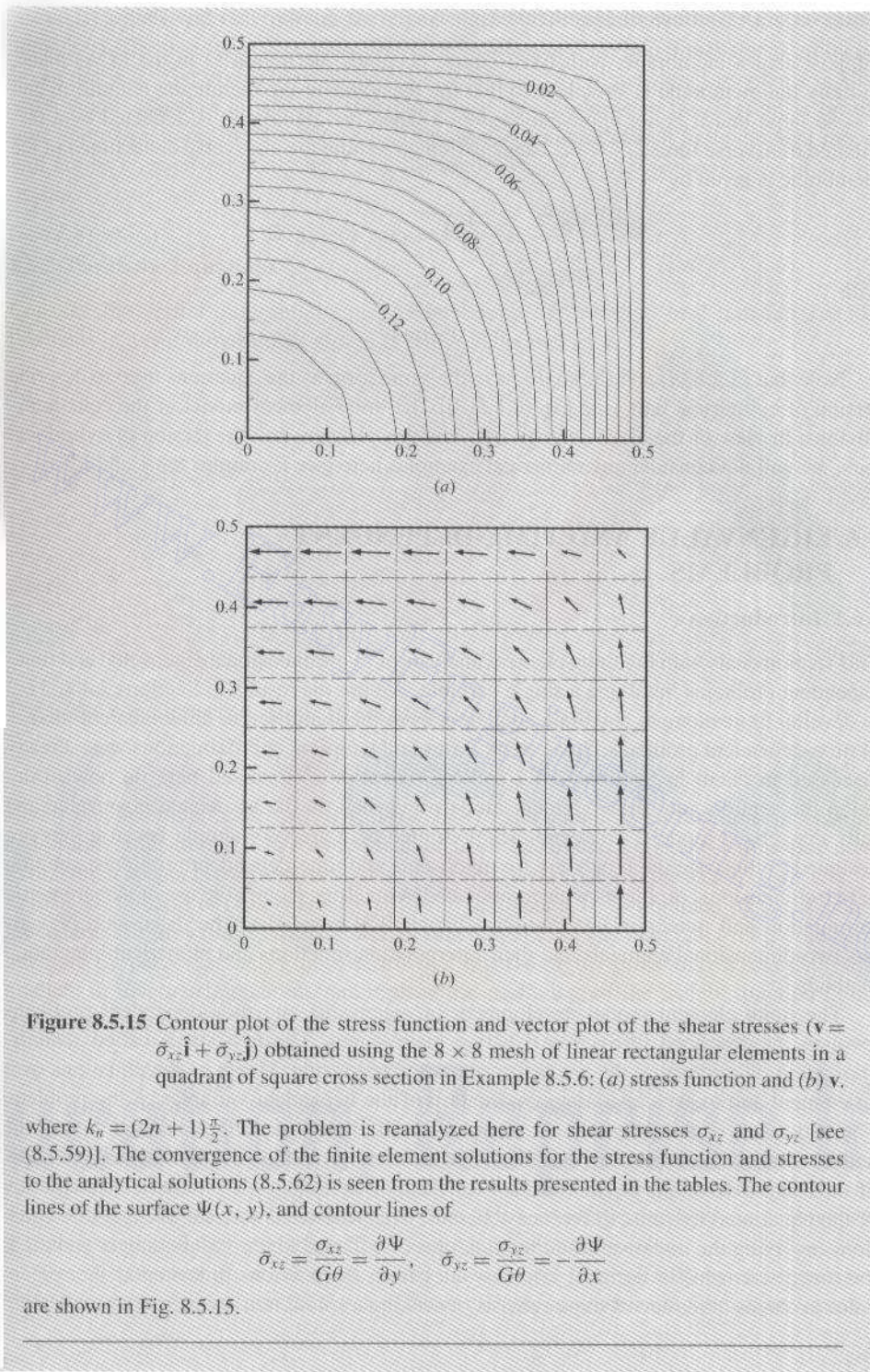


Figure 8.5.15 Contour plot of the stress function and vector plot of the shear stresses ($\mathbf{v} = \bar{\sigma}_{xz}\hat{\mathbf{i}} + \bar{\sigma}_{yz}\hat{\mathbf{j}}$) obtained using the 8×8 mesh of linear rectangular elements in a quadrant of square cross section in Example 8.5.6: (a) stress function and (b) \mathbf{v} .

where $k_n = (2n + 1)\frac{\pi}{2}$. The problem is reanalyzed here for shear stresses σ_{xz} and σ_{yz} [see (8.5.59)]. The convergence of the finite element solutions for the stress function and stresses to the analytical solutions (8.5.62) is seen from the results presented in the tables. The contour lines of the surface $\Psi(x, y)$, and contour lines of

$$\bar{\sigma}_{xz} = \frac{\sigma_{xz}}{G\theta} = \frac{\partial \Psi}{\partial y}, \quad \bar{\sigma}_{yz} = \frac{\sigma_{yz}}{G\theta} = -\frac{\partial \Psi}{\partial x}$$

are shown in Fig. 8.5.15.

Transverse Deflections of Membranes

Suppose that a membrane, with fixed edges, occupies the region Ω in the (x, y) plane. Initially the membrane is stretched so that the tension a in the membrane is uniform and a is so large that it is not appreciably altered when the membrane is deflected by a distributed transverse force, $f(x, y)$. The equation governing the transverse deflection u of the membrane is given by

$$-a \left(\frac{\partial^2 u}{\partial x^2} + \frac{\partial^2 u}{\partial y^2} \right) = f(x, y) \quad \text{in } \Omega \quad (8.5.63a)$$

with

$$u = 0 \quad \text{on } \Gamma \quad (8.5.63b)$$

Note that (8.5.63a) and (8.5.63b) have the same form as the equations used to describe torsion of cylindrical bars [see Eq. (8.5.60)]. The finite element model of the equation is obvious. In view of the close analogy between this problem and the torsion of cylindrical bars, we will not consider any numerical examples here (see Examples 8.3.1 and 8.5.6).

8.6 EIGENVALUE AND TIME-DEPENDENT PROBLEMS

8.6.1 Introduction

This section deals with the finite element analysis of two-dimensional eigenvalue and time-dependent problems involving a single variable. We use the results of Sections 2.4 and 6.2 to develop finite element algebraic equations from the semidiscrete finite element models of time-dependent problems. Since weak forms and temporal approximations were already discussed in detail in Sections 2.4.2 and 6.2, attention is focussed here on how to develop the semidiscrete finite element models and then on the associated eigenvalue and fully discretized models. The examples presented here are very simple because they are designed to illustrate the procedure for eigenvalue and time-dependent problems; solution of two-dimensional problems with complicated geometries require the use of isoparametric formulation and numerical integration. Chapter 9 is devoted to the discussion of various two-dimensional elements and their interpolation functions and numerical integration methods.

The finite element model development of eigenvalue and time-dependent problems involves, as described in Section 6.2, two main stages. The first stage, called *semidiscretization*, is to develop the weak form or weighted-residual form of the equations over an element and to seek spatial approximation of the dependent variables of the problem. The end result of this step is a set of ordinary differential equations in time among the nodal values of the dependent variables. For transient problems, the second stage consists of time approximations of the ordinary differential equations (i.e., numerical integration of the equations) by finite difference schemes. This step leads to a set of algebraic equations involving the nodal values at time $t_{s+1} [= (s + 1)\Delta t]$, where s is an integer and Δt is the time increment] in terms of known values from the previous time step(s). For eigenvalue problems, the second stage consists of seeking a solution of the form $u_j(t) = U_j e^{-\lambda_j t}$

for nodal values and determining the eigenvalues λ and eigenfunctions $U_j \psi_j(x, y)$ (no sum on j). The two-stage procedure was clearly illustrated for one-dimensional problems in Section 6.2. The procedure will be applied here to two-dimensional problems involving a single equation in a single variable. Since the emphasis in this section is on the time approximations, the development of the weak form and spatial finite element model will not be covered explicitly here, and the reader is referred to Sections 8.2 and 8.3 for details.

8.6.2 Parabolic Equations

Consider the partial differential equation governing the transient heat transfer and like problems in a two-dimensional region Ω with total boundary Γ ,

$$c \frac{\partial u}{\partial t} - \frac{\partial}{\partial x} \left(a_{11} \frac{\partial u}{\partial x} \right) - \frac{\partial}{\partial y} \left(a_{22} \frac{\partial u}{\partial y} \right) + a_0 u = f(x, y, t) \quad (8.6.1)$$

with the boundary conditions

$$u = \hat{u} \text{ or } q_n = \hat{q}_n \quad \text{on } \Gamma \quad (t \geq 0) \quad (8.6.2a)$$

where

$$q_n = a_{11} \frac{\partial u}{\partial x} n_x + a_{22} \frac{\partial u}{\partial y} n_y \quad (8.6.2b)$$

The initial conditions (i.e., at $t = 0$) are of the form

$$u(x, y, 0) = u_0(x, y) \quad \text{in } \Omega \quad (8.6.3)$$

Here t denotes time, and $c, a_{11}, a_{22}, a_0, \hat{u}, u_0, f$, and \hat{q}_n are given functions of position and/or time. Equation (8.6.1) is a modification of (8.2.1) in that it contains a time derivative term, which accounts for time variations of the physical process represented by (8.2.1).

The weak form of (8.6.1) and (8.6.2) over an element Ω_e is obtained by the standard procedure: Multiply (8.6.1) with the weight function $v(x, y)$ and integrate over the element, integrate by parts (spatially) those terms that involve higher-order derivatives using the gradient or divergence theorem, and replace the coefficient of the weight function in the boundary integral with the secondary variable [i.e., use (8.6.2b)]. We obtain

$$0 = \int_{\Omega_e} \left[v \left(c \frac{\partial u}{\partial t} + a_0 u - f \right) + a_{11} \frac{\partial v}{\partial x} \frac{\partial u}{\partial x} + a_{22} \frac{\partial v}{\partial y} \frac{\partial u}{\partial y} \right] dx dy - \oint_{\Gamma_e} q_n v ds \quad (8.6.4)$$

Note that the procedure to obtain the weak form for time-dependent problems is not much different from that used for steady-state problems in Section 8.2.3. The difference is that all terms of the equations may be functions of time. Also, no integration by parts with respect to time is used, and the weight function v is not a function of time.

The *semidiscrete* finite element model is obtained from (8.6.4) by substituting a finite element approximation for the dependent variable, u . In selecting the approximation

for u , once again we assume that the time dependence can be separated from the space variation,

$$u(x, y, t) \approx \sum_{j=1}^n u_j^e(t) \psi_j^e(x, y) \quad (8.6.5)$$

where u_j^e denotes the value of $u(x, y, t)$ at the spatial location (x_j, y_j) at time t . The i th differential equation (in time) of the finite element model is obtained by substituting $v = \psi_i^e(x, y)$ and replacing u by (8.6.5) in (8.6.4):

$$0 = \sum_{j=1}^n \left(M_{ij}^e \frac{du_j^e}{dt} + K_{ij}^e u_j^e \right) - f_i^e - Q_i^e \quad (8.6.6a)$$

or, in matrix form

$$[M^e]\{\dot{u}^e\} + [K^e]\{u^e\} = \{f^e\} + \{Q^e\} \quad (8.6.6b)$$

where a superposed dot on u denotes a derivative with time ($\dot{u} = \partial u / \partial t$), and

$$\begin{aligned} M_{ij}^e &= \int_{\Omega_e} c \psi_i^e \psi_j^e dx dy \\ K_{ij}^e &= \int_{\Omega_e} \left(a_{11} \frac{\partial \psi_i^e}{\partial x} \frac{\partial \psi_j^e}{\partial x} + a_{22} \frac{\partial \psi_i^e}{\partial y} \frac{\partial \psi_j^e}{\partial y} + a_0 \psi_i^e \psi_j^e \right) dx dy \\ f_i^e &= \int_{\Omega_e} f(x, y, t) \psi_i^e dx dy \end{aligned} \quad (8.6.6c)$$

This completes the semidiscretization step.

Eigenvalue Analysis

The problem of finding $u_j^e(t) = U_j e^{-\lambda t}$ such that (8.6.6) holds for homogeneous boundary and initial conditions and $f = 0$ is called an *eigenvalue problem*. Substituting for $u_j^e(t)$ into (8.6.6b), we obtain

$$(-\lambda[M^e] + [K^e])\{u^e\} = \{Q^e\} \quad (8.6.7)$$

Upon assembly of the element equations (8.6.7), the right column vector of the condensed equations is zero (because of the homogeneous boundary conditions), giving rise to the global eigenvalue problem

$$([K] - \lambda[M])\{U\} = \{0\} \quad (8.6.8)$$

The order of the matrix equations is $N \times N$, where N is the number of nodes at which the solution is not known. A nontrivial solution to (8.6.8) exists only if the determinant of the coefficient matrix is zero:

$$|[K] - \lambda[M]| = 0$$

which, when expanded, results in an N th-degree polynomial in λ . The N roots λ_j ($j = 1, 2, \dots, N$) of this polynomial give the first N eigenvalues of the discretized system (the continuous system, in general, has an infinite number of eigenvalues). There exist standard eigenvalue routines to solve (8.6.8), which give N eigenvalues and eigenvectors.

Transient Analysis

Note that the form of (8.6.6b) is the same as the parabolic equation discussed in Section 6.2 [see Eq. (6.2.21a)]. Whether a problem is one-dimensional, two-dimensional, or three-dimensional, the form of the semidiscrete finite element model is the same. Therefore, the time approximation schemes discussed in Section 6.2 for parabolic equations can be readily applied.

Using the α -family of approximation

$$\{u\}_{s+1} = \{u\}_s + \Delta t[(1 - \alpha)\{\dot{u}\}_s + \alpha\{\dot{u}\}_{s+1}] \quad (0 \leq \alpha \leq 1) \quad (8.6.9)$$

we can transform the ordinary differential equations (8.6.6b) into a set of algebraic equations at time t_{s+1} :

$$[\hat{K}]_{s+1}\{u\}_{s+1} = \{\hat{F}\}_{s,s+1} \quad (8.6.10a)$$

where

$$\begin{aligned} [\hat{K}]_{s+1} &= [M] + a_1[K]_{s+1} \\ \{\hat{F}\} &= \Delta t(\alpha\{F\}_{s+1} + (1 - \alpha)\{F\}_s) + ([M] - a_2[K]_s)\{u\}_s \quad (8.6.10b) \\ a_1 &= \alpha\Delta t, \quad a_2 = (1 - \alpha)\Delta t \end{aligned}$$

Equation (8.6.10a), after assembly and imposition of boundary conditions, is solved at each time step for the nodal values u_j at time $t_{s+1} = (s + 1)\Delta t$. At time $t = 0$ (i.e., $s = 0$), the right-hand side of (8.6.10a) is computed using the initial values $\{u\}_0$; the vector $\{F\}$, which is the sum of the source vector $\{f\}$ and internal flux vector $\{Q\}$, is always known for both times t_s and t_{s+1} , at all nodes at which the solution is unknown [because $f(x, t)$ is a known function of time and the sum of Q_j^e at these nodes is zero].

It should be recalled from Section 6.2 that, for different values of α , we obtain the following well-known time approximation schemes [see Eq. (6.2.20)]:

$$\alpha = \begin{cases} 0, & \text{the forward difference scheme (conditionally stable); } O(\Delta t) \\ \frac{1}{2}, & \text{the Crank–Nicolson scheme (unconditionally stable); } O(\Delta t)^2 \\ \frac{2}{3}, & \text{the Galerkin scheme (unconditionally stable); } O(\Delta t)^2 \\ 1, & \text{the backward difference scheme (unconditionally stable); } O(\Delta t) \end{cases}$$

For the forward difference scheme the stability requirement is

$$\Delta t < \Delta t_{\text{cri}} = \frac{2}{(1 - 2\alpha)\lambda_{\max}}, \quad \alpha < \frac{1}{2} \quad (8.6.11)$$

where λ_{\max} is the largest eigenvalue of the finite element equations (8.6.8).

We consider examples of an eigenvalue problem and a time-dependent problem next.

Example 8.6.1 (Eigenvalue Analysis)

Consider the differential equation,

$$\frac{\partial u}{\partial t} - \left(\frac{\partial^2 u}{\partial x^2} + \frac{\partial^2 u}{\partial y^2} \right) = f \quad (8.6.12a)$$

in a unit square, subjected to the boundary conditions

$$\frac{\partial u}{\partial x}(0, y, t) = 0, \quad \frac{\partial u}{\partial y}(x, 0, t) = 0, \quad u(x, 1, t) = 0, \quad u(1, y, t) = 0 \quad (8.6.12b)$$

and initial conditions

$$u(x, y, 0) = 0 \quad (8.6.12c)$$

As a first choice we may choose a 1×1 mesh of two triangular elements. Alternatively, for the choice of triangles, we can use the diagonal symmetry and model the domain with one triangular element (see Fig. 8.3.1c). The element matrices for a right-angle triangle with $a = b$ are:

$$[K^e] = \frac{1}{2} \begin{bmatrix} 1 & -1 & 0 \\ -1 & 2 & -1 \\ 0 & -1 & 1 \end{bmatrix}, \quad [M^e] = \frac{a^2}{24} \begin{bmatrix} 2 & 1 & 1 \\ 1 & 2 & 1 \\ 1 & 1 & 2 \end{bmatrix}$$

The eigenvalue problem becomes ($a = 1.0$)

$$\left(-\frac{\lambda}{24} \begin{bmatrix} 2 & 1 & 1 \\ 1 & 2 & 1 \\ 1 & 1 & 2 \end{bmatrix} + \frac{1}{2} \begin{bmatrix} 1 & -1 & 0 \\ -1 & 2 & -1 \\ 0 & -1 & 1 \end{bmatrix} \right) \begin{Bmatrix} U_1 \\ U_2 \\ U_3 \end{Bmatrix} = \begin{Bmatrix} Q_1^1 \\ Q_2^1 \\ Q_3^1 \end{Bmatrix}$$

The boundary conditions require $U_2 = U_3 = 0$ and $Q_i^1 = 0$. Hence, we have

$$\left(-\frac{\lambda}{12} + \frac{1}{2} \right) U_1 = 0 \quad \text{or} \quad \lambda = 6$$

The eigenfunction becomes

$$U(x, y) = \psi_1(x, y) = 1 - x$$

which is defined over the octant of the domain. For a quadrant of the domain, by symmetry, the eigenfunction becomes $U(x, y) = (1 - x)(1 - y)$.

For a mesh of single rectangular element with $a = b$ (see Fig. 8.3.1b), we have

$$[K^e] = \frac{1}{6} \begin{bmatrix} 4 & -1 & -2 & -1 \\ -1 & 4 & -1 & 2 \\ -2 & -1 & 4 & -1 \\ -1 & -2 & -1 & 4 \end{bmatrix}, \quad [M^e] = \frac{a^2}{36} \begin{bmatrix} 4 & 2 & 1 & 2 \\ 2 & 4 & 2 & 1 \\ 1 & 2 & 4 & 2 \\ 2 & 1 & 2 & 4 \end{bmatrix}$$

and

$$\left(-\frac{\lambda}{36} \begin{bmatrix} 4 & 2 & 1 & 2 \\ 2 & 4 & 2 & 1 \\ 1 & 2 & 4 & 2 \\ 2 & 1 & 2 & 4 \end{bmatrix} + \frac{1}{6} \begin{bmatrix} 4 & -1 & -2 & -1 \\ -1 & 4 & -1 & 2 \\ -2 & -1 & 4 & -1 \\ -1 & -2 & -1 & 4 \end{bmatrix} \right) \begin{Bmatrix} U_1 \\ U_2 \\ U_3 \\ U_4 \end{Bmatrix} = \begin{Bmatrix} Q_1^1 \\ Q_2^1 \\ Q_3^1 \\ Q_4^1 \end{Bmatrix}$$

Table 8.6.1 Comparison of finite element solutions for eigenvalues, obtained using various meshes, with the analytical solution (Example 8.6.1).

λ	Triangles				Rectangles				Analytical solution [†]
	1 × 1	2 × 2	4 × 4	8 × 8	1 × 1	2 × 2	4 × 4	8 × 8	
$\lambda_1(\lambda_{11})$	6.000	5.415	5.068	4.969	6.000	5.193	4.999	4.951	4.935
$\lambda_2(\lambda_{13})$	—	32.000	27.250	25.340	—	34.290	27.370	25.330	24.674
$\lambda_3(\lambda_{31})$	—	38.200	28.920	25.730	—	34.290	27.370	25.330	24.674
$\lambda_4(\lambda_{33})$	—	76.390	58.220	48.080	—	63.380	49.740	45.710	44.413
$\lambda_4(\lambda_{15})$	—	—	85.350	69.780	—	—	84.570	69.260	64.152
$\lambda_5(\lambda_{51})$	—	—	86.790	69.830	—	—	84.570	69.260	64.152

[†]The analytical solution is $\lambda_{mn} = \frac{1}{4}\pi^2(m^2 + n^2)$ ($m, n = 1, 3, 5, \dots$)

Using the boundary conditions $U_2 = U_3 = U_4 = 0$ and $Q_i^1 = 0$, we obtain

$$\left(-\frac{\lambda}{36} \times 4 + \frac{4}{6} \right) U_1 = 0, \quad \text{or } \lambda = 6$$

The eigenfunction over the quadrant of the domain is given by

$$U(x, y) = \psi_1(x, y) = (1 - x)(1 - y)$$

For this problem, the one-element mesh of triangles in an octant of the domain gives the same solution as the one-element mesh of rectangular elements in a quadrant of the domain.

Table 8.6.1 contains eigenvalues obtained with various meshes of triangular and rectangular elements, along with the analytical solution of the problem. It is clear that the convergence of the minimum eigenvalue obtained with the finite element method to the analytical value is rapid compared to the convergence of the higher eigenvalues, i.e., error in the higher eigenvalues is always larger than that in the minimum eigenvalue. Also, the minimum eigenvalue converges faster with mesh refinements.

Example 8.6.2 (Transient Analysis)

We wish to solve the transient heat conduction equation

$$\frac{\partial T}{\partial t} - \left(\frac{\partial^2 T}{\partial x^2} + \frac{\partial^2 T}{\partial y^2} \right) = 1 \quad (8.6.13a)$$

subject to the boundary conditions (see Fig. 8.6.1a), for $t \geq 0$,

$$\begin{aligned} \frac{\partial T}{\partial x}(0, y, t) &= 0, & \frac{\partial T}{\partial y}(x, 0, t) &= 0 \\ T(1, y, t) &= 0, & T(x, 1, t) &= 0 \end{aligned} \quad (8.6.13b)$$

and the initial conditions

$$T(x, y, 0) = 0 \quad \text{for all } (x, y) \text{ in } \Omega \quad (8.6.13c)$$

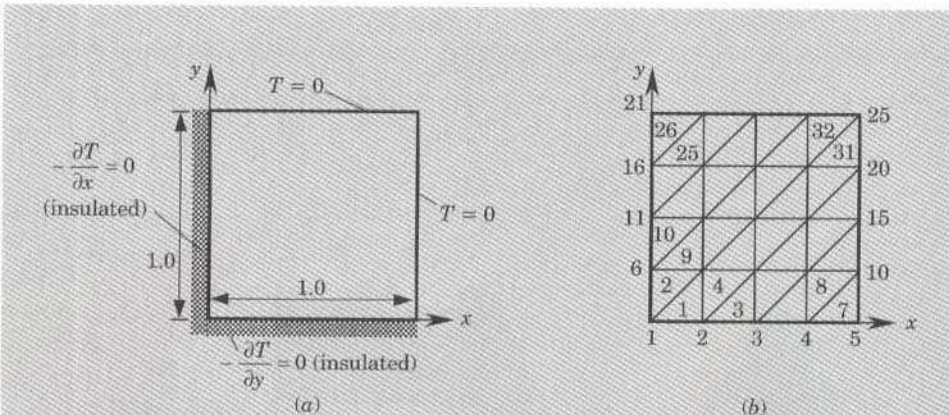


Figure 8.6.1 (a) Domain, boundary conditions and (b) finite element mesh for the transient heat conduction problem of Example 8.6.2.

We choose a 4×4 mesh of linear triangular elements (see Fig. 8.6.1b) to model the domain, and investigate the stability and accuracy of the Crank–Nicolson method (i.e., $\alpha = 0.5$) and the forward difference scheme ($\alpha = 0.0$) for the temporal approximation. Since the Crank–Nicolson method is unconditionally stable, we can choose any value of Δt . However, for large values of Δt the solution may not be accurate. The forward difference scheme is conditionally stable; it is stable if $\Delta t < \Delta t_{\text{cri}}$, where

$$\Delta t_{\text{cri}} = \frac{2}{\lambda_{\max}} = \frac{2}{386.4} = 0.00518$$

where the maximum eigenvalue of (8.6.13a) for the 4×4 mesh of triangles is 386.4.

The element equations are given by (8.6.6b), with $[M^c]$, $[K^c]$, and $\{f^c\}$ defined by (8.6.6c), wherein $c = 1$, $a_{11} = 1$, $a_{22} = 1$, $a_0 = 0$, and $f = 1$. The boundary conditions of the problem for the 4×4 mesh are given by

$$U_5 = U_{10} = U_{15} = U_{20} = U_{21} = U_{22} = U_{33} = U_{24} = U_{25} = 0.0$$

Beginning with the initial conditions $U_i = 0$ ($i = 1, 2, \dots, 25$), we solve the assembled set of equations associated with (8.6.10).

The forward difference scheme would be unstable for $\Delta t > 0.00518$. To illustrate this point, the equations are solved using $\alpha = 0$, $\Delta t = 0.01$ and $\alpha = 0.5$, $\Delta t = 0.01$. The Crank–Nicolson method gives stable and accurate solution, while the forward difference scheme yields unstable solution (i.e., the solution error grows unboundedly with time), as can be seen from Fig. 8.6.2. For $\Delta t = 0.005$, the forward difference scheme yields stable solution.

The Crank–Nicolson method gives a stable and accurate solution for even $\Delta t = 0.05$. The temperature $T(x, 0, t)$ versus x for various values of time are shown in Fig. 8.6.3(a). The steady state is reached at time $t = 1.0$. The temperature $T(0, 0, t)$ versus time, predicted by the Crank–Nicolson method, is shown in Fig. 8.6.3(b), which indicates the evolution of the temperature from zero to the steady state. A comparison of the transient solution at $t = 1.0$ is given in Table 8.6.2 with the steady-state finite element, the finite difference, and the analytical solutions. Table 8.6.3 contains the finite element solutions for temperature predicted by 4×4 meshes of triangles and rectangles and various values of Δt and $\alpha = 0.5$.

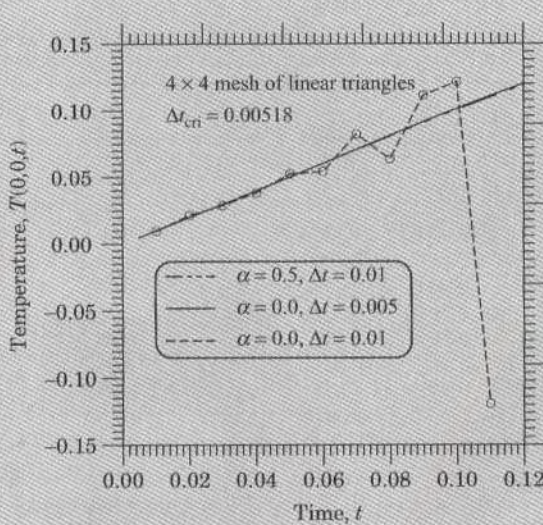


Figure 8.6.2 Stability of the transient solutions of the heat conduction problem in Example 8.6.2 analyzed using a 4×4 mesh of linear triangular elements and the Crank-Nicolson ($\alpha = 0.5$) and forward difference ($\alpha = 0.0$) time integration schemes.

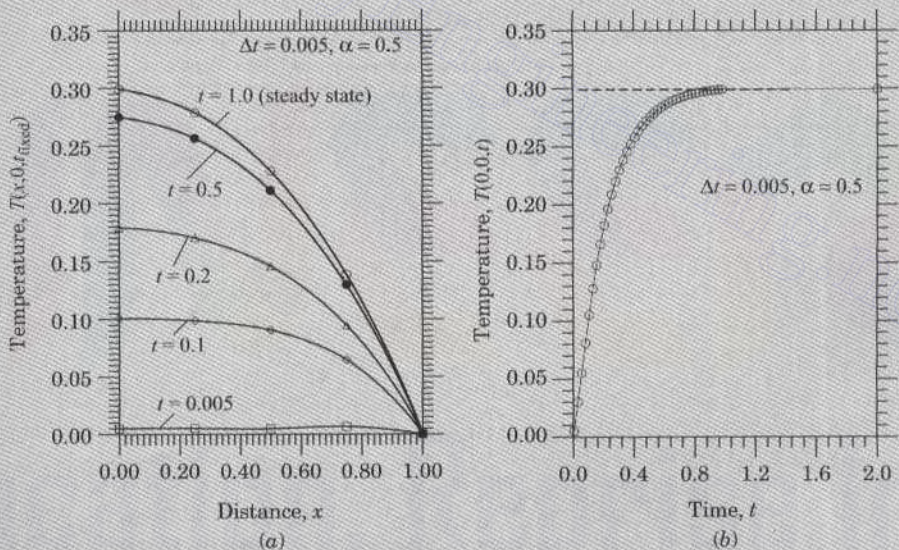


Figure 8.6.3 Variation of the temperature as a function of position x and time t for the transient heat conduction problem of Example 8.6.2 (4×4 mesh of linear triangles).

Table 8.6.2 Comparison of finite difference method (FDM) and finite element method (FEM) solutions with the exact solution of the heat conduction problem in Example 8.6.2.

Node	Exact (steady)	FDM (steady)	Error	FEM (steady)	Error	(FEM) at $t = 1.0^{\dagger}$
1	0.2947	0.2911	0.0036	0.3013	-0.0066	0.2993
2	0.2789	0.2755	0.0034	0.2805	-0.0016	0.2786
3	0.2293	0.2266	0.0027	0.2292	0.0001	0.2278
4	0.1397	0.1381	0.0016	0.1392	0.0005	0.1385
5	0.0000	0.0000	0.0000	0.0000	0.0000	0.0000
7	0.2642	0.2609	0.0033	0.2645	-0.0003	0.2628
8	0.2178	0.2151	0.0027	0.2172	0.0006	0.2159
9	0.1333	0.1317	0.0016	0.1327	0.0006	0.1320
10	0.0000	0.0000	0.0000	0.0000	0.0000	0.0000
13	0.1811	0.1787	0.0024	0.1801	0.0010	0.1791
14	0.1127	0.1110	0.0017	0.1117	0.0010	0.1111
15	0.0000	0.0000	0.0000	0.0000	0.0000	0.0000
19	0.0728	0.0711	0.0017	0.0715	0.0013	0.0712
20	0.0000	0.0000	0.0000	0.0000	0.0000	0.0000
25	0.0000	0.0000	0.0000	0.0000	0.0000	0.0000

[†]Obtained with the Crank–Nicolson scheme with $\Delta t = 0.005$

Table 8.6.3 Comparison of transient solutions of (8.6.13a) and (8.6.13b) obtained using meshes of triangular and rectangular elements.

Time t	Element [†]	Temperature along the line $y = 0$: $T(x, 0, t) \times 10$			
		$x = 0.0$	$x = 0.25$	$x = 0.5$	$x = 0.75$
0.1	T1	0.9758	0.9610	0.9063	0.7104
	R1	0.9684	0.9556	0.8956	0.6887
	T2	0.9928	0.9798	0.9168	0.6415
	R2	0.9841	0.9718	0.9020	0.6323
0.2	T1	1.8003	1.7238	1.4891	0.9321
	R1	1.7723	1.7216	1.4829	0.9367
	T2	1.7979	1.7060	1.4644	0.9462
	R2	1.7681	1.6990	1.4626	0.9469
0.3	T1	2.3130	2.1671	1.7961	1.1466
	R1	2.2747	2.1650	1.8084	1.1499
	T2	2.2829	2.1448	1.7943	1.1249
	R2	2.2479	2.1432	1.8018	1.1319
1.0	T1	2.9960	2.7871	2.2804	1.3843
	R1	2.9648	2.8053	2.3090	1.4059
	T2	2.9925	2.7862	2.2776	1.3849
	R2	2.9621	2.8037	2.3065	1.4053

[†]T1, triangular element mesh with $\Delta t = 0.1$; T2, triangular element mesh with $\Delta t = 0.05$; R1, rectangular element mesh with $\Delta t = 0.1$; R2, rectangular element mesh with $\Delta t = 0.05$. In all cases, $\alpha = 0.5$.

8.6.3 Hyperbolic Equations

The transverse motion of a membrane, for example, is governed by the partial differential equation of the form,

$$c \frac{\partial^2 u}{\partial t^2} - \frac{\partial}{\partial x} \left(a_{11} \frac{\partial u}{\partial x} \right) - \frac{\partial}{\partial y} \left(a_{22} \frac{\partial u}{\partial y} \right) + a_0 u = f(x, y, t) \quad (8.6.14a)$$

where $u(x, y, t)$ denotes the transverse deflection, c the material density of the membrane, a_{11} and a_{22} are the tensions in the x and y directions of the membrane, a_0 is the modulus of elastic foundation on which the membrane is stretched (often $a_0 = 0$, i.e., there is no foundation), and $f(x, y, t)$ is the transversely distributed force. Equation (8.6.14a) is known as the *wave equation* and is classified mathematically as an hyperbolic equation. The function u must be determined such that it satisfies (8.6.14a) in a region Ω and the following boundary and initial conditions:

$$u = \hat{u} \quad \text{on } \Gamma \quad \text{or} \quad q_n = \hat{q}_n \quad \text{on } \Gamma \quad (t \geq 0) \quad (8.6.14b)$$

$$u(x, y, 0) = u_0(x, y), \quad \frac{\partial u}{\partial t}(x, y, 0) = v_0(x, y) \quad (8.6.14c)$$

where \hat{u} and \hat{q}_n are specified boundary values of u and q_n [see (8.6.2b)], and u_0 and v_0 are specified initial values of u and its time derivative, respectively.

The weak form of (8.6.14a) and (8.6.14b) over a typical element Ω_e is similar to that of (8.6.1) [see Eq. (8.6.4)], except that here we have the second time derivative of u :

$$0 = \int_{\Omega_e} \left[v \left(c \frac{\partial^2 u}{\partial t^2} + a_0 u - f \right) + a_{11} \frac{\partial v}{\partial x} \frac{\partial u}{\partial x} + a_{22} \frac{\partial v}{\partial y} \frac{\partial u}{\partial y} \right] dx dy - \oint_{\Gamma_e} q_n v ds \quad (8.6.15)$$

where $v = v(x, y)$ is the weight function.

The semidiscrete finite element model is obtained by substituting the finite element approximation (8.6.5) for u and $v = \psi_i$ into (8.6.15):

$$0 = \sum_{j=1}^n \left(M_{ij}^e \frac{d^2 u_j^e}{dt^2} + K_{ij}^e u_j^e \right) - f_i^e - Q_i^e \quad (8.6.16a)$$

or, in matrix form, we have

$$[M^e]\{\ddot{u}^e\} + [K^e]\{u^e\} = \{f^e\} + \{Q^e\} \quad (8.6.16b)$$

The coefficients M_{ij}^e , K_{ij}^e , and f_i^e are the same as those in (8.6.6c).

Eigenvalue Analysis

The problem of finding $u_j(t) = U_j e^{-i\omega t}$ ($i = \sqrt{-1}$) such that (8.6.16a) and (8.6.16b) hold for homogeneous boundary and initial conditions and $f = 0$ is called an eigenvalue problem associated with (8.6.14a). We obtain,

$$(-\omega^2[M^e] + [K^e])\{u^e\} = \{Q^e\} \quad (8.6.17)$$

The eigenvalues ω^2 and eigenfunctions $\sum_j^n U_j \psi_j(x, y)$ are determined from the assembled equations associated with (8.6.17), after imposing the homogeneous boundary conditions.

For a membrane problem, ω denotes the frequency of natural vibration. The number of eigenvalues of the discrete system (8.6.17) of the problem is equal to the number of unknown nodal values of U in the mesh.

Example 8.6.3 (Natural Vibration Analysis)

Consider the free vibrations of a homogeneous-material rectangular membrane of dimension a by b (in ft.), material density ρ (in slugs/ft.²), and fixed on all its edges, i.e., $u = 0$ on Γ . Although the problem has symmetry about the center horizontal line and center vertical lines of the domain (see Fig. 8.6.4), use of any symmetry in the finite element analysis will eliminate the unsymmetric modes of vibration of the membrane. For example, if we consider a quadrant of the domain in the finite element analysis, the frequencies ω_{mn} ($m, n \neq 1, 3, 5, \dots$) and associated eigenfunctions will be missed in the results [i.e., we can only obtain ω_{mn} ($m, n = 1, 3, 5, \dots$)]. By considering the full domain, the first N frequencies allowed by the mesh can be computed, where N is the number of unknown nodal values in the mesh.

If only the first eigenvalue ω_{11} is of interest or only symmetric frequencies are required, we can use a quadrant of the domain in the analysis. Indeed, results of Example 8.6.1 are applicable here, with $\lambda_{mn} = \omega_{mn}^2$. The results presented in Table 8.6.1 can be interpreted as the squares of the symmetric natural frequencies of a square $a = b = 2$ membrane with $\rho = 1$ and $a_{11} = a_{22} \equiv T = 1$. The exact natural frequencies of a rectangular membrane of dimension a by b , with tensions $a_{11} = a_{22} = T$ and density ρ are:

$$\omega_{mn} = \pi \sqrt{\frac{T}{\rho} \sqrt{\frac{m^2}{a^2} + \frac{n^2}{b^2}}} \quad (m, n = 1, 2, \dots)$$

To obtain all the frequencies, the full domain must be modeled.

Table 8.6.4 contains the first nine frequencies of a rectangular membrane of 4 ft. by 2 ft., tension $T = 12.5$ lb/ft., and density $\rho = 2.5$ slugs/ft.², as computed using various meshes of linear triangular and rectangular elements in the total domain. The convergence of the finite element results to the analytical solution is clear. The accuracy of frequencies associated with the symmetric modes is the same when $(n/2) \times (n/2)$ mesh used in a quadrant as when $n \times n$ mesh is used the total domain. The mesh of linear rectangular element yields more accurate results compared with the mesh of linear triangular elements.

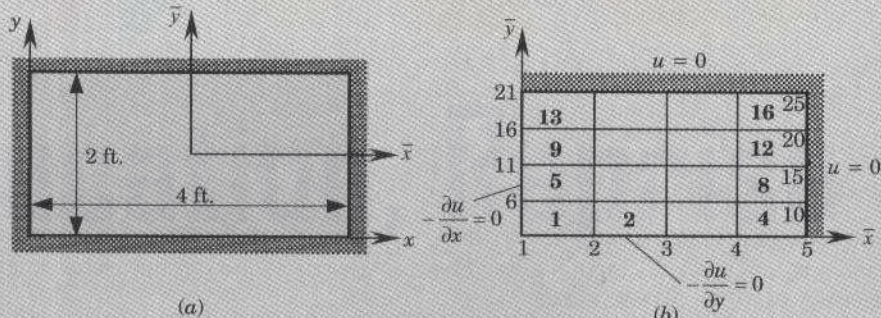


Figure 8.6.4 Analysis of a rectangular membrane: (a) actual geometry and (b) computational domain with finite element mesh of rectangular elements and boundary conditions (4×4 mesh of linear elements or 2×2 mesh of nine-node quadratic elements).

Table 8.6.4 Comparison of natural frequencies computed using various meshes of linear triangular and rectangular elements with the analytical solution of a rectangular membrane fixed on all its sides ($a_{11} = a_{22} = 12.5$, $\rho = T = 2.5$).

ω_{mn}	Triangular (linear)			Rectangular (linear)			Analytical
	2×2	4×4	8×8	2×2	4×4	8×8	
ω_{11}	5.0000	4.2266	4.0025	4.3303	4.0285	3.9522	3.9270
ω_{21}	—	5.9083	5.2068	—	5.2899	5.0478	4.9673
ω_{31}	—	8.2392	6.8788	—	7.2522	6.6020	6.3321
ω_{12}	—	8.3578	7.5271	—	7.9527	7.4200	7.2410
ω_{22}	—	10.0618	8.4565	—	8.6603	8.0571	7.8540
ω_{41}	—	12.1021	8.8856	—	9.9805	8.5145	7.8540
ω_{32}	—	13.2011	9.9280	—	12.7157	9.1117	8.7810
ω_{51}	—	14.6942	11.1193	—	13.1700	10.5797	9.4574
ω_{42}	—	15.8117	11.4425	—	14.0734	10.7280	9.9346

Transient Analysis

The hyperbolic equation (8.6.16b) can be reduced to a system of algebraic equations by approximating the second-order time derivative. As discussed in Section 6.2, the Newmark time integration schemes are the most commonly used ones in structural dynamics. Since Eq. (8.6.16b) is a special case (with $[C] = [0]$) of Eq. (6.2.28a), the results in Eqs. (6.2.38)–(6.2.40) hold with $[C] = [0]$. For ready reference, the main results are summarized here.

Newmark's Scheme

$$\begin{aligned}\{u\}_{s+1} &= \{u\}_s + \Delta t \{\dot{u}\}_s + \frac{(\Delta t)^2}{2} \{\ddot{u}\}_{s+\gamma} \\ \{\dot{u}\}_{s+1} &= \{\dot{u}\}_s + \Delta t \{\ddot{u}\}_{s+\alpha} \\ \{\ddot{u}\}_{s+\theta} &= (1 - \theta) \{\ddot{u}\}_s + \theta \{\ddot{u}\}_{s+1}\end{aligned}\quad (8.6.18a)$$

where

$$\alpha = \frac{1}{2}, \gamma = \frac{1}{2} : \text{ constant-average acceleration method (stable scheme)}$$

$$\alpha = \frac{1}{2}, \gamma = \frac{1}{3} : \text{ linear acceleration method (conditionally stable)} \quad (8.6.18b)$$

$$\alpha = \frac{1}{2}, \gamma = 0 : \text{ central difference method (conditionally stable)}$$

Stability Criterion

$$\Delta t < \Delta t_{\text{cri}} = \left[\frac{1}{2} \omega_{\max}^2 (\alpha - \gamma) \right]^{-\frac{1}{2}}, \quad \alpha \geq \frac{1}{2}, \quad \gamma < \alpha \quad (8.6.19)$$

where ω_{\max}^2 is the maximum eigenvalue of the corresponding discrete eigenvalue problem (8.6.17) (i.e., the same mesh and element type used in the transient analysis must be used in the eigenvalue analysis). Note that a more refined mesh will yield a higher maximum eigenvalue and a lower Δt_{cri} .

Time Marching Scheme

$$[\hat{K}^e]_{s+1}\{u^e\}_{s+1} = \{\hat{F}^e\}_{s+1} \quad (8.6.20a)$$

where (the superscript e is omitted for brevity in the following),

$$[\hat{K}]_{s+1} = [K]_{s+1} + a_3[M]_{s+1}$$

$$\{\hat{F}\}_{s,s+1} = \{F\}_{s+1} + [M]_{s+1}(a_3\{u\}_s + a_4\{\dot{u}\}_s + a_5\{\ddot{u}\}_s) \quad (8.6.20b)$$

$$a_3 = \frac{2}{\gamma(\Delta t)^2}, \quad a_4 = \Delta t a_3, \quad a_5 = \frac{1}{\gamma} - 1$$

Once $\{u\}_{s+1}$ is calculated from (8.6.20a), the velocities and accelerations at time $t_{s+1} = \Delta t(s+1)$ are calculated from

$$\begin{aligned} \{\ddot{u}\}_{s+1} &= a_3(\{u\}_{s+1} - \{u\}_s) - a_4\{\dot{u}\}_s - a_5\{\ddot{u}\}_s \\ \{\dot{u}\}_{s+1} &= \{\dot{u}\}_s + a_2\{\ddot{u}\}_s + a_1\{\ddot{u}\}_{s+1} \\ a_1 &= \alpha \Delta t, \quad a_2 = (1 - \alpha) \Delta t \end{aligned} \quad (8.6.21)$$

For the centered difference scheme ($\gamma = 0$), the alternative formulation of Problem 6.23 must be used.

Note that (8.6.20a) is valid for an element. Therefore, operations indicated in (8.6.20b) are carried out for an element, and $[\hat{K}^e]$ and $\{\hat{F}^e\}$ are assembled as in a static analysis. For the first time step, the initial conditions on u and $\partial u / \partial t$ are used to compute $\{u\}_0$ and $\{\dot{u}\}_0$ for each element of the entire mesh. The acceleration vector $\{\ddot{u}\}_0$ is computed from (8.6.16b) at $t = 0$:

$$\{\ddot{u}\}_0 = [M]^{-1}(\{F\}_0 - [K]\{u\}_0) \quad (8.6.22)$$

Often, it is assumed that $\{F\}_0 = \{0\}$. If the initial conditions are zero, $\{u\}_0 = \{0\}$, and the applied force is assumed to be zero at $t = 0$, we then take $\{\ddot{u}\}_0 = \{0\}$.

Example 8.6.4 (Transient Analysis)

Consider a homogeneous rectangular membrane of sides $a = 4$ ft. and $b = 2$ ft. fixed on all its four edges. Assume that the tension in the membrane is 12.5 lb/ft. (i.e., $a_{11} = a_{22} = 12.5$) and the density is $\rho = c = 2.5$ slugs/ft.². The initial deflection of the membrane is assumed to be

$$u_0(x, y) = 0.1(4x - x^2)(2y - y^2) \quad (8.6.23)$$

and the initial velocity is $v_0 = 0$. We wish to determine the deflection $u(x, y, t)$ of the membrane as a function of time using the finite element method. The analytical solution of this problem

is [see Kreyszig (1988), p. 684)],

$$u(x, y, t) = \frac{409.6}{\pi^6} \sum_{m,n=1,3,\dots} \frac{1}{m^3 n^3} \cos \omega_{mn} t \sin \frac{m\pi x}{4} \sin \frac{n\pi y}{2} \quad (8.6.24a)$$

$$\omega_{mn} = \frac{\pi}{4} \sqrt{5(m^2 + 4n^2)} \quad (8.6.24b)$$

where the origin of the (x, y) coordinate system is located at the lower corner of the domain [see Fig. 8.6.4(a)].

In the finite element analysis, we can utilize the biaxial symmetry of the problem and model one quadrant of the domain [see Fig. 8.6.4(b)]. We set up a new coordinate system (\bar{x}, \bar{y}) for the computational domain. The initial displacement in the new coordinates is given by (8.6.23) with x and y replaced in terms of \bar{x} and \bar{y} : $x = \bar{x} + 2$, $y = \bar{y} + 1$. The initial values of \bar{u} are calculated using (8.6.22) with $\{F\}_0 = \{0\}$ and $\{u\}_0$ as given in (8.6.23) by $u_0(x, y)$. At $\bar{x} = 2$ and $\bar{y} = 1$, all nodal values for the function u and its time derivatives are zero.

As for the critical time step, we calculate λ_{\max} from the solution of (8.6.17) using the same mesh as that used for the transient analysis and then use (8.6.19) to compute Δt_{cri} . Of course, for $\alpha = \frac{1}{2}$ and $\gamma = \frac{1}{2}$, there is no restriction on the time step for a stable solution. For a 4×4 mesh of linear rectangular elements in a quadrant, the maximum eigenvalue is found to be $\lambda_{\max} = 1072.68$, which yields $\Delta t_{\text{cri}} = 0.1058$ for the linear acceleration scheme ($\alpha = 0.5$, $\gamma = \frac{1}{3}$).

Stability characteristics of the solutions computed using the constant-average acceleration ($\alpha = 0.5$, $\gamma = 0.5$) and linear acceleration ($\alpha = 0.5$, $\gamma = \frac{1}{3}$) schemes for $\Delta t = 0.25 > \Delta t_{\text{cri}}$ are shown in Fig. 8.6.5. Plots of the center deflection $u(0, 0, t)$ versus time t are shown in Fig. 8.6.6. The finite element solutions are in good agreement with the analytical solution (8.6.24a) and (8.6.24b).

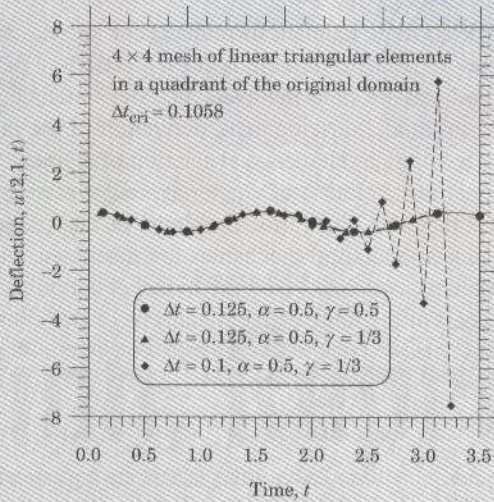


Figure 8.6.5 Stability characteristics of the constant-average acceleration and linear acceleration schemes (a 4×4 mesh of linear rectangular elements is used in a quadrant of the domain).

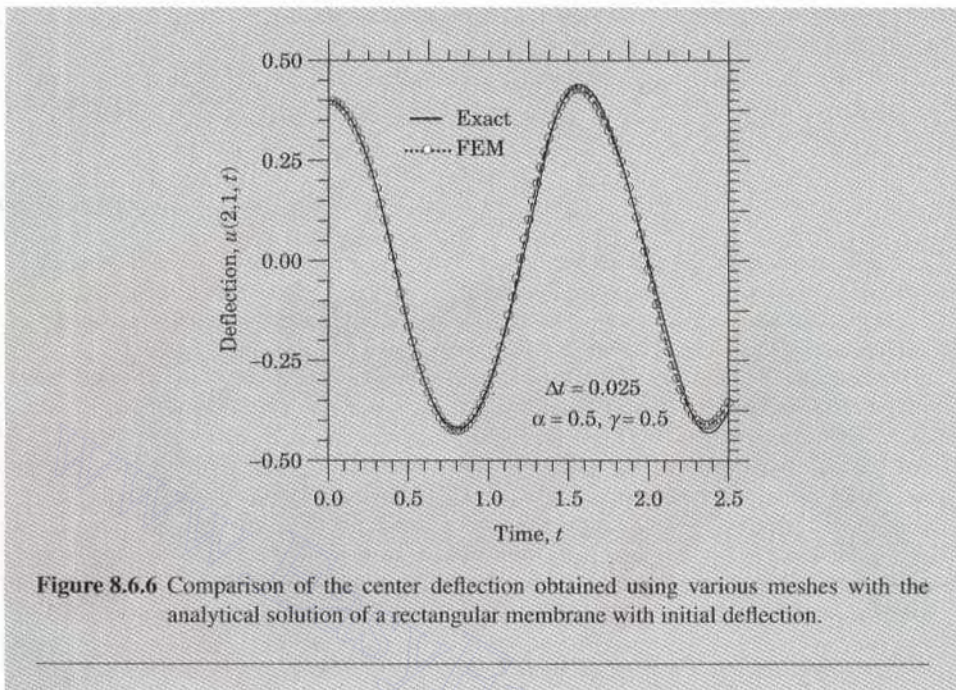


Figure 8.6.6 Comparison of the center deflection obtained using various meshes with the analytical solution of a rectangular membrane with initial deflection.

8.7 SUMMARY

A step by step procedure for finite element formulation of second-order equations in two dimensions with a single dependent variable is presented. The Poisson equation in two dimensions is used to illustrate the steps involved. The steps include: weak formulation of the equation, finite element model development, derivation of the interpolation functions for linear triangular and rectangular elements, evaluation of element matrices and vectors, assembly of element equations, solution of equations, and postcomputation of the gradient of the solution. A number of illustrative problems of heat transfer (conduction and convection), fluid mechanics, and solid mechanics are discussed. Finally, the eigenvalue and time-dependent problems associated with the model equation are also discussed. This chapter constitutes the heart of the finite element analysis of two-dimensional problems in Chapters 10–12.

PROBLEMS

Note: Most problems require some formulative effort (sketching a mesh when it is not given, calculations of element matrices and source vectors in some cases, assembling equations, identifying the boundary conditions in terms of the nodal variables, writing condensed equations, and so on). In some cases, a complete solution is required. When the problem size is large, essential steps of setting up the problem are required. Many of these problems will be solved by FEM2D in Chapter 13.

- 8.1 For a linear triangular element, show that

$$\sum_{i=1}^3 \alpha_i^e = 2A_e, \quad \sum_{i=1}^3 \beta_i^e = 0, \quad \sum_{i=1}^3 \gamma_i^e = 0$$

$$\alpha_i^e + \beta_i^e \hat{x}^e + \gamma_i^e \hat{y}^e = \frac{2}{3} A_e \text{ for any } i$$

where

$$\hat{x}^e = \sum_{i=1}^3 x_i^e, \quad \hat{y}^e = \sum_{i=1}^3 y_i^e$$

and (x_i^e, y_i^e) are the coordinates of the i th node of the element ($i = 1, 2, 3$).

- 8.2 Consider the partial differential equation over a typical element Ω_e with boundary Γ_e

$$-\nabla^2 u + cu = 0 \quad \text{in } \Omega_e, \quad \text{with} \quad \frac{\partial u}{\partial n} + \beta u = q_n \quad \text{on } \Gamma_e$$

Develop the weak form and finite element model of the equation over an element Ω_e .

- 8.3 Assuming that c and β are constant in Problem 8.2, write the element coefficient matrix and source vector for a linear (a) rectangular element and (b) triangular element.
- 8.4 Calculate the linear interpolation functions for the linear triangular and rectangular elements shown in Fig. P8.4. Answer: (a) $\psi_1 = (12.25 - 2.5x - 1.5y)/8.25$.

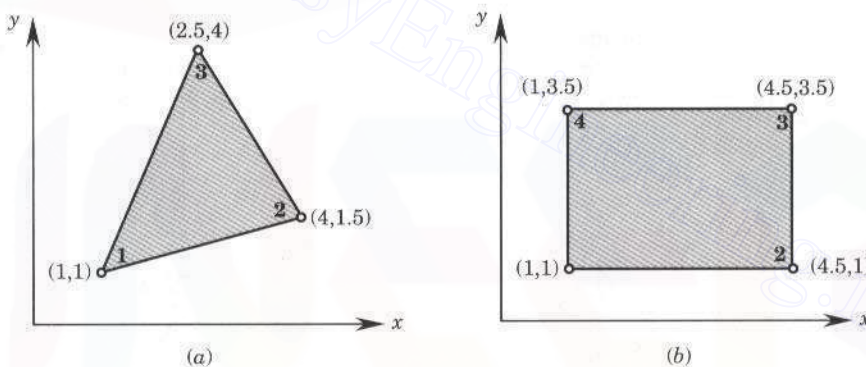


Figure P8.4

- 8.5 The nodal values of a triangular element in the finite element analysis of a field problem, $-\nabla^2 u = f_0$, are:

$$u_1 = 389.79, \quad u_2 = 337.19, \quad u_3 = 395.08$$

The interpolation functions of the element are given by

$$\psi_1 = \frac{1}{8.25}(12.25 - 2.5x - 1.5y), \quad \psi_2 = \frac{1}{8.25}(-1.5 + 3x - 1.5y)$$

$$\psi_3 = \frac{1}{8.25}(-2.5 - 0.5x + 3y)$$

506 AN INTRODUCTION TO THE FINITE ELEMENT METHOD

- (a) Find the component of the flux in the direction of the vector $4\hat{i} + 3\hat{j}$ at $x = 3$ and $y = 2$.
- (b) A point source of magnitude Q_0 is located at point $(x_0, y_0) = (3, 2)$ inside the triangular element. Determine the contribution of the point source to the element source vector. Express your answer in terms of Q_0 .
- 8.6** The nodal values of an element in the finite element analysis of a field problem $-\nabla^2 u = f_0$ are $u_1 = 389.79$, $u_2 = 337.19$, and $u_3 = 395.08$ (see Fig. P8.6). (a) Find the gradient of the solution, and (b) Determine where the 392 isoline intersects the boundary of the element in Fig. P8.6.
- Answer:* $\nabla u_h = 10.58\hat{e}_1 - 105.2\hat{e}_2$.

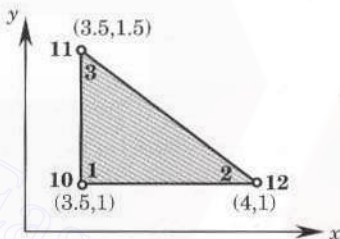


Figure P8.6

- 8.7** If the nodal values of the elements shown in Fig. P8.7 are $u_1 = 0.2645$, $u_2 = 0.2172$, and $u_3 = 0.1800$ for the triangular element and $u_1 = 0.2173$, $u_3 = 0.1870$, and $u_2 = u_4 = 0.2232$ for the rectangular element, compute u , $\partial u / \partial x$, and $\partial u / \partial y$ at the point $(x, y) = (0.375, 0.375)$.

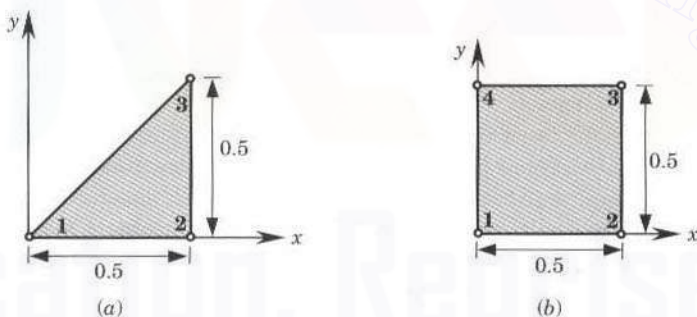


Figure P8.7

- 8.8** Compute the contribution of the pump 2 discharge to the nodes of element 43 in the groundwater flow problem of Example 8.5.4.
- 8.9** Find the coefficient matrix associated with the Laplace operator when the rectangular element in Fig. P8.9(a) is divided into two triangles by joining node 1 to node 3 [see Fig. P8.9(b)]. Compare the resulting matrix with that of the rectangular element in Eq. (8.2.54).

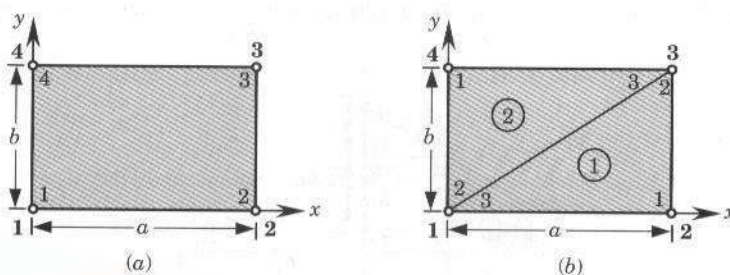


Figure P8.9

8.10 Compute the element matrices

$$S_{ij}^{01} = \int_0^a \int_0^b \psi_i \frac{d\psi_j}{dx} dx dy, \quad S_{ij}^{02} = \int_0^a \int_0^b \psi_i \frac{d\psi_j}{dy} dx dy$$

where $\psi_i(x, y)$ are the linear interpolation functions of a rectangular element with sides a and b .

8.11 Give the assembled coefficient matrix for the finite element meshes shown in Figs. P8.11(a) and P8.11(b). Assume one degree of freedom per node, and let $[K^e]$ denote the element coefficient matrix for the e th element. The answer should be in terms of element matrices K_{ij}^e .

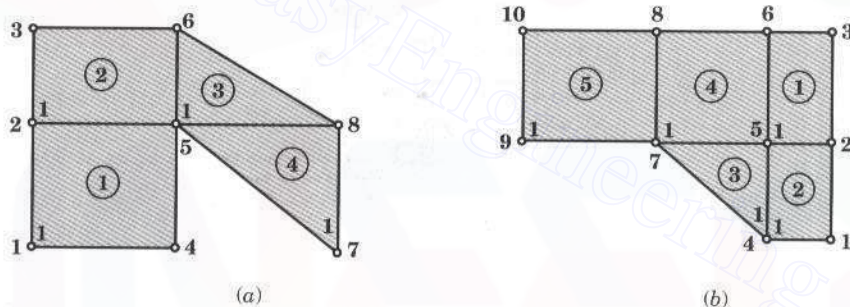


Figure P8.11

8.12 Repeat Problem 8.11 for the mesh shown in Fig. P8.12.

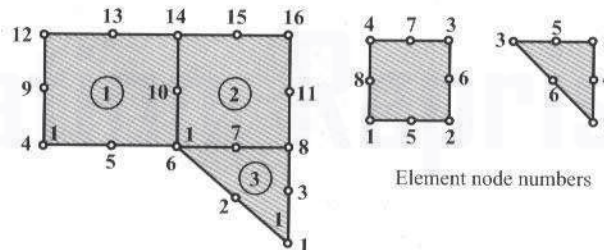


Figure P8.12

- 8.13 Compute the global source vector corresponding to the nonzero specified boundary flux for the finite element meshes of linear elements shown in Fig. P8.13.

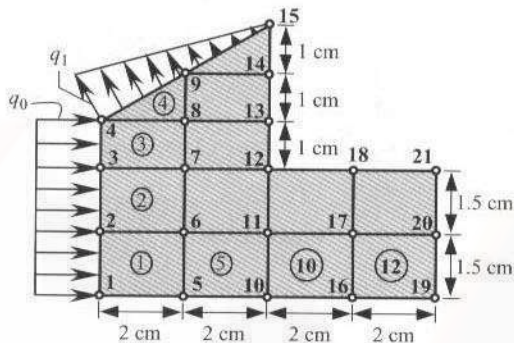


Figure P8.13

- 8.14 Repeat Problem 8.13 for the finite element mesh of quadratic elements shown in Fig. P8.14.

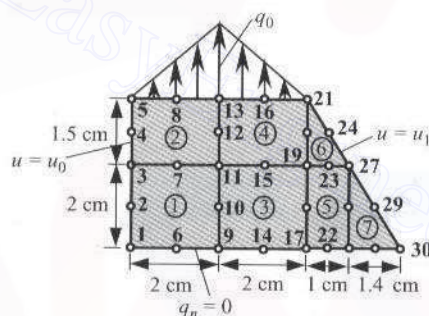


Figure P8.14

- 8.15 A line source of intensity q_0 is located across the triangular element shown in Fig. P8.15. Compute the element source vector.

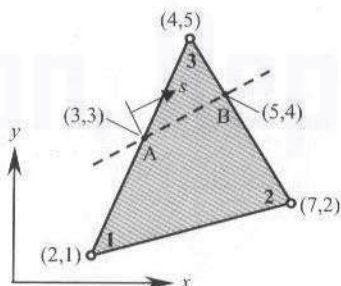


Figure P8.15

8.16 Repeat Problem 8.15 when the line source has varying source, $q(s) = q_0 s/L$, where s is the coordinate along the line source.

8.17 Consider the following partial differential equation governing the variable u :

$$c \frac{\partial u}{\partial t} - \frac{\partial}{\partial x} \left(a \frac{\partial u}{\partial x} \right) - \frac{\partial}{\partial y} \left(b \frac{\partial u}{\partial y} \right) - f_0 = 0$$

where c, a, b , and f_0 are constants. Assume an approximation of the form

$$u_h(x, y, t) = (1-x)y u_1(t) + x(1-y) u_2(t)$$

where u_1 and u_2 are nodal values of u at time t .

(a) Develop the fully discretized finite element model of the equation.

(b) Evaluate the element coefficient matrices and source vector for a square element of dimension 1 unit by 1 unit (so that the evaluation of the integrals is made easy).

Note: You should not be concerned with this nonconventional approximation of the dependent unknown but just use it as given to answer the question.

8.18 Solve the Laplace equation

$$-\left(\frac{\partial^2 u}{\partial x^2} + \frac{\partial^2 u}{\partial y^2}\right) = 0 \quad \text{in } \Omega$$

on a rectangle, when $u(0, y) = u(a, y) = u(x, 0) = 0$ and $u(x, b) = u_0(x)$. Use the symmetry and (a) a mesh of 2×2 triangular elements and (b) a mesh of 2×2 rectangular elements (see Fig. P8.18). Compare the finite element solution with the exact solution

$$u(x, y) = \sum_{n=1}^{\infty} A_n \sin \frac{n\pi x}{a} \sinh \frac{n\pi y}{b}$$

where

$$A_n = \frac{2}{a \sinh(n\pi b/a)} \int_0^a u_0(x) \sin \frac{n\pi x}{a} dx$$

Take $a = b = 1$, and $u_0(x) = \sin \pi x$ in the computations. For this case, the exact solution becomes

$$u(x, y) = \frac{\sin \pi x \sinh \pi y}{\sinh \pi}$$

Answer: For a 2×2 mesh of triangles, $U_4 = 0.23025$ and $U_5 = 0.16281$; for a 2×2 mesh of rectangles, $U_4 = 0.1520$ and $U_5 = 0.1075$.

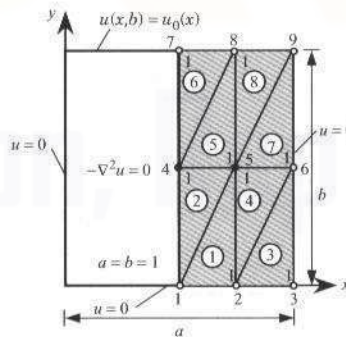


Figure P8.18

510 AN INTRODUCTION TO THE FINITE ELEMENT METHOD

- 8.19** Solve Problem 8.18 when $u_0(x) = 1$. The analytical solution is given by

$$u(x, y) = \frac{4}{\pi} \sum_{n=0}^{\infty} \frac{\sin(2n+1)\pi x \sinh(2n+1)\pi y}{(2n+1) \sinh(2n+1)\pi}$$

Answer: (a) $U_4 = 0.2647$ and $U_5 = 0.2059$.

- 8.20** Solve Problem 8.18 when $u_0(x) = 4(x - x^2)$. Answer: (a) $U_4 = 0.2353$ and $U_5 = 0.1691$; (b) $U_4 = 0.1623$ and $U_5 = 0.1068$

- 8.21** Solve the Laplace equation for the unit square domain and boundary conditions given in Fig. P8.21. Use one rectangular element.

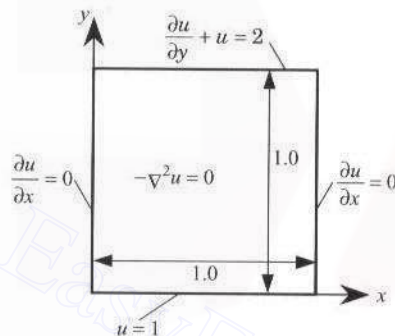


Figure P8.21

- 8.22** Use two triangular elements to solve the problem in Fig. P8.21. Use the mesh obtained by joining points $(1,0)$ and $(0,1)$.

- 8.23** Consider the steady-state heat transfer (or other phenomenon) in a square region shown in Fig. P8.23. The governing equation is given by

$$-\frac{\partial}{\partial x} \left(k \frac{\partial u}{\partial x} \right) - \frac{\partial}{\partial y} \left(k \frac{\partial u}{\partial y} \right) = f_0$$

The boundary conditions for the problem are:

$$u(0, y) = y^2, \quad u(x, 0) = x^2, \quad u(1, y) = 1 - y, \quad u(x, 1) = 1 - x$$

Assuming $k = 1$ and $f_0 = 2$, determine the unknown nodal value of u using the uniform 2×2 mesh of rectangular elements. Answer: $U_5 = 0.625$.

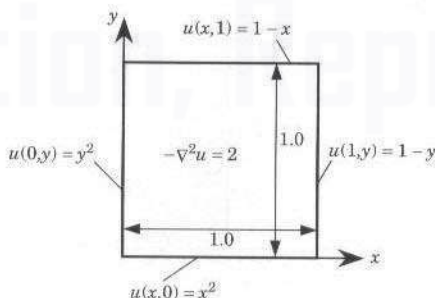


Figure P8.23

- 8.24** Solve Problem 8.23 using the mesh of a rectangle and two triangles, as shown in Fig. P8.24.
Answer: $U_5 = 0.675$.

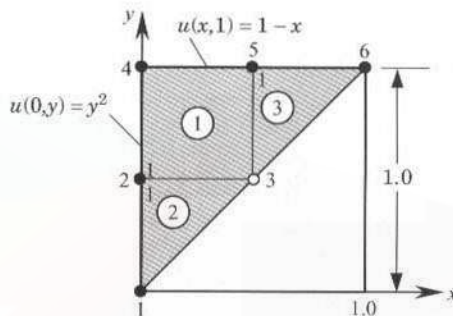


Figure P8.24

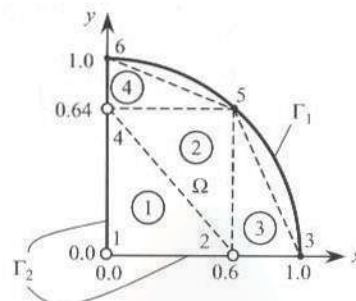


Figure P8.25

- 8.25** Solve the Poisson equation $-\nabla^2 u = 2$ in Ω , $u = 0$ on Γ_1 , $\partial u / \partial n = 0$ on Γ_2 , where Ω is the first quadrant bounded by the parabola $y = 1 - x^2$ and the coordinate axes (see Fig. P8.25), and Γ_1 and Γ_2 are the boundaries shown in Fig. P8.25.
- 8.26** Solve the axisymmetric field problem shown in Fig. P8.26 for the mesh shown there. Note that the problem has symmetry about any $z = \text{constant}$ line. Hence, the problem is essentially one dimensional. You are only required to determine the element matrix and source vector for element 1 and give the known boundary conditions on the primary and secondary variables.

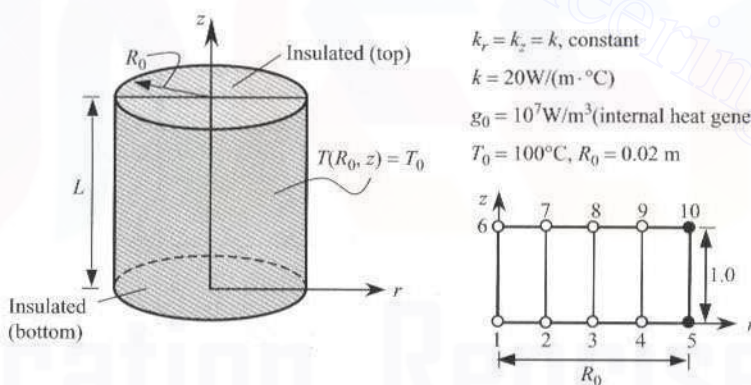


Figure P8.26

- 8.27** Formulate the axisymmetric field problem shown in Fig. P8.27 for the mesh shown. You are only required to give the known boundary conditions on the primary and secondary variables and compute the secondary variable at $r = R_0/2$ using equilibrium and the definition. Use the element at the left of the node.

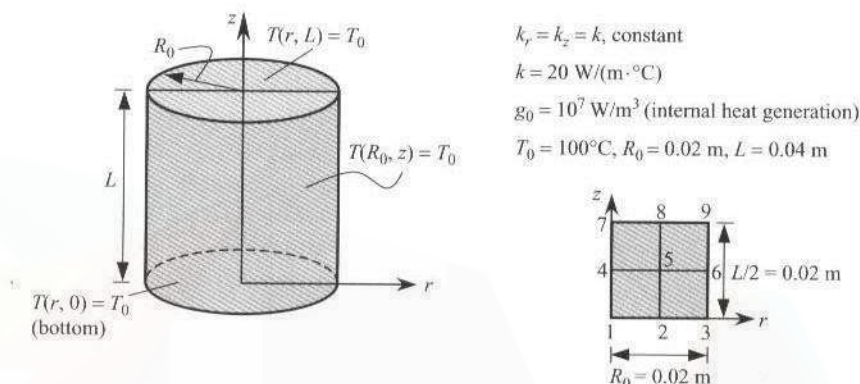


Figure P8.27

- 8.28** A series of heating cables have been placed in a conducting medium, as shown in Fig. P8.28. The medium has conductivities of $k_x = 10 \text{ W}/(\text{cm} \cdot ^\circ\text{C})$ and $k_y = 15 \text{ W}/(\text{cm} \cdot ^\circ\text{C})$, the upper surface is exposed to a temperature of -5°C , and the lower surface is bounded by an insulating medium. Assume that each cable is a point source of $250 \text{ W}/\text{cm}$. Take the convection coefficient between the medium and the upper surface to be $\beta = 5 \text{ W}/(\text{cm}^2 \cdot \text{K})$. Use a 8×8 mesh of linear rectangular (or triangular) elements in the computational domain (use any symmetry available in the problem), and formulate the problem (i.e., give element matrices for a typical element, give boundary conditions on primary and secondary variables, and compute convection boundary contributions).

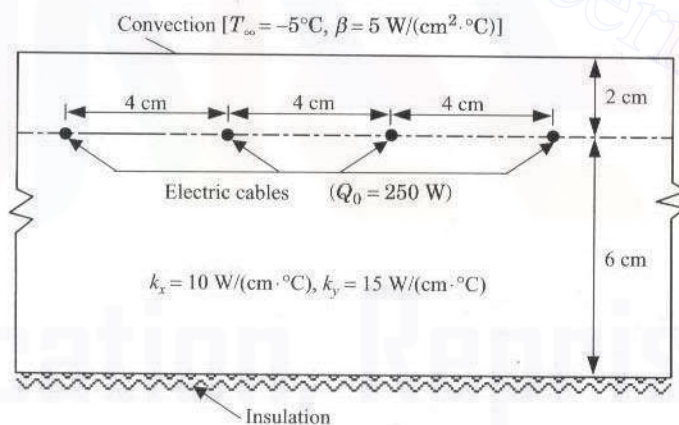


Figure P8.28

- 8.29** Formulate the finite element analysis information to determine the temperature distribution in the molded asbestos insulation shown in Fig. P8.29. Use the symmetry to identify a computational domain and give the specified boundary conditions at the nodes of the mesh. What is the connectivity of matrix for the mesh shown?

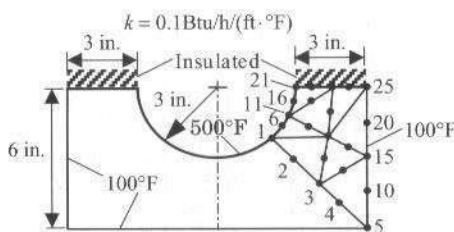


Figure P8.29

- 8.30 Consider steady-state heat conduction in a square region of side $2a$. Assume that the medium has conductivity of k (in $\text{W}/(\text{m} \cdot ^\circ\text{C})$) and uniform heat (energy) generation of g_0 (in W/m^3). For the boundary conditions and mesh shown in Fig. P8.30, write the finite element algebraic equations for nodes 1, 3, and 7.

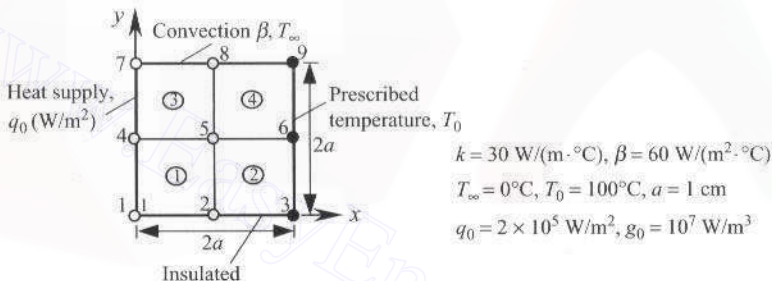


Figure P8.30

- 8.31 For the convection heat transfer problem shown in Fig. P8.31, write the four finite element equations for the unknown temperatures. Assume that the thermal conductivity of the material is $k = 5 \text{ W}/(\text{m} \cdot ^\circ\text{C})$, the convection heat transfer coefficient on the left surface is $\beta = 28 \text{ W}/(\text{m}^2 \cdot ^\circ\text{C})$, and the internal heat generation is zero. Compute the heats at nodes 2, 4 and 9 using (a) element equations (i.e., equilibrium), and (b) definition in Eq. (8.2.19b) (use the temperature field of elements 1 and 2).

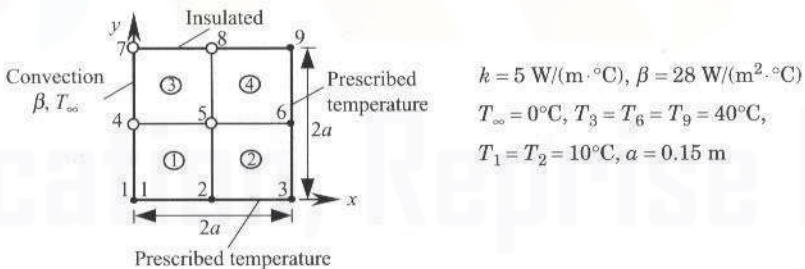


Figure P8.31

- 8.32 Write the finite element equations for the unknown temperatures of the problem shown in Fig. P8.32.

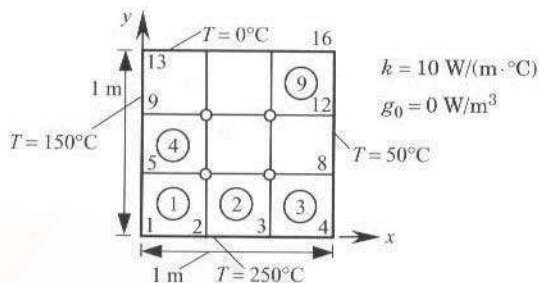


Figure P8.32

8.33 Write the finite element equations for the heats at nodes 1 and 13 of Problem 8.32. The answer should be in terms of the nodal temperatures T_1, T_2, \dots, T_{16} .

8.34 Write the finite element equations associated with nodes 13, 16, and 19 for the problem shown in Fig. P8.34.

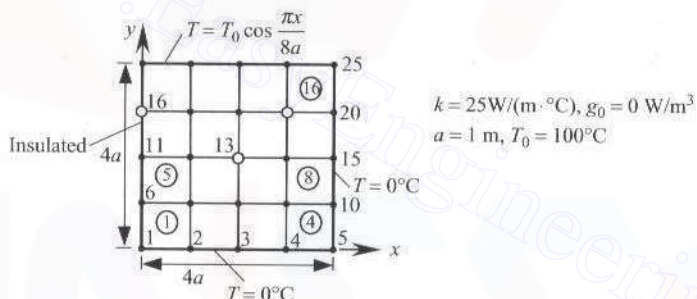


Figure P8.34

8.35 The fin shown in Fig. P8.35 has its base maintained at 300°C and exposed to convection on its remaining boundary. Write the finite element equations at nodes 7 and 10.

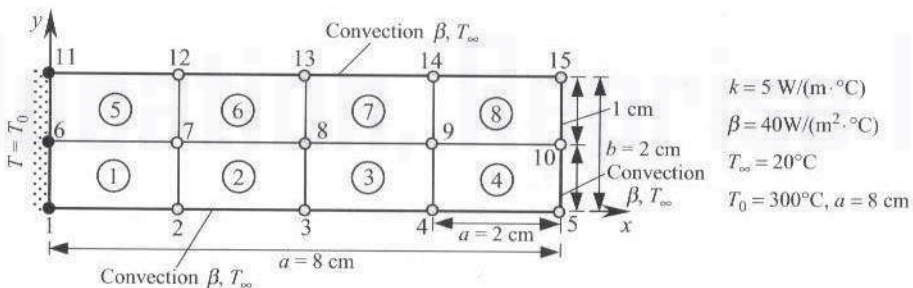


Figure P8.35

8.36 Compute the heat loss at nodes 10 and 13 of Problem 8.35.

- 8.37** Consider the problem of the flow of groundwater beneath a coffer dam. Solve the problem using the velocity potential formulation. The geometry and boundary conditions are shown in Fig. P8.37.

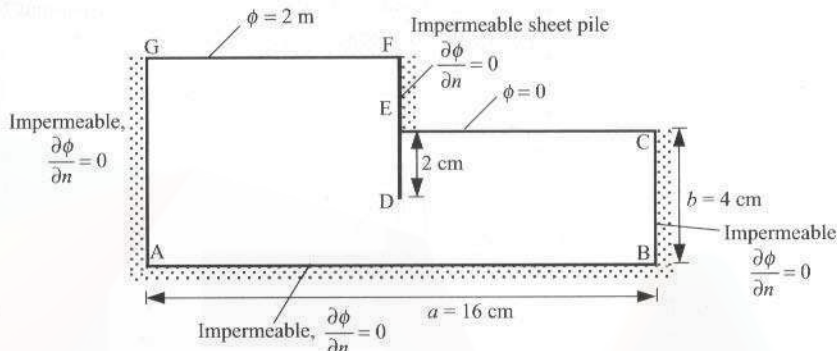


Figure P8.37

- 8.38** Formulate the groundwater flow problem of the domain shown in Fig. P8.38 for finite element analysis. The pump is located at $(x, y) = (787.5, 300)$ m.

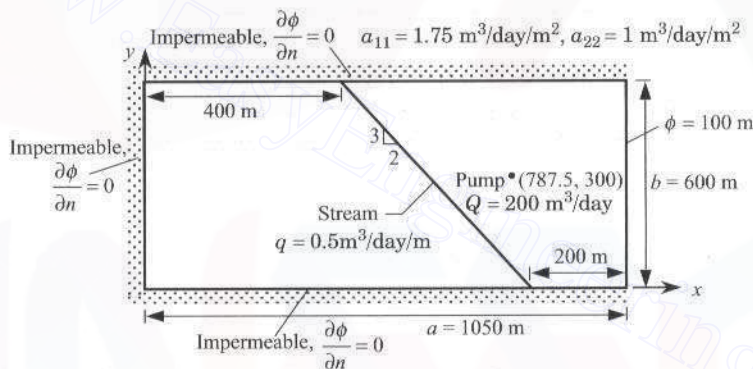


Figure P8.38

- 8.39** Repeat Problem 8.38 for the domain shown in Fig. P8.39.

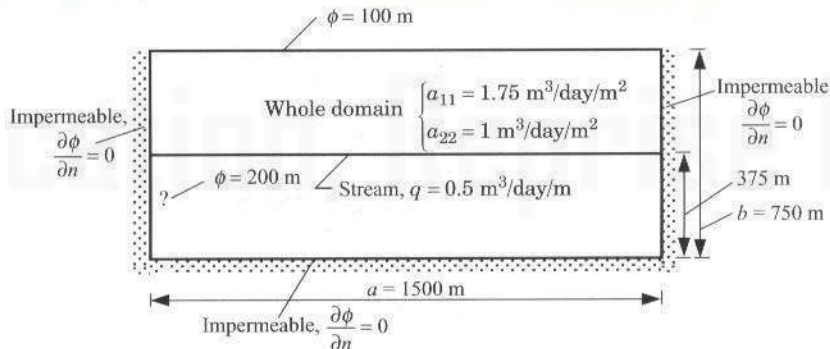


Figure P8.39

516 AN INTRODUCTION TO THE FINITE ELEMENT METHOD

- 8.40** Consider the steady confined flow through the foundation soil of a dam (see Fig. P8.40). Assuming that the soil is isotropic ($k_x = k_y$), formulate the problem for finite element analysis (identify the specified primary and secondary variables and their contribution to the nodes). In particular, write the finite element equations at nodes 8 and 11. Write the finite element equations for the horizontal velocity component in 5th and 10th elements.

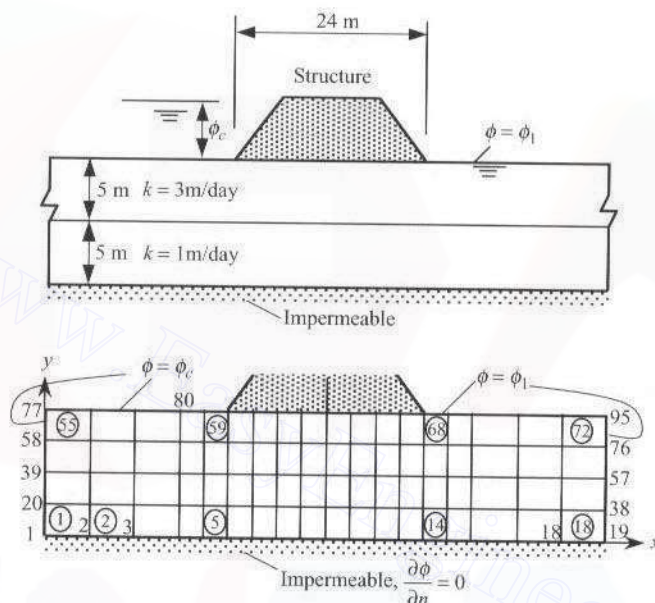


Figure P8.40

- 8.41** Formulate the problem of the flow about an elliptical cylinder using the (a) stream function and (b) velocity potential. The geometry and boundary conditions are shown in Fig. P8.41.

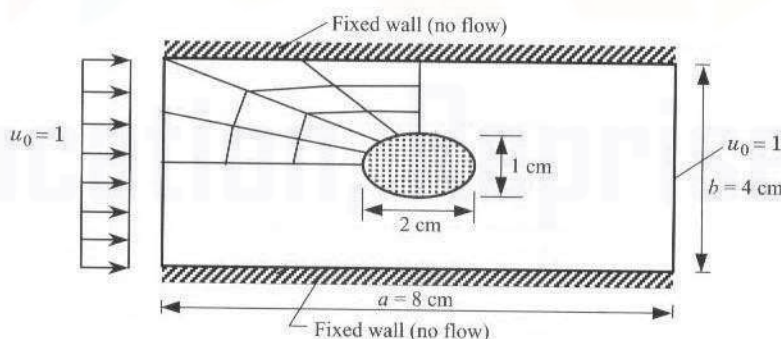


Figure P8.41

8.42 Repeat Problem 8.41 for the domain shown in Fig. P8.42.

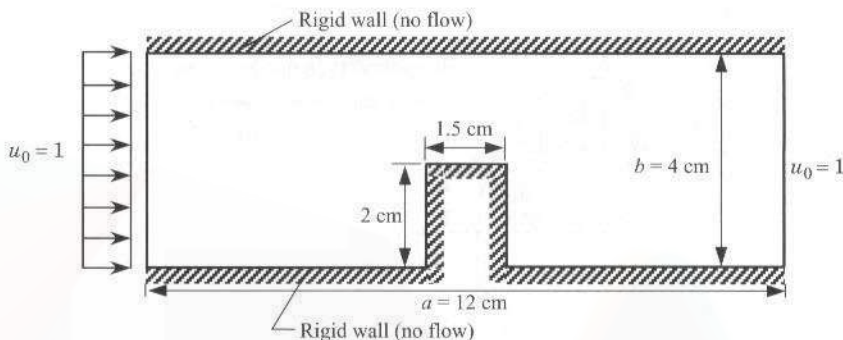


Figure P8.42

8.43 The Prandtl theory of torsion of a cylindrical member leads to

$$-\nabla^2 u = 2G\theta \quad \text{in } \Omega; \quad u = 0 \quad \text{on } \Gamma$$

where Ω is the cross section of the cylindrical member being twisted, Γ is the boundary of Ω , G is the shear modulus of the material of the member, θ is the angle of twist, and u is the stress function. Solve the equation for the case in which Ω is a circular section (see Fig. P8.43) using the mesh of linear triangular elements. Compare the finite element solution with the exact solution (valid for elliptical sections with axes a and b):

$$u = \frac{G\theta a^2 b^2}{a^2 + b^2} \left(1 - \frac{x^2}{a^2} - \frac{y^2}{b^2} \right)$$

Use $a = 1$, $b = 1$, and $f_0 = 2G\theta = 10$.

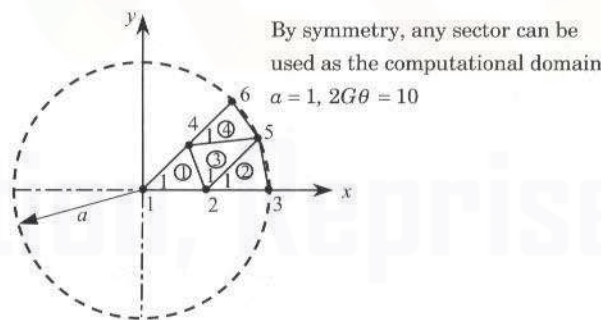


Figure P8.43

- 8.44** Repeat Problem 8.43 for an elliptical section member (see Fig. P8.44). Use $a = 1$ and $b = 1.5$.

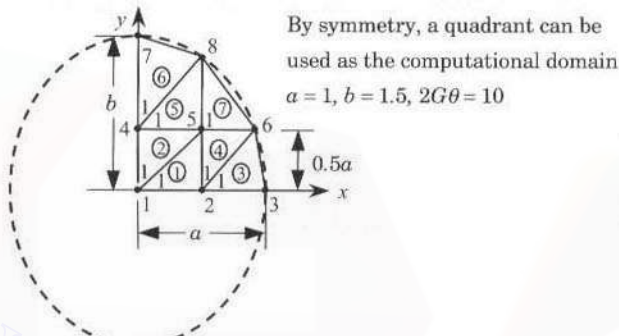


Figure P8.44

- 8.45** Repeat Problem 8.43 for the case in which Ω is an equilateral triangle (see Fig. P8.45). The exact solution is given by

$$u = -G\theta \left[\frac{1}{2}(x^2 + y^2) - \frac{1}{2a}(x^3 - 3xy^2) - \frac{2}{27}a^2 \right]$$

Take $a = 1$ and $f_0 = 2G\theta = 10$. Give the finite element equation for node 5.

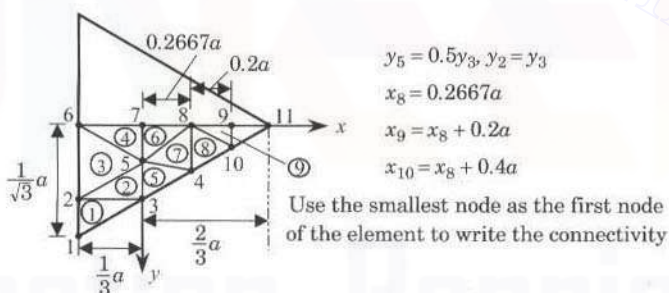


Figure P8.45

- 8.46** Consider the torsion of a hollow square cross-sectional member. The stress function Ψ is required to satisfy the Poisson equation in (8.5.60) and the following boundary conditions:

$$\Psi = 0 \quad \text{on the outer boundary; } \quad \Psi = 2r^2 \quad \text{on the inner boundary}$$

where r is the ratio of the outside dimension to the inside dimension, $r = 6a/2a$. Formulate the problem for finite element analysis using the mesh shown in Fig. P8.46.

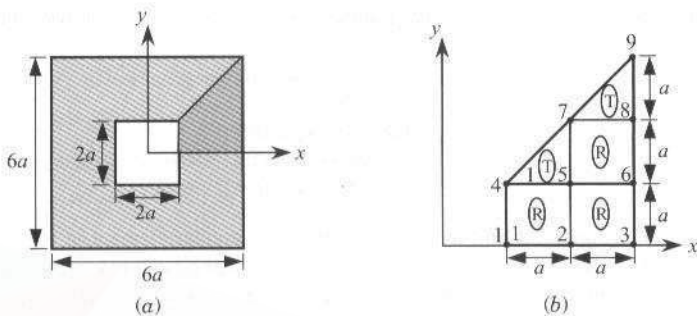


Figure P8.46

- 8.47** Repeat Problem 8.46 with the mesh of linear triangles [join nodes 1 and 5, 2 and 6, and 5 and 8 in Fig. P8.46(b)].
- 8.48** The membrane shown in Fig. P8.48 is subjected to uniformly distributed transverse load of intensity f_0 (in N/m²). Write the condensed equations for the unknown displacements.

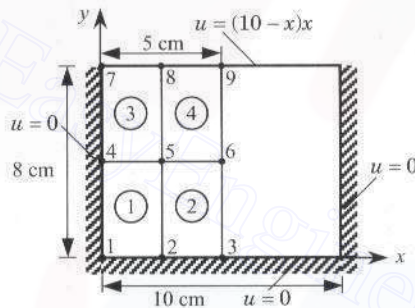


Figure P8.48

- 8.49** The circular membrane shown in Fig. P8.49 is subjected to uniformly distributed transverse load of intensity f_0 (in N/m²). Write the condensed equations for the unknown displacements.

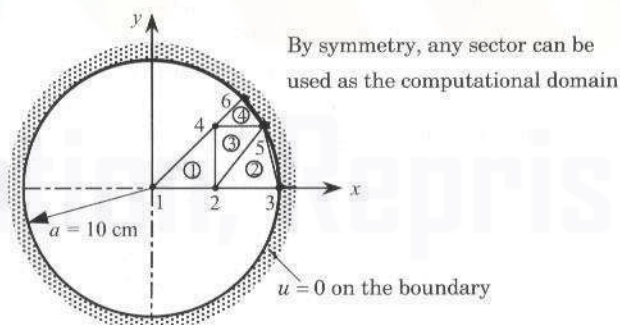


Figure P8.49

- 8.50** Determine the critical time step for the transient analysis (with $\alpha \leq \frac{1}{2}$) of the problem

$$\frac{\partial u}{\partial t} - \nabla^2 u = 1 \quad \text{in } \Omega; \quad u = 0 \quad \text{in } \Omega \text{ at } t = 0$$

by determining the maximum eigenvalue of the problem

$$-\nabla^2 u = \lambda u \quad \text{in } \Omega; \quad u = 0 \quad \text{on } \Gamma$$

The domain is a square of unit length. Use (a) one triangular element in the octant, (b) four linear elements in the octants, and (c) a 2×2 mesh of linear rectangular elements in a quadrant (see Fig. P8.50). Determine the critical time step for the forward difference scheme. Answer: (a) $\lambda = 24$. (b) $\lambda_{max} = 305.549$.

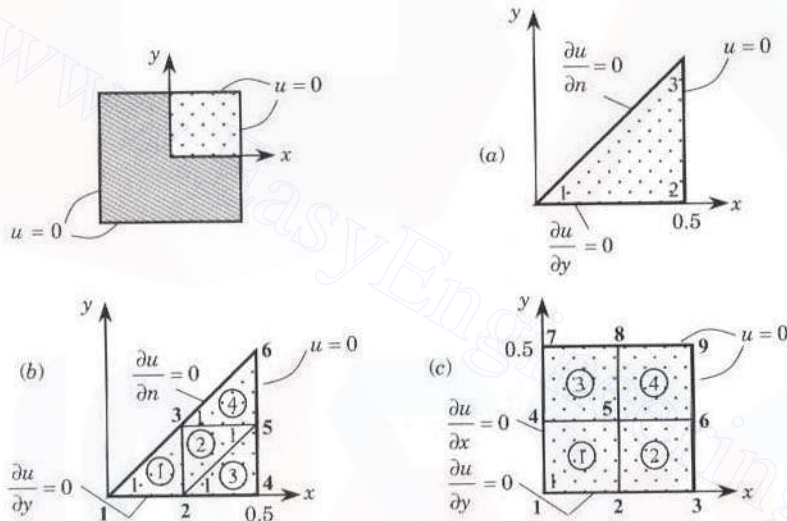


Figure P8.50

- 8.51** Set up the condensed equations for the transient problem in Problem 8.50 for the α -family of approximation. Use the mesh shown in Fig. P8.50(b).
- 8.52** Set up the condensed equations for the time-dependent analysis of the circular membrane in Problem 8.49.
- 8.53** Determine the fundamental natural frequency of the rectangular membrane in Problem 8.48.
- 8.54** Determine the critical time step based on the forward difference scheme for the time-dependent analysis of the circular membrane in Problem 8.49.
- 8.55** (*Central difference method*) Consider the following matrix differential equation in time:

$$[M]\{\ddot{U}\} + [C]\{\dot{U}\} + [K]\{U\} = \{F\}$$

where the superposed dot indicates differentiation with respect to time. Assume

$$\{\ddot{U}\}_n = \frac{1}{(\Delta t)^2} (\{U\}_{n-1} - 2\{U\}_n + \{U\}_{n+1}), \quad \{\dot{U}\}_n = \frac{1}{2(\Delta t)} (\{U\}_{n+1} - \{U\}_{n-1})$$

and derive the algebraic equations for the solution of $\{U\}_{n+1}$ in the form

$$[A]\{U\}_{n+1} = \{F\}_n - [B]\{U\}_n - [D]\{U\}_{n-1}$$

Define $[A]$, $[B]$, and $[D]$ in terms of $[M]$, $[C]$, and $[K]$.

8.56 Consider the first-order differential equation in time

$$a \frac{du}{dt} + bu = f$$

Using linear approximation, $u(t) = u_1\psi_1(t) + u_2\psi_2(t)$, $\psi_1 = 1 - t/\Delta t$, and $\psi_2 = t/\Delta t$, derive the associated algebraic equation and compare with that obtained using the α -family of approximation.

8.57 (*Space-time element*) Consider the differential equation

$$c \frac{\partial u}{\partial t} - \frac{\partial}{\partial x} \left(a \frac{\partial u}{\partial x} \right) = f \quad \text{for } 0 < x < L, \quad 0 \leq t \leq T$$

with

$$u(0, t) = u(L, t) = 0 \quad \text{for } 0 \leq t \leq T, \quad u(x, 0) = u_0(x) \quad \text{for } 0 < x < L$$

where $c = c(x)$, $a = a(x)$, $f = f(x, t)$, and u_0 are given functions. Consider the rectangular domain defined by

$$\Omega = \{(x, t) : 0 < x < L, \quad 0 \leq t \leq T\}$$

A finite element discretization of Ω by rectangles is a time-space rectangular element (with y replaced by t). Give a finite element formulation of the equation over a time-space element, and discuss the *mathematical/practical* limitations of such a formulation. Compute the element matrices for a linear element.

8.58 (*Space-time finite element*) Consider the time-dependent problem

$$\begin{aligned} \frac{\partial^2 u}{\partial x^2} &= c \frac{\partial u}{\partial t}, \quad \text{for } 0 < x < 1, \quad t > 0 \\ u(0, t) &= 0, \quad \frac{\partial u}{\partial x}(1, t) = 1, \quad u(x, 0) = x \end{aligned}$$

Use linear rectangular elements in the (x, t) -plane to model the problem. Note that the finite element model is given by $[K^e]\{u^e\} = \{Q^e\}$, where

$$K_{ij}^e = \int_0^{\Delta t} \int_{x_a}^{x_b} \left(\frac{\partial \psi_i^e}{\partial x} \frac{\partial \psi_j^e}{\partial x} + c \psi_i^e \frac{\partial \psi_j^e}{\partial t} \right) dx dt$$

$$Q_1^e = \left(- \int_0^{\Delta t} \frac{\partial u}{\partial x} dt \right) \Big|_{x=x_a}, \quad Q_2^e = \left(\int_0^{\Delta t} \frac{\partial u}{\partial x} dt \right) \Big|_{x=x_b}$$

8.59 The collocation time approximation methods are defined by the following relations:

$$\begin{aligned} \{\ddot{u}\}_{n+\alpha} &= (1 - \alpha)\{\ddot{u}\}_n + \alpha\{\ddot{u}\}_{n+1} \\ \{\dot{u}\}_{n+\alpha} &= \{\dot{u}\}_n + \alpha\Delta t[(1 - \gamma)\{\ddot{u}\}_n + \gamma\{\ddot{u}\}_{n+\alpha}] \\ \{u\}_{n+\alpha} &= \{u\}_n + \alpha\Delta t\{\dot{u}\}_n + \frac{\alpha(\Delta t)^2}{2} [(1 - 2\beta)\{\ddot{u}\}_n + 2\beta\{\ddot{u}\}_{n+\alpha}] \end{aligned}$$

The collocation scheme contains two of the well-known schemes: $\alpha = 1$ gives the Newmark's scheme; and $\beta = \frac{1}{6}$ and $\gamma = \frac{1}{2}$ gives the Wilson scheme. The collocation scheme is unconditionally stable, second-order accurate for the following values of the parameters:

$$\alpha \geq 1, \quad \gamma = \frac{1}{2}, \quad \frac{\alpha}{2(1+\alpha)} \geq \beta \geq \frac{2\alpha^2 - 1}{4(2\alpha^3 - 1)}$$

Formulate the algebraic equations associated with the matrix differential equation

$$[M]\{\ddot{u}\} + [C]\{\dot{u}\} + [K]\{u\} = \{F\}$$

using the collocation scheme.

8.60 Consider the following pair of coupled partial differential equations:

$$-\frac{\partial}{\partial x} \left(a \frac{\partial u}{\partial x} \right) - \frac{\partial}{\partial y} \left[b \left(\frac{\partial u}{\partial y} + \frac{\partial v}{\partial x} \right) \right] + \frac{\partial u}{\partial t} - f_x = 0 \quad (i)$$

$$-\frac{\partial}{\partial x} \left[b \left(\frac{\partial u}{\partial y} + \frac{\partial v}{\partial x} \right) \right] - \frac{\partial}{\partial y} \left(c \frac{\partial v}{\partial y} \right) + \frac{\partial v}{\partial t} - f_y = 0 \quad (ii)$$

where u and v are the dependent variables (unknown functions), a , b , and c are known functions of x and y , and f_x and f_y are known functions of position (x, y) and time t .

- (a) Use the three-step procedure on each equation with a different weight function for each equation (say, w_1 and w_2) to develop the (semidiscrete) weak form.
- (b) Assume finite element approximation of (u, v) in the following form

$$u(x, y) = \sum_{j=1}^n \psi_j(x, y) U_j(t), \quad v(x, y) = \sum_{j=1}^n \psi_j(x, y) V_j(t) \quad (iii)$$

and develop the (semidiscrete) finite element model in the form

$$0 = \sum_{j=1}^n M_{ij}^{11} \dot{U}_j + \sum_{j=1}^n K_{ij}^{11} U_j + \sum_{j=1}^n K_{ij}^{12} V_j - F_i^1 \quad (iv)$$

$$0 = \sum_{j=1}^n M_{ij}^{22} \dot{V}_j + \sum_{j=1}^n K_{ij}^{21} U_j + \sum_{j=1}^n K_{ij}^{22} V_j - F_i^2$$

You must define the algebraic form of the element coefficients K_{ij}^{11} , K_{ij}^{12} , F_i^1 etc.

- (c) Give the fully discretized finite element model of the model (in the standard form; you are not required to derive it).

REFERENCES FOR ADDITIONAL READING

1. Eskinazi, S., *Principles of Fluid Mechanics*, Allyn and Bacon, Boston, MA, 1962.
2. Holman, J. P., *Heat Transfer*, 6th ed., McGraw-Hill, New York, 1986.
3. Kohler, W. and Pitt, J., "Calculation of Transient Temperature Fields with Finite Elements in Space and Time Dimensions," *International Journal for Numerical Methods in Engineering*, **8**, 625–631, 1974.
4. Kreyszig, E., *Advanced Engineering Mathematics*, 6th ed., John Wiley, New York, 1988.
5. Mikhlin, S. G., *Variational Methods in Mathematical Physics*, (translated from the Russian by T. Boddington), Pergamon Press, Oxford, UK, 1964.

6. Mikhlin, S. G., *The Numerical Performance of Variational Methods*, (translated from the Russian by R. S. Anderssen), Wolters-Noordhoff, The Netherlands, 1971.
7. Oden, J. T. and Reddy, J. N., *Variational Methods in Theoretical Mechanics*, 2nd ed., Springer-Verlag, Berlin, 1983.
8. Özisik, M. N., *Heat Transfer A Basic Approach*, McGraw-Hill, New York, 1985.
9. Reddy, J. N., *Applied Functional Analysis and Variational Methods in Engineering*, McGraw-Hill, New York, 1986; reprinted by Krieger, Melbourne, FL, 1991.
10. Reddy, J. N., *Energy Principles and Variational Methods in Applied Mechanics*, 2nd ed., John Wiley, New York, 2002.
11. Reddy, J. N. and Rasmussen, M. L., *Advanced Engineering Analysis*, John Wiley, New York, 1982; reprinted by Krieger, Melbourne, FL, 1990.
12. Rektorys, K., *Variational Methods in Mathematics, Science and Engineering*, D. Reidel Publishing Co., Boston, MA, 1980.
13. Schlichting, H., *Boundary-Layer Theory* (translated by J. Kestin), 7th ed., McGraw-Hill, New York, 1979.
14. Sobey, R. J., "Hermitian Space-Time Finite Elements for Estuarine Mass Transport," *International Journal for Numerical Methods in Fluids*, 2, 277–297, 1982.
15. Timoshenko, S. P. and Goodier, J. N., *Theory of Elasticity*, 3rd ed., McGraw-Hill, New York, 1970.
16. Ugural, A. C. and Fenster, S. K., *Advanced Strength and Applied Elasticity*, 4th ed., Prentice Hall, Upper Saddle River, NJ, 2003.

Chapter 9

INTERPOLATION FUNCTIONS, NUMERICAL INTEGRATION, AND MODELING CONSIDERATIONS

9.1 INTRODUCTION

In the previous chapter we studied the finite element analysis of a model second-order equation and its analogues in the fields of heat transfer, fluid mechanics, and solid mechanics. As part of this study we developed the interpolation functions for the basic elements, namely, the linear triangular and rectangular elements. These elements, which were developed in connection with the finite element analysis of a second-order partial differential equation in a single variable, are useful in all finite element models that admit Lagrange interpolation of the primary variables of the weak formulation. Thus, if a library of interpolation functions is available, then we can select admissible functions for the model from the library.

The objective of this chapter is to develop a library of two-dimensional triangular and rectangular elements of the Lagrange family, i.e., elements over which only the function—not its derivatives—are interpolated. The Hermite cubic interpolation functions are also presented, without a derivation, for the sake of completeness and reference. Once we have elements of different shapes and order at our disposal, we can choose appropriate elements and associated interpolation functions for a given problem. The regularly shaped elements, called *master elements*, for which interpolation functions are developed here, can be used for numerical evaluation of integrals defined on irregular elements. Of course, this requires a transformation of the geometry from the actual element shape to an associated master element. Section 9.3 deals with the transformation and numerical integration.

9.2 ELEMENT LIBRARY

9.2.1 Triangular Elements

The linear (three-node) triangular element was developed in Section 8.2.5. Higher-order triangular elements (i.e., triangular elements with interpolation functions of higher degree) can be systematically developed with the help of the so-called *Pascal's triangle*, which

Pascal's triangle	Degree of the complete polynomial	Number of terms in the polynomial	Element with nodes
1	0	1	
$x \quad y$	1	3	
$x^2 \quad xy \quad y^2$	2	6	
$x^3 \quad x^2y \quad xy^2 \quad y^3$	3	10	
$x^4 \quad x^3y \quad x^2y^2 \quad xy^3 \quad y^4$	4	15	
$x^5 \quad x^4y \quad x^3y^2 \quad x^2y^3 \quad xy^4 \quad y^5$	5	21	(Figure not shown)

Figure 9.2.1 Topmost six rows of Pascal's triangle for the generation of the Lagrange family of triangular elements.

contains the terms of polynomials of various degrees in the two coordinates x and y , as shown in Fig. 9.2.1. Here x and y denote some local coordinates; they do not, in general, represent the global coordinates of the problem. We can view the position of the terms as the nodes of the triangle, with the constant term and the first and last terms of a given row being the vertices of the triangle. Of course, the shape of the triangle is arbitrary—not necessarily an equilateral triangle, as might appear from the position of the terms in Pascal's triangle. For example, a triangular element of order 2 (i.e., the degree of the polynomial is 2) contains six nodes, as can be seen from the third row of Pascal's triangle. The position of the six nodes in the triangle is at the three vertices and at the midpoints of the three sides. The polynomial involves six constants, which can be expressed in terms of the nodal values of the variable being interpolated:

$$u = \sum_{i=1}^6 u_i \psi_i(x, y) \quad (9.2.1)$$

where ψ_i are the quadratic interpolation functions obtained following the same procedure as that used for the linear element in Section 8.2. In general, a p th-order triangular element has a number of n nodes

$$n = \frac{1}{2}(p+1)(p+2) \quad (9.2.2)$$

and a complete polynomial of p th degree is given by

$$u(x, y) = \sum_{i=1}^n a_i x^r y^s = \sum_{j=1}^n u_j \psi_j, \quad r + s \leq p \quad (9.2.3)$$

The location of the entries in Pascal's triangle gives a symmetric location of nodal points in elements that will produce exactly the right number of nodes to define a Lagrange interpolation of any degree. It should be noted that the Lagrange family of triangular elements (of order greater than zero) should be used for second-order problems that require only the dependent variables (not their derivatives) of the problem to be continuous at interelement boundaries. It can be easily seen that the p th-degree polynomial associated with the p th-order Lagrange element, when evaluated on the boundary of the element, yields a p th-degree polynomial in the boundary coordinate. For example, the quadratic polynomial associated with the quadratic (six-node) triangular element shown in Fig. 9.2.2(a) is given by

$$u^e(x, y) = a_1 + a_2x + a_3y + a_4xy + a_5x^2 + a_6y^2 \quad (9.2.4)$$

The derivatives of u^e are

$$\frac{\partial u^e}{\partial x} = a_2 + a_4y + 2a_5x, \quad \frac{\partial u^e}{\partial y} = a_3 + a_4x + 2a_6y \quad (9.2.5)$$

The element shown in Fig. 9.2.2(a) is an arbitrary quadratic triangular element. By rotating and translating the (x, y) coordinate system, we obtain the (s, t) coordinate system [see Fig. 9.2.2(b)]. Since the transformation from the (x, y) system to the (s, t) system involves only rotation (which is linear) and translation, a k th-degree polynomial in the (x, y)

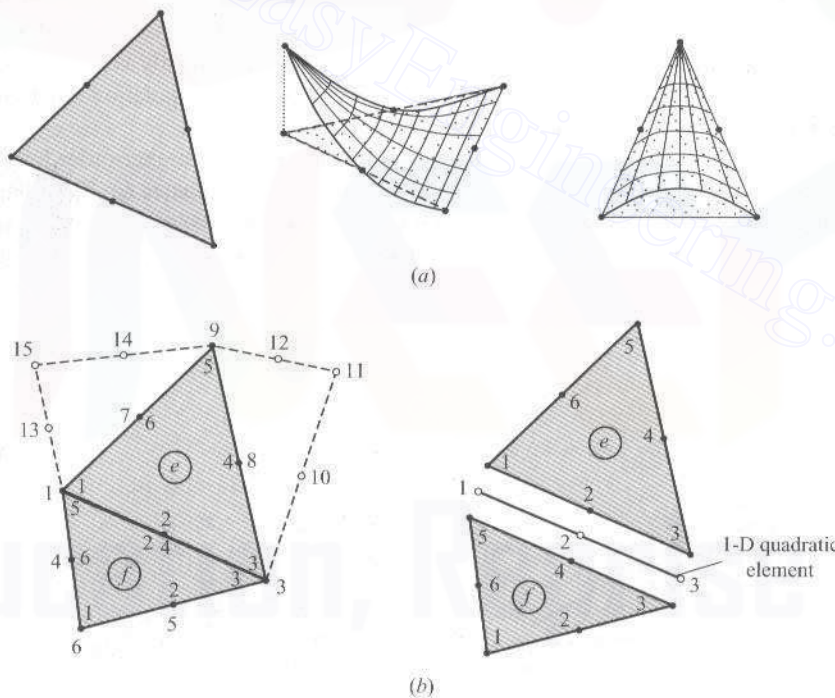


Figure 9.2.2 Variation of a function along the interelement boundaries of higher-order Lagrange elements: (a) a quadratic triangular element and (b) interelement continuity of a quadratic interpolation function.

coordinate system is still a k th-degree polynomial in the (s, t) system:

$$u^e(s, t) = \hat{a}_1 + \hat{a}_2 s + \hat{a}_3 t + \hat{a}_4 s t + \hat{a}_5 s^2 + \hat{a}_6 t^2 \quad (9.2.6)$$

where \hat{a}_i ($i = 1, 2, \dots, 6$) are constants that depend on a_i and the angle of rotation α . Now by setting $t = 0$, we get the restriction of u to side 1–2–3 of element Ω_e :

$$u^e(s, 0) = \hat{a}_1 + \hat{a}_2 s + \hat{a}_5 s^2 \quad (9.2.7)$$

which is a quadratic polynomial in s . If a neighboring element Ω_f has its side 5–4–3 in common with side 1–2–3 of element Ω_e , then the function u on side 5–4–3 of element Ω_f is also a quadratic polynomial

$$u^f(s, 0) = \hat{b}_1 + \hat{b}_2 s + \hat{b}_5 s^2 \quad (9.2.8)$$

Since the polynomials are uniquely defined by the same nodal values $U_1 = u_1^e = u_5^f$, $U_2 = u_2^e = u_4^f$, and $U_3 = u_3^e = u_3^f$, we have $u^e(s, 0) = u^f(s, 0)$ and hence the function u is uniquely defined on the interelement boundary of elements e and f .

The ideas discussed above can be easily extended to three dimensions, in which case Pascal's triangle takes the form of a Christmas tree and the elements are of a pyramid shape, called tetrahedral elements. We shall not elaborate on this any further because the scope of the present study is limited to two-dimensional elements only. A brief introduction to three-dimensional elements is presented in Chapter 14.

Recall from (8.2.21)–(8.2.25) that the procedure for deriving the interpolation functions involves the inversion of a $n \times n$ matrix, where n is the number of terms in the polynomial used to represent a function. When $n > 3$, this procedure is algebraically very tedious, and therefore we should devise an alternative way of developing the interpolation functions, as was discussed for one-dimensional elements in Chapter 3.

The alternative derivation of the interpolation functions for the higher-order Lagrange family of triangular elements is simplified by use of the *area* coordinates L_i . For triangular elements it is possible to construct three nondimensionalized coordinates L_i ($i = 1, 2, 3$) that relate respectively to the sides directly opposite nodes 1, 2, and 3 such that (see Fig. 9.2.3)

$$L_i = \frac{A_i}{A} \quad A = \sum_{i=1}^3 A_i \quad (9.2.9)$$

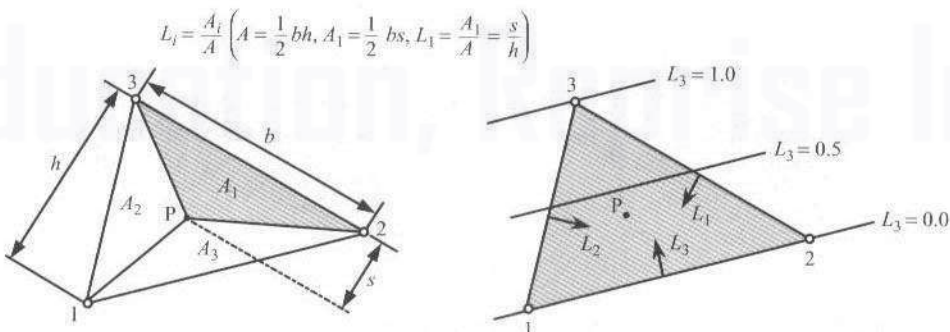


Figure 9.2.3 Definition of the natural coordinates of a triangular element.

where A_i is the area of the triangle formed by nodes j and k and an arbitrary point P in the element, and A is the total area of the element. For example, A_1 is the area of the shaded triangle, which is formed by nodes 2 and 3 and point P . The point P is at a perpendicular distance of s from the side connecting nodes 2 and 3. We have $A_1 = \frac{1}{2}bs$ and $A = \frac{1}{2}bh$. Hence,

$$L_1 = \frac{A_1}{A} = \frac{s}{h}$$

Clearly, L_1 is zero on side 2–3 (hence, zero at nodes 2 and 3) and has a value of unity at node 1. Thus, L_1 is the interpolation function associated with node 1. Similarly, L_2 and L_3 are the interpolation functions associated with nodes 2 and 3, respectively. In summary, we have

$$\psi_i = L_i \quad (9.2.10)$$

for a linear triangular element. We shall use L_i to construct interpolation functions for higher-order triangular elements.

Consider a higher-order element with k nodes (equally spaced) per side [see Fig. 9.2.4(a)]. Then the total number of nodes in the element is given by

$$n = \sum_{i=0}^{k-1} (k-i) = k + (k-1) + \cdots + 1 = \frac{1}{2}k(k+1) \quad (9.2.11)$$

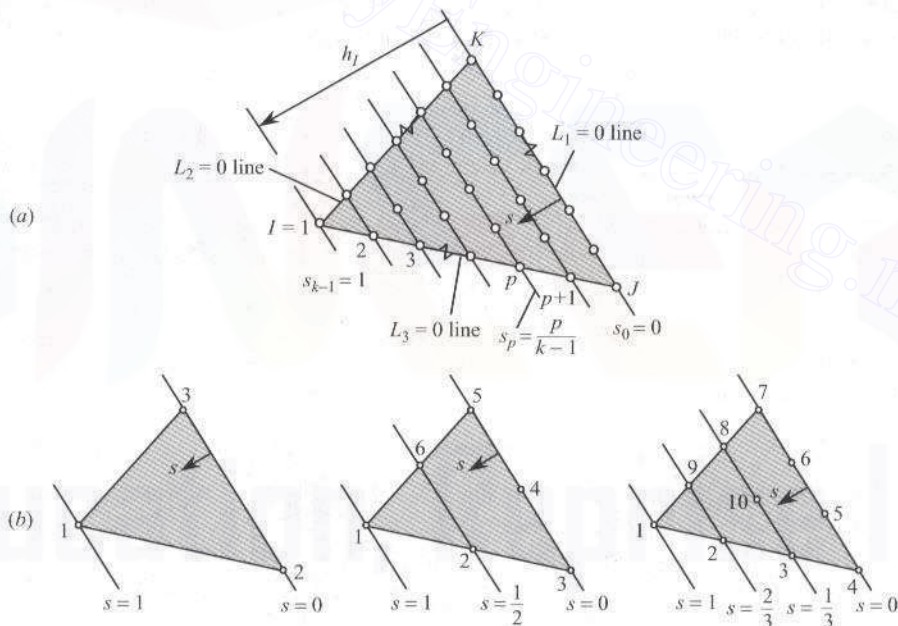


Figure 9.2.4 Construction of the element interpolation functions of the Lagrange triangular elements: (a) an arbitrary $(k-1)$ th-order element; and (b) linear, quadratic, and cubic elements.

and the degree of the interpolation functions is equal to $k - 1$. For example, for the quadratic element we have $k - 1 = 2$ and $n = 6$. Let the corner (i.e., vertex) nodes be denoted by I , J , and K , and let h_I be the perpendicular distance of the node I from the side connecting J and K . Then the distance s_p to the p th row parallel to side $J-K$ (under the assumption that the nodes are equally spaced along the sides and the rows) is given in nondimensional form by

$$s_p = \frac{p}{k-1}, \quad s_0 = 0, \quad s_{k-1} = 1 \quad (9.2.12)$$

The interpolation function ψ_I should be zero at the nodes on the lines $L_I = 0, 1/k, 2/k, \dots, (p-1)/k$ ($p = 0, 1, \dots, k-2$), and ψ_I should be equal to 1 at $L_I = s_{k-1}$. Thus, we have the necessary information for constructing the interpolation function ψ_I for vertex node I ($I = 1, 2, 3$):

$$\psi_I = \frac{(L_I - s_0)(L_I - s_1)(L_I - s_2) \cdots (L_I - s_{k-2})}{(s_{k-1} - s_0)(s_{k-1} - s_1) \cdots (s_{k-1} - s_{k-2})} = \prod_{p=0}^{k-2} \frac{L_I - s_p}{s_{k-1} - s_p} \quad (9.2.13)$$

Similar expressions can be derived for nodes located at other than the vertices. In general, ψ_i for node i is given by

$$\psi_i = \prod_{j=1}^{k-1} \frac{f_j^i}{f_j} \quad (9.2.14)$$

where f_j are functions of L_1 , L_2 , and L_3 , and f_j^i is the value of f_j at node i . The functions f_j are derived from the equations of $k-1$ lines that pass through all the nodes except node i . The procedure is illustrated below via an example.

Example 9.2.1

First, consider the triangular element that has two nodes per side (i.e., $k = 2$). This is the linear triangular element with the total number of nodes equal to three ($n = 3$). For node 1 [see Fig. 9.2.4(b)], we have $k - 2 = 0$ and

$$s_0 = 0, \quad s_1 = 1, \quad \psi_1 = \frac{L_1 - s_0}{s_1 - s_0} = L_1 \quad (9.2.15a)$$

Similarly, for ψ_2 and ψ_3 , we obtain

$$\psi_2 = L_2, \quad \psi_3 = L_3 \quad (9.2.15b)$$

Next, consider the triangular element with three nodes per side ($k = 3$). The total number of nodes is equal to six. For node 1, we have

$$s_0 = 0, \quad s_1 = \frac{1}{2}, \quad s_2 = 1$$

$$\psi_1 = \frac{L_1 - s_0}{s_2 - s_0} \frac{L_1 - s_1}{s_2 - s_1} = L_1(2L_1 - 1) \quad (9.2.16a)$$

The function ψ_2 [see Fig. 9.2.4(b)] should vanish at nodes 1, 3, 4, 5, and 6, and should be equal to 1 at node 2. Equivalently, ψ_2 should vanish along the lines connecting nodes 1 and 5, and 3 and 5. These two lines are given in terms of L_1 and L_2 (note that the subscripts of L refer to the nodes in the three-node triangular element) as $L_2 = 0$ and $L_1 = 0$. Hence, we have

$$\psi_2 = \frac{L_2 - s_0}{s_1 - s_0} \frac{L_1 - s_0}{s_1 - s_0} = \frac{L_2 - 0}{\frac{1}{2}} \frac{L_1 - 0}{\frac{1}{2}} = 4L_1 L_2 \quad (9.2.16b)$$

Similarly,

$$\psi_3 = L_2(2L_2 - 1), \quad \psi_4 = 4L_2 L_3, \quad \psi_5 = L_3(2L_3 - 1), \quad \psi_6 = 4L_1 L_3 \quad (9.2.16c)$$

As a last example, consider the cubic element (i.e., $k = 1 = 3$). For ψ_1 we note that it must vanish along lines $L_1 = 0$, $L_1 = \frac{1}{3}$, and $L_1 = \frac{2}{3}$. Therefore, we have

$$\psi_1 = \frac{L_1 - 0}{1 - 0} \frac{L_1 - \frac{1}{3}}{1 - \frac{1}{3}} \frac{L_1 - \frac{2}{3}}{1 - \frac{2}{3}} = \frac{1}{2} L_1 (3L_1 - 1)(3L_1 - 2)$$

The function ψ_2 must vanish along lines $L_1 = 0$, $L_2 = 0$, and $L_1 = 1/3$ (and node 2 is at a distance of $2/3$ along L_1 and a distance of $1/3$ along L_2)

$$\psi_2 = \frac{L_1 - 0}{\frac{2}{3} - 0} \frac{L_2 - 0}{\frac{1}{3} - 0} \frac{L_1 - \frac{1}{3}}{\frac{2}{3} - \frac{1}{3}} = \frac{9}{2} L_2 L_1 (3L_1 - 1)$$

Similarly, we can derive other functions. Thus, we have

$$\begin{aligned} \psi_1 &= \frac{1}{2} L_1 (3L_1 - 1)(3L_1 - 2), & \psi_2 &= \frac{9}{2} L_2 L_1 (3L_1 - 1) \\ \psi_3 &= \frac{9}{2} L_1 L_2 (3L_2 - 1), & \psi_4 &= \frac{1}{2} L_2 (3L_2 - 1)(3L_2 - 2) \\ \psi_5 &= \frac{9}{2} L_2 L_3 (3L_3 - 1), & \psi_6 &= \frac{9}{2} L_2 L_3 (3L_3 - 1) \\ \psi_7 &= \frac{1}{2} L_3 (3L_3 - 1)(3L_3 - 2), & \psi_8 &= \frac{9}{2} L_3 L_1 (3L_3 - 1) \\ \psi_9 &= \frac{9}{2} L_1 L_3 (3L_1 - 1), & \psi_{10} &= 27 L_1 L_2 L_3 \end{aligned} \quad (9.2.17)$$

It should be pointed out that the area coordinates L_i facilitate not only the construction of the interpolation functions for the higher-order elements but also the integration of functions of L_i over line paths and areas. The following exact integration formulas prove to be useful:

$$\int_a^b L_1^m L_2^n ds = \frac{m!n!}{(m+n+1)!} (b-a) \quad (9.2.18a)$$

$$\int \int_{\text{area}} L_1^m L_2^n L_3^p dA = \frac{m!n!p!}{(m+n+p+2)!} 2A \quad (9.2.18b)$$

where m , n , and p are arbitrary (positive) integers, A is the area of the domain of integration, and $m!$ denotes the factorial of m ($0! = 1$). Of course, we should transform the integrals from the x and y coordinates to L_i coordinates using the transformation,

$$x = \sum_{i=1}^n x_i L_i \quad y = \sum_{i=1}^n y_i L_i \quad (9.2.19)$$

where (x_i, y_i) are the global coordinates of the i th node of the element.

9.2.2 Rectangular Elements

Analogous to the Lagrange family of triangular elements (see Fig. 9.2.1), the Lagrange family of rectangular elements can be developed from a rectangular array as shown in Fig. 9.2.5. Since a linear rectangular element has four corners (hence, four nodes), the polynomial should have the first four terms $1, x, y$, and xy (which form a parallelogram in Pascal's triangle and a rectangle in the array given in Fig. 9.2.5). The coordinates (x, y) are usually taken to be the element (i.e., local) coordinates. In general, a p th-order Lagrange rectangular element has n nodes, with

$$n = (p + 1)^2 \quad (p = 0, 1, \dots)$$

and the associated polynomial contains the terms from the p th parallelogram or the p th rectangle in Fig. 9.2.5. When $p = 0$, it is understood (as in triangular elements) that the node is at the center of the element (i.e., the variable is a constant on the entire element). The Lagrange quadratic rectangular element has nine nodes, and the associated polynomial is given by

$$\begin{aligned} u(x, y) = & a_1 + a_2x + a_3y + a_4xy + a_5x^2 + a_6y^2 \\ & + a_7x^2y + a_8xy^2 + a_9x^2y^2 \end{aligned} \quad (9.2.20a)$$

$$\begin{aligned} \frac{\partial u}{\partial x} = & a_2 + a_4y + 2a_5x + 2a_7xy + a_8y^2 + 2a_9xy^2 \\ \frac{\partial u}{\partial y} = & a_3 + a_4x + 2a_6y + a_7x^2 + 2a_8xy + 2a_9x^2y \end{aligned} \quad (9.2.20b)$$

The polynomial contains the complete polynomial of the second degree plus the third-degree terms x^2y and xy^2 and also the x^2y^2 term. Four of the nine nodes are placed at the four corners, four at the midpoints of the sides, and one at the center of the element. The polynomial is uniquely determined by specifying its values at each of the nine nodes. Moreover, along the sides of the element, the polynomial is quadratic (with three terms—as can be seen by setting $y = 0$) and is determined by its values at the three nodes on that side. If two rectangular elements share a side and the polynomial is required to have the same values from both elements at the three nodes of the elements, then u is uniquely defined along the entire side (shared by the two elements). Note that the normal derivatives of u approximated by the quadratic Lagrange polynomials is quadratic in the tangential direction and linear in the normal direction (i.e., $\partial u / \partial x$ is quadratic in y and linear in x , and $\partial u / \partial y$ is quadratic in x and linear in y). Plots of ψ_1 , ψ_2 , and ψ_5

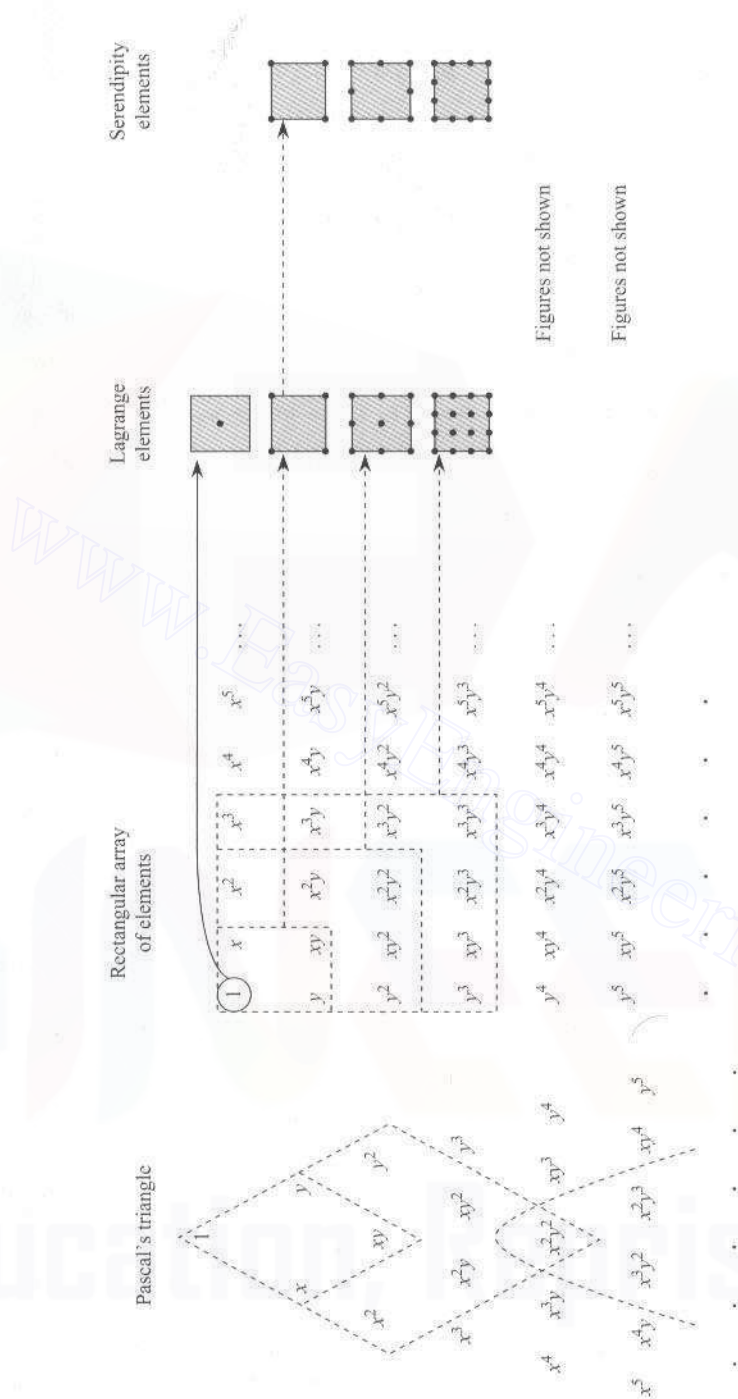


Figure 9.2.5 Lagrange and serendipity families of rectangular finite elements.

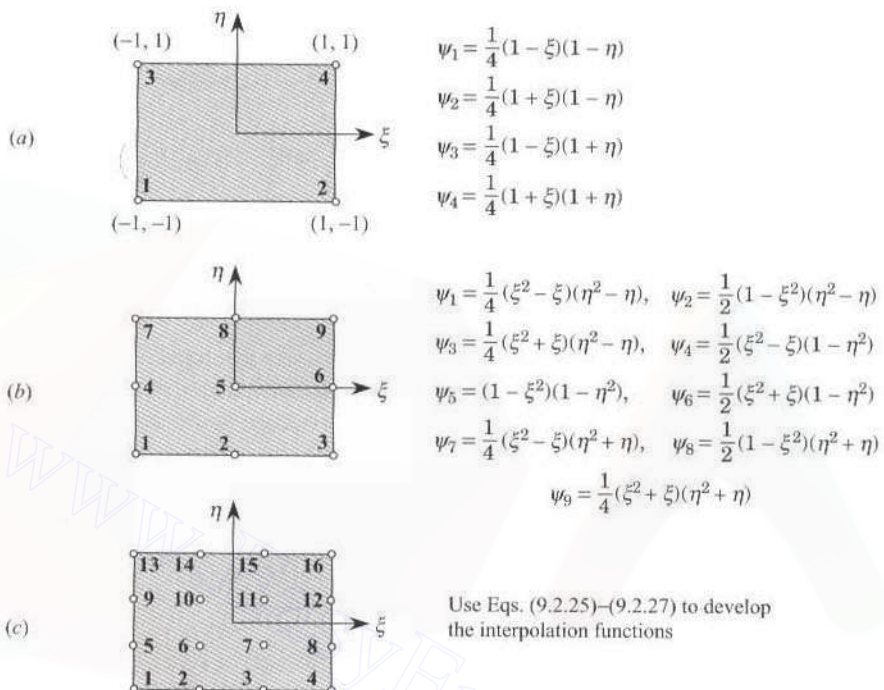


Figure 9.2.6 Node numbers and interpolation functions for the rectangular elements of the Lagrange family.

(the node numbers correspond to those in Fig. 9.2.6) of the nine-node rectangular element are shown in Fig. 9.2.7.

The p th-order Lagrange rectangular element has the p th-degree polynomial

$$\begin{aligned} u(x, y) &= \sum_{i=1}^n a_i x^i y^k & (j+k \leq p+1; j, k \leq p) \\ &= \sum_{i=1}^n u_i \psi_i \end{aligned} \quad (9.2.21)$$

and ψ_i are called the p th-order Lagrange interpolation functions.

The Lagrange interpolation functions associated with rectangular elements can be obtained from corresponding one-dimensional Lagrange interpolation functions by taking the tensor product of the x direction (one-dimensional) interpolation functions with the y direction (one-dimensional) interpolation functions. Let the x and y coordinates be taken along element sides with the origin of the coordinate system at the lower left corner of the rectangle. Then for an element with dimensions a and b along the x and y directions, respectively, the interpolation functions are given as follows:

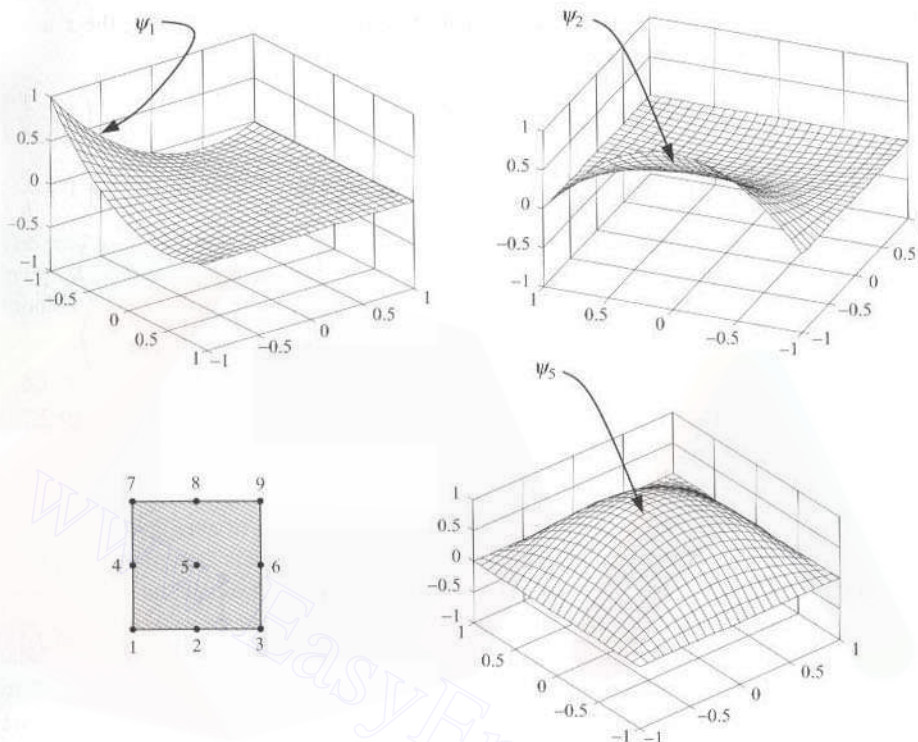


Figure 9.2.7 Geometric variation of the Lagrange interpolation functions at nodes 1, 2, and 5 (see Fig. 9.2.6) of the nine-node quadratic element.

Linear ($p = 1$)

$$\begin{bmatrix} \psi_1 & \psi_3 \\ \psi_2 & \psi_4 \end{bmatrix} = \begin{Bmatrix} 1 - \frac{x}{a} \\ \frac{x}{a} \end{Bmatrix} \begin{Bmatrix} 1 - \frac{y}{b} & \frac{y}{b} \end{Bmatrix}$$

$$= \begin{bmatrix} \left(1 - \frac{x}{a}\right)\left(1 - \frac{y}{b}\right) & \left(1 - \frac{x}{a}\right)\frac{y}{b} \\ \frac{x}{a}\left(1 - \frac{y}{b}\right) & \frac{x}{a}\frac{y}{b} \end{bmatrix} \quad (9.2.22)$$

Quadratic ($p = 2$)

$$\begin{bmatrix} \psi_1 & \psi_4 & \psi_7 \\ \psi_2 & \psi_5 & \psi_8 \\ \psi_3 & \psi_6 & \psi_9 \end{bmatrix} = \left\{ \begin{array}{l} \frac{(x - \frac{1}{2}a)(x - a)}{(-\frac{1}{2}a)(-a)} \\ \frac{x(x - a)}{\frac{1}{2}a(\frac{1}{2}a - a)} \\ \frac{x(x - \frac{1}{2}a)}{a(\frac{1}{2}a)} \end{array} \right\} \left\{ \begin{array}{l} \frac{(y - \frac{1}{2}b)(y - b)}{\frac{1}{2}b^2} \\ \frac{y(y - b)}{-\frac{1}{4}b^2} \\ \frac{y(y - b/2)}{\frac{1}{2}b^2} \end{array} \right\}^T \quad (9.2.23)$$

where the two vectors are the one-dimensional interpolation functions along the x and y directions, respectively. We obtain

$$\begin{aligned}\psi_1 &= \left(1 - \frac{2x}{a}\right)\left(1 - \frac{x}{a}\right)\left(1 - \frac{2y}{b}\right)\left(1 - \frac{y}{b}\right), & \psi_2 &= \frac{4x}{a}\left(1 - \frac{x}{a}\right)\left(1 - \frac{2y}{b}\right)\left(1 - \frac{y}{b}\right) \\ \psi_3 &= \frac{x}{a}\left(\frac{2x}{a} - 1\right)\left(1 - \frac{2y}{b}\right)\left(1 - \frac{y}{b}\right), & \psi_4 &= \left(1 - \frac{2x}{a}\right)\left(1 - \frac{x}{a}\right)\frac{4y}{b}\left(1 - \frac{y}{b}\right) \\ \psi_5 &= \frac{4x}{a}\left(1 - \frac{x}{a}\right)\frac{4y}{b}\left(1 - \frac{y}{b}\right), & \psi_6 &= \frac{x}{a}\left(\frac{2x}{a} - 1\right)\frac{4y}{b}\left(1 - \frac{y}{b}\right) \\ \psi_7 &= \left(1 - \frac{2x}{a}\right)\left(1 - \frac{x}{a}\right)\frac{y}{b}\left(\frac{2y}{b} - 1\right), & \psi_8 &= \frac{4x}{a}\left(1 - \frac{x}{a}\right)\frac{y}{b}\left(\frac{2y}{b} - 1\right) \\ \psi_9 &= \frac{x}{a}\left(\frac{2x}{a} - 1\right)\frac{y}{b}\left(\frac{2y}{b} - 1\right)\end{aligned}\quad (9.2.24)$$

p th Order

$$\begin{bmatrix} \psi_1 & \psi_{p+2} & \dots & \psi_k \\ \psi_2 & & & \\ \vdots & & \ddots & \vdots \\ \psi_p & & & \\ \psi_{p+1} & \psi_{2p+2} & \dots & \psi_n \end{bmatrix} = \begin{Bmatrix} f_1 \\ f_2 \\ \vdots \\ f_{p+1} \end{Bmatrix} \begin{Bmatrix} g_1 \\ g_2 \\ \vdots \\ g_{p+1} \end{Bmatrix}^T \quad (9.2.25)$$

$$k = (p + 1)p + 1, \quad n = (p + 1)^2$$

where $f_i(x)$ and $g_i(y)$ are the p th-order interpolants in x and y , respectively. For example, the polynomial

$$f_i(\xi) = \frac{(\xi - \xi_1)(\xi - \xi_2) \cdots (\xi - \xi_{i-1})(\xi - \xi_{i+1}) \cdots (\xi - \xi_{p+1})}{(\xi_i - \xi_1)(\xi_i - \xi_2) \cdots (\xi_i - \xi_{i-1})(\xi_i - \xi_{i+1}) \cdots (\xi_i - \xi_{p+1})} \quad (9.2.26)$$

(where ξ_i is the ξ coordinate of node i) is the p th-degree interpolation polynomial in ξ that vanishes at points $\xi_1, \xi_2, \dots, \xi_{i-1}, \xi_{i+1}, \dots, \xi_{p+1}$. We recall that (x, y) are the element coordinates.

It is convenient (for numerical integration purposes) to express the interpolation functions in (9.2.22)–(9.2.25) in terms of the natural coordinates ξ and η :

$$\xi = \frac{2(x - x_1) - a}{a}, \quad \eta = \frac{2(y - y_1) - b}{b} \quad (9.2.27)$$

where x_1 and y_1 are the global coordinates of node 1 in the local x and y coordinates. For a coordinate system with origin fixed at node 1 and coordinates parallel to the sides of the element, we have $x_1 = y_1 = 0$. In this case, the quadratic interpolation functions in (9.2.24) can be written in terms of the natural coordinates ξ and η as

$$\begin{aligned}\psi_1 &= \frac{1}{4}(\xi - \xi^2)(\eta - \eta^2), & \psi_5 &= (1 - \xi^2)(1 - \eta^2) \\ \psi_2 &= -\frac{1}{2}(1 - \xi^2)(\eta - \eta^2), & \psi_6 &= \frac{1}{2}(\xi + \xi^2)(1 - \eta^2)\end{aligned}$$

$$\begin{aligned}\psi_3 &= -\frac{1}{4}(\xi + \xi^2)(\eta - \eta^2), & \psi_7 &= -\frac{1}{4}(\xi - \xi^2)(\eta + \eta^2) \\ \psi_4 &= -\frac{1}{2}(\xi - \xi^2)(1 - \eta^2), & \psi_8 &= \frac{1}{2}(1 - \xi^2)(\eta + \eta^2) \\ \psi_9 &= \frac{1}{4}(\xi + \xi^2)(\eta + \eta^2)\end{aligned}\quad (9.2.28)$$

The reader should be cautioned that the subscripts of ψ_i refer to the node numbering used in Fig. 9.2.6. For any renumbering of the nodes, the subscripts of the interpolation functions should be changed accordingly.

9.2.3 The Serendipity Elements

Since the internal nodes of the higher-order elements of the Lagrange family do not contribute to the interelement connectivity, they can be condensed out at the element level so that the size of the element matrices is reduced. Alternatively, we can use the so-called serendipity elements to avoid the internal nodes present in the Lagrange elements. The serendipity elements are those rectangular elements which have no interior nodes. In other words, all the node points are on the boundary of the element. The interpolation functions for serendipity elements cannot be obtained using tensor products of one-dimensional interpolation functions. Instead, an alternative procedure that employs the interpolation properties in (8.2.33) is used. Here we illustrate how to construct the interpolation functions for the eight-node (quadratic) element using the natural coordinates (ξ, η) .

The interpolation function for node 1 should take on a value of zero at nodes 2, 3, ..., 8, and a value of unity at node 1. Equivalently, ψ_1 should vanish on the sides defined by the equations $1 - \xi = 0$, $1 - \eta = 0$, and $1 + \xi + \eta = 0$ (see Fig. 9.2.8). Therefore, ψ_1 is of the

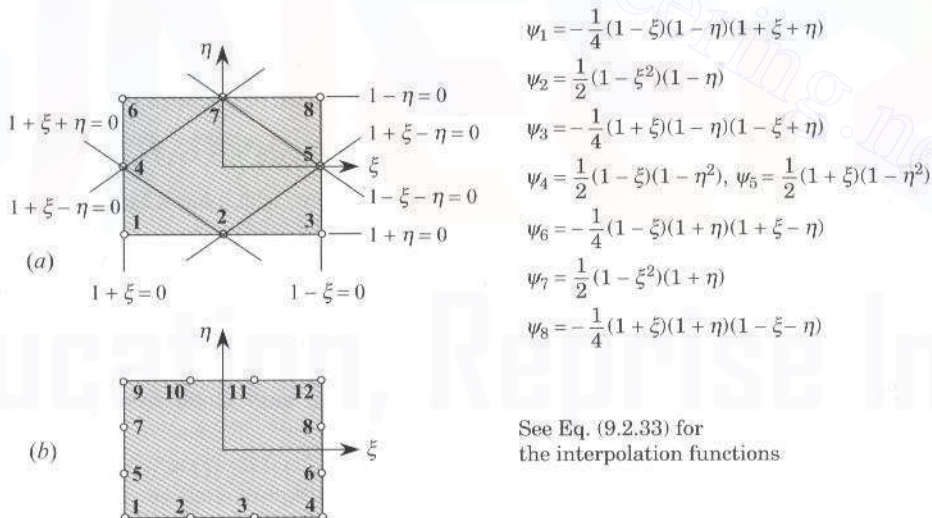


Figure 9.2.8 Node numbers and interpolation functions associated with the serendipity family of elements.

form

$$\psi_1(\xi, \eta) = c(1 - \xi)(1 - \eta)(1 + \xi + \eta) \quad (9.2.29a)$$

where c is a constant that should be determined so as to yield $\psi_1(-1, -1) = 1$. We obtain $c = -\frac{1}{4}$, and therefore

$$\psi_1(\xi, \eta) = -\frac{1}{4}(1 - \xi)(1 - \eta)(1 + \xi + \eta) \quad (9.2.29b)$$

We can construct other interpolation functions in a similar manner. We have

$$\begin{aligned} \psi_1 &= -\frac{1}{4}(1 - \xi)(1 - \eta)(1 + \xi + \eta), & \psi_2 &= \frac{1}{2}(1 - \xi^2)(1 - \eta) \\ \psi_3 &= \frac{1}{4}(1 + \xi)(1 - \eta)(-1 + \xi - \eta), & \psi_4 &= \frac{1}{2}(1 - \xi)(1 - \eta^2) \\ \psi_5 &= \frac{1}{2}(1 + \xi)(1 - \eta^2), & \psi_6 &= \frac{1}{4}(1 - \xi)(1 + \eta)(-1 - \xi + \eta) \\ \psi_7 &= \frac{1}{2}(1 - \xi^2)(1 + \eta), & \psi_8 &= \frac{1}{4}(1 + \xi)(1 + \eta)(-1 + \xi + \eta) \end{aligned} \quad (9.2.30)$$

Note that all the ψ_i for the eight-node element have the form

$$\psi_i = c_1 + c_2\xi + c_3\eta + c_4\xi\eta + c_5\xi^2 + c_6\eta^2 + c_7\xi^2\eta + c_8\xi\eta^2 \quad (9.2.31a)$$

The derivatives of ψ_i with respect to ξ and η are of the form,

$$\begin{aligned} \frac{\partial \psi_i}{\partial \xi} &= c_2 + c_4\eta + 2c_5\xi + 2c_7\xi\eta + c_8\eta^2 \\ \frac{\partial \psi_i}{\partial \eta} &= c_3 + c_4\xi + 2c_6\eta + c_7\xi^2 + 2c_8\xi\eta \end{aligned} \quad (9.2.31b)$$

Plots of ψ_1 and ψ_2 (the node numbers correspond to those in Fig. 9.2.8) for the eight-node serendipity element are shown in Fig. 9.2.9. It should be noted that ψ_2 of the nine-node element is zero at the element center, whereas ψ_2 of the eight-node element is nonzero there. The interpolation functions ψ_i for the twelve-node element are of the form

$$\psi_i = \text{terms of the form in (9.2.31a)} + c_9\xi^3 + c_{10}\eta^3 + c_{11}\xi^3\eta + c_{12}\xi\eta^3 \quad (9.2.32)$$

The interpolation functions for the cubic serendipity element, which has 12 nodes, are

$$\begin{aligned} \psi_1 &= \frac{1}{32}(1 - \xi)(1 - \eta)[-10 + 9(\xi^2 + \eta^2)], & \psi_2 &= \frac{9}{32}(1 - \eta)(1 - \xi^2)(1 - 3\xi) \\ \psi_3 &= \frac{9}{32}(1 - \eta)(1 - \xi^2)(1 + 3\xi), \\ \psi_4 &= \frac{1}{32}(1 + \xi)(1 - \eta)[-10 + 9(\xi^2 + \eta^2)] \\ \psi_5 &= \frac{9}{32}(1 - \xi)(1 - \eta^2)(1 - 3\eta), & \psi_6 &= \frac{9}{32}(1 + \xi)(1 - \eta^2)(1 - 3\eta) \\ \psi_7 &= \frac{9}{32}(1 - \xi)(1 - \eta^2)(1 + 3\eta), & \psi_8 &= \frac{9}{32}(1 + \xi)(1 - \eta^2)(1 + 3\eta) \end{aligned}$$

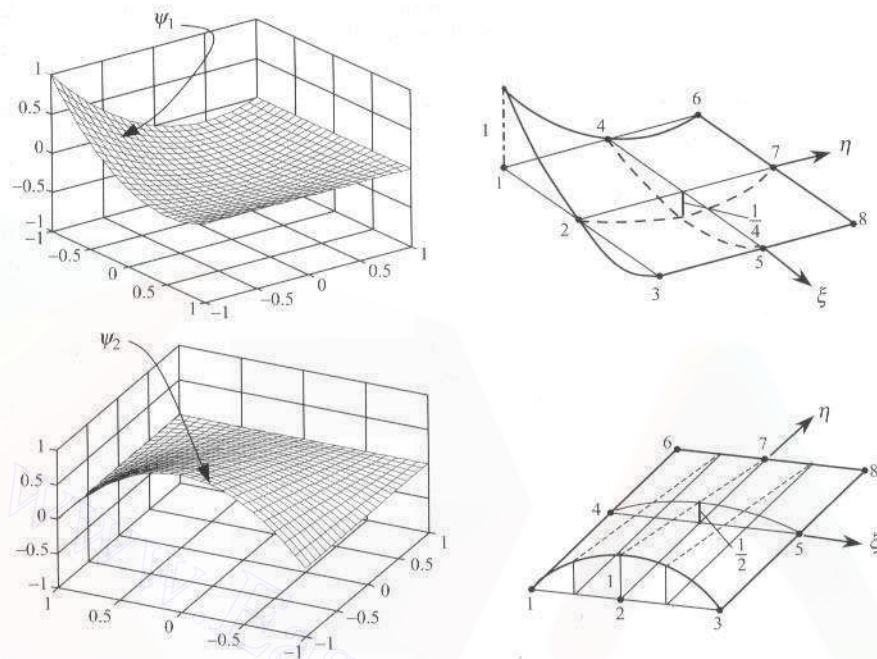


Figure 9.2.9 Graphical representation of the interpolation functions associated with nodes 1 and 2 of the eight-node serendipity element (see Fig. 9.2.8).

$$\begin{aligned}\psi_9 &= \frac{1}{32}(1-\xi)(1+\eta)[-10 + 9(\xi^2 + \eta^2)], & \psi_{10} &= \frac{9}{32}(1+\eta)(1-\xi^2)(1-3\xi) \\ \psi_{11} &= \frac{9}{32}(1+\eta)(1-\xi^2)(1+3\xi), \\ \psi_{12} &= \frac{1}{32}(1+\xi)(1+\eta)[-10 + 9(\xi^2 + \eta^2)]\end{aligned}\quad (9.2.33)$$

9.2.4 Hermite Cubic Interpolation Functions

In the above discussion, we developed only the Lagrange interpolation functions for triangular and rectangular elements. The Hermite family of interpolation functions (which interpolate the function and its derivatives) were not discussed. We recall that such functions are required in the finite element formulation of fourth-order (or higher-order) differential equations (e.g., the Euler–Bernoulli beam theory of Chapter 4 and the classical or Kirchhoff plate theory of Chapter 12). For the sake of completeness, while not presenting the details of the derivation, the Hermite cubic interpolation functions for two rectangular elements are summarized in Table 9.2.1. The first one is based on the interpolation of $(u, \partial u / \partial x, \partial u / \partial y, \partial^2 u / \partial x \partial y)$ at each node, and the second one is based on the interpolation

Table 9.2.1 Interpolation functions for the linear and quadratic Lagrange rectangular elements, quadratic serendipity element, and Hermite cubic rectangular elements.[†]

Element type	Interpolation functions	Remarks
Lagrange element		
<i>Linear</i>	$\frac{1}{4}(1 + \xi_0)(1 + \eta_0)$	Node $i = 1, \dots, 4$
<i>Quadratic</i>	$\psi_i = \frac{1}{4}\xi_0(1 + \xi_0)\eta_0(1 + \eta_0)$ $\psi_i = \frac{1}{2}\eta_0(1 + \eta_0)(1 - \xi^2)$ $\psi_i = \frac{1}{2}\xi_0(1 + \xi_0)(1 - \eta^2)$ $\psi_i = (1 - \xi^2)(1 - \eta^2)$	Corner node i Side node i , $\xi_i = 0$ Side node i , $\eta_i = 0$ Interior node i
Serendipity element		
<i>Quadratic</i>	$\psi_i = \frac{1}{4}(1 + \xi_0)(1 + \eta_0)(\xi_0 + \eta_0 - 1)$ $\psi_i = \frac{1}{2}(1 - \xi^2)(1 + \eta_0)$ $\psi_i = \frac{1}{2}(1 + \xi_0)(1 - \eta^2)$	Corner node i Side node i , $\xi_i = 0$ Side node i , $\eta_i = 0$
Hermite cubic element		
<i>Nonconforming element</i>	$[I = 4(i - 1) + 1, i = 1, \dots, 4]$ $\varphi_I = \frac{1}{16}(\xi + \xi_i)^2(\xi_0 - 2)(\eta + \eta_i)^2(\eta_0 - 2)$ $\varphi_{I+1} = -\frac{1}{16}\xi_i(\xi + \xi_i)^2(\xi_0 - 1)(\eta + \eta_i)^2(\eta_0 - 2)$ $\varphi_{I+2} = -\frac{1}{16}(\xi + \xi_i)^2(\xi_0 - 2)\eta_i(\eta + \eta_i)^2(\eta_0 - 1)$ $\varphi_{I+3} = \frac{1}{16}\xi_i(\xi + \xi_i)^2(\xi_0 - 1)\eta_i(\eta + \eta_i)^2(\eta_0 - 1)$	
<i>Conforming element</i>	$[I = 3(i - 1) + 1, i = 1, \dots, 4]$ $\varphi_I = \frac{1}{8}(\xi_0 + 1)(\eta_0 + 1)(2 + \xi_0 + \eta_0 - \xi^2 - \eta^2)$ $\varphi_{I+1} = \frac{1}{8}\xi_i(\xi_0 + 1)^2(\xi_0 - 1)(\eta_0 + 1)$ $\varphi_{I+2} = \frac{1}{8}\eta_i(\xi_0 + 1)(\eta_0 + 1)^2(\eta_0 - 1)$	
	$\xi = (x - x_c)/a$, $\eta = (y - y_c)/b$, $\xi_0 = \xi\xi_i$, $\eta_0 = \eta\eta_i$	

[†] See Fig. 9.2.10 for the coordinate system; (ξ_i, η_i) denote the natural coordinates of the i th node of the element; (x_c, y_c) are the global coordinates of the center of the element; and $2a$ and $2b$ are the sides of the rectangular element.

of $(u, \partial u / \partial x, \partial u / \partial y)$ at each node. The node numbering system in Table 9.2.1 refers to that used in Fig. 9.2.10.

9.3 NUMERICAL INTEGRATION

9.3.1 Preliminary Comments

An accurate representation of irregular domains (i.e., domains with curved boundaries) can be accomplished by the use of refined meshes and/or irregularly shaped curvilinear elements. For example, a nonrectangular region cannot be represented accurately using rectangular elements; however, it can be represented by quadrilateral elements. Since the interpolation functions are easily derivable for a rectangular element and it is easier to evaluate integrals over rectangular geometries, we transform the finite element integral statements defined over quadrilaterals to a rectangle. The transformation results in complicated expressions in terms of the coordinates used for the rectangular element. Therefore, numerical integration is used to evaluate such complicated expressions. Numerical integration schemes, such as the Gauss-Legendre numerical integration scheme, require the integral to be evaluated on a specific domain or with respect to a specific coordinate system. The Gauss-Legendre quadrature, for example, requires the integral to be expressed over a square region $\hat{\Omega}$ of

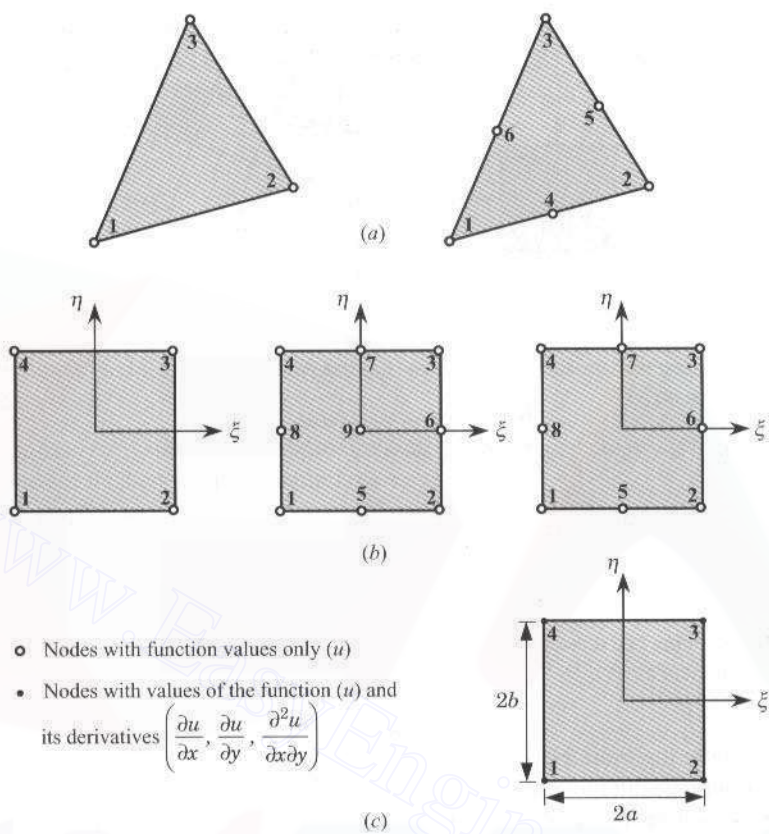


Figure 9.2.10 Triangular and rectangular elements with the standard node numbering system. (a) Linear and quadratic triangular elements; (b) linear and quadratic Lagrange elements; and (c) Hermite cubic element.

dimension 2 by 2 and the coordinate system (ξ, η) to be such that $-1 \leq (\xi, \eta) \leq 1$. The transformation of the geometry and the variable coefficients of the differential equation from the problem coordinates (x, y) to the coordinates (ξ, η) results in algebraically complex expressions, and they preclude analytical (i.e., exact) evaluation of the integrals. Thus, the transformation of a given integral expression, defined over element Ω_e , to one on the domain $\hat{\Omega}$ facilitates the numerical integration. Each element of the finite element mesh is transformed to $\hat{\Omega}$ only for the purpose of numerically evaluating the integrals. The element $\hat{\Omega}$ is called a *master element*. For example, every quadrilateral element can be transformed to a square element with side 2 that facilitates the use of Gauss-Legendre quadrature to evaluate integrals defined over the quadrilateral element.

The transformation between Ω_e and $\hat{\Omega}$ [or equivalently, between (x, y) and (ξ, η)] is accomplished by a coordinate transformation of the form

$$x = \sum_{j=1}^m x_j^e \hat{\psi}_j^e(\xi, \eta) \quad y = \sum_{j=1}^m y_j^e \hat{\psi}_j^e(\xi, \eta) \quad (9.3.1)$$

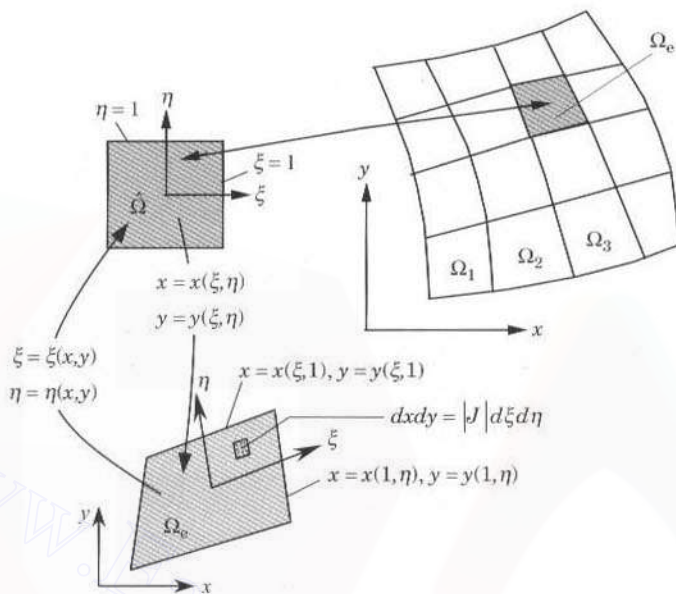


Figure 9.3.1 Mapping of a master rectangular element to an arbitrary quadrilateral element of a finite element mesh.

where $\hat{\psi}_j^e$ denote the finite element interpolation functions of the master element $\hat{\Omega}$. Although the Lagrange interpolation of the geometry is implied by Eq. (9.3.1), we can also use Hermite interpolation. Consider, as an example, the master element shown in Fig. 9.3.1. The coordinates in the master element are chosen to be the natural coordinates (ξ, η) such that $-1 \leq (\xi, \eta) \leq 1$. This choice is dictated by the limits of integration in the Gauss-Legendre quadrature rule, which is used to evaluate the integrals. For this case, the $\hat{\psi}_j^e$ denote the interpolation functions of the four-node rectangular element shown in Fig. 9.3.1 (i.e., $m = 4$). The transformation (9.3.1) maps a point (ξ, η) in the master element $\hat{\Omega}$ onto a point (x, y) in element Ω_e and vice versa if the Jacobian of the transformation is positive-definite. The transformation maps the line $\xi = 1$ in $\hat{\Omega}$ to the line defined parametrically by $x = x(1, \eta)$ and $y = y(1, \eta)$ in the (x, y) plane. For instance, consider the line $\xi = 1$ in the master element $\hat{\Omega}$. We have

$$\begin{aligned} x(1, \eta) &= \sum_{i=1}^4 x_i \hat{\psi}_i(1, \eta) = x_1 \cdot 0 + \frac{1}{2} x_2(1 - \eta) + \frac{1}{2} x_3(1 + \eta) + x_4 \cdot 0 \\ &= \frac{1}{2}(x_2 + x_3) + \frac{1}{2}(x_3 - x_2)\eta \end{aligned} \quad (9.3.2)$$

$$y(1, \eta) = \sum_{i=1}^4 y_i \hat{\psi}_i(1, \eta) = \frac{1}{2}(y_2 + y_3) + \frac{1}{2}(y_3 - y_2)\eta$$

Clearly, x and y are linear functions of η . Therefore, they define a straight line. Similarly, the lines $\xi = -1$ and $\eta = \pm 1$ are mapped into straight lines in the element Ω_e . In other words, the master element $\hat{\Omega}$ is transformed, under the linear transformation, into a quadrilateral element (i.e., a four-sided element whose sides are not parallel) in the (x, y) plane.

Conversely, every quadrilateral element of a mesh can be transformed to the same four-node square (master) element $\hat{\Omega}$ in the (ξ, η) plane (see Fig. 9.3.1).

In general, the dependent variable(s) of the problem are approximated by expressions of the form,

$$u(x, y) = \sum_{j=1}^n u_j^e \psi_j^e(x, y) \quad (9.3.3)$$

The interpolation functions ψ_j^e used for the approximation of the dependent variable are, in general, different from $\hat{\psi}_j^e$ used in the approximation of the geometry. Depending on the relative degree of approximations used for the geometry [see Eq. (9.3.1)] and the dependent variable(s) [see Eq. (9.3.3)], the finite element formulations are classified into three categories.

1. *Superparametric* ($m > n$): The approximation used for the geometry is higher order than that used for the dependent variable.
2. *Isoparametric* ($m = n$): Equal degree of approximation is used for both geometry and dependent variables.
3. *Subparametric* ($m < n$): Higher-order approximation of the dependent variable is used. (9.3.4)

For example, in the finite element analysis of the Euler–Bernoulli beams, we used linear Lagrange interpolation of the geometry,

$$x = \sum_{j=1}^2 x_j^e \hat{\psi}_j^e(\xi) = x_A + \frac{1}{2} h_e (1 + \xi) \quad (9.3.5)$$

whereas the Hermite cubic interpolation was used to approximate the transverse deflection. Such formulation falls into the subparametric category. Since the axial displacement is approximated by the linear Lagrange interpolation functions, it can be said that isoparametric formulation is used for the axial displacement. Superparametric formulations are rarely used. Also, the approximation of the geometry by Hermite family of interpolation functions is not common.

9.3.2 Coordinate Transformations

It should be noted that the transformation of a quadrilateral element of a mesh to the master element $\hat{\Omega}$ is solely for the purpose of numerically evaluating the integrals. *No transformation of the physical domain or elements is involved in the finite element analysis.* The resulting algebraic equations of the finite element formulation are always among the nodal values of the physical domain. Different elements of the finite element mesh can be generated from the same master element by assigning the global coordinates of the elements (see Fig. 9.3.1). Master elements of different order define different transformations and hence different collections of finite element meshes. For example, a cubic-order master rectangular element can be used to generate a mesh of cubic curvilinear quadrilateral elements. Thus, with the help of an appropriate master element, any arbitrary element of a mesh can be generated. However, the transformations of a master element should be such that there exist no spurious gaps between elements and no element overlaps occur. The elements in Figs. 9.2.6 and 9.2.8 can be used as master elements.

When a typical element of the finite element mesh is transformed to its master element for the purpose of numerically evaluating integrals, the integrand also must be expressed in terms of the coordinates (ξ, η) of the master element. For example, consider the element coefficients

$$K_{ij}^e = \int_{\Omega^e} \left[a(x, y) \frac{\partial \psi_i^e}{\partial x} \frac{\partial \psi_j^e}{\partial x} + b(x, y) \frac{\partial \psi_i^e}{\partial y} \frac{\partial \psi_j^e}{\partial y} + c(x, y) \psi_i^e \psi_j^e \right] dx dy \quad (9.3.6)$$

The integrand (i.e., the expression in the square brackets under the integral) is a function of the global coordinates x and y . We must rewrite it in terms of ξ and η using the transformation (9.3.1). Note that the integrand contains not only functions but also derivatives with respect to the global coordinates (x, y) . Therefore, we must relate $\partial \psi_i^e / \partial x$ and $\partial \psi_i^e / \partial y$ to $\partial \psi_i^e / \partial \xi$ and $\partial \psi_i^e / \partial \eta$ using the transformation (9.3.1).

The functions $\psi_i^e(x, y)$ can be expressed in terms of the local coordinates ξ and η by means of Eq. (9.3.1). Hence, by the chain rule of partial differentiation, we have

$$\begin{aligned} \frac{\partial \psi_i^e}{\partial \xi} &= \frac{\partial \psi_i^e}{\partial x} \frac{\partial x}{\partial \xi} + \frac{\partial \psi_i^e}{\partial y} \frac{\partial y}{\partial \xi} \\ \frac{\partial \psi_i^e}{\partial \eta} &= \frac{\partial \psi_i^e}{\partial x} \frac{\partial x}{\partial \eta} + \frac{\partial \psi_i^e}{\partial y} \frac{\partial y}{\partial \eta} \end{aligned} \quad (9.3.7a)$$

or, in matrix notation

$$\begin{Bmatrix} \frac{\partial \psi_i^e}{\partial \xi} \\ \frac{\partial \psi_i^e}{\partial \eta} \end{Bmatrix} = \begin{bmatrix} \frac{\partial x}{\partial \xi} & \frac{\partial y}{\partial \xi} \\ \frac{\partial x}{\partial \eta} & \frac{\partial y}{\partial \eta} \end{bmatrix}^e \begin{Bmatrix} \frac{\partial \psi_i^e}{\partial x} \\ \frac{\partial \psi_i^e}{\partial y} \end{Bmatrix} \equiv [J] \begin{Bmatrix} \frac{\partial \psi_i^e}{\partial x} \\ \frac{\partial \psi_i^e}{\partial y} \end{Bmatrix} \quad (9.3.7b)$$

which gives the relation between the derivatives of ψ_i^e with respect to the global and local coordinates. The matrix $[J]$ is called the *Jacobian matrix* of the transformation (9.3.1):

$$[J] = \begin{bmatrix} \frac{\partial x}{\partial \xi} & \frac{\partial y}{\partial \xi} \\ \frac{\partial x}{\partial \eta} & \frac{\partial y}{\partial \eta} \end{bmatrix}^e \quad (9.3.8)$$

Note from the expression given for K_{ij}^e in Eq. (9.3.6) that we must relate $\partial \psi_i^e / \partial x$ and $\partial \psi_i^e / \partial y$ to $\partial \psi_i^e / \partial \xi$ and $\partial \psi_i^e / \partial \eta$, whereas Eq. (9.3.7) provides the inverse relations. Therefore, Eq. (9.3.7b) must be inverted

$$\begin{Bmatrix} \frac{\partial \psi_i^e}{\partial x} \\ \frac{\partial \psi_i^e}{\partial y} \end{Bmatrix} = [J]^{-1} \begin{Bmatrix} \frac{\partial \psi_i^e}{\partial \xi} \\ \frac{\partial \psi_i^e}{\partial \eta} \end{Bmatrix} \quad (9.3.9)$$

This requires that the Jacobian matrix $[J]$ be nonsingular.

Although it is possible to write the relationship (9.3.9) directly by means of the chain rule,

$$\begin{aligned} \frac{\partial \psi_i^e}{\partial x} &= \frac{\partial \psi_i^e}{\partial \xi} \frac{\partial \xi}{\partial x} + \frac{\partial \psi_i^e}{\partial \eta} \frac{\partial \eta}{\partial x} \\ \frac{\partial \psi_i^e}{\partial y} &= \frac{\partial \psi_i^e}{\partial \xi} \frac{\partial \xi}{\partial y} + \frac{\partial \psi_i^e}{\partial \eta} \frac{\partial \eta}{\partial y} \end{aligned} \quad (9.3.10)$$

it is not possible to evaluate $\partial\xi/\partial x$, $\partial\xi/\partial y$, $\partial\eta/\partial x$, and $\partial\eta/\partial y$ directly from the transformation equation (9.3.1). The transformation equation (9.3.1) allows direct evaluation of $\partial x/\partial\xi$, $\partial x/\partial\eta$, $\partial y/\partial\xi$, and $\partial y/\partial\eta$, and therefore $[J]$, as discussed next.

Using the transformation (9.3.1), we can write

$$\begin{aligned}\frac{\partial x}{\partial\xi} &= \sum_{j=1}^m x_j \frac{\partial\hat{\psi}_j^e}{\partial\xi}, & \frac{\partial y}{\partial\xi} &= \sum_{j=1}^m y_j \frac{\partial\hat{\psi}_j^e}{\partial\xi} \\ \frac{\partial x}{\partial\eta} &= \sum_{j=1}^m x_j \frac{\partial\hat{\psi}_j^e}{\partial\eta}, & \frac{\partial y}{\partial\eta} &= \sum_{j=1}^m y_j \frac{\partial\hat{\psi}_j^e}{\partial\eta}\end{aligned}\quad (9.3.11a)$$

and

$$\begin{aligned}[J] &= \begin{bmatrix} \frac{\partial x}{\partial\xi} & \frac{\partial y}{\partial\xi} \\ \frac{\partial x}{\partial\eta} & \frac{\partial y}{\partial\eta} \end{bmatrix} = \begin{bmatrix} \sum_{i=1}^m x_i \frac{\partial\hat{\psi}_i}{\partial\xi} & \sum_{i=1}^m y_i \frac{\partial\hat{\psi}_i}{\partial\xi} \\ \sum_{i=1}^m x_i \frac{\partial\hat{\psi}_i}{\partial\eta} & \sum_{i=1}^m y_i \frac{\partial\hat{\psi}_i}{\partial\eta} \end{bmatrix} \\ &= \begin{bmatrix} \frac{\partial\hat{\psi}_1}{\partial\xi} & \frac{\partial\hat{\psi}_2}{\partial\xi} & \dots & \frac{\partial\hat{\psi}_m}{\partial\xi} \\ \frac{\partial\hat{\psi}_1}{\partial\eta} & \frac{\partial\hat{\psi}_2}{\partial\eta} & \dots & \frac{\partial\hat{\psi}_m}{\partial\eta} \end{bmatrix} \begin{bmatrix} x_1 & y_1 \\ x_2 & y_2 \\ \vdots & \vdots \\ x_m & y_m \end{bmatrix}\end{aligned}\quad (9.3.11b)$$

Thus, given the global coordinates (x_j, y_j) of element nodes and the interpolation functions $\hat{\psi}_j^e$ used for geometry, the Jacobian matrix can be evaluated using Eq. (9.3.8). Note that $\hat{\psi}_j^e$ are different, in general, from ψ_i^e used in the approximation of the dependent variables.

In order to compute the global derivatives of ψ_i^e (i.e., derivatives of ψ_i^e with respect to x and y), Eq. (9.3.9) requires inversion of the Jacobian matrix. A necessary and sufficient condition for $[J]^{-1}$ to exist is that the determinant $|J|$, called the Jacobian J , be nonzero at every point (ξ, η) in $\hat{\Omega}$:

$$J \equiv \det[J] = \frac{\partial x}{\partial\xi} \frac{\partial y}{\partial\eta} - \frac{\partial x}{\partial\eta} \frac{\partial y}{\partial\xi} > 0 \quad (9.3.12)$$

From Eq. (9.3.12) it is clear that the functions $\xi = \xi(x, y)$ and $\eta = \eta(x, y)$ must be continuous, differentiable, and invertible. Moreover, the transformation should be algebraically simple so that the Jacobian matrix can be easily evaluated. Transformations of the form in Eq. (9.3.1) satisfy these requirements and the requirement that no spurious gaps between elements or overlapping of elements should occur. We consider an example to illustrate the invertibility requirements.

Example 9.3.1

Consider the three-element mesh of quadrilaterals shown in Fig. 9.3.2. The master element is the four-node square. Elements 1 and 2 have counterclockwise element node numbering consistent with the node numbering in the master element, and element 3 has node numbering

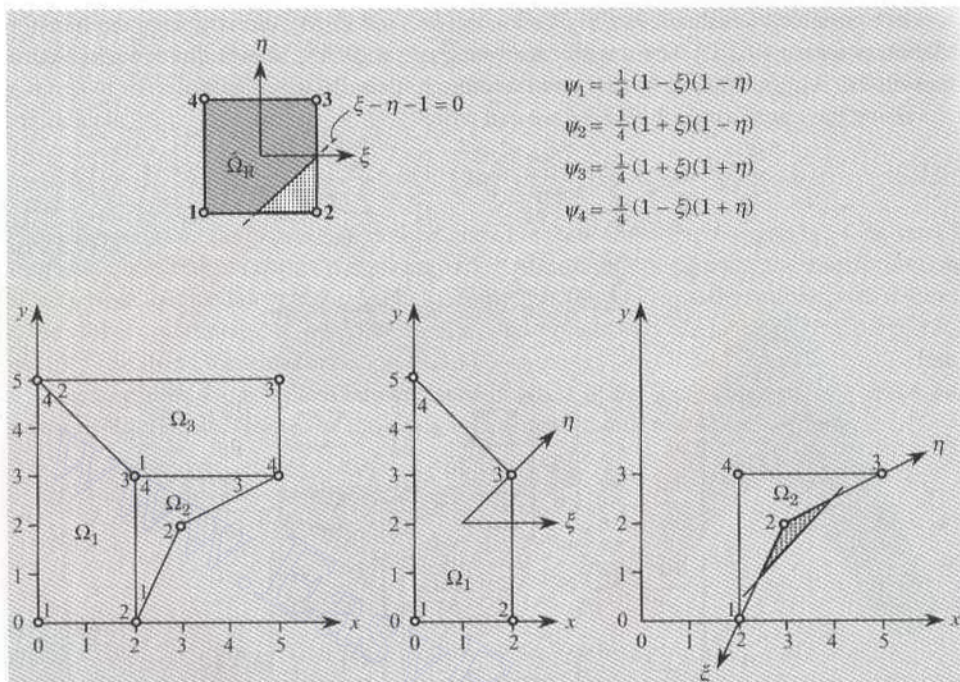


Figure 9.3.2 Examples of transformations of the master rectangular element $\hat{\Omega}_M$.

opposite to that of the master element. Elements 1 and 3 are *convex* domains in the sense that the line segment connecting any two arbitrary points of a convex domain lies entirely in the element. Clearly, element 2 is not convex because, for example, the line segment joining nodes 1 and 3 is not entirely inside the element. In the following paragraphs, we investigate the effect of node numbering and element convexity on the transformations from the master element to each of the three elements.

First, we compute the elements of the Jacobian matrix (the interpolation functions are given in Fig. 9.3.2)

$$\begin{aligned}
 \frac{\partial x}{\partial \xi} &= \sum_{i=1}^4 x_i \frac{\partial \hat{\psi}_i}{\partial \xi} = \frac{1}{4} [-x_1(1-\eta) + x_2(1-\eta) + x_3(1+\eta) - x_4(1+\eta)] \\
 \frac{\partial x}{\partial \eta} &= \sum_{i=1}^4 x_i \frac{\partial \hat{\psi}_i}{\partial \eta} = \frac{1}{4} [-x_1(1-\xi) - x_2(1+\xi) + x_3(1+\xi) + x_4(1+\xi)] \\
 \frac{\partial y}{\partial \xi} &= \sum_{i=1}^4 y_i \frac{\partial \hat{\psi}_i}{\partial \xi} = \frac{1}{4} [-y_1(1-\eta) + y_2(1-\eta) + y_3(1+\eta) - y_4(1+\eta)] \\
 \frac{\partial y}{\partial \eta} &= \sum_{i=1}^4 y_i \frac{\partial \hat{\psi}_i}{\partial \eta} = \frac{1}{4} [-y_1(1-\xi) - y_2(1+\xi) + y_3(1+\xi) + y_4(1+\xi)]
 \end{aligned} \tag{9.3.13}$$

Next, we evaluate the Jacobian for each of the elements.

Element 1. We have $x_1 = x_4 = 0$, $x_2 = x_3 = 2$; $y_1 = y_2 = 0$, $y_3 = 3$, $y_4 = 5$. The transformation and Jacobian are given by

$$x = 2\hat{\psi}_2 + 2\hat{\psi}_3 = 1 + \xi, \quad y = 3\hat{\psi}_3 + 5\hat{\psi}_4 = (1 + \eta)(2 - \frac{1}{2}\xi) \quad (9.3.14a)$$

$$J = \det[J] = \begin{vmatrix} \frac{\partial x}{\partial \xi} & \frac{\partial y}{\partial \xi} \\ \frac{\partial x}{\partial \eta} & \frac{\partial y}{\partial \eta} \end{vmatrix} = \begin{vmatrix} 1 & -\frac{1}{2}(1 + \eta) \\ 0 & 2 - \frac{1}{2}\xi \end{vmatrix} = \frac{1}{2}(4 - \xi) > 0 \quad (9.3.14b)$$

Clearly, the Jacobian is linear in ξ , and for all values of ξ in $-1 \leq \xi \leq 1$, it is positive. Therefore, the transformation (9.3.14a) is invertible:

$$1 + \xi = x, \quad 1 + \eta = \frac{2y}{5 - x}$$

Element 2. Here we have $x_1 = x_4 = 2$, $x_2 = 3$, $x_3 = 5$, $y_1 = 0$, $y_2 = 2$, and $y_3 = y_4 = 3$. The transformation and the Jacobian are given by

$$x = 3 + \xi + \frac{1}{2}\eta + \frac{1}{2}\xi\eta, \quad y = 2 + \frac{1}{2}\xi + \eta - \frac{1}{2}\xi\eta \quad (9.3.15a)$$

$$J = \begin{vmatrix} \frac{\partial x}{\partial \xi} & \frac{\partial y}{\partial \xi} \\ \frac{\partial x}{\partial \eta} & \frac{\partial y}{\partial \eta} \end{vmatrix} = \begin{vmatrix} 1 + \frac{1}{2}\eta & \frac{1}{2}(1 - \eta) \\ \frac{1}{2}(1 + \xi) & 1 - \frac{1}{2}\xi \end{vmatrix} = \frac{3}{4}(1 + \eta - \xi) \quad (9.3.15b)$$

The Jacobian is *not* nonzero everywhere in the master element. It is zero along the line $\xi = 1 + \eta$, and it is negative in the shaded area of the master element (see Fig. 9.3.2). Moreover, this area is mapped into the shaded area outside element 2. Thus, elements with any interior angle greater than π should not be used in any finite element mesh.

Element 3. We have $x_1 = 2$, $x_2 = 0$, $x_3 = x_4 = 5$, $y_1 = y_4 = 3$, and $y_2 = y_3 = 5$. The transformation and the Jacobian become (note that the nodes are numbered clockwise)

$$x = 3 - \frac{1}{2}\xi + 2\eta + \frac{1}{2}\xi\eta, \quad y = 4 + \xi \quad (9.3.16a)$$

$$J = \begin{vmatrix} \frac{\partial x}{\partial \xi} & \frac{\partial y}{\partial \xi} \\ \frac{\partial x}{\partial \eta} & \frac{\partial y}{\partial \eta} \end{vmatrix} = \begin{vmatrix} -\frac{1}{2}(1 - \eta) & 1 \\ 2 + \frac{1}{2}\xi & 0 \end{vmatrix} = -\left(2 + \frac{1}{2}\xi\right) < 0 \quad (9.3.16b)$$

The negative Jacobian indicates that a right-hand coordinate system is mapped into a left-hand coordinate system. Such coordinate transformations should be avoided.

The above example illustrates, for the four-node master element, that nonconvex elements are not admissible in finite element meshes. In general, any interior angle θ (see Fig. 9.3.3) should not be too small or too large because the Jacobian $J = (|dr_1||dr_2| \sin \theta)/d\xi d\eta$ will be very small. Similar restrictions hold for higher-order master elements. Additional restrictions also exist for higher-order elements. For example, for higher-order triangular and rectangular elements, the placing of the side and interior nodes is restricted.

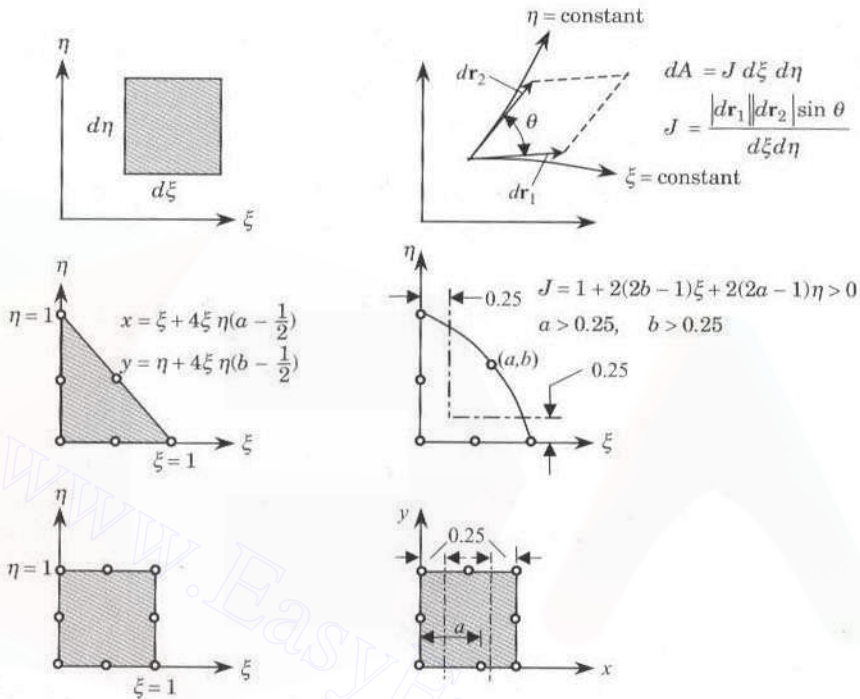


Figure 9.3.3 Some restrictions on element transformations.

For the eight-node rectangular element, it can be shown that the side nodes should be placed at a distance greater than or equal to a quarter of the length of the side from either corner node (see Fig. 9.3.3).

Returning to numerical evaluation of integrals, we have from Eq. (9.3.9),

$$\begin{Bmatrix} \frac{\partial \psi_i^e}{\partial x} \\ \frac{\partial \psi_i^e}{\partial y} \end{Bmatrix} = [J]^{-1} \begin{Bmatrix} \frac{\partial \psi_i^e}{\partial \xi} \\ \frac{\partial \psi_i^e}{\partial \eta} \end{Bmatrix} \equiv [J^*] \begin{Bmatrix} \frac{\partial \psi_i^e}{\partial \xi} \\ \frac{\partial \psi_i^e}{\partial \eta} \end{Bmatrix} \quad (9.3.17)$$

where J_{ij}^* is the element in position (i, j) of the inverse of the Jacobian matrix,

$$[J]^{-1} \equiv [J^*] = \begin{bmatrix} J_{11}^* & J_{12}^* \\ J_{21}^* & J_{22}^* \end{bmatrix} \quad (9.3.18)$$

The element area $dA = dx dy$ in element Ω_e is transformed to

$$dA \equiv dx dy = J d\xi d\eta \quad (9.3.19)$$

in the master element $\hat{\Omega}$.

Equations (9.3.9), (9.3.11), (9.3.18), and (9.3.19) provide the necessary relations to transform integral expressions on any element Ω_e to an associated master element $\hat{\Omega}$. For instance, consider the integral expression in Eq. (9.3.6) where $a = a(x, y)$, $b = b(x, y)$, and $c = c(x, y)$ are functions of x and y . Suppose that the mesh of finite elements is generated

by a master element $\hat{\Omega}$. Under the transformation (9.3.1), we can write

$$\begin{aligned}
 K_{ij}^e &= \int_{\Omega_e} \left(a \frac{\partial \psi_i}{\partial x} \frac{\partial \psi_j}{\partial x} + b \frac{\partial \psi_i}{\partial y} \frac{\partial \psi_j}{\partial y} + c \psi_i \psi_j \right) dx dy \\
 &= \int_{\hat{\Omega}} \left[\hat{a} \left(J_{11}^* \frac{\partial \psi_i}{\partial \xi} + J_{12}^* \frac{\partial \psi_i}{\partial \eta} \right) \left(J_{11}^* \frac{\partial \psi_j}{\partial \xi} + J_{12}^* \frac{\partial \psi_j}{\partial \eta} \right) \right. \\
 &\quad \left. + \hat{b} \left(J_{21}^* \frac{\partial \psi_i}{\partial \xi} + J_{22}^* \frac{\partial \psi_i}{\partial \eta} \right) \left(J_{21}^* \frac{\partial \psi_j}{\partial \xi} + J_{22}^* \frac{\partial \psi_j}{\partial \eta} \right) + \hat{c} \psi_i \psi_j \right] J d\xi d\eta \\
 &\equiv \int_{\hat{\Omega}} F(\xi, \eta) d\xi d\eta \tag{9.3.20}
 \end{aligned}$$

where J_{ij}^* are the elements of the inverse of the Jacobian matrix in (9.3.18), and $\hat{a} = a(\xi, \eta)$, and so on. Equations (9.3.9), (9.3.11), and (9.3.18)–(9.3.20) are valid for master elements of both rectangular and triangular geometry. The master triangular and rectangular elements for linear and quadratic triangular and quadrilateral elements are shown in Fig. 9.3.4.

9.3.3 Integration over a Master Rectangular Element

Quadrature formulas for integrals defined over a rectangular master element $\hat{\Omega}_R$ (such as that shown in Fig. 9.3.4) can be derived from the one-dimensional quadrature formulae presented in Section 7.6.4. We have

$$\begin{aligned}
 \int_{\hat{\Omega}_R} F(\xi, \eta) d\xi d\eta &= \int_{-1}^1 \left[\int_{-1}^1 F(\xi, \eta) d\eta \right] d\xi \approx \int_{-1}^1 \left[\sum_{J=1}^N F(\xi, \eta_J) W_J \right] d\xi \\
 &\approx \sum_{I=1}^M \sum_{J=1}^N F(\xi_I, \eta_J) W_I W_J \tag{9.3.21}
 \end{aligned}$$

where M and N denote the number of quadrature points in the ξ and η directions, (ξ_I, η_J) denote the Gauss points, and W_I and W_J denote the corresponding Gauss weights (see Table 7.1.2). The selection of the number of Gauss points is based on the same formula as that given in Section 7.1.5: A polynomial of degree p is integrated exactly employing $N = \text{int}[\frac{1}{2}(p+1)]$, i.e., the smallest integer greater than $\frac{1}{2}(p+1)$. In most cases, the interpolation functions are of the same degree in both ξ and η , and therefore $M = N$. When the integrand is of different degree in ξ and η , the number of Gauss points is selected on the basis of the largest-degree polynomial. The minimum allowable quadrature rule is one that computes the mass of the element exactly when the density is constant.

Table 9.3.1 contains information on the selection of the integration order and the location of the Gauss points for linear, quadratic, and cubic elements. The maximum degree of the polynomial refers to the degree of the highest polynomial in ξ or η that is present in the integrands of the element matrices of the type in Eq. (9.3.20). Note that the polynomial degree of coefficients as well as J_{ij}^* and J should be accounted for in determining the total polynomial degree of the integrand. Of course, the coefficients a , b , and c , and J_{ij}^* in general may not be polynomials. In those cases, their functional variations must be approximated

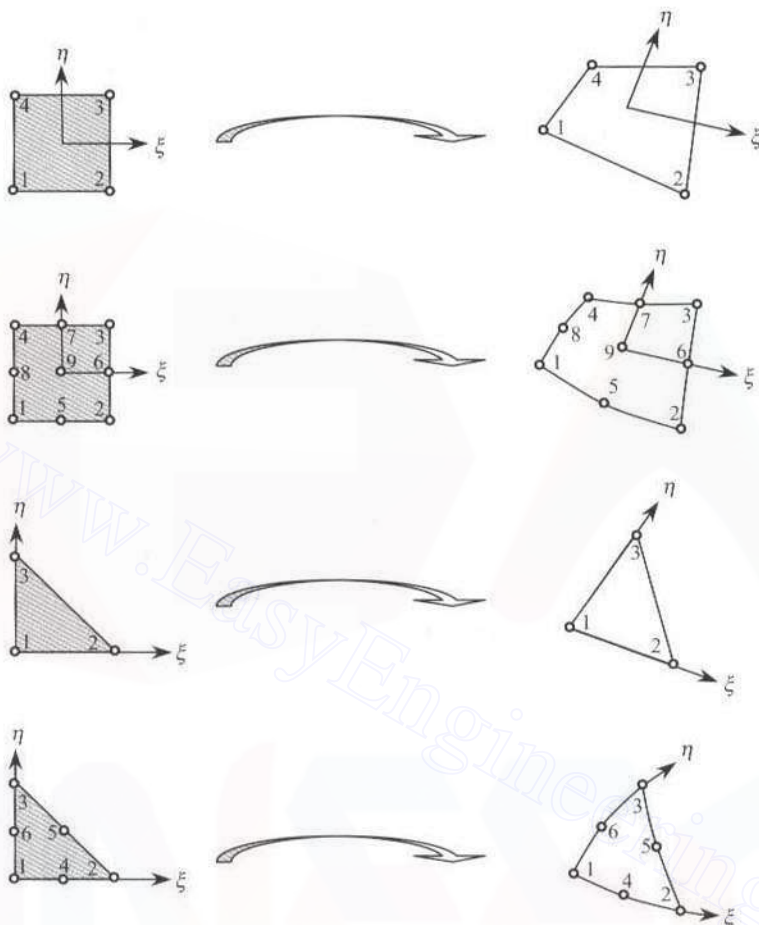


Figure 9.3.4 Linear and quadratic master finite elements and their typical counterparts in the problem coordinate system.

by a suitable polynomial (for example, by a binomial series) in order to determine the polynomial degree of the integrand.

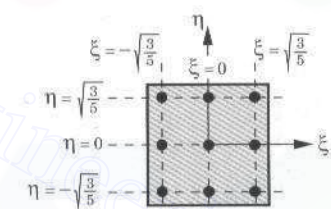
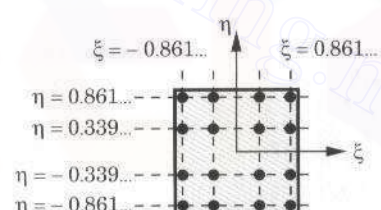
The $N \times N$ Gauss point locations are given by the *tensor product* of one-dimensional Gauss points ξ_I :

$$\begin{Bmatrix} \xi_1 \\ \xi_2 \\ \vdots \\ \xi_N \end{Bmatrix} \{ \xi_1, \xi_2, \dots, \xi_N \} \equiv \begin{bmatrix} (\xi_1, \xi_1) & (\xi_1, \xi_2) & \dots & (\xi_1, \xi_N) \\ (\xi_2, \xi_1) & \ddots & & \vdots \\ \vdots & & & \\ (\xi_N, \xi_1) & \dots & & (\xi_N, \xi_N) \end{bmatrix} \quad (9.3.22)$$

The values of ξ_I ($I = 1, 2, \dots, N$) are presented in Table 9.3.1 (also, see Table 7.1.2).

The next two examples illustrate the evaluation of the Jacobian and element matrices on rectangular elements.

Table 9.3.1 Selection of the integration order and location of the Gauss points for linear, quadratic, and cubic quadrilateral elements (nodes not shown).

Element type	Maximum polynomial degree	Order of integration ($r \times r$)	Order of the residual	Location of integration points* in master element
Constant ($r = 1$)	0	1×1	$O(h^2)$	
Linear ($r = 2$)	2	2×2	$O(h^4)$	
Quadratic ($r = 3$)	4	(3×3)	$O(h^6)$	
Cubic ($r = 4$)	6	(4×4)	$O(h^8)$	

*See Table 6.1.2 for the integration points and weights for each coordinate direction.

Example 9.3.2

Consider the quadrilateral element Ω_1 shown in Fig. 9.3.2. We wish to evaluate $\partial\psi_i/\partial x$ and $\partial\psi_i/\partial y$ at $(\xi, \eta) = (0, 0)$ and $(\frac{1}{2}, \frac{1}{2})$ using the isoparametric formulation (i.e., $\hat{\psi}_i = \psi_i$). From

Eq. (9.3.11b) we have

$$\begin{aligned} [J] &= \begin{bmatrix} \frac{\partial x}{\partial \xi} & \frac{\partial y}{\partial \xi} \\ \frac{\partial x}{\partial \eta} & \frac{\partial y}{\partial \eta} \end{bmatrix} = \frac{1}{4} \begin{bmatrix} -(1-\eta) & 1-\eta & 1+\eta & -(1+\eta) \\ -(1-\xi) & -(1+\xi) & 1+\xi & 1-\xi \end{bmatrix} \begin{bmatrix} 0.0 & 0.0 \\ 2.0 & 0.0 \\ 2.0 & 3.0 \\ 0.0 & 5.0 \end{bmatrix} \\ &= \begin{bmatrix} 1 & -\frac{1}{2}(1+\eta) \\ 0 & \frac{1}{2}(4-\xi) \end{bmatrix} \end{aligned}$$

The inverse of the Jacobian matrix is given by

$$[J]^{-1} = \begin{bmatrix} 1 & \frac{1+\eta}{4-\xi} \\ 0 & \frac{2}{4-\xi} \end{bmatrix}, \quad J_{11}^* = 1, \quad J_{21}^* = 0, \quad J_{12}^* = \frac{1+\eta}{4-\xi}, \quad J_{22}^* = \frac{2}{4-\xi}$$

From (9.3.9), we have

$$\frac{\partial \psi_i}{\partial x} = \frac{\partial \psi_i}{\partial \xi} + \frac{1+\eta}{4-\xi} \frac{\partial \psi_i}{\partial \eta}, \quad \frac{\partial \psi_i}{\partial y} = \frac{2}{4-\xi} \frac{\partial \psi_i}{\partial \eta}$$

where

$$\psi_i = \frac{1}{4}(1+\xi\xi_i)(1+\eta\eta_i), \quad \frac{\partial \psi_i}{\partial \xi} = \frac{1}{4}\xi_i(1+\eta\eta_i), \quad \frac{\partial \psi_i}{\partial \eta} = \frac{1}{4}\eta_i(1+\xi\xi_i) \quad (9.3.23)$$

(ξ_i, η_i) being the coordinates of the i th node in the master element (see Fig. 9.3.2);

Node	ξ_i	η_i
1	-1	-1
2	1	-1
3	1	1
4	-1	1

Thus, we have

$$\begin{aligned} \frac{\partial \psi_i}{\partial x} &= \frac{1}{4}\xi_i(1+\eta\eta_i) + \frac{1}{4} \left(\frac{1+\eta}{4-\xi} \right) \eta_i(1+\xi\xi_i) \\ \frac{\partial \psi_i}{\partial y} &= \frac{1}{4} \frac{2}{(4-\xi)} \eta_i(1+\xi\xi_i) \end{aligned}$$

In particular, at $(\xi, \eta) = (0, 0)$ the derivatives of ψ_i with respect to the global coordinates (x, y) are

$$\frac{\partial \psi_i}{\partial x} = \frac{1}{4}\xi_i + \frac{1}{16}\eta_i, \quad \frac{\partial \psi_i}{\partial y} = \frac{1}{8}\eta_i$$

and at $(\xi, \eta) = (0.5, 0.5)$ they are

$$\frac{\partial \psi_i}{\partial x} = \frac{1}{8} \xi_i (2 + \eta_i) + \frac{3}{56} \eta_i (2 + \xi_i), \quad \frac{\partial \psi_i}{\partial y} = \frac{1}{14} \eta_i (2 + \xi_i)$$

Example 9.3.3

Consider the quadrilateral element in Fig. 9.3.5. We wish to compute the following element matrices using the Gauss-Legendre quadrature:

$$\begin{aligned} S_{ij}^{00} &= \int_{\Omega} \psi_i \psi_j dx dy, & S_{ij}^{11} &= \int_{\Omega} \frac{\partial \psi_i}{\partial x} \frac{\partial \psi_j}{\partial x} dx dy \\ S_{ij}^{22} &= \int_{\Omega} \frac{\partial \psi_i}{\partial y} \frac{\partial \psi_j}{\partial y} dx dy, & S_{ij}^{12} &= \int_{\Omega} \frac{\partial \psi_i}{\partial x} \frac{\partial \psi_j}{\partial y} dx dy \end{aligned} \quad (9.3.24)$$

The transformation equations are

$$\begin{aligned} x &= 0 \cdot \hat{\psi}_1 + 5\hat{\psi}_2 + 4\hat{\psi}_3 + 1 \cdot \hat{\psi}_4 = \frac{1}{4} (10 + 8\xi - 2\xi\eta) \\ y &= 0 \cdot \hat{\psi}_1 - 1 \cdot \hat{\psi}_2 + 5\hat{\psi}_3 + 4\hat{\psi}_4 = \frac{1}{4} (8 + 10\eta + 2\xi\eta) \end{aligned}$$

the Jacobian matrix and its inverse are

$$\begin{aligned} [J] &= \begin{bmatrix} \frac{\partial x}{\partial \xi} & \frac{\partial x}{\partial \eta} \\ \frac{\partial y}{\partial \xi} & \frac{\partial y}{\partial \eta} \end{bmatrix} = \frac{1}{4} \begin{bmatrix} 8 - 2\eta & 2\eta \\ -2\xi & 10 + 2\xi \end{bmatrix}, \quad J = \frac{1}{4} [(4 - \eta)(5 + \xi) + \xi\eta] = \frac{1}{4} (20 + 4\xi - 5\eta) \\ [J]^{-1} &= \frac{1}{4J} \begin{bmatrix} 10 + 2\xi & -2\eta \\ 2\xi & 8 - 2\eta \end{bmatrix}, \quad J_{11}^* = \frac{10 + 2\xi}{20 + 4\xi - 5\eta}, \quad J_{12}^* = -\frac{2\eta}{20 + 4\xi - 5\eta} \\ J_{21}^* &= \frac{2\xi}{20 + 4\xi - 5\eta}, \quad J_{22}^* = \frac{8 - 2\eta}{20 + 4\xi - 5\eta} \end{aligned}$$

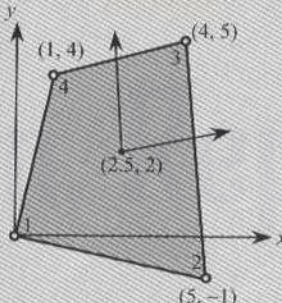


Figure 9.3.5 Geometry of the bilinear element used in Example 9.3.3.

The matrix $[J]$ transforms base vectors $\hat{\mathbf{e}}_x = (1, 0)$ and $\hat{\mathbf{e}}_y = (0, 1)$ in the xy system to the base vectors $\hat{\mathbf{e}}_\xi$ and $\hat{\mathbf{e}}_\eta$ in the $\xi\eta$ system

$$\frac{1}{4} \begin{bmatrix} 8 - 2\eta & 2\eta \\ -2\xi & 10 + 2\xi \end{bmatrix} \begin{Bmatrix} 1 \\ 0 \end{Bmatrix} = \frac{1}{4} \begin{Bmatrix} 8 - 2\eta \\ 2\eta \end{Bmatrix}, \quad \frac{1}{4} \begin{bmatrix} 8 - 2\eta & 2\eta \\ -2\xi & 10 + 2\xi \end{bmatrix} \begin{Bmatrix} 0 \\ 1 \end{Bmatrix} = \frac{1}{4} \begin{Bmatrix} -2\xi \\ 10 + 2\xi \end{Bmatrix}$$

or

$$\hat{\mathbf{e}}_\xi = \frac{1}{4} [(8 - 2\eta)\hat{\mathbf{e}}_x + 2\eta\hat{\mathbf{e}}_y], \quad \hat{\mathbf{e}}_\eta = \frac{1}{4} [-2\xi\hat{\mathbf{e}}_x + (10 + 2\xi)\hat{\mathbf{e}}_y]$$

Hence, the area element $dxdy$ in the xy system is related to the area element $d\xi d\eta$ in the $\xi\eta$ system by

$$dxdy = \frac{1}{16} \begin{vmatrix} 8 - 2\eta & -2\xi \\ 2\eta & 10 + 2\xi \end{vmatrix} d\xi d\eta = J d\xi d\eta \quad (9.3.25)$$

The coefficients S_{ij}^{00} and S_{ij}^{11} , for example, can be expressed in natural coordinates (for numerical evaluation) as

$$\begin{aligned} S_{ij}^{00} &= \int_{\Omega_e} \psi_i \psi_j dx dy = \int_{-1}^1 \int_{-1}^1 \psi_i \psi_j J d\xi d\eta \\ S_{ij}^{11} &= \int_{\Omega_e} \frac{\partial \psi_i}{\partial x} \frac{\partial \psi_j}{\partial x} dx dy \\ &= \int_{-1}^1 \int_{-1}^1 \left(J_{11}^* \frac{\partial \psi_i}{\partial \xi} + J_{12}^* \frac{\partial \psi_i}{\partial \eta} \right) \left(J_{11}^* \frac{\partial \psi_j}{\partial \xi} + J_{12}^* \frac{\partial \psi_j}{\partial \eta} \right) J d\xi d\eta \end{aligned}$$

where $\partial \psi_i / \partial \xi$ and $\partial \psi_i / \partial \eta$ are given by Eqs. (9.3.23). Note that the integrand of S_{ij}^{00} is a polynomial of the order $p=3$ in each coordinate ξ and η . Hence, $N=M=[(p+1)/2]=2$ will evaluate S_{ij} exactly. For example, consider the coefficient S_{11}^{00}

$$\begin{aligned} S_{11}^{00} &= \int_{\Omega_e} \psi_1 \psi_1 dx dy = \int_{-1}^1 \int_{-1}^1 \psi_1 \psi_1 J d\xi d\eta \\ &= \frac{1}{64} \int_{-1}^1 \int_{-1}^1 (1-\xi)^2 (1-\eta)^2 (20 + 4\xi - 5\eta) d\xi d\eta \\ &= \frac{1}{64} \sum_{i,j=1}^2 (1-\xi_i)^2 (1-\eta_j)^2 (20 + 4\xi_i - 5\eta_j) \end{aligned}$$

where (ξ_i, η_i) are the Gauss points

$$(\xi_1, \eta_2) = \left(-\frac{1}{\sqrt{3}}, \frac{1}{\sqrt{3}} \right), \quad (\xi_2, \eta_2) = \left(\frac{1}{\sqrt{3}}, \frac{1}{\sqrt{3}} \right)$$

$$(\xi_1, \eta_1) = \left(-\frac{1}{\sqrt{3}}, -\frac{1}{\sqrt{3}} \right), \quad (\xi_2, \eta_1) = \left(\frac{1}{\sqrt{3}}, -\frac{1}{\sqrt{3}} \right)$$

We have

$$\begin{aligned} S_{11}^{00} &= \frac{1}{64} \left[\left(1 + \frac{1}{\sqrt{3}}\right)^4 \left(20 - \frac{4}{\sqrt{3}} + \frac{5}{\sqrt{3}}\right) + \left(1 + \frac{1}{\sqrt{3}}\right)^2 \left(1 - \frac{1}{\sqrt{3}}\right)^2 \left(20 - \frac{4}{\sqrt{3}} - \frac{5}{\sqrt{3}}\right) \right. \\ &\quad \left. + \left(1 - \frac{1}{\sqrt{3}}\right)^2 \left(1 + \frac{1}{\sqrt{3}}\right)^2 \left(20 + \frac{4}{\sqrt{3}} + \frac{5}{\sqrt{3}}\right) + \left(1 - \frac{1}{\sqrt{3}}\right)^4 \left(20 + \frac{4}{\sqrt{3}} - \frac{5}{\sqrt{3}}\right) \right] \\ &= \frac{1}{64} \left[\frac{1120}{9} + \frac{160}{9} + \frac{32}{3\sqrt{3}} \left(-\frac{4}{\sqrt{3}} + \frac{5}{\sqrt{3}} \right) \right] = \frac{1312}{576} = 2.27778 \end{aligned}$$

Similarly, consider the coefficient S_{12}^{11} :

$$\begin{aligned} S_{12}^{11} &= \int_{\Omega_e} \frac{\partial \psi_1}{\partial x} \frac{\partial \psi_2}{\partial x} dx dy \\ &= \int_{-1}^1 \int_{-1}^1 \left(J_{11}^* \frac{\partial \psi_1}{\partial \xi} + J_{12}^* \frac{\partial \psi_1}{\partial \eta} \right) \left(J_{11}^* \frac{\partial \psi_2}{\partial \xi} + J_{12}^* \frac{\partial \psi_2}{\partial \eta} \right) J d\xi d\eta \\ &= \frac{1}{64} \int_{-1}^1 \int_{-1}^1 [-(10+2\xi)(1-\eta) + 2\eta(1-\xi)] [(10+2\xi)(1-\eta) + 2\eta(1-\xi)] \\ &\quad \times \frac{1}{(20+4\xi-5\eta)} d\xi d\eta \\ &= \frac{1}{64} \int_{-1}^1 \int_{-1}^1 [-(10+2\xi)^2(1-\eta)^2 + 4\eta^2(1-\xi)^2] \frac{1}{(20+4\xi-5\eta)} d\xi d\eta \end{aligned}$$

which is a ratio of polynomials. Hence, we do not expect to evaluate the integral exactly. The integrand varies, approximately, as a quadratic polynomial in each ξ and η . Hence, we may use the two-point Gauss integration to evaluate the integral

$$\begin{aligned} S_{12}^{11} &= \frac{1}{64} \int_{-1}^1 \int_{-1}^1 [-(10+2\xi)^2(1-\eta)^2 + 4\eta^2(1-\xi)^2] \frac{1}{(20+4\xi-5\eta)} d\xi d\eta \\ &\approx \sum_{i,j=1}^2 [-(10+2\xi_i)^2(1-\eta_j)^2 + 4\eta_j^2(1-\xi_i)^2] \frac{1}{64(20+4\xi_i-5\eta_j)} \\ &= \left[-\left(10 - \frac{2}{\sqrt{3}}\right)^2 \left(1 + \frac{1}{\sqrt{3}}\right)^2 + \frac{4}{3} \left(1 + \frac{1}{\sqrt{3}}\right)^2 \right] \frac{1}{64 \left(20 + \frac{1}{\sqrt{3}}\right)} \\ &\quad + \left[-\left(10 + \frac{2}{\sqrt{3}}\right)^2 \left(1 + \frac{1}{\sqrt{3}}\right)^2 + \frac{4}{3} \left(1 - \frac{1}{\sqrt{3}}\right)^2 \right] \frac{1}{64 \left(20 + \frac{9}{\sqrt{3}}\right)} \\ &\quad + \left[-\left(10 - \frac{2}{\sqrt{3}}\right)^2 \left(1 - \frac{1}{\sqrt{3}}\right)^2 + \frac{4}{3} \left(1 + \frac{1}{\sqrt{3}}\right)^2 \right] \frac{1}{64 \left(20 - \frac{9}{\sqrt{3}}\right)} \\ &\quad + \left[-\left(10 + \frac{2}{\sqrt{3}}\right)^2 \left(1 - \frac{1}{\sqrt{3}}\right)^2 + \frac{4}{3} \left(1 - \frac{1}{\sqrt{3}}\right)^2 \right] \frac{1}{64 \left(20 - \frac{1}{\sqrt{3}}\right)} = -0.36892 \end{aligned}$$

A three-point integration gives $S_{11}^{00} = -0.36998$.

Evaluating the integrals in Eq. (9.3.24) using 2×2 quadrature rule, we obtain

$$[S^{00}] = \begin{bmatrix} 2.27778 & 1.25000 & 0.55556 & 1.00000 \\ 1.25000 & 2.72222 & 1.22222 & 0.55556 \\ 0.55556 & 1.22222 & 2.16667 & 0.97222 \\ 1.00000 & 0.55556 & 0.97222 & 1.72222 \end{bmatrix} \text{ (exact)}$$

$$[S^{11}] = \begin{bmatrix} 0.40995 & -0.36892 & -0.20479 & 0.16376 \\ -0.36892 & 0.34516 & 0.25014 & -0.22639 \\ -0.20479 & 0.25014 & 0.43155 & -0.47690 \\ 0.16376 & -0.22639 & -0.47690 & 0.53953 \end{bmatrix} \text{ (inexact)}$$

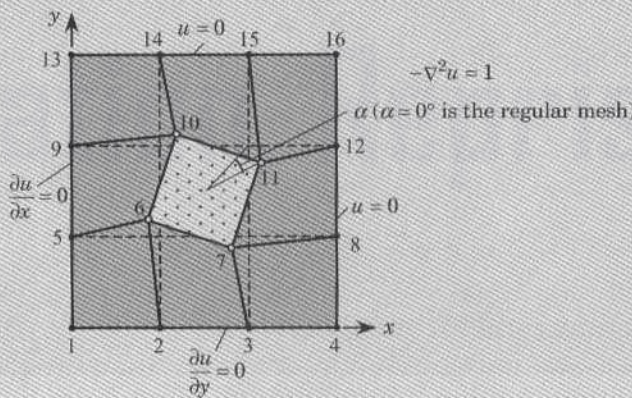
$$[S^{22}] = \begin{bmatrix} 0.26237 & 0.16389 & -0.13107 & -0.29520 \\ 0.16389 & 0.22090 & -0.23991 & -0.14489 \\ -0.13107 & -0.23991 & 0.27619 & 0.09478 \\ -0.29520 & -0.14489 & 0.09478 & 0.34530 \end{bmatrix} \text{ (inexact)}$$

$$[S^{12}] = \begin{bmatrix} 0.24731 & 0.25156 & -0.25297 & -0.24589 \\ -0.24844 & -0.25090 & 0.25172 & 0.24762 \\ -0.25297 & -0.24828 & 0.24671 & 0.25454 \\ 0.25411 & 0.24762 & -0.24546 & -0.25627 \end{bmatrix} \text{ (inexact)}$$

These matrices would have been exact if the element had its sides parallel to the coordinate system (i.e., for a rectangular element). The values are accurate enough to yield good solutions for most problems (depends on the problem).

To see the effect of skewed elements on the accuracy of the results, we revisit the problem in Example 8.3.1. We consider the nine-element mesh shown in the figure below and investigate the effect of skewness (measured in terms of the angle α) on the solution accuracy. The same number of Gauss points (2×2) as in the case of a regular mesh are used. The results are summarized below (compare with the results in Table 8.3.1). The results are not very sensitive to the mesh distortion.

$\alpha = 0^\circ$	$\alpha = 15^\circ$	$\alpha = 30^\circ$	$\alpha = 45^\circ$
0.3014	0.2972	0.3017	0.2972



9.3.4 Integration over a Master Triangular Element

In the preceding section we discussed numerical integration on quadrilateral elements that can be used to represent very general geometries as well as field variables in a variety of problems. Here we discuss numerical integration on triangular elements. Since quadrilateral elements can be geometrically distorted, it is possible to distort a quadrilateral element to obtain a required triangular element by moving the position of the corner nodes to one of the neighboring nodes. In actual computation, this is achieved by assigning the same global node number to two corner nodes of the quadrilateral element. Thus, master triangular elements can be obtained in a natural way from associated master rectangular elements. Here we discuss the transformations from an arbitrary triangular element to an arbitrary triangular element.

We choose the unit right isosceles triangle [see Fig. 9.3.6(a)] as the master element. An arbitrary triangular element Ω_e can be generated from the master triangular element $\hat{\Omega}_T$ by transformation of the form (9.3.1). The coordinate lines $\xi = 0$ and $\eta = 0$ in $\hat{\Omega}_T$ correspond to the skew curvilinear coordinate lines 1–3 and 1–2 in Ω_e . For the three-node triangular element, the transformation (9.3.1) is taken to be

$$x = \sum_{i=1}^3 x_i \hat{\psi}_i(\xi, \eta), \quad y = \sum_{i=1}^3 y_i \hat{\psi}_i(\xi, \eta) \quad (9.3.26)$$

where $\hat{\psi}_i(\xi, \eta)$ are the interpolation functions of the master three-node triangular element [see Fig. 9.3.6(b)],

$$\hat{\psi}_1 = 1 - \xi - \eta, \quad \hat{\psi}_2 = \xi, \quad \hat{\psi}_3 = \eta \quad (9.3.27)$$

The inverse transformation from element Ω_e to $\hat{\Omega}_T$ is given by inverting Eqs. (9.3.26):

$$\begin{aligned} \xi &= \frac{1}{2A} [(x - x_1)(y_3 - y_1) - (y - y_1)(x_3 - x_1)] \\ \eta &= \frac{1}{2A} [(x - x_1)(y_1 - y_2) + (y - y_1)(x_2 - x_1)] \end{aligned} \quad (9.3.28)$$

where A is the area of Ω_e .

With the help of (9.3.28), we can show that the interpolation functions in (8.2.25b) are equivalent to the $\hat{\psi}_i$ in Eqs. (9.3.27). Moreover, the area coordinates L_i in (9.2.9) are also equivalent to $\hat{\psi}_i$. The interpolation functions for the linear and higher-order triangular elements can be obtained from the area coordinates, as described in Section 9.2.

The Jacobian matrix for the linear triangular element is given by

$$[J]^{-1} = \begin{bmatrix} x_2 - x_1 & y_2 - y_1 \\ x_3 - x_1 & y_3 - y_1 \end{bmatrix} = \begin{bmatrix} \gamma_3 & -\beta_3 \\ -\gamma_2 & \beta_2 \end{bmatrix} \quad (9.3.29)$$

where β_i and γ_i are the constants defined in (8.2.24b). The inverse of the Jacobian matrix is given by

$$[J]^{-1} = \frac{1}{J} \begin{bmatrix} \beta_2 & \beta_3 \\ \gamma_2 & \gamma_3 \end{bmatrix}, \quad J = \beta_2 \gamma_3 - \gamma_2 \beta_3 = 2A \quad (9.3.30)$$

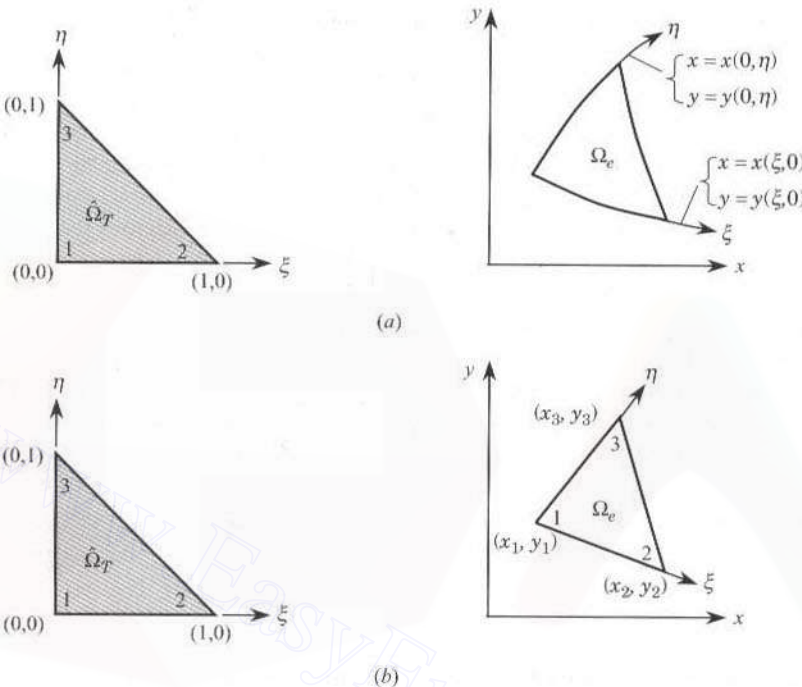


Figure 9.3.6 Triangular master finite element and its transformations: (a) general transformation; and (b) linear transformation of a master element to a triangular element.

The relations in (9.3.9) for isoparametric formulation with linear triangular elements have the explicit form,

$$\begin{aligned} \frac{\partial \psi_1}{\partial x} &= -\frac{\beta_2 + \beta_3}{2A} = \frac{\beta_1}{2A}, & \frac{\partial \psi_1}{\partial y} &= -\frac{\gamma_2 + \gamma_3}{2A} = \frac{\gamma_1}{2A} \\ \frac{\partial \psi_2}{\partial x} &= \frac{\beta_2}{2A}, & \frac{\partial \psi_2}{\partial y} &= \frac{\gamma_2}{2A}, & \frac{\partial \psi_3}{\partial x} &= \frac{\beta_3}{2A}, & \frac{\partial \psi_3}{\partial y} &= \frac{\gamma_3}{2A} \end{aligned} \quad (9.3.31)$$

In a general case, the derivatives of ψ_i with respect to the global coordinates can be computed from Eqs.(9.3.9), which take the form

$$\begin{aligned} \frac{\partial \psi_i}{\partial x} &= \frac{\partial \psi_i}{\partial L_1} \frac{\partial L_1}{\partial x} + \frac{\partial \psi_i}{\partial L_2} \frac{\partial L_2}{\partial x} \\ \frac{\partial \psi_i}{\partial y} &= \frac{\partial \psi_i}{\partial L_1} \frac{\partial L_1}{\partial y} + \frac{\partial \psi_i}{\partial L_2} \frac{\partial L_2}{\partial y} \end{aligned} \quad (9.3.32a)$$

or

$$\left\{ \begin{array}{l} \frac{\partial \psi_i}{\partial x} \\ \frac{\partial \psi_i}{\partial y} \end{array} \right\} = [J]^{-1} \left\{ \begin{array}{l} \frac{\partial \psi_i}{\partial L_1} \\ \frac{\partial \psi_i}{\partial L_2} \end{array} \right\}, [J] = \begin{bmatrix} \frac{\partial x}{\partial L_1} & \frac{\partial y}{\partial L_1} \\ \frac{\partial x}{\partial L_2} & \frac{\partial y}{\partial L_2} \end{bmatrix} \quad (9.3.32b)$$

Note that only L_1 and L_2 are treated as linearly independent coordinates, because $L_3 = 1 - L_1 - L_2$.

After transformation, integrals on $\hat{\Omega}_T$ have the form

$$\int_{\hat{\Omega}_T} G(\xi, \eta) d\xi d\eta = \int_{\hat{\Omega}_T} \hat{G}(L_1, L_2, L_3) dL_1 dL_2 \quad (9.3.33)$$

which can be approximated by the quadrature formula

$$\int_{\hat{\Omega}_T} \hat{G}(L_1, L_2, L_3) dL_1 dL_2 \approx \frac{1}{2} \sum_{I=1}^N W_I \hat{G}(\mathbf{S}_I) \quad (9.3.34)$$

where W_I and \mathbf{S}_I denote the weights and integration points of the quadrature rule. Table 9.3.2 contains the location of integration points and weights for one-, three-, and seven-point quadrature rules over triangular elements. For evaluation of integrals whose integrands are polynomials of degree higher than five (in any of the area coordinates), the reader should consult books on numerical integration [e.g., see Froberg (1969) and Carnahan, et al. (1969)].

Table 9.3.2 Quadrature points and weights for triangular elements.

Number of integration points	Degree of polynomial and order of the residual	Integration points and weights				Nodes	Geometric locations
		L_1	L_2	L_3	W		
1	1; $O(h^2)$	$\frac{1}{3}$	$\frac{1}{3}$	$\frac{1}{3}$	1	a	
3	2; $O(h^3)$	$\frac{1}{2}$	0	$\frac{1}{2}$	$\frac{1}{3}$	a	
		$\frac{1}{2}$	$\frac{1}{2}$	0	$\frac{1}{3}$	b	
		0	$\frac{1}{2}$	$\frac{1}{2}$	$\frac{1}{3}$	c	
4	3; $O(h^4)$	$\frac{1}{3}$	$\frac{1}{3}$	$\frac{1}{3}$	$-\frac{27}{48}$	a	
		0.6	0.2	0.2	$\frac{25}{48}$	b	
		0.2	0.6	0.2	$\frac{25}{48}$	c	
		0.2	0.2	0.6	$\frac{25}{48}$	d	
7	5; $O(h^6)$	$\frac{1}{3}$	$\frac{1}{3}$	$\frac{1}{3}$	0.225	a	
		α_1^+	β_1	β_1	W_2	b	
		β_1	α_1	β_1		c	
		α_2	β_2	β_2	W_3	d	
		β_2	α_2	β_2		e	
		β_2	β_2	α_2		f	
						g	

[†] $\alpha_1 = 0.797\ 426\ 985\ 353$, $\beta_1 = 0.101\ 286\ 507\ 323$, $\alpha_2 = 0.059\ 715\ 871\ 789$, $\beta_2 = 0.470\ 142\ 064\ 105$, $W_2 = 0.125\ 939\ 180\ 544$, $W_3 = 0.132\ 394\ 152\ 788$.

Example 9.3.4

Consider the quadratic triangular element shown in Fig. 9.3.7. We wish to calculate $\partial\psi_1/\partial x$, $\partial\psi_1/\partial y$, $\partial\psi_4/\partial x$, and $\partial\psi_4/\partial y$ at the point $(x, y) = (2, 4)$ and evaluate the integral of the product $(\partial\psi_1/\partial x)(\partial\psi_4/\partial x)$.

Since the element has straight edges, its geometry is defined by the interpolation functions of the corner nodes (i.e., subparametric formulation can be used). Note that if the element is curvilinear, we cannot use three corner nodes only to describe the geometry exactly (hence, the isoparametric formulation must be used). For the element at hand, we have

$$\begin{aligned} x &= \sum_{i=1}^3 x_i L_i = 7L_2 + 2L_3 = 2 - 2L_1 + 5L_2 \\ y &= \sum_{i=1}^3 y_i L_i = 2L_2 + 6L_3 = 6 - 6L_1 - 4L_2 \end{aligned} \quad (9.3.35a)$$

$$[J] = \begin{bmatrix} -2 & -6 \\ 5 & -4 \end{bmatrix}, \quad [J]^{-1} = \frac{1}{38} \begin{bmatrix} -4 & 6 \\ -5 & -2 \end{bmatrix}$$

$$\begin{aligned} \begin{Bmatrix} \frac{\partial\psi_1}{\partial x} \\ \frac{\partial\psi_1}{\partial y} \end{Bmatrix} &= \frac{1}{38} \begin{bmatrix} -4 & 6 \\ -5 & -2 \end{bmatrix} \begin{Bmatrix} \frac{\partial\psi_1}{\partial L_1} \\ \frac{\partial\psi_1}{\partial L_2} \end{Bmatrix} = \begin{Bmatrix} \frac{-4(4L_1 - 1)}{38} \\ \frac{-5(4L_1 - 1)}{38} \end{Bmatrix} \\ \begin{Bmatrix} \frac{\partial\psi_4}{\partial x} \\ \frac{\partial\psi_4}{\partial y} \end{Bmatrix} &= \frac{1}{38} \begin{bmatrix} -4 & 6 \\ -5 & -2 \end{bmatrix} \begin{Bmatrix} \frac{\partial\psi_4}{\partial L_1} \\ \frac{\partial\psi_4}{\partial L_2} \end{Bmatrix} = \frac{1}{38} \begin{Bmatrix} -16L_2 + 24L_1 \\ -20L_2 - 8L_1 \end{Bmatrix} \end{aligned} \quad (9.3.35b)$$

where $\psi_1 = L_1(2L_1 - 1)$ and $\psi_4 = 4L_1L_2$ [see Eq. (9.2.16) and Fig. 9.2.4(b)], so that

$$\frac{\partial\psi_1}{\partial L_1} = L_1 - 1, \quad \frac{\partial\psi_1}{\partial L_2} = 0, \quad \frac{\partial\psi_4}{\partial L_1} = 4L_2, \quad \frac{\partial\psi_4}{\partial L_2} = 4L_1$$

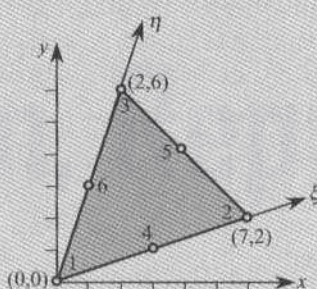


Figure 9.3.7 A quadratic triangular element in the global (x, y) and local coordinate systems (Example 9.3.4).

For the point (2, 4), the area coordinates can be calculated from Eqs. (9.3.35a):

$$2 = 7L_2 + 2L_3, \quad 4 = 2L_2 + 6L_3$$

Once L_2 and L_3 are computed from the above relations, L_1 is found from the relation $L_1 = 1 - L_2 - L_3$. We have

$$L_1 = \frac{5}{19}, \quad L_2 = \frac{2}{19}, \quad L_3 = \frac{12}{19}$$

Evaluating $\partial\psi_1/\partial x$ and $\partial\psi_4/\partial y$ at the point (2, 4), we obtain

$$\begin{aligned} \frac{\partial\psi_1}{\partial x} &= -\frac{2}{19}\left(\frac{20}{19}-1\right) = -\frac{2}{361} \\ \frac{\partial\psi_1}{\partial y} &= -\frac{5}{38}\left(4\times\frac{5}{19}-1\right) = -\frac{5}{722} \\ \frac{\partial\psi_4}{\partial x} &= -\frac{16}{(19)^2} + \frac{60}{(19)^2} = \frac{44}{361} \\ \frac{\partial\psi_4}{\partial y} &= -\frac{20}{(19)^2} - \frac{20}{(19)^2} = -\frac{40}{361} \end{aligned} \quad (9.3.36)$$

The integral of $(\partial\psi_1/\partial x)(\partial\psi_4/\partial y)$ over the quadratic element is ($J = 38$)

$$\int_{\Omega_T} \frac{\partial\psi_1}{\partial x} \frac{\partial\psi_4}{\partial y} dx dy = -\frac{4J}{361} \int_0^1 \int_0^{1-L_2} (4L_1 - 1)(6L_1 - 4L_2) dL_1 dL_2$$

Since the integrand is quadratic in L_1 and bilinear in L_1 and L_2 , we use the three-point quadrature (see Table 9.3.2) to evaluate the integral exactly [see Eq. (9.3.34)]:

$$\begin{aligned} &-\frac{4J}{361} \int_0^1 \int_0^{1-L_2} (4L_1 - 1)(6L_1 - 4L_2) dL_1 dL_2 \\ &= -\frac{1}{2} \frac{4 \times 38}{361} \left[\left(\frac{4}{2}-1\right)\left(\frac{6}{2}-0\right) + \left(\frac{4}{2}-1\right)\left(\frac{6}{2}-\frac{4}{2}\right) + (0-1)\left(0-\frac{4}{2}\right) \right] \\ &= -\frac{8}{19} \end{aligned} \quad (9.3.37)$$

The result can be verified using the exact integration formula in (9.2.18b):

$$\int_{\Omega_T} \frac{\partial\psi_1}{\partial x} \frac{\partial\psi_4}{\partial y} dx dy = \frac{4}{361} \left[6 \times \frac{1}{3!} - 4 \times \frac{1}{3!} - 24 \times \frac{2!}{4!} + 16 \times \frac{1}{4!} \right] 2A = -\frac{8}{19}$$

The area A of the triangle is equal to 19, and therefore we obtain the same result as above.

9.4 MODELING CONSIDERATIONS

9.4.1 Preliminary Comments

Numerical simulation of a physical processes requires (a) a mathematical model that describes the process and (b) a numerical method to analyze the mathematical model. In

the development of a mathematical model we often make a set of assumptions about the process (e.g., constitutive behavior, loads, and boundary conditions) to derive the mathematical relationships governing the system. The mathematical model, which is often in the form of differential equations, is used to gain an understanding of how the corresponding process works. If the relationships are simple, it is possible to obtain *exact* information on the quantities of interest. This is known as the *analytic* solution. However, most practical problems are too complicated to allow analytical solutions of the models. Hence, these mathematical models must be studied by numerical methods, such as the finite element method.

Finite element analysis is a numerical simulation of a physical process. Therefore, finite element modeling involves assumptions concerning the representation of the system and/or its behavior. Valid assumptions can be made only if we have a qualitative understanding of how the process or system works. A good knowledge of the basic principles governing the process and the finite element theory enable the development of a good numerical model of the actual process.

Here we discuss several aspects of development of finite element models. Guidelines concerning element geometries, mesh refinements, and load representations are given.

9.4.2 Element Geometries

Recall from Section 9.3 that the numerical evaluation of integrals over actual elements involves a coordinate transformation from the actual element to a master element. The transformation is acceptable if and only if every point in the actual element is mapped uniquely into a point in the master element, and vice versa. Such mappings are termed *one-to-one*. This requirement can be expressed as [see Eq. (9.3.12)]

$$J^e \equiv \det[J^e] > 0 \quad \text{everywhere in the element } \Omega_e \quad (9.4.1)$$

where $[J^e]$ is the Jacobian matrix in Eq. (9.3.11b). Geometrically, the Jacobian J^e represents the ratio of an area element in the real element to the corresponding area element in the master element,

$$dA \equiv dx dy = J^e d\xi d\eta$$

If J^e is zero, then a nonzero area element in the real element is mapped into zero area in the master element, which is unacceptable. Also, if $J^e < 0$, a right-handed coordinate system is mapped into a left-handed coordinate system.

In general, the Jacobian is a function of ξ and η , implying that the real element is nonuniformly mapped into the master element, i.e., the element is distorted. Excessive distortion of elements is not good because a nonzero area element can be mapped into a zero or nearly zero area.

To ensure $J^e > 0$ and keep within the extreme limits of acceptable distortion, certain geometric shapes of real elements must be avoided. For example, the interior angle at each vertex of a triangular element should not be equal to either 0° or 180° . Indeed, in practice the angle should reasonably be larger than 0° and smaller than 180° to avoid numerical ill-conditioning of element matrices. Although the acceptable range depends on the problem, the range $15^\circ - 165^\circ$ can be used as a guide. Figure 9.4.1 shows elements with unacceptable vertex angles for straight-sided and curved-sided elements.

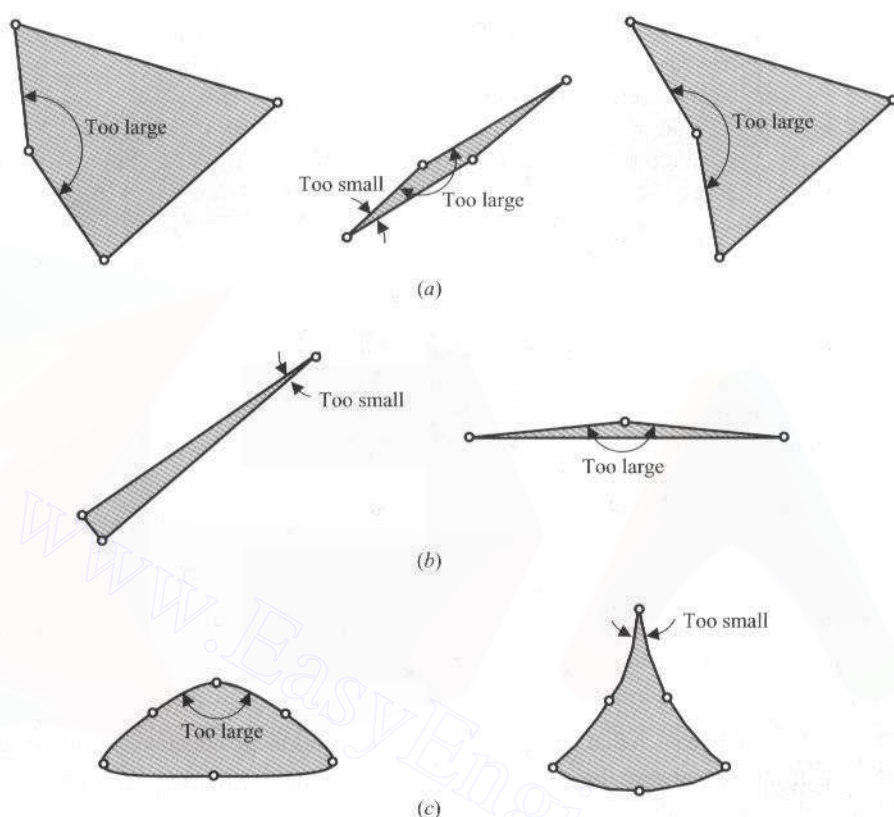


Figure 9.4.1 Finite elements with unacceptable vertex angles: (a) linear quadrilateral elements; (b) linear triangular elements; and (c) quadratic triangular elements. The angles marked are either too small compared with 0° or too large compared with 180° .

For higher-order Lagrange elements (also called the C^0 elements), the locations of the interior nodes contribute to the element distortion, and therefore they are constrained to lie within certain distance from the vertex nodes. For example, in the case of a quadratic element the midside node should be at a distance not less than one-fourth of the length of the side from the vertex nodes (see Fig. 9.4.2). When the midside node is located exactly at a distance of one-fourth of the side length from a vertex, the element exhibits special properties (see Problem 9.19). Such elements, called *quarter-point elements*, are used in fracture mechanics problems to represent an inverse square-root singularity in the gradient of the solution at the nearest vertex node.

9.4.3 Mesh Generation

Generation of a finite element mesh for a given problem should follow the guidelines listed below:

1. The mesh should represent the geometry of the computational domain and load representation accurately.

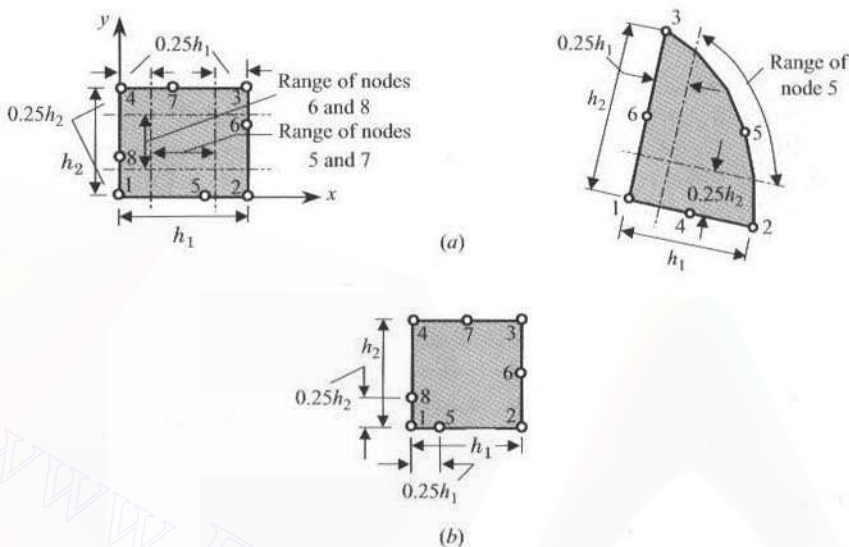


Figure 9.4.2 Range of acceptable locations of the midside nodes for quadratic elements: (a) eight-node quadratic element and six-node quadratic triangular element; and (b) the quarter-point quadrilateral element.

2. The mesh should be such that large gradients in the solution are adequately represented.
3. The mesh should not contain elements with unacceptable geometries, especially in regions of large gradients.

Within the above guidelines, the mesh used can be *coarse* (i.e., have few elements) or *refined* (i.e., have many elements), and may consist of one or more orders and types of elements (e.g., linear and quadratic, triangular and quadrilateral). A judicious choice of element order and type could save computational cost while giving accurate results. It should be noted that the choice of elements and mesh is problem-dependent. What works well for one problem may not work well for another problem. An analyst with physical insight into the process being simulated can make a better choice of elements and mesh for the problem at hand. We should start with a coarse mesh that meets the three requirements listed above, exploit symmetries available in the problem, and evaluate the results thus obtained in light of physical understanding and approximate analytical and/or experimental information. These results can be used to guide subsequent mesh refinements and analyses.

Generation of meshes of single element type is easy because elements of the same degree are compatible with each other (see Fig. 9.4.3). Mesh refinements involve several options. Refine the mesh by subdividing existing elements into two or more elements of the same type [see Fig. 9.4.4(a)]. This is called the *h-version mesh refinement*. Alternatively, existing elements can be replaced by elements of higher order [see Fig. 9.4.4(b)]. This type of refinement is called the *p-version mesh refinement*. The *h, p-version mesh refinement*, in which elements are subdivided into two or more elements in some places and replaced with higher-order elements in other places. Generally, local mesh refinements should be such that very small elements are not placed adjacent to very large ones (see Fig. 9.4.5).

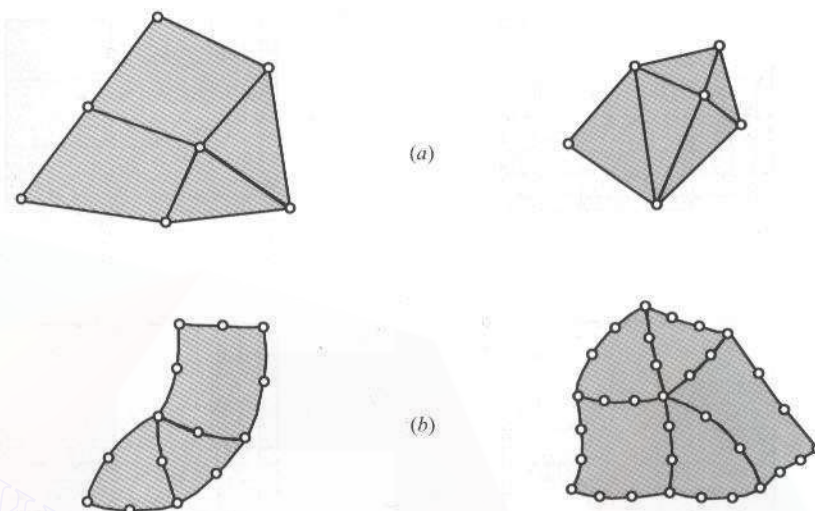


Figure 9.4.3 Connecting elements of the same order. The C^0 elements of the same order ensure the C^0 continuity along the element interfaces: (a) linear elements; and (b) quadratic and cubic elements.

Combining elements of different *kinds* naturally arises in solid and structural mechanics problems. For example, plate bending elements (2-D) can be connected to a beam element (1-D). If the plate element is based on the classical plate theory (see Chapter 12), the beam element should be one based on the Euler–Bernoulli beam theory so that they have the same degrees of freedom at the connecting node. When a plane elasticity element (see Chapter 11) is connected to a beam element, which are not compatible with the former

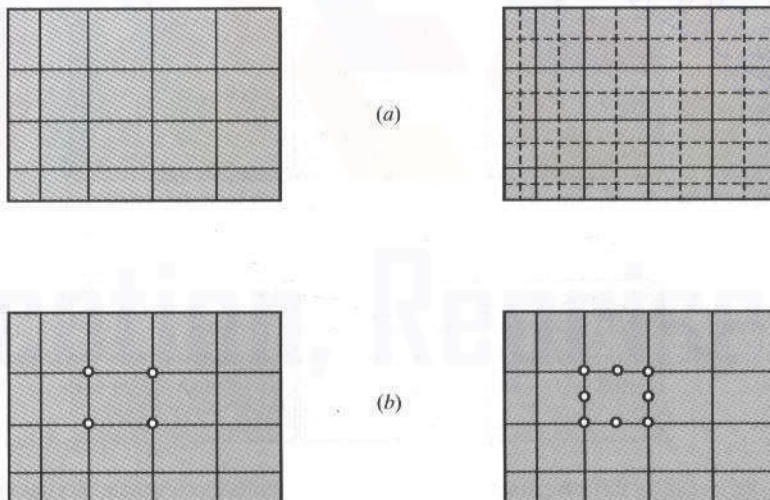


Figure 9.4.4 The (a) *h*-version and (b) *p*-version mesh refinements.

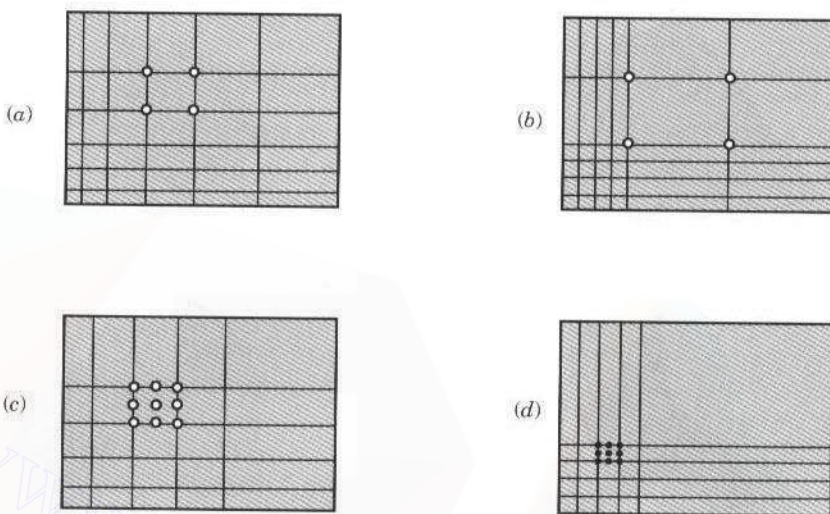


Figure 9.4.5 Finite element mesh refinements. Meshes shown in (a) and (c) are acceptable, and those shown in (b) and (d) are unacceptable.

in terms of the degrees of freedom at the nodes, we must construct a special element that makes the transition from the 2-D plane elasticity element to the 1-D beam element (see Problem 11.8). Such elements are called *transition elements*.

Combining elements of different order, say linear to quadratic elements, may be necessary to accomplish local mesh refinements. There are two ways to do this. One way is to use a transition element, which has different number of nodes on different sides [see Fig. 9.4.6(a)]. The other way is to impose a condition that constrains the midside node

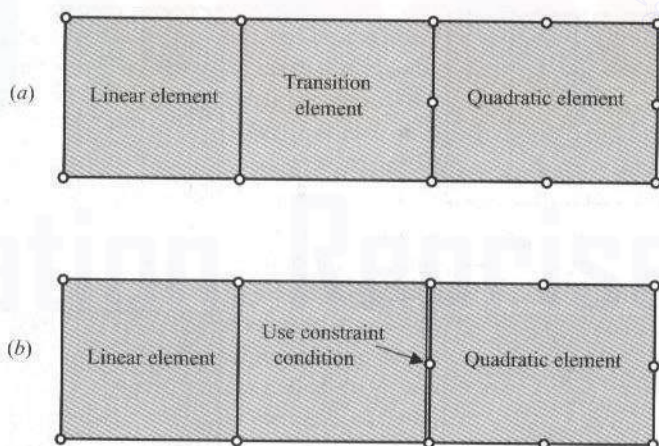


Figure 9.4.6 Combining different order elements: (a) use of a transition element that has three sides linear and one side quadratic; and (b) use of a linear constraint equation to connect a linear side to a quadratic side.

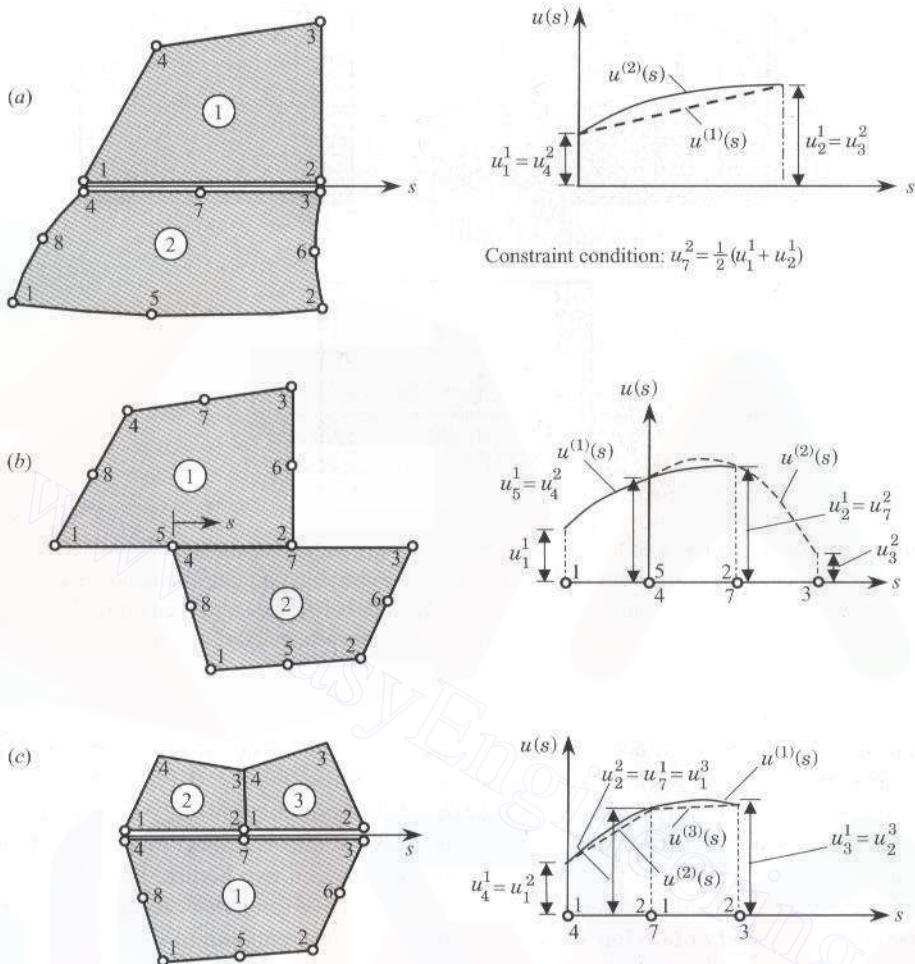


Figure 9.4.7 Various types of incompatible connections of finite elements. In all cases the interelement continuity of the function is violated along the connecting side.

to have the same value as that experienced at the node by the lower-order element [see Fig. 9.4.6(b)]. However, such combinations do not enforce interelement continuity of the solution along the entire interface. Figure 9.4.7 contains element connections that do not satisfy the C^0 continuity along the connecting sides. Use of transition elements and constraint conditions in local mesh refinements is a common practice. Figure 9.4.8 shows a few examples of such refinements.

9.4.4 Load Representation

Computation of the nodal contributions of a distributed boundary source was discussed in Chapter 8 [see Eq. (8.2.56)]. The accuracy of the result depends on the element and mesh used to represent the domain. For example, in heat transfer problems the boundary source

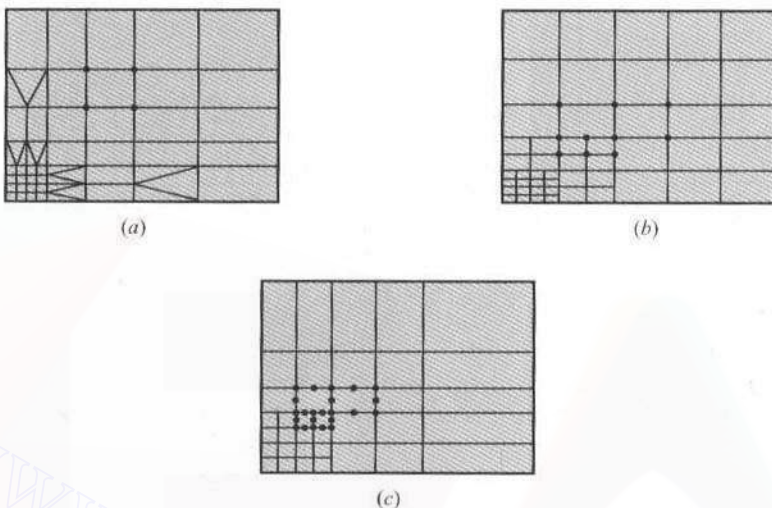


Figure 9.4.8 Some examples of local mesh refinements; (a) with compatible (C^0 -continuous) elements; (b) with transition elements (or when constraint conditions are imposed) between linear elements; and (c) with transition elements between quadratic elements. In (b) and (c), the transition elements can be between linear and quadratic, and quadratic and cubic elements, respectively.

is the heat flux across (i.e., normal to) the boundary. Use of linear elements, for example, to represent the boundary will change the actual distribution (see Fig. 9.4.9). Of course, h -version or p -version mesh refinements will improve the representation of the boundary flux.

Another situation where representation of boundary forces is subject to different interpretations is found when the force is due to contact between two bodies. For example, a solid plate in contact with a circular disc generates a reactive force that can be represented either as a point load or as a locally distributed force. Representation of the contact force

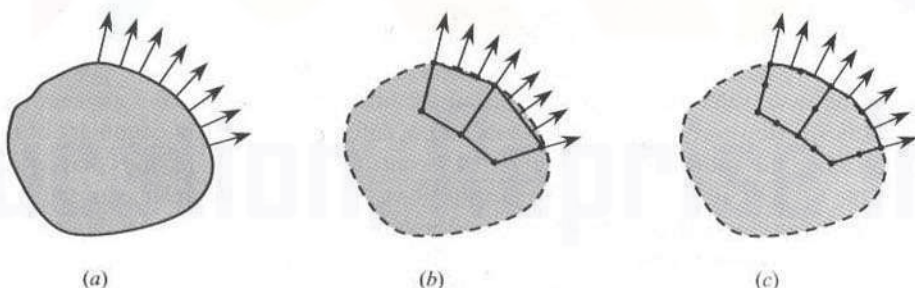


Figure 9.4.9 Approximation of the boundary fluxes in the finite element method; (a) actual geometry of the domain and distribution of flux; (b) approximation of the domain by linear finite elements and associated representation of the boundary flux; and (c) approximation of the domain by quadratic finite elements and associated representation of the boundary flux.

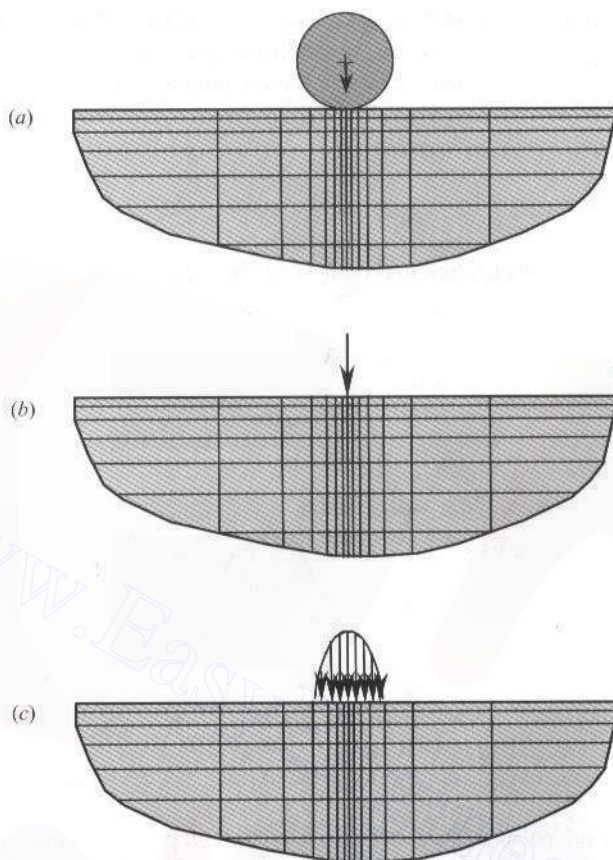


Figure 9.4.10 Representation of contact pressure developed between two bodies; (a) geometry of the bodies in contact; (b) representation of the contact pressure as a point load; and (c) representation of the contact pressure as a distributed surface load. In the latter case, often the surface area of the distributed force is unknown.

between deformable bodies as a point load is an approximation of the true distribution. A sine distribution might be more realistic representation of the actual force (see Fig. 9.4.10).

9.5 SUMMARY

In this chapter three major topics have been discussed: (1) Lagrange interpolation functions for triangular and rectangular elements; (2) numerical integration to evaluate integral expressions over triangular and rectangular elements; and (3) some modeling guidelines. Interpolation functions for linear, quadratic, and cubic triangular elements are developed using the area coordinates. Linear, quadratic, and cubic interpolation functions for Lagrange and serendipity family of rectangular elements are also developed. A systematic description of numerical evaluation of integral expressions involving interpolation functions and their derivatives with respect to global coordinates has been presented. This development is

suitable for computer implementation, as will be seen in Chapter 13. Modeling is an art that can be improved by experience and understanding of physical interactions involved in the process. It is necessary to critically evaluate the computed results before using them. The guidelines are given to encourage good modeling practice, and they should be followed to determine the actual “working” model.

PROBLEMS

- 9.1** Show that the interpolation functions for the three-node equilateral triangular element given in Fig. P9.1 are

$$\psi_1 = \frac{1}{2} \left(1 - \xi - \frac{1}{\sqrt{34}} \eta \right), \quad \psi_2 = \frac{1}{2} \left(1 + \xi - \frac{1}{\sqrt{34}} \eta \right), \quad \psi_3 = \frac{1}{\sqrt{34}} \eta$$

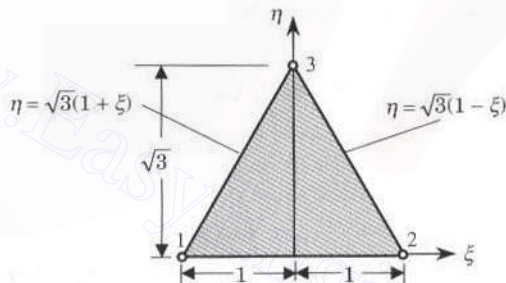


Figure P9.1

- 9.2** Show that the interpolation functions that involve the term $\xi^2 + \eta^2$ for the five-node rectangular element shown in Fig. P9.2 are given by

$$\begin{aligned}\psi_1 &= 0.25(-\xi - \eta + \xi\eta) + 0.125(\xi^2 + \eta^2) \\ \psi_2 &= 0.25(\xi - \eta - \xi\eta) + 0.125(\xi^2 + \eta^2) \\ \psi_3 &= 0.25(\xi + \eta + \xi\eta) + 0.125(\xi^2 + \eta^2) \\ \psi_4 &= 0.25(-\xi + \eta - \xi\eta) + 0.125(\xi^2 + \eta^2) \\ \psi_5 &= 1 - 0.5(\xi^2 + \eta^2)\end{aligned}$$

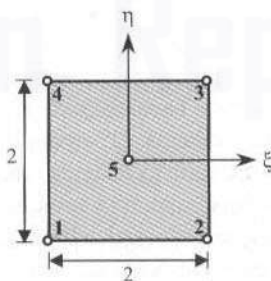


Figure P9.2

- 9.3 Calculate the interpolation functions $\psi_i(x, y)$ for the quadratic triangular element shown in Fig. P9.3. Hint: Use Eq. (9.2.16), where L_i are given by Eq. (9.2.9).

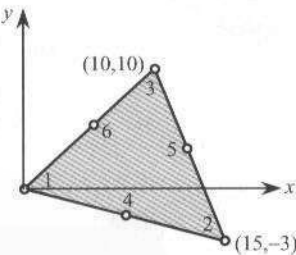


Figure P9.3

- 9.4 Determine the interpolation function ψ_{14} in terms of the area coordinates, L_i for the triangular element shown in Fig. P9.4.

Answer: $32L_1L_2L_3(4L_2 - 1)$.

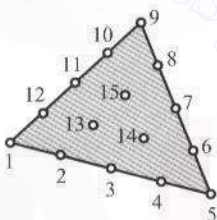


Figure P9.4

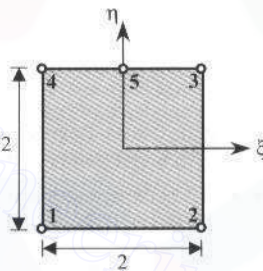


Figure P9.6

- 9.5 Derive the interpolation function of a corner node in a cubic serendipity element.

- 9.6 Consider the five-node element shown in Fig. P9.6. Using the basic linear and quadratic interpolations along the coordinate directions ξ and η , derive the interpolation functions for the element. Note that the element can be used as a transition element connecting four-node elements to eight- or nine-node elements.

- 9.7 (*Nodeless variables*) Consider the four-node rectangular element with interpolation of the form

$$u = \sum_{i=1}^4 u_i \psi_i + \sum_{i=1}^4 c_i \phi_i$$

where u_i are the nodal values and c_i are arbitrary constants. Determine the form of ψ_i and ϕ_i for the element.

- 9.8–9.10 Determine the Jacobian matrix and the transformation equations for the elements given in Fig. P9.8–P9.10.

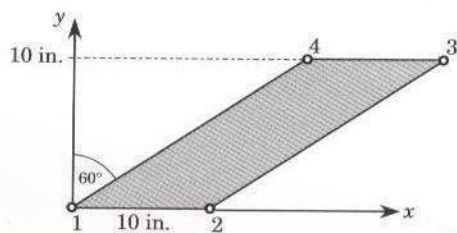


Figure P9.8

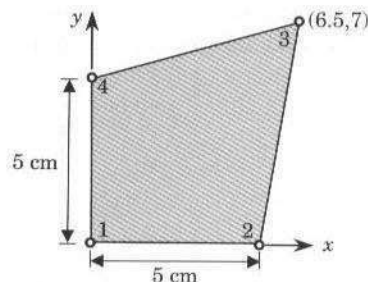


Figure P9.9

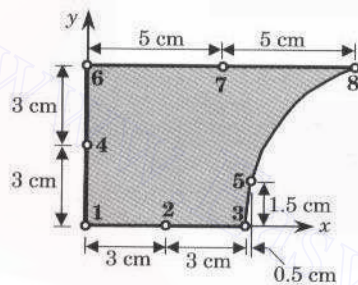


Figure P9.10

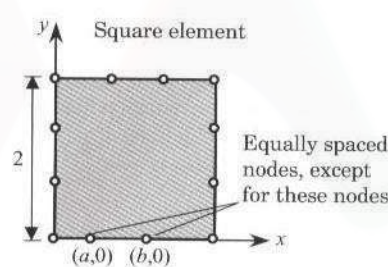


Figure P9.12

9.11 Using the Gauss-Legendre quadrature, determine the contribution of a constant distributed source to nodal points of the four-node finite element in Fig. P9.9.

9.12 For a 12-node serendipity (cubic) element, as illustrated in Fig. P9.12, show that the Jacobian $J = J_{11}$ is

$$\begin{aligned} J &= 0.4375 + 0.84375(b-a) + 0.5625\eta - 0.84375(b-a)\eta \\ &\quad + 1.125\xi - 0.5625(a+b)\xi - 1.125\eta\xi + 0.5625(a+b)\eta\xi \\ &\quad + 1.6875\xi^2 - 2.53125(b-a)\xi^2 - 1.6875\eta\xi^2 + 2.53125(b-a)\eta\xi^2 \end{aligned}$$

What can you conclude from the requirement $J > 0$?

9.13 Determine the Jacobian of the eight-node rectangular element of Fig. P9.13 in terms of the parameter a .

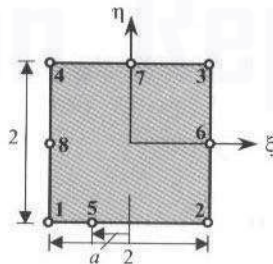


Figure P9.13

- 9.14** Determine the conditions on the location of node 3 of the quadrilateral element shown in Fig. P9.14. Show that the transformation equations are given by

$$x = \frac{1}{4}(1+\xi)[2(1-\eta) + a(1+\eta)]$$

$$y = \frac{1}{4}(1+\eta)[2(1-\xi) + b(1+\xi)]$$

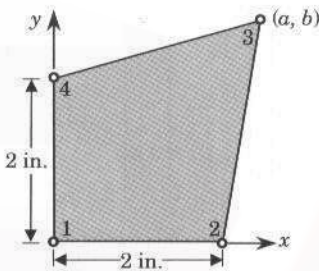


Figure P9.14

- 9.15** Determine the global derivatives of the interpolation functions for node 3 of the element shown in Fig. P9.9.

- 9.16** Let the transformation between the global coordinates (x, y) and local normalized coordinates (ξ, η) in a Lagrange element Ω_e be

$$x = \sum_{i=1}^m x_i \hat{\psi}_i(\xi, \eta), \quad y = \sum_{i=1}^m y_i \hat{\psi}_i(\xi, \eta)$$

where (x_i, y_i) denote the global coordinates of the element nodes. The differential lengths in the two coordinates are related by

$$dx_e = \frac{\partial x_e}{\partial \xi} d\xi + \frac{\partial x_e}{\partial \eta} d\eta, \quad dy_e = \frac{\partial y_e}{\partial \xi} \xi + \frac{\partial y_e}{\partial \eta} d\eta$$

or

$$\begin{Bmatrix} dx_e \\ dy_e \end{Bmatrix} = \begin{bmatrix} \frac{\partial x_e}{\partial \xi} & \frac{\partial x_e}{\partial \eta} \\ \frac{\partial y_e}{\partial \xi} & \frac{\partial y_e}{\partial \eta} \end{bmatrix} \begin{Bmatrix} d\xi \\ d\eta \end{Bmatrix} = [\mathcal{T}] \begin{Bmatrix} d\xi \\ d\eta \end{Bmatrix}$$

In the finite element literature, the transpose of $[\mathcal{T}]$ is called the Jacobian matrix, $[J]$. Show that the derivatives of the interpolation function $\psi_i^e(\xi, \eta)$ with respect to the global coordinates (x, y) are related to their derivatives with respect to the local coordinates (ξ, η) by

$$\begin{Bmatrix} \frac{\partial \psi_i^e}{\partial x} \\ \frac{\partial \psi_i^e}{\partial y} \end{Bmatrix} = [J]^{-1} \begin{Bmatrix} \frac{\partial \psi_i^e}{\partial \xi} \\ \frac{\partial \psi_i^e}{\partial \eta} \end{Bmatrix}$$

and

$$\begin{aligned} \begin{Bmatrix} \frac{\partial^2 \psi_i^e}{\partial x^2} \\ \frac{\partial^2 \psi_i^e}{\partial y^2} \\ \frac{\partial^2 \psi_i^e}{\partial x \partial y} \end{Bmatrix} &= \begin{bmatrix} \left(\frac{\partial x_e}{\partial \xi}\right)^2 & \left(\frac{\partial y_e}{\partial \xi}\right)^2 & 2\frac{\partial x_e}{\partial \xi} \frac{\partial y_e}{\partial \xi} \\ \left(\frac{\partial x_e}{\partial \eta}\right)^2 & \left(\frac{\partial y_e}{\partial \eta}\right)^2 & 2\frac{\partial x_e}{\partial \eta} \frac{\partial y_e}{\partial \eta} \\ \frac{\partial x_e}{\partial \xi} \frac{\partial x_e}{\partial \eta} & \frac{\partial y_e}{\partial \xi} \frac{\partial y_e}{\partial \eta} & \frac{\partial x_e}{\partial \eta} \frac{\partial y_e}{\partial \xi} + \frac{\partial x_e}{\partial \xi} \frac{\partial y_e}{\partial \eta} \end{bmatrix}^{-1} \\ &\times \begin{pmatrix} \frac{\partial^2 \psi_i^e}{\partial \xi^2} \\ \frac{\partial^2 \psi_i^e}{\partial \eta^2} \\ \frac{\partial^2 \psi_i^e}{\partial \xi \partial \eta} \end{pmatrix} - \begin{bmatrix} \frac{\partial^2 x_e}{\partial \xi^2} & \frac{\partial^2 y_e}{\partial \xi^2} \\ \frac{\partial^2 x_e}{\partial \eta^2} & \frac{\partial^2 y_e}{\partial \eta^2} \\ \frac{\partial^2 x_e}{\partial \xi \partial \eta} & \frac{\partial^2 y_e}{\partial \xi \partial \eta} \end{bmatrix} \begin{Bmatrix} \frac{\partial \psi_i^e}{\partial x} \\ \frac{\partial \psi_i^e}{\partial y} \end{Bmatrix} \end{aligned}$$

9.17 (Continuation of Problem 9.16) Show that the Jacobian can be computed from the equation

$$[J] = \begin{Bmatrix} \frac{\partial \psi_1^e}{\partial \xi} & \frac{\partial \psi_2^e}{\partial \xi} & \dots & \frac{\partial \psi_n^e}{\partial \xi} \\ \frac{\partial \psi_1^e}{\partial \eta} & \frac{\partial \psi_2^e}{\partial \eta} & \dots & \frac{\partial \psi_n^e}{\partial \eta} \end{Bmatrix} \begin{bmatrix} x_1^e & y_1^e \\ x_2^e & y_2^e \\ \vdots & \vdots \\ x_n^e & y_n^e \end{bmatrix}$$

9.18 Find the Jacobian matrix for the nine-node quadrilateral element shown in Fig. P9.18. What is the determinant of the Jacobian matrix?

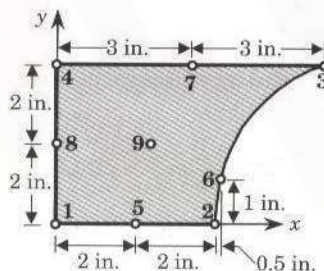


Figure P9.18

9.19 For the eight-node element shown in Fig. P9.19, show that the x coordinate along the side 1–2 is related to the ξ coordinate by the relation

$$x = -\frac{1}{2}\xi(1-\xi)x_1^e + \frac{1}{2}\xi(1+\xi)x_2^e + (1-\xi^2)x_5^e$$

and that the following relations hold:

$$\xi = 2\left(\frac{x}{a}\right)^{1/2} - 1, \quad \frac{\partial x}{\partial \xi} = (xa)^{1/2}$$

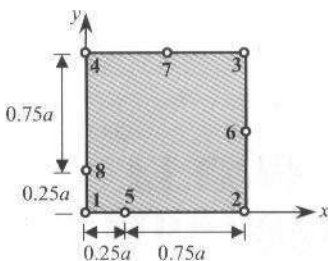


Figure P9.19

Also, show that

$$\begin{aligned}
 u_h(x, 0) &= -\left[2\left(\frac{x}{a}\right)^{1/2} - 1\right]\left[1 - \left(\frac{x}{a}\right)^{1/2}\right]u_1^e \\
 &\quad + \left[-1 + 2\left(\frac{x}{a}\right)^{1/2}\right]\left(\frac{x}{a}\right)^{1/2}u_2^e + 4\left[\left(\frac{x}{a}\right)^{1/2} - \frac{x}{a}\right]u_5^e \\
 \frac{\partial u_h}{\partial x} \Big|_{(x,0)} &= -\frac{1}{(xa)^{1/2}}\left\{\frac{1}{2}\left[3 - 4\left(\frac{x}{a}\right)^{1/2}\right]u_1^e + \frac{1}{2}\left[-1 + 4\left(\frac{x}{a}\right)^{1/2}\right]u_2^e\right. \\
 &\quad \left.+ 2\left[1 - 2\left(\frac{x}{a}\right)^{1/2}\right]u_5^e\right\}
 \end{aligned}$$

Thus, $\partial u_h / \partial x$ grows at a rate of $(xa)^{-1/2}$ as x approaches zero along the side 1–2. In other words, we have a $x^{-1/2}$ singularity at node 1. Such elements are used in fracture mechanics problems.

- 9.20** Using the tensor product of the one-dimensional Hermite cubic interpolation functions, obtain the Hermite cubic interpolation functions (16 of them) for the four-node rectangular element.

REFERENCES FOR ADDITIONAL READING

- Burnett, D. S., *Finite Element Analysis from Concepts to Applications*, Addison-Wesley Publishing Company, Reading, MA, 1987.
- Carnahan, B., Luther, H. A., and Wilkes, J. O., *Applied Numerical Methods*, John Wiley, New York, 1969.
- Cowper, G. R., "Gaussian Quadrature Formulas for Triangles," *International Journal for Numerical Methods in Engineering*, **7**, 405–408, 1973.
- Froberg, C. E., *Introduction to Numerical Analysis*, Addison-Wesley, Reading, MA, 1969.
- Hammer, P. C., Marlowe, O. P., and Stroud, A. H., "Numerical Integration over Simplexes and Cones," *Mathematics Tables Aids Comp.*, National Research Council (Washington), **10**, 130–137, 1956.
- Irons, B. M., "Quadrature Rules for Brick-Based Finite Elements," *International Journal for Numerical Methods in Engineering*, **3**, 293–294, 1971.
- Loxan, A. N., Davids, N., and Levenson, A., "Table of the Zeros of the Legendre Polynomials of Order 1–16 and the Weight Coefficients for Gauss' Mechanical Quadrature Formula," *Bulletin of the American Mathematical Society*, **48**, 739–743, 1942.
- Reddy, C. T. and Shippy, D. J., "Alternative Integration Formulae for Triangular Finite Elements," *International Journal for Numerical Methods in Engineering*, **17**, 133–139, 1981.
- Silvester, P., "Newton–Cotes Quadrature Formulae for N -Dimensional Simplexes," *Proceedings of 2nd Canadian Congress of Applied Mechanics* (Waterloo, Ontario, Canada), 1969.
- Stroud, A. H. and Secrest, D., *Gaussian Quadrature Formulas*, Prentice-Hall, Engelwood Cliffs, NJ, 1966.

Chapter 10

FLows OF VISCOUS INCOMPRESSIBLE FLUIDS

10.1 PRELIMINARY COMMENTS

In Chapter 8, we considered the finite element analysis of second-order partial differential equations in one dependent unknown. Such equations arise in two-dimensional heat transfer, torsion of a cylindrical members of arbitrary cross section, deflection of membranes in a plane, and inviscid flows in two dimensions. In this chapter, we consider flows of viscous incompressible fluids in two dimensions whose governing equations are described by a set of three *coupled* partial differential equations expressed in terms of three dependent variables, namely, two velocity components and pressure. The word “coupled” is used here to imply that the same dependent variables appear in more than one equation of the set, and no equation can be solved independently of the other(s) in the set.

A brief introduction to fluids was given in Sections 4.4 and 8.5.2. The finite element analysis of fluid flow problems that can be described as one-dimensional systems was discussed in Section 4.4. In Section 8.5.2, finite element models of two-dimensional flows of inviscid, incompressible fluids (i.e., potential flows) were considered. The potential flow problems were cast in terms of either the stream function or the velocity potential, and the governing equation in each case was shown to be the Laplace equation, $\nabla^2 u = 0$.

In this chapter we consider the finite element analysis of two-dimensional flows of viscous, incompressible fluids. We begin with a review of the pertinent equations governing low-speed, laminar flows of viscous incompressible fluids.

10.2 GOVERNING EQUATIONS

Consider the *slow* flow of a *viscous* and *incompressible fluid* in a closed domain Ω :

Slow (inertial effects are negligible): $\mathbf{v} \cdot \nabla \mathbf{v} \approx 0$

Viscous: $\mu \neq 0$

Incompressible: $\frac{D\rho}{Dt} = 0$ ($\rho = \text{constant}$)

Assume that one of the dimensions, say, along the z direction (into the plane of the paper) of the domain is very long and there is no flow along that direction, and the velocity components in the other two directions (v_x and v_y) do not vary with the z direction. Under these conditions, the flow can be approximated by a two-dimensional model. The governing equations of such flows in rectangular Cartesian coordinates (x, y) are summarized below.

Conservation of Linear Momentum

$$\rho \frac{\partial v_x}{\partial t} - \frac{\partial \sigma_{xx}}{\partial x} - \frac{\partial \sigma_{xy}}{\partial y} - f_x = 0 \quad (10.2.1)$$

$$\rho \frac{\partial v_y}{\partial t} - \frac{\partial \sigma_{xy}}{\partial x} - \frac{\partial \sigma_{yy}}{\partial y} - f_y = 0 \quad (10.2.2)$$

Conservation of Mass (or Continuity Equation)

$$\frac{\partial v_x}{\partial x} + \frac{\partial v_y}{\partial y} = 0 \quad (10.2.3)$$

Constitutive Equations

$$\sigma_{xx} = \tau_{xx} - P, \quad \sigma_{xy} = \tau_{xy}, \quad \sigma_{yy} = \tau_{yy} - P \quad (10.2.4)$$

$$\tau_{xx} = 2\mu \frac{\partial v_x}{\partial x}, \quad \tau_{xy} = \mu \left(\frac{\partial v_x}{\partial y} + \frac{\partial v_y}{\partial x} \right), \quad \tau_{yy} = 2\mu \frac{\partial v_y}{\partial y} \quad (10.2.5)$$

Boundary Conditions. Specify one element of each of the following pairs at each point on the boundary Γ :

$$(v_x, t_x), \quad (v_y, t_y) \quad \text{for any } t > 0 \quad (10.2.6)$$

$$t_x = \sigma_{xx} n_x + \sigma_{xy} n_y, \quad t_y = \sigma_{xy} n_x + \sigma_{yy} n_y \quad (10.2.7)$$

Initial Conditions. Specify velocities at time $t = 0$ at each point in the domain Ω and on the boundary Γ :

$$v_x(x, y, 0) = v_x^0(x, y), \quad v_y(x, y, 0) = v_y^0(x, y) \quad (10.2.8)$$

Here (v_x, v_y) are the velocity components, $(\sigma_{xx}, \sigma_{yy}, \sigma_{xy})$ the Cartesian components of the total stress tensor σ , P the pressure, $(\tau_{xx}, \tau_{xy}, \tau_{yy})$ the Cartesian components of the viscous stress tensor τ , μ the viscosity, f_x and f_y the components of body force vector, (t_x, t_y) the components of stress vector on the boundary, and (v_x^0, v_y^0) the specified initial values of the velocity components.

Using the constitutive relations (10.2.4) and (10.2.5), the momentum and continuity equations in a flow domain Ω can be expressed as

$$\rho \frac{\partial v_x}{\partial t} - \frac{\partial}{\partial x} \left(2\mu \frac{\partial v_x}{\partial x} \right) - \frac{\partial}{\partial y} \left[\mu \left(\frac{\partial v_x}{\partial y} + \frac{\partial v_y}{\partial x} \right) \right] + \frac{\partial P}{\partial x} - f_x = 0 \quad (10.2.9)$$

$$\rho \frac{\partial v_y}{\partial t} - \frac{\partial}{\partial x} \left[\mu \left(\frac{\partial v_x}{\partial y} + \frac{\partial v_y}{\partial x} \right) \right] - \frac{\partial}{\partial y} \left(2\mu \frac{\partial v_y}{\partial y} \right) + \frac{\partial P}{\partial y} - f_y = 0 \quad (10.2.10)$$

$$\frac{\partial v_x}{\partial x} + \frac{\partial v_y}{\partial y} = 0 \quad (10.2.11)$$

and the boundary stress components in (10.2.7) become

$$\begin{aligned} t_x &= \left(2\mu \frac{\partial v_x}{\partial x} - P \right) n_x + \mu \left(\frac{\partial v_x}{\partial y} + \frac{\partial v_y}{\partial x} \right) n_y && \text{on } \Gamma \\ t_y &= \mu \left(\frac{\partial v_x}{\partial y} + \frac{\partial v_y}{\partial x} \right) n_x + \left(2\mu \frac{\partial v_y}{\partial y} - P \right) n_y \end{aligned} \quad (10.2.12)$$

Thus, we have three partial differential equations (10.2.9)–(10.2.11) in three unknowns (v_x , v_y , P).

In the present study, we shall consider two different finite element models of Eqs. (10.2.9)–(10.2.11). The first one is a natural and direct formulation of Eqs. (10.2.9)–(10.2.11) in (v_x, v_y, P) and is known as the *velocity-pressure formulation* or *mixed formulation*. The second model is based on the interpretation that the continuity equation (10.2.11) is an additional relation among the velocity components (i.e., a constraint on v_x and v_y); the constraint is satisfied in a least-squares (i.e., approximate) sense. This particular method of including the constraint in the formulation is known as the *penalty function method*, and the formulation is termed the *penalty formulation*. It is informative to note that the velocity-pressure formulation is the same as the Lagrange multiplier formulation, and the Lagrange multiplier turns out to be the negative of the pressure.

10.3 VELOCITY-PRESSURE FORMULATION

10.3.1 Weak Formulation

The weak forms of Eqs. (10.2.9)–(10.2.11) over an element Ω_e can be obtained by the three-step procedure discussed in Chapter 8. We multiply the three equations, (10.2.1)–(10.2.3) wherein $(\sigma_{xx}, \sigma_{xy}, \sigma_{yy})$ are known in terms of (v_x, v_y, P) through Eqs. (10.2.4) and (10.2.5), with three different weight functions (w_1, w_2, w_3) , integrate over the element, and integrate by parts (i.e., apply the Green–Gauss theorem) to obtain the following weak forms:

$$\begin{aligned} 0 &= \int_{\Omega_e} w_1 \left[\rho \frac{\partial v_x}{\partial t} - \frac{\partial \sigma_{xx}}{\partial x} - \frac{\partial \sigma_{xy}}{\partial y} - f_x \right] dx dy \\ &= \int_{\Omega_e} \left[\rho w_1 \frac{\partial v_x}{\partial t} + \frac{\partial w_1}{\partial x} \sigma_{xx} + \frac{\partial w_1}{\partial y} \sigma_{xy} - w_1 f_x \right] dx dy \\ &\quad + \oint_{\Gamma_e} w_1 (\sigma_{xx} n_x + \sigma_{xy} n_y) ds \end{aligned} \quad (10.3.1)$$

$$\begin{aligned} 0 &= \int_{\Omega_e} w_2 \left[\rho \frac{\partial v_y}{\partial t} - \frac{\partial \sigma_{xy}}{\partial x} - \frac{\partial \sigma_{yy}}{\partial y} - f_y \right] dx dy \\ &= \int_{\Omega_e} \left[\rho w_2 \frac{\partial v_y}{\partial t} + \frac{\partial w_2}{\partial x} \sigma_{xy} + \frac{\partial w_2}{\partial y} \sigma_{yy} - w_2 f_y \right] dx dy \\ &\quad + \oint_{\Gamma_e} w_2 (\sigma_{xy} n_x + \sigma_{yy} n_y) ds \end{aligned} \quad (10.3.2)$$

$$0 = \int_{\Omega_e} w_3 \left(\frac{\partial v_x}{\partial x} + \frac{\partial v_y}{\partial y} \right) dx dy \quad (10.3.3)$$

The weight functions (w_1, w_2, w_3) can be interpreted physically as follows: Since the first equation is the momentum equation and $f_x dx dy$ denotes the force, w_1 must be like the x component of velocity v_x so that the product $f_x w_1$ gives the power. Similarly, w_2 must be like the y component of velocity v_y . The third equation represents the volume change in an element of dimensions dx and dy . Therefore, w_3 must be like a force that causes the volume change. Volume changes occur under the action of hydrostatic pressure, hence, w_3 is like $-P$:

$$w_1 \sim u, w_2 \sim v, \text{ and } w_3 \sim -P \quad (10.3.4)$$

This interpretation is useful in developing the finite element model because w_1 , for example, will be replaced by the i th interpolation function used in the approximation of v_x . Similarly, w_3 will be replaced by the i th interpolation function used in the approximation of P . When different interpolations are used for (v_x, v_y) and P , this interpretation becomes necessary. Expressing the equations in terms of (v_x, v_y, P) , the weak forms (10.3.1)–(10.3.3) become

$$\begin{aligned} 0 &= \int_{\Omega_e} \left[\rho w_1 \frac{\partial v_x}{\partial t} + \frac{\partial w_1}{\partial x} \left(2\mu \frac{\partial v_x}{\partial x} - P \right) + \mu \frac{\partial w_1}{\partial y} \left(\frac{\partial v_x}{\partial y} + \frac{\partial v_y}{\partial x} \right) - w_1 f_x \right] dx dy \\ &\quad - \oint_{\Gamma_e} w_1 t_x ds \end{aligned} \quad (10.3.5)$$

$$\begin{aligned} 0 &= \int_{\Omega_e} \left[\rho w_2 \frac{\partial v_y}{\partial t} + \mu \frac{\partial w_2}{\partial x} \left(\frac{\partial v_x}{\partial y} + \frac{\partial v_y}{\partial x} \right) + \frac{\partial w_2}{\partial y} \left(2\mu \frac{\partial v_y}{\partial y} - P \right) - w_2 f_y \right] dx dy \\ &\quad - \oint_{\Gamma_e} w_2 t_y ds \end{aligned} \quad (10.3.6)$$

$$0 = - \int_{\Omega_e} w_3 \left(\frac{\partial v_x}{\partial x} + \frac{\partial v_y}{\partial y} \right) dx dy \quad (10.3.7)$$

Note that there is no boundary integral involving w_3 because no integration by parts is used. This implies that P is not a primary variable; it is a part of the secondary variables (t_x and t_y). This in turn requires that P not be made continuous across interelement boundaries. If P by itself is not specified in a problem (but t_x and t_y are specified), then P is arbitrarily set to a value at some node to determine the constant state of the pressure. Thus, P can be determined only within an arbitrary constant. The minus sign in the third statement is inserted because $P \sim -w_3$, which makes the resulting finite element model symmetric.

The problem described by weak forms (10.3.5)–(10.3.7) can be restated as a variational problem of finding (v_x, v_y, P) such that

$$\begin{aligned} B_t(\mathbf{w}, \mathbf{v}) + B_v(\mathbf{w}, \mathbf{v}) - \bar{B}_p(\mathbf{w}, P) &= l(\mathbf{w}) \\ -B_p(w_3, \mathbf{v}) &= 0 \end{aligned} \quad (10.3.8)$$

holds for all (w_1, w_2, w_3) and $t > 0$. Here, we have used the notation

$$\mathbf{w} = \begin{Bmatrix} w_1 \\ w_2 \end{Bmatrix}, \quad \mathbf{v} = \begin{Bmatrix} v_x \\ v_y \end{Bmatrix}, \quad \mathbf{f} = \begin{Bmatrix} f_x \\ f_y \end{Bmatrix}, \quad \mathbf{t} = \begin{Bmatrix} t_x \\ t_y \end{Bmatrix} \quad (10.3.9)$$

Since w_i are linearly independent of each other, the sum of the three equations in (10.3.5)–(10.3.7) is the same as the three individual equations. Thus, the bilinear forms $B_t(\mathbf{w}, \mathbf{v})$, $B_v(\mathbf{w}, \mathbf{v})$, $\bar{B}_p(\mathbf{w}, P)$, and $B_p(w_3, \mathbf{v})$, and the linear form $l(\mathbf{w})$ are defined by

$$\begin{aligned} B_t(\mathbf{w}, \mathbf{v}) &= \int_{\Omega_e} \rho \mathbf{w}^T \dot{\mathbf{v}} d\mathbf{x} \\ B_v(\mathbf{w}, \mathbf{v}) &= \int_{\Omega_e} (\mathbf{D}\mathbf{w})^T \mathbf{C} (\mathbf{D}\mathbf{v}) d\mathbf{x} \\ \bar{B}_p(\mathbf{w}, P) &= \int_{\Omega_e} (\mathbf{D}_1^T \mathbf{w})^T P d\mathbf{x} \\ B_p(w_3, \mathbf{v}) &= \int_{\Omega_e} (w_3)^T (\mathbf{D}_1^T \mathbf{v}) d\mathbf{x} \\ l(\mathbf{w}) &= \int_{\Omega_e} \mathbf{w}^T \mathbf{f} d\mathbf{x} + \oint_{\Gamma_e} \mathbf{w}^T \mathbf{t} ds \end{aligned} \quad (10.3.10a)$$

where

$$\mathbf{D} = \begin{bmatrix} \frac{\partial}{\partial x} & 0 \\ 0 & \frac{\partial}{\partial y} \\ \frac{\partial}{\partial y} & \frac{\partial}{\partial x} \end{bmatrix}, \quad \mathbf{D}_1 = \begin{Bmatrix} \frac{\partial}{\partial x} \\ \frac{\partial}{\partial y} \end{Bmatrix}, \quad \mathbf{C} = \mu \begin{bmatrix} 2 & 0 & 0 \\ 0 & 2 & 0 \\ 0 & 0 & 1 \end{bmatrix} \quad (10.3.10b)$$

The transpose of a scalar (or 1×1 matrix) used in the Eq. (10.3.10a) may look a bit strange at the moment, but it is necessary to obtain the correct form of the finite element model, as will be seen shortly.

10.3.2 Finite Element Model

An examination of the weak form reveals that v_x and v_y are the primary variables that should be made continuous at interelement boundaries, while P is a nodal variable that need not be made continuous across the interelement boundaries. Therefore, the Lagrange family of finite elements can be used for (v_x, v_y, P) . The weak form shows that the minimum continuity requirements on (v_x, v_y, P) are:

$$(v_x, v_y) \text{ linear in } x \text{ and } y, \quad P \text{ constant}$$

Thus, there are different continuity requirements on the interpolation of the velocity field and pressure. Let (the element label “ e ” on the variables is omitted)

$$v_x(x, y, t) = \sum_{j=1}^n v_x^j(t) \psi_j(x, y), \quad v_y(x, y, t) = \sum_{j=1}^n v_y^j(t) \psi_j(x, y) \quad (10.3.11a)$$

$$P(x, y, t) = \sum_{J=1}^m P_J(t) \phi_J(x, y) \quad (10.3.11b)$$

where ψ_j ($j = 1, 2, \dots, n$) and ϕ_J ($J = 1, 2, \dots, m$) are interpolation functions of different order. In view of the fact that pressure appears without a derivative while (v_x, v_y) appear with derivatives with respect to x and y , we often take $n = m + 1$. If the degree of the approximation functions is high, we may use the same degree of interpolation for P and (v_x, v_y) .

Substituting (10.3.11a) and (10.3.11b) into Eqs. (10.3.5)–(10.3.7), we obtain the following finite element model:

$$\begin{aligned} & \left[\begin{array}{ccc} 2[S^{11}] + [S^{22}] & [S^{21}] & -[S^{10}] \\ [S^{12}] & [S^{11}] + 2[S^{22}] & -[S^{20}] \\ -[S^{10}]^T & -[S^{20}]^T & [0] \end{array} \right] \begin{Bmatrix} \{v_x\} \\ \{v_y\} \\ \{P\} \end{Bmatrix} \\ & + \left[\begin{array}{ccc} [M] & [0] & [0] \\ [0] & [M] & [0] \\ [0] & [0] & [0] \end{array} \right] \begin{Bmatrix} \{\dot{v}_x\} \\ \{\dot{v}_y\} \\ \{\dot{P}\} \end{Bmatrix} = \begin{Bmatrix} \{F^1\} \\ \{F^2\} \\ \{0\} \end{Bmatrix} \end{aligned} \quad (10.3.12)$$

The coefficient matrices shown in Eqs. (10.3.12) are defined by

$$\begin{aligned} M_{ij} &= \int_{\Omega_e} \rho \psi_i^e \psi_j^e dx dy \\ S_{ij}^{\alpha\beta} &= \int_{\Omega_e} \mu \frac{\partial \psi_i^e}{\partial x_\alpha} \frac{\partial \psi_j^e}{\partial x_\beta} dx dy; \quad \alpha, \beta = 1, 2 \\ S_{ij}^{\alpha 0} &= \int_{\Omega_e} \mu \frac{\partial \psi_i^e}{\partial x_\alpha} \phi_j^e dx dy; \quad \alpha = 1, 2 \\ F^1 &= \int_{\Omega_e} \psi_i^e f_x dx dy + \oint_{\Gamma_e} \psi_i^e t_x ds \\ F^2 &= \int_{\Omega_e} \psi_i^e f_y dx dy + \oint_{\Gamma_e} \psi_i^e t_y ds \end{aligned} \quad (10.3.13)$$

We note that $[K^{33}] = [0]$ because the continuity equation does not contain P . Therefore, the assembled equations will also have zeros in diagonal elements corresponding to the nodal values of P (i.e., the system of equations is not positive-definite).

The vector form of the finite element model (10.3.12) can be obtained as follows: The finite element approximations (10.3.11a) and (10.3.11b) is expressed as

$$\begin{aligned} \mathbf{v} &= \begin{Bmatrix} v_x \\ v_y \end{Bmatrix} = \Psi \Delta, \quad \mathbf{w} = \begin{Bmatrix} w_1 \\ w_2 \end{Bmatrix} = \Psi \delta \Delta \\ P &= \Phi^T \mathbf{P}, \quad w_3 = \Phi^T \delta \mathbf{P} \end{aligned} \quad (10.3.14a)$$

where δ denotes the variational symbol, $\mathbf{w} = \delta \mathbf{v}$ denotes the virtual variation of \mathbf{v} , and δP_i is the virtual variation of P_i . Various symbols used in Eq. (10.3.14a) are defined as

$$\begin{aligned}\Psi &= \begin{bmatrix} \psi_1 & 0 & \psi_2 & 0 & \cdots & \psi_n & 0 \\ 0 & \psi_1 & 0 & \psi_2 & \cdots & 0 & \psi_n \end{bmatrix} \\ \Delta &= \{v_x^1 \ v_y^1 \ v_x^2 \ v_y^2 \ \cdots \ v_x^n \ v_y^n\}^T \\ \Phi &= \{\phi_1 \ \phi_2 \ \cdots \ \phi_m\}^T, \quad \mathbf{P} = \{P_1 \ P_2 \ \cdots \ P_m\}^T\end{aligned}\quad (10.3.14b)$$

Substituting (10.3.14a) into Eq. (10.3.8) and noting that δv_x^i and δv_y^i are arbitrary and linearly independent, we obtain

$$\mathbf{M} \dot{\Delta} + \mathbf{K}^{11} \Delta + \mathbf{K}^{12} \mathbf{P} = \mathbf{F}^1, \quad \mathbf{K}^{21} \Delta = \mathbf{0} \quad (10.3.15)$$

where

$$\begin{aligned}\mathbf{M} &= \int_{\Omega_e} \rho \Psi^T \Psi \, d\mathbf{x}, \quad \mathbf{K}^{11} = \int_{\Omega_e} \mathbf{B}_v^T \mathbf{C} \mathbf{B}_v \, d\mathbf{x} \\ \mathbf{K}^{12} &= \int_{\Omega_e} \mathbf{B}_p^T \Phi^T \, d\mathbf{x}, \quad \mathbf{K}^{21} = \int_{\Omega_e} \Phi \mathbf{B}_p \, d\mathbf{x} \\ \mathbf{F}^1 &= \int_{\Omega_e} \Psi^T \mathbf{f} \, d\mathbf{x} + \oint_{\Gamma_e} \Psi^T \mathbf{t} \, ds \\ \mathbf{B}_v &= \mathbf{D} \Psi, \quad \mathbf{B}_p = \mathbf{D}_1^T \Psi\end{aligned}\quad (10.3.16)$$

Note that \mathbf{M} and \mathbf{K}^{11} are of the order $2n \times 2n$, \mathbf{K}^{12} is of the order $2n \times m$, \mathbf{K}^{21} is of the order $m \times 2n$, and \mathbf{F}^1 is of the order $2n \times 1$.

10.4 PENALTY FUNCTION FORMULATION

10.4.1 Preliminary Comments

The penalty function method was introduced in Section 4.6.4 in connection with algebraic constraint equations. It can also be used to reformulate a problem with differential constraints as one without constraints. Since the basic idea of the method was already introduced (see Example 4.6.2), we proceed directly to its application to the viscous flow problem at hand. The question we may ask is: Where is the constraint in the flow problem? There are no constraint conditions in the way the equations were presented. We have three equations (10.2.9)–(10.2.11) in three unknowns (v_x , v_y , P). Since the pressure P is uncoupled from the continuity equation (10.2.11) [which has the consequence of yielding a nonpositive-definite system of finite element equations (10.3.12)], we would like to eliminate it from the set of governing equations. The elimination of pressure leads to a constraint equation among the velocity components, as described next.

10.4.2 Formulation of the Flow Problem as a Constrained Problem

The equations governing flows of viscous incompressible fluids can be viewed as equivalent to minimizing a quadratic functional with a constraint. Here we present the formulation, in

the interest of simplicity, for the static case since the constraint condition does not involve time derivative terms. Then, we add the time derivative terms to study transient problems.

We begin with unconstrained problem described by the weak forms of the mixed model, namely, Eqs. (10.3.8) without the time-derivative terms

$$\begin{aligned} B_v(\mathbf{w}, \mathbf{v}) - \bar{B}_p(\mathbf{w}, P) &= l(\mathbf{w}) \\ -B_p(w_3, \mathbf{v}) &= 0 \end{aligned} \quad (10.4.1)$$

where $B_v(\cdot, \cdot)$, $\bar{B}_p(\cdot, \cdot)$, $B_p(\cdot, \cdot)$, and $l(\cdot)$ are defined in Eqs. (10.3.10a) and (10.3.10b). Now, suppose that the velocity field (v_x, v_y) is such that the continuity equation (10.2.3) is satisfied identically. Then the weight functions (w_1, w_2) , being (virtual) variations of the velocity components, also satisfy the continuity equation

$$\frac{\partial w_1}{\partial x} + \frac{\partial w_2}{\partial y} = 0 \quad (10.4.2)$$

As a result, variational problem (10.4.1) now can be stated as follows: Among all (v_x, v_y) that satisfy the continuity equation (10.2.3), find the one that satisfies the variational problem

$$B_v(\mathbf{w}, \mathbf{v}) = l(\mathbf{w}) \quad (10.4.3)$$

for all admissible weight functions (w_1, w_2) , i.e., the one that satisfies condition (10.4.2).

The variational problem in Eq. (10.4.3) is a constrained variational problem because the solution (v_x, v_y) is constrained to satisfy the continuity equation (10.2.3). We note that $B_v(\cdot, \cdot)$ is symmetric (because \mathbf{C} is symmetric)

$$B_v(\mathbf{w}, \mathbf{v}) = B_v(\mathbf{v}, \mathbf{w}) \quad (10.4.4)$$

and it is linear in \mathbf{w} as well as \mathbf{v} , while $l(\cdot)$ is linear in \mathbf{w} . Hence, the quadratic functional is given by the expression [see Eq. (2.4.19)]

$$I_v(\mathbf{v}) = \frac{1}{2} B_v(\mathbf{v}, \mathbf{v}) - l(\mathbf{v}) \quad (10.4.5)$$

Now we can state that the equations governing steady flows of viscous incompressible fluids are equivalent to

$$\text{minimize } I_v(\mathbf{v}) \quad (10.4.6)$$

$$\text{subjected to the constraint } G(\mathbf{v}) \equiv \frac{\partial v_x}{\partial x} + \frac{\partial v_y}{\partial y} = 0$$

The constrained problem (10.4.6) can be reformulated as an unconstrained problem using the Lagrange multiplier method or the penalty function method. These are discussed next.

10.4.3 Lagrange Multiplier Model

In the Lagrange multiplier method the constrained problem (10.4.6) is reformulated as one of finding the stationary points of the unconstrained functional

$$I_L(\mathbf{v}, \lambda) \equiv I_v(\mathbf{v}) + \int_{\Omega_e} \lambda G(\mathbf{v}) \, dx dy \quad (10.4.7)$$

where $\lambda(x, y)$ is the *Lagrange multiplier*. The necessary condition for I_L to have a stationary value is that

$$\delta I_L = \delta_{v_x} I_L + \delta_{v_y} I_L + \delta_\lambda I_L = 0 \rightarrow \delta_{v_x} I_L = 0, \quad \delta_{v_y} I_L = 0, \quad \delta_\lambda I_L = 0 \quad (10.4.8)$$

where δ_{v_x} , δ_{v_y} , and δ_λ denote the partial variations (see Section 2.3) with respect to v_x , v_y , and λ , respectively. Calculating the first variations in (10.4.8), we obtain

$$\begin{aligned} 0 &= \int_{\Omega_e} \left[\frac{\partial \delta v_x}{\partial x} \left(2\mu \frac{\partial v_x}{\partial x} + \lambda \right) + \mu \frac{\partial \delta v_x}{\partial y} \left(\frac{\partial v_x}{\partial y} + \frac{\partial v_y}{\partial x} \right) \right] dx dy \\ &\quad - \int_{\Omega_e} \delta v_x f_x dx dy - \oint_{\Gamma_e} \delta v_x t_x ds \end{aligned} \quad (10.4.9)$$

$$\begin{aligned} 0 &= \int_{\Omega_e} \left[\mu \frac{\partial \delta v_y}{\partial x} \left(\frac{\partial v_x}{\partial y} + \frac{\partial v_y}{\partial x} \right) + \frac{\partial \delta v_y}{\partial y} \left(2\mu \frac{\partial v_y}{\partial y} + \lambda \right) \right] dx dy \\ &\quad - \int_{\Omega_e} \delta v_y f_y dx dy - \oint_{\Gamma_e} \delta v_y t_y ds \end{aligned} \quad (10.4.10)$$

$$0 = \int_{\Omega_e} \delta \lambda \left(\frac{\partial v_x}{\partial x} + \frac{\partial v_y}{\partial y} \right) dx dy \quad (10.4.11)$$

where

$$\begin{aligned} t_x &= \left(2\mu \frac{\partial v_x}{\partial x} + \lambda \right) n_x + \mu \left(\frac{\partial v_x}{\partial y} + \frac{\partial v_y}{\partial x} \right) n_y \\ t_y &= \mu \left(\frac{\partial v_x}{\partial y} + \frac{\partial v_y}{\partial x} \right) n_x + \left(2\mu \frac{\partial v_y}{\partial y} + \lambda \right) n_y \end{aligned} \quad (10.4.12)$$

or, in vector form

$$B_v(\mathbf{w}, \mathbf{v}) + \bar{B}_p(\mathbf{w}, \lambda) = l(\mathbf{w}), \quad B_p(\delta \lambda, \mathbf{v}) = 0 \quad (10.4.13)$$

and the bilinear forms are the same as those in Eqs. (10.3.10a) and (10.3.10b). A comparison of Eq. (10.4.13) with Eq. (10.3.8) [or comparison of Eqs. (10.3.5)–(10.3.7) with (10.4.9)–(10.4.11)] reveals that $\lambda = -P$. Hence, the Lagrange multiplier formulation is the same as the velocity-pressure formulation.

10.4.4 Penalty Model

In the penalty function method, the constrained problem (10.4.6) is reformulated as an unconstrained problem as follows: Minimize the modified functional

$$I_P(\mathbf{v}) \equiv I_v(\mathbf{v}) + \frac{\gamma_e}{2} \int_{\Omega_e} [G(\mathbf{v})]^2 d\mathbf{x} \quad (10.4.14)$$

where γ_e is called the *penalty parameter*. Note that the constraint is included in a least-squares sense into the functional. Seeking the minimum of the modified functional $I_P(\mathbf{v})$ is equivalent to seeking the minimum of both $I_v(\mathbf{v})$ and $G(\mathbf{v})$, the latter with respect to the weight γ_e . The larger the value of γ_e , the more exactly the constraint is satisfied. The necessary condition for the minimum of I_P is

$$\delta I_P = 0 \quad (10.4.15)$$

We have

$$\begin{aligned} 0 &= \int_{\Omega_e} \left[2\mu \frac{\partial \delta v_x}{\partial x} \frac{\partial v_x}{\partial x} + \mu \frac{\partial \delta v_x}{\partial y} \left(\frac{\partial v_x}{\partial y} + \frac{\partial v_y}{\partial x} \right) - \delta v_x f_x \right] dx dy \\ &\quad - \oint_{\Gamma_e} \delta v_x t_x ds + \int_{\Omega_e} \gamma_e \frac{\partial \delta v_x}{\partial x} \left(\frac{\partial v_x}{\partial x} + \frac{\partial v_y}{\partial y} \right) dx dy \end{aligned} \quad (10.4.16)$$

$$\begin{aligned} 0 &= \int_{\Omega_e} \left[2\mu \frac{\partial \delta v_y}{\partial y} \frac{\partial v_y}{\partial y} + \mu \frac{\partial \delta v_y}{\partial x} \left(\frac{\partial v_x}{\partial y} + \frac{\partial v_y}{\partial x} \right) - \delta v_y f_y \right] dx dy \\ &\quad - \oint_{\Gamma_e} \delta v_y t_y ds + \int_{\Omega_e} \gamma_e \frac{\partial \delta v_y}{\partial y} \left(\frac{\partial v_x}{\partial x} + \frac{\partial v_y}{\partial y} \right) dx dy \end{aligned} \quad (10.4.17)$$

or, in vector form,

$$B_p(\mathbf{w}, \mathbf{v}) = l(\mathbf{w}) \quad (10.4.18)$$

where ($w_1 = \delta v_x$ and $w_2 = \delta v_y$)

$$\begin{aligned} B_p(\mathbf{w}, \mathbf{v}) &= B_v(\mathbf{w}, \mathbf{v}) + \int_{\Omega_e} \gamma_e (\mathbf{D}_1^T \mathbf{w})^T \mathbf{D}_1^T \mathbf{v} dx \\ l(\mathbf{w}) &= \int_{\Omega_e} \mathbf{w}^T \mathbf{f} dx dy + \oint_{\Gamma_e} \mathbf{w}^T \mathbf{t} ds \end{aligned} \quad (10.4.19)$$

and $B_v(\cdot, \cdot)$ and \mathbf{D}_1 are defined in Eqs. (10.3.10a) and (10.3.10b). We note that the pressure does not appear explicitly in the weak forms (10.4.16) and (10.4.17), although it is a part of the boundary stresses [see Eq. (10.4.12), $\lambda = -P$].

A comparison of the weak forms in (10.4.16) and (10.4.17) with those in (10.4.9) and (10.4.10) show that

$$\lambda = \gamma_e \left(\frac{\partial v_x}{\partial x} + \frac{\partial v_y}{\partial y} \right) = -P \quad \text{or} \quad P = -\gamma_e \mathbf{D}_1^T \mathbf{v} \quad (10.4.20)$$

where $\mathbf{v} = \mathbf{v}(\gamma_e)$ is the solution of Eqs. (10.4.16) and (10.4.17). Thus, an approximation for the pressure can be postcomputed using (10.4.20).

The time derivative terms can be added to equations (10.4.9)–(10.4.11) as well as to (10.4.16) and (10.4.17) without affecting the above discussion. For the penalty model, we have

$$\begin{aligned} 0 &= \int_{\Omega_e} \left[\rho \delta v_x \frac{\partial v_x}{\partial t} + 2\mu \frac{\partial \delta v_x}{\partial x} \frac{\partial v_x}{\partial x} + \mu \frac{\partial \delta v_x}{\partial y} \left(\frac{\partial v_x}{\partial y} + \frac{\partial v_y}{\partial x} \right) \right. \\ &\quad \left. + \gamma_e \frac{\partial \delta v_x}{\partial x} \left(\frac{\partial v_x}{\partial x} + \frac{\partial v_y}{\partial y} \right) \right] dx dy - \int_{\Omega_e} \delta v_x f_x dx dy - \oint_{\Gamma_e} \delta v_x t_x ds \end{aligned} \quad (10.4.21)$$

$$\begin{aligned} 0 &= \int_{\Omega_e} \left[\rho \delta v_y \frac{\partial v_y}{\partial t} + 2\mu \frac{\partial \delta v_y}{\partial y} \frac{\partial v_y}{\partial y} + \mu \frac{\partial \delta v_y}{\partial x} \left(\frac{\partial v_x}{\partial y} + \frac{\partial v_y}{\partial x} \right) \right. \\ &\quad \left. + \gamma_e \frac{\partial \delta v_y}{\partial y} \left(\frac{\partial v_x}{\partial x} + \frac{\partial v_y}{\partial y} \right) \right] dx dy - \int_{\Omega_e} f_y \delta v_y dx dy - \oint_{\Gamma_e} \delta v_y t_y ds \end{aligned} \quad (10.4.22)$$

or

$$B_t(\mathbf{w}, \mathbf{v}) + B_p(\mathbf{w}, \mathbf{v}) = l(\mathbf{w}) \quad (10.4.23)$$

where $B_t(\cdot, \cdot)$ is defined in Eq. (10.3.10a), and $B_p(\cdot, \cdot)$ and $l(\cdot)$ are defined in Eq. (10.4.19).

The penalty finite element model can be constructed using Eqs. (10.4.21) and (10.4.22) [or Eq. (10.4.23)] by substituting $\delta v_x = \psi_i$ and $\delta v_y = \psi_i$ and approximations (10.3.11a) for (v_x, v_y) . We obtain

$$\begin{bmatrix} [M] & [0] \\ [0] & [M] \end{bmatrix} \begin{Bmatrix} \{\dot{v}_x\} \\ \{\dot{v}_y\} \end{Bmatrix} + \begin{bmatrix} [K^{11}] & [K^{12}] \\ [K^{21}] & [K^{22}] \end{bmatrix} \begin{Bmatrix} \{v_x\} \\ \{v_y\} \end{Bmatrix} = \begin{Bmatrix} \{F^1\} \\ \{F^2\} \end{Bmatrix} \quad (10.4.24)$$

where

$$\begin{aligned} [K^{11}] &= 2[S^{11}] + [S^{22}] + [\bar{S}^{11}], & [K^{12}] &= [S^{21}] + [\bar{S}^{12}] \\ [K^{22}] &= [S^{11}] + 2[S^{22}] + [\bar{S}^{22}], & [K^{21}] &= [S^{12}] + [\bar{S}^{21}] \end{aligned} \quad (10.4.25)$$

with the coefficients

$$\begin{aligned} M_{ij} &= \int_{\Omega_e} \rho \psi_i^e \psi_j^e dx dy \\ S_{ij}^{\alpha\beta} &= \int_{\Omega_e} \mu \frac{\partial \psi_i^e}{\partial x_\alpha} \frac{\partial \psi_j^e}{\partial x_\beta} dx dy ; \quad \alpha, \beta = 1, 2 \\ S_{ij}^{\alpha 0} &= \int_{\Omega_e} \mu \frac{\partial \psi_i^e}{\partial x_\alpha} \psi_j^e dx dy ; \quad \alpha = 1, 2 \\ \bar{S}_{ij}^{\alpha\beta} &= \int_{\Omega_e} \gamma_e \frac{\partial \psi_i^e}{\partial x_\alpha} \frac{\partial \psi_j^e}{\partial x_\beta} dx dy ; \quad \alpha, \beta = 1, 2 \\ \bar{S}_{ij}^{\alpha 0} &= \int_{\Omega_e} \gamma_e \frac{\partial \psi_i^e}{\partial x_\alpha} \psi_j^e dx dy ; \quad \alpha = 1, 2 \\ F^1 &= \int_{\Omega_e} \psi_i^e f_x dx dy + \oint_{\Gamma_e} \psi_i^e t_x ds \\ F^2 &= \int_{\Omega_e} \psi_i^e f_y dx dy + \oint_{\Gamma_e} \psi_i^e t_y ds \end{aligned} \quad (10.4.26)$$

In vector form, the finite element model is given by

$$\mathbf{M}\dot{\Delta} + (\mathbf{K}_v + \mathbf{K}_p)\Delta = \mathbf{F} \quad (10.4.27)$$

where (\mathbf{M} , \mathbf{K}_v , and \mathbf{K}_p are of the order $2n \times 2n$, and \mathbf{F} is of the order $2n \times 1$)

$$\begin{aligned} \mathbf{M} &= \int_{\Omega_e} \rho \Psi^T \Psi d\mathbf{x}, & \mathbf{K}_v &= \int_{\Omega_e} \mathbf{B}_v^T \mathbf{C} \mathbf{B}_v d\mathbf{x} \\ \mathbf{K}_p &= \int_{\Omega_e} \gamma_e \mathbf{B}_p^T \mathbf{B}_p d\mathbf{x}, & \mathbf{F} &= \int_{\Omega_e} \Psi^T \mathbf{f} d\mathbf{x} + \oint_{\Gamma_e} \Psi^T \mathbf{t} ds \\ \mathbf{B}_v &= \mathbf{D}\Psi, & \mathbf{B}_p &= \mathbf{D}_1^T \Psi \end{aligned} \quad (10.4.28)$$

10.4.5 Time Approximation

For the unsteady case, Eqs. (10.3.15) and (10.4.27) are further approximated using a time approximation scheme. Equations (10.3.15) and (10.4.27) are of the form [see (6.2.21a)]

$$\mathbf{M}\dot{\Delta} + \mathbf{K}\Delta = \mathbf{F} \quad (10.4.29)$$

where $\{\Delta\}$ denotes the vector of nodal velocities and pressure in the velocity-pressure formulation and only velocities in the penalty formulation. Using the α -family of approximation we reduce Eq. (10.4.27) (with $\mathbf{K} = \mathbf{K}_v + \mathbf{K}_p$) to [see Eqs. (6.2.21a)–(6.2.24b)],

$$\hat{\mathbf{K}}\Delta_{s+1} = \tilde{\mathbf{K}}\Delta_s + \hat{\mathbf{F}}_{s,s+1} \quad (10.4.30)$$

where

$$\hat{\mathbf{K}} = \mathbf{M} + a_1 \mathbf{K}_{s+1}, \quad \tilde{\mathbf{K}}_s = \mathbf{M} - a_2 \mathbf{K}_s \quad (10.4.31)$$

$$\hat{\mathbf{F}}_{s,s+1} = a_1 \mathbf{F}_{s+1} + a_2 \mathbf{F}_s, \quad a_1 = \alpha \Delta t, \quad a_2 = (1 - \alpha) \Delta t \quad (10.4.32)$$

where \mathbf{M} and \mathbf{K} for the penalty model are defined in Eqs. (10.4.28).

10.5 COMPUTATIONAL ASPECTS

10.5.1 Properties of the Matrix Equations

Some of the properties of the matrix equations in (10.3.15) and (10.4.27) are listed below.

1. The matrix equations (10.3.15) and (10.4.27) represent discrete analogs of conservation of mass and momentum. An inspection of the structure of the individual matrices shows that \mathbf{M} and \mathbf{K} are symmetric.
2. A negative aspect of the mixed finite element model is the presence of zeroes on the matrix diagonals corresponding to the pressure variables [see Eq. (10.3.15)]. Direct equation-solving methods must use some type of pivoting strategy, while the use of iterative solvers is severely handicapped by poor convergence behavior.
3. The computer implementation of the mixed model is somewhat complicated by the fact that the element contains variable degrees of freedom, e.g., in the quadratic approximation of the velocity field and bilinear continuous approximation of the pressure, the element has three degrees of freedom (v_x, v_y, P) at the corner nodes and two degrees of freedom (v_x, v_y) at the interior and midside nodes. This complicates the calculation of element matrices as well as the assembly of element equations.
4. Equations (10.3.15) and (10.4.27) represent a set of ordinary differential equations in time. The fact that the pressure does not appear explicitly in the continuity equation makes the system time-singular in pressure and precludes the use of purely explicit time-integration methods.
5. The choice of the penalty parameter is largely dictated by the ratio of the magnitude of penalty terms to the viscous terms, the mesh, and the precision of the computer. Generally, a value of $\gamma = 10^4 \mu$ to $10^{12} \mu$, where μ denotes the viscosity, gives good results. It is found that the pressure is more sensitive to the value of γ than the velocity field.

10.5.2 Choice of Elements

As is clear from the weak forms, both finite element models require only the C^0 -continuous functions to approximate the field variables (i.e., velocities and pressure). Thus, any of the Lagrange and serendipity family of interpolation functions are admissible for the interpolation of the velocity field in mixed and penalty finite element models.

The choice of interpolation functions used for the pressure variable in the mixed finite element model is further constrained by the special role that pressure plays in incompressible flows. Recall that the pressure can be interpreted as a Lagrange multiplier that serves to enforce the incompressibility constraint on the velocity field. From Eq. (10.3.11b) it is seen that the approximation functions ϕ_j used for pressure is the weighting function for the continuity equation. In order to prevent an overconstrained system of discrete equations, the interpolation used for pressure must be at least one order lower than that used for the velocity field (i.e., unequal order interpolation). Furthermore, the pressure need not be made continuous across elements because the pressure variable does not constitute a primary variable of the weak form presented in Eqs. (10.3.5)–(10.3.7).

Commonly used elements for two-dimensional flows of viscous incompressible fluids are shown in Fig. 10.5.1. In the case of linear elements, pressure is treated as discontinuous between elements; otherwise, the whole domain will have the same pressure. Two different pressure approximations have been used when the velocities are approximated by quadratic Lagrange functions. The first is a continuous bilinear approximation in which the pressure is defined at the corner nodes of the element and is made continuous across element boundaries. The second pressure approximation involves a discontinuous (between elements) linear variation defined on the element by $\Phi = [1 \ x \ y]^T$. Here the unknowns are not nodal point values of the pressure but correspond to the coefficients in $P = a \cdot 1 + b \cdot x + c \cdot y$.

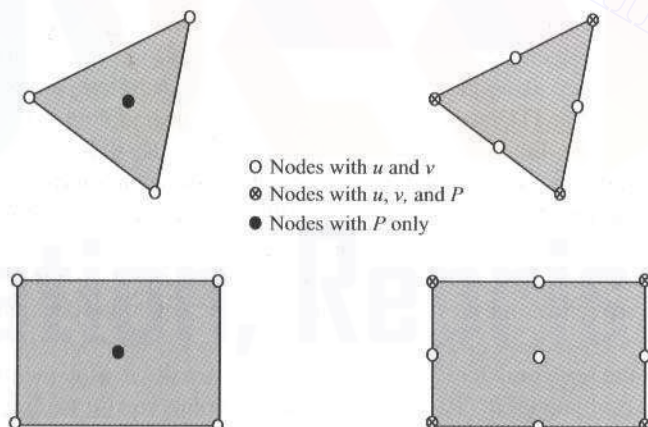


Figure 10.5.1 The triangular and quadrilateral elements used for the mixed and penalty finite element models.

When the eight-node quadratic element is used to represent the velocity field, a continuous, bilinear pressure approximation may be selected. When a discontinuous pressure variation is utilized with this element, the constant pressure representation over each element must be used. The quadratic quadrilateral elements shown in Fig. 10.5.1 are known to give reliable solutions for velocity and pressure fields. Other elements may yield acceptable solutions for the velocity field, but the pressure field is often in error.

10.5.3 Evaluation of Element Matrices in the Penalty Model

The numerical evaluation of the coefficient matrices appearing in equation (10.4.27) requires special consideration. This aspect is discussed here for the steady-state case. For the steady-state flows with constant material properties, Eq. (10.4.27) is of the form

$$(\mathbf{K}_v + \mathbf{K}_p)\Delta = \mathbf{F} \quad (10.5.1)$$

where \mathbf{K}_v is the contribution from the viscous terms and \mathbf{K}_p is the contribution from the penalty terms (and depends on γ), which comes from the incompressibility constraint. In theory, as we increase the value of γ , the conservation of mass is satisfied more exactly. However, in practice, for some large value of γ , the contribution from the viscous terms would be negligibly small compared to the penalty terms. Thus, if \mathbf{K}_p is a nonsingular (i.e., invertible) matrix, the solution of Eq. (10.5.1) for a large value of γ is trivial, $\Delta = \mathbf{0}$. While the solution satisfies the continuity equation, it does not satisfy the momentum equations. In this case the discrete problem (10.5.1) is said to be overconstrained or “locked.” If \mathbf{K}_p is singular, then the sum $(\mathbf{K}_v + \mathbf{K}_p)$ is nonsingular (because \mathbf{K}_v is nonsingular), and a nontrivial solution to the problem is obtained.

The numerical problem described above is eliminated by proper evaluation of the integrals in \mathbf{K}_v and \mathbf{K}_p . It is found that if the coefficients of \mathbf{K}_p (i.e., penalty matrix coefficients) are evaluated using a numerical integration rule where the order is one less than that required to integrate them exactly, the finite element equations (10.5.1) give acceptable solutions for the velocity field. This technique of underintegrating the penalty terms is known in the literature as *reduced integration*. For example, if a linear quadrilateral element is used to approximate the velocity field, the matrix coefficients \mathbf{K}_v (as well as \mathbf{M} for unsteady problems) are evaluated using the 2×2 Gauss-Legendre quadrature, and \mathbf{K}_p is evaluated using the one-point (1×1) Gauss-Legendre quadrature. The one-point quadrature yields a singular \mathbf{K}_p . Therefore, Eq. (10.5.1) can be solved because $(\mathbf{K}_v + \mathbf{K}_p)$ is nonsingular and can be inverted (after assembly and imposition of boundary conditions) to obtain a good finite element solution of the original problem. When a quadratic quadrilateral element is used, the 3×3 Gauss-Legendre quadrature is used to evaluate \mathbf{K}_v and \mathbf{M} , and the 2×2 Gauss-Legendre quadrature is used to evaluate \mathbf{K}_p . Of course, as the degree of interpolation goes up, or as very refined meshes are used, the resulting equations become less sensitive to locking.

Concerning the postcomputation of pressure in the penalty model, the pressure should be computed by evaluating Eq. (10.4.20) at integration points corresponding to the reduced Gauss rule. This is equivalent to using an interpolation for pressure that is one order less than the one used for the velocity field. The pressure computed using equation (10.4.20) at the reduced integration points is not always reliable and accurate. The pressures predicted

using the linear elements, especially for coarse meshes, are seldom acceptable. Quadratic elements are known to yield more reliable results.

10.5.4 Postcomputation of Stresses

The analysis of a flow problem generally includes calculation of not only the velocity field and pressure but also the computation of the stress field. A brief discussion of the stress calculation is presented next.

For a plane two-dimensional flow, the stress components (σ_{xx} , σ_{yy} , σ_{xy}) are given by

$$\sigma_{xx} = 2\mu \frac{\partial v_x}{\partial x} - P, \quad \sigma_{yy} = 2\mu \frac{\partial v_y}{\partial y} - P, \quad \sigma_{xy} = \mu \left(\frac{\partial v_x}{\partial y} + \frac{\partial v_y}{\partial x} \right) \quad (10.5.2)$$

where μ is the viscosity of the fluid. Substitution of the finite element approximations (10.3.11a) and (10.3.11b) for the velocity field and pressure into Eqs. (10.5.2) yields

$$\begin{aligned} \sigma_{xx} &= 2\mu \sum_{j=1}^n \frac{\partial \psi_j}{\partial x} v_x^j - P, \quad \sigma_{yy} = 2\mu \sum_{j=1}^n \frac{\partial \psi_j}{\partial y} v_y^j - P \\ \sigma_{xy} &= \mu \sum_{j=1}^n \left(\frac{\partial \psi_j}{\partial y} v_x^j + \frac{\partial \psi_j}{\partial x} v_y^j \right) \end{aligned} \quad (10.5.3)$$

where P is calculated from

$$P(x, y) = \sum_{J=1}^m \phi_J(x, y) P_J \quad (10.5.4)$$

for the mixed model and from

$$P_Y(x, y) = -\gamma \sum_{j=1}^n \left(\frac{\partial \psi_j}{\partial x} v_x^j + \frac{\partial \psi_j}{\partial y} v_y^j \right) \quad (10.5.5)$$

for the penalty model.

The spatial derivatives of the interpolation functions in Eqs. (10.5.3) and (10.5.5) must be evaluated using the reduced Gauss point rule. Thus, the stresses (as well as the pressure) are computed using the one-point Gauss rule for linear elements and with the 2×2 Gauss rule for the quadratic elements. The stresses computed at interior integration points can be extrapolated to the nodes by a simple linear extrapolation procedure, and they may be appropriately averaged between adjacent elements to produce a continuous stress field.

10.6 NUMERICAL EXAMPLES

A number of simple examples of two-dimensional Stokes flows of viscous incompressible fluids are presented in this section [see Reddy (2004)]. The examples presented herein were solved using the mixed and *reduced integration penalty* finite element models. The objective here is to evaluate the accuracy of the penalty and mixed finite element models by comparing with the available analytical results and to illustrate the effect of the penalty parameter on the accuracy of the solutions.

Example 10.6.1 (Viscous Fluid Squeezed between Parallel Plates)

Consider the slow flow of a viscous incompressible material squeezed between two long parallel plates [see Fig. 10.6.1(a)]. When the length of the plates is very large compared to both the width and the distance between the plates, we have a case of plane flow. Although this is a moving boundary problem, we wish to determine the velocity and pressure fields for a fixed distance between the plates, assuming that a state of plane flow exists.

Let v_0 be the velocity with which the two plates are moving toward each other (i.e., squeezing out the fluid), and let $2b$ and $2a$ denote, respectively, the distance between and the length of the plates [see Fig. 10.6.1(a)]. Due to the biaxial symmetry present in the problem, it suffices to model only a quadrant of the domain. As a first mesh, we use a 5×3 nonuniform mesh of nine-node quadratic elements in the mixed model, and a 10×6 mesh of the four-node linear elements and 5×3 mesh of nine-node quadratic elements in the penalty model [see Fig. 10.6.1(b)]. The nonuniform mesh, with smaller elements near the free surface (i.e., at $x = a$), is used to approximate accurately the singularity in the shear stress at the point $(a, b) = (6, 2)$. The mesh used for the penalty model has exactly the same number of nodes as the mesh used for the nine-node mesh of the mixed model.

The velocity boundary conditions are shown in Fig. 10.6.1(b). The velocity field at $x = 6$ (outflow boundary) is not known; if we do not impose any boundary conditions there, it amounts to requiring $t_x = t_y = 0$ in the integral sense. In the mixed finite element model, it is necessary to specify the pressure at least at one node. In the present case, the node at $(x, y) = (a, 0)$ is specified to have zero pressure. An approximate analytical solution to this two-dimensional problem is provided by Nadai (1963), and it is given by

$$\begin{aligned} v_x(x, y) &= \frac{3V_0x}{2b} \left(1 - \frac{y^2}{b^2}\right), \quad v_y(x, y) = -\frac{3V_0y}{2b} \left(3 - \frac{y^2}{b^2}\right) \\ P(x, y) &= \frac{3\mu V_0}{2b^3} (a^2 + y^2 - x^2) \end{aligned} \quad (10.6.1)$$

The velocities $v_x(x, 0)$ obtained with the two finite element models compare well with the analytical solution, as shown in Table 10.6.1. The nine-node element gives very good results for both the penalty and mixed models. The influence of the penalty parameter on the accuracy of

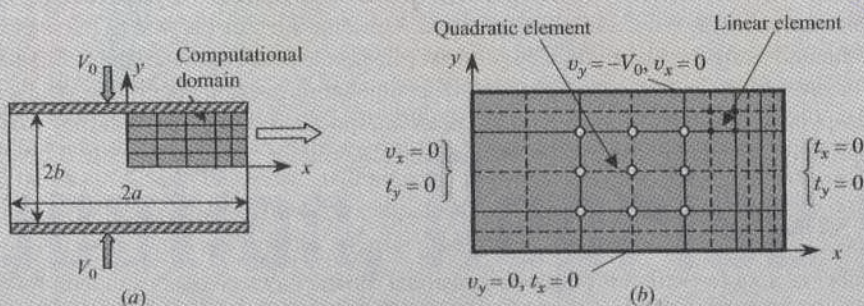


Figure 10.6.1 (a) Geometry, computational domain, and (b) the finite element mesh used for the analysis of the slow flow of viscous incompressible fluid between parallel plates.

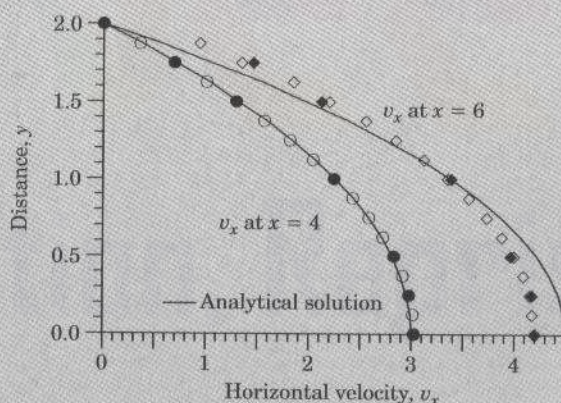
Table 10.6.1 Comparison of finite element solution $v_x(x, 0)$ with the analytical solution for fluid squeezed between plates.

x	$\gamma = 1.0$		$\gamma = 100$		$\gamma = 10^8$		Mixed model	
	Four-node	Nine*-node	Four-node	Nine-node	Four-node	Nine-node	Nine-node	Series solution
1.00	0.0303	0.0310	0.6563	0.6513	0.7576	0.7505	0.7497	0.7500
2.00	0.0677	0.0691	1.3165	1.3062	1.5135	1.4992	1.5031	1.5000
3.00	0.1213	0.1233	1.9911	1.9769	2.2756	2.2557	2.2561	2.2500
4.00	0.2040	0.2061	2.6960	2.6730	3.0541	3.0238	3.0203	3.0000
4.50	0.2611	0.2631	3.0718	3.0463	3.4648	3.4307	3.4292	3.3750
5.00	0.3297	0.3310	3.4347	3.3956	3.8517	3.8029	3.8165	3.7500
5.25	0.3674	0.3684	3.6120	3.5732	4.0441	3.9944	3.9893	3.9375
5.50	0.4060	0.4064	3.7388	3.6874	4.1712	4.1085	4.1204	4.1250
5.75	0.4438	0.4443	3.8316	3.7924	4.2654	4.2160	4.2058	4.3125
6.00	0.4793	0.4797	3.8362	3.7862	4.2549	4.1937	4.2364	4.5000

*The 3×3 Gauss rule is used for nonpenalty terms, and the 2×2 Gauss rule for penalty terms is used for quadratic elements.

the solution is clear from the results. Whether the element is linear or quadratic, it is necessary to use a large value of the penalty parameter.

Figure 10.6.2 contains plots of the velocity $v_x(x, y)$ for $x = 4$ and $x = 6$, and Fig. 10.6.3 contains plots of pressure $P(x, y)$, for $y = y_0$, where y_0 is the y coordinate of the Gauss point nearest to the centerline or top plate. These results were obtained with two different meshes: 5×3 and 10×8 . The pressure in the penalty model was computed using Eq. (10.5.5) with the 2×2 Gauss rule for the quadratic rectangular element and the one-point formula for the linear element, whereas in the mixed model (as well as the analytical solution) it is computed at the nodes. If the pressure in the penalty model were computed using the full quadrature

**Figure 10.6.2** Velocity fields for fluid squeezed between parallel plates.

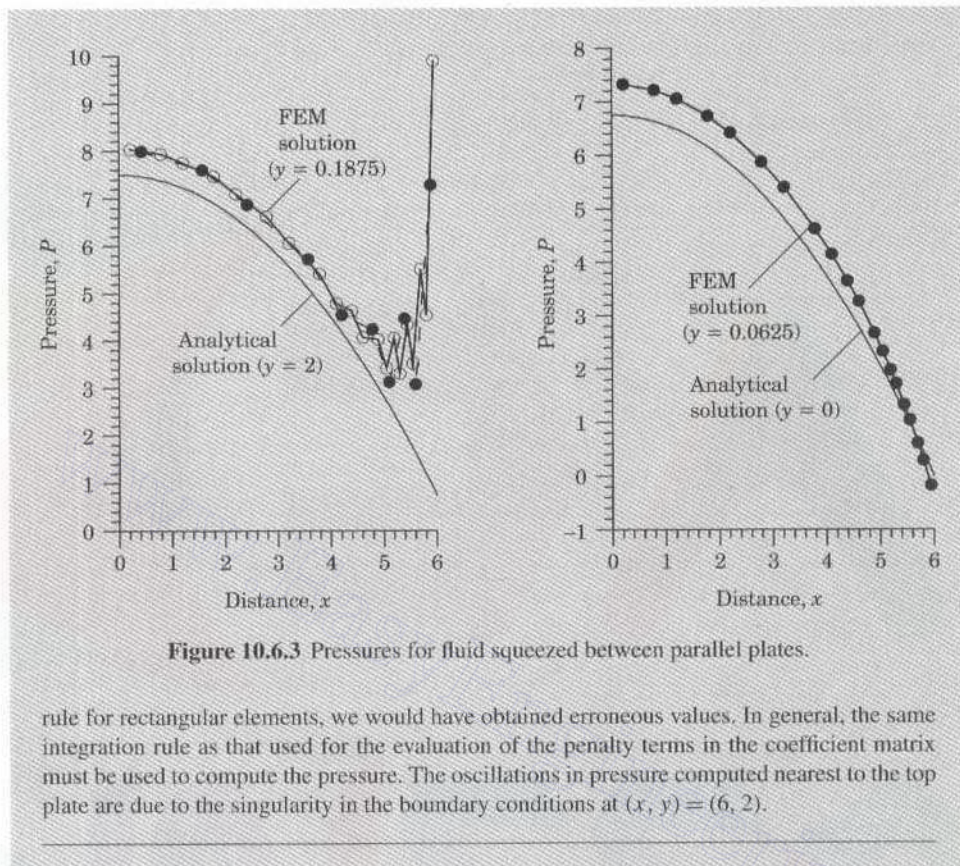


Figure 10.6.3 Pressures for fluid squeezed between parallel plates.

rule for rectangular elements, we would have obtained erroneous values. In general, the same integration rule as that used for the evaluation of the penalty terms in the coefficient matrix must be used to compute the pressure. The oscillations in pressure computed nearest to the top plate are due to the singularity in the boundary conditions at $(x, y) = (6, 2)$.

Example 10.6.2 (Flow of a Viscous Lubricant in a Slider Bearing)

The slider (or slipper) bearing consists of a short sliding pad moving at a velocity $u = V_0$ relative to a stationary pad inclined at a small angle with respect to the stationary pad, and the small gap between the two pads is filled with a lubricant [see Fig. 10.6.4(a)]. Since the ends of the bearing are generally open, the pressure there is atmospheric, P_0 . If the upper pad is parallel to the base plate, the pressure everywhere in the gap must be atmospheric (because dP/dx is a constant for flow between parallel plates), and the bearing cannot support any transverse load. If the upper pad is inclined to the base pad, a pressure distribution, in general, a function of x and y , is set up in the gap. For large values of V_0 , the pressure generated can be of sufficient magnitude to support heavy loads normal to the base pad.

When the width of the gap and the angle of inclination are small, we may assume that $v_y = 0$ and the pressure is not a function of y . Assuming a two-dimensional state of flow and a small angle of inclination, and neglecting the normal stress gradient (in comparison with the shear stress gradient), the equations governing the flow of the lubricant between the pads

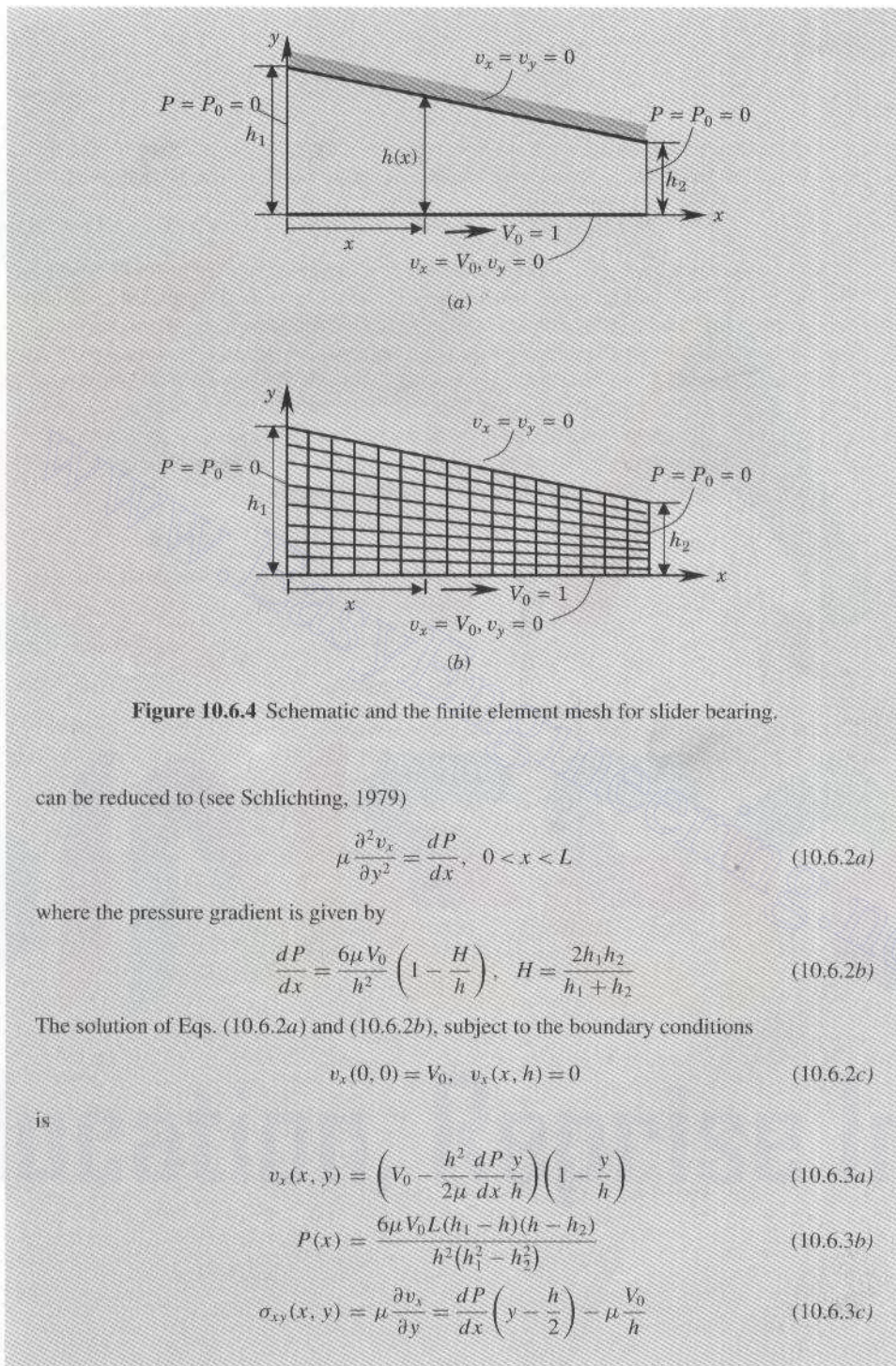


Figure 10.6.4 Schematic and the finite element mesh for slider bearing.

can be reduced to (see Schlichting, 1979)

$$\mu \frac{\partial^2 v_x}{\partial y^2} = \frac{dP}{dx}, \quad 0 < x < L \quad (10.6.2a)$$

where the pressure gradient is given by

$$\frac{dP}{dx} = \frac{6\mu V_0}{h^2} \left(1 - \frac{H}{h} \right), \quad H = \frac{2h_1 h_2}{h_1 + h_2} \quad (10.6.2b)$$

The solution of Eqs. (10.6.2a) and (10.6.2b), subject to the boundary conditions

$$v_x(0, 0) = V_0, \quad v_x(x, h) = 0 \quad (10.6.2c)$$

is

$$v_x(x, y) = \left(V_0 - \frac{h^2}{2\mu} \frac{dP}{dx} \frac{y}{h} \right) \left(1 - \frac{y}{h} \right) \quad (10.6.3a)$$

$$P(x) = \frac{6\mu V_0 L (h_1 - h)(h - h_2)}{h^2 (h_1^2 - h_2^2)} \quad (10.6.3b)$$

$$\sigma_{xy}(x, y) = \mu \frac{\partial v_x}{\partial y} = \frac{dP}{dx} \left(y - \frac{h}{2} \right) - \mu \frac{V_0}{h} \quad (10.6.3c)$$

where

$$h(x) = h_1 + \frac{h_2 - h_1}{L}x \quad (10.6.4)$$

In the finite element analysis we do not make any assumptions concerning v_y and the pressure gradient, and solve the Stokes equations with the following choice of parameters:

$$h_1 = 2h_2 = 8 \times 10^{-4} \text{ ft.}, \quad L = 0.36 \text{ ft.}, \quad \mu = 8 \times 10^{-4} \text{ lb/ft.}^2, \quad V_0 = 30 \text{ ft.} \quad (10.6.5)$$

We use a mesh (mesh 1) of 18×8 linear quadrilateral elements to analyze the problem. The mesh and boundary conditions are shown in Fig. 10.6.4(b). The penalty parameter is chosen to be $\gamma = \mu \times 10^8$. Table 10.6.2 contains a comparison of the finite element solutions and analytical solutions for the velocity, pressure, and shear stress. Figure 10.6.5 contains plots of the horizontal velocity v_x at $x = 0, 0.18$, and 0.36 ft. Figure 10.6.6 contains plots of pressure and shear stress as a function of x at $y = 0$. The finite element solutions for the pressure and shear stress were computed at the center of the first row of elements along the moving block. The results are in good agreement with the analytical solutions (10.6.3a)–(10.6.3c), validating the assumptions made in the development of the analytical solution.

Table 10.6.2 Comparison of finite element solutions velocities with the analytical solutions for viscous fluid in a slider bearing.

\bar{y}	$v_x(0, y)$				$v_x(0.18, y)$				$v_x(0.36, y)$	
	FEM	Analy.	\bar{y}	FEM	Analy.	\bar{y}	FEM	Analy.		
0.0	30.000	30.000	0.00	30.000	30.000	0.00	30.000	30.000		
1.0	22.923	22.969	0.75	25.139	25.156	0.50	29.564	29.531		
2.0	16.799	16.875	1.50	20.596	20.625	1.00	28.182	28.125		
3.0	11.626	11.719	2.25	16.372	16.406	1.50	25.853	25.781		
4.0	7.403	7.500	3.00	12.465	12.500	2.00	22.577	22.500		
5.0	4.130	4.219	3.75	8.874	8.906	2.50	18.354	18.281		
6.0	1.805	1.875	4.50	5.600	5.625	3.00	13.184	13.125		
7.0	0.429	0.469	5.25	2.642	2.656	3.50	7.066	7.031		
8.0	0.000	0.000	6.00	0.000	0.000	4.00	0.000	0.000		

x	Analytical solution			FEM Solution			
	$\bar{P}(x, 0)$	$-\sigma_{xy}(x, 0)$	\bar{x}	\bar{y}	\bar{P}	$-\sigma_{xy}$	
0.01	7.50	59.99	0.1125	0.4922	8.46	56.61	
0.03	22.46	59.89	0.3375	0.4766	25.46	56.60	
0.05	37.29	59.67	0.5625	0.4609	42.31	56.47	
0.07	51.89	59.30	0.7875	0.4453	58.76	56.17	
0.09	66.12	58.77	1.0125	0.4297	74.69	55.69	
0.27	129.60	38.40	2.5875	0.3203	134.40	41.77	
0.29	118.57	32.71	2.8125	0.3047	125.60	36.93	
0.31	99.58	25.70	3.0375	0.2891	107.60	30.76	
0.33	70.30	17.04	3.2625	0.2734	77.39	22.89	
0.35	27.61	6.31	3.4875	0.2578	30.80	12.82	

$$\bar{x} = 10x, \quad \bar{y} = y \times 10^4, \quad \bar{P} = P \times 10^{-2}.$$

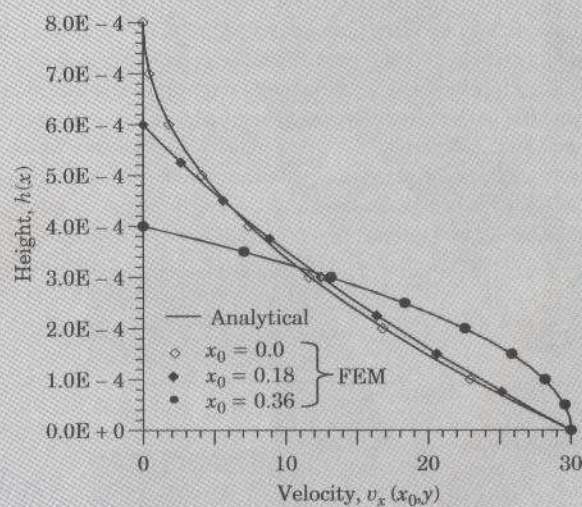


Figure 10.6.5 Velocity distributions for the slider bearing problem.

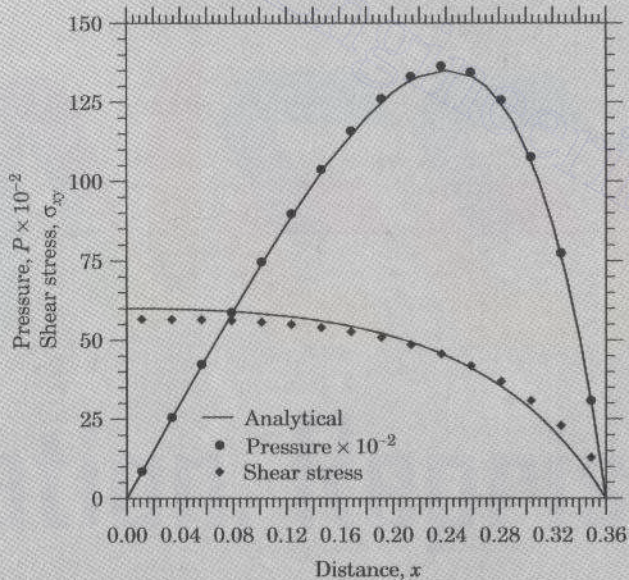


Figure 10.6.6 Pressure and shear stress distributions for the slider bearing problem.

Example 10.6.3 (Lid-Driven Cavity Flow)

Consider the laminar flow of a viscous, incompressible fluid in a square cavity bounded by three motionless walls and a lid moving at a constant velocity in its own plane (see Fig. 10.6.7). Singularities exist at each corner where the moving lid meets a fixed wall. This example is one that has been extensively studied by analytical, numerical, and experimental methods, and it is often used as a benchmark problem to test a new numerical method or formulation.

Assuming a unit square and a unit velocity of the top wall, we can discretize the flow region using a uniform 8×8 mesh of linear elements or 4×4 of nine-node quadratic elements. At the singular points, namely at the top corners of the lid, we assume that $v_x(x, 1) = v_0 = 1.0$. The linear solution for the horizontal velocity along the vertical centerline obtained with the two meshes is shown in Fig. 10.6.8, and the variation of pressure along the top wall (computed

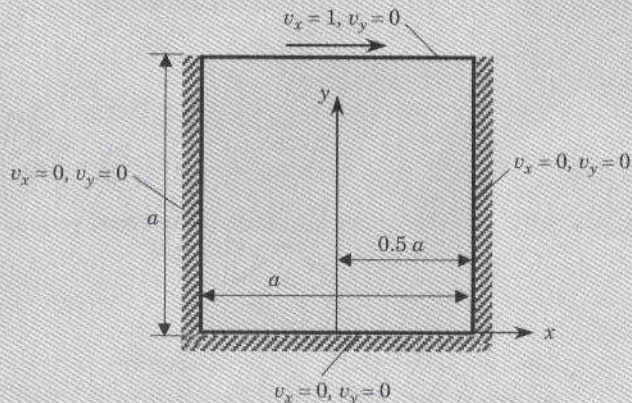


Figure 10.6.7 Boundary conditions for lid-driven cavity problem.

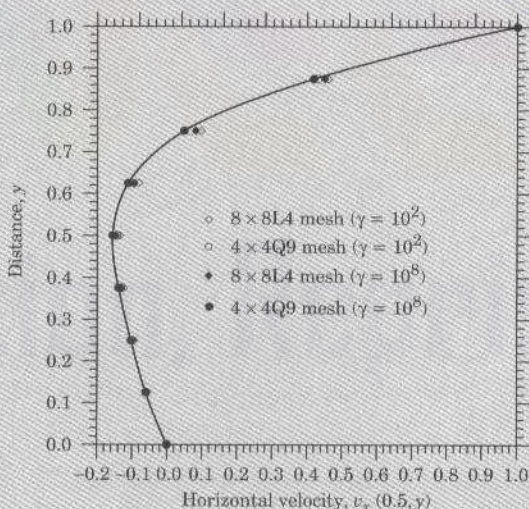


Figure 10.6.8 Plots of horizontal velocity $v_x(0.5, y)$ along the vertical centerline of the cavity.

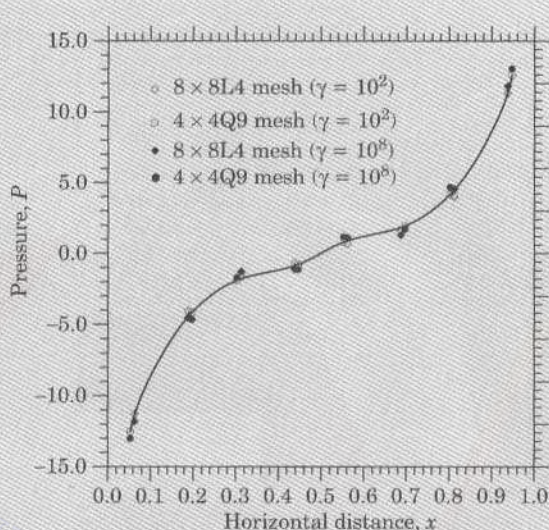


Figure 10.6.9 Plots of pressure $P(x, y_0)$ along the top wall of the cavity.

at the reduced Gauss points) is shown in Fig. 10.6.9. The numerical values of the velocity field are tabulated in Table 10.6.3. It is clear that the value of the penalty parameter between $\gamma = 10^2$ and 10^8 has a small effect on the accuracy of the solution. Figure 10.6.10 contains plots of center velocity $v_x(0.5, y)$ as a function of y for 8×8 and 16×20 meshes of bilinear elements.

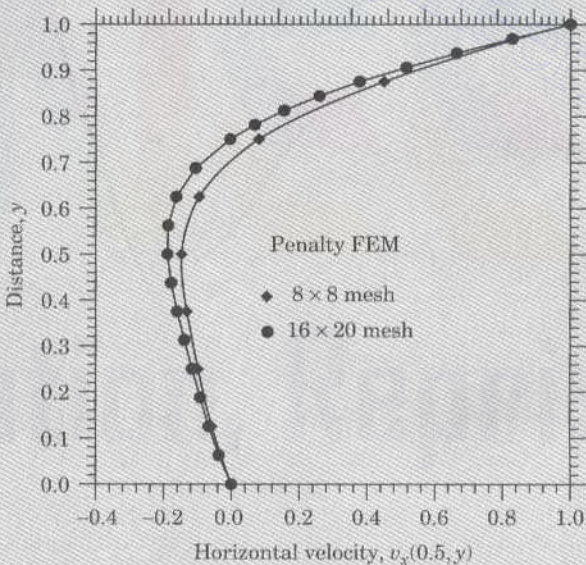


Figure 10.6.10 Velocity $v_x(0.5, y)$ versus y for 8×8 and 16×20 meshes of bilinear elements.

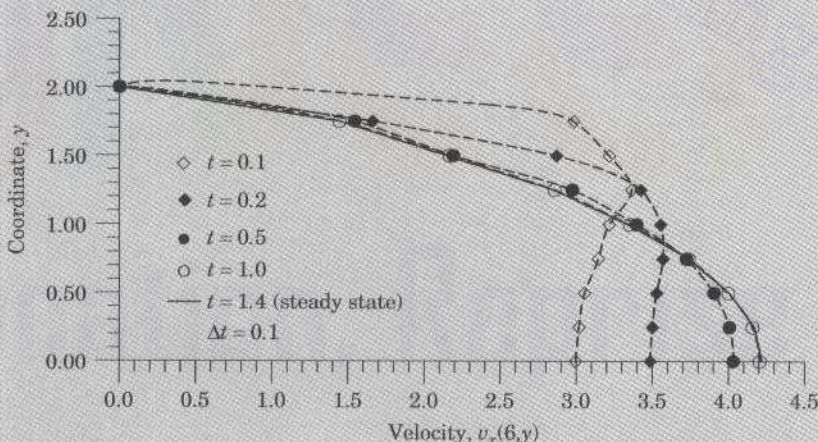
Table 10.6.3 Velocity $v_x(0.5, y)$ obtained with various values of the penalty parameter γ .

y	Mesh: 8×8 L4		Mesh: 4×4 Q9	
	$\gamma = 10^2$	$\gamma = 10^8$	$\gamma = 10^2$	$\gamma = 10^8$
0.125	-0.0557	-0.0579	-0.0589	-0.0615
0.250	-0.0938	-0.0988	-0.0984	-0.1039
0.375	-0.1250	-0.1317	-0.1320	-0.1394
0.500	-0.1354	-0.1471	-0.1442	-0.1563
0.625	-0.0818	-0.0950	-0.0983	-0.1118
0.750	0.0958	0.0805	0.0641	0.0481
0.875	0.4601	0.4501	0.4295	0.4186

Example 10.6.4 (Transient Analysis of Fluid Squeezed between Plates)

Consider the unsteady flow of a viscous fluid squeezed between two parallel plates [see Fig. 10.6.1(a)]. The flow is induced by the uniform motion of the plates toward each other. The boundary conditions of the model are the same as shown in Fig. 10.6.1(b). The initial boundary conditions are assumed to be zero.

We use the 6×4 mesh of nine-node quadratic elements, employed in Example 10.6.1, to model the problem. Figure 10.6.11 contains plots of the horizontal velocity $v_x(6, y)$ as a

**Figure 10.6.11** Velocity $v_x(6, y)$ versus y for various times (6×4 mesh of nine-node quadratic elements using penalty FEM).

function of y for various times and for two different time steps. The transient solution reaches a steady state around $t = 1.4$ (for a difference of 10^{-3} between the solutions at two consecutive time steps with $\Delta t = 0.1$).

Example 10.6.5 (Transient Analysis of the Lid-Driven Cavity)

Lastly, we study the motion of a viscous fluid inside a lid-driven cavity. We use 16×20 Q4 nonuniform mesh (of four-node rectangular elements) in the domain. The element sizes in each coordinate direction are given by

$$\{\text{DX}\} = \{0.0625, 0.0625, \dots, 0.0625\}$$

$$\{\text{DY}\} = \{0.0625, \dots, 0.0625, 0.03125, \dots, 0.03125\}$$

The Crank–Nicolson method ($\alpha = 0.5$) with two different time steps $\Delta t = 0.01$ and $\Delta t = 0.001$ are used. Table 10.6.4 contains the velocity field $v_x(0.5, y, t) \times 10$ for times $t = 0.01, 0.05$, and 0.1 . The solution reaches the steady state ($\epsilon = 10^{-2}$) at time $t = 0.1$ when $\Delta t = 0.01$ is used. The evolution of the horizontal velocity component $v_x(0.5, y, t)$ is shown in Fig. 10.6.12 ($\Delta t = 0.01$).

Table 10.6.4 The horizontal velocity field $v_x(0.5, y, t) \times 10$ versus time t for the wall-driven cavity problem (16×20 Q4 mesh).

y	$t = 0.01$	$t = 0.01$	$t = 0.05$	$t = 0.05$	$t = 0.10$	Steady state
	$\Delta t = 0.01$	$\Delta t = 0.001$	$\Delta t = 0.01$	$\Delta t = 0.001$	$\Delta t = 0.01$	
0.0625	-0.1342	-0.1953	-0.3103	-0.3247	-0.3655	-0.3688
0.1250	-0.1936	-0.3140	-0.5624	-0.5841	-0.6558	-0.6631
0.1875	-0.2314	-0.3940	-0.7888	-0.8163	-0.9108	-0.9198
0.2500	-0.2691	-0.4651	-1.0122	-1.0435	-1.1499	-1.1593
0.3125	-0.3157	-0.5475	-1.2346	-1.2746	-1.3802	-1.3886
0.3750	-0.3759	-0.6536	-1.4790	-1.5053	-1.5967	-1.6028
0.4375	-0.4516	-0.7902	-1.6964	-1.7151	-1.7793	-1.7820
0.5000	-0.5435	-0.9605	-1.8536	-1.8643	-1.8906	-1.8895
0.5625	-0.6465	-1.1577	-1.8846	-1.8878	-1.8700	-1.8652
0.6250	-0.7474	-1.3479	-1.7011	-1.6946	-1.6336	-1.6250
0.6875	-0.8097	-1.4428	-1.1889	-1.1653	-1.0700	-1.0572
0.7500	-0.7536	-1.1523	-0.2093	-0.1693	-0.0520	-0.0382
0.7813	-0.6325	-0.7744	0.5100	0.5471	0.6713	0.6820
0.8125	-0.4077	-0.1695	1.4014	1.4197	1.5467	1.5526
0.8438	-0.0054	0.7336	2.4885	2.4716	2.5918	2.5965
0.8750	0.6329	1.9318	3.7259	3.6716	3.7646	3.7824
0.9063	1.7000	3.5232	5.1185	5.0707	5.1198	5.1616
0.9375	3.3334	5.3837	6.5139	6.5756	6.6082	6.6410
0.9688	5.9470	7.5970	7.9975	8.2488	8.3805	8.2838

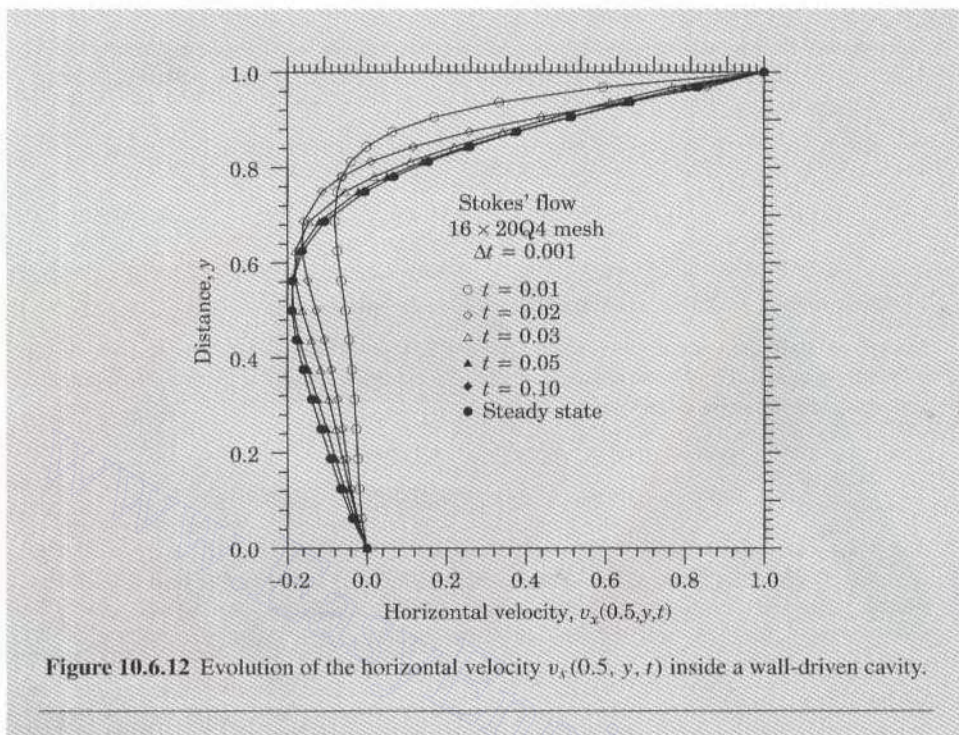


Figure 10.6.12 Evolution of the horizontal velocity $v_x(0.5, y, t)$ inside a wall-driven cavity.

10.7 SUMMARY

Finite element models of the equations governing two-dimensional flows of viscous, incompressible fluids are developed. Two different types of finite element models are presented: (1) the velocity-pressure finite element model, with (v_x, v_y, P) as the primary nodal degrees of freedom and (2) the penalty finite element model with (v_x, v_y) as the primary nodal degrees of freedom. In the penalty function method, the pressure is calculated from the velocity field in the postcomputation. The coefficient matrix in the penalty finite element model is evaluated using mixed integration: full integration for the viscous terms and reduced integration for the penalty terms (i.e., terms associated with the incompressibility or divergence-free condition on the velocity field). Both triangular and rectangular elements are discussed. In general, triangular elements do not yield accurate pressure fields. The linear and quadratic quadrilateral elements are more reliable for pressure as well as for velocity fields in the penalty finite element model.

A more complete treatment of finite element models of fluid flow can be found in the books by Gresho and Sani (1998), Reddy and Gartling (2001), and Reddy (2004). These books also contain extensive references to the literature on finite element analysis of fluid flow problems.

PROBLEMS

- 10.1** Consider Eqs. (10.2.1) and (10.2.2) in cylindrical coordinates (r, θ, z) . For axisymmetric flows of viscous incompressible fluids (i.e., flow field is independent of θ coordinate), we have

$$\rho \frac{\partial u}{\partial t} = \frac{1}{r} \frac{\partial}{\partial r} (r \sigma_{rr}) - \frac{\sigma_{\theta\theta}}{r} + \frac{\partial \sigma_{rz}}{\partial z} + f_r \quad (1)$$

$$\rho \frac{\partial w}{\partial t} = \frac{1}{r} \frac{\partial}{\partial r} (r \sigma_{rz}) + \frac{\partial \sigma_{zz}}{\partial z} + f_z \quad (2)$$

$$\frac{1}{r} \frac{\partial}{\partial r} (ru) + \frac{\partial w}{\partial z} = 0 \quad (3)$$

where

$$\sigma_{rr} = -P + 2\mu \frac{\partial u}{\partial r}, \quad \sigma_{\theta\theta} = -P + 2\mu \frac{u}{r}, \quad \sigma_{zz} = -P + 2\mu \frac{\partial w}{\partial z}, \quad \sigma_{rz} = \mu \left(\frac{\partial u}{\partial z} + \frac{\partial w}{\partial r} \right) \quad (4)$$

Develop the semidiscrete finite element model of the equation by the pressure-velocity formulation.

- 10.2** Develop the semidiscrete finite element model of the equations in Problem 10.1 using the penalty function formulation.
10.3 Write the fully discretized finite element equations of the finite element models in Problems 10.1 and 10.2. Use the α -family of approximation.
10.4 The equations governing unsteady slow flow of viscous, incompressible fluids in the (x, y) plane can be expressed in terms of vorticity ζ and stream function ψ :

$$\rho \frac{\partial \zeta}{\partial t} - \mu \nabla^2 \zeta = 0, \quad -2\zeta - \nabla^2 \psi = 0$$

Develop the semidiscrete finite element model of the equations. Discuss the meaning of the secondary variables. Use α -family of approximation to reduce the ordinary differential equations to algebraic equations.

- 10.5–10.7** For the viscous flow problems given in Figs. P10.5–P10.7, give the specified primary and secondary degrees of freedom and their values.

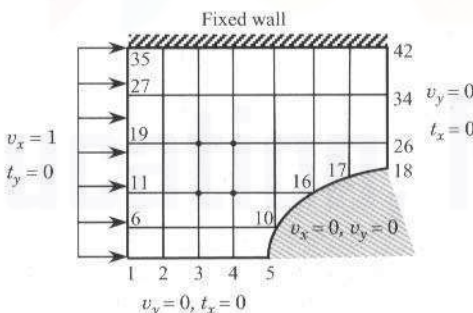


Figure P10.5

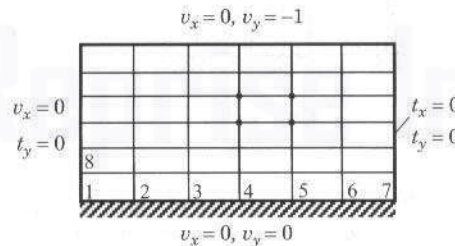


Figure P10.6

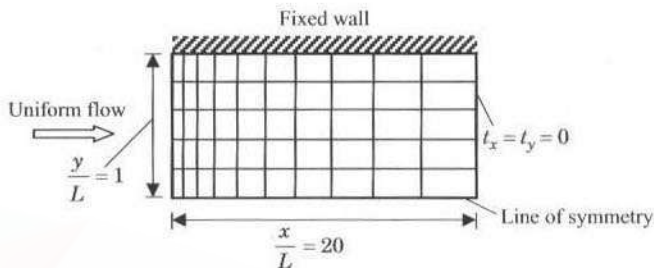


Figure P10.7

- 10.8.** Consider the flow of a viscous incompressible fluid in a square cavity (Fig. P10.8). The flow is induced by the movement of the top wall (or lid) with a velocity $v_x = \sin \pi x$. For a 5×4 mesh of linear elements, give the primary and secondary degrees of freedom.

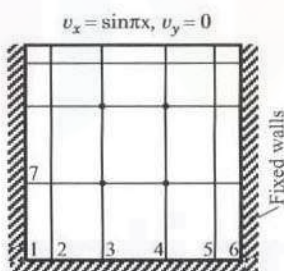


Figure P10.8

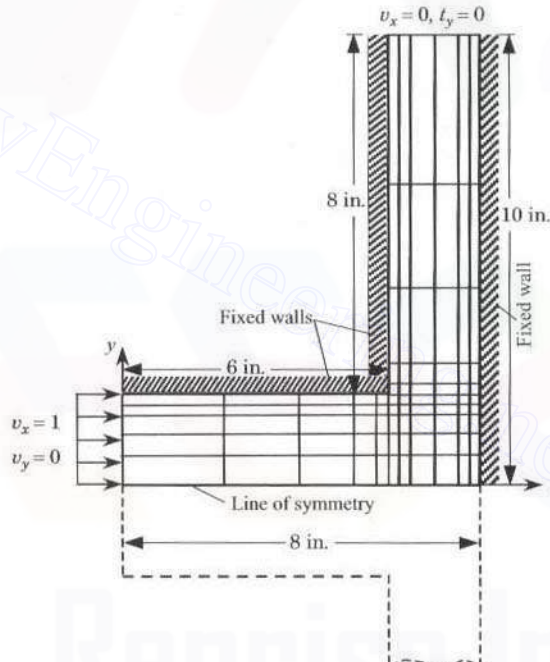


Figure P10.9

- 10.9.** Consider the flow of a viscous incompressible fluid in a 90° plane tee. Using the symmetry and the mesh shown in Fig. P10.9. Write the specified primary and secondary variables for the computational domain.
- 10.10.** Repeat Problem 10.9 for the geometry shown in Fig. P10.10.

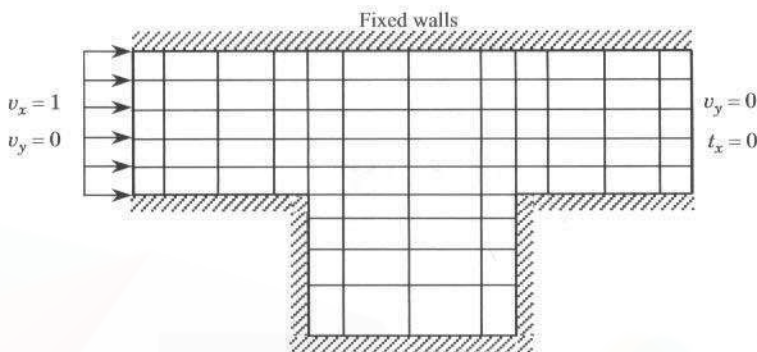


Figure P10.10

REFERENCES FOR ADDITIONAL READING

1. Bird, R. B., Stewart, W. E., and Lightfoot, E. N., *Transport Phenomena*, John Wiley, New York, 1960.
2. Gresho, P. M. and Sani, R. L., *Incompressible Flow and the Finite Element Method*, John Wiley, West Sussex, UK, 2000.
3. Nadai, A, *Theory of Flow and Fracture of Solids*, Vol. II, McGraw-Hill, New York, 1963.
4. Oden, J. T., "RIP Methods for Stokesian Flows," in Gallagher, R. H., Zienkiewicz, O. C., Oden, J. T., and Norrie, D. (eds.), *Finite Element Method in Flow Problems*, Vol. IV, John Wiley, London, UK, 1982.
5. Reddy, J. N., "On the Accuracy and Existence of Solutions to Primitive Variable Models of Viscous Incompressible Fluids," *International Journal Engineering Science*, **16**, 921–929, 1978.
6. Reddy, J. N., "On the Finite Element Method with Penalty for Incompressible Fluid Flow Problems," in Whiteman, J. R. (ed.), *The Mathematics of Finite Elements and Applications III*, Academic Press, New York, 1979.
7. Reddy, J. N., *Applied Functional Analysis and Variational Methods in Engineering*, McGraw-Hill, New York, 1986; reprinted by Krieger, Melbourne, FL, 1991.
8. Reddy, J. N., *An Introduction to Nonlinear Finite Element Analysis*, Oxford University Press, Oxford, UK, 2004.
9. Reddy, J. N. and Gartling, D. K., *The Finite Element Method in Heat Transfer and Fluid Dynamics*, 2nd ed., CRC Press, Boca Raton, FL, 2001.
10. Roache, P. J., *Fundamentals of Computational Fluid Dynamics*, 2nd ed., Hermosa, Albuquerque, NM, 1998.
11. Schlichting, H., *Boundary Layer Theory* (translated by J. Kestin), 7th ed., McGraw-Hill, New York, 1979.

Chapter 11

PLANE ELASTICITY

11.1 INTRODUCTION

Elasticity is the part of solid mechanics that deals with stress and deformation of solid continua. Linearized elasticity is concerned with small deformations (i.e., strains and displacements that are very small compared to unity) in linear elastic solids (i.e., obey Hooke's law). There is a class of problems in elasticity whose solutions (i.e., displacements and stresses) are not dependent on one of the coordinates because of their geometry, boundary conditions, and external applied loads. Such problems are called plane elasticity problems. The plane elasticity problems considered here are grouped into *plane strain* and *plane stress* problems. Both classes of problems are described by a set of two *coupled* partial differential equations expressed in terms of two dependent variables that represent the two components of the displacement vector. The governing equations of plane strain problems differ from those of the plane stress problems only in the coefficients of the differential equations.

The primary objective of this chapter is three-fold: (1) review the governing equations in the Cartesian rectangular coordinate system (x, y, z), (2) develop the weak forms, and (3) construct finite element model of the plane elasticity equations. The treatment of topics (2) and (3) proceeds along the same lines as the discussion in Chapter 10 on viscous incompressible fluids. In fact, the governing equations of the two fields are quite similar, as we shall see shortly. We utilize suitable approximation functions from the library of two-dimensional finite element interpolation functions already developed in Chapters 8 and 9 to derive finite element equations.

11.2 GOVERNING EQUATIONS

11.2.1 Plane Strain

Plane strain problems are characterized by the displacement field

$$u_x = u_x(x, y), \quad u_y = u_y(x, y), \quad u_z = 0 \quad (11.2.1)$$

where (u_x, u_y, u_z) denote the components of the displacement vector \mathbf{u} in the (x, y, z) coordinate system. The displacement field (11.2.1) results in the following strain field:

$$\begin{aligned} \varepsilon_{xz} &= \varepsilon_{yz} = \varepsilon_{zz} = 0 \\ \varepsilon_{xx} &= \frac{\partial u_x}{\partial x}, \quad 2\varepsilon_{xy} = \frac{\partial u_x}{\partial y} + \frac{\partial u_y}{\partial x}, \quad \varepsilon_{yy} = \frac{\partial u_y}{\partial y} \end{aligned} \quad (11.2.2)$$

Clearly, the body is in a state of plane strain. For an orthotropic material, with principal material axes (x_1, x_2, x_3) coinciding with the (x, y, z) coordinates, the stress components are given by

$$\sigma_{xz} = \sigma_{yz} = 0, \quad \sigma_{zz} = E_3 \left(\frac{\nu_{13}}{E_1} \sigma_{xx} + \frac{\nu_{23}}{E_2} \sigma_{yy} \right) \quad (11.2.3a)$$

$$\begin{Bmatrix} \sigma_{xx} \\ \sigma_{yy} \\ \sigma_{xy} \end{Bmatrix} = \begin{bmatrix} \bar{c}_{11} & \bar{c}_{12} & 0 \\ \bar{c}_{12} & \bar{c}_{22} & 0 \\ 0 & 0 & \bar{c}_{66} \end{bmatrix} \begin{Bmatrix} \varepsilon_{xx} \\ \varepsilon_{yy} \\ 2\varepsilon_{xy} \end{Bmatrix} \quad (11.2.3b)$$

where \bar{c}_{ij} are the elastic stiffnesses

$$\begin{aligned} \bar{c}_{11} &= \frac{E_1(1-\nu_{12})}{(1+\nu_{12})(1-\nu_{12}-\nu_{21})} \\ \bar{c}_{22} &= \frac{E_2(1-\nu_{21})}{(1+\nu_{21})(1-\nu_{12}-\nu_{21})} \\ \bar{c}_{12} &= \nu_{12}\bar{c}_{22}, \quad \bar{c}_{66} = G_{12} \end{aligned} \quad (11.2.4)$$

and E_1 and E_2 are principal (Young's) moduli in the x and y directions, respectively, G_{12} the shear modulus in the xy plane, and ν_{12} and ν_{21} the Poisson ratio (i.e., the negative of the ratio of the transverse strain in the y direction to the strain in the x direction when stress is applied in the x direction). The Poisson ratio ν_{21} can be computed from the reciprocal relation

$$\nu_{21} = \nu_{12} \frac{E_2}{E_1} \quad (11.2.5)$$

Additional engineering constants E_3 , ν_{23} , and ν_{13} are required to compute σ_{zz} . For an isotropic material, we have

$$E_1 = E_2 = E_3 = E, \quad \nu_{12} = \nu_{21} = \nu_{13} = \nu_{23} = \nu, \quad G_{12} = G = \frac{E}{2(1+\nu)} \quad (11.2.6)$$

The equations of motion of three-dimensional linear elasticity, $\sigma_{ij,j} + f_i = \rho \ddot{u}_i$ with the body force components $f_3 = f_z = 0$, $f_1 = f_x = f_x(x, y)$, and $f_2 = f_y = f_y(x, y)$, and ρ the density of the material, reduce to the following two plane strain equations of motion

$$\rho \frac{\partial^2 u_x}{\partial t^2} - \frac{\partial \sigma_{xx}}{\partial x} - \frac{\partial \sigma_{xy}}{\partial y} - f_x = 0 \quad (11.2.7)$$

$$\rho \frac{\partial^2 u_y}{\partial t^2} - \frac{\partial \sigma_{xy}}{\partial x} - \frac{\partial \sigma_{yy}}{\partial y} - f_y = 0 \quad (11.2.8)$$

An example of a plane strain problem is provided by the long cylindrical member under external loads that are independent of z , as shown in Fig. 11.2.1. For cross sections sufficiently far from the ends, it is clear that the displacement u_z is zero and that u_x and u_y are independent of z , i.e., a state of plane strain exists.

11.2.2 Plane Stress

A state of plane stress is defined as one in which the following stress field exists:

$$\begin{aligned} \sigma_{xz} &= \sigma_{yz} = \sigma_{zz} = 0 \\ \sigma_{xx} &= \sigma_{xx}(x, y), \quad \sigma_{xy} = \sigma_{xy}(x, y), \quad \sigma_{yy} = \sigma_{yy}(x, y) \end{aligned} \quad (11.2.9a)$$

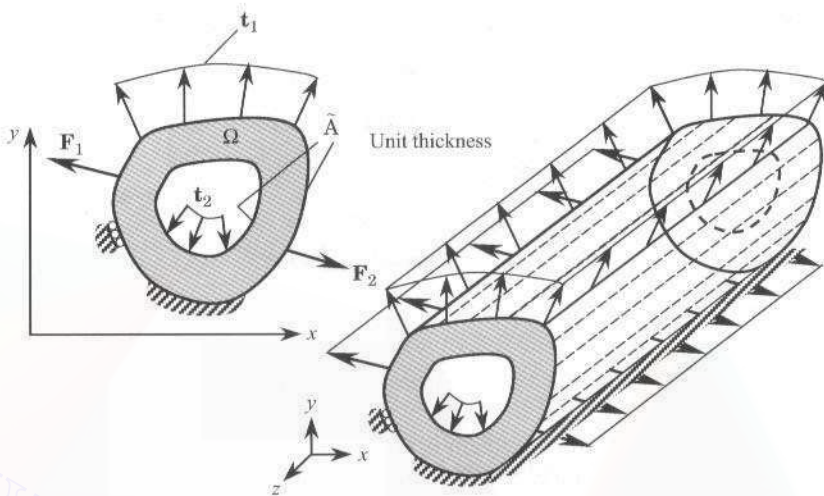


Figure 11.2.1 A hollow cylindrical member with internal and external applied loads.

The strain field associated with the stress field in (11.2.9a) is

$$\begin{Bmatrix} \varepsilon_{xx} \\ \varepsilon_{yy} \\ 2\varepsilon_{xy} \end{Bmatrix} = \begin{bmatrix} s_{11} & s_{12} & 0 \\ s_{12} & s_{22} & 0 \\ 0 & 0 & s_{66} \end{bmatrix} \begin{Bmatrix} \sigma_{xx} \\ \sigma_{yy} \\ \sigma_{xy} \end{Bmatrix} \quad (11.2.9b)$$

$$\varepsilon_{xz} = \varepsilon_{yz} = 0, \quad \varepsilon_{zz} = s_{13}\sigma_{xz} + s_{23}\sigma_{yz} \quad (11.2.9c)$$

where s_{ij} are the elastic compliances

$$\begin{aligned} s_{11} &= \frac{1}{E_1}, & s_{22} &= \frac{1}{E_2}, & s_{33} &= \frac{1}{E_3} \\ s_{12} &= -\nu_{21}s_{22} = -\nu_{12}s_{11}, & s_{66} &= \frac{1}{G_{12}} \\ s_{13} &= -\nu_{31}s_{33} = -\nu_{13}s_{11}, & s_{23} &= -\nu_{32}s_{33} = -\nu_{23}s_{22} \end{aligned} \quad (11.2.10)$$

The inverse of (11.2.9b) is given by

$$\begin{Bmatrix} \sigma_{xx} \\ \sigma_{yy} \\ \sigma_{xy} \end{Bmatrix} = \begin{bmatrix} \hat{c}_{11} & \hat{c}_{12} & 0 \\ \hat{c}_{12} & \hat{c}_{22} & 0 \\ 0 & 0 & \hat{c}_{66} \end{bmatrix} \begin{Bmatrix} \varepsilon_{xx} \\ \varepsilon_{yy} \\ 2\varepsilon_{xy} \end{Bmatrix} \quad (11.2.11)$$

where \hat{c}_{ij} are the elastic stiffnesses

$$\begin{aligned} \hat{c}_{11} &= \frac{E_1}{(1 - \nu_{12}\nu_{21})}, & \hat{c}_{22} &= \frac{E_2}{(1 - \nu_{12}\nu_{21})} \\ \hat{c}_{12} &= \nu_{12}\hat{c}_{22} = \nu_{21}\hat{c}_{11}, & \hat{c}_{66} &= G_{12} \end{aligned} \quad (11.2.12)$$

The equations of motion of a plane stress problem are the same as those listed in Eqs. (11.2.7) and (11.2.8). Note that the equations of motion of plane stress and plane strain differ from each other only on account of the difference in the constitutive equations for the two cases.

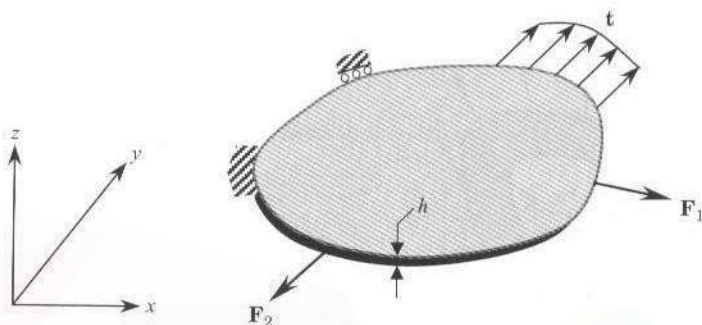


Figure 11.2.2 A thin plate in a state of plane stress.

An example of a plane stress problem is provided by a thin plate under external loads applied in the xy plane (or parallel to it) that are independent of z , as shown in Fig. 11.2.2. The top and bottom surfaces of the plate are assumed to be traction free, and the specified boundary forces are in the xy plane so that $f_z = 0$ and $u_z = 0$.

11.2.3 Summary of Equations

The governing equations for the two types of plane elasticity problems discussed above are summarized below, both in expanded form and vector form.

Equations of Motion

$$\begin{aligned}\frac{\partial \sigma_{xx}}{\partial x} + \frac{\partial \sigma_{xy}}{\partial y} + f_x &= \rho \frac{\partial^2 u_x}{\partial t^2} \\ \frac{\partial \sigma_{xy}}{\partial x} + \frac{\partial \sigma_{yy}}{\partial y} + f_y &= \rho \frac{\partial^2 u_y}{\partial t^2}\end{aligned}\quad (11.2.13a)$$

or

$$\mathbf{D}^* \boldsymbol{\sigma} + \mathbf{f} = \rho \ddot{\mathbf{u}} \quad (11.2.13b)$$

where f_x and f_y denote the components of the body force vector (measured per unit volume) along the x and y directions, respectively, ρ is the density of the material, and

$$\mathbf{D}^* = \begin{bmatrix} \partial/\partial x & 0 & \partial/\partial y \\ 0 & \partial/\partial y & \partial/\partial x \end{bmatrix}, \quad \boldsymbol{\sigma} = \begin{Bmatrix} \sigma_{xx} \\ \sigma_{yy} \\ \sigma_{xy} \end{Bmatrix}, \quad \mathbf{f} = \begin{Bmatrix} f_x \\ f_y \end{Bmatrix}, \quad \mathbf{u} = \begin{Bmatrix} u_x \\ u_y \end{Bmatrix} \quad (11.2.13c)$$

Strain-Displacement Relations

$$\varepsilon_{xx} = \frac{\partial u_x}{\partial x}, \quad \varepsilon_{yy} = \frac{\partial u_y}{\partial y}, \quad 2\varepsilon_{xy} = \frac{\partial u_x}{\partial y} + \frac{\partial u_y}{\partial x} \quad (11.2.14a)$$

or

$$\boldsymbol{\varepsilon} = \mathbf{D}\mathbf{u}, \quad \boldsymbol{\varepsilon} = \begin{Bmatrix} \varepsilon_{xx} \\ \varepsilon_{yy} \\ 2\varepsilon_{xy} \end{Bmatrix}, \quad \mathbf{D} = (\mathbf{D}^*)^T \quad (11.2.14b)$$

Stress-Strain (or Constitutive) Relations

$$\begin{Bmatrix} \sigma_{xx} \\ \sigma_{yy} \\ \sigma_{xy} \end{Bmatrix} = \begin{bmatrix} c_{11} & c_{12} & 0 \\ c_{12} & c_{22} & 0 \\ 0 & 0 & c_{66} \end{bmatrix} \begin{Bmatrix} \varepsilon_{xx} \\ \varepsilon_{yy} \\ 2\varepsilon_{xy} \end{Bmatrix} \quad (11.2.15a)$$

or

$$\boldsymbol{\sigma} = \mathbf{C}\boldsymbol{\varepsilon}, \quad \mathbf{C} = \begin{bmatrix} c_{11} & c_{12} & 0 \\ c_{12} & c_{22} & 0 \\ 0 & 0 & c_{66} \end{bmatrix} \quad (11.2.15b)$$

where c_{ij} ($c_{ji} = c_{ij}$) are the elasticity (material) constants for an orthotropic medium with the material principal directions (x_1, x_2, x_3) coinciding with the coordinate axes (x, y, z) used to describe the problem. The c_{ij} can be expressed in terms of the engineering constants (E_1, E_2, v_{12}, G_{12}) for an orthotropic material by Eqs. (11.2.3b) for plane strain problems ($c_{ij} = \bar{c}_{ij}$) and by Eqs. (11.2.11) for plane stress problems ($c_{ij} = \hat{c}_{ij}$).

Boundary Conditions

Natural boundary conditions are

$$\left. \begin{aligned} t_x &\equiv \sigma_{xx}n_x + \sigma_{xy}n_y = \hat{t}_x \\ t_y &\equiv \sigma_{xy}n_x + \sigma_{yy}n_y = \hat{t}_y \end{aligned} \right\} \quad \text{on } \Gamma_\sigma \quad (11.2.16a)$$

or

$$\mathbf{t} \equiv \bar{\sigma}\mathbf{n} = \hat{\mathbf{t}} \quad \text{on } \Gamma_\sigma, \quad \mathbf{n} = \begin{Bmatrix} n_x \\ n_y \end{Bmatrix}, \quad \bar{\sigma} = \begin{bmatrix} \sigma_{xx} & \sigma_{xy} \\ \sigma_{xy} & \sigma_{yy} \end{bmatrix} \quad (11.2.16b)$$

Essential boundary conditions are

$$u_x = \hat{u}_x, \quad u_y = \hat{u}_y \quad \text{on } \Gamma_u \quad (11.2.17a)$$

or

$$\mathbf{u} = \hat{\mathbf{u}} \quad \text{on } \Gamma_u \quad (11.2.17b)$$

where (n_x, n_y) denote the components (or direction cosines) of the unit normal vector on the boundary Γ ; Γ_σ and Γ_u are (disjoint) portions of the boundary; \hat{t}_x and \hat{t}_y denote the components of the specified traction vector; and \hat{u}_x and \hat{u}_y are the components of specified displacement vector. Only one element of each pair, (u_x, t_x) and (u_y, t_y) , may be specified at a boundary point.

Equations (11.2.7) and (11.2.8) can be expressed in terms of only the displacements u_x and u_y by substituting Eqs. (11.2.14) into Eqs. (11.2.15), and the result into Eqs. (11.2.13):

$$\begin{aligned} -\frac{\partial}{\partial x} \left(c_{11} \frac{\partial u_x}{\partial x} + c_{12} \frac{\partial u_y}{\partial y} \right) - \frac{\partial}{\partial y} \left[c_{66} \left(\frac{\partial u_x}{\partial y} + \frac{\partial u_y}{\partial x} \right) \right] &= f_x - \rho \frac{\partial^2 u_x}{\partial t^2} \\ -\frac{\partial}{\partial x} \left[c_{66} \left(\frac{\partial u_x}{\partial y} + \frac{\partial u_y}{\partial x} \right) \right] - \frac{\partial}{\partial y} \left(c_{12} \frac{\partial u_x}{\partial x} + c_{22} \frac{\partial u_y}{\partial y} \right) &= f_y - \rho \frac{\partial^2 u_y}{\partial t^2} \end{aligned} \quad (11.2.18a)$$

or

$$-\mathbf{D}^* \mathbf{C} \mathbf{D} \mathbf{u} = \mathbf{f} + \rho \ddot{\mathbf{u}} \quad (11.2.18b)$$

The boundary stress components (or tractions) can also be expressed in terms of the displacements:

$$\begin{aligned} t_x &= \left(c_{11} \frac{\partial u_x}{\partial x} + c_{12} \frac{\partial u_y}{\partial y} \right) n_x + c_{66} \left(\frac{\partial u_x}{\partial y} + \frac{\partial u_y}{\partial x} \right) n_y \\ t_y &= c_{66} \left(\frac{\partial u_x}{\partial y} + \frac{\partial u_y}{\partial x} \right) n_x + \left(c_{12} \frac{\partial u_x}{\partial x} + c_{22} \frac{\partial u_y}{\partial y} \right) n_y \end{aligned} \quad (11.2.19a)$$

or

$$\mathbf{t} = \bar{\mathbf{n}} \mathbf{C} \mathbf{D} \mathbf{u}, \quad \bar{\mathbf{n}} = \begin{bmatrix} n_x & 0 & n_y \\ 0 & n_y & n_x \end{bmatrix} \quad (11.2.19b)$$

This completes the review of the governing equations of a plane elastic body undergoing small deformations. Next, we discuss the finite element model development of the equations.

11.3 WEAK FORMULATIONS

11.3.1 Preliminary Comments

Here, we study two different ways of constructing the weak forms and associated finite element model of the plane elasticity equations (11.2.18a) and (11.2.19a). The first one uses the principle of virtual displacements (or the principle of minimum total potential energy), expressed in terms of matrices relating displacements to strains, strains to stresses, and the equations of motion. This approach is used in most finite element texts on solid mechanics. The second approach follows a procedure consistent with the previous sections and employs the weak formulation of Eqs. (11.2.18a) and (11.2.19a) to construct the finite element model. Of course, both methods give, mathematically, the *same* finite element model, but differ in their algebraic forms.

11.3.2 Principle of Virtual Displacements in Vector Form

Here, we use the (dynamic version of) the principle of virtual displacements [see Reddy (2002)] applied to a plane elastic finite element Ω_e with volume $V_e = h_e \Omega_e$ (see Fig. 11.3.1)

$$0 = \int_{V_e} (\sigma_{ij} \delta \varepsilon_{ij} + \rho \ddot{u}_i \delta u_i) dV - \int_{V_e} f_i \delta u_i dV - \oint_{S_e} \hat{t}_i \delta u_i ds \quad (11.3.1)$$

where S_e is the surface of the volume element V_e , h_e is the thickness of the element, δ denotes the variational operator, σ_{ij} and ε_{ij} are the components of stress and strain tensors, respectively, and f_i and \hat{t}_i are the components of the body force and boundary stress vectors, respectively. The correspondence between the (x, y) components and (x_1, x_2) components is given by

$$\begin{aligned} \sigma_{11} &= \sigma_{xx}, \quad \sigma_{12} = \sigma_{xy}, \quad \sigma_{22} = \sigma_{yy}, \quad \varepsilon_{11} = \varepsilon_{xx}, \quad \varepsilon_{12} = \varepsilon_{xy}, \quad \varepsilon_{22} = \varepsilon_{yy} \\ u_1 &= u_x, \quad u_2 = u_y, \quad h_e f_1 = f_x, \quad h_e f_2 = f_y, \quad h_e t_1 = t_x, \quad h_e t_2 = t_y \end{aligned} \quad (11.3.2)$$

The first term in Eq. (11.3.1) corresponds to the virtual strain energy stored in the body, the second term corresponds to the kinetic energy stored in the body, the third term represents the virtual work done by the body forces, and the fourth term represents the virtual work done by the surface tractions. We assume that all quantities are independent of the

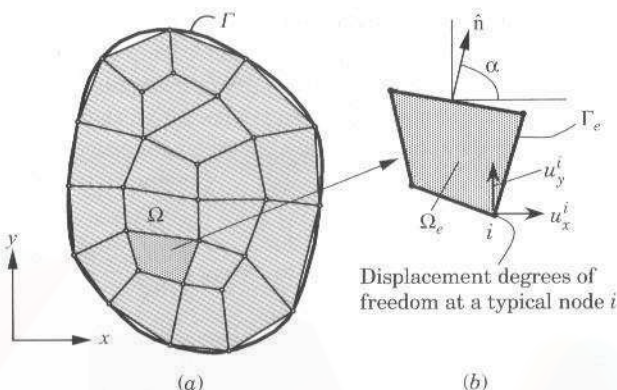


Figure 11.3.1 (a) Finite element discretization of a plane elastic domain and (b) a typical finite element.

thickness coordinate, z . Hence,

$$\begin{aligned} 0 = & \int_{\Omega_e} h_e [\sigma_{xx} \delta \varepsilon_{xx} + \sigma_{yy} \delta \varepsilon_{yy} + 2\sigma_{xy} \delta \varepsilon_{xy} + \rho(\ddot{u}_x \delta u_x + \ddot{u}_y \delta u_y)] dx dy \\ & - \int_{\Omega_e} (f_x \delta u_x + f_y \delta u_y) dx dy - \oint_{\Gamma_e} (t_x \delta u_x + t_y \delta u_y) ds \end{aligned} \quad (11.3.3)$$

wherein, now, f_x and f_y are body forces per unit area and t_x and t_y are boundary forces per unit length. When the stresses are expressed in terms of strains through Eq. (11.2.15a) and strains in terms of displacements by Eq. (11.2.14a), Eq. (11.3.3) takes the form associated with minimizing the total potential energy, $\delta \Pi_e = 0$.

Equation (11.3.3) can be rewritten using the notation introduced in Eqs. (11.2.13)–(11.2.15) (note that $\delta \varepsilon = \mathbf{D} \delta \mathbf{u}$ and $(\mathbf{AB})^T = \mathbf{B}^T \mathbf{A}^T$)

$$0 = \int_{\Omega_e} h_e [(\mathbf{D} \delta \mathbf{u})^T \mathbf{C} (\mathbf{D} \mathbf{u}) + \rho \mathbf{u}^T \ddot{\mathbf{u}}] dx - \int_{\Omega_e} (\delta \mathbf{u})^T \mathbf{f} dx - \oint_{\Gamma_e} (\delta \mathbf{u})^T \mathbf{t} ds \quad (11.3.4)$$

11.3.3 Weak Form of the Governing Differential Equations

Here we present an alternative procedure to develop the weak form of the plane elasticity equations (11.2.18a) and (11.2.18b). The present approach, which has been used throughout the book thus far, does not require knowledge of the principles of virtual displacements or the total minimum potential energy but only needs the governing differential equations of the problem. We use the three-step procedure for each of the two differential equations: multiply the first equation with a weight function w_1 and integrate by parts to trade the differentiation equally between the weight function and the dependent variables (u_x, u_y). We have

$$\begin{aligned} 0 = & \int_{\Omega_e} h_e \left(\frac{\partial w_1}{\partial x} \sigma_{xx} + \frac{\partial w_1}{\partial y} \sigma_{xy} - w_1 f_x + \rho w_1 \ddot{u}_x \right) dx dy \\ & - \oint_{\Gamma_e} h_e w_1 (\sigma_{xx} n_x + \sigma_{xy} n_y) ds \end{aligned} \quad (11.3.5)$$

Similarly, for the second equation, we have

$$0 = \int_{\Omega_e} h_e \left(\frac{\partial w_2}{\partial x} \sigma_{xy} + \frac{\partial w_2}{\partial y} \sigma_{yy} - w_2 f_y + \rho w_2 \ddot{u}_y \right) dx dy \\ - \oint_{\Gamma_e} h_e w_2 (\sigma_{xy} n_x + \sigma_{yy} n_y) ds \quad (11.3.6)$$

where

$$\begin{aligned} \sigma_{xx} &= c_{11} \frac{\partial u_x}{\partial x} + c_{12} \frac{\partial u_y}{\partial y}, & \sigma_{xy} &= c_{66} \left(\frac{\partial u_x}{\partial y} + \frac{\partial u_y}{\partial x} \right) \\ \sigma_{yy} &= c_{12} \frac{\partial u_x}{\partial x} + c_{22} \frac{\partial u_y}{\partial y} \end{aligned} \quad (11.3.7)$$

The last step of the development is to identify the primary and secondary variables of the formulation and rewrite the boundary integrals in terms of the secondary variables. Examination of the boundary integrals in Eqs. (11.3.5) and (11.3.6) reveals that the expressions in the parentheses constitute the secondary variables. By comparing these expressions with those in Eq. (11.2.16a), it follows that the boundary forces t_x and t_y are the secondary variables. The weight functions w_1 and w_2 are the first variations of u_x and u_y , respectively. Thus, the final weak forms are given by

$$0 = \int_{\Omega_e} h_e \left[\frac{\partial w_1}{\partial x} \left(c_{11} \frac{\partial u_x}{\partial x} + c_{12} \frac{\partial u_y}{\partial y} \right) + c_{66} \frac{\partial w_1}{\partial y} \left(\frac{\partial u_x}{\partial y} + \frac{\partial u_y}{\partial x} \right) + \rho w_1 \ddot{u}_x \right] dx dy \\ - \int_{\Omega_e} h_e w_1 f_x dx dy - \oint_{\Gamma_e} h_e w_1 t_x ds \quad (11.3.8a)$$

$$0 = \int_{\Omega_e} h_e \left[c_{66} \frac{\partial w_2}{\partial x} \left(\frac{\partial u_x}{\partial y} + \frac{\partial u_y}{\partial x} \right) + \frac{\partial w_2}{\partial y} \left(c_{12} \frac{\partial u_x}{\partial x} + c_{22} \frac{\partial u_y}{\partial y} \right) + \rho w_2 \ddot{u}_y \right] dx dy \\ - \int_{\Omega_e} h_e w_2 f_y dx dy - \oint_{\Gamma_e} h_e w_2 t_y ds \quad (11.3.8b)$$

This completes the development of the weak formulation of the plane elasticity equations in (11.2.18a). The alternative formulation in Eqs. (11.3.8a) and (11.3.8b) is exactly the same as that in Eq. (11.3.4); one is in vector form and the other is in explicit form. Therefore, the finite element models developed using the weak forms (11.3.4) and (11.3.8a) and (11.3.8b) would be the same.

11.4 FINITE ELEMENT MODEL

11.4.1 General Model

Here, we develop the finite element model of the plane elasticity equations using both the expanded forms (11.3.8a) and (11.3.8b) as well as the vector form (11.3.4) so that readers with different backgrounds can follow the development. An examination of the weak forms (11.3.8a) and (11.3.8b) reveals that: (a) u_x and u_y are the primary variables, which must be carried as the primary nodal degrees of freedom, and (b) only first derivatives of u_x and u_y with respect to x and y , respectively, appear. Therefore, u_x and u_y must be approximated by the Lagrange family of interpolation functions, and at least bilinear (i.e., linear both in x

and y) interpolation is required. The simplest elements that satisfy those requirements are the linear triangular and linear quadrilateral elements. Although u_x and u_y are independent of each other, they are the components of the displacement vector. Therefore, both components should be approximated using the same type and degree of interpolation.

Let u_x and u_y be approximated by the finite element interpolations (the element label e is omitted in the interest of brevity)

$$u_x \approx \sum_{j=1}^n u_x^j \psi_j(x, y), \quad u_y \approx \sum_{j=1}^n u_y^j \psi_j(x, y) \quad (11.4.1a)$$

or

$$\mathbf{u} = \begin{Bmatrix} u_x \\ u_y \end{Bmatrix} = \Psi \Delta, \quad \mathbf{w} = \delta \mathbf{u} = \begin{Bmatrix} w_1 = \delta u_x \\ w_2 = \delta u_y \end{Bmatrix} = \Psi \delta \Delta \quad (11.4.1b)$$

where

$$\begin{aligned} \Psi &= \begin{bmatrix} \psi_1 & 0 & \psi_2 & 0 & \dots & \psi_n & 0 \\ 0 & \psi_1 & 0 & \psi_2 & \dots & 0 & \psi_n \end{bmatrix} \\ \Delta &= [u_x^1 \quad u_y^1 \quad u_x^2 \quad u_y^2 \quad \dots \quad u_x^n \quad u_y^n]^T \end{aligned} \quad (11.4.2)$$

At the moment, we will not restrict ψ_j to any specific element so that the finite element formulation to be developed is valid for any admissible element. For example, if a linear triangular element ($n = 3$) is used, we have two (u_x^i, u_y^i) ($i = 1, 2, 3$) degrees of freedom per node and a total of six nodal displacements per element [see Fig. 11.4.1(a)]. For a linear quadrilateral element, there are a total of eight nodal displacements per element [see Fig. 11.4.1(b)]. Since the first derivatives of ψ_i for a triangular element are elementwise constant, all the strains ($\epsilon_{xx}, \epsilon_{yy}, \epsilon_{xy}$) computed for the linear triangular element are elementwise constant. Therefore, the linear triangular element for plane elasticity problems is known as the *constant-strain triangular (CST) element*. For a quadrilateral element the first derivatives of ψ_i are not constant: $\partial \psi_i^e / \partial \xi$ is linear in η and constant in ξ , and $\partial \psi_i^e / \partial \eta$ is linear in ξ and constant in η .

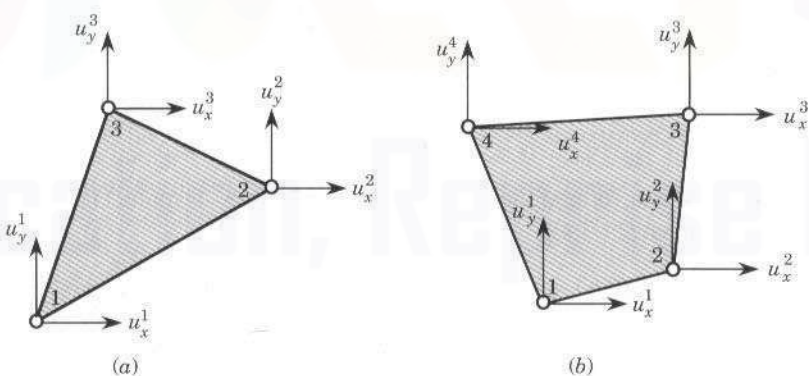


Figure 11.4.1 (a) Linear triangular element and (b) linear quadrilateral element for plane elasticity problems.

The strains are

$$\boldsymbol{\varepsilon} = \mathbf{D}\mathbf{u} = \mathbf{D}\Psi\Delta \equiv \mathbf{B}\Delta, \quad \boldsymbol{\sigma} = \mathbf{C}\mathbf{B}\Delta \quad (11.4.3)$$

where \mathbf{D} is defined earlier in Eq. (11.2.14b) and \mathbf{B} is a $3 \times 2n$ matrix

$$\mathbf{B} = \mathbf{D}\Psi = \begin{bmatrix} \frac{\partial \psi_1}{\partial x} & 0 & \frac{\partial \psi_2}{\partial x} & 0 & \dots & \frac{\partial \psi_n}{\partial x} & 0 \\ 0 & \frac{\partial \psi_1}{\partial y} & 0 & \frac{\partial \psi_2}{\partial y} & \dots & 0 & \frac{\partial \psi_n}{\partial y} \\ \frac{\partial \psi_1}{\partial y} & \frac{\partial \psi_1}{\partial x} & \frac{\partial \psi_2}{\partial y} & \frac{\partial \psi_2}{\partial x} & \dots & \frac{\partial \psi_n}{\partial y} & \frac{\partial \psi_n}{\partial x} \end{bmatrix} \quad (11.4.4)$$

Substituting Eq. (11.4.1) for u_x and u_y , setting $w_1 = \psi_i$ and $w_2 = \psi_i$ [to obtain the i th algebraic equation associated with each of the weak statements in Eqs. (11.3.8a) and (11.3.8b)], and writing the resulting algebraic equations in matrix form, we obtain

$$\begin{bmatrix} [M] & [0] \\ [0] & [M] \end{bmatrix} \begin{Bmatrix} \{\bar{u}_x\} \\ \{\bar{u}_y\} \end{Bmatrix} + \begin{bmatrix} [K^{11}] & [K^{12}] \\ [K^{12}]^T & [K^{22}] \end{bmatrix} \begin{Bmatrix} \{u_x\} \\ \{u_y\} \end{Bmatrix} = \begin{Bmatrix} \{F^1\} \\ \{F^2\} \end{Bmatrix} \quad (11.4.5)$$

where

$$\begin{aligned} M_{ij} &= \int_{\Omega_e} \rho h \psi_i \psi_j dx dy \\ K_{ij}^{11} &= \int_{\Omega_e} h \left(c_{11} \frac{\partial \psi_i}{\partial x} \frac{\partial \psi_j}{\partial x} + c_{66} \frac{\partial \psi_i}{\partial y} \frac{\partial \psi_j}{\partial y} \right) dx dy \\ K_{ij}^{12} &= K_{ji}^{21} = \int_{\Omega_e} h \left(c_{12} \frac{\partial \psi_i}{\partial x} \frac{\partial \psi_j}{\partial y} + c_{66} \frac{\partial \psi_i}{\partial y} \frac{\partial \psi_j}{\partial x} \right) dx dy \\ K_{ij}^{22} &= \int_{\Omega_e} h \left(c_{66} \frac{\partial \psi_i}{\partial x} \frac{\partial \psi_j}{\partial x} + c_{22} \frac{\partial \psi_i}{\partial y} \frac{\partial \psi_j}{\partial y} \right) dx dy \\ F_i^1 &= \int_{\Omega_e} h \psi_i f_x dx dy + \oint_{\Gamma_e} h \psi_i t_x ds, \quad F_i^2 = \int_{\Omega_e} h \psi_i f_y dx dy + \oint_{\Gamma_e} h \psi_i t_y ds \end{aligned} \quad (11.4.6)$$

The body forces f_x and f_y are measured per unit area where the coefficient matrix $[K^{12}]$, for example, corresponds to the coefficient of u_y (second variable) in the first equation, i.e., the first superscript corresponds to the equation number and the second one to the variable number.

To obtain the vector form of the finite element model, we substitute (11.4.1b) into the virtual work statement (11.3.4)

$$\begin{aligned} 0 &= \int_{\Omega_e} h(\delta\Delta)^T (\mathbf{B}^T \mathbf{C} \mathbf{B} \{\Delta\} + \rho \Psi^T \Psi \ddot{\Delta}) d\mathbf{x} - \int_{\Omega_e} h(\delta\Delta)^T \Psi^T \mathbf{f} d\mathbf{x} - \oint_{\Gamma_e} h(\delta\Delta)^T \Psi^T \mathbf{t} ds \\ &= (\delta\Delta)^T (\mathbf{K}^e \Delta^e + \mathbf{M}^e \dot{\Delta}^e - \mathbf{F}^e - \mathbf{Q}^e) \end{aligned} \quad (11.4.7)$$

Since the above equation holds for any *arbitrary* variations $\delta\Delta$, it follows (from the fundamental lemma of variational calculus) that the coefficient of $\delta\Delta$ in the expression (11.4.7)

should be identical to zero, giving the result

$$\mathbf{M}^e \ddot{\Delta}^e + \mathbf{K}^e \Delta^e = \mathbf{F}^e + \mathbf{Q}^e \quad (11.4.8)$$

where

$$\begin{aligned} \mathbf{K}^e &= \int_{\Omega_e} h_e \mathbf{B}^T \mathbf{C} \mathbf{B} dx, & \mathbf{M}^e &= \int_{\Omega_e} \rho h_e \Psi^T \Psi dx \\ \mathbf{F}^e &= \int_{\Omega_e} h_e \Psi^T \mathbf{f} dx, & \mathbf{Q}^e &= \oint_{\Gamma_e} h_e \Psi^T \mathbf{t} ds \end{aligned} \quad (11.4.9)$$

The element mass matrix \mathbf{M}^e and stiffness matrix \mathbf{K}^e are of order $2n \times 2n$, and the element load vector \mathbf{F}^e and the vector of internal forces \mathbf{Q}^e are of order $2n \times 1$, where n is the number of nodes in a Lagrange finite element [see Eq. (11.4.1)].

11.4.2 Eigenvalue and Transient Problems

For natural vibration study of plane elastic bodies, we seek a periodic solution of the form

$$\{\Delta\} = \{\Delta_0\} e^{-i\omega t} \quad (11.4.10)$$

where ω is the frequency of natural vibration and $i = \sqrt{-1}$. Then Eq. (11.4.5) or (11.4.8) reduces to an eigenvalue problem

$$(-\omega^2 \mathbf{M}^e + \mathbf{K}^e) \Delta_0^e = \mathbf{Q}^e \quad (11.4.11)$$

For transient analysis, using the time-approximation method discussed in Section 6.2.4 (Newmark integration scheme), Eq. (11.4.5) or (11.4.8) can be reduced to the following system of algebraic equations:

$$\hat{\mathbf{K}}_{s+1}^e \Delta_{s+1}^e = \hat{\mathbf{F}}_{s,s+1}^e \quad (11.4.12a)$$

where

$$\begin{aligned} \hat{\mathbf{K}}_{s+1}^e &= \mathbf{K}_{s+1}^e + a_3 \mathbf{M}_{s+1}^e \\ \hat{\mathbf{F}}_{s,s+1}^e &= \bar{\mathbf{F}}_{s+1}^e + \mathbf{M}_{s+1}^e (a_3 \Delta_s^e + a_4 \dot{\Delta}_s^e + a_5 \ddot{\Delta}_s^e) \end{aligned} \quad (11.4.12b)$$

$$a_3 = \frac{2}{\gamma(\Delta t)^2}, \quad a_4 = \Delta t a_3, \quad a_5 = \frac{1}{\gamma} - 1$$

where \mathbf{K}^e , \mathbf{M}^e , and $\bar{\mathbf{F}}^e$ ($= \mathbf{F}^e + \mathbf{Q}^e$) are the vectors appearing in Eq. (11.4.9) and γ is the parameter in the Newmark scheme [see Eqs. (6.2.29)–(6.2.31)]. For $\gamma = 0$ (centered difference scheme), the alternative formulation of Problem 6.23 must be used. For additional details, the reader should consult Section 6.2.4.

11.5 EVALUATION OF INTEGRALS

For the linear triangular (i.e., CST) element, the ψ_i^e and its derivatives are given by

$$\psi_i^e = \frac{1}{2A_e} (\alpha_i^e + \beta_i^e x + \gamma_i^e y), \quad \frac{\partial \psi_i^e}{\partial x} = \frac{\beta_i^e}{2A_e}, \quad \frac{\partial \psi_i^e}{\partial y} = \frac{\gamma_i^e}{2A_e} \quad (11.5.1)$$

Since the derivatives of ψ_i^e are constant, we have

$$\mathbf{B}^e = \frac{1}{2A_e} \begin{bmatrix} \beta_1^e & 0 & \beta_2^e & 0 & \cdots & \beta_n^e & 0 \\ 0 & \gamma_1^e & 0 & \gamma_2^e & \cdots & 0 & \gamma_n^e \\ \gamma_1^e & \beta_1^e & \gamma_2^e & \beta_2^e & \cdots & \gamma_n^e & \beta_n^e \end{bmatrix} \quad (3 \times 2n) \quad (11.5.2)$$

where A_e is the area of the triangular element. Since \mathbf{B}^e and \mathbf{C}^e are independent of x and y , the element stiffness matrix in (11.4.9) for the CST element is given by

$$\mathbf{K}^e = h_e A_e (\mathbf{B}^e)^T \mathbf{C}^e \mathbf{B}^e \quad (2n \times 2n) \quad (11.5.3)$$

For the case in which the body force components f_x and f_y are elementwise constant (say, equal to f_{x0}^e and f_{y0}^e , respectively), the load vector \mathbf{F}^e has the form

$$\mathbf{F}^e = \int_{\Omega_e} h_e (\Psi^e)^T \mathbf{f}_0^e \, d\mathbf{x} = \frac{A_e h_e}{3} \begin{Bmatrix} f_{x0}^e \\ f_{y0}^e \\ f_{x0}^e \\ f_{y0}^e \\ f_{x0}^e \\ f_{y0}^e \end{Bmatrix} \quad (6 \times 1) \quad (11.5.4)$$

For a general quadrilateral element, it is not easy to compute the coefficients of the stiffness matrix by hand. In such cases we use the numerical integration method discussed in Section 9.2. However, for a linear rectangular element of sides a and b , the element coefficient matrices in Eq. (8.2.52) can be used to obtain the stiffness matrix. For a linear quadrilateral element with constant body force components (f_{x0}, f_{y0}) , the load vector is given by

$$\mathbf{F}^e = \frac{A_e h_e}{4} \begin{Bmatrix} f_{x0} \\ f_{y0} \\ f_{x0} \\ f_{y0} \\ \vdots \end{Bmatrix} \quad (8 \times 1) \quad (11.5.5)$$

The vector \mathbf{Q}^e is computed only when the element Ω_e falls on the boundary of the domain on which tractions are specified (i.e., known). Computation of \mathbf{Q}^e involves the evaluation of line integrals (for any type of element), as explained in Sec. 8.2.6; also, see Example 8.2.4. For plane elasticity problems, the surface tractions t_x and t_y take the place of q_n in the single-variable problems [see Eq. (8.2.56)]. However, it should be noted that t_x and t_y are the horizontal and vertical components (i.e., parallel to the coordinate lines x and y), respectively, of the traction vector \mathbf{t} , which, in general, is oriented at an angle to the boundary. In practice, it is convenient to express the surface traction \mathbf{t} in the element coordinates. In that case, \mathbf{Q}^e can be evaluated in the element coordinates and then transformed to the global coordinates for assembly. If \mathbf{Q}^e denotes the element load vector referred to the element coordinates, then the corresponding load vector referred to the global coordinates is given by

$$\mathbf{F}^e = \mathbf{R}^T \mathbf{Q}^e \quad (11.5.6a)$$

where \mathbf{R} is the transformation matrix

$$\mathbf{R}^e = \begin{bmatrix} \cos \alpha & \sin \alpha & 0 & 0 \\ -\sin \alpha & \cos \alpha & 0 & 0 \\ 0 & 0 & \cos \alpha & \sin \alpha \\ 0 & 0 & -\sin \alpha & \cos \alpha \end{bmatrix} \quad (2n \times 2n) \quad (11.5.6b)$$

and α is the angle between the global x axis and the traction vector \mathbf{t} .

Example 11.5.1

As a specific example, first consider the structure shown in Fig. 11.5.1(a). Side 2–3 of element 7 is subjected to linearly varying normal force:

$$t_n \neq 0, \quad t_s = 0$$

where the subscripts n and s refer to normal and tangential directions, respectively. We have (for $e = 7$)

$$\mathbf{Q}^e = \oint_{\Gamma_e} h_e \Psi^T \begin{Bmatrix} t_n \\ t_s \end{Bmatrix} ds = \int_{\Gamma_{12}^e} h_e \Psi^T \begin{Bmatrix} t_n \\ t_s \end{Bmatrix} ds + \int_{\Gamma_{23}^e} h_e \Psi^T \begin{Bmatrix} t_n \\ 0 \end{Bmatrix} ds + \int_{\Gamma_{31}^e} h_e \Psi^T \begin{Bmatrix} t_n \\ t_s \end{Bmatrix} ds \quad (11.5.7a)$$

The first and third integrals cannot be evaluated because we do not know t_n and t_s on these sides of the element. However, because of internal stress equilibrium, contributions of these integrals cancel with like contributions from the neighboring elements (elements 4 and 5) in the assembled force vector of the structure. Thus, we must compute only the integral over side

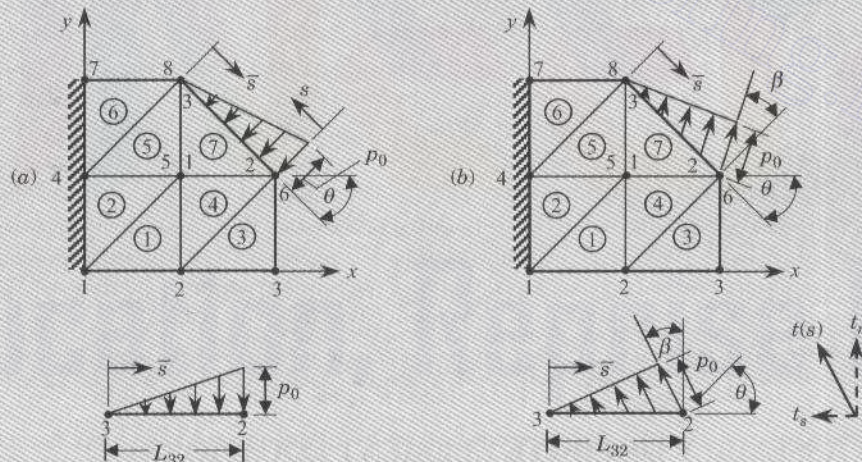


Figure 11.5.1 Plane elasticity problem with (a) traction normal to the boundary and (b) traction in an arbitrary direction.

2–3 of the element. We have (for $e = 7$)

$$\mathbf{Q}_{2-3}^{(7)} = \int_0^{L_{23}} h \Psi^T \begin{Bmatrix} t_n \\ 0 \end{Bmatrix} d\bar{s}, \quad t_n = -p_0 \left(1 - \frac{\bar{s}}{L_{23}} \right) \quad (11.5.7b)$$

where the minus sign in front of p_0 is added to account for the direction of the applied traction, which is acting toward the body in the present case. The local coordinate system \bar{s} used in the above expression is chosen along the side connecting node 2 to node 3, with its origin at node 2. We are not restricted to this choice. If we feel that it is convenient to choose the local coordinate system \bar{s} , which is taken along side 3–2, with its origin at node 3 of element 7, we can write

$$\mathbf{Q}_{3-2}^{(7)} = \int_0^{L_{32}} h \Psi^T \begin{Bmatrix} t_n \\ 0 \end{Bmatrix} d\bar{s}, \quad t_n = -\frac{p_0 \bar{s}}{L_{32}} \quad (11.5.7c)$$

wherein now Ψ^e is expressed in terms of the local coordinate \bar{s} . We have ($L_{32} = L_{23}$)

$$\mathbf{Q}_{3-2}^{(7)} = \int_0^{L_{32}} h \begin{Bmatrix} 0 \\ 0 \\ \psi_2^T t_n \\ 0 \\ \psi_3^T t_n \\ 0 \end{Bmatrix} d\bar{s} = -\frac{L_{32} p_0 h}{6} \begin{Bmatrix} 0 \\ 0 \\ 2 \\ 0 \\ 1 \\ 0 \end{Bmatrix} \quad (11.5.8a)$$

The global components of this force vector are [set $\alpha = 90^\circ - \theta$ in Eq. (11.5.6b)]

$$\mathbf{Q}_{3-2}^{(7)} = -\frac{L_{32} p_0 h}{6} \begin{Bmatrix} 0 \\ 0 \\ 2 \sin \theta \\ 2 \cos \theta \\ \sin \theta \\ \cos \theta \end{Bmatrix} \quad (11.5.8b)$$

Next, consider the case in which the tractions are oriented at an angle β , as shown in Fig. 11.5.1(b). Then, we may resolve the applied traction into normal and tangential components.

$$t_n = t(s) \cos \beta, \quad t_s = t(s) \sin \beta \quad (11.5.9)$$

and repeat the procedure described above.

The same procedure applies to linear quadrilateral elements. In general, the loads due to specified boundary stresses can be computed using an appropriate local coordinate system and one-dimensional interpolation functions. When higher-order elements are involved, the corresponding order of one-dimensional interpolation functions must be used.

11.6 ASSEMBLY OF FINITE ELEMENT EQUATIONS

The assembly procedure for problems with many degrees of freedom is the same as that used for a single degree of freedom problem (see Section 8.2), except that the procedure should be applied to both degrees of freedom at each node. For example, consider the plane

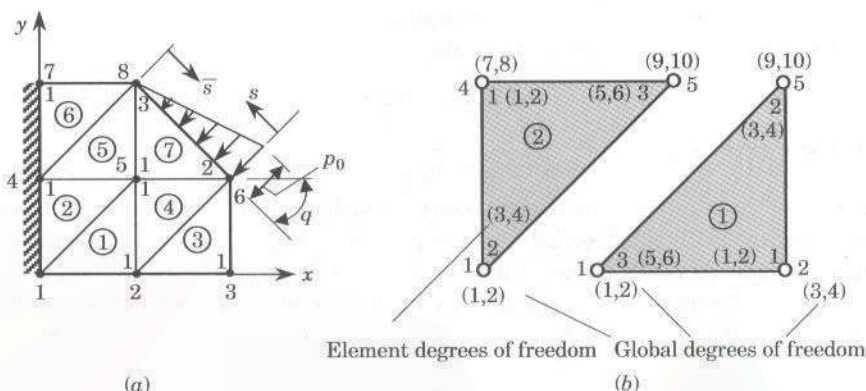


Figure 11.6.1 Plane elasticity problem with global degrees of freedom.

elastic structure and the finite element mesh used in Fig. 11.6.1(a). There are eight nodes in the mesh; hence, the total size of the assembled stiffness matrix will be 16×16 , and the force vector will be 16×1 . The first two rows and columns of the global stiffness matrix, for example, correspond to the global degrees (1, 2) of freedom at global node 1, which has contributions from nodes 2 and 3 of elements 1 and 2, respectively, as indicated in Fig. 11.6.1(b). Thus, the contributions to global coefficients K_{IJ} ($I, J = 1, 2$) come from K_{ij}^1 ($i, j = 3, 4$) and K_{ij}^2 ($i, j = 5, 6$).

For instance, the global stiffness matrix coefficients K_{11} , K_{12} , K_{13} , K_{15} , K_{22} , K_{33} , and K_{34} are known in terms of the element coefficients as follows:

$$\begin{aligned} K_{11} &= K_{55}^1 + K_{33}^2, \quad K_{22} = K_{66}^1 + K_{44}^2, \quad K_{12} = K_{56}^1 + K_{34}^2, \quad K_{13} = K_{51}^1 \\ K_{33} &= K_{11}^1 + K_{55}^3 + K_{33}^4, \quad K_{34} = K_{12}^1 + K_{56}^3 + K_{34}^4, \quad K_{15} = 0 \end{aligned} \quad (11.6.1)$$

Note that K_{34} , for example, denotes the coupling stiffness coefficient between the third (u_x) and fourth (u_y) global displacement degrees of freedom, both of which are at global node 2. On the other hand, K_{13} denotes the coupling coefficient between the first displacement degree of freedom (u_x) at global node 1 and third global displacement degree (u_x) of freedom at global node 2. Similar arguments apply for the assembly of the force vector.

With regard to the specification of the displacements (the primary degrees of freedom) and forces (the secondary degrees of freedom) in a finite element mesh, we have the following four distinct possibilities:

- Case 1: u_x and u_y are specified (and t_x and t_y are unknown)
- Case 2: u_x and t_y are specified (and t_x and u_y are unknown)
- Case 3: t_x and u_y are specified (and u_x and t_y are unknown)
- Case 4: t_x and t_y are specified (and u_x and u_y are unknown)

In general, only one of the quantities of each of the pairs (u_x, t_x) and (u_y, t_y) is known at a nodal point in the mesh. As discussed in Chapter 9, we are required to make a decision as to which degree of freedom is known when singular points (i.e., points at which both displacement and force degrees of freedom are known or when two different values of the same degree of freedom are specified) are encountered.

For time-dependent problems, the initial displacement and velocity must be specified for each component of the displacement field:

$$\mathbf{u} = \mathbf{u}^0, \quad \dot{\mathbf{u}} = \mathbf{v}^0 \quad (11.6.2)$$

11.7 EXAMPLES

Next, we consider a couple of computational examples of plane elasticity problems to illustrate the load computation and imposition of boundary conditions. The stresses are evaluated at reduced Gauss points of the elements [see Section 10.5.4 and Barlow (1976, 1989)]. These examples are actually analyzed using the program **FEM2D**, which is discussed in Chapter 13.

Example 11.7.1

Consider a thin elastic plate subjected to a uniformly distributed edge load, as shown in Fig. 11.7.1. We wish to determine the static solution to the problem. First, we consider a two-element discretization of the plate by triangular elements and perform the required algebra to obtain the nodal displacements.

The assembly of element matrices for two *degree-of-freedom* (DOF) elements is described in Section 11.6. For the finite element mesh at hand, the correspondence between the global and local nodes and stiffness is given in Table 11.7.1. If two global nodes correspond to two (local) nodes of the same element, then the corresponding stiffness coefficient is nonzero; otherwise, it is zero.

The specified global degrees of freedom for the problem are

$$U_1 = U_2 = U_5 = U_6 = 0 \quad (11.7.1)$$

The known forces are

$$F_3 = F_4 = \frac{p_0 b h}{2}, \quad F_7 = F_8 = F_5 + F_3 = \frac{p_0 b h}{2}, \quad F_9 = F_{10} = F_6 + F_4 = 0 \quad (11.7.2)$$

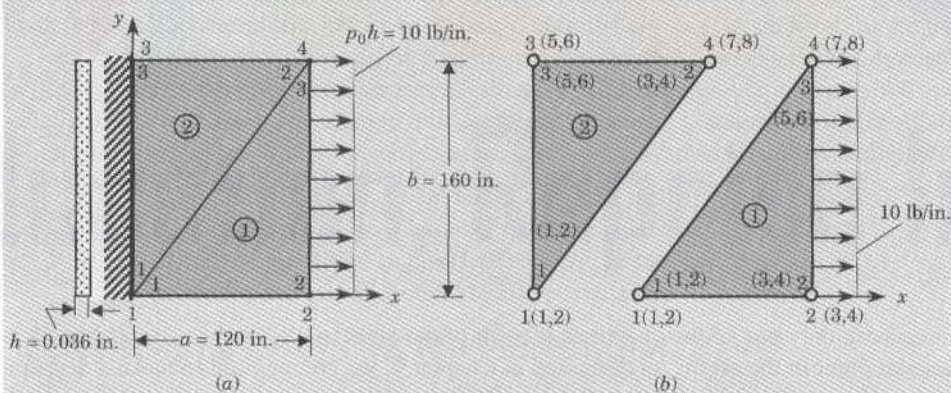


Figure 11.7.1 Geometry and finite element mesh of a plane elasticity problem by the CST elements.

Table 11.7.1 Correspondence between the global and element nodes of the mesh shown in Fig. 11.7.1.

Nodal correspondence		Stiffness correspondence	
Global Node (DOF)	Local Node (DOF)	Global	Local
1 (1, 2)	1 of element 1 (1, 2)	K_{11}	$K_{11}^1 + K_{11}^2$
	1 of element 2 (1, 2)	K_{22} K_{12}	$K_{22}^1 + K_{22}^2$ $K_{12}^1 + K_{12}^2$
2 (3, 4)	2 of element 1 (3, 4)	K_{33}	K_{33}^1
		K_{44}	K_{44}^1
		K_{34}	K_{34}^1
3 (5, 6)	3 of element 2 (5, 6)	K_{55}	K_{55}^2
		K_{66}	K_{66}^2
		K_{56}	K_{56}^2
4 (7, 8)	2 of element 2 (3, 4) 3 of element 1 (5, 6)	K_{77}	$K_{77}^1 + K_{77}^2$
		K_{88}	$K_{88}^1 + K_{88}^2$
		K_{78}	$K_{78}^1 + K_{78}^2$

The first two rows and columns and the last two rows and columns of the assembled $[K]$ can be deleted (since the specified boundary conditions are homogeneous) to obtain the following condensed equations

$$\begin{bmatrix} K_{33}^1 & K_{34}^1 & K_{35}^1 & K_{36}^1 \\ K_{43}^1 & K_{44}^1 & K_{45}^1 & K_{46}^1 \\ K_{53}^1 & K_{54}^1 & K_{55}^1 + K_{53}^2 & K_{56}^1 + K_{54}^2 \\ K_{63}^1 & K_{64}^1 & K_{65}^1 + K_{43}^2 & K_{66}^1 + K_{44}^2 \end{bmatrix} \begin{bmatrix} U_3 \\ U_4 \\ U_7 \\ U_8 \end{bmatrix} = \begin{bmatrix} \frac{p_0 b h}{2} \\ 0 \\ \frac{p_0 b h}{2} \\ 0 \end{bmatrix} \quad (11.7.3)$$

or (using $a = 120$ in., $b = 160$ in., $h = 0.036$ in., $v = 0.25$, $E = 30 \times 10^6$ psi, and $p_0 = 10$ lb/in.)

$$10^4 \begin{bmatrix} 93.0 & -36.0 & -16.2 & 14.4 \\ -36.0 & 72.0 & 21.6 & -43.2 \\ -16.2 & 21.6 & 93.0 & 0.0 \\ 14.4 & -43.2 & 0.0 & 72.0 \end{bmatrix} \begin{bmatrix} U_3 \\ U_4 \\ U_7 \\ U_8 \end{bmatrix} = \begin{bmatrix} 800.0 \\ 0.0 \\ 800.0 \\ 0.0 \end{bmatrix} \quad (11.7.4)$$

Inverting the matrix, we obtain

$$\begin{aligned} \begin{bmatrix} U_3 \\ U_4 \\ U_7 \\ U_8 \end{bmatrix} &= \frac{10^{-6}}{3} \begin{bmatrix} 4.07 & 2.34 & 0.17 & 0.59 \\ 2.24 & 8.65 & -1.60 & 4.72 \\ 0.17 & -1.60 & 3.63 & -0.99 \\ 0.59 & 4.72 & -0.99 & 6.88 \end{bmatrix} \begin{bmatrix} 800.0 \\ 0.0 \\ 800.0 \\ 0.0 \end{bmatrix} \\ &= 10^{-4} \begin{bmatrix} 11.291 \\ 1.964 \\ 10.113 \\ -1.080 \end{bmatrix} \text{ in} \end{aligned} \quad (11.7.5)$$

Table 11.7.2 Finite element results for a thin plate (plane stress assumption) using various meshes of triangular and rectangular elements and material properties.[†]

Mesh	Material	U_3 ($\times 10^{-4}$)	U_4 ($\times 10^{-4}$)	U_7 ($\times 10^{-4}$)	U_8 ($\times 10^{-4}$)
1 × 1	Isotropic: $E = 30 \times 10^6$ psi $v = 0.25$ $G = E/[2(1 + v)]$	11.291 10.853	1.964 2.326	10.113 10.853	-1.080 -2.326
1 × 1	Orthotropic: $E_1 = 31 \times 10^6$ psi $E_2 = 2.7 \times 10^6$ psi $G_{12} = 0.75 \times 10^6$ psi $v_{12} = 0.28$	10.767 10.728	1.666 2.675	10.651 10.728	-1.579 -2.675

[†]For each mesh, the first row corresponds to triangular elements and the second row to one rectangular element.

Table 11.7.2 contains the finite element solutions (deflections and stresses) for the displacements at the points (120, 0) and (120, 160) of isotropic and orthotropic plates for the meshes shown. The results were obtained using the computer code **FEM2D**. Note that the finite element solutions (e.g., displacements) obtained with two-element meshes do not yield symmetric results (i.e., $U_3 = U_7$ and $U_4 = -U_8$). This is because of the lack of symmetry of the meshes used. As the mesh is refined, even with unsymmetric meshes, the solution will become symmetric about $y = b/2$ line within a certain degree of accuracy.

Table 11.7.3 Deflections and stresses in an isotropic plate subjected to uniform edge load (Example 11.7.1).

Mesh	$u_x(120, 0)$ ($\times 10^{-4}$)	$u_y(120, 0)$ ($\times 10^{-4}$)	σ_{xx}	σ_{yy}	σ_{xy}	
Triangles	1 × 1	11.291	1.964	285.9 (80, 53.33) [†]	67.42 (40, 106.7)	10.80 (80, 53.33)
	2 × 2	11.372	2.175	294.1 (40, 26.67)	69.36 (20, 53.33)	23.20 (40, 26.67)
	4 × 4	11.284	2.126	306.2 (20, 13.33)	69.59 (10, 26.67)	35.93 (20, 13.33)
	16 × 16	11.179	2.014	372.5 (5, 3.33)	75.39 (2.5, 6.67)	58.90 (5, 3.33)
Rectangles	1 × 1	10.853	2.326	277.8 (60, 80)	25.84 (60, 80)	0.0 (60, 80)
	2 × 2	11.372	2.175	29418 (40, 26.67)	69.36 (20, 53.33)	23.20 (40, 26.67)
	4 × 4	11.150	2.009	288.1 (15, 20)	64.77 (45, 20)	27.73 (15, 20)
	16 × 16	11.166	1.992	339.5 (3.75, 5)	61.2 (3.75, 75)	53.14 (3.75, 5)

[†]Location of the stress.

Deflections and stresses obtained with various uniform meshes of triangular elements or rectangular elements are presented in Table 11.7.3. Mesh $m \times n$ means that m elements in the x direction and n elements in the y direction are used.

Example 11.7.2

Consider the cantilever beam ($E = 30 \times 10^6$ psi, $\nu = 0.25$, $a = 10$ in., $b = 2$ in., $h = 1$ in.) shown in Fig. 11.7.2(a). We wish to determine, using the elasticity equations, the maximum deflection and bending stress in the beam when it is subjected to a uniformly distributed shear stress $\tau_0 = 150$ psi. The boundary conditions of the problem are

$$\begin{aligned} u_x(a, y) &= 0, \quad u_y(a, b/2) = 0, \quad t_y(a, y) = 0 \text{ except at } y = b/2 \\ t_x = t_y &= 0 \text{ at } y = 0, b \text{ for any } x, \quad t_x = 0, \quad t_y = -h\tau_0 \text{ at } x = 0 \text{ for any } y \end{aligned} \quad (11.7.6)$$

We shall solve the problem using the plane stress assumption. The elastic coefficients c_{ij} for the plane stress case are defined (assuming that steel is isotropic) as

$$c_{11} = c_{12} = \frac{E}{1 - \nu^2}, \quad c_{22} = \frac{E\nu}{1 - \nu^2}, \quad c_{66} = \frac{E}{2(1 + \nu)} (= G) \quad (11.7.7)$$

Three different, increasingly refined finite element meshes are shown in Fig. 11.7.2(b). The meshes shown are those consisting of linear rectangular elements. Equivalent triangular

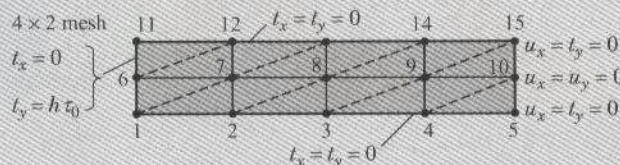
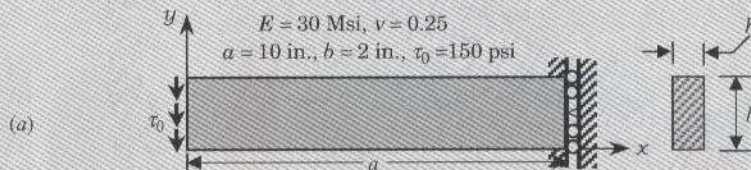


Figure 11.7.2 Finite element meshes for an end-loaded cantilever beam.

Table 11.7.4 Comparison of the finite element solution with the elasticity solution for a cantilever beam subjected to a uniform shear load at the free end (Example 11.7.2).

Number of nodes	Tip deflection, $-u_y \times 10^{-2}$			Normal stress, σ_{xx}		
	LT*	LR	QR	LT	LR	QR
15	0.1611	0.3134	0.5031	1209 (15) ^j	1196 (8.75, 1.5) ^j	2196 (8.943, 1.577)
27	0.2662	0.4388	0.5129	2270 (31)	1793 (9.375, 1.5)	2439 (9.471, 1.577)
51	0.3166	0.4878	0.5137	2829 (63)	2056 (9.6875, 1.5)	226 (9.736, 1.577)
Elasticity ^k	0.5188 (0.0, 1.0)			2876 (9.583, 1.667)	2180 (9.6875, 1.5)	2528 (9.736, 1.577)

*LT = linear triangular elements; LR = linear rectangular elements; and

QR = quadratic rectangular elements.

^jElement number.

ⁱQuadrature points.

^kFrom Reddy (1984), p. 53:

$$u_y(0, 1) = -(PL^3/3EI)(1 + 3(1 + v)/L^2), \quad \sigma_{xx} = Py(1 - y)/I, \quad I = \frac{2}{3}$$

element meshes are obtained by joining node 1 to node 3 of each rectangular element, as indicated by the dotted lines. Equivalent meshes of nine-node quadratic Lagrange elements are obtained by considering a 2×2 mesh of linear Lagrange elements equivalent to a quadratic element.

For the finite element model, the boundary conditions on the primary and secondary variables, e.g., for the 15-node mesh, are given by

$$U_0 = U_{19} = U_{20} = U_{29} = 0.0 \\ F_1^y = -\frac{(t_0 h)b}{4} = -75.0, \quad F_6^y = -150.0, \quad F_{11}^y = -75.0 \quad (11.7.8)$$

and all other forces are zero on the boundary.

Table 11.7.4 contains a comparison of the finite element solutions with the elasticity solutions for the tip deflection (i.e., deflection at the center node of the left end) and bending stress σ_{xx} , obtained using two-dimensional elasticity theory [see Reddy (1984)]. The linear triangular element mesh has the slowest convergence compared to the linear and quadratic rectangular elements.

The last example of this chapter deals with free vibration and transient analysis of the cantilever beam of Example 11.7.2.

Example 11.7.3

Consider the cantilever beam shown in Fig. 11.7.2(a). We wish to determine the natural frequencies and transient response using the plane elements. We use the finite element meshes of linear triangular and rectangular elements shown in Fig. 11.7.2(b) and their nodal equivalent meshes of quadratic elements to analyze the problem (mass density of steel is taken

Table 11.7.5 Comparison of first ten frequencies of the cantilever beam of Example 11.7.3 as computed using various meshes of linear and quadratic triangular and rectangular elements.

ω	Triangular elements				Rectangular elements			
	Linear element		Quadratic element		Linear element		Quadratic element	
	4×2	8×2	2×1	4×1	4×2	8×2	2×1	4×1
1	2,019.4	1,583.0	1,186.4	1,156.7	1,465.5	1,242.3	1,169.9	1,151.8
2	9,207.4	8,264.0	7,896.6	6,496.5	8,457.9	6,845.8	7,197.7	6,341.4
3	10,449.6	9,177.7	9,158.2	9,156.0	9,218.4	9,171.7	9,158.2	9,156.0
4	25,339.2	19,540.5	18,369.1	16,219.9	22,334.0	16,887.7	17,890.8	15,572.7
5	29,193.2	27,843.9	27,805.3	27,441.7	29,113.3	27,836.8	27,869.8	27,226.3
6	42,363.4	32,727.8	40,399.2	28,696.9	40,309.7	29,433.6	39,583.7	27,442.2
7	52,937.0	46,840.4	50,469.6	39,762.6	52,991.9	44,231.1	50,964.4	39,302.3
8	67,964.6	48,014.4	66,260.9	45,815.6	66,842.5	47,441.0	67,015.3	45,839.9
9	76,833.2	61,560.4	74,582.1	57,429.5	74,523.3	60,078.3	74,064.6	56,949.9
10	79,443.0	68,257.4	79,241.8	64,867.4	76,515.5	67,813.3	80,029.3	64,636.0

to be $\rho = 8,8255 \times 10^{-3}$ slugs/in.³). Table 11.7.5 contains a comparison of first ten natural frequencies obtained with various meshes. The convergence of the natural frequencies with mesh refinement is clear.

For transient analysis, the time step Δt used in the linear acceleration scheme ($\alpha = 0.5$, $\gamma = 1/3$) is restricted by the stability requirement

$$\Delta t < \Delta t_{\text{crit}} = \sqrt{\frac{12}{\lambda_{\max}}} \quad (11.7.9)$$

For the 4×2 mesh of rectangular elements, for example, we have $\Delta t_{\text{crit}} = 1.617 \times 10^{-5}$. The load, $h\tau_0$ lb/in., is used with zero initial conditions. The load at the nodes of the free end are

$$\begin{aligned} -75.0 \text{ lb}, \quad -150.0 \text{ lb}, \quad -75 \text{ lb} &\quad \text{for linear element mesh} \\ -50.0 \text{ lb}, \quad -200.0 \text{ lb}, \quad -50 \text{ lb} &\quad \text{for quadratic element mesh} \end{aligned}$$

Figure 11.7.3 contains plots of the tip deflection $u_y(0, 0, t)$ versus time as predicted by the 4×2 mesh of linear rectangular elements and the two time approximation schemes: (1) $\alpha = \gamma = \frac{1}{2}$ and (2) $\alpha = \frac{1}{3}$, $\gamma = \frac{1}{3}$. The time step used in these computations is greater than the critical time step for the mesh, i.e., $\Delta t = 2.5 \times 10^{-4} > \Delta t_{\text{crit}}$. Therefore, the second scheme yields unstable transient response. Note that the solution predicted by the linear acceleration scheme is stable for the first several time steps, but it eventually becomes unstable. Figures 11.7.4 contains plots of the tip deflection as a function of time as predicted by various meshes of linear and quadratic rectangular elements. The notation *L4* implies a mesh of four-node linear elements, and *Q9* indicates a mesh of nine-node quadratic elements. Clearly, the solution gets refined as the mesh is refined. Obviously, mesh 4×2 *L4* is too crude to predict the right wavelength of the time response.

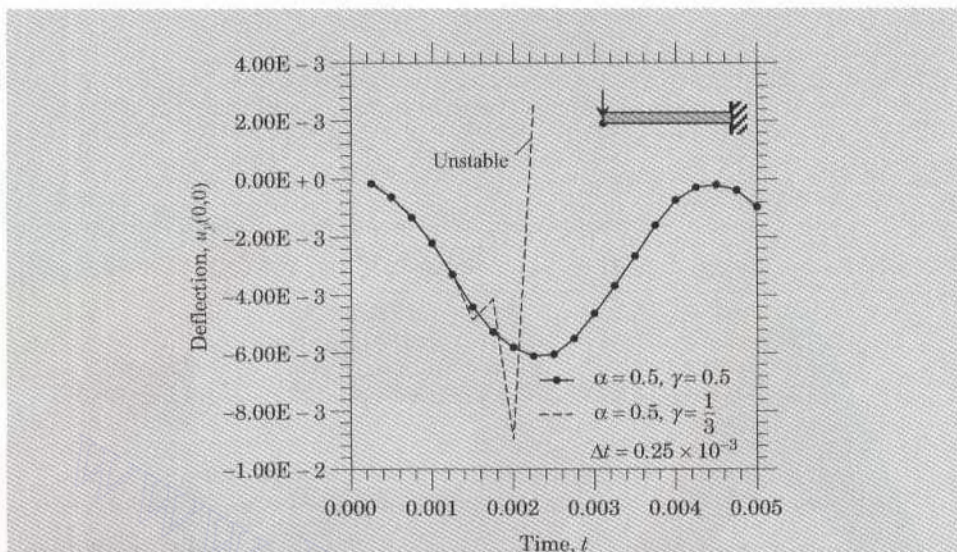


Figure 11.7.3 Stability of the finite element solutions predicted by two different time integration schemes (Example 11.7.3). The 4×2 mesh of linear rectangular elements is used.

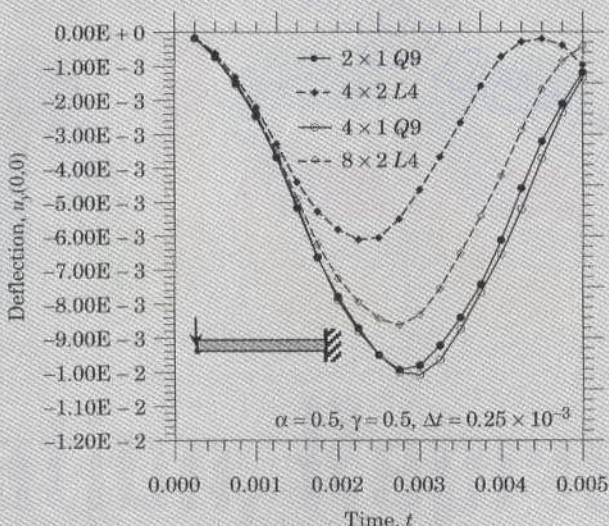


Figure 11.7.4 Tip deflection versus times, as predicted by various meshes of rectangular elements: L4, 4×2 mesh of linear elements; L8, 8×2 mesh of linear elements; Q2, 2×1 mesh of nine-node quadratic elements; and Q4, 4×1 mesh of nine-node quadratic elements.

11.8 SUMMARY

In this chapter equations of the plane elasticity (i.e., two-dimensional problems of elasticity) are introduced and their finite element models are formulated. The plane strain and plane stress problems, which differ only in the use of constitutive relations, are discussed. The governing equations are expressed in terms of the displacements, and their weak form and finite element model are developed in two alternative ways:

1. The vector/matrix formulation ($\mathbf{B}^T \mathbf{C} \mathbf{B}$) using the principle virtual displacements, which is most common in finite element books on solid and structural mechanics and
2. The weak-form formulation, which is used throughout the book.

Triangular and rectangular elements are developed. The eigenvalue and time-dependent problems of plane elasticity are also discussed. Several numerical examples are presented to illustrate the evaluation of element stiffness matrices and load vectors.

PROBLEMS

- 11.1–11.3** Compute the contribution of the boundary forces to the global force DOF in the plane elasticity problems given in Figs. P11.1–P11.3. Give nonzero forces for at least two global nodes. *Answer for Problem 11.1: $F_{7}^x = \frac{17p_1 + p_0}{72}$ and $F_{14}^x = \frac{5p_1 + p_0}{12}$.*

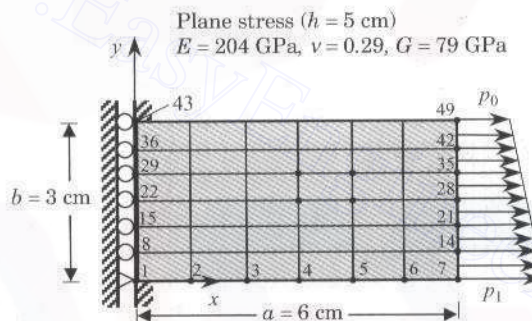


Figure P11.1

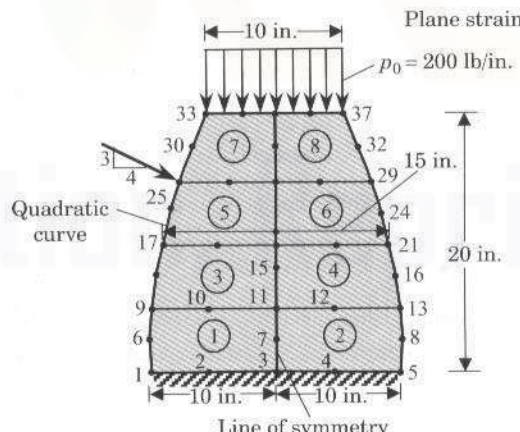


Figure P11.2

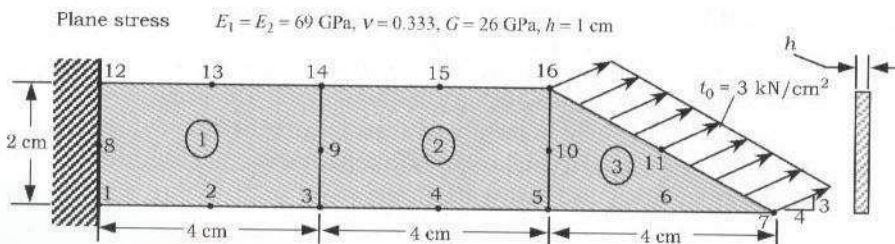


Figure P11.3

11.4–11.6 Give the connectivity matrices and the specified primary degrees of freedom for the plane elasticity problems given in Figs. P11.1–P11.3. Give only the first three rows of the connectivity matrix.

11.7 Consider the cantilevered beam of length 6 cm, height 2 cm, thickness 1 cm, and material properties $E = 3 \times 10^7 \text{ N/cm}^2$ and $\nu = 0.3$, and subjected to a bending moment of 600 N-cm at the free end, (as shown in P11.7). Replace the moment by an equivalent distributed force at $x = 6 \text{ cm}$, and model the domain by a nonuniform 10×4 mesh of linear rectangular elements. Identify the special displacements and global forces. Answer: $F_{11}^x = -187.5 \text{ N}$ and $F_{22}^x = -225 \text{ N}$.

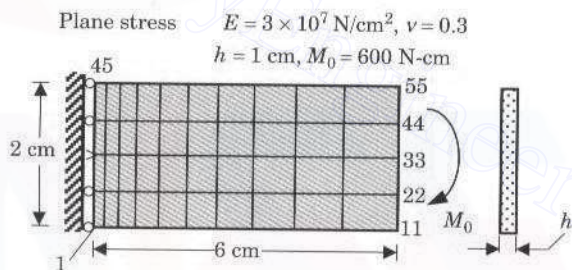


Figure P11.7

11.8 Consider the (“transition”) element shown in Fig. P11.8. Define the generalized displacement vector of the element by

$$\{u\} = \{u_1, v_1, \Theta_1, u_2, v_2, u_3, v_3\}^T$$

and represent the displacement components u and v by

$$u = \psi_1 u_1 + \psi_2 u_2 + \psi_3 u_3 + \frac{b}{2} \eta \psi_1 \theta_1, \quad v = \psi_1 v_1 + \psi_2 v_2 + \psi_3 v_3$$

where ψ_1 is the interpolation function for the beam, and ψ_2 and ψ_3 are the interpolation functions for nodes 2 and 3:

$$\psi_1 = \frac{1}{2}(1-\xi), \quad \psi_2 = \frac{1}{4}(1+\xi)(1-\eta), \quad \psi_3 = \frac{1}{4}(1+\xi)(1+\eta)$$

Derive the stiffness matrix for the element.

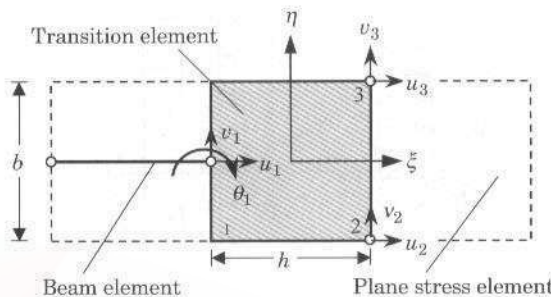


Figure P11.8

- 11.9** Consider a square, isotropic, elastic body of thickness h shown in Fig. P11.9. Suppose that the displacements are approximated by

$$u_x(x, y) = (1 - x)y u_x^1 + x(1 - y) u_x^2, \quad u_y(x, y) = 0$$

Assuming that the body is in a plane state of stress, derive the 2×2 stiffness matrix for the unit square

$$[K] \begin{Bmatrix} u_x^1 \\ u_x^2 \end{Bmatrix} = \begin{Bmatrix} F_1 \\ F_2 \end{Bmatrix}$$

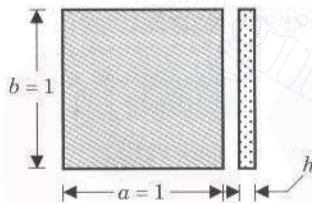


Figure P11.9

- 11.10–11.14.** For the plane elasticity problems shown in Figs. P11.10–11.14, give the boundary DOF and compute the contribution of the specified forces to the nodes. *Answer for Problem 11.11:* $F_{37}^y = -37.5$ kN and $F_{38}^y = -75$ kN.

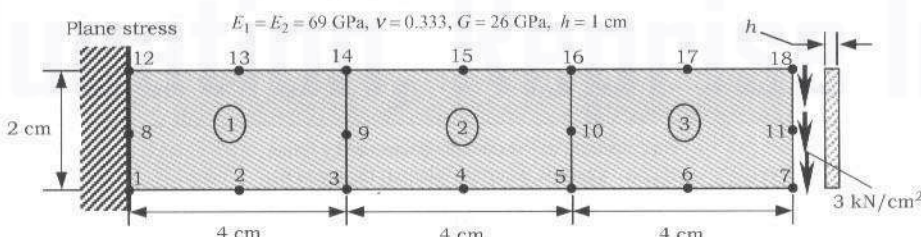


Figure P11.10

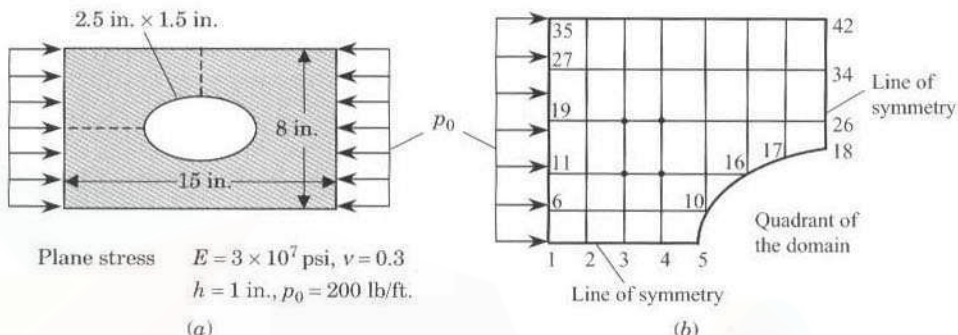


Figure P11.11

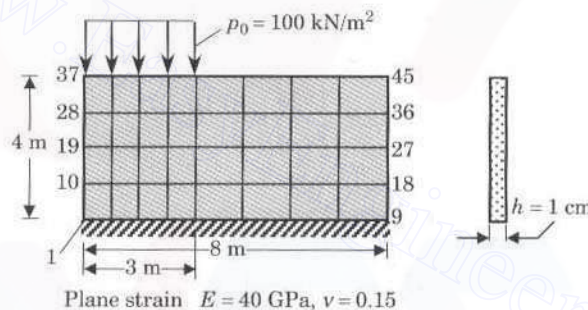


Figure P11.12

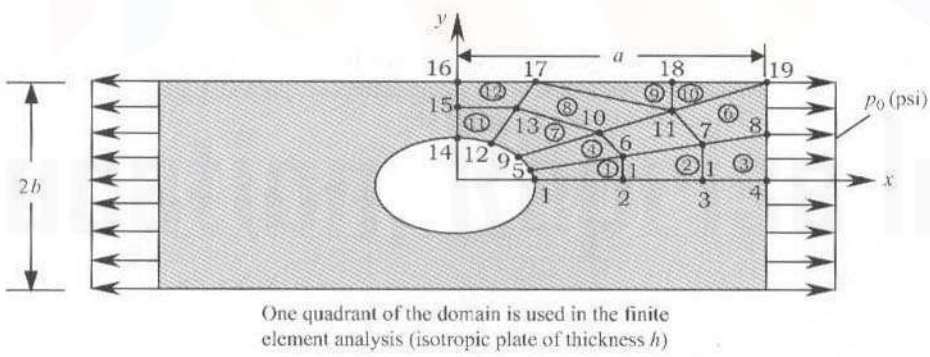


Figure P11.13

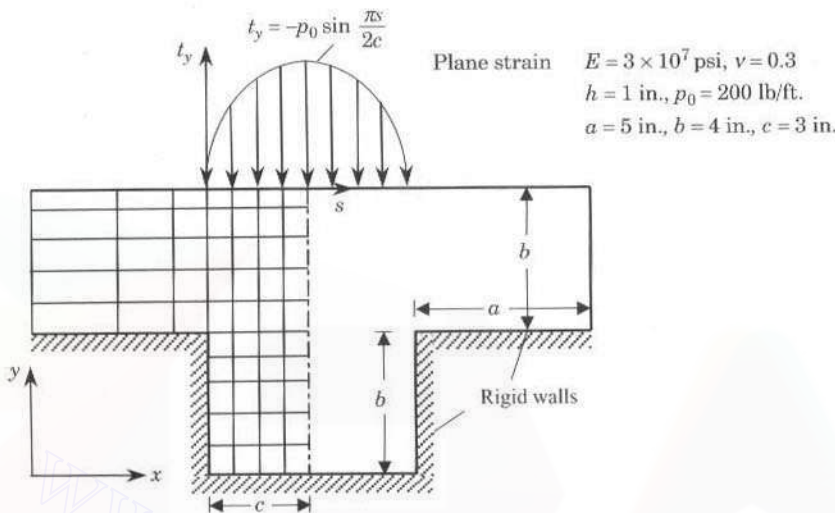


Figure P11.14

REFERENCES FOR ADDITIONAL READING

1. Barlow, J., "Optimal Stress Locations in Finite Element Models," *Int. Journal for Numerical Methods in Engineering*, **10**, 243–251, 1976.
2. Barlow, J., "More on Optimal Stress Points—Reduced Integration Element Distortions and Error Estimation," *Int. Journal for Numerical Methods in Engineering*, **28**, 1487–1504, 1989.
3. Budynas, R. G., *Advanced Strength and Applied Stress Analysis*, 2nd ed., McGraw-Hill, New York, 1999.
4. Reddy, J. N. and Rasmussen, M. L., *Advanced Engineering Analysis*, John Wiley, New York, 1982.
5. Reddy, J. N., *Energy and Variational Methods in Applied Mechanics*, (with an Introduction to the Finite Element Method), John Wiley, New York, 1984.
6. Reddy, J. N., *Energy Principles and Variational Methods in Applied Mechanics*, 2nd ed., John Wiley, New York, 2002.
7. Rektorys, K., *Variational Methods in Mathematics, Science and Engineering*, D. Reidel Publishing, Boston, MA, 1980.
8. Rektorys, K., *The Method of Discretization in Time*, D. Reidel Publishing, Boston, MA, 1982.
9. Shames, I. H., and Dym, C. L., *Energy and Finite Element Methods in Structural Mechanics*, Taylor and Francis, Philadelphia, PA, 1995.
10. Slaughter, W. S., *The Linearized Theory of Elasticity*, Birkhäuser, Boston, MA, 2002.
11. Timoshenko, S. P. and Goodier, J. N., *Theory of Elasticity*, 3rd ed., McGraw-Hill, New York, 1970.
12. Ugural, A. C. and Fenster, S. K., *Advanced Strength and Applied Elasticity*, Prentice Hall, Upper Saddle River, NJ, 1995.
13. Volterra, E. and Gaines, J. H., *Advanced Strength of Materials*, Prentice-Hall, Engelwood Cliffs, NJ, 1971.

Chapter 12

BENDING OF ELASTIC PLATES

12.1 INTRODUCTION

The term “plate” refers to solid bodies that are bounded by two parallel planes whose lateral dimensions are large compared with the separation between them (i.e., thickness of the plate), as shown in Fig. 12.1.1. In most cases, the thickness is no greater than one-tenth of the smallest in-plane dimension. Geometrically, plate problems are similar to the plane stress problems considered in Chapter 11 except that plates are also subjected to transverse loads (i.e., loads perpendicular to the plane of the plate) that cause bending about axes in the plane of the plate. In other words, a plate is a two-dimensional analog of a beam (see Chapter 5). Because of the smallness of the thickness dimension, it is often not necessary to model plates using three-dimensional elasticity theory. Simple two-dimensional theories that account for the kinematics of bending deformation of thin bodies subjected to transverse loads have been developed, and they are known as *plate theories*. An overview of plate theories can be found in Reddy (1999, 2002, 2004a).

Governing equations of displacement-based plate theories are derived using the principle of virtual displacements [see Reddy (1999, 2002)]. As we shall see shortly (and has already been shown in Chapter 11), the principle of virtual displacements directly yields the weak forms of the governing equations. The starting point in the development of the governing equations of a plate theory is to choose a displacement field. Typically, the displacement components are selected in the form of a linear combination of unknown functions and powers of the thickness coordinate z so that certain kinematics (i.e., geometry of deformation) of the plate are represented. For example, if $u_i(x, y, z, t)$ is the i th displacement component in the plate, it is expanded in the form

$$u_i(x, y, z, t) = \sum_{k=0}^N (z)^k u_i^{(k)}(x, y, t) \quad (12.1.1)$$

where $u_i^{(k)}$ are functions of (x, y) that are to be determined, (x, y) are the in-plane coordinates, z is the thickness coordinate, and t denotes time.

The principle of virtual displacements or Hamilton’s principle [see Reddy (1999, 2002)] requires

$$0 = \int_{t_1}^{t_2} [\delta K - (\delta U + \delta V)] dt \quad (12.1.2)$$

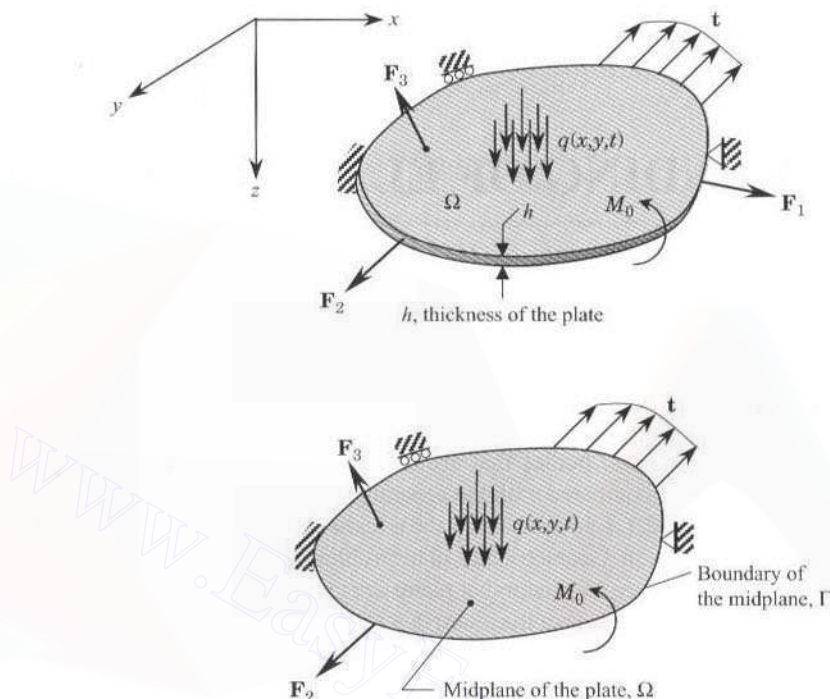


Figure 12.1.1 A plate structure subjected to external applied loads.

where δU , δV , and δK denote the virtual strain energy, virtual work done by external applied forces, and virtual kinetic energy, respectively (see Section 2.3.6). These quantities are expressed in terms of actual stresses and virtual strains, which depend on the assumed displacement functions, $u_i^{(k)}$, and their variations. For plate structures, the integration over the domain of the plate is represented as the (tensor) product of integration over the plane of the plate and integration over the thickness of the plate (volume integral = integral over the plane \times integral over the thickness). This is possible because of the explicit nature of the assumed displacement field (12.1.1) in the thickness coordinate. Thus, we can write

$$\int_V (\cdot) dV = \int_{-\frac{h}{2}}^{\frac{h}{2}} \int_{\Omega_0} (\cdot) d\Omega dz \quad (12.1.3)$$

where h denotes the total thickness of the plate and Ω denotes the undeformed midplane of the plate, which is assumed to coincide with the xy plane. Since all undetermined variables are explicit functions of the thickness coordinate, integration over the plate thickness is carried out explicitly, reducing the problem to a two-dimensional one. Consequently, the governing equations associated with the assumed expansion in Eq. (12.1.1) consist of differential equations involving the dependent variables $u_i^{(k)}(x, y, t)$ and thickness-averaged stress resultants, $R_{ij}^{(m)}$:

$$R_{ij}^{(m)} = \int_{-\frac{h}{2}}^{\frac{h}{2}} (z)^m \sigma_{ij} dz \quad (12.1.4)$$

The resultants can be written in terms of $u_i^{(k)}$ with the help of the assumed constitutive equations (stress-strain relations) and strain-displacement relations. More complete development of this procedure can be found in the textbooks by Reddy (1999, 2002, 2004a).

The two most commonly used displacement-based plate theories are the *classical plate theory* (CPT) and *first-order shear deformation theory* (SDT). CPT is an extension of the Euler–Bernoulli beam theory (see Section 5.2) from one dimension to two dimensions and is also known as the *Kirchhoff plate theory*. SDT is an extension of the Timoshenko beam theory (see Section 5.3) and is often known as the *Hencky–Mindlin plate theory*. A review of these plate theories and other refined plate theories can be found in Reddy (1999, 2004a). In this study, we shall review the governing equations and develop the finite element models of only the CPT and SDT.

For a linear theory based on infinitesimal strains and orthotropic material properties, the in-plane displacements (u_x, u_y) are uncoupled from the transverse deflection $u_z = w$. The in-plane displacements (u_x, u_y) are governed by the plane elasticity equations discussed in Chapter 11. If there are no in-plane forces, the inplane displacements will be zero. Hence, we discuss only the equations governing the bending deformation and the associated finite element models.

12.2 CLASSICAL PLATE THEORY

12.2.1 Displacement Field

The CPT is based on the assumptions that a straight line perpendicular to the plane of the plate is (1) inextensible, (2) remains straight, and (3) rotates such that it remains perpendicular to the tangent to the deformed surface [see Fig. 12.2.1(a)]. These assumptions are equivalent to specifying

$$\varepsilon_{zz} = 0, \quad \varepsilon_{yz} = 0, \quad \varepsilon_{xz} = 0 \quad (12.2.1)$$

The following assumed displacement field satisfies the assumptions

$$\begin{aligned} u_1(x, y, z, t) &= u_x(x, y, t) - z \frac{\partial w}{\partial x} \\ u_2(x, y, z, t) &= u_y(x, y, t) - z \frac{\partial w}{\partial y} \\ u_3(x, y, z, t) &= u_z(x, y, t) \equiv w(x, y, t) \end{aligned} \quad (12.2.2)$$

where (u_1, u_2, u_3) denote the total displacements of the point (x, y, z) along the x , y , and z directions, respectively, and (u_x, u_y, u_z) represent displacements of a point on the midplane $(x, y, 0)$ at time t .

The linear bending strains (due to the displacement w only) in (12.2.2) are (virtual strains are also listed)

$$\begin{Bmatrix} \varepsilon_{xx} \\ \varepsilon_{yy} \\ 2\varepsilon_{xy} \end{Bmatrix} = -z \begin{Bmatrix} \frac{\partial^2 w}{\partial x^2} \\ \frac{\partial^2 w}{\partial y^2} \\ 2\frac{\partial^2 w}{\partial x \partial y} \end{Bmatrix}, \quad \begin{Bmatrix} \delta\varepsilon_{xx} \\ \delta\varepsilon_{yy} \\ 2\delta\varepsilon_{xy} \end{Bmatrix} = -z \begin{Bmatrix} \frac{\partial^2 \delta w}{\partial x^2} \\ \frac{\partial^2 \delta w}{\partial y^2} \\ 2\frac{\partial^2 \delta w}{\partial x \partial y} \end{Bmatrix} \quad (12.2.3)$$

and $\varepsilon_{xz} = 0$, $\varepsilon_{yz} = 0$, and $\varepsilon_{zz} = 0$.

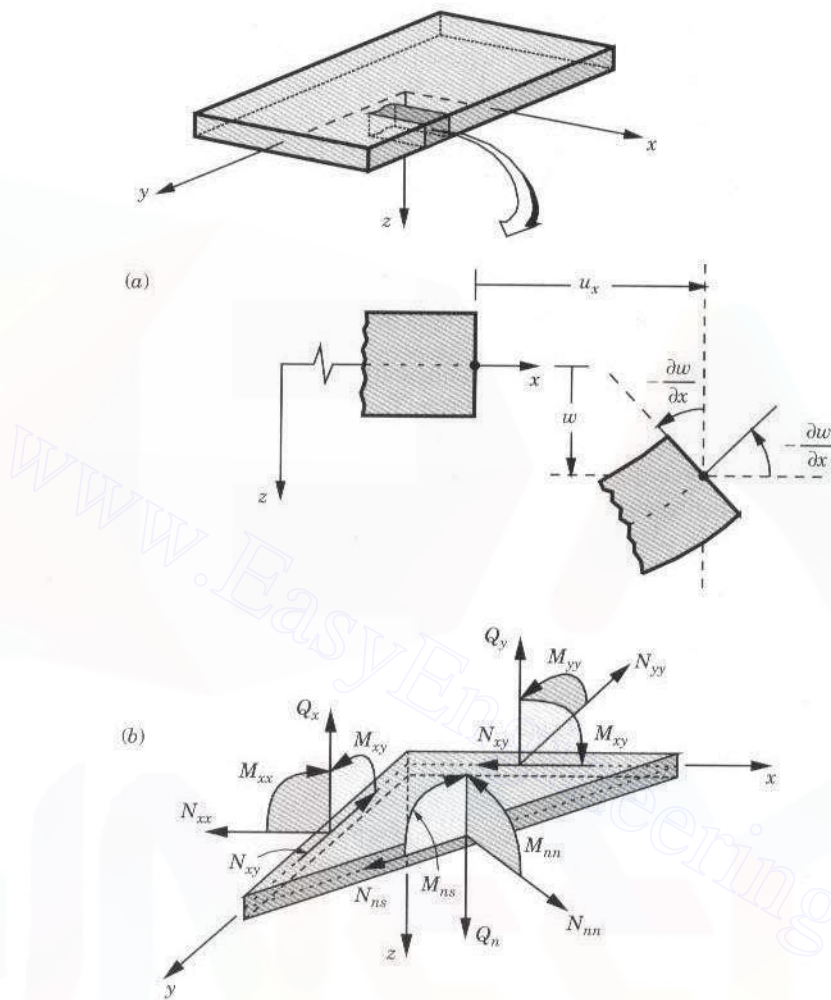


Figure 12.2.1 (a) Undeformed and deformed geometries of an edge in CPT. (b) Bending moments and shear forces on a plate element.

12.2.2 Virtual Work Statement

The principle of virtual displacements (12.1.2) applied to a plate finite element occupying a volume V_e and whose midplane is Ω_e takes the form [Reddy (1999, 2002)]

$$\begin{aligned}
 0 = & \int_{V_e} \left[\rho z^2 \left(\frac{\partial \delta w}{\partial x} \frac{\partial^3 w}{\partial x \partial t^2} + \frac{\partial \delta w}{\partial y} \frac{\partial^3 w}{\partial y \partial t^2} \right) + \rho \delta w \frac{\partial^2 w}{\partial t^2} \right. \\
 & \left. + \delta \varepsilon_{xx} \sigma_{xx} + \delta \varepsilon_{yy} \sigma_{yy} + 2 \delta \varepsilon_{xy} \sigma_{xy} \right] dV \\
 & - \int_{\Omega_e} q \delta w \, dx \, dy - \oint_{\Gamma_e} \left(-M_{nn} \frac{\partial \delta w}{\partial n} + V_n \delta w \right) ds
 \end{aligned} \tag{12.2.4}$$

The first three terms in (12.2.4) represent the virtual work done by the inertial forces in the three coordinate directions, while the remaining terms in the volume integral represent the virtual strain energy stored in the plate. The last two integrals, one defined on the midplane Ω_e and the other on the boundary Γ_e , denote the virtual work done by the transversely distributed load q , edge bending moment M_{nn} and shear force V_n [see Fig. 12.2.1(b)]. Since $V_e = \Omega_e \times (-\frac{h_e}{2}, \frac{h_e}{2})$ and the integrand is separable into functions of x and y alone and functions of z

$$F(x, y, z) = g(x, y) f(z) \quad (12.2.5)$$

we can carry out integration with respect to z (through thickness) explicitly.

Substitution of (12.2.3) for virtual displacements and strains into (12.2.4) and integrating with respect to z , we obtain

$$\begin{aligned} 0 = & \int_{\Omega_e} \left(I_0 \delta w \frac{\partial^2 w}{\partial t^2} + I_2 \frac{\partial \delta w}{\partial x} \frac{\partial^3 w}{\partial x \partial t^2} + I_2 \frac{\partial \delta w}{\partial y} \frac{\partial^3 w}{\partial y \partial t^2} \right. \\ & \left. - M_{xx} \frac{\partial^2 \delta w}{\partial x^2} - M_{yy} \frac{\partial^2 \delta w}{\partial y^2} - 2M_{xy} \frac{\partial^2 \delta w}{\partial x \partial y} - q \delta w \right) dx dy \\ & - \oint_{\Gamma_e} \left(-M_{nn} \frac{\partial \delta w}{\partial n} + V_n \delta w \right) ds \end{aligned} \quad (12.2.6)$$

where (M_{xx}, M_{yy}, M_{xy}) are the bending moments [see Fig. 12.2.1(b)],

$$\begin{aligned} M_{xx} &= \int_{-h/2}^{h/2} \sigma_{xx} z dz = - \left(D_{11} \frac{\partial^2 w}{\partial x^2} + D_{12} \frac{\partial^2 w}{\partial y^2} \right) \\ M_{yy} &= \int_{-h/2}^{h/2} \sigma_{yy} z dz = - \left(D_{12} \frac{\partial^2 w}{\partial x^2} + D_{22} \frac{\partial^2 w}{\partial y^2} \right) \\ M_{xy} &= \int_{-h/2}^{h/2} \sigma_{xy} z dz = -2D_{66} \frac{\partial^2 w}{\partial x \partial y} \end{aligned} \quad (12.2.7)$$

I_0 and I_2 are the mass moments of inertia (the rotatory inertia I_2 is neglected often)

$$I_0 = \int_{-h/2}^{h/2} \rho dz = \rho h, \quad I_2 = \int_{-h/2}^{h/2} \rho z^2 dz = \frac{1}{12} \rho h^3 \quad (12.2.8a)$$

and D_{ij} are the plate material stiffnesses

$$\begin{aligned} D_{11} &= \frac{E_1 h^3}{12(1 - \nu_{12}\nu_{21})}, \quad D_{22} = \frac{E_2 h^3}{12(1 - \nu_{12}\nu_{21})} \\ D_{12} &= \frac{\nu_{12} E_2 h^3}{12(1 - \nu_{12}\nu_{21})}, \quad D_{66} = \frac{G_{12} h^3}{12} \end{aligned} \quad (12.2.8b)$$

where the plane-stress reduced constitutive equations (11.2.11) are used in arriving at the expressions (12.2.7); M_{nn} and M_{ns} denote the normal and twisting moments, respectively, on an edge with unit normal vector \hat{n} , and V_n is the shear force. The moment M_{nn} and

shear force V_n on an edge with unit normal $\hat{\mathbf{n}}$ can be related to moments M_{xx} , M_{yy} , and M_{xy} on edges $x = \text{constant}$ and $y = \text{constant}$ by [see Reddy (2000)]

$$M_{nn} = M_{xx}n_x^2 + M_{yy}n_y^2 + 2M_{xy}n_xn_y, \quad V_n = \hat{Q}_n + \frac{\partial M_{ns}}{\partial s} \\ \hat{Q}_n = Q_x n_x + Q_y n_y + I_2 \left(\frac{\partial^3 w}{\partial x \partial t^2} n_x + \frac{\partial^3 w}{\partial y \partial t^2} n_y \right) \quad (12.2.9a)$$

$$M_{ns} = (M_{yy} - M_{xx})n_xn_y + M_{xy}(n_x^2 - n_y^2) \\ Q_x = \frac{\partial M_{xx}}{\partial x} + \frac{\partial M_{xy}}{\partial y}, \quad Q_y = \frac{\partial M_{xy}}{\partial x} + \frac{\partial M_{yy}}{\partial y} \quad (12.2.9b)$$

where (n_x, n_y) are the direction cosines of the unit normal, $\hat{\mathbf{n}} = n_x \hat{\mathbf{i}} + n_y \hat{\mathbf{j}}$, on the boundary Γ_e .

Substituting (12.2.7) into (12.2.6) yields the following weak form of the problem:

$$0 = \int_{\Omega_e} \left[I_0 \delta w \frac{\partial^2 w}{\partial t^2} + I_2 \frac{\partial \delta w}{\partial x} \frac{\partial^3 w}{\partial x \partial t^2} + I_2 \frac{\partial \delta w}{\partial y} \frac{\partial^3 w}{\partial y \partial t^2} + 4D_{66} \frac{\partial^2 w}{\partial x \partial y} \frac{\partial^2 \delta w}{\partial x \partial y} \right. \\ \left. + \left(D_{11} \frac{\partial^2 w}{\partial x^2} + D_{12} \frac{\partial^2 w}{\partial y^2} \right) \frac{\partial^2 \delta w}{\partial x^2} + \left(D_{12} \frac{\partial^2 w}{\partial x^2} + D_{22} \frac{\partial^2 w}{\partial y^2} \right) \frac{\partial^2 \delta w}{\partial y^2} \right. \\ \left. - \delta w q \right] dx dy - \oint_{\Gamma_e} \left(-M_{nn} \frac{\partial \delta w}{\partial n} + V_n \delta w \right) ds \quad (12.2.10)$$

The differential equation [i.e., the Euler–Lagrange equation resulting from (12.2.10)] governing w is

$$\frac{\partial^2}{\partial x^2} \left(D_{11} \frac{\partial^2 w}{\partial x^2} + D_{12} \frac{\partial^2 w}{\partial y^2} \right) + \frac{\partial^2}{\partial y^2} \left(D_{12} \frac{\partial^2 w}{\partial x^2} + D_{22} \frac{\partial^2 w}{\partial y^2} \right) \\ + 2 \frac{\partial^2}{\partial x \partial y} \left(2D_{66} \frac{\partial^2 w}{\partial x \partial y} \right) = q - I_0 \frac{\partial^2 w}{\partial t^2} + I_2 \frac{\partial^2}{\partial t^2} \left(\frac{\partial^2 w}{\partial x^2} + \frac{\partial^2 w}{\partial y^2} \right) \quad (12.2.11)$$

Note that the expressions in parentheses in the first three terms are the bending moments $-M_{xx}$, $-M_{yy}$, and $-M_{xy}$, respectively [see (12.2.7)]. The boundary conditions for the CPT are given below:

$$\begin{aligned} \text{clamped: } w &= 0, & \frac{\partial w}{\partial n} &= 0 \\ \text{simply supported: } w &= 0, & M_{nn} &= 0 \\ \text{free: } V_n &= 0, & M_{nn} &= 0 \end{aligned} \quad (12.2.12)$$

We do not need Eq. (12.2.11) but only the weak form (12.2.10) to develop the finite element model. Alternatively, we can construct the weak form of the governing equation (12.2.11) using the usual procedure. We obtain

$$0 = \int_{\Omega_e} \left[\frac{\partial^2 v}{\partial x^2} \left(D_{11} \frac{\partial^2 w}{\partial x^2} + D_{12} \frac{\partial^2 w}{\partial y^2} \right) + \frac{\partial^2 v}{\partial y^2} \left(D_{12} \frac{\partial^2 w}{\partial x^2} + D_{22} \frac{\partial^2 w}{\partial y^2} \right) \right. \\ \left. + 4D_{66} \frac{\partial^2 v}{\partial x \partial y} \frac{\partial^2 w}{\partial x \partial y} - vq + I_0 v \frac{\partial^2 w}{\partial t^2} + I_2 \left(\frac{\partial v}{\partial x} \frac{\partial^3 w}{\partial x \partial t^2} + \frac{\partial v}{\partial y} \frac{\partial^3 w}{\partial y \partial t^2} \right) \right] dx dy$$

$$\begin{aligned}
 & -\oint_{\Gamma_e} v \left[\left(\frac{\partial M_{xx}}{\partial x} + \frac{\partial M_{xy}}{\partial y} \right) n_x + \left(\frac{\partial M_{xy}}{\partial x} + \frac{\partial M_{yy}}{\partial y} \right) n_y \right. \\
 & \quad \left. + I_2 \left(\frac{\partial^3 w}{\partial x \partial t^2} n_x + \frac{\partial^3 w}{\partial y \partial t^2} n_y \right) \right] ds \\
 & + \oint_{\Gamma_e} \left[\frac{\partial v}{\partial x} (M_{xx} n_x + M_{xy} n_y) + \frac{\partial v}{\partial y} (M_{xy} n_x + M_{yy} n_y) \right] ds \tag{12.2.13}
 \end{aligned}$$

where v denotes the weight function, which can be interpreted as the first variation, $\delta w = v$. Next, we convert the derivatives of w with respect to the rectangular coordinates (x, y) to those with respect to the local (normal and tangential) coordinates (n, s) . We use the identities

$$\frac{\partial}{\partial x} = n_x \frac{\partial}{\partial n} - n_y \frac{\partial}{\partial s}, \quad \frac{\partial}{\partial y} = n_x \frac{\partial}{\partial s} + n_y \frac{\partial}{\partial n} \tag{12.2.14}$$

and the definitions (12.2.9) to rewrite the boundary integrals of (12.2.13) as

$$-\oint_{\Gamma_e} v \hat{Q}_n ds + \oint_{\Gamma_e} \left(\frac{\partial v}{\partial n} M_{nn} + \frac{\partial v}{\partial s} M_{ns} \right) ds$$

The second term in the second integral is integrated by parts to yield the expression

$$-\oint_{\Gamma_e} \left[v \left(\hat{Q}_n + \frac{\partial M_{ns}}{\partial s} \right) - \frac{\partial v}{\partial n} M_{nn} \right] ds \tag{12.2.15}$$

The expression in parenthesis (\cdot) is denoted by V_n , and its specification is known as the *Kirchhoff free-edge condition*. We have made the assumption that $[v M_{ns}]_s = 0$, which holds only when the boundary is smooth. It is clear that the weak form in (12.2.13), with the boundary integrals replaced by (12.2.15), is the same as that in (12.2.10).

The weak form (12.2.10) can be expressed in vector form as ($\mathbf{w} = w$ and $\delta \mathbf{w} = \delta w$)

$$\begin{aligned}
 0 = & \int_{\Omega_e} [I_0(\delta \mathbf{w})^T \ddot{\mathbf{w}} + I_2(\mathbf{D}_1 \delta \mathbf{w})^T (\mathbf{D}_1 \ddot{\mathbf{w}}) + (\mathbf{D}_2 \delta \mathbf{w})^T \mathbf{C} (\mathbf{D}_2 \mathbf{w}) - (\delta \mathbf{w})^T q] d\mathbf{x} \\
 & - \oint_{\Gamma_e} [-(\delta \mathbf{w}_{,n})^T M_{nn} + (\delta \mathbf{w})^T V_n] ds \tag{12.2.16}
 \end{aligned}$$

where $\mathbf{w}_{,n} = (\partial \mathbf{w} / \partial n)$ and

$$\mathbf{D}_1 = \begin{Bmatrix} \frac{\partial}{\partial x} \\ \frac{\partial}{\partial y} \end{Bmatrix}, \quad \mathbf{D}_2 = \begin{Bmatrix} \frac{\partial^2}{\partial x^2} \\ \frac{\partial^2}{\partial y^2} \\ 2 \frac{\partial^2}{\partial x \partial y} \end{Bmatrix}, \quad \mathbf{C} = \begin{bmatrix} D_{11} & D_{12} & 0 \\ D_{12} & D_{22} & 0 \\ 0 & 0 & D_{66} \end{bmatrix} \tag{12.2.17}$$

This completes the development of the CPT and its variational (or weak) form. Next, we develop the finite element model based on Eqs. (12.2.10) and (12.2.16).

12.2.3 Finite Element Model

An examination of the boundary terms in the weak form (12.2.10) suggests that the essential boundary conditions involve specifying the transverse deflection w and the normal derivative of w , which constitute the primary variables of the problem (like in the Euler–Bernoulli beam model). Hence, the finite element interpolation of w must be such that w and $\partial w / \partial n$ are continuous across the interelement boundaries in CPT elements. Note that $\partial / \partial n$ and $\partial / \partial s$ are related to the global derivatives $\partial / \partial x$ and $\partial / \partial y$ by the relations [the inverse of those in (12.2.14)]

$$\frac{\partial}{\partial n} = n_x \frac{\partial}{\partial x} + n_y \frac{\partial}{\partial y}, \quad \frac{\partial}{\partial s} = n_x \frac{\partial}{\partial y} - n_y \frac{\partial}{\partial x} \quad (12.2.18)$$

Thus, the primary variables at the nodes of a rectangular element with sides parallel to the x and y axes should be

$$w, \quad \frac{\partial w}{\partial x}, \quad \frac{\partial w}{\partial y}$$

Finite elements that require continuity of w and its first derivatives are called C^1 elements.

Towards developing the CPT finite element model, we assume that w is interpolated over a typical element Ω_e by expressions of the form

$$w(x, y, t) = \sum_{j=1}^n \Delta_j(t) \varphi_j(x, y) \quad (12.2.19a)$$

or

$$\mathbf{w} = \Phi^T \Delta, \quad \Phi^T = \{\varphi_1 \varphi_2 \dots \varphi_n\} \quad (12.2.19b)$$

where Δ_j denote the nodal values of w and its derivatives, and $\varphi_j(x, y)$ are the Hermite interpolation functions (see Table 9.2.1). The nature of the interpolation functions φ_j will be discussed in the sequel. Substitution of (12.2.19a) for w and $\delta w = \varphi_i$ ($i = 1, 2, \dots, n$) into (12.2.10) gives the finite element model

$$[M^e][\ddot{\Delta}^e] + [K^e]\{\Delta^e\} = \{F^e\} + \{Q^e\} \quad (12.2.20)$$

where

$$\begin{aligned} M_{ij}^e &= \int_{\Omega_e} \left[I_0 \varphi_i \varphi_j + I_2 \left(\frac{\partial \varphi_i}{\partial x} \frac{\partial \varphi_j}{\partial x} + \frac{\partial \varphi_i}{\partial y} \frac{\partial \varphi_j}{\partial y} \right) \right] dx dy \\ K_{ij}^e &= \int_{\Omega_e} \left[D_{11} \frac{\partial^2 \varphi_i}{\partial x^2} \frac{\partial^2 \varphi_j}{\partial x^2} + D_{12} \left(\frac{\partial^2 \varphi_i}{\partial x^2} \frac{\partial^2 \varphi_j}{\partial y^2} + \frac{\partial^2 \varphi_i}{\partial y^2} \frac{\partial^2 \varphi_j}{\partial x^2} \right) \right. \\ &\quad \left. + D_{22} \frac{\partial^2 \varphi_i}{\partial y^2} \frac{\partial^2 \varphi_j}{\partial y^2} + 4D_{66} \frac{\partial^2 \varphi_i}{\partial x \partial y} \frac{\partial^2 \varphi_j}{\partial x \partial y} \right] dx dy \\ F_i^e &= \int_{\Omega_e} q \varphi_i dx dy, \quad Q_i^e = \oint_{\Gamma_e} \left(-M_{nn} \frac{\partial \varphi_i}{\partial n} + V_n \varphi_i \right) ds \end{aligned} \quad (12.2.21)$$

The vector form of the finite element model is obtained by substituting (12.2.19b) into Eq. (12.2.16) and setting the coefficient of $\delta \Delta^T$ to zero:

$$\mathbf{M}^e \ddot{\Delta}^e + \mathbf{K}^e \Delta^e = \mathbf{F}^e + \mathbf{Q}^e \quad (12.2.22)$$

where [see Eq. (12.2.17) for the definitions of \mathbf{D}_1 , \mathbf{D}_2 , and \mathbf{C}]

$$\begin{aligned}\mathbf{M}^e &= \int_{\Omega_e} (I_0 \Phi \Phi^T + I_2 \mathbf{B}_1^T \mathbf{B}_1) d\mathbf{x} \\ \mathbf{K}^e &= \int_{\Omega_e} \mathbf{B}_2^T \mathbf{C} \mathbf{B}_2 d\mathbf{x}, \quad \mathbf{F}^e = \int_{\Omega_e} \Phi q d\mathbf{x} \\ \mathbf{Q}^e &= \oint_{\Gamma_e} (-\Phi_{,n} M_n + \Phi V_n) ds \\ \mathbf{B}_1 = \mathbf{D}_1 \Phi^T &= \left[\begin{array}{cccc} \frac{\partial \varphi_1}{\partial x} & \frac{\partial \varphi_2}{\partial x} & \dots & \frac{\partial \varphi_n}{\partial x} \\ \frac{\partial \varphi_1}{\partial y} & \frac{\partial \varphi_2}{\partial y} & \dots & \frac{\partial \varphi_n}{\partial y} \end{array} \right]_{(2 \times n)} \quad (12.2.23) \\ \mathbf{B}_2 = \mathbf{D}_2 \Phi^T &= \left[\begin{array}{cccc} \frac{\partial^2 \varphi_1}{\partial x^2} & \frac{\partial^2 \varphi_2}{\partial x^2} & \dots & \frac{\partial^2 \varphi_n}{\partial x^2} \\ \frac{\partial^2 \varphi_1}{\partial y^2} & \frac{\partial^2 \varphi_2}{\partial y^2} & \dots & \frac{\partial^2 \varphi_n}{\partial y^2} \\ 2 \frac{\partial^2 \varphi_1}{\partial x \partial y} & 2 \frac{\partial^2 \varphi_2}{\partial x \partial y} & \dots & 2 \frac{\partial^2 \varphi_n}{\partial x \partial y} \end{array} \right]_{(3 \times n)}\end{aligned}$$

12.2.4 Plate Bending Elements

A number of C^1 rectangular and triangular plate bending elements with $(w, \partial w / \partial x, \partial w / \partial y)$ or with $(w, \partial w / \partial x, \partial w / \partial y, \partial^2 w / \partial x \partial y)$ as the degrees of freedom at each node exist in the literature. A rectangular element with four nodes, with $(w, \partial w / \partial x, \partial w / \partial y)$ at each node, requires the 12-term ($n = 12$) polynomial approximation of w

$$\begin{aligned}w &= a_1 + a_2x + a_3y + a_4xy + a_5x^2 + a_6y^2 + a_7x^2y \\ &\quad + a_8xy^2 + a_9x^3 + a_{10}y^3 + a_{11}x^3y + a_{12}xy^3 \quad (12.2.24)\end{aligned}$$

The polynomial is *not* a complete fourth-order polynomial; it is a complete third-order polynomial. For a three-node triangular element with $(w, \partial w / \partial x, \partial w / \partial y)$ at each node, the following nine-term ($n = 9$) polynomial is selected

$$w = a_1 + a_2x + a_3y + a_4xy + a_5x^2 + a_6y^2 + a_7(x^2y + xy^2) + a_8x^3 + a_9y^3 \quad (12.2.25)$$

This is an incomplete third-order polynomial because x^2y and y^2x do not vary independently.

Some comments are in order on the interelement continuity of w and $\partial w / \partial n$ for the four-node rectangular element ($n = 12$) and three-node triangular element ($n = 9$). We note from (12.2.24) that w varies as a cubic along any line $x = \text{constant}$ or $y = \text{constant}$. Along a given side, there are two nodes and two values (w and its normal derivative) per node to define the cubic variation uniquely. Hence, w is uniquely defined along the element boundary and is continuous along interelement boundaries. The normal derivative, say, $\partial w / \partial x$ on a line $x = \text{constant}$, also varies as a cubic function of y along the side. Since only two values of $\partial w / \partial x$ are available on the side, the cubic variation cannot be uniquely defined and the normal slope continuity is not satisfied. In addition, $\partial^2 w / \partial x \partial y$ is not single-valued at the corner points of the element. Elements that violate any of the continuity conditions are known as

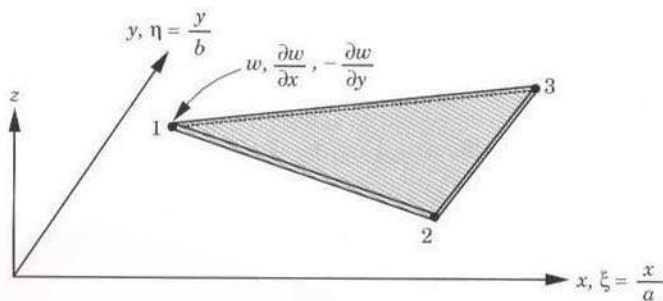


Figure 12.2.2 A nonconforming triangular element with three degrees of freedom (w , $\partial w / \partial x$, $\partial w / \partial y$) per node.

nonconforming elements. Thus, the four-node rectangular element with w represented by (12.2.24) is a nonconforming element. Despite this deficiency, the element is known to give good results. A similar discussion leads to the conclusion that the three-node triangular element is nonconforming. In addition, the triangular element is found to have convergence problems and singular behavior for certain meshes.

Triangular Elements

An effective nonconforming triangular element (the BCIZ triangle) was developed by Bazeley, Cheung, Irons, and Zienkiewicz (1965), and it consists of three degrees of freedom (w , $-\partial w / \partial y$, $\partial w / \partial x$) at the three vertex nodes (see Fig. 12.2.2). The interpolation functions for the triangular element can be expressed in terms of the area coordinates as

$$\left\{ \begin{array}{l} \varphi_1 \\ \varphi_2 \\ \varphi_3 \\ \varphi_4 \\ \varphi_5 \\ \varphi_6 \\ \varphi_7 \\ \varphi_8 \\ \varphi_9 \end{array} \right\} = \left\{ \begin{array}{l} L_1 + L_1^2 L_2 + L_1^2 L_3 - L_1 L_2^2 - L_1 L_3^2 \\ x_{31}(L_3 L_1^2 - 0.5 L_{123}) - x_{12}(L_1^2 L_2 + 0.5 L_{123}) \\ y_{31}(L_3 L_1^2 + 0.5 L_{123}) - y_{12}(L_1^2 L_2 + 0.5 L_{123}) \\ L_2 + L_2^2 L_3 + L_2^2 L_1 - L_2 L_3^2 - L_2 L_1^2 \\ x_{12}(L_1 L_2^2 - 0.5 L_{123}) - x_{23}(L_2^2 L_3 + 0.5 L_{123}) \\ y_{12}(L_1 L_2^2 + 0.5 L_{123}) - y_{23}(L_2^2 L_3 + 0.5 L_{123}) \\ L_3 + L_3^2 L_1 + L_3^2 L_2 - L_3 L_1^2 - L_3 L_2^2 \\ x_{23}(L_2 L_3^2 - 0.5 L_{123}) - x_{31}(L_3^2 L_1 + 0.5 L_{123}) \\ y_{23}(L_2 L_3^2 + 0.5 L_{123}) - y_{31}(L_3^2 L_1 + 0.5 L_{123}) \end{array} \right\} \quad (12.2.26)$$

where $L_{123} = L_1 L_2 L_3$, $x_{ij} = x_i - x_j$, and $y_{ij} = y_i - y_j$, (x_i, y_i) being the global coordinates of the i th node.

A conforming triangular element due to Clough and Tocher (1965) is an assemblage of three triangles as shown in Fig. 12.2.3 [Clough and Felippa (1968) developed a quadrilateral element by dividing it into four triangles and each triangle divided into three subtriangles]. The normal slope continuity is enforced at the midside nodes between the subtriangles. In the i th subtriangle, the transverse deflection is represented by the polynomial

$$w^i(x, y) = a_1^i + a_2^i \xi + a_3^i \eta + a_4^i \xi^2 + a_5^i \xi \eta + a_6^i \eta^2 + a_7^i \xi^3 + a_8^i \xi \eta^2 + a_9^i \eta \xi^2 + a_{10}^i \eta^3 \quad (12.2.27)$$

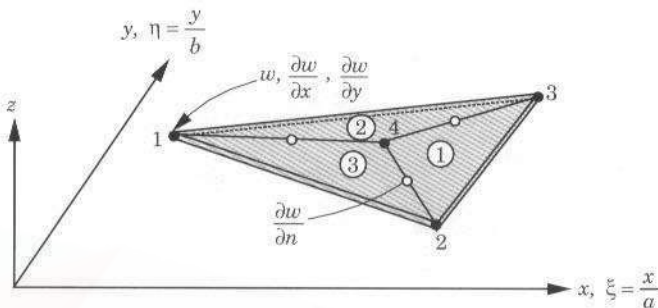


Figure 12.2.3 A conforming triangular element with three degrees of freedom.

where ($i = 1, 2, 3$) and (ξ, η) are the local coordinates, as shown in the Fig. 12.2.3. The thirty coefficients are reduced to nine, three $(w, \partial w / \partial x, \partial w / \partial y)$ at each vertex of the triangle, by equating the variables from the vertices of each subtriangle at the common points and normal slope between the midside points of the subtriangles.

Rectangular Elements

A nonconforming rectangular element with 12 degrees of freedom [see Eq. (12.2.24)] with w , $\partial w / \partial x$, and $\partial w / \partial y$ as the nodal variables [see Fig. 12.2.4(a)] is based on the work of Melosh (1963) and Zienkiewicz and Cheung (1964). The normal slope varies cubically along an edge whereas there are only two values of $\partial w / \partial n$ available on the edge. Therefore, the cubic polynomial for the normal derivative of w is not the same on the edge common to two elements. The interpolation functions for this element can be expressed compactly as

$$\begin{aligned}\varphi_i^e &= g_{i1} \quad (i = 1, 4, 7, 10); \quad \varphi_i^e = g_{i2} \quad (i = 2, 5, 8, 11) \\ \varphi_i^e &= g_{i3} \quad (i = 3, 6, 9, 12)\end{aligned}\quad (12.2.28a)$$

where

$$\begin{aligned}g_{i1} &= \frac{1}{8}(1 + \xi_0)(1 + \eta_0)(2 + \xi_0 + \eta_0 - \xi^2 - \eta^2) \\ g_{i2} &= \frac{1}{8}\xi_i(\xi_0 - 1)(1 + \eta_0)(1 + \xi_0)^2 \\ g_{i3} &= \frac{1}{8}\eta_i(\eta_0 - 1)(1 + \xi_0)(1 + \eta_0)^2 \\ \xi &= (x - x_c)/a, \quad \eta = (y - y_c)/b, \quad \xi_0 = \xi\xi_i, \quad \eta_0 = \eta\eta_i\end{aligned}\quad (12.2.28b)$$

$2a$ and $2b$ are the sides of the rectangle, and (x_c, y_c) are the global coordinates of the center of the rectangle. We denote this element as the CPT(N) element.

A conforming rectangular element with w , $\partial w / \partial x$, $\partial w / \partial y$, and $\partial^2 w / \partial x \partial y$ as the nodal variables (a total of 16 degrees of freedom) was developed by Bogner, Fox, and Schmidt (1965). The interpolation functions (obtained from the tensor products of the one-dimensional Hermite cubic polynomials) for this element [see Fig. 12.2.4(b) and Table 9.2.1]

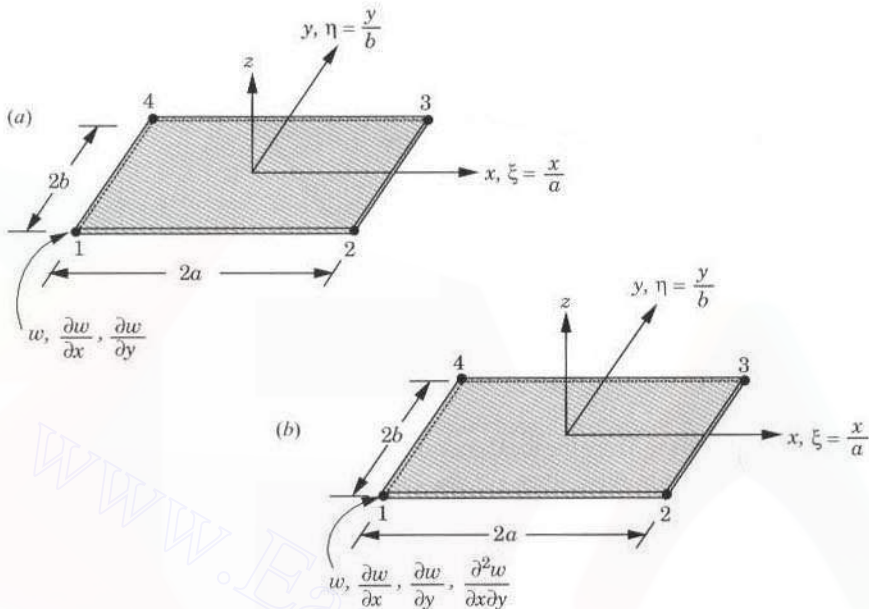


Figure 12.2.4 (a) A nonconforming rectangular element with three degrees of freedom ($w, \frac{\partial w}{\partial x}, \frac{\partial w}{\partial y}$) per node. (b) A conforming rectangular element with four degrees of freedom ($w, \frac{\partial w}{\partial x}, \frac{\partial w}{\partial y}, \frac{\partial^2 w}{\partial x \partial y}$) per node.

are

$$\begin{aligned}\varphi_i^e &= g_{i1} \quad (i = 1, 5, 9, 13); & \varphi_i^e &= g_{i2} \quad (i = 2, 6, 10, 14) \\ \varphi_i^e &= g_{i3} \quad (i = 3, 7, 11, 15); & \varphi_i^e &= g_{i4} \quad (i = 4, 8, 12, 16)\end{aligned}\quad (12.2.29a)$$

where

$$\begin{aligned}g_{i1} &= \frac{1}{16}(\xi + \xi_i)^2(\xi_0 - 2)(\eta + \eta_i)^2(\eta_0 - 2) \\ g_{i2} &= \frac{1}{16}\xi_i(\xi + \xi_i)^2(1 - \xi_0)(\eta + \eta_i)^2(\eta_0 - 2) \\ g_{i3} &= \frac{1}{16}\eta_i(\xi + \xi_i)^2(\xi_0 - 2)(\eta + \eta_i)^2(1 - \eta_0) \\ g_{i4} &= \frac{1}{16}\xi_i\eta_i(\xi + \xi_i)^2(1 - \xi_0)(\eta + \eta_i)^2(1 - \eta_0)\end{aligned}\quad (12.2.29b)$$

This element is denoted as CPT(C).

12.3 SHEAR DEFORMATION PLATE THEORY

12.3.1 Displacement Field

In the SDT, we relax the normality assumption of CPT, i.e., transverse normals may rotate without remaining normal to the midplane (see Fig. 12.3.1). SDT is based on the

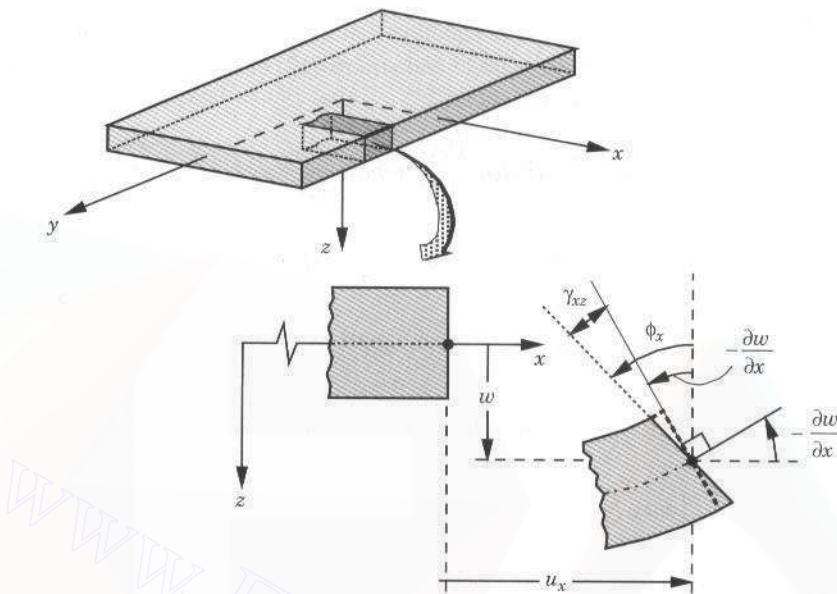


Figure 12.3.1 Undeformed and deformed geometries of an edge in SDT.

displacement field

$$\begin{aligned} u_1(x, y, z, t) &= u_x(x, y, t) + z\phi_x(x, y, t) \\ u_2(x, y, z, t) &= u_y(x, y, t) + z\phi_y(x, y, t) \\ u_3(x, y, z, t) &= u_z(x, y, t) \equiv w(x, y, t) \end{aligned} \quad (12.3.1)$$

where $(u_x, u_y, u_z = w)$ are the displacements of a point on the midplane in the (x, y, z) coordinate directions, and ϕ_x and ϕ_y are rotations of the transverse normal about the y and $-x$ axes, respectively. Since (u_x, u_y) are uncoupled from (w, ϕ_x, ϕ_y) , we develop the equations governing (w, ϕ_x, ϕ_y) .

The bending strains associated with (12.3.1) are

$$\begin{Bmatrix} \varepsilon_{xx} \\ \varepsilon_{yy} \\ 2\varepsilon_{xy} \\ 2\varepsilon_{xz} \\ 2\varepsilon_{yz} \end{Bmatrix} = \begin{Bmatrix} z \frac{\partial \phi_x}{\partial x} \\ z \frac{\partial \phi_y}{\partial y} \\ z \left(\frac{\partial \phi_x}{\partial y} + \frac{\partial \phi_y}{\partial x} \right) \\ \phi_x + \frac{\partial w}{\partial x} \\ \phi_y + \frac{\partial w}{\partial y} \end{Bmatrix}, \quad \begin{Bmatrix} \delta\varepsilon_{xx} \\ \delta\varepsilon_{yy} \\ 2\delta\varepsilon_{xy} \\ 2\delta\varepsilon_{xz} \\ 2\delta\varepsilon_{yz} \end{Bmatrix} = \begin{Bmatrix} z \frac{\partial \delta\phi_x}{\partial x} \\ z \frac{\partial \delta\phi_y}{\partial y} \\ z \left(\frac{\partial \delta\phi_x}{\partial y} + \frac{\partial \delta\phi_y}{\partial x} \right) \\ \delta\phi_x + \frac{\partial \delta w}{\partial x} \\ \delta\phi_y + \frac{\partial \delta w}{\partial y} \end{Bmatrix} \quad (12.3.2)$$

Note that the transverse shear strains are nonzero and $\varepsilon_{zz} = 0$.

12.3.2 Virtual Work Statement

Substituting the displacement field (12.3.1) and strains (12.3.2) into the statement of the principle of virtual displacements, we obtain

$$0 = \int_{V_e} \left(\rho z^2 \delta \phi_x \frac{\partial^2 \phi_x}{\partial t^2} + \rho z^2 \delta \phi_y \frac{\partial^2 \phi_y}{\partial t^2} + \rho \delta w \frac{\partial^2 w}{\partial t^2} + \delta \varepsilon_{xx} \sigma_{xx} + \delta \varepsilon_{yy} \sigma_{yy} \right. \\ \left. + 2\delta \varepsilon_{xy} \sigma_{xy} + 2\delta \varepsilon_{xz} \sigma_{xz} + 2\delta \varepsilon_{yz} \sigma_{yz} \right) dV - \int_{\Omega_e} \delta w q \, dx \, dy \\ - \oint_{\Gamma_e} (\delta \phi_n M_{nn} + \delta \phi_s M_{ns} + \delta w Q_n) \, ds$$

Carrying out the integration with respect to z , we arrive at

$$0 = \int_{\Omega_e} \left[I_0 \delta w \frac{\partial^2 w}{\partial t^2} + I_2 \left(\delta \phi_x \frac{\partial^2 \phi_x}{\partial t^2} + \delta \phi_y \frac{\partial^2 \phi_y}{\partial t^2} \right) \right. \\ \left. + M_{xx} \frac{\partial \delta \phi_x}{\partial x} + M_{yy} \frac{\partial \delta \phi_y}{\partial y} + M_{xy} \left(\frac{\partial \delta \phi_x}{\partial y} + \frac{\partial \delta \phi_y}{\partial x} \right) \right. \\ \left. + Q_x \left(\delta \phi_x + \frac{\partial \delta w}{\partial x} \right) + Q_y \left(\delta \phi_y + \frac{\partial \delta w}{\partial y} \right) - \delta w q \right] dx \, dy \\ - \oint_{\Gamma_e} (\delta \phi_n M_{nn} + \delta \phi_s M_{ns} + \delta w Q_n) \, ds \quad (12.3.3)$$

where M_{nn} , M_{ns} , and Q_n are defined in Eq. (12.2.9a) with

$$Q_x = K_s \int_{-h/2}^{h/2} \sigma_{xz} \, dz = K_s A_{55} \left(\phi_x + \frac{\partial w}{\partial x} \right) \quad (12.3.4)$$

$$Q_y = K_s \int_{-h/2}^{h/2} \sigma_{yz} \, dz = K_s A_{44} \left(\phi_y + \frac{\partial w}{\partial y} \right)$$

$$M_{xx} = D_{11} \frac{\partial \phi_x}{\partial x} + D_{12} \frac{\partial \phi_y}{\partial y}, \quad M_{yy} = D_{12} \frac{\partial \phi_x}{\partial x} + D_{22} \frac{\partial \phi_y}{\partial y} \quad (12.3.5)$$

$$M_{xy} = D_{66} \left(\frac{\partial \phi_x}{\partial y} + \frac{\partial \phi_y}{\partial x} \right)$$

$$Q_n = Q_x n_x + Q_y n_y, \quad \phi_n = \phi_x n_x + \phi_y n_y, \quad \phi_s = \phi_y n_x - \phi_x n_y \quad (12.3.6)$$

$$A_{44} = G_{23} h, \quad A_{55} = G_{13} h$$

Here K_s denotes the shear correction coefficient. This coefficient is introduced to account for the discrepancy between the distribution of transverse shear stresses in SDT and the actual distribution (see Section 5.3 on the Timoshenko beam element).

The virtual work statement (12.3.3) contains three weak forms for the three displacements (w , ϕ_x , ϕ_y). They are identified by collecting the terms involving δw , $\delta\phi_x$, and $\delta\phi_y$ separately and equating them to zero:

$$0 = \int_{\Omega_e} \left(I_0 \delta w \frac{\partial^2 w}{\partial t^2} + Q_x \frac{\partial \delta w}{\partial x} + Q_y \frac{\partial \delta w}{\partial y} - q \delta w \right) dx dy - \oint_{\Gamma_e} \delta w Q_n ds \quad (12.3.7a)$$

$$0 = \int_{\Omega_e} \left(I_2 \delta \phi_x \frac{\partial^2 \phi_x}{\partial t^2} + M_{xx} \frac{\partial \delta \phi_x}{\partial x} + M_{xy} \frac{\partial \delta \phi_x}{\partial y} + Q_x \delta \phi_x \right) dx dy - \oint_{\Gamma_e} \delta \phi_x (M_{nn} n_x - M_{ns} n_y) ds \quad (12.3.7b)$$

$$0 = \int_{\Omega_e} \left(I_2 \delta \phi_y \frac{\partial^2 \phi_y}{\partial t^2} + M_{xy} \frac{\partial \delta \phi_y}{\partial x} + M_{yy} \frac{\partial \delta \phi_y}{\partial y} + Q_y \delta \phi_y \right) dx dy - \oint_{\Gamma_e} \delta \phi_y (M_{nn} n_y + M_{ns} n_x) ds \quad (12.3.7c)$$

The governing differential equations of SDT are [obtained from the weak forms (12.3.7a)–(12.3.7c)]

$$\frac{\partial Q_x}{\partial x} + \frac{\partial Q_y}{\partial y} + q = I_0 \frac{\partial^2 w}{\partial t^2} \quad (12.3.8a)$$

$$\frac{\partial M_{xx}}{\partial x} + \frac{\partial M_{xy}}{\partial y} - Q_x = I_2 \frac{\partial^2 \phi_x}{\partial t^2} \quad (12.3.8b)$$

$$\frac{\partial M_{xy}}{\partial x} + \frac{\partial M_{yy}}{\partial y} - Q_y = I_2 \frac{\partial^2 \phi_y}{\partial t^2} \quad (12.3.8c)$$

The boundary conditions for the CPT are given below.

$$\begin{aligned} \text{clamped: } & w = 0, \quad \phi_n = 0 \\ \text{simply supported: } & w = 0, \quad M_{nn} = 0 \\ \text{free: } & Q_n = 0, \quad M_{nn} = 0 \end{aligned} \quad (12.3.9)$$

The three-step procedure can be used to develop the weak forms of (12.3.8a)–(12.3.8c), which will be equivalent to those listed in (12.3.7a)–(12.3.7c). To see the equivalence, the following identities must be used:

$$\begin{aligned} M_{nn} n_x - M_{ns} n_y &= M_{xx} n_x + M_{xy} n_y \equiv \hat{M}_{nn} \\ M_{nn} n_y + M_{ns} n_x &= M_{xy} n_x + M_{yy} n_y \equiv \hat{M}_{ns} \\ \phi_x &= \phi_n n_x - \phi_s n_y, \quad \phi_y = \phi_n n_y + \phi_s n_x \end{aligned} \quad (12.3.10)$$

The vector form of the virtual work statement (12.3.3) [after replacing the stress resultants Q_x , Q_y , M_{xx} , M_{xy} , and M_{yy} in terms of the generalized displacements (w , ϕ_x , ϕ_y)

using Eqs. (12.3.4) and (12.3.5)] is given by

$$0 = \int_{\Omega_e} [I_0(\delta \mathbf{w})^T \ddot{\mathbf{w}} + I_2 \delta \Phi^T \ddot{\Phi} + (\delta \Phi + \mathbf{D}_1 \delta \mathbf{w})^T \mathbf{A} (\Phi + \mathbf{D}_1 \mathbf{w}) \\ + (\mathbf{D} \delta \Phi)^T \mathbf{C} (\mathbf{D} \Phi) - \mathbf{w}^T q] d\mathbf{x} - \oint_{\Gamma_e} (\delta \Phi_n^T \mathbf{M}_n + \mathbf{w}^T Q_n) ds \quad (12.3.11)$$

where

$$\Phi = \begin{Bmatrix} \phi_x \\ \phi_y \end{Bmatrix}, \quad \Phi_n = \begin{Bmatrix} \phi_n \\ \phi_s \end{Bmatrix}, \quad \mathbf{M}_n = \begin{Bmatrix} M_n \\ M_s \end{Bmatrix}, \quad \mathbf{D}_1 = \begin{Bmatrix} \frac{\partial}{\partial x} \\ \frac{\partial}{\partial y} \end{Bmatrix} \quad (12.3.12a)$$

$$\mathbf{D} = \begin{bmatrix} \frac{\partial}{\partial x} & 0 \\ 0 & \frac{\partial}{\partial y} \\ \frac{\partial}{\partial y} & \frac{\partial}{\partial x} \end{bmatrix}, \quad \mathbf{A} = \begin{bmatrix} A_{55} & 0 \\ 0 & A_{44} \end{bmatrix}, \quad \mathbf{C} = \begin{bmatrix} D_{11} & D_{12} & 0 \\ D_{12} & D_{22} & 0 \\ 0 & 0 & D_{66} \end{bmatrix} \quad (12.3.12b)$$

12.3.3 Finite Element Model

We note from the boundary integrals in (12.3.7a)–(12.3.7c) that the primary variables of the theory are (w, ϕ_x, ϕ_y) and the secondary variables are (Q_n, M_{nn}, M_{ns}) (or a linear combination of Q_x, Q_y, M_{xx}, M_{yy} , and M_{xy}). Therefore, the Lagrange interpolation of w , ϕ_x and ϕ_y is admissible for SDT.

We assume finite element interpolation of w , ϕ_x , and ϕ_y in the form

$$w(x, y, t) = \sum_{j=1}^n w_j(t) \psi_j^1(x, y) \\ \phi_x(x, y, t) = \sum_{j=1}^m S_j^x(t) \psi_j^2(x, y), \quad \phi_y(x, y, t) = \sum_{j=1}^m S_j^y(t) \psi_j^2(x, y) \quad (12.3.13)$$

or

$$w(x, y, t) = (\Psi^1)^T \mathbf{W}, \quad \Phi = \begin{Bmatrix} \phi_x \\ \phi_y \end{Bmatrix} = \Psi^2 \mathbf{S} \quad (12.3.14)$$

where

$$(\Psi^1)^T = \{\psi_1^1 \ \psi_2^1 \ \dots \ \psi_n^1\}, \quad \Psi^2 = \begin{bmatrix} \psi_1^2 & 0 & \psi_2^2 & \dots & \psi_n^2 & 0 \\ 0 & \psi_1^2 & 0 & \psi_2^2 & \dots & \psi_n^2 \end{bmatrix} \\ \mathbf{S}^T = \{S_1^x \ S_1^y \ S_2^x \ S_2^y \ \dots \ S_m^x \ S_m^y\}, \quad \mathbf{W}^T = \{w_1 \ w_2 \ w_3 \ \dots \ w_n\} \quad (12.3.15)$$

and ψ_j^1 and ψ_j^2 are interpolation functions used for w and (ϕ_x, ϕ_y) , respectively. In general, ψ_j^1 and ψ_j^2 are polynomials of different degree. However, in the present study, we take $\psi_j^1 = \psi_j^2 \equiv \psi_j$. This choice, as discussed for the Timoshenko beam element, requires the use of reduced integration for the evaluation of stiffness coefficients associated with the transverse shear strains.

Substituting (12.3.13) into (12.3.7a)–(12.3.7c), we obtain the finite element model in expanded form

$$\begin{aligned} & \left[\begin{array}{ccc} [M^{11}] & [0] & [0] \\ & [M^{22}] & [0] \\ \text{symmetric} & & [M^{33}] \end{array} \right] \left\{ \begin{array}{l} \{\ddot{w}\} \\ \{\ddot{S}^x\} \\ \{\ddot{S}^y\} \end{array} \right\} \\ & + \left[\begin{array}{ccc} [K^{11}] & [K^{12}] & [K^{13}] \\ & [K^{22}] & [K^{23}] \\ \text{symmetric} & & [K^{33}] \end{array} \right] \left\{ \begin{array}{l} \{w\} \\ \{S^x\} \\ \{S^y\} \end{array} \right\} = \left\{ \begin{array}{l} \{F^1\} \\ \{F^2\} \\ \{F^3\} \end{array} \right\} \quad (12.3.16) \end{aligned}$$

where

$$M_{ij}^{11} = I_0 M_{ij}, \quad M_{ij}^{22} = M_{ij}^{33} = I_2 M_{ij}, \quad M_{ij} = \int_{\Omega_e} \psi_i \psi_j \, dx \, dy$$

$$K_{ij}^{11} = \int_{\Omega_e} \left(A_{55} \frac{\partial \psi_i}{\partial x} \frac{\partial \psi_j}{\partial x} + A_{44} \frac{\partial \psi_i}{\partial y} \frac{\partial \psi_j}{\partial y} \right) dx \, dy$$

$$K_{ij}^{12} = \int_{\Omega_e} A_{55} \frac{\partial \psi_i}{\partial x} \psi_j \, dx \, dy$$

$$K_{ij}^{13} = \int_{\Omega_e} A_{44} \frac{\partial \psi_i}{\partial y} \psi_j \, dx \, dy$$

$$K_{ij}^{22} = \int_{\Omega_e} \left(D_{11} \frac{\partial \psi_i}{\partial x} \frac{\partial \psi_j}{\partial x} + D_{66} \frac{\partial \psi_i}{\partial y} \frac{\partial \psi_j}{\partial y} + A_{55} \psi_i \psi_j \right) dx \, dy$$

$$K_{ij}^{23} = \int_{\Omega_e} \left(D_{12} \frac{\partial \psi_i}{\partial x} \frac{\partial \psi_j}{\partial y} + D_{66} \frac{\partial \psi_i}{\partial y} \frac{\partial \psi_j}{\partial x} \right) dx \, dy$$

$$K_{ij}^{33} = \int_{\Omega_e} \left(D_{66} \frac{\partial \psi_i}{\partial x} \frac{\partial \psi_j}{\partial x} + D_{22} \frac{\partial \psi_i}{\partial y} \frac{\partial \psi_j}{\partial y} + A_{44} \psi_i \psi_j \right) dx \, dy$$

$$F_i^1 = \int_{\Omega_e} q \psi_i \, dx \, dy + \oint_{\Gamma_e} Q_n \psi_i \, ds$$

$$F_i^2 = \oint_{\Gamma_e} \hat{M}_{nn} \psi_i \, ds, \quad F_i^3 = \oint_{\Gamma_e} \hat{M}_{ns} \psi_i \, ds \quad (12.3.17)$$

The vector of the finite element model is obtained by substituting (12.3.14) into (12.3.11):

$$\left[\begin{array}{cc} \mathbf{M}^{11} & \mathbf{0} \\ \mathbf{0} & \mathbf{M}^{22} \end{array} \right] \left\{ \begin{array}{l} \ddot{\mathbf{W}} \\ \ddot{\mathbf{S}} \end{array} \right\} + \left[\begin{array}{cc} \mathbf{K}^{11} & \mathbf{K}^{12} \\ \mathbf{K}^{21} & \mathbf{K}^{22} \end{array} \right] \left\{ \begin{array}{l} \mathbf{W} \\ \mathbf{S} \end{array} \right\} = \left\{ \begin{array}{l} \mathbf{F}^1 \\ \mathbf{F}^2 \end{array} \right\} \quad (12.3.18)$$

where [see Eqs. (12.3.12a) and (12.3.12b) for the definitions of \mathbf{D} , \mathbf{D}_1 , etc.]

$$\begin{aligned} \mathbf{M}^{11} &= \int_{\Omega_e} I_0 \Psi^1 (\Psi^1)^T \, d\mathbf{x}, \quad \mathbf{M}^{22} = \int_{\Omega_e} I_2 (\Psi^2)^T (\Psi^2) \, d\mathbf{x} \\ \mathbf{K}^{11} &= \int_{\Omega_e} \mathbf{B}_1^T \mathbf{A} \mathbf{B}_1 \, d\mathbf{x}, \quad \mathbf{K}^{12} = \int_{\Omega_e} \mathbf{B}_1^T \mathbf{A} \Psi^2 \, d\mathbf{x} = (\mathbf{K}^{21})^T \\ \mathbf{K}^{22} &= \int_{\Omega_e} [(\Psi^2)^T \mathbf{A} \Psi^2 + \mathbf{B}^T \mathbf{C} \mathbf{B}] \, d\mathbf{x} \quad (12.3.19) \end{aligned}$$

$$\mathbf{F}^1 = \int_{\Omega_e} \Psi^1 q \, d\mathbf{x} + \oint_{\Gamma_e} \Psi^1 Q_n \, ds, \quad \mathbf{F}^2 = \oint_{\Gamma_e} (\Psi^2)^T \mathbf{M}_{nn} \, ds$$

$$\mathbf{B}_1 = \mathbf{D}_1 (\Psi^1)^T = \begin{bmatrix} \psi_{1,x}^1 & \psi_{2,x}^1 & \dots & \psi_{n,x}^1 \\ \psi_{1,y}^1 & \psi_{2,y}^1 & \dots & \psi_{n,y}^1 \end{bmatrix}_{(2 \times n)}$$

$$\mathbf{B} = \mathbf{D} \Psi^2 = \begin{bmatrix} \psi_{1,x}^2 & 0 & \psi_{2,x}^2 & 0 & \dots & \psi_{m,x}^2 & 0 \\ 0 & \psi_{1,y}^2 & 0 & \psi_{2,y}^2 & \dots & 0 & \psi_{m,y}^2 \\ \psi_{1,y}^2 & \psi_{1,x}^2 & \psi_{2,y}^2 & \psi_{2,x}^2 & \dots & \psi_{m,y}^2 & \psi_{m,x}^2 \end{bmatrix}_{(3 \times 2m)}$$

The element equations (12.3.16) and (12.3.18) both can be written in compact form as

$$\mathbf{M}\ddot{\Delta} + \mathbf{K}\Delta = \mathbf{F} \quad (12.3.20)$$

where $\Delta = [\mathbf{W} \ \mathbf{S}]^T$. The element stiffness matrix \mathbf{K} and mass matrix \mathbf{M} in (12.3.20) are of order $(n + 2m) \times (n + 2m)$, where n is the number of nodes per the Lagrange element used for w and m is the number of nodes per the Lagrange element used for ϕ_x and ϕ_y . The individual matrices in (12.3.18) have the following dimensions: \mathbf{M}^{11} is $n \times n$; \mathbf{M}^{22} is $2m \times 2m$; \mathbf{K}^{11} is $n \times n$; \mathbf{K}^{12} is $n \times 2m$; \mathbf{K}^{22} is $2m \times 2m$; \mathbf{F}^1 is $n \times 1$; and \mathbf{F}^2 is $2m \times 1$. When equal interpolation is used, $\psi_i^1 = \psi_i^2$, the four-node quadrilateral element has a total of 12 degrees of freedom and the nine-node quadrilateral element has 27 degrees of freedom (see Fig. 12.3.2).

12.3.4 Shear Locking and Reduced Integration

The transverse shear strains (i.e., terms involving A_{44} and A_{55}) in the element equations of SDT present computational difficulties when the side-to-thickness ratio, a/h , of the plate

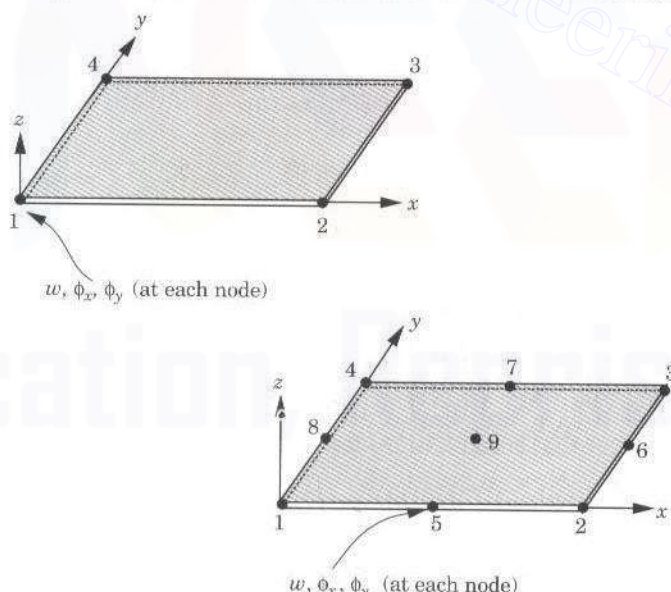


Figure 12.3.2 Linear and quadratic rectangular elements for SDT with three degrees of freedom (w, ϕ_x, ϕ_y) per node.

is large (i.e., when the plate becomes thin, say $a/h \geq 50$). For thin plates, the transverse shear strains $2\varepsilon_{xz} = \gamma_{xz} = \phi_x + \partial w/\partial x$ and $2\varepsilon_{yz} = \gamma_{yz} = \phi_y + \partial w/\partial y$ are negligible, and consequently the element stiffness matrix becomes stiff and yields erroneous results for the generalized displacements (w_i , S_i^x , S_i^y). This phenomenon is known as *shear locking*, and it can be interpreted as being caused by the inclusion of the following constraints into the variational form [see Reddy (1980) and Averill and Reddy (1990)]:

$$\phi_x + \frac{\partial w}{\partial x} = 0, \quad \phi_y + \frac{\partial w}{\partial y} = 0 \quad (12.3.21)$$

The energy due to transverse shear strains in the total potential energy of SDT is given by

$$\frac{1}{2} \int_{\Omega_e} \left[A_{44} \left(\phi_y + \frac{\partial w}{\partial y} \right)^2 + A_{55} \left(\phi_x + \frac{\partial w}{\partial x} \right)^2 \right] dx dy \quad (12.3.22)$$

The locking observed in the displacement finite element model of SDT is the result of the fact that the discrete form of (12.3.21) is not satisfied when the plate is very thin. Of course, when the plate is thick, the relations (12.3.21) do not have to be satisfied, and the locking does not occur (at least, it is not severe enough to give completely wrong results). However, for thin plates, the constraints (12.3.21) are valid but not satisfied in the numerical model, and we therefore face the same problem as in the Timoshenko beam finite element. Therefore, we use the same remedy as before: reduced integration to evaluate stiffness coefficients involving the transverse shear terms [see Zienkiewicz, et al. (1971) and Hughes, et al. (1977)]. For example, when a four-node rectangular element is used, the one-point Gauss rule should be used to evaluate the shear energy terms (i.e., terms involving A_{44} and A_{55}) while the two-point Gauss rule should be used for all other terms. When an eight- or nine-node rectangular element is used, the two- and three-point Gauss rules should be used to evaluate the shear and bending terms, respectively. For the triangular elements, we use one- and three-point integrations for transverse shear stiffnesses in the linear and quadratic elements, respectively. However, in the present study, we shall not consider triangular plate bending elements.

12.4 EIGENVALUE AND TIME-DEPENDENT PROBLEMS

The differential equations in (12.2.20) and (12.3.20) can be reduced to various special cases depending on the type of analysis. In both cases, the finite element equations have the same vector form, namely (12.3.20), facilitating the discussion of the eigenvalue and transient analysis for both CPT and SDT.

Static Analysis

For static analysis, we set the inertia term $\{\ddot{\Delta}\}$ equal to zero and solve the problem

$$\mathbf{K}^e \boldsymbol{\Delta}^e = \mathbf{F}^e \quad (12.4.1)$$

Natural Vibration

For natural vibration problems, we replace the inertia term by

$$\ddot{\boldsymbol{\Delta}}^e = -\omega^2 \boldsymbol{\Delta}_0^e \quad (\text{or } \boldsymbol{\Delta}^e = \boldsymbol{\Delta}_0^e e^{-i\omega t}) \quad (12.4.2)$$

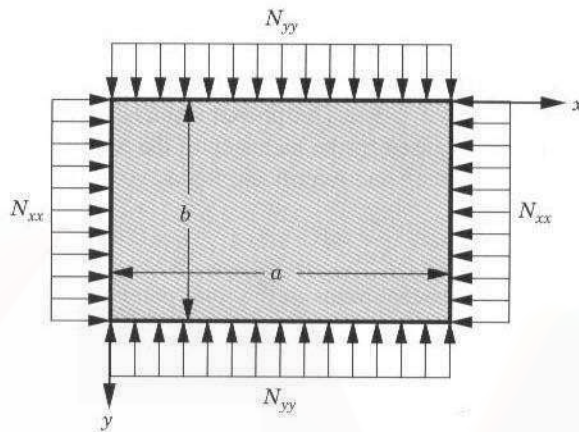


Figure 12.4.1 Biaxial compression of a rectangular plate.

Then Eq. (12.3.20) takes the form of an eigenvalue problem:

$$(\mathbf{K}^e - \omega^2 \mathbf{M}^e) \Delta_0^e = \mathbf{0} \quad (12.4.3)$$

Buckling Analysis

For buckling analysis (i.e., to determine the value of the in-plane compressive forces at which the plate buckles; also see Fig. 12.4.1), we replace the mass matrix in (12.4.3) with the stability matrix \mathbf{G} and ω^2 with the buckling load λ . This expression comes from the in-plane force due to the nonlinear inplane strains (underlined):

$$\begin{aligned} \underline{\varepsilon_{xx}} &= \frac{1}{2} \left(\frac{\partial w}{\partial x} \right)^2 - z \frac{\partial^2 w}{\partial x^2}, & \underline{\varepsilon_{yy}} &= \frac{1}{2} \left(\frac{\partial w}{\partial y} \right)^2 - z \frac{\partial^2 w}{\partial y^2} \\ \underline{2\varepsilon_{xy}} &= \frac{\partial w}{\partial x} \frac{\partial w}{\partial y} - 2z \frac{\partial^2 w}{\partial x \partial y} \end{aligned} \quad (12.4.4)$$

For CPT, \mathbf{G} is given by

$$G_{ij} = \int_{\Omega_e} \left[\bar{N}_{xx} \frac{\partial \varphi_i}{\partial x} \frac{\partial \varphi_j}{\partial x} + \bar{N}_{yy} \frac{\partial \varphi_i}{\partial y} \frac{\partial \varphi_j}{\partial y} + \bar{N}_{xy} \left(\frac{\partial \varphi_i}{\partial x} \frac{\partial \varphi_j}{\partial y} + \frac{\partial \varphi_i}{\partial y} \frac{\partial \varphi_j}{\partial x} \right) \right] dx dy \quad (12.4.5)$$

where \bar{N}_{xx} , \bar{N}_{yy} , and \bar{N}_{xy} are the applied in-plane force resultants. The eigenvalue λ represents the ratio of the actual buckling load to the applied in-plane forces:

$$\lambda = \frac{N_{xx}}{\bar{N}_{xx}} = \frac{N_{yy}}{\bar{N}_{yy}} = \frac{N_{xy}}{\bar{N}_{xy}} \quad (12.4.6)$$

For SDT, only \mathbf{M}^{11} [see Eq. (12.3.18)] is replaced by \mathbf{G} , where

$$G_{ij} = \int_{\Omega_e} \left[\bar{N}_{xx} \frac{\partial \psi_i}{\partial x} \frac{\partial \psi_j}{\partial x} + \bar{N}_{yy} \frac{\partial \psi_i}{\partial y} \frac{\partial \psi_j}{\partial y} + \bar{N}_{xy} \left(\frac{\partial \psi_i}{\partial x} \frac{\partial \psi_j}{\partial y} + \frac{\partial \psi_i}{\partial y} \frac{\partial \psi_j}{\partial x} \right) \right] dx dy \quad (12.4.7)$$

and \mathbf{M}^{22} is set equal to zero. Hence, the stability matrix is non-positive-definite, requiring special eigenvalue solvers for SDT.

Transient Analysis

To solve a time-dependent problem, we must approximate the time derivatives in (12.2.20) or (12.3.20) to obtain algebraic equations relating solution Δ_{s+1} at time $t + \Delta t$ to solution Δ_s at time t , where Δt is the time step. In the Newmark integration scheme (see Section 6.2.4), the vectors Δ_{s+1} and $\ddot{\Delta}_{s+1}$ at time $t = (s + 1)\Delta t$ are approximated by the expressions

$$\begin{aligned}\dot{\Delta}_{s+1} &= \dot{\Delta}_s + a_1 \ddot{\Delta}_s + a_2 \ddot{\Delta}_{s+1} \\ \Delta_{s+1} &= \Delta_s + \dot{\Delta}_s \Delta t + \frac{1}{2}[(1 - \gamma)\ddot{\Delta}_s + \gamma \ddot{\Delta}_{s+1}](\Delta t)^2\end{aligned}\quad (12.4.8)$$

where $a_1 = (1 - \alpha)\Delta t$ and $a_2 = \alpha\Delta t$, (α and γ are parameters that control the accuracy and stability of the scheme), and the subscript s indicates that the vectors are evaluated at the s th time step (i.e., at time $t = s\Delta t$).

Rearranging (12.3.20) and (12.4.8), we obtain

$$\hat{\mathbf{K}}_{s+1} \Delta_{s+1} = \hat{\mathbf{F}}_{s,s+1} \quad (12.4.9a)$$

where

$$\begin{aligned}\hat{\mathbf{K}}_{s+1} &= \mathbf{K}_{s+1} + a_3 \mathbf{M}_{s+1} \\ \hat{\mathbf{F}}_{s,s+1} &= \mathbf{F}_{s+1} + \mathbf{M}_{s+1}(a_3 \Delta_s + a_4 \dot{\Delta}_s + a_5 \ddot{\Delta}_s) \\ a_3 &= \frac{2}{\gamma(\Delta t)^2}, \quad a_4 = a_3 \Delta t, \quad a_5 = \frac{1}{\gamma} - 1\end{aligned}\quad (12.4.9b)$$

Once the solution Δ_{s+1} at time $t_{s+1} = (s + 1)\Delta t$ is known, the velocity and acceleration at t_{s+1} are computed from

$$\begin{aligned}\ddot{\Delta}_{s+1} &= a_3(\Delta_{s+1} - \Delta_s) - a_4 \dot{\Delta}_s - a_5 \ddot{\Delta}_s, \\ \dot{\Delta}_{s+1} &= \dot{\Delta}_s + a_1 \ddot{\Delta}_s + a_2 \ddot{\Delta}_{s+1}\end{aligned}\quad (12.4.10)$$

12.5 EXAMPLES

Here we consider several numerical examples of rectangular plates with different boundary conditions. We will use the conforming CPT(C) and nonconforming CPT(N) rectangular elements and the linear and quadratic SDT elements to present numerical results. Various types of boundary conditions on an edge of a plate element are given in Eqs. (12.2.12) and (12.3.9) for CPT and SDT, respectively. When the edge is parallel to the x (or y) axis, the normal and tangential components of a variable become the y and x (or x and y) components, respectively, of the variable. For CPT, ϕ_n and ϕ_s of SDT must be replaced with $-\partial w/\partial n$ and $-\partial w/\partial s$, respectively. In all cases, the stresses are computed at the reduced Gauss points.

The first example deals with the bending of a simply supported plate using CPT and SDT. The effect of reduced integration on the deflections and stresses of a simply supported plate as computed using the SDT plate element is investigated.

Example 12.5.1

Consider a simply supported, isotropic ($\nu = 0.25$), square plate subjected to a uniformly distributed transverse load of intensity q_0 . We shall solve the problem using CPT and SDT plate bending elements. Owing to the biaxial symmetry, we need to model only a quadrant of the plate. The essential (i.e., geometric) boundary conditions at simply supported edges ($x = \frac{1}{2}a$ and $y = \frac{1}{2}a$), for SDT, are (see Fig. 12.5.1)

$$\begin{aligned} w &= 0, \quad \phi_y = 0 \quad \text{at} \quad x = a/2 \\ w &= 0, \quad \phi_x = 0 \quad \text{at} \quad y = a/2 \end{aligned} \quad (12.5.1)$$

The essential boundary conditions along the symmetry lines ($x = 0$ and $y = 0$) are

$$\phi_x(0, y) = \phi_y(x, 0) = 0 \quad (12.5.2)$$

The natural (i.e., force) boundary conditions, which enter the finite element equations through the forces $\{F\}$, are

$$\begin{aligned} Q_u &= 0 \quad \text{along} \quad x = 0 \quad \text{and} \quad y = 0 \\ M_{xx} &= 0 \quad \text{along} \quad y = 0 \quad \text{and} \quad x = a/2 \\ M_{yy} &= 0 \quad \text{along} \quad x = 0 \quad \text{and} \quad y = a/2 \end{aligned} \quad (12.5.3)$$

The essential boundary conditions for a quadrant, when using the CPT element, are shown in Fig. 12.5.1.

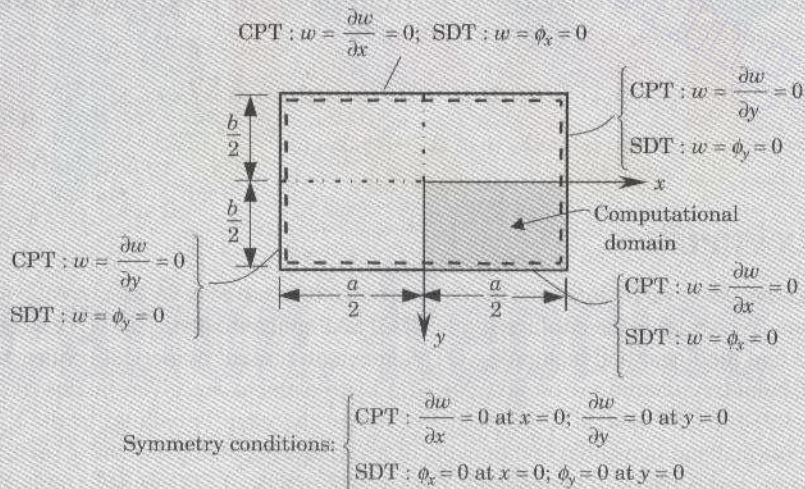


Figure 12.5.1 Geometry and coordinate system used for a rectangular plate. Boundary and symmetry conditions in CPT and SDT for simply supported plates.

For a linear (four-node) rectangular element of SDT, the contribution of a uniformly distributed load q_0 is given by

$$f_i = \int_0^{h_x} \int_0^{h_y} q_0 \psi_i \, dx \, dy = \frac{1}{4} h_x h_y q_0 \quad (12.5.4)$$

where h_x and h_y are the plane-form dimensions of the element. This contribution goes to the first, fourth, seventh, and tenth nodal degrees of freedom of the element (corresponding to w). For CPT, the nodal forces due to the uniform transverse load of intensity q_0 are computed using the definition

$$f_i = \int_{\Omega_e} q_0 \varphi_i \, dx \, dy \quad (12.5.5)$$

The effect of reduced integration, thickness, and mesh on the center deflection and normal stress σ_{xx} is investigated, and the results are presented in Table 12.5.1. The displacement and stress are nondimensionalized as

$$\bar{w} = \frac{w(0, 0) E h^3 \times 10^2}{q_0 a^4}, \quad \bar{\sigma}_{xx} = \left(\frac{h}{a}\right)^2 \frac{1}{q_0} \sigma_{xx} \left(A, A, \pm \frac{1}{2}h\right) \quad (12.5.6)$$

where A is the Gauss-point location with respect to the (x, y) system located at the center of the plate (see Fig. 12.5.1). Q4 denotes the four-node rectangular element, and Q9

Table 12.5.1 The effect of reduced integration, thickness, and mesh refinement on the center deflections and stresses† of a simply supported, isotropic ($v = 0.25$), square plate under a uniform transverse load of intensity q_0 (Example 12.5.1).

a/h	Integ.	1 × 1		2 × 2		4 × 4		2 × 2		Exact‡	
		Linear	\bar{w}	Linear	\bar{w}	Linear	\bar{w}	Quadratic	\bar{w}	Exact	\bar{w}
10	F	0.964	0.018	2.474	0.119	3.883	0.216	4.770	0.290	4.791	0.276
	M	3.950	0.095	4.712	0.235	4.773	0.266	4.799	0.272		
20	F	0.270	0.005	0.957	0.048	2.363	0.138	4.570	0.268	4.625	0.276
	M	3.669	0.095	4.524	0.235	4.603	0.266	4.633	0.272		
40	F	0.070	0.001	0.279	0.014	0.944	0.056	4.505	0.270	4.584	0.276
	M	3.599	0.095	4.375	0.235	4.560	0.266	4.592	0.271		
50	F	0.005	0.000	0.182	0.009	0.652	0.039	4.496	0.267	4.579	0.276
	M	3.590	0.095	4.472	0.235	4.555	0.266	4.587	0.271		
100	F	0.011	0.000	0.047	0.002	0.182	0.011	4.482	0.266	4.572	0.276
	M	3.579	0.095	4.465	0.235	4.548	0.266	4.580	0.272		
CPT(N)		5.643	0.260	4.857	0.274	4.643	0.276	—	—	4.570	0.276
CPT(C)		4.638	0.262	4.574	0.272	4.570	0.275	—	—	4.570	0.276

† $\bar{w} = w E h^3 \times 10^2 / q_0 a^4$, $\bar{\sigma}_x = \sigma_x (A, A, \pm h) h^2 / q_0 a^2$, $A = \frac{1}{4} a (1 \times 1 \text{ linear})$, $\frac{1}{8} a (2 \times 2 \text{ linear})$, $\frac{1}{16} a (4 \times 4 \text{ linear})$, $0.05283 a$ (2×2 quadratic).

‡ From Reddy (2002).

the nine-node rectangular element. The Gauss point locations for various meshes are given below.

$2 \times 2Q4$	$4 \times 4Q4$	$2 \times 2Q9$
$0.125a$	$0.0625a$	$0.05283a$

In Table 12.5.1, F denotes full integration for all terms, and M denotes mixed integration: full integration for bending terms and reduced integration for the shear terms. The following observations can be made from the results of Table 12.5.1:

1. The nine-node element gives virtually the same results for full (3×3 Gauss rule) and mixed (3×3 and 2×2 Gauss rules for bending and shear terms, respectively) integrations. However, the results obtained using the mixed integration are closest to the exact solution.
2. Full integration gives less accurate results than mixed integration, and the error increases with an increase in side-to-thickness ratio (a/h). This implies that mixed integration is essential for thin plates, especially when modeled by lower-order elements.
3. Full integration results in smaller errors for quadratic elements and refined meshes than for linear elements and/or coarser meshes.
4. The conforming plate finite element CPT(C) gives more accurate results when compared with the nonconforming plate element CPT(N).

The next example deals with a clamped square plate under a distributed transverse load. The mixed integration rule is used in the evaluation of stiffness coefficients of the SDT model.

Example 12.5.2

Consider an isotropic ($\nu = 0.3$) square plate under a uniform load of intensity q_0 . We shall consider clamped boundary conditions (see Fig. 12.5.2). Note that, for the case of the conforming displacement model based on CPT, we must also specify the boundary conditions on the cross-derivative $\partial^2 w / \partial x \partial y$. Once again, we exploit the biaxial symmetry and model only a quadrant of the plate.

The center deflection $\bar{w} = w(0, 0)D \times 10^2/q_0a^4$ [where $D = Eh^3/12(1 - \nu^2)$] and center normal stress $\sigma_z = \sigma_z(A, A) \times 10/q_0$ as obtained using uniform meshes of the two types of elements, CPT(N) and CPT(C), are presented in Table 12.5.2. In both models, the values of A used are given in the following table.

Element type	Location A			
	1×1	2×2	4×4	8×8
Mesh for CPT & SDT(L)				
Mesh for SDT(Q)		1×1	2×2	4×4
CPT model	0.05635a	0.02817a	0.01409a	0.03125a
SDT model	linear	0.25a	0.125a	0.0625a
	quadratic	—	0.1057a	0.0528a
				0.02642a

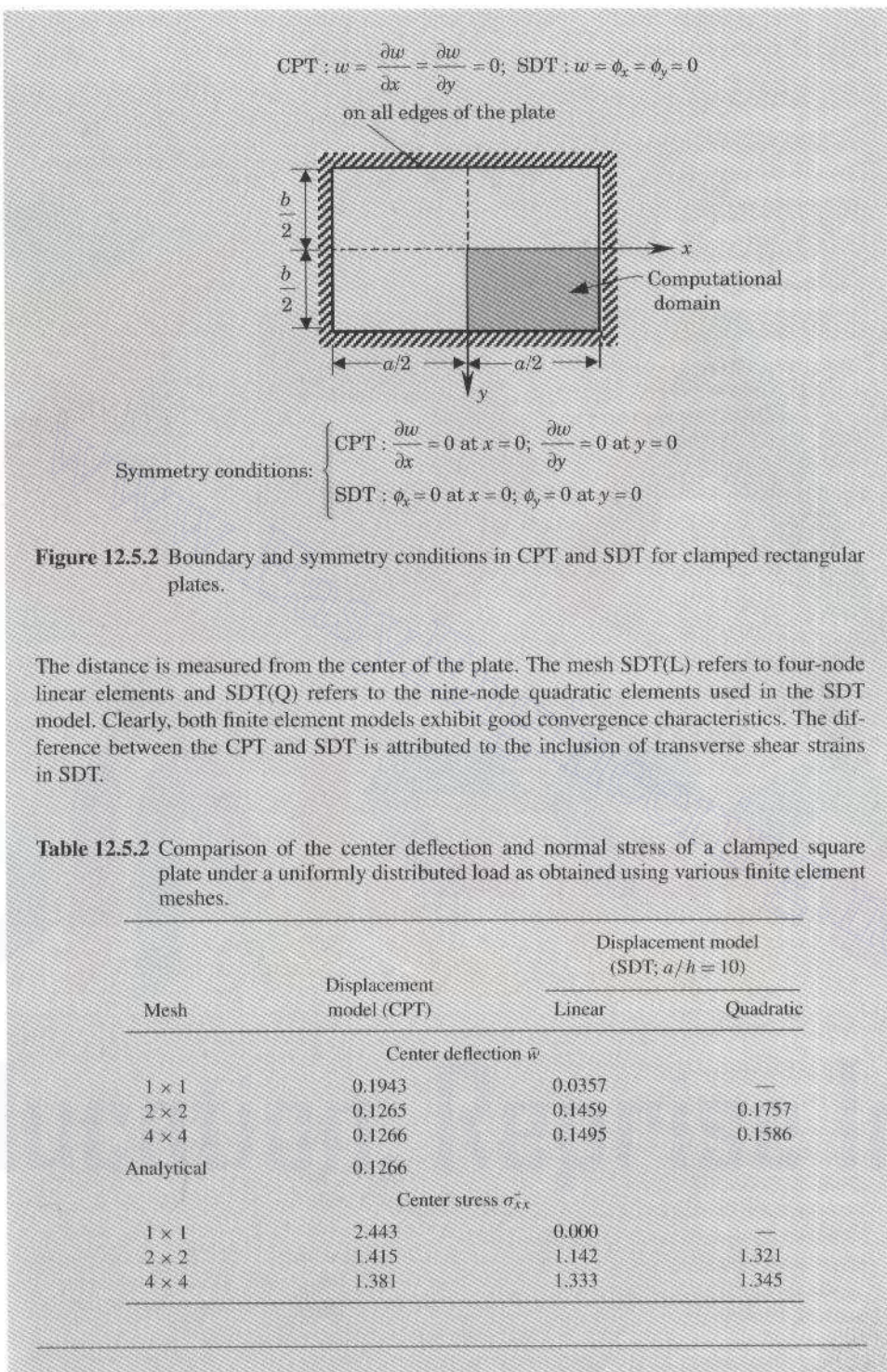


Figure 12.5.2 Boundary and symmetry conditions in CPT and SDT for clamped rectangular plates.

The distance is measured from the center of the plate. The mesh SDT(L) refers to four-node linear elements and SDT(Q) refers to the nine-node quadratic elements used in the SDT model. Clearly, both finite element models exhibit good convergence characteristics. The difference between the CPT and SDT is attributed to the inclusion of transverse shear strains in SDT.

Table 12.5.2 Comparison of the center deflection and normal stress of a clamped square plate under a uniformly distributed load as obtained using various finite element meshes.

Mesh	Displacement model (CPT)	Displacement model (SDT; $a/h = 10$)	
		Linear	Quadratic
Center deflection \bar{w}			
1 × 1	0.1943	0.0357	—
2 × 2	0.1265	0.1459	0.1757
4 × 4	0.1266	0.1495	0.1586
Analytical	0.1266		
Center stress σ_{xx}^*			
1 × 1	2.443	0.000	—
2 × 2	1.415	1.142	1.321
4 × 4	1.381	1.333	1.345

The next example deals with a simply supported orthotropic plate under a uniformly distributed transverse load.

Example 12.5.3

Here we consider an orthotropic square plate with the following material (graphite-epoxy) properties ($\nu_{21} = \nu_{12} E_2 / E_1$, $\text{Mpsi} = 10^6 \text{ psi}$):

$$E_1 = 31.8 \text{ Mpsi}, \quad E_2 = 1.02 \text{ Mpsi}, \quad \nu_{12} = 0.31, \quad G_{12} = G_{23} = G_{13} = 0.96 \text{ Mpsi} \quad (12.5.7)$$

The nondimensionalized center deflection \bar{w} and normal stress $\bar{\sigma}_{xx}$ obtained using the conforming CPT(C) element and the SDT element are compared in Table 12.5.3.

Table 12.5.3 Comparison of the center deflection [$\bar{w} = w \times 10^3 (H/q_0 a^4)$] and normal stress [$\bar{\sigma}_{xx} = \sigma_{xx} \times 10(h^2/q_0 a^2)$] of a graphite-epoxy, simply supported square plate under a uniform transverse load (Example 12.5.3).

Mesh	Displacement model (CPT)	Displacement model (SDT; $a/h = 10$)	
		Linear	Quadratic
Center deflection \bar{w}			
2 × 2	0.9220	1.2545	1.2715
4 × 4	0.9224	1.2186	1.2147
8 × 8	0.9224	1.2152	1.2147
Exact [†]	0.9225		1.215
Center stress $\bar{\sigma}_{xx}$			
2 × 2	7.678	6.277	7.192
4 × 4	7.616	7.256	7.399
8 × 8	7.600	7.449	7.478
Exact [†]	7.595		7.512

[†]From Reddy (2002); $H = D_{12} + 2D_{66}$.

The next example deals with natural vibration of the plate of Example 12.5.1.

Example 12.5.4

Consider the simply supported, isotropic, square plate of Example 12.5.1. We wish to determine the natural frequencies of the plate. Once again, a quadrant of the plate is used as the computational domain to obtain the first few symmetric natural frequencies. To obtain all the frequencies (i.e., symmetric as well as antisymmetric), we must use the full plate model. The geometric boundary conditions used are shown in Fig. 12.5.1.

The natural frequencies of the simply supported plate, obtained using various meshes of CPT and SDT elements, are presented in Table 12.5.4. It is clear that CPT overpredicts the natural frequencies for the side-to-thickness ratio of $a/h = 10$ (i.e., thick plate) when compared to SDT. The difference is attributed to the inclusion of transverse shear strains, γ_{xz} and γ_{yz} , in SDT. In other words, the normality assumption (or neglecting transverse shear strains) in CPT amounts to overestimating the stiffness of the plate.

Table 12.5.4 The first three symmetric vibrational frequencies ($\bar{\omega} \times 10^{-2}$)ⁱ of an isotropic, simply supported square plate obtained using CPT and SDT ($a/h = 10$).

Theory	Mesh	$\bar{\omega}_{11}$	$\bar{\omega}_{13}$	$\bar{\omega}_{33}$
SDT	1×1 Q4	0.0746	—	—
	2×2 Q4	0.0608	0.4473	0.4810
	4×4 Q4	0.0579	0.2913	0.4654
	1×1 Q9	0.0575	0.4030	0.5476
	3×2 Q9	0.0570	0.2651	0.4342
	Exact	0.0569	0.2552	0.4217
CPT(N)	1×1	0.0535	0.3118	0.3565
CPT(C)	1×1	0.0597	0.2912	0.3360
CPT(N)	2×2	0.0567	0.2762	0.4406
CPT(C)	2×2	0.0584	0.4842	0.4842
CPT(N)	4×4	0.0579	0.2792	0.4665
CPT(C)	4×4	0.0584	0.2821	0.4900
Exact		0.0584	0.2829	0.4943

ⁱ $\bar{\omega} = \omega(\rho/E)^{1/2} a^2/h$.

The final example deals with the transient response of an isotropic plate subjected to a sudden uniform patch loading at the center of the plate (an idealization of impact load).

Example 12.5.5

Consider an isotropic ($\nu = 0.3$, $\rho = 1.0$), simply supported, rectangular plate ($a/b = \sqrt{2}$, $h/b = 0.2$) under a suddenly applied, uniformly distributed load on a square ($c/b = 0.4$) area at the center (see Fig. 12.5.3):

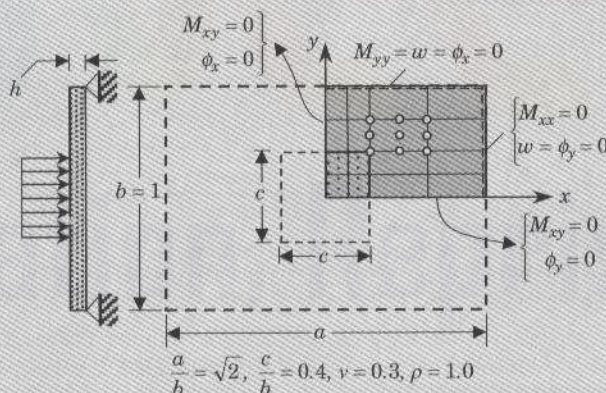


Figure 12.5.3 Domain, boundary conditions, and finite element mesh for the bending of a rectangular plate under a suddenly applied pulse loading at the central square area.

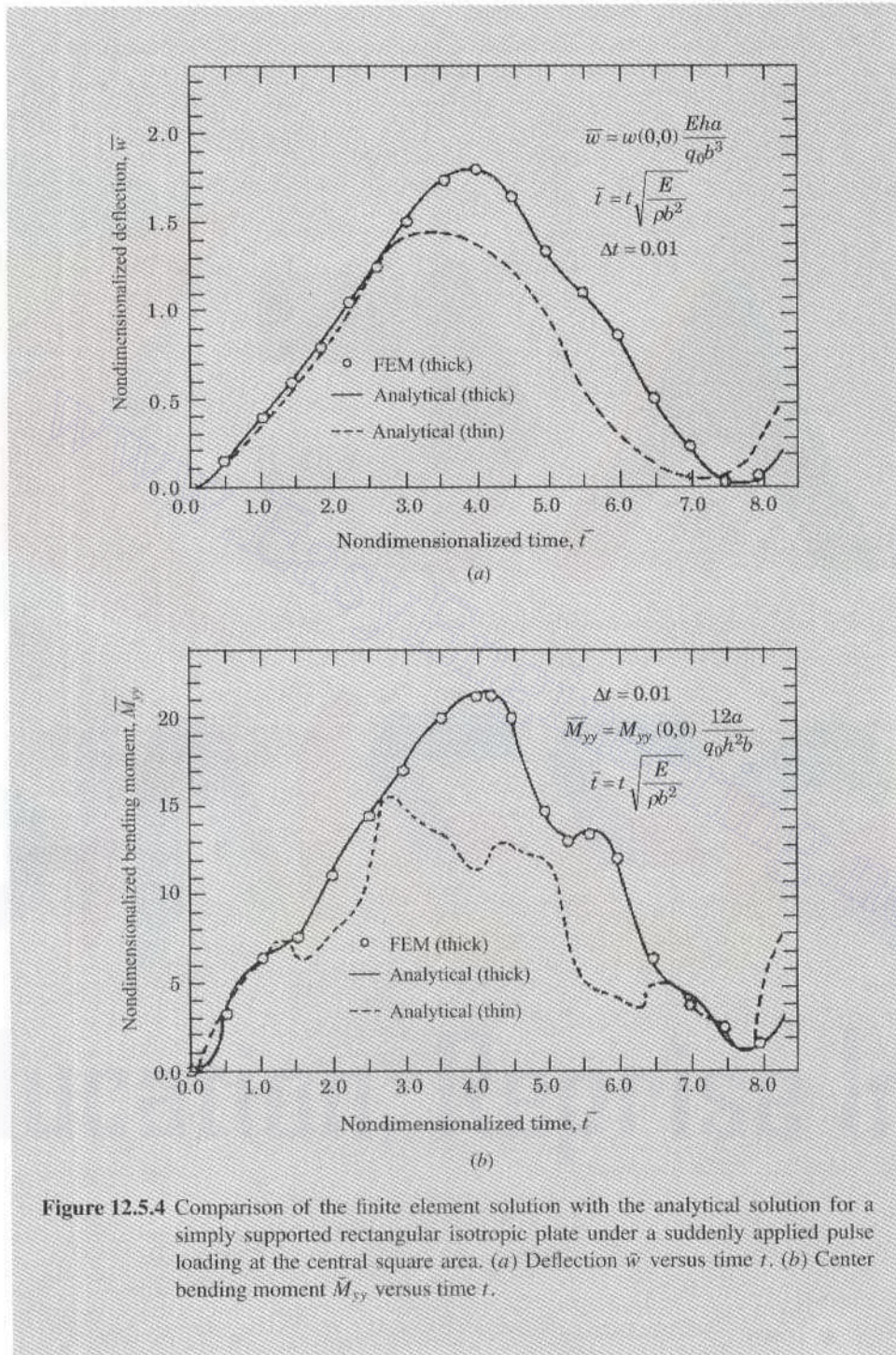


Figure 12.5.4 Comparison of the finite element solution with the analytical solution for a simply supported rectangular isotropic plate under a suddenly applied pulse loading at the central square area. (a) Deflection \bar{w} versus time \bar{t} . (b) Center bending moment \bar{M}_{yy} versus time \bar{t} .

$$a/b = \sqrt{2}, \quad \Delta t = 0.01$$

$$q(x, y, t) = q_0(x, y)H(t) \quad \text{where} \quad q_0(x, y) = \begin{cases} 1 & \text{for } 0 < x, y \leq 0.2 \\ 0 & \text{for } x, y > 0.2 \end{cases} \quad (12.5.8)$$

and $H(t)$ is the Heaviside unit step function. The geometry and boundary conditions are shown in Fig. 12.5.3. A nonuniform mesh of 4×4 nine-node shear deformation elements is used in a quadrant of the plate.

The center deflection and bending moments of the present linear analysis are compared with the analytical thick- and thin-plate solutions of Reismann and Lee (1969) in Fig. 12.5.4. We note significant difference between the solutions of the two theories. The present finite element solutions for the center deflection and bending moment are in excellent agreement with the thick-plate solution of Reismann and Lee (1969). Since the bending moment in the finite element method is calculated at the Gauss points, it is not expected to match exactly with the analytical solution at the center of the plate.

12.6 SUMMARY

Finite element models of the CPT and SDT have been developed in this chapter. C^1 continuity of the transverse deflection w (i.e., the deflection and its derivatives are continuous between elements) is required in CPT, whereas C^0 continuity (i.e., only the variables are continuous between elements) of the generalized displacements (w, ϕ_x, ϕ_y) is required in SDT. Triangular and rectangular elements with C^1 continuity have been discussed. Two four-node rectangular elements, one with $(w, \partial w / \partial x, \partial w / \partial y)$ and another with $(w, \partial w / \partial x, \partial w / \partial y, \partial^2 w / \partial x \partial y)$ as degrees of freedom, have been presented for CPT. The first one is a nonconforming element that does not satisfy continuity of the normal derivative along element sides, and the second is a conforming element. Linear and quadratic rectangular elements of SDT have been developed. They require selective evaluation of the stiffness coefficients. The bending stiffness coefficients are evaluated using full integration, and the transverse shear stiffness coefficients are evaluated using reduced integration to avoid the shear locking that occurs when these elements are used to model thin plates. Finite element equations of vibration, stability, and static and dynamic responses have been developed and numerical results are presented.

PROBLEMS

- 12.1** Investigate the displacement and slope compatibility of the nonconforming rectangular element CPT(N). *Hint:* Use the edge connecting nodes 1 and 2 and check if the displacement w and slopes $\partial w / \partial x$ and $\partial w / \partial y$ are continuous.
- 12.2–12.10** For the plate bending problems (CPT and SDT) given in Figs. P12.2–P12.10, give the specified primary and secondary degrees of freedom and their values for the meshes shown. The dashed lines in the figures indicate simply supported boundary conditions. You are required to give values of the loads for at least a couple of representative loads.

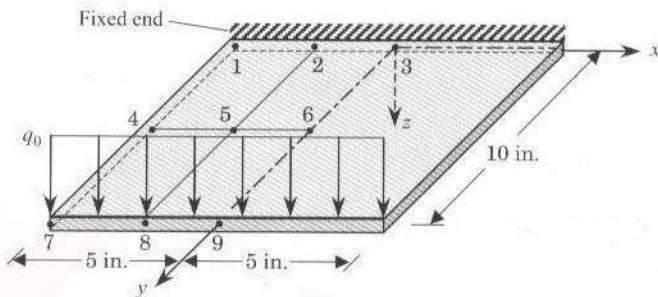
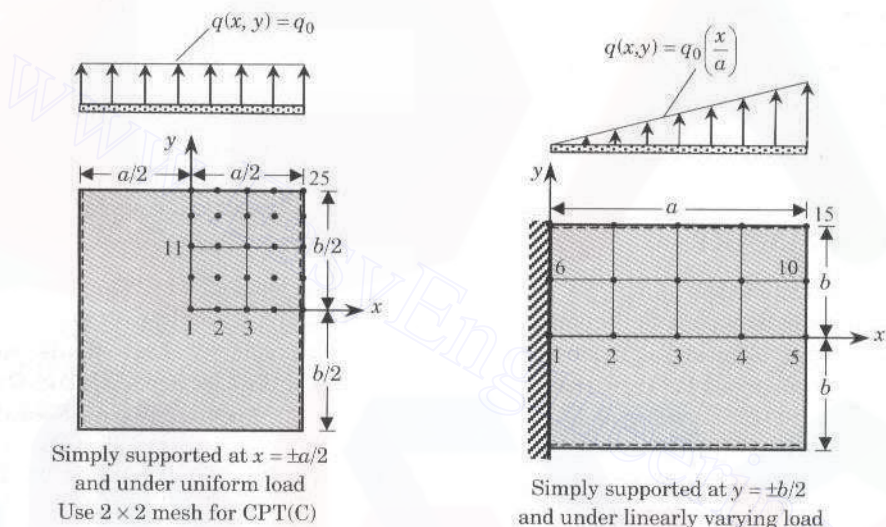


Figure P12.2

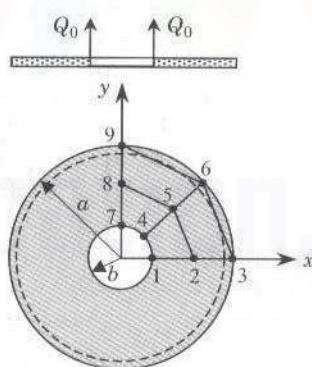


Simply supported at $x = \pm a/2$
and under uniform load
Use 2×2 mesh for CPT(C)

Simply supported at $y = \pm b/2$
and under linearly varying load

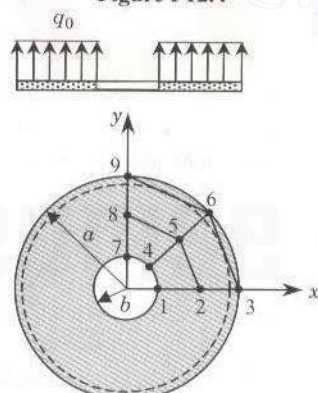
Figure P12.3

Figure P12.4



Simply supported at $r = a$
and under line load at $r = b$

Figure P12.5



Simply supported at $r = a$
and under uniform load

Figure P12.6

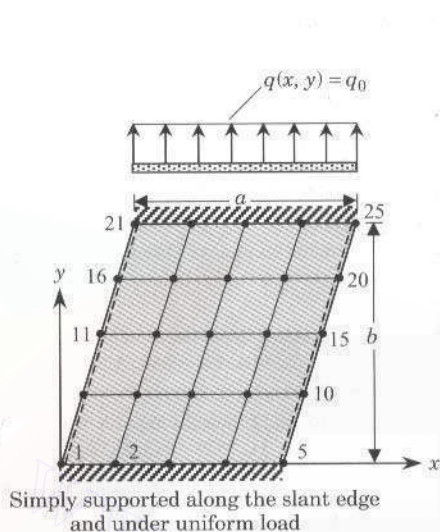


Figure P12.7

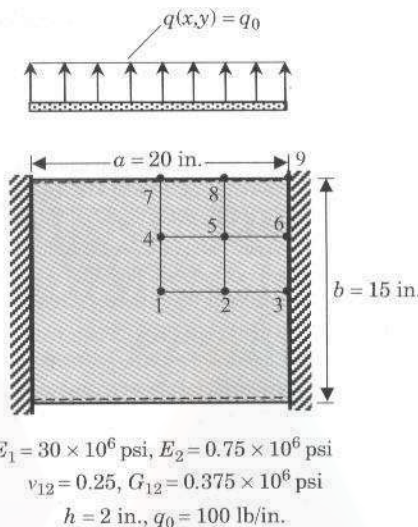


Figure P12.8

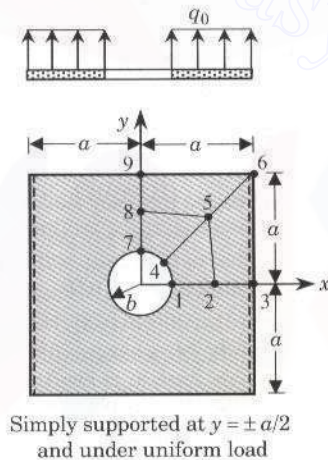


Figure P12.9

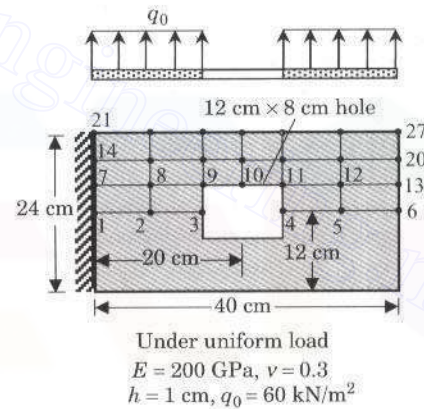


Figure P12.10

REFERENCES FOR ADDITIONAL READING

1. Averill, R. C. and Reddy, J. N., "On the Behavior of Plate Elements Based on the First-Order Shear Deformation Theory," *Engineering Computations*, **7**(1), 57–74, 1990.
2. Bathe, K. J. and Dvorkin, E. N., "A Four-Node Plate Bending Element Based on Mindlin/Reissner Plate Theory and a Mixed Interpolation," *International Journal for Numerical Methods in Engineering*, **21**, 367–383, 1985.
3. Bazeley, G. P., Cheung, Y. K., Irons, B. M., and Zienkiewicz, O. C., "Triangular Elements in Plate Bending—Conforming and Non-Conforming Solutions," *Proceedings of the First Conference on Matrix Methods in*

- Structural Mechanics*, AFFDL-TR-66-80, Air Force Institute of Technology, Wright-Patterson Air Force Base, Ohio, 547-576, 1965.
4. Belytschko, T., Tsay, C. S., and Liu, W. K., "Stabilization Matrix for the Bilinear Mindlin Plate Element," *Computer Methods in Applied Mechanics and Engineering*, **29**, 313-327, 1981.
 5. Bogner, F. K., Fox, R. L., and Schmidt, Jr. L. A., "The Generation of Inter-Element-Compatible Stiffness and Mass Matrices by the Use of Interpolation Formulas," *Proceedings of the First Conference on Matrix Methods in Structural Mechanics*, AFFDL-TR-66-80, Air Force Institute of Technology, Wright-Patterson Air Force Base, Ohio, 397-443, 1965.
 6. Clough, R. W. and Felippa, C. A., "A Refined Quadrilateral Element for Analysis of Plate Bending," *Proceedings of the Second Conference on Matrix Methods in Structural Mechanics*, Air Force Institute of Technology, Wright-Patterson Air Force Base, Ohio, 399-440, 1968.
 7. Clough, R. W. and Tocher, J. L., "Finite Element Stiffness Matrices for Analysis of Plate Bending," *Proceedings of the First Conference on Matrix Methods in Structural Mechanics*, AFFDL-TR-66-80, Air Force Institute of Technology, Wright-Patterson Air Force Base, Ohio, 515-545, 1965.
 8. Hughes, T. J. R., Taylor, R. L., and Kanoknukulchai, W., "A Simple and Efficient Finite Element for Plate Bending," *International Journal for Numerical Methods in Engineering*, **11**, 1529-1543, 1977.
 9. Hughes, T. J. R., Cohen, M., and Haroun, M., "Reduced and Selective Integration Techniques in the Finite Element Analysis of Plates," *Nuclear Engineering and Design*, **46**, 203-222, 1978.
 10. Melosh, R. J., "Basis of Derivation of Matrices for the Direct Stiffness Method," *AIAA Journal*, **1**, 1631-1637, 1963.
 11. Reddy, J. N., "A Penalty Plate-Bending Element for the Analysis of Laminated Anisotropic Composite Plates," *International Journal for Numerical Methods in Engineering*, **15**(8), 1187-1206, 1980.
 12. Reddy, J. N., "On the Solutions to Forced Motions of Rectangular Composite Plates," *Journal of Applied Mechanics*, **49**, 403-408, 1982.
 13. Reddy, J. N., *Theory and Analysis of Elastic Plates*, Taylor and Francis, Philadelphia, PA, 1999.
 14. Reddy, J. N., *Energy Principles and Variational Methods in Applied Mechanics*, 2nd ed., John Wiley, New York, 2002.
 15. Reddy, J. N., *Mechanics of Laminates Composite Plates and Shells: Theory and Analysis*, CRC Press, 2nd ed., Boca Raton, FL, 2004a.
 16. Reddy, J. N., *An Introduction to Nonlinear Finite Element Analysis*, Oxford University Press, Oxford, UK, 2004b.
 17. Reismann, H. and Lee, Y., "Forced Motions of Rectangular Plates," in *Developments in Theoretical and Applied Mechanics*, Vol. 4, Frederick, D. (ed.), Pergamon Press, New York, pp. 3-18, 1969.
 18. Tsay, C. S. and Reddy, J. N., "Bending, Stability, and Free Vibration of Thin Orthotropic Plates by Simplified Mixed Finite Elements," *Journal of Sound and Vibration*, **59**, 307-311, 1978.
 19. Zienkiewicz, O. C. and Cheung, Y. K., "The Finite Element Method for Analysis of Elastic Isotropic and Orthotropic Slabs," *Proceeding of the Institute of Civil Engineers*, London, **28**, 471-488, 1964.
 20. Zienkiewicz, O. C., Taylor, R. L., and Too, J. M., "Reduced Integration Technique in General Analysis of Plates and Shells," *International Journal for Numerical Methods in Engineering*, **3**, 275-290, 1971.

Chapter 13

COMPUTER IMPLEMENTATION OF TWO-DIMENSIONAL PROBLEMS

13.1 INTRODUCTION

In Chapter 7, we discussed some basic ideas concerning the development of a typical finite element program, and the use of **FEM1D** in the solution of one-dimensional problems was illustrated via many example problems. Specific details of various logical units of a finite element program for one-dimensional problems were given. Most of the ideas presented there are also valid for two-dimensional problems. The imposition of the boundary conditions and the solution of the equations remain the same as in one-dimensional problems. Here we focus attention on the computer implementation of two-dimensional elements. The use of a model program **FEM2D** is discussed. The program **FEM2D** contains linear and quadratic triangular and rectangular elements, and it can be used for the solution of heat conduction and convection problems, laminar flows of viscous incompressible fluids using the penalty function formulation, plane elasticity problems, and plate-bending problems using classical and shear deformation theories. A flow chart of **FEM2D** is given in Fig. 13.1.1.

In two dimensions, the element calculations are more involved than in one dimension, owing to the following considerations:

1. Various geometric shapes of elements
2. Single as well as multivariable problems
3. Integrations performed over areas as opposed to along lines (for one-dimensional elements)
4. Mixed-order integrations used in certain formulations (shear-deformable plates and penalty function formulations of viscous incompressible fluids)

A brief description of the function of each subroutine from program **FEM2D** is given below.

BOUNDARY: Subroutine to impose specified (essential, natural, and mixed) boundary conditions on the primary and secondary variables.

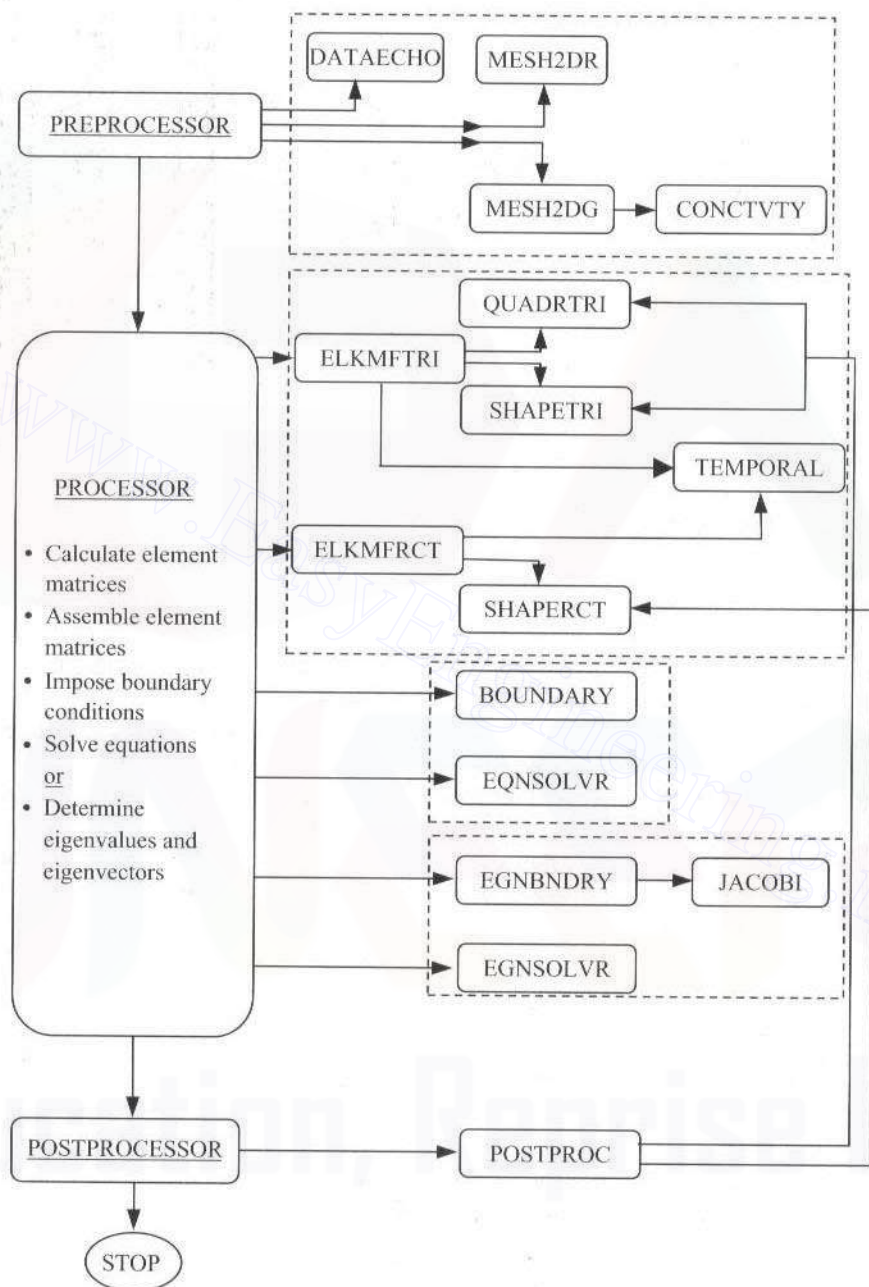


Figure 13.1.1 Flow chart of the computer program FEM2D.

CONCTVTY: Subroutine called from the mesh generator **MESH2DG**.

DATAECHO: Subroutine to echo the input data to the program (to facilitate the user to check the input data).

EGNBNDRY: Subroutine to impose specified homogeneous (essential and mixed) boundary conditions on the primary variables when an eigenvalue problem is solved.

EGNSOLVR: Subroutine to determine eigenvalues and eigenvectors.

ELKMFRC: Subroutine to compute the element matrices $[K]$, $[M]$, and $\{F\}$ for various field problems when rectangular elements are used.

ELKMFTR: Subroutine to compute the element matrices $[K]$, $[M]$, and $\{F\}$ for various field problems when triangular elements are used.

EQNSOLVR: Subroutine to solve a banded, symmetric system of algebraic equations using the Gauss elimination method.

INVERSE: Subroutine to invert a 3×3 matrix explicitly.

JACOBI: Subroutine called inside **EGNSOLVR**.

MESH2DG: Subroutine to generate mesh for nonrectangular domains.

MESH2DR: Subroutine to generate mesh for rectangular domains only.

POSTPROC: Subroutine to postcompute the solution, gradient of solution, and stresses for various field problems.

QUADRTRI: Subroutine to generate the quadrature points and weights for triangular elements.

SHAPERCT: Subroutine to compute the shape (interpolation) functions for linear and quadratic (eight- and nine-node) rectangular elements.

SHAPETRI: Subroutine to compute the shape (interpolation) functions for linear and quadratic triangular elements.

TEMPORAL: Subroutine to compute the equivalent coefficient matrices and column vectors for parabolic and hyperbolic equations when time-dependent analysis is carried (matrices of fully discretized system).

13.2 PREPROCESSOR

In the preprocessor unit, the program **MESH2DR** is used to generate triangular- and rectangular-element meshes of rectangular domains. The subroutine requires minimal input but is not general enough to generate finite element meshes of arbitrary domains. The subroutine **MESH2DG** is more general and can be used to generate meshes for nonrectangular domains. Of course, we can use any other mesh generation program in place of **MESH2DR** or **MESH2DG**. The subroutines **MESH2DR** and **MESH2DG** generate the connectivity matrix (array **NOD**) and the global coordinates of the nodes (array **GLXY**). When the mesh generators cannot be used, the mesh information should be read in.

13.3 ELEMENT COMPUTATIONS (PROCESSOR)

The two-dimensional problems of interest in this book require the evaluation of element matrices that involve products of interpolation functions and their derivatives with respect

to the global coordinates. Since the integrals are evaluated numerically, the integrands must be evaluated at the quadrature points and summed over the number of integration points. Thus, evaluation of the interpolation functions and their derivatives must be carried out inside the do-loops.

Element calculations for linear and quadratic triangular (**ELKMFTRI**) and quadrilateral (**ELKMFRCT**) elements can be carried out according to the concepts presented in Chapters 8 and 9. The principal steps involved are as follows.

1. Development of a subroutine for the evaluation of the interpolation functions and their derivatives with respect to the global coordinates [see Eqs. (9.3.7)–(9.3.11)].
2. Numerical integration of the coefficients of the element matrices using numerical quadrature formulas [see Eqs. (9.3.21) and (9.3.34)].
3. Setting up of the element matrices required for the class of problems being solved (e.g., static, transient, and eigenvalue problems).

We begin with the notation used for shape functions and their derivatives with respect to the natural (local) coordinates (ξ, η) and global coordinates (x, y) for rectangular elements. The variable names adopted are very transparent, and thus it is easy to see how the theoretical developments are translated into Fortran statements. We use the following notation:

XI(I)	Natural coordinate ξ_I of element node I
ETA(I)	Natural coordinate η_I of element node I
ELXY(I, 1)	Global coordinate x of element node I
ELXY(I, 2)	Global coordinate y of element node I
GLXY(I, 1)	Global coordinate x of the Ith node of the mesh
GLXY(I, 2)	Global coordinate y of the Ith node of the mesh
SF(I)	Interpolation function ψ_I of the Ith node of an element
DSF(1, I)	Derivative of SF(I) with respect to ξ : $DSF(1, I) = \partial\psi_I / \partial\xi$
DSF(2, I)	Derivative of SF(I) with respect to η : $DSF(2, I) = \partial\psi_I / \partial\eta$
GDSF(1, I)	Derivative of SF(I) with respect to x : $GDSF(1, I) = \partial\psi_I / \partial x$
GDSF(2, I)	Derivative of SF(I) with respect to y : $GDSF(2, I) = \partial\psi_I / \partial y$
DET	Determinant J of the Jacobian matrix [J]
CONST	Product of Jacobian J with the weights corresponding to the Gauss integration point $(\xi_{NI}, \eta_{NJ}) =$ DET * GAUSWT(NI, NGP) * GAUSWT(NJ, NGP)

The subroutines **SHAPETRI** and **SHAPERCT** (called in a do-loop based on the number of quadrature points) contain the expressions of the interpolation functions and their derivatives for various-order triangular (TRI) and rectangular (RCT) elements, respectively. The derivatives of the interpolation functions with respect to global coordinates [see Eq. (9.3.9)] are also computed in these subroutines. The Fortran statements to carry out the operations in Eqs. (9.3.7)–(9.3.11) is summarized in Box 13.3.1.

Once the arrays SF and GDSF are available in do-loops on a number of Gauss points in each coordinate direction, it is easy to evaluate the matrix coefficients using the Gauss

Box 13.3.1 Fortran statements for the calculation of the Jacobian matrix and local and global derivatives of shape functions.

Given the interpolation functions (SF) and their derivatives with respect to the natural coordinates (array DSF), the Jacobian matrix (GJ), its determinant (DET) and inverse (matrix GJINV), and global derivative of the shape functions (array GDSF) can be computed as follows:

```

DO 40 I = 1, 2
DO 40 J = 1, 2
GJ(I, J) = 0.0
DO 40 K = 1, NPE
40   GJ(I, J) = GJ(I, J) + DSF(I, K)*ELXY(K, J)

DET = GJ(1, 1)*GJ(2, 2) - GJ(1, 2)*GJ(2, 1)
GJINV(1, 1) = GJ(2, 2)/DET
GJINV(2, 2) = GJ(1, 1)/DET
GJINV(1, 2) = -GJ(1, 2)/DET
GJINV(2, 1) = -GJ(2, 1)/DET

DO 50 I = 1, 2
DO 50 J = 1,NPE
GDSF(I, J) = 0.0
DO 50 K = 1, 2
50   GDSF(I, J) = GDSF(I, J) + GJINV(I, K)*DSF(K, J)

```

quadrature formula (9.3.21). For example, $S_{ij}^{\alpha\beta}$ of Eq. (8.2.39)

$$S_{ij}^{\alpha\beta} = \int_{\Omega^e} \frac{\partial \psi_i}{\partial x_\alpha} \frac{\partial \psi_j}{\partial x_\beta} dx dy \quad (13.3.1)$$

where $x_1 = x$ and $x_2 = y$, can be translated into Fortran statement by

$$\begin{aligned}
 S00(I, J) &= S00(I, J) + SF(I) * SF(J) * CONST \\
 S11(I, J) &= S11(I, J) + GDSF(1, I) * GDSF(1, J) * CONST \\
 S12(I, J) &= S12(I, J) + GDSF(1, I) * GDSF(2, J) * CONST \\
 S22(I, J) &= S22(I, J) + GDSF(2, I) * GDSF(2, J) * CONST
 \end{aligned} \quad (13.3.2)$$

The summed values of $S00(I, J)$, $S11(I, J)$, and so on, over the number of Gauss points yields the numerical values of the integral coefficients in (13.3.1). The Fortran statements listed in Box 13.3.2 summarize the discussion.

To set up the element coefficient matrices of a given problem, we make use of the element matrices defined above. As an example, consider the problem described by the Poisson equation in Eq. (8.2.1). The element coefficient matrix and the column vectors for the problem are given by Eqs. (8.2.19b). The element matrix K_{ij} [denoted ELK(I, J)] can be expressed in terms of S_{ji}^{00} , S_{ij}^{11} , ... by

$$\begin{aligned}
 ELK(I, J) &= A00 * S00(I, J) + A11 * S11(I, J) + A12 * S12(I, J) \\
 &\quad + A21 * S12(J, I) + A22 * S22(I, J)
 \end{aligned}$$

Box 13.3.2 Fortran statements to compute matrix coefficients $S_{ij}^{\alpha\beta}$.

NPE = Number of nodes per elements

IPDF = Number of integration points (i.e., Gauss points)

DIMENSION GAUSPT(5, 5), GAUSWT(5, 5), SF(9), GDSF(2, 9),

1 ELXY(9, 2), S00(9, 9), S11(9, 9), S12(9, 9), S22(9, 9)

DATA GAUSPT/5*0.0D0, -0.57735027D0, 0.57735027D0, 3*0.0D0,

2 -0.77459667D0, 0.0D0, 0.77459667D0, 2*0.0D0, -0.86113631D0,

3 -0.33998104D0, 0.33998104D0, 0.86113631D0, 0.0D0, -0.90617984D0,

4 -0.53846931D0, 0.0D0, 0.53846931D0, 0.90617984D0/

DATA GAUSWT/2.0D0, 4*0.0D0, 2*1.0D0, 3*0.0D0, 0.55555555D0,

2 0.88888888D0, 0.55555555D0, 2*0.0D0, 0.34785485D0,

3 2*0.65214515D0, 0.34785485D0, 0.0D0, 0.23692688D0,

4 0.47862867D0, 0.56888888D0, 0.47862867D0, 0.23692688D0/

Initialize the arrays

```
DO 120 I = 1, NPE
DO 120 J = 1, NPE
    S00(I, J) = 0.0
    S11(I, J) = 0.0
    S12(I, J) = 0.0
    S21(I, J) = 0.0
    S22(I, J) = 0.0
120 CONTINUE
```

DO-loops on numerical (Gauss) integration begin here:

```
DO 200 NI = 1, IPDF
DO 200 NJ = 1, IPDF
XI = GAUSPT(NI, IPDF)
ETA = GAUSPT(NJ, IPDF)
```

Subroutine SHAPERCT (SHAPE functions for ReCTangular elements) is called to compute arrays SF and GDSF:

```
CALL SHPRCT (NPE,XI,ETA,ELXY,DET,SF,GDSF)
CNST = DET*GAUSWT(NI,IPDF)*GAUSWT(NJ,IPDF)
```

Compute $S_{ij}^{\alpha\beta}$ of Eq. (13.3.1):

```
DO 180 I = 1, NPE
DO 180 J = 1, NPE
    S00(I, J) = S00(I, J) + SF(I)*SF(J)*CNST
    S11(I, J) = S11(I, J) + GDSF(1, I)*GDSF(1, J)*CNST
    S12(I, J) = S12(I, J) + GDSF(1, I)*GDSF(2, J)*CNST
    S21(I, J) = S21(I, J) + GDSF(2, I)*GDSF(1, J)*CNST
    S22(I, J) = S22(I, J) + GDSF(2, I)*GDSF(2, J)*CNST
180 CONTINUE
200 CONTINUE
```

where $a_{00} = A00$, $a_{11} = A11$, $a_{12} = A12$, $a_{21} = A21$, and $a_{22} = A22$ are the constant coefficients of the differential equation (8.2.1).

In multivariable problems, the element matrices are themselves defined in terms of submatrices, as was the case for plane fluid flow, elasticity, and plate bending. In such cases, the nodal degrees of freedom should be renumbered to reduce the half-bandwidth of the assembled coefficient matrix. For example, consider the element equations (10.4.24) associated with the penalty formulation of two-dimensional viscous flow problems, which have a close resemblance to the finite element model of the plane elasticity problem; see Eq. (11.4.5). The element nodal variables Δ_i are given (say, for a linear rectangular element) by

$$\begin{Bmatrix} \Delta_1 \\ \Delta_2 \\ \Delta_3 \\ \vdots \\ \Delta_8 \end{Bmatrix} = \begin{Bmatrix} v_x^1 \\ v_x^2 \\ v_x^3 \\ v_x^4 \\ v_y^1 \\ v_y^2 \\ v_y^3 \\ v_y^4 \end{Bmatrix} \quad (13.3.3)$$

Thus, at any node, the difference between the label number of the first degree of freedom and that of the second degree of freedom is 4 (in a general case, the difference is n , where n is the number of nodes per element). This difference contributes to an increase in the half-bandwidth of the assembled coefficient matrix and hence in computational cost when Gauss elimination methods are used to solve the equations. To remedy this situation, we reorder the element nodal degrees of freedom as follows:

$$\begin{Bmatrix} \Delta_1 \\ \Delta_2 \\ \Delta_3 \\ \Delta_4 \\ \vdots \\ \Delta_{2n-1} \\ \Delta_{2n} \end{Bmatrix} = \begin{Bmatrix} v_x^1 \\ v_y^1 \\ v_x^2 \\ v_y^2 \\ \vdots \\ v_x^n \\ v_y^n \end{Bmatrix} \quad (13.3.4)$$

In reordering the nodal degrees of freedom, we must retain the symmetry, if one is present, of the system of algebraic equations. This is accomplished by renumbering the equations in the same way as the nodal degrees of freedom. To illustrate how this can be done, we consider the matrix equation

$$\begin{bmatrix} [S^{11}] & [S^{12}] \\ [S^{21}] & [S^{22}] \end{bmatrix} \begin{Bmatrix} \{u\} \\ \{v\} \end{Bmatrix} = \begin{Bmatrix} \{F^1\} \\ \{F^2\} \end{Bmatrix} \quad (13.3.5a)$$

which is a set of four equations in four unknowns. In expanded form, we have

$$\begin{aligned} S_{11}^{11}u_1 + S_{12}^{11}u_2 + S_{11}^{12}v_1 + S_{12}^{12}v_2 &= F_1^1 \\ S_{21}^{11}u_1 + S_{22}^{11}u_2 + S_{21}^{12}v_1 + S_{22}^{12}v_2 &= F_2^1 \\ S_{11}^{21}u_1 + S_{12}^{21}u_2 + S_{11}^{22}v_1 + S_{12}^{22}v_2 &= F_1^2 \\ S_{21}^{21}u_1 + S_{22}^{21}u_2 + S_{21}^{22}v_1 + S_{22}^{22}v_2 &= F_2^2 \end{aligned} \quad (13.3.5b)$$

Box 13.3.3 Fortran statements to rearrange the degrees of freedom to reduce the bandwidth of the coefficient matrix.

Rearrangement of element equations for problems with multiple degrees of freedom per node (Illustrated using plane elasticity model, NDF = 2).

NDF = Number of degrees of freedom per node

NPE = Number of nodes per element

CMAT(I, J) = Matrix of elastic coefficients

ELK(I, J) = Element stiffness matrix coefficients

Dimension the arrays: ELK(NN, NN) and CMAT(3, 3), where

NN = NPE*NDF

Computation of coefficients ELK11(I, J), ELK12(I, J), ELK21(I, J), and ELK22(I, J) of Eqs. (11.4.5) and (11.4.6) using numerical integration.

Initialize arrays ELK11(I, J), ELK12(I, J), ELK21(I, J) and ELK22(I, J).

Initialization loops are not included here. The following statements

go inside the Gauss-Legendre quadrature loops; see Box 13.3.2 for

evaluation of $S_{ij}^{\alpha\beta}$:

```

DO 140 I = 1, NPE
DO 120 J = 1, NPE
  ELK11(I, J) = ELK11(I, J) + CMAT(1, 1)*S11(I, J) + CMAT(3, 3)*S22(I, J)
  ELK12(I, J) = ELK12(I, J) + CMAT(1, 2)*S12(I, J) + CMAT(3, 3)*S21(I, J)
  ELK21(I, J) = ELK21(I, J) + CMAT(1, 2)*S21(I, J) + CMAT(3, 3)*S12(I, J)
  ELK22(I, J) = ELK22(I, J) + CMAT(3, 3)*S11(I, J) + CMAT(2, 2)*S22(I, J)
120  CONTINUE
140  CONTINUE

```

Rearrange the coefficients

```

II = 1
DO 180 I = 1, NN
  JJ = 1
  DO 160 J = 1, NN
    ELK(II, JJ) = ELK11(I, J)
    ELK(II, JJ+1) = ELK12(I, J)
    ELK(II+1, JJ) = ELK21(I, J)
    ELK(II+1, JJ+1) = ELK22(I, J)
160 JJ = NDF*J+1
180 II = NDF*I+1

```

Here (u_i, v_i) are the degrees of freedom at element node i . Now letting

$$\Delta_1 = u_1, \quad \Delta_2 = v_1, \quad \Delta_3 = u_2, \quad \Delta_4 = v_2 \quad (13.3.6)$$

(i.e., the third nodal variable is renamed as the second, and vice versa) and rearranging (13.3.5a) (i.e., the third equation becomes the second equation, and vice versa), we obtain

$$\begin{aligned} S_{11}^{11}\Delta_1 + S_{11}^{12}\Delta_2 + S_{12}^{11}\Delta_3 + S_{12}^{12}\Delta_4 &= F_1^1 \\ S_{11}^{21}\Delta_1 + S_{11}^{22}\Delta_2 + S_{12}^{21}\Delta_3 + S_{12}^{22}\Delta_4 &= F_1^2 \\ S_{21}^{11}\Delta_1 + S_{21}^{12}\Delta_2 + S_{22}^{11}\Delta_3 + S_{22}^{12}\Delta_4 &= F_2^1 \\ S_{21}^{21}\Delta_1 + S_{21}^{22}\Delta_2 + S_{22}^{21}\Delta_3 + S_{22}^{22}\Delta_4 &= F_2^2 \end{aligned} \quad (13.3.7a)$$

or, in matrix form,

$$\mathbf{S}\Delta = \mathbf{F} \quad (13.3.7b)$$

where

$$\begin{aligned} S_{ij} &= S_{\alpha\beta}^{11}, \quad S_{i,j+1} = S_{\alpha\beta}^{12}, \quad S_{i+1,j} = S_{\alpha\beta}^{21}, \quad S_{i+1,j+1} = S_{\alpha\beta}^{22} \\ F_i &= F_\alpha^1, \quad F_{i+1} = F_\alpha^2 \\ i &= 2\alpha - 1, \quad j = 2\beta - 1, \quad \alpha, \beta = 1, 2 \end{aligned} \quad (13.3.7c)$$

The above discussion applies to any number of degrees of freedom per node (NDF). Computer implementation of the rearrangement of nodal degrees of freedom and the associated equations [see Eqs.(13.3.7c)] is straightforward, and the Fortran statements of the procedure are given in Box 13.3.3.

The Fortran statements provided in Boxes 13.3.1 through 13.3.3 should help the reader see the ease with which finite element models can be implemented in a computer. No attempt is made here to discuss equation solver and eigenvalue solver. These are considered to be extraneous to the method. The Fortran source code of **FEM2D** gives a more complete idea as to how various computational steps of finite element analysis are carried out. The program can be modified to include one's own finite element formulation. In the next section, we illustrate the capabilities and limitations of the educational program **FEM2D**.

13.4 APPLICATIONS OF THE COMPUTER PROGRAM FEM2D

13.4.1 Introduction

The computer program **FEM2D** is developed to solve the following four types of problems:

Case 1. Single-variable problems, including convective-type boundary conditions for heat transfer problems

$$c_t \left(\frac{\partial u}{\partial t} + \frac{\partial^2 u}{\partial t^2} \right) - \frac{\partial}{\partial x} \left(a_x \frac{\partial u}{\partial x} \right) - \frac{\partial}{\partial y} \left(a_y \frac{\partial u}{\partial y} \right) + a_0 u = f \quad (13.4.1a)$$

with

$$\begin{aligned} c_t &= c_0 + c_x x + c_y y, & a_x &= a_{10} + a_{1x} x + a_{1y} y \\ a_y &= a_{20} + a_{2x} x + a_{2y} y, & f_0 &= f_0 + f_x x + f_y y \\ a_0 &= \text{constant} \end{aligned} \quad (13.4.1b)$$

Case 2. Viscous incompressible fluid flows using the penalty function formulation of Chapter 10 [Eqs. (10.2.9) and (10.2.10) with P replaced by (10.4.20)]

Case 3. The plane elasticity problems of Chapter 11 [Eq. (11.2.18a)]

Case 4. Plate bending problems using classical plate theory [Eq. (12.2.11)] and shear deformation plate theory [Eqs. (12.3.8a)–(12.3.8c)] of Chapter 12; only rectangular elements are included

The first category of problems is quite general and includes, as special cases, many other field problems of engineering and science. As a special case, axisymmetric problems can also be analyzed. The last three categories are specialized to linear (i.e., Stokes) viscous incompressible fluid flow, linear elasticity, and linear plate bending, respectively.

The type of gradient of the solution computed (in subroutine **POSTPROC**) for single-variable problems (Case 1) differs for different physical problems. For heat transfer problems, we wish to compute the x and y components of heat flux

$$q_x = -a_x \frac{\partial u}{\partial x}, \quad q_y = -a_y \frac{\partial u}{\partial y} \quad (13.4.2)$$

The same definition applies to the calculation of the velocity components in the velocity potential formulation of inviscid fluid flows [i.e., q_x and q_y of Eq. (13.4.2) are the velocity components v_x and v_y , respectively]. In the stream function formulation, the velocity components (v_x, v_y) are defined by

$$v_x = a_x \frac{\partial u}{\partial y}, \quad v_y = -a_x \frac{\partial u}{\partial x} \quad (13.4.3)$$

The (total) stresses for multivariable problems are computed using the constitutive equations, with the strains (or strain rates for fluid flow problems) computed at the reduced Gauss points using the strain-displacement relations.

For heat transfer problems (i.e., $\text{ITYPE} = 0$), the variable **ICONV** is used to indicate the presence (**ICONV** = 1) or absence (**ICONV** = 0) of convective boundaries. When convective boundaries are involved (i.e., **ICONV** = 1), the elements whose boundaries coincide with such a boundary will have additional contributions to their coefficient matrices [see Eqs. (8.5.6)–(8.5.10)]. The array **IBN** is used to store elements that have convective boundaries, and the array **INOD** is used to store the pairs of element local nodes (of elements in array **IBN**) that are on the convective boundary (to specify the side of the element on the convective boundary). If an element has more than one of its sides on the convective boundary, it should be repeated as many times as the number of sides on the convective boundary.

A complete list of the input variables of the program **FEM2D** is included in Table 13.4.1, which contains an explanation of the key variables for the six classes ($\text{ITYPE} = 0, 1, 2, \dots, 5$) of problems.

Table 13.4.1 Description of the input variables to the program **FEM2D**.**• Data Card 1**

TITLE Title of the problem being solved (80 characters)

• Data Card 2

ITYPE Problem type

ITYPE = 0 Single variable problems

ITYPE = 1 Viscous incompressible flow problems

ITYPE = 2 Plane elasticity problems

ITYPE = 3 Plate bending problems by FSDT

ITYPE = 4 Plate bending problems by CPT(N)

ITYPE = 5 Plate bending problems by CPT(C)

IGRAD Indicator for computing the gradient of the solution or stresses in the postprocessor

IGRAD = 0 No postprocessing is required

IGRAD > 0 Postprocessing is required

When ITYPE = 0 and IGRAD = 1, the gradient is computed as in Eq. (13.4.2);
for ITYPE = 0 and IGRAD > 1 the gradient is computed by Eq. (13.4.3)

ITEM Indicator for dynamic analysis

ITEM = 0 Static analysis is required

ITEM > 0 Either eigenvalue or transient analysis is required:

ITEM = 1 Parabolic equation

ITEM = 2 Hyperbolic equation

NEIGN Indicator for eigenvalue analysis

NEIGN = 0 Static or transient analysis

NEIGN > 0 Eigenvalue analysis:

NEIGN = 1 Vibration analysis

NEIGN > 1 Stability of plates

Skip card 3 if NEIGN = 0.

• Data Card 3

NVALU Number of eigenvalues to be printed

NVCTR Indicator for printing eigenvectors:

NVCTR = 0 Do not print eigenvectors

NVCTR > 0 Print eigenvectors

• Data Card 4

IELTYP Element type used in the analysis

IELTYP = 0 Triangular elements

IELTYP > 0 Quadrilateral elements

NPE Nodes per element

NPE = 3 Linear triangle (IELTYP = 0)

NPE = 4 Linear quadrilateral (IELTYP > 0)

NPE = 6 Quadratic triangle (IELTYP = 0)

NPE = 8 or 9 Quadratic quadrilateral (IELTYP > 0)

MESH Indicator for mesh generation by the program

MESH = 0 Mesh is not generated by the program

MESH = 1 Mesh is generated by the program for rectangular domains
by **MESH2DR**

MESH > 1 Mesh is generated by the program for nonrectangular domains
by **MESH2DG**

NPRNT Indicator for printing certain output

NPRNT = 0 Not print array NOD, element matrices or global matrices

NPRNT = 1 Print array NOD and element 1 matrices ELK and ELF

(Table 13.4.1 continued)

NPRNT = 2 Print array NOD and assembled matrices GLK and GLF

NPRNT > 2 Combination of NPRNT = 1 and 2

Skip card 5 if MESH = 1.

• Data Card 5

NEM Number of elements in the mesh when the user inputs the mesh or the mesh is generated by **MESH2DG**

NNM Number of nodes in the mesh when the user inputs the mesh or the mesh is generated by **MESH2DG**

Skip cards 6 and 7 if MESH ≠ 0; otherwise, read card 6 in a loop on the number of elements (N = 1, NEM) and card 7 in loops on I and J.

• Data Card 6

NOD(N, I) Connectivity for the Nth element (I=1, NPE)

• Data Card 7

GLXY(I, J) Global *x* and *y* coordinates of the Ith global node in the mesh (J = 1, *x* coordinate; J = 2, *y* coordinate)

Loops on I and J are: [(J = 1, 2), I = 1, NNM]; the NNM pairs of (*x*, *y*) coordinates are read sequentially

Cards 8–11 are read in **MESH2DG**. Skip them unless MESH > 1.

• Data Card 8

NRECL Number of line records to be read in the mesh

• Data Card 9

Read the following variables NRECL times:

NOD1 First global node number of the line segment

NODL Last global node number of the line segment

NODINC Node increment on the line

X1 The global *x* coordinate of the NOD1

Y1 The global *y* coordinate of the NOD1

XL The global *x* coordinate of NODL

YL The global *y* coordinate of NODL

RATIO The ratio of the first element length to the last element length

• Data Card 10

NRECEL Number of rows of elements to be read in the mesh

• Data Card 11

Read the following variables NRECEL times:

NEL1 First element number of the row

NELL Last element number of the row

IELINC Increment of element number in the row

NODINC Increment of the global node number in the row

NPE Number of nodes in each element

NODE(I) Connectivity array of the first element in the row (I=1, NPE)

Skip cards 12–14 if MESH ≠ 1.

• Data Card 12

NX Number of elements in the *x* direction

NY Number of elements in the *y* direction

• Data Card 13

X0 The *x* coordinate of global node 1

DX(I) The *x* dimension of the Ith element (I = 1, NX)

(Table 13.4.1 continued)

• Data Card 14

- Y0 The y coordinate of global node 1
 DY(I) The y dimension of the Ith element ($I = 1, NY$)

• Data Card 15

- NSPV The number of specified primary variables

Skip card 16 if NSPV = 0

• Data Card 16

- ISPV(I, J) Node number and local degree of freedom (DOF) number of the Ith specified primary variable
 ISPV(I, 1) = Node number
 ISPV(I, 2) = Local DOF number
 The do-loops on I and J are: $[(J = 1, 2), I = 1, NSPV]$

Skip card 17 if NSPV = 0 or NEIGN ≠ 0.

• Data Card 17

- VSPV(I) Specified value of the Ith primary variable ($I = 1, NSPV$)

Skip card 18 if NEIGN ≠ 0.

• Data Card 18

- NSSV Number of (nonzero) specified secondary variables

Skip card 19 if NSSV = 0 or NEIGN ≠ 0.

• Data Card 19

- ISSV(I, J) Node number and local DOF number of the Ith specified secondary variable
 ISSV(I, 1) = Node number
 ISSV(I, 2) = Local DOF number
 The loops on I and J are: $((J = 1, 2), I = 1, NSSV)$

Skip card 20 if NSSV = 0 or NEIGN ≠ 0.

• Data Card 20

- VSSV(I) Specified value of the Ith secondary variable ($I = 1, NSSV$)

Data Cards 21–27 are for the single variable problems (ITYPE = 0).

• Data Card 21

- A10 Coefficients of the differential equation
 A1X
 A1Y $a_{11} = A10 + A1X*X + A1Y*Y$

• Data Card 22

- A20 Coefficients of the differential equation
 A2X
 A2Y $a_{22} = A20 + A2X*X + A2Y*Y$

• Data Card 23

- A00 Coefficient of the differential equation

• Data Card 24

- ICONV Indicator for convection boundary conditions
 ICONV = 0 No convection boundary conditions
 ICONV > 0 Convection boundary conditions present

• Data Card 25

- NBE Number elements with convection

• Data Card 26

- The following cards are read for each I, $I = 1, NBE$:

- IBN(I) Ith element number with convection
 BETA(I) Film coefficient for convection on Ith element
 TINF(I) Ambient temperature of the Ith element

(Table 13.4.1 continued)

• Data Card 27

INOD(I, J) Local node numbers of the side with convection
 $(J = 1, 2; \text{ for quadratic elements, give end nodes})$
 Loops on I and J are: $[(J = 1, 2), I = 1, \text{NBE}]$

Data Card 28 is for viscous fluid flows (ITYPE = 1) only.

• Data Card 28

VISCOSITY Viscosity of the fluid
 PENALTY Value of the penalty parameter

Data Cards 29 and 30 are for plane elasticity problems (ITYPE = 2) only.

• Data Card 29

LNSTRS Flag for plane stress or plane strain problems
 $\text{LNSTRS} = 0$ Plane strain elastic problems
 $\text{LNSTRS} > 0$ Plane stress elastic problems

• Data Card 30

E1	Young's moduli along the global x axis
E2	Young's moduli along the global y axis
ANU12	Poisson's ratio in the xy plane
G12	Shear modulus in the xy plane
THKNS	Thickness of the plane elastic body analyzed

Data Card 31 is for plate bending problems (ITYPE = 3 to 5) only.

• Data Card 31

E1	Young's moduli along the global x axis
E2	Young's moduli along the global y axis
ANU12	Poisson's ratio in the xy plane
G12	Shear modulus in the xy plane
G13	Shear modulus in the xz plane
G23	Shear modulus in the yz plane
THKNS	Thickness of the plate analyzed

*** Remaining data cards are for all problem types. ***

Skip card 32 if NEIGN $\neq 0$.

• Data Card 32

F0 Coefficients to define the source term
 FX
 FY $f(x, y) = F0 + FX*x + FY*y$

*** Cards 33–37 are for transient analysis (ITEM $\neq 0$) only. ***

Skip card 33 if ITEM = 0.

• Data Card 33

C0 Coefficients defining the temporal parts of the
 differential equations, as defined below:
 CX
 CY
 $CT = C0 + CX*X + CY*Y$ when ITYPE = 0 or 1
 $CT = (C0 + CX*X + CY*Y)*THKNS$ when ITYPE = 2
 $I0 = C0*THKNS, I2 = C0*(THKNS**3)/12$
 and CX and CY are not used (when NEIGH ≤ 1 and ITYPE = 3 to 5)
 C0, CX, and CY denote the buckling parameters when ITYPE = 3 and NEIGN > 1

Skip card 34 if ITEM = 0 or NEIGN $\neq 0$.

(Table 13.4.1 continued)

• Data Card 34

NTIME	Number of time steps for the transient solution
NSTP	Time step number at which the source is removed
INTVL	Time step interval at which to print the solution
INTIAL	Indicator for nature of initial conditions
	INTIAL = 0 Zero initial conditions are used
	INTIAL > 0 Nonzero initial conditions are used

Skip card 35 if ITEM = 0 or NEIGN ≠ 0.

• Data Card 35

DT	Time step used for the transient solution
ALFA	Parameter in the alfa-family of time approximation used for parabolic equations: ALFA = 0 The forward difference scheme (C.S.) [†] ALFA = 0.5 The Crank–Nicolson scheme (stable) ALFA = 2/3 The Galerkin scheme (stable) ALFA = 1 The backward difference scheme (stable)
	[†] C.S. = conditionally stable; for all schemes with $ALFA < 0.5$, the time step DT is restricted to $DT < 2/[MAXEGN*(1-2*ALFA)]$, where MAXEGN is the maximum eigenvalue of the discrete problem
GAMA	Parameter in the Newmark time integration scheme used for hyperbolic equations: GAMA = 0.5 Constant-average acceleration (stable) GAMA = 1/3 Linear acceleration scheme (C.S.) GAMA = 0.0 The central difference scheme (C.S.) ALFA = 0.5 for all schemes; For schemes for which $ALFA \leq 0.5$ and $GAMA < ALFA$, DT is restricted to: $DT < 2/SQRT[MAXEGN*(ALFA-GAMA)]$, MAXEGN being the maximum eigenvalue of the discrete system
EPSLN	A small parameter to check if the solution has reached a steady state

Skip card 36 if ITEM or INTIAL = 0, or NEIGN ≠ 0.

• Data Card 36

GLU(I)	Vector of initial value of the primary variables (I = 1, NEQ), where NEQ = Number of nodal values in the mesh
--------	--

Skip card 37 if ITEM ≤ 1, NEIGN ≠ 0, or INTIAL = 0.

• Data Card 37

GLV(I)	Vector of the initial values of the first derivative of the primary variables (velocity) (I = 1, NEQ)
--------	--

13.4.2 Description of Mesh Generators

A major limitation of the program **FEM2D** lies in the mesh generation [i.e., the computation of arrays NOD(I, J) and GLXY(I, J) for arbitrary domains]. For such problems, the user is required to input the mesh information, which can be a tedious job if many elements are used. Of course, the program can be modified to accept other mesh generation subroutines. Here we discuss the input data to the two mesh generators, namely, **MESH2DR** and **MESH2DG**.

First, let us consider **MESH2DR**. The program is restricted to rectangular domains with sides parallel to the global x and y axes. The subroutine requires the following input data:

NX	Number of elements in the x direction
NY	Number of elements in the y direction
(X_0, Y_0)	Global coordinates of global node 1, which is located at the lower left corner of the domain (see Fig. 13.4.1)
DX(I)	The array of element lengths along the x direction
DY(I)	The array of element lengths along the y direction

The node and element numbering schemes for triangular and rectangular element meshes generated by **MESH2DR** are shown in Fig. 13.4.1.

Next, we consider **MESH2DG**, which is relatively more general than **MESH2DR**. The program, based on the straight line generation logic used by Akay, Willhite, and Didandeh (1987), requires the user to sketch a desired mesh with certain regularity of node and element numbering. It exploits the regularity to generate the mesh. The program **MESH2DG** requires the following input (except for NEM and NNM, all other variables are read from the subroutine):

NEM	Number of total elements in the mesh
NNM	Number of total nodes in the mesh
NRECL	Number of line-segment records

For each line segment, read the following variables:

NOD1	First node number on the line segment
NODL	Last node number on the line segment
NODINC	Increment between two consecutive nodes on the line
(X_1, Y_1)	Global coordinates of the first node, NOD1 on the line
(X_N, Y_N)	Global coordinates of the last node, NODL on the line
RATIO	Ratio of the first element length to the last element length

Similar information on the elements is read as follows:

NRECEL	Number of rows of elements
--------	----------------------------

For each row of elements, read the following variables:

NEL1	First element number in the row
NELL	Last element number in the row
NODINC	Increment between respective nodes of consecutive elements in the row
NPE	Number of nodes per element
NODE(I) ($I = 1, NPE$)	Nodal connectivity for element NEL1

The type of data being read in **MESH2DG** should give some indication of the restrictions of the program. The node and element numbering should be regular along the lines and rows being read. Figures 13.4.2(a)–13.4.2(d) show typical examples of meshes of linear and quadratic triangular and quadrilateral elements. For each of these meshes, the input data required for **MESH2DG** is listed in Boxes 13.4.1 and 13.4.2.

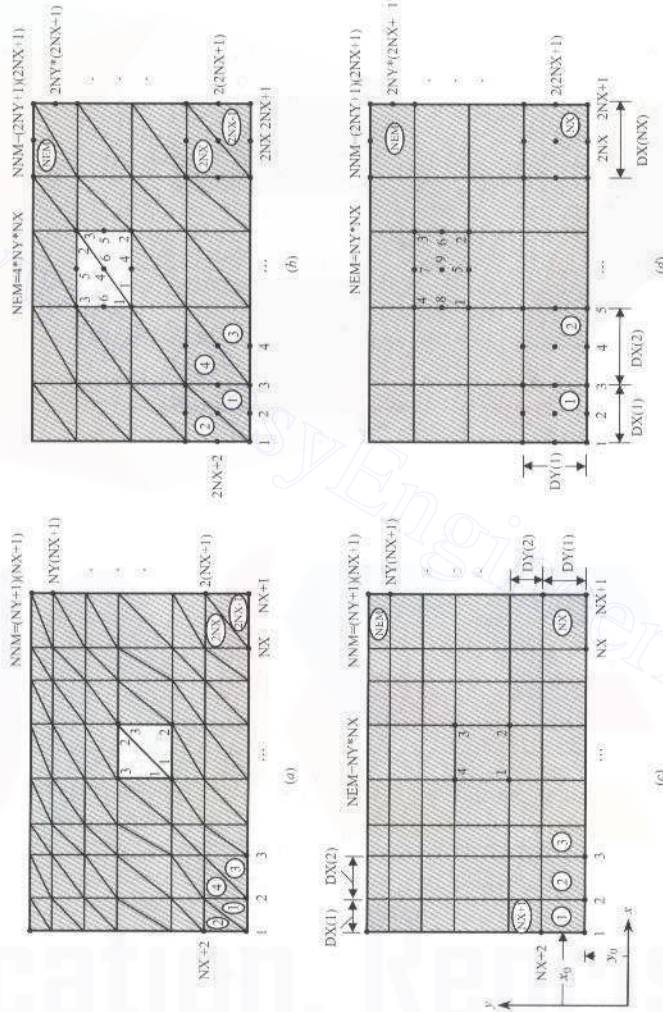


Figure 13.4.1 Element numbering and global and element node numbering system used in subroutine **MESH2DR** for the generation of meshes for rectangular domains. (a) Mesh of linear triangles, (b) Mesh of quadratic triangles, (c) Mesh of linear rectangles, (d) Mesh of quadratic (nine-node) rectangles.

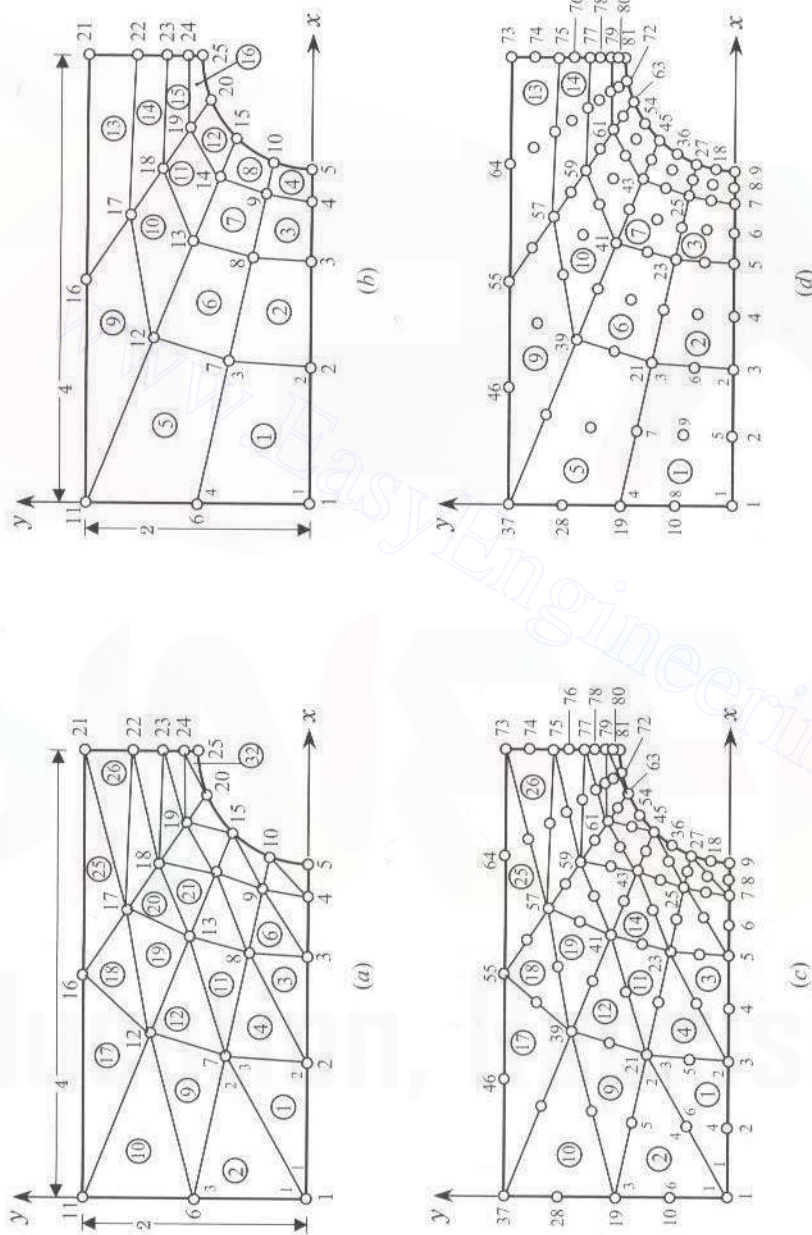


Figure 13.4.2 Typical examples of mesh generation in irregular domains using subroutine **MESH2DG**. (a) Mesh of linear triangles. (b) Mesh of linear quadrilaterals. (c) Mesh of quadratic triangles. (d) Mesh of quadratic (nine-node) quadrilateral elements.

Box 13.4.1 The input data to program **FEM2D** to generate the finite element meshes shown in Figs. 13.4.2(a) and 13.4.2(b).

(a) Mesh of linear triangles [see Figure 13.4.2(a)]

32 25	NEM, NNM
5	NRECL
1 5 1 0.0 0.0 3.0 0.0 6.0	NOD1, NODL, NODINC,
6 10 1 0.0 1.0 3.07612 0.38268 6.0	X1, Y1, XL, YL, RATIO
11 15 1 0.0 2.0 3.29289 0.7071 6.0	for each of the five
16 20 1 2.0 2.0 3.61732 0.92388 6.0	line segments
21 25 1 4.0 2.0 4.0 1.0 6.0	
8	NRECEL
1 7 2 1 3 1 2 7	NELL, NELL, IELINC,
2 8 2 1 3 1 7 6	NODINC, NPE, NOD(I,J)
9 15 2 1 3 6 7 12	for each of the
10 16 2 1 3 6 12 11	eight rows of
17 23 2 1 3 11 12 16	elements
18 24 2 1 3 12 17 16	
25 31 2 1 3 16 17 21	
26 32 2 1 3 17 22 21	

(b) Mesh of linear quadrilaterals [see Figure 13.4.2(b)]

16 25	NEM, NNM
5	NRECL
1 5 1 0.0 0.0 3.0 0.0 6.0	NOD1, NODL, NODINC,
6 10 1 0.0 1.0 3.07612 0.38268 6.0	etc.
11 15 1 0.0 2.0 3.29289 0.7071 6.0	
16 20 1 2.0 2.0 3.61732 0.92388 6.0	
21 25 1 4.0 2.0 4.0 1.0 6.0	
4	NRECEL
1 4 1 1 4 1 2 7 6	NELL, NELL, IELINC,
5 8 1 1 4 6 7 12 11	etc.
9 12 1 1 4 11 12 17 16	
13 16 1 1 4 16 17 22 21	

Box 13.4.2 The input data to program **FEM2D** to generate the finite element meshes shown in Figs. 13.4.2(c) and 13.4.2(d).

(c) Mesh of quadratic triangles [see Fig. 13.4.2(c)]

32 81	NEM, NNM
9	NRECL
1 9 1 0.0 0.0 3.0 0.0 6.0	
10 18 1 0.0 0.5 3.01921 0.19509 6.0	
19 27 1 0.0 1.0 3.07612 0.38268 6.0	
28 36 1 0.0 1.5 3.16853 0.55557 6.0	NOD1, NODL, NODINC,
37 45 1 0.0 2.0 3.29289 0.7071 6.0	X1, Y1, XL, YL, RATIO
46 54 1 1.0 2.0 3.44443 0.83147 6.0	for each line segment
55 63 1 2.0 2.0 3.61732 0.92388 6.0	
64 72 1 3.0 2.0 3.80491 0.98078 6.0	
73 81 1 4.0 2.0 4.0 1.0 6.0	

(Box 13.4.2 is continued from the previous page)

8										NRECEL			
1	7	2	2	6	1	3	21	2	12	11			
2	8	2	2	6	1	21	19	11	20	10			
9	15	2	2	6	19	21	39	20	30	29			
10	16	2	2	6	19	39	37	29	38	28			
17	23	2	2	6	37	39	55	38	47	46			
18	24	2	2	6	39	57	55	48	56	47			
25	31	2	2	6	55	57	73	56	65	64			
26	32	2	2	6	57	75	73	66	74	65			
(d) Mesh of quadratic (nine-node) quadrilaterals [see Fig. 13.4.2(d)]:													
16	81									NEM, NNM			
9										NRECL			
1	9	1	0.0	0.0	3.0	0.0		6.0					
10	18	1	0.0	0.5	3.01921	0.19509	6.0						
19	27	1	0.0	1.0	3.07612	0.38268	6.0						
28	36	1	0.0	1.5	3.16853	0.55557	6.0						
37	45	1	0.0	2.0	3.29289	0.7071	6.0						
46	54	1	1.0	2.0	3.44443	0.83147	6.0						
55	63	1	2.0	2.0	3.61732	0.92388	6.0						
64	72	1	3.0	2.0	3.80491	0.98078	6.0						
73	81	1	4.0	2.0	4.0	1.0		6.0					
4										NRECEL			
1	4	1	2	9	1	3	21	19	2	12	20	10	11
5	8	1	2	9	19	21	39	37	20	30	38	28	29
9	12	1	2	9	37	39	57	55	38	48	56	46	47
13	16	1	2	9	55	57	75	73	56	66	74	64	65

13.4.3 Applications (Illustrative Examples)

In this section, the input data to **FEM2D** for several example problems are discussed. The example problems are selected from those discussed in Chapters 8–12. For a description of the variables used in the input data, see Table 13.4.1.

Example 13.4.1 (Poisson's Equation)

We consider the Poisson equation

$$-\nabla^2 u = 1 \text{ in } \Omega, \quad u = 0 \text{ on } \Gamma$$

where Ω is a square of two units and Γ denotes the boundary of Ω . Due to the biaxial symmetry, we can use a quadrant of the domain to solve the problem using the finite element method. We represent the computational domain by two different meshes (1) mesh of linear triangles [Fig. 13.4.3(a)], and (2) mesh of linear rectangles [Fig. 13.4.3(b)].

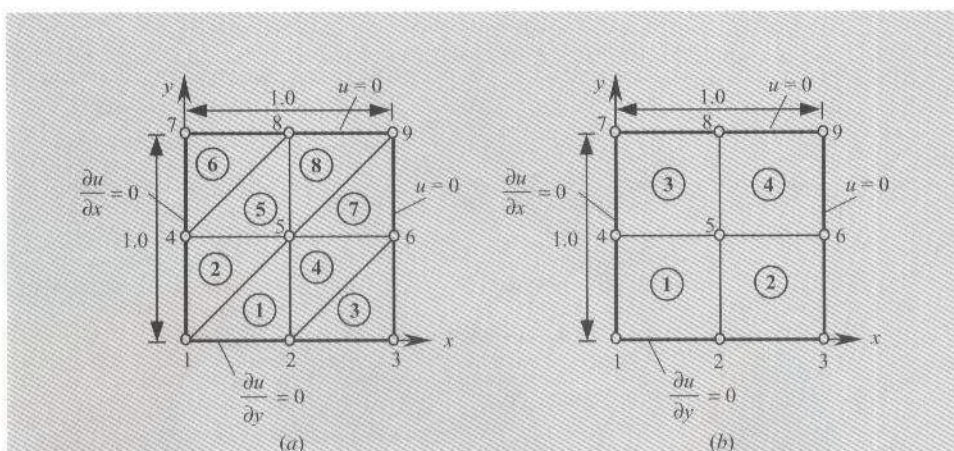


Figure 13.4.3 Finite element meshes of (a) linear triangles and (b) linear rectangles.

Triangular elements. We use the 2×2 mesh shown in Fig. 13.4.3(a). We have

```
ITYPE = 0,    IGRAD = 1,    ITEM = 0,    NEIGN = 0
IELTYP = 0,    NPE = 3,    MESH = 1,    NPRNT = 0
```

Note that we chose to generate the mesh using the subroutine **MESH2DR**. Therefore, we must specify the number of subdivisions and their lengths along each direction:

```
NX = 2,    NY = 2,    X0 = 0.0,    Y0 = 0.0
DX(1) = 0.5,    DX(2) = 0.5,    DY(1) = 0.5,    DY(2) = 0.5
```

The number of specified primary variables (NSPV), the node numbers and the specified local degree of freedom (ISPV), and their specified values (VSPV) for the problem are: NSPV = 5, ISPV(I, J) = (3, 1; 6, 1; 7, 1; 8, 1; 9, 1), and VSPV(I) = (0.0, 0.0, 0.0, 0.0, 0.0). There are no specified secondary variables, NSSV = 0.

The coefficients a_x and a_y of the differential equation (13.4.1a) are unity, $a_0 = 0$, the source term f is unity, and there is no convection:

```
A10 = 1.0,    A1X = 0.0,    A1Y = 0.0,    A20 = 1.0,    A2X = 0.0
A2Y = 0.0,    A00 = 0.0,    ICONV = 0,    FO = 1.0,    FX = 0.0,    FY = 0.0
```

Rectangular elements. For the 2×2 (four-element) mesh of rectangular elements [see Fig. 13.4.3(b)], the data input to the program differ only in the specification of the element type and the number of nodes per element: IELTYP = 1 and NPE = 4.

The input data to **FEM2D** for these two meshes are presented in Box 13.4.3, and the corresponding (edited) output in Box 13.4.4. The numerical results of this problem were discussed in Example 8.3.1.

Box 13.4.3 The input data to program **FEM2D** for the Poisson equation of Example 13.4.1.

```

Example 13.4.1: Solution of the Poisson equation (mesh of triangles)
0   1   0   0
0   3   1   0
2   2
0.0  0.5  0.5
0.0  0.5  0.5
5
3 1    6 1    7 1    8 1    9 1
0.0  0.0  0.0  0.0  0.0
0
1.0  0.0  0.0
1.0  0.0  0.0
0.0
0
1.0  0.0  0.0

```

ITYPE, IGRAD, ITEM, NEIGN
IELTYP, NPE, MESH, NPRINT
NX, NY
X0,DX(I)
Y0,DY(I)
NSPV
ISPV(I,J)
VSPV(I)
NSSV
A10, A1X, A1Y
A20, A2X, A2Y
A00
ICONV
F0, FX, FY

Example 13.4.1: Solution of the Poisson equation (mesh of rectangles)

```

0   1   0   0
1   4   1   0
2   2
0.0  0.5  0.5
0.0  0.5  0.5
5
3 1    6 1    7 1    8 1    9 1
0.0  0.0  0.0  0.0  0.0
0
1.0  0.0  0.0
1.0  0.0  0.0
0.0
0
1.0  0.0  0.0

```

ITYPE, IGRAD, ITEM, NEIGN
IELTYP, NPE, MESH, NPRINT
NX, NY
X0,DX(I)
Y0,DY(I)
NSPV
ISPV(I,J)
VSPV(I)
NSSV
A10, A1X, A1Y
A20, A2X, A2Y
A00
ICONV
F0, FX, FY

Box 13.4.4 The output from program **FEM2D** for the Poisson equation of Example 13.4.1.

Example 13.4.1: Solution of the Poisson equation on a square domain
OUTPUT from program FEM2DV2.5 by J. N. REDDY
ANALYSIS OF A POISSON/LAPLACE EQUATION COEFFICIENTS OF THE DIFFERENTIAL EQUATION Coefficient, A10 = 0.1000E+01 Coefficient, A1X = 0.0000E+00 Coefficient, A1Y = 0.0000E+00 Coefficient, A20 = 0.1000E+01 Coefficient, A2X = 0.0000E+00 Coefficient, A2Y = 0.0000E+00 Coefficient, A00 = 0.0000E+00

Coefficient, A10	=	0.1000E+01
Coefficient, A1X	=	0.0000E+00
Coefficient, A1Y	=	0.0000E+00
Coefficient, A20	=	0.1000E+01
Coefficient, A2X	=	0.0000E+00
Coefficient, A2Y	=	0.0000E+00
Coefficient, A00	=	0.0000E+00

(Box 13.4.4 is continued from the previous page)

CONTINUOUS SOURCE COEFFICIENTS:

Coefficient, F0 = 0.1000E+01
 Coefficient, FX = 0.0000E+00
 Coefficient, FY = 0.0000E+00

***** A STEADY-STATE PROBLEM is analyzed *****
 *** A mesh of TRIANGLES is chosen by user ***

FINITE ELEMENT MESH INFORMATION:

Element type: 0 = Triangle; >0 = Quad.) .. = 0
 Number of nodes per element, NPE = 3
 No. of primary deg. of freedom/node, NDF = 1
 Number of elements in the mesh, NEM = 8
 Number of nodes in the mesh, NNM = 9
 Number of equations to be solved, NEQ = 9
 Half-bandwidth of the matrix GLK, NHBW ... = 5
 Mesh subdivisions, NX and NY = 2 2
 No. of specified PRIMARY variables, NSPV = 5

Node	x-coord.	y-coord.	Speci. primary & secondary variables (0, unspecified; >0, specified)	Primary DOF	Secondary DOF
------	----------	----------	---	-------------	---------------

1	0.0000E+00	0.0000E+00		0	0
2	0.5000E+00	0.0000E+00		0	0
3	0.1000E+01	0.0000E+00		1	0
4	0.0000E+00	0.5000E+00		0	0
5	0.5000E+00	0.5000E+00		0	0
6	0.1000E+01	0.5000E+00		1	0
7	0.0000E+00	0.1000E+01		1	0
8	0.5000E+00	0.1000E+01		1	0
9	0.1000E+01	0.1000E+01		1	0

NUMERICAL INTEGRATION DATA:

Full integration polynomial degree, IPDF = 3
 Number of full integration points, NIPF = 4
 Reduced integration polynomial deg., IPDR = 1
 No. of reduced integration points, NIPR = 1
 Integ. poly. deg. for stress comp., ISTR = 1
 No. of integ. pts. for stress comp., NSTR = 1

(Box 13.4.4 is continued from the previous page)

SOLUTION:

Node	x-coord.	y-coord.	Primary DOF
1	0.00000E+00	0.00000E+00	0.31250E+00
2	0.50000E+00	0.00000E+00	0.22917E+00
3	0.10000E+01	0.00000E+00	0.00000E+00
4	0.00000E+00	0.50000E+00	0.22917E+00
5	0.50000E+00	0.50000E+00	0.17708E+00
6	0.10000E+01	0.50000E+00	0.00000E+00
7	0.00000E+00	0.10000E+01	0.00000E+00
8	0.50000E+00	0.10000E+01	0.00000E+00
9	0.10000E+01	0.10000E+01	0.00000E+00

The orientation of gradient vector is measured from the positive x-axis

x-coord.	y-coord.	-a11(du/dx)	-a22(du/dy)	Flux	Mgntd	Orientation
0.3333E+00	0.1667E+00	0.1667E+00	0.1042E+00	0.1965E+00	32.01	
0.1667E+00	0.3333E+00	0.1042E+00	0.1667E+00	0.1965E+00	57.99	
0.8333E+00	0.1667E+00	0.4583E+00	0.0000E+00	0.4583E+00	0.00	
0.6667E+00	0.3333E+00	0.3542E+00	0.1042E+00	0.3692E+00	16.39	
0.3333E+00	0.6667E+00	0.1042E+00	0.3542E+00	0.3692E+00	73.61	
0.1667E+00	0.8333E+00	0.0000E+00	0.4583E+00	0.4583E+00	90.00	
0.8333E+00	0.6667E+00	0.3542E+00	0.0000E+00	0.3542E+00	0.00	
0.6667E+00	0.8333E+00	0.0000E+00	0.3542E+00	0.3542E+00	90.00	

Example 13.4.2 (Convective Heat Transfer)

Consider a square region of $1\text{ m} \times 1\text{ m}$. The left side of the region (i.e., $x = 0$) is maintained at 100°C , while the boundary $y = 1\text{ m}$ is maintained at 500°C . The boundaries $x = 1\text{ m}$ and $y = 0$ are exposed to an ambient temperature of 100°C , and the film coefficient $\beta = 10\text{ W}/(\text{m}^2 \cdot ^\circ\text{C})$. There is no internal heat generation ($f = 0$). The conductivity is taken to be $k_x = k_y = 12.5\text{ W}/(\text{m} \cdot ^\circ\text{C})$.

The input variables associated with convective boundary conditions are

$\text{ICONV} = 1$, $\text{NBE} = 16$ (for an 8×8 mesh of linear rectangular elements)

$[\text{IBN}(I), \text{BETA}(I), \text{TINF}(I)] = [1, 10.0, 100.0; 2, 10.0, 100.0, \dots]$

$[\text{INOD}(I, J)] = [1, 2; 1, 2; \dots]$

$A10 = 12.5$, $A1X = 0.0$, $A1Y = 0.0$, $A20 = 12.5$,

$A2X = 0.0$, $A2Y = 0.0$, $A00 = 0.0$

Box 13.4.5 contains the input data for the 8×8 mesh of linear rectangular elements. The output for this problem is not included here, but the results are included in the form of figures. Plots of temperature variations and heat flow

$$q_x = -k_x \frac{\partial T}{\partial x}, \quad q_y = -k_y \frac{\partial T}{\partial y}$$

along the boundaries are shown in Fig 13.4.4 and 13.4.5, respectively. Note that q_x is linear in x and constant in y , and q_y is linear in y and constant in x (for constant k_x and k_y). A nonuniform mesh with smaller elements in the high-gradient region gives more accurate results:

$$\{DY(I)\} = \{DX(I)\} = (0.25, 0.125, 0.125, 0.125, 0.125, 0.125, 0.125, 0.0625, 0.0625)$$

Box 13.4.5 The input data to program **FEM2D** for the convective heat transfer problem of Example 13.4.2.

```

Example 13.4.2: Convective heat transfer in a square region
0   1   0   0                                     ITYPE, IGRAD, ITEM, NEIGN
1   4   1   0                                     IELTYP, NPE, MESH, NPNRT
8   8                                     NX, NY
0.0  0.125  0.125  0.125  0.125  0.125  0.125
          0.125  0.125                                     X0, DX(I)
0.0  0.125  0.125  0.125  0.125  0.125  0.125
          0.125  0.125                                     Y0, DY(I)

17                                     NSPV
1 1   10 1   19 1   28 1   37 1   46 1   55 1   64 1   73 1
74 1   75 1   76 1   77 1   78 1   79 1   80 1   81 1   ISPV(I,J)
100.0 100.0 100.0 100.0 100.0 100.0 100.0 100.0 500.0
500.0 500.0 500.0 500.0 500.0 500.0 500.0 500.0  VSPV(I)
0                                     NSSV

12.5  0.0  0.0                                     A10, A1X, A1Y
12.5  0.0  0.0                                     A20, A2X, A2Y
0.0                                         A00

1                                     ICONV
16                                     NBE, IBN, BETA, TINF
1 10.0  100.0  2 10.0  100.0  3 10.0  100.0  4 10.0  100.0
5 10.0  100.0  6 10.0  100.0  7 10.0  100.0  8 10.0  100.0
8 10.0  100.0  16 10.0  100.0  24 10.0  100.0  32 10.0  100.0
40 10.0  100.0  48 10.0  100.0  56 10.0  100.0  64 10.0  100.0
1 2 1 2 1 2 1 2 1 2 1 2 1 2 1 2 1 2 1 2 1 2 1 2 1 2 1 2 1 2 1 2
2 3 2 3 2 3 2 3 2 3 2 3 2 3 2 3 2 3 2 3 2 3 2 3 2 3 2 3 2 3 2 3
                                         INOD(I,J)

0.0  0.0  0.0                                     F0, FX, FY

```

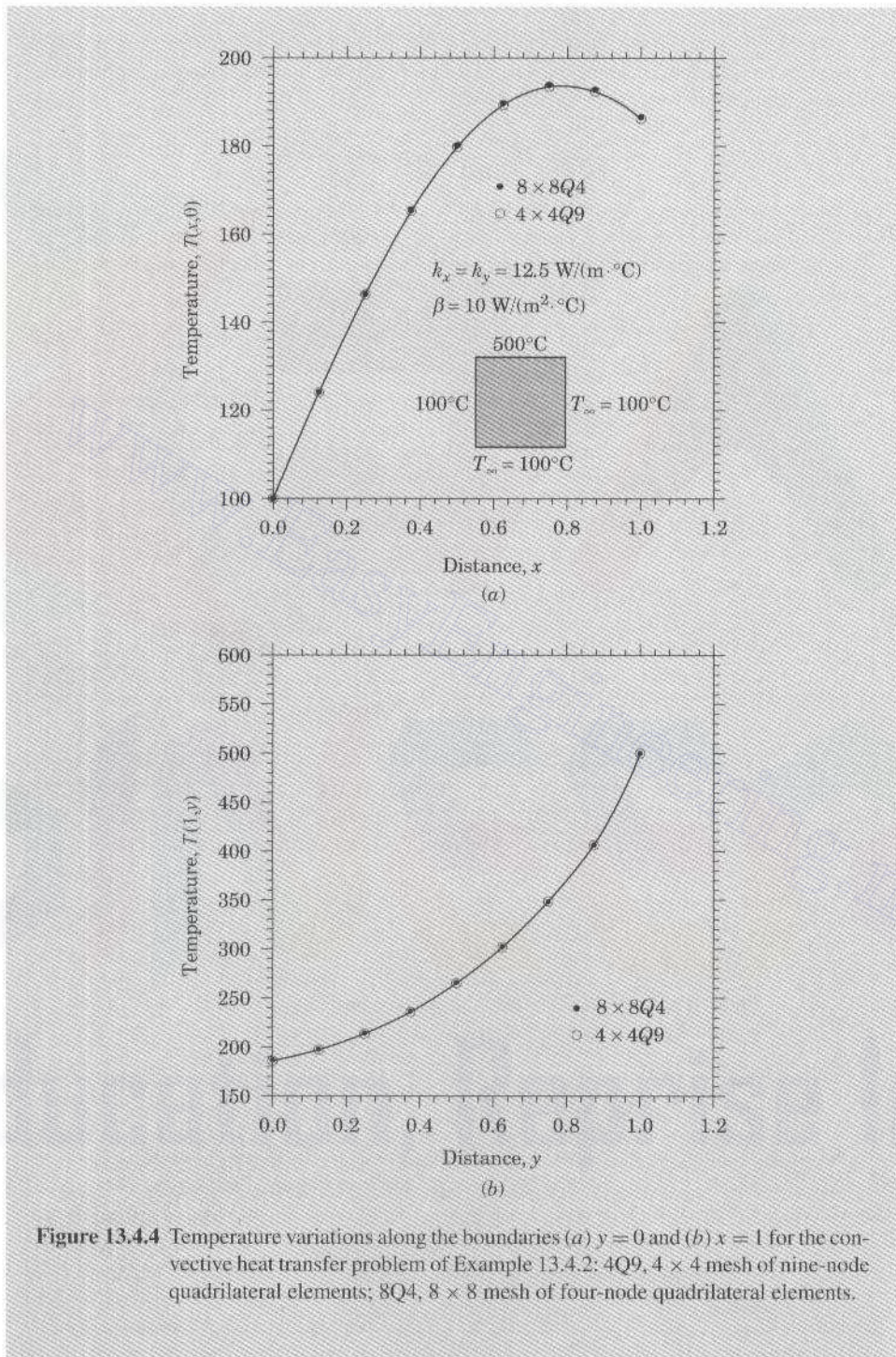


Figure 13.4.4 Temperature variations along the boundaries (a) $y = 0$ and (b) $x = 1$ for the convective heat transfer problem of Example 13.4.2: 4Q9, 4×4 mesh of nine-node quadrilateral elements; 8Q4, 8×8 mesh of four-node quadrilateral elements.

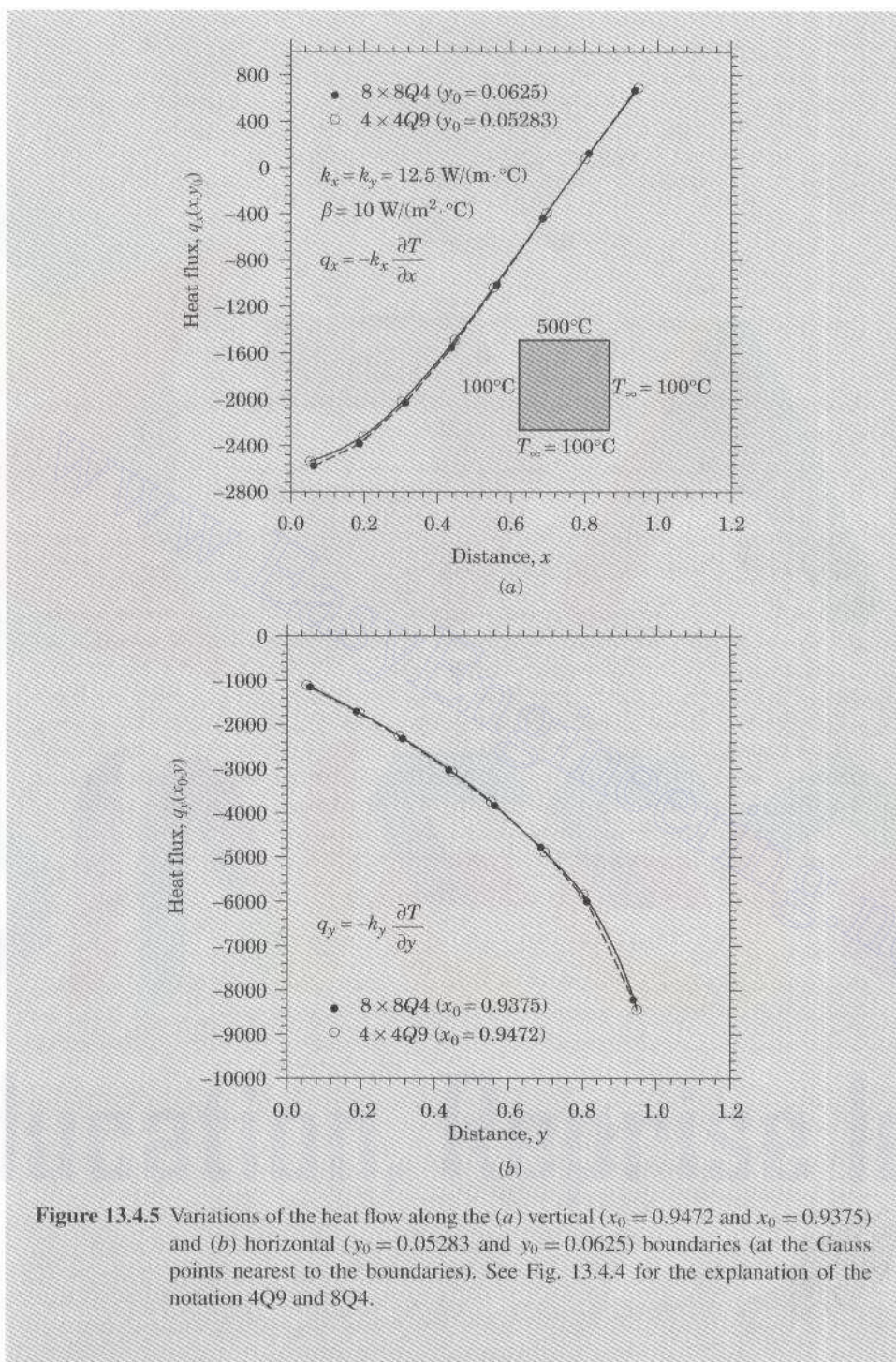


Figure 13.4.5 Variations of the heat flow along the (a) vertical ($x_0 = 0.9472$ and $x_0 = 0.9375$) and (b) horizontal ($y_0 = 0.05283$ and $y_0 = 0.0625$) boundaries (at the Gauss points nearest to the boundaries). See Fig. 13.4.4 for the explanation of the notation 4Q9 and 8Q4.

The program can also be used to analyze axisymmetric problems. For example, consider a finite cylinder of radius $R_0 = 1$ m and length $L = 1$ m. The bottom and top of the cylinder are maintained at $T_0 = 100^\circ\text{C}$, while the surface is exposed to an ambient temperature $T_\infty = 100^\circ\text{C}$ ($\beta = 10\text{W}/(\text{m}^2 \cdot \text{C})$). For this case, the governing differential equation is given by (8.5.11). The coefficients A10, A1X, A1Y, A20, A2X, A2Y, and A00 for **FEM2D** are

$$\begin{aligned} A10 &= 0.0, & A1X &= 2\pi k_r, & A1Y &= 0.0 \\ A20 &= 0.0, & A2X &= 2\pi k_z, & A2Y &= 0.0 \\ A00 &= 0.0 \end{aligned}$$

The uniform heat generation f_0 (if not zero) is entered as

$$F0 = 0.0, \quad FX = 2\pi f_0, \quad FY = 0.0$$

For a mesh of $m \times n$ mesh of linear elements, the number of elements with convective boundary will be n .

Example 13.4.3 (Flow around a Circular Cylinder)

Consider the flow of an inviscid fluid around a cylinder. We shall use the stream function and velocity potential formulations to determine the velocity fields. Since the domain is not rectangular, we should use subroutine **MESH2DG** (i.e., set MESH = 2). We consider the mesh of 25 nodes and 32 triangular elements shown in Fig. 13.4.2. We have ITYPE = 0; IGRAD = 1 in the velocity potential formulation and IGRAD = 2 in the stream function formulation; ITEM = 0 and NEIGN = 0; IELTYP = 0 for triangles and IELTYP = 1 for quadrilaterals; and MESH = 2 and NPRNT = 0. The input for **MESH2DG** is given in Box 13.4.1 for triangular as well as quadrilateral elements. The partial input of the problem is given in Box 13.4.6.

In the stream function formulation, we have NSPV = 13 and NSSV = 0; and in the velocity potential formulation, we have NSPV = 5 and NSSV = 3. The coefficients are

$$\begin{aligned} A10 &= 1.0, & A20 &= 1.0, & A1X &= 0.0, & A1Y &= 0.0, & A2X &= 0.0, & A2Y &= 0.0 \\ A00 &= 0.0, & F0 &= 0.0, & FX &= 0.0, & FY &= 0.0 \end{aligned}$$

The partial input of the problem is given in Box 13.4.6 (see Box 13.4.1 for the mesh data). A detailed discussion of the numerical results is presented in Example 8.5.5.

Example 13.4.4 (Eigenvalue and Transient Analysis)

We consider the eigenvalue and transient problems discussed in Examples 8.6.1 and 8.6.2. The governing differential equation is [see Eqs. (8.6.12a)–(8.6.12c)]

$$\begin{aligned} \frac{\partial u}{\partial t} - \left(\frac{\partial^2 u}{\partial x^2} + \frac{\partial^2 u}{\partial y^2} \right) &= 1 \\ \frac{\partial u}{\partial x}(0, y, t) &= 0, \quad \frac{\partial u}{\partial y}(x, 0, t) = 0, \quad u(x, 1, t) = 0, \quad u(1, y, t) = 0 \\ u(x, y, 0) &= 0 \end{aligned}$$

Box 13.4.6 The input data to program FEM2D for the flow of an inviscid fluid around a cylinder.

Example 13.4.3(a): Flow around a circular cylinder (VEL.POTENTIAL)																		
0	1	0	0						ITYPE, IGRAD, ITEM, NEIGN									
0	3	2	0						IEL, NPE, MESH, NPRNT									
 *** See TABLE 13.4.1(a) for the MESH2DG input ***																		
5									NSPV									
21	1	22	1	23	1	24	1	25	1									
0.0		0.0		0.0		0.0		0.0	ISPV(I,J)									
3									VSPV(I)									
1	1	6	1	11	1				NSSV									
0.5		1.0		0.5					ISSV(I,J)									
1.0	0.0	0.0							VSSV(I)									
1.0	0.0	0.0							A10, A1X, A1Y									
0.0									A20, A2X, A2Y									
0.0									A00									
0									ICONV									
0.0	0.0	0.0							F0, FX, FY									
 Example 13.4.3(b): Flow around a circular cylinder (STRM FUNCN)																		
0	2	0	0						ITYPE, IGRAD, ITEM, NEIGN									
0	3	2	0						IELTYP, NPE, MESH, NPRNT									
 *** See TABLE 13.4.1(a) for the MESH2DG input ***																		
13									NSPV									
1	1	2	1	3	1	4	1	5	1	10	1	15	1	20	1	25	1	
6	1	11	1	16	1	21	1											ISPV(I,J)
0.0		0.0		0.0		0.0		0.0		0.0		0.0		0.0		0.0		VSPV(I)
1.0		2.0		2.0		2.0												NSSV
0																		
 *** Remaining data is the same as in Example 13.4.3(a) above ***																		

For eigenvalue analysis, we set ITEM = 1 and NEIGN = 1; for the transient analysis, we set ITEM = 1 (parabolic equation) and NEIGN = 0. In addition, we must input the following parameters:

Eigenvalue Analysis

NVALU (number of eigenvalues to be printed) and NVCTR (if eigenvectors to be printed).

Transient Analysis

NTIME = 20, NSTP = 21, ($>$ NTIME), INTVL = 1

INTIAL = 0, DT = 0.05, ALFA = 0.5, GAMA = 0.5 (not used)

C0 = 1.0, CX = 0.0, CY = 0.0

The parameter **NSTP** allows removal of the source (i.e., f) at a given time step. For example, if **NSTP = 5**, then at the fifth time step and at each subsequent time step f will be set equal to zero. In the present case, the source $f = 1$ is kept at all times; hence, we must choose **NSTP** to be greater than **NTIME** (say **NSTP = 21**).

The input files and partial output for the eigenvalue and transient analyses are presented in Boxes 13.4.7 and 13.4.8, respectively. For a discussion of the numerical results of these two problems, see Examples 8.6.1 and 8.6.2.

The problems in Examples 8.6.3 and 8.6.4 can be analyzed using **FEM2D**, with minor changes to the input data given in Boxes 13.4.7 and 13.4.8. The input data for the two problems of Examples 8.6.3 and 8.6.4 is included in Box 13.4.9.

Box 13.4.7 The input data and partial output of program **FEM2D** for the eigenvalue analysis of a parabolic equation (Example 13.4.4).

```

Example 13.4.4: EIGENVALUE ANALYSIS of a parabolic equation
      0   0   1   1                           ITYPE, IGRAD, ITEM, NEIGN
      16   0                           NVALU, NVCTR
      1   4   1   0                           IELTYP, NPE, MESH, NPRNT
      4   4                           NX, NY
      0.0  0.25  0.25  0.25  0.25          X0,DX(I)
      0.0  0.25  0.25  0.25  0.25          Y0,DY(I)
      9                           NSPV
      5 1   10 1   15 1   20 1   21 1          ISPV
      22 1   23 1   24 1   25 1               A10, A1X, A1Y
      1.0  0.0   0.0               A20, A2X, A2Y
      1.0  0.0   0.0               A00
      0                           ICONV
      1.0  0.0   0.0               C0, CX, CY

S O L U T I O N (from FEM2D):
Number of Jacobi iterations ..... NROT = 371
E I G E N V A L U E (1) = 0.343256E+03
E I G E N V A L U E (2) = 0.253701E+03
E I G E N V A L U E (3) = 0.253701E+03
E I G E N V A L U E (4) = 0.196500E+03
E I G E N V A L U E (5) = 0.196500E+03
E I G E N V A L U E (6) = 0.174127E+03
E I G E N V A L U E (7) = 0.174127E+03
E I G E N V A L U E (8) = 0.164145E+03
E I G E N V A L U E (9) = 0.106945E+03
E I G E N V A L U E (10) = 0.106945E+03
E I G E N V A L U E (11) = 0.845720E+02
E I G E N V A L U E (12) = 0.845720E+02
E I G E N V A L U E (13) = 0.497442E+02
E I G E N V A L U E (14) = 0.273714E+02
E I G E N V A L U E (15) = 0.273714E+02
E I G E N V A L U E (16) = 0.499854E+01

```

Box 13.4.8 The input data and partial output of program **FEM2D** for the transient analysis of a parabolic equation (Example 13.4.4).

```

Example 13.4.4: TRANSIENT ANALYSIS of a parabolic equation
 0   0   1   0           ITYPE,IGRAD,ITEM,NEIGN
 1   4   1   0           IELTYP,NPE,MESH,NPRNT
 4   4           NX,NY
 0.0  0.25  0.25  0.25  0.25  X0,DX(I)
 0.0  0.25  0.25  0.25  0.25  Y0,DY(I)
 9           NSPV
 5 1  10 1  15 1  20 1  21 1  22 1
23 1  24 1  25 1           ISPV
 0.0 0.0 0.0 0.0 0.0 0.0 0.0 0.0 0.0 0.0  VSPV
 0           NSSV
 1.0 0.0 0.0           A10, A1X, A1Y
 1.0 0.0 0.0           A20, A2X, A2Y
 0.0           A00
 0           ICONV
 1.0 0.0 0.0           F0, FX, FY
 1.0 0.0 0.0           C0, CX, CY
 20  21  1   0           NTIME,NSTP,INTVL,INTIAL
 0.05 0.5  0.5  1.0E-3  DT,ALFA,GAMA,EPSLN

```

Edited output from FEM2D

TIME = 0.50000E-01 Time Step Number = 1
 S O L U T I O N :

Node	x-coord.	y-coord.	Primary DOF
1	0.00000E+00	0.00000E+00	0.49867E-01
2	0.25000E+00	0.00000E+00	0.49718E-01
3	0.50000E+00	0.00000E+00	0.48620E-01
4	0.75000E+00	0.00000E+00	0.41808E-01

TIME= 0.10000E+01 Time Step Number = 20
 S O L U T I O N :

Node	x-coord.	y-coord.	Primary DOF
1	0.00000E+00	0.00000E+00	0.29621E+00
2	0.25000E+00	0.00000E+00	0.28037E+00
3	0.50000E+00	0.00000E+00	0.23065E+00
4	0.75000E+00	0.00000E+00	0.14053E+00

Box 13.4.9 The input data and partial output of program **FEM2D** for vibration and transient analysis of the rectangular membrane of Examples 8.6.3 and 8.6.4.

Example 13.4.4: Natural vibration of a rectangular membrane																		
0	0	2	1						ITYPE, IGRAD, ITEM, NEIGN									
10	0								NVALU, NVCTR									
1	4	1	0						IELTYP, NPE, MESH, NPRNT									
4	4								NX, NY									
0.0	1.0	1.0	1.0	1.0					X0, DX(I)									
0.0	0.5	0.5	0.5	0.5					Y0, DY(I)									
16									NSPV									
1	1	2	1	3	1	4	1	5	1	6	1	10	1	11	1			
15	1	16	1	20	1	21	1	22	1	23	1	24	1	25	1			
12.5	0.0	0.0								A10, A1X, A1Y								
12.5	0.0	0.0								A20, A2X, A2Y								
0.0										A00								
0										ICONV								
2.5	0.0	0.0								C0, CX, CY								
Example 13.4.4: Transient analysis of a rectangular membrane																		
0	0	2	0						ITYPE, IGRAD, ITEM, NEIGN									
1	4	1	0						IELTYP, NPE, MESH, NPRNT									
4	4								NX, NY									
0.0	0.5	0.5	0.5	0.5	0.5				X0, DX(I) (a quadrant)									
0.0	0.25	0.25	0.25	0.25	0.25				Y0, DY(I) (is used)									
9									NSPV									
5	1	10	1	15	1	20	1	21	1	22	1	23	1	24	1	25	1	ISPV
0.0	0.0	0.0	0.0	0.0	0.0	0.0	0.0	0.0	0.0	0.0	0.0	0.0	0.0	0.0	0.0	VSPV		
0										NSSV								
12.5	0.0	0.0								A10, A1X, A1Y								
12.5	0.0	0.0								A20, A2X, A2Y								
0.0										A00								
0										ICONV								
0.0	0.0	0.0								FO, FX, FY								
2.5	0.0	0.0								C0, CX, CY								
20	21	1	1							NTIME, NSTP, INTVL, INTIAL								
0.025	0.5	0.5	1.0E-3							DT, ALFA, GAMA, EPSLN								
0.400	0.375	0.300		0.175		0.0												
0.375	0.35156	0.28125		0.16406		0.0												
0.300	0.28125	0.225		0.13125		0.0												
0.175	0.16406	0.13125		0.076563		0.0												
0.0	0.0	0.0		0.0		0.0				Ini. cond., GLU(I)								
0.0	0.0	0.0		0.0		0.0												
0.0	0.0	0.0		0.0		0.0												
0.0	0.0	0.0		0.0		0.0												
0.0	0.0	0.0		0.0		0.0												

Example 13.4.5 (Fluid Squeezed between Parallel Plates)

We set up the data for a 12×8 uniform mesh of linear rectangular elements and the equivalent 6×4 mesh of nine-node elements. Most of the data is exactly the same for both meshes. We have

```
ITYPE = 1, IGRAD = 1, ITEM = 0 (for static analysis)
ITEM = 1 (for transient analysis), NEIGN = 0
NX = 6, NY = 4, NSPV = 47
AMU(=  $\mu$ ) = 1.0, PENLTY(=  $\gamma$ ) = 108
```

Box 13.4.10 contains the complete input data for the 6×4 mesh of nine-node elements for the transient case. For additional details, see Examples 10.6.1 and 10.6.4.

Box 13.4.10 The input data to program **FEM2D** for the transient analysis of fluid squeezed between plates (Example 13.4.5).

Example 13.4.5: TRANSIENT ANALYSIS of fluid squeezed between plates												
1	1	1	0									ITYPE, IGRAD, ITEM, NEIGN
2	9	1	0									IEL, NPE, MESH, NPRINT
6	4											NX, NY
0.0	1.0	1.0	1.0	1.0	1.0	1.0	1.0					X0, DX(I)
0.0	0.5	0.5	0.5	0.5								Y0, DY(I)
47												NSPV
1 1	1 2	2 2	3 2	4 2	5 2	6 2	7 2	8 2	9 2			
10 2	11 2	12 2	13 2	14 1	27 1	40 1	53 1	66 1	79 1			
92 1	105 1	105 2	106 1	106 2	107 1	107 2	108 1	108 2	109 1			
109 2	110 1	110 2	111 1	111 2	112 1	112 2	113 1	113 2	114 1			
114 2	115 1	115 2	116 1	116 2	117 1	117 2				ISPV(I,J)		
0.0	0.0	0.0	0.0	0.0	0.0	0.0	0.0	0.0	0.0			
0.0	0.0	0.0	0.0	0.0	0.0	0.0	0.0	0.0	0.0			
0.0	0.0	-1.0	0.0	-1.0	0.0	-1.0	0.0	-1.0	0.0			
-1.0	0.0	-1.0	0.0	-1.0	0.0	-1.0	0.0	-1.0	0.0			
-1.0	0.0	-1.0	0.0	-1.0	0.0	-1.0	VSPV(I)					
0										NNSV		
1.0	1.0E8									AMU, PENLTY		
0.0	0.0	0.0								FO, FX, FY		
1.0	0.0	0.0								CO, CX, CY		
20	50	1	0							NTIME, NSTP, INTVL, INTIAL		
0.1	0.5	0.25	1.0D-3							DT, ALFA, GAMMA, EPSLN		

The next example deals with plane elasticity problem of Examples 11.7.2 and 11.7.3.

Example 13.4.6 (Elasticity Problem)

This is a plane elasticity problem with plane stress assumption (i.e., LNSTRS = 1). Here we consider both triangular and rectangular element meshes (see Fig. 13.4.6); MESH2DR can be used to generate the meshes (i.e., MESH = 1). For the 8×2 mesh of linear elements, we have the following input parameters:

$$\text{ITYPE} = 2, \quad \text{IGRAD} = 1 \quad (\text{or } > 0), \quad \text{ITEM} = 0$$

for static analysis and ITEM = 2 for dynamic analysis. There are four specified primary variables and three nonzero specified forces for the mesh:

$$\text{NSSV} = 4, \quad \text{ISVP}(I, J) = (9, 1; 18, 1; 18, 2; 27, 1)$$

$$\text{VSPV}(I) = (0.0, 0.0, 0.0, 0.0)$$

$$\text{NSSV} = 3, \quad \text{ISSV}(I, J) = (1, 2; 10, 2; 19, 2), \quad \text{VSSV}(I) = (-75.0, -150.0, -75.0)$$

For the 4×1 mesh of nine-node quadratic elements, the data remains the same as above, except for the values of the specified forces ($-50.0, -200.0, -50.0$).

Box 13.4.11 contains the data sets for natural vibration and transient analysis for the 4×1 mesh of nine-node quadratic elements. The data for the static case follows easily from the transient case. The results were discussed in Examples 11.7.2 and 11.7.3.

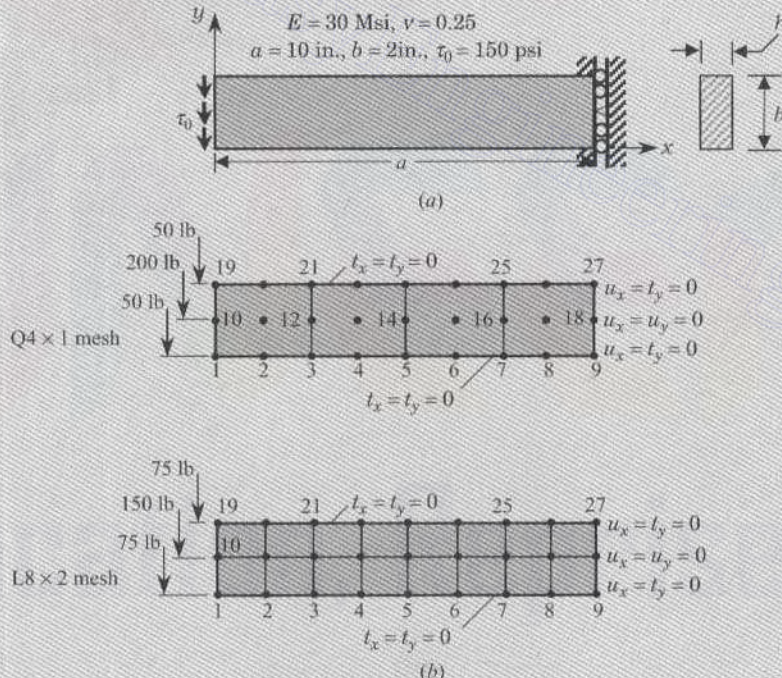


Figure 13.4.6 Bending of a cantilever plate using the elasticity equations: (a) geometry and loading; and (b) meshes of four-node linear elements (8×2) and nine-node quadratic elements (4×1).

Box 13.4.11 The input data to program **FEM2D** for natural vibration and transient analysis of a cantilever plate (Example 13.4.6).

```

Example 13.4.6: Natural vibration of a beam by plane elasticity
 2   0   2   1           ITYPE,IGRAD,ITEM,NEIGN
 10  0                   NVALU,NVCTR
 2   9   1   0           IELTYP,NPE,MESH,NPRNT
 4   1                   NX, NY
 0.0  2.5   2.5   2.5   2.5   X0, DX(I)
 0.0  2.0               Y0, DY(I)
 4                   NSPV
 9 1   18 1   18 2   27  1   ISPV
 1                   LNSTRS
 30.0E06  30.0E06  0.25  12.0E06  1.0   E1,E2,ANU12,G12,THKNS
 8.8255E-03  0.0   0.0   C0, CX, CY

Example 13.4.6: Transient analysis of a beam by plane elasticity
 2   1   2   0           ITYPE,IGRAD,ITEM,NEIGN
 2   9   1   0           IELTYP,NPE,MESH,NPRNT
 4   1                   NX, NY
 0.0  2.5   2.5   2.5   2.5   X0,DX(I)
 0.0  2.0               Y0,DY(I)
 4                   NSPV
 9 1   18 1   18 2   27  1   ISPV
 0.0  0.0   0.0   0.0   VSPV
 3                   NSSV
 1   2   10  2   19  3   ISSV
 -50.0 -200.0 -50.0   VSSV
 1                   LNSTRS
 30.0E06  30.0E06  0.25  12.0E06  1.0   E1,E2,ANU12,G12,THKNS
 0.0   0.0   0.0   F0, FX, FY
 8.8255E-03  0.0   0.0   C0, CX, CY
 20   21   1   0       NTIME,NSTP,INTVL,INITIAL
 0.25E-03      0.5   0.5   1.0E-3   DT,ALFA,GAMA,EPSLN

```

The next two examples are concerned with plate bending problems (see Chapter 12).

Example 13.4.7 (Bending of a Plate)

Consider bending of a square plate under uniformly distributed load. The 1×1 mesh of Hermite elements and 4×4 mesh of nine-node elements are used to model the square plate. Only rectangular elements are allowed:

Classical Plate Theory (CPT) (ITYPE = 4 or 5)

ITYPE = 5 (conforming element), IGRAD = 1

Shear Deformation Theory (SDT)

ITYPE = 3, IGRAD = 1

The classical plate model has three degrees of freedom per node when the nonconforming element is used (i.e., ITYPE = 4), and four degrees of freedom per node for the conforming element (i.e., ITYPE = 5). This must be taken into consideration in specifying boundary conditions. For additional details, see Example 12.5.1.

The input data for static analysis of a simply supported, square, isotropic plate using CPT(C) and SDT models is presented in Box 13.4.12. A quadrant of the plate is used as the computational domain. For the nonconforming element, the data is the same as that used for the shear deformation model, except that ITYPE = 4. For free vibration (NEIGN = 1) and stability analysis (NEIGN = 2), most of the data remain the same. For transient analysis, the time step used for unconditionally stable schemes is arbitrary, but should be small enough to give a complete and accurate response curve.

Box 13.4.12 The input data to program **FEM2D** for (static) bending analysis of a simply supported, square, isotropic plate (see Fig. 12.5.1).

```
Example 13.4.7: Bending of a simply-supported plate (SDT)
 3   1   0   0                               ITYPE, IGRAD, ITEM, NEIGN
 1   4   1   0                               IEL, NPE, MESH, NPRNT
 4   4                               NX, NY
 0.0  1.25   1.25   1.25   1.25           X0, DX(I)
 0.0  1.25   1.25   1.25   1.25           Y0, DY(I)
 27                               NSPV
 1 2   1 3   2 3   3 3   4 3   5 1   5 3   6 2   10 1
 10 3   11 2   15 1   15 3   16 2   20 1   20 3   21 1   21 2
 22 1   22 2   23 1   23 2   24 1   24 2   25 1   25 2   25 3
 0.0   0.0   0.0   0.0   0.0   0.0   0.0   0.0   0.0
 0.0   0.0   0.0   0.0   0.0   0.0   0.0   0.0   0.0
 0.0   0.0   0.0   0.0   0.0   0.0   0.0   0.0   0.0
 0                               NSSV
 1.0E7  1.0E7  0.25  0.4E7  0.4E7  1.0   E1,E2,ANU12,G12, etc.
 1.0   0.0   0.0                               FO, FX, FY
```

```
Example 13.4.7: Bending of a simply-supported plate [CPT(C)]
 5   1   0   0                               ITYPE, IGRAD, ITEM, NEIGN
 1   4   1   0                               IEL, NPE, MESH, NPRNT
 1   1                               NX, NY
 0.0  5.0                               X0, DX(I)
 0.0  5.0                               Y0, DY(I)
 12                               NSPV
 1 2   1 3   2 1   2 3   3 1   3 2   4 1   4 2
 4 3   1 4   2 4   3 4                           ISPV(I,J)
 0.0   0.0   0.0   0.0   0.0   0.0   0.0   0.0
 0.0   0.0   0.0   0.0                           VSPV(I)
 0                               NSSV
 1.0E7  1.0E7  0.25  0.4E7  0.4E7  0.4E7  1.0   E1,E2,ANU12,G12,etc.
 1.0   0.0   0.0                               FO, FX, FY
```

Example 13.4.8 (Transient Response of a Clamped Circular Plate)

Consider a clamped circular plate of radius $R = 100$ in., thickness $h = 20$ in., modulus $E = 100$ psi, Poisson's ratio $\nu = 0.3$, and density $\rho = 10$ slug/in.³, and subjected to a suddenly applied pressure load of intensity $q_0 = 1$ psi. We analyze the problem by modeling one quadrant (using the symmetry) of the plate by five nine-node elements (see Fig. 13.4.7) and $\Delta t = 2.5$ s. The input data to **FEM2D** is presented in Box 13.4.13. Plots of the center deflection and stress versus time are shown in Fig. 13.4.8.

Box 13.4.13 The input data to program **FEM2D** for transient analysis of a clamped, circular, isotropic plate under uniform load.

```

Example 13.4.8: Transient analysis of a circular plate (SDT)
 3   1   2   0          ITYPE, IGRAD, ITEM, NEIGN
 2   9   0   0          TEL, NPE, MESH, NPRNT
 5   29          NEM, NNM
 1   5   7   9   2   6   8   4   3          NOD(1,I), I=1,NPE
 5   15  17  7   10  16  12   6  11          NOD(2,I), I=1,NPE
 9   7   17  19   8  12  18  14  13          NOD(3,I), I=1,NPE
 15  25  27  17  20  26  22  16  21          NOD(4,I), I=1,NPE
 19  17  27  29  18  22  28  24  23          NOD(5,I), I=1,NPE
 0.0000  0.0000  16.5000  0.0000  11.6673  11.6673
 0.0000  16.5      33.0      0.0      30.488   12.6286
 23.3345 23.3345  12.6286  30.488    0.0      33.0
 49.5     0.0      45.732   18.9428  35.0      35.0
 18.9428 45.732    0.0      49.5      66.0      0.0
 60.976   25.2571  46.669   46.669  25.2571  60.976
 0.0      66.0      83.0      0.0      76.682   31.7627
 58.6898 58.6898  31.7627  76.682    0.0      83.0
 100.0    0.0      92.388   38.2683  70.7107  70.7107
 38.2683 92.388    0.0      100.0    GLXY(I,J)
 27          NSDPV
 1 2   1 3   2 3   4 2   5 3   9 2   10 3   14 2   15 3
 19 2  20 3  24 2  25 1  25 2  25 3  26 1  26 2  26 3
 27 1  27 2  27 3  28 1  28 2  28 3  29 1  29 2  29 3
 0.0  0.0  0.0  0.0  0.0  0.0  0.0  0.0  0.0  0.0  0.0  0.0
 0.0  0.0  0.0  0.0  0.0  0.0  0.0  0.0  0.0  0.0  0.0  0.0
 0.0  0.0  0.0  0.0  0.0  0.0  0.0  0.0  0.0  0.0  0.0  0.0
 0          NSSV
 1.0E2 1.0E2  0.3  0.3845E2  0.3845E2  0.3845E2  20.0 E1,E2, etc.
 1.0  0.0  0.0          FO, FX, FY
 10.0 0.0  0.0          CO, CX, CY
 200  201  10  0          NTIME, NSTP, INTVL, INITIAL
 2.5  0.5  0.5  1.0E-03 DT, ALFA, GAMMA, EPSLN

```

13.5 SUMMARY

A description of finite element computer program **FEM2D** and its application to problems discussed in Chapters 8–12 have been presented. The program can be used to analyze two-dimensional field problems and problems of plane elasticity, two-dimensional flows of viscous incompressible fluids, and plate bending. It allows static, eigenvalue, and time-dependent analyses. Linear and quadratic, and triangular and rectangular elements can be used. The program **FEM2D** is a true reflection of the theory presented in Chapters 8–12, and it can be extended to analyze other field problems with appropriate modifications.

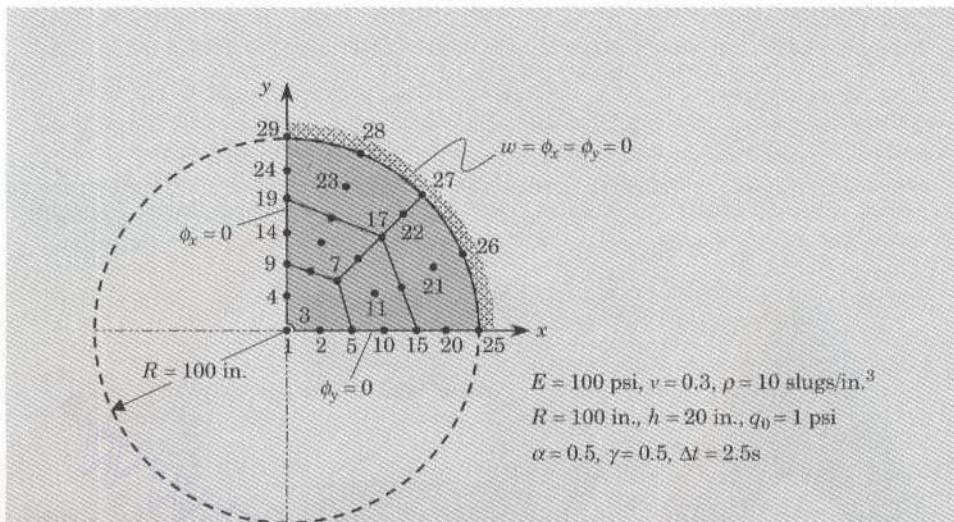


Figure 13.5.7 The geometry, boundary conditions, and finite element mesh of the clamped circular plate of Example 13.4.8.

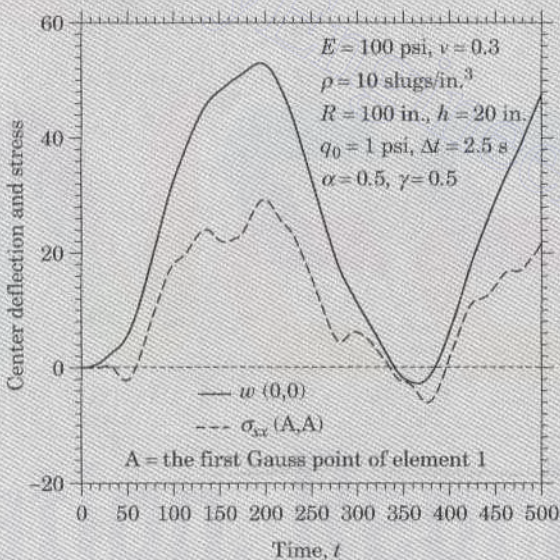


Figure 13.5.8 Center deflection and stress versus time for the clamped circular plate of Example 13.4.8.

PROBLEMS

Note that most of the problems may be analyzed using **FEM2D**. The results obtained from the program should be evaluated for their accuracy in the light of analytical solutions for qualitative understanding of the solutions of the problems. New problems can be generated from those given here by changing the problem data, mesh, type of element, etc. For time-dependent problems, the time step (whose order of magnitude is given by the critical time step) and number of time steps should be chosen such that the solution pattern is established or a steady state is reached. When specific material properties are not given, use values such that the solution can be interpreted as the nondimensional solution of the problem.

General Field Problems (Chapter 8)

- 13.1 Investigate the convergence of solutions to Problem 8.18 using 2×2 , 4×4 , and 8×8 meshes of linear triangular elements, and compare the results (in graphical or tabular form) with the analytical solution.
- 13.2 Repeat Problem 13.1 with rectangular elements.
- 13.3 Repeat Problem 13.1 for the case $u_0(x) = 1$ (see Problem 8.19 for the analytical solution).
- 13.4 Repeat Problem 13.3 with rectangular elements.
- 13.5 Investigate the convergence of the solution to Problem 8.23 using 2×2 , 4×4 , and 8×8 meshes of linear triangular elements and equivalent meshes of quadratic triangular elements.
Answer: For a 4×4 mesh of quadratic triangles, the values of $u(x, 0.125)$ at nodes 11 through 17 are 0.1145, 0.1977, 0.2829, 0.3787, 0.4880, 0.6111, and 0.7436.
- 13.6 Repeat Problem 13.5 using rectangular elements. *Answer:* For a 4×4 mesh of quadratic rectangles, the values of $u(x, 0.125)$ at nodes 11 through 17 are 0.1165, 0.1982, 0.2834, 0.3789, 0.4884, 0.6114, and 0.7449.
- 13.7 Analyze the axisymmetric problem in Problem 8.26 using 4×1 and 8×1 linear rectangular elements, and compare the solution with the exact solution. *Answer:* For a 8×1 mesh the values at $r = 0, 0.005, 0.01, 0.015$ and 0.02 are: $U_1 = 150.53$, $U_3 = 147.05$, $U_5 = 137.59$, and $U_7 = 121.91$. The exact values are $T_1 = 150.0$, $T_2 = 146.875$, $T_3 = 137.50$, and $T_4 = 121.875$.
- 13.8 Analyze the axisymmetric problem in Problem 8.27 using 4×4 and 8×8 meshes of linear rectangular elements.
- 13.9 Analyze Problem 8.18 for eigenvalues (take $c = 1.0$), using a 4×4 uniform mesh of triangular elements. Calculate the critical time step for a parabolic equation. *Answer:* $\Delta t_{\text{cr}} = 2.172 \times 10^{-3}$.
- 13.10 Analyze Problem 8.18 using a 4×4 mesh of triangles for transient response. Assume zero initial conditions. Use $\alpha = 0.5$ and $\Delta t = 0.001$. Investigate the stability of the solution when $\alpha = 0.0$ and $\Delta t = 0.0025$. The number of time steps should be such that the solution reaches its peak value or a steady state.
- 13.11 Analyze Problem 8.23 for transient response (take $c = 1.0$) using a 4×4 mesh of linear rectangular elements and a 2×2 mesh of nine-node quadratic rectangular elements. Assume zero initial conditions. Investigate the stability and accuracy of the Crank–Nicolson scheme ($\alpha = 0.5$) and the forward difference scheme ($\alpha = 0$).
- 13.12 Repeat Problem 13.11 for the axisymmetric problem in Fig. P8.27. Assume zero initial conditions.

Heat Transfer (Chapter 8)

- 13.13 Analyze the heat transfer problem in Problem 8.28 using an 8×16 mesh of linear triangular elements and an equivalent mesh of linear rectangular elements.
- 13.14 Analyze the heat transfer problem in Fig. P8.29.
- 13.15 Analyze Problem 8.30 for nodal temperatures and heat flow across the boundaries. Use the following data: $k = 30 \text{ W}/(\text{m} \cdot ^\circ\text{C})$, $\beta = 60 \text{ W}/(\text{m}^2 \cdot ^\circ\text{C})$, $T_\infty = 0^\circ\text{C}$, $T_0 = 100^\circ\text{C}$, $q_0 = 2 \times 10^5 \text{ W}/\text{m}^2$, $g_0 = 10^7 \text{ W}/\text{m}^3$, and $a = 1 \text{ cm}$.
- 13.16 Repeat Problem 13.15 with an equivalent mesh of triangular elements.
- 13.17 Analyze Problem 8.35 for nodal temperature and heat flows across the boundary. Take $k = 5 \text{ W}/(\text{m} \cdot ^\circ\text{C})$.
- 13.18 Consider heat transfer in a rectangular domain with a central heated circular cylinder (see Fig. P13.18 for the geometry). Analyze the problem using the mesh of linear quadrilateral elements shown in Fig. 13.4.2(b).

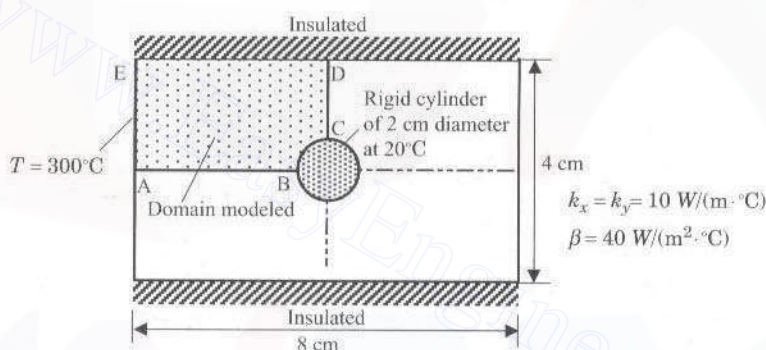


Figure P13.18

- 13.19 Analyze the heat transfer problem in Fig. P8.31 with (a) 2×2 and (b) 4×4 meshes of linear rectangular elements.
- 13.20 Repeat Problem 13.19 with triangular elements.
- 13.21 Analyze the problem in Fig. P8.32 with (a) 3×3 , and (b) 6×6 meshes of linear rectangular elements. Take $k = 10 \text{ W}/(\text{m} \cdot ^\circ\text{C})$.
- 13.22 Repeat Problem 13.21 with linear triangular elements.
- 13.23 Analyze the heat transfer problem in Fig. P8.34 with a 4×4 mesh of linear rectangular elements and an equivalent mesh of quadratic (nine-node) elements. Take $a = 1 \text{ cm}$, $T_0 = 100^\circ\text{C}$, and $k = 3 \text{ W}/(\text{m} \cdot ^\circ\text{C})$.
- 13.24 Analyze the problem in Fig. P8.35 for transient response using (a) $\alpha = 0$ and (b) $\alpha = 0.5$. Use $c = \rho c_p = 1.0$.
- 13.25 Analyze the axisymmetric problem in Fig. P8.26 using the Crank–Nicolson method. Use an 8×1 mesh of linear rectangular elements. Use $c = \rho c_p = 3.6 \times 10^6 \text{ J}/(\text{m}^3 \cdot \text{K})$.

Groundwater and Inviscid Flows (Chapter 8)

- 13.26 Analyze the groundwater flow in Problem 8.38 using the mesh of linear quadrilateral elements in Fig. 8.3.8 (remove the diagonal lines to obtain the mesh of quadrilateral elements).

- 13.27** Repeat Problem 13.26 with the mesh of linear triangular elements shown in Fig. 8.3.8.
- 13.28** Analyze Problem 8.39 with an 8×4 mesh of (a) linear triangular elements and (b) linear quadrilateral elements.
- 13.29** Repeat Problem 8.39 with a 4×2 mesh of (a) quadratic triangular elements and (b) quadratic (nine-node) quadrilateral elements.
- 13.30** Analyze Problem 8.37 using linear rectangular elements and an equivalent mesh of quadratic rectangular elements. Use an 8×6 mesh in the first rectangle and an 8×4 mesh in the second. The meshes should be refined in the horizontal direction to have smaller elements around the sheet pile.
- 13.31** Analyze the flow around a cylinder of elliptical cross section (see Fig. P8.41). Use the symmetry and an appropriate mesh of linear triangular elements. Use the stream function approach.
- 13.32** Repeat Problem 13.31 using the velocity potential formulation.

Membrane and Torsion Problems (Chapter 8)

- 13.33** Analyze the torsion of a member of circular cross section (see Fig. P8.43) for the state of shear stress distribution. Investigate the accuracy with mesh refinements (by subdividing the mesh in Fig. P8.43 with horizontal and vertical lines).
- 13.34** Analyze the torsion problem in Fig. P8.45.
- 13.35** Analyze the hollow-cross-section torsion problem in Fig. P8.46 using a mesh of (a) linear triangular elements in an octant and (b) linear rectangular elements in a quadrant. The meshes should be nodewise equivalent.
- 13.36** Analyze the rectangular membrane problem in Fig. P8.48 with 4×4 and 8×8 meshes of linear rectangular elements in the computational domain. Take $a_{11} = a_{22} = 1$ and $f_0 = 1$.
- 13.37** Repeat Problem 13.36 with equivalent meshes of quadratic elements.
- 13.38** Determine the eigenvalues of the rectangular membrane in Fig. P8.48 using a 4×4 mesh of linear rectangular elements in the half-domain. Use $c = 1.0$.
- 13.39** Determine the eigenvalues of the circular membrane problem in Fig. P8.49 with a mesh of four quadratic triangular elements. Use $c = 1.0$.
- 13.40** Determine the transient response of the problem in Fig. P8.49 (see Problem 13.39). Assume zero initial conditions, $c = 1$ and $f_0 = 1$. Use $\alpha = \gamma = 0.5$ and $\Delta t = 0.05$, and plot the center deflection versus time t for $t = 0$ to $t = 2.4$.

Viscous Incompressible Fluids (Chapter 10)

- 13.41** Analyze the viscous flow problem in Problem 10.8 using an 8×8 mesh of linear rectangular elements. Plot the horizontal velocity $u(0.5, y)$ versus y , and the pressure along the top surface of the cavity. Investigate the effect of the penalty parameter on the solution (see Fig. P10.8).
- 13.42** Repeat Problem 13.41 with nine-node quadratic elements.
- 13.43** Analyze the slider bearing problem of Example 10.6.2 to investigate the effect of the penalty parameter on the velocity and pressure fields. Use an 8×8 mesh of linear rectangular elements.
- 13.44** Repeat Problem 13.43 with nine-node quadratic elements.
- 13.45** Analyze the problem of a viscous incompressible fluid being squeezed through a 4:1 contraction, as shown in Fig. P13.45. Take $L_1 = 10$, $L = 6$, $R_1 = 4$, and $R_2 = 1$, and linear quadrilateral elements. The inlet velocity $v_x(y)$ is the fully developed solution of the flow between parallel plates. Plot the velocity $v_x(x, y)$ and pressure along the horizontal centerline.

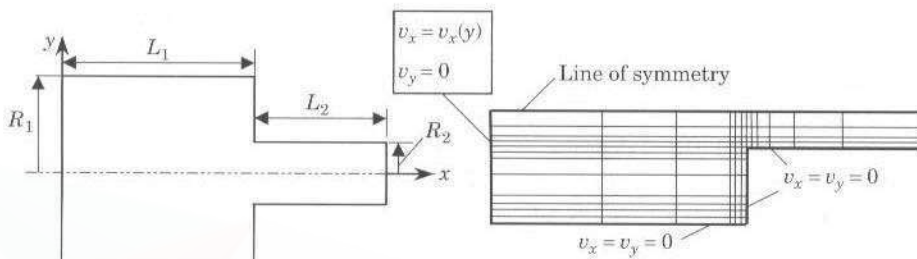


Figure P13.45

- 13.46** Analyze the cavity problem in Problem 13.41 for its transient solution. Use $\rho = 1.0$, zero initial conditions, penalty parameter $\gamma = 10^8$, time parameter $\alpha = 0.5$, and a time step of $\Delta t = 0.005$ to capture the evolution of $v_x(0.5, y)$ with time.
- 13.47** Analyze the slider bearing problem of Example 10.6.2 for its transient solution. Use $p = 20$, zero initial conditions, $\gamma = 10^8$, $\alpha = 0.5$, and a time step of 10^{-4} .

Plane Elasticity (Chapter 11)

- 13.48** Analyze the plane elasticity problem in Fig. P11.7 using 10×4 mesh of linear rectangular elements. Evaluate the results (i.e., displacements and stresses) qualitatively. Use the plane stress assumption.
- 13.49** Repeat Problem 13.48 using triangular elements.
- 13.50–13.59** Analyze the plane elasticity problems shown in Figs. P11.1–11.3 and P10.10–P10.16 using suitable meshes of triangular or rectangular elements (the instructor should specify the element type and mesh).
- 13.60** Analyze the plane elasticity problem in Fig. P11.7 for natural frequencies. Use a density of $\rho = 0.0088 \text{ kg/cm}^3$.
- 13.61** Repeat Problem 13.60 with triangular elements.
- 13.62** Analyze the plane elasticity problem in Fig. P11.7 for the transient response. Use $\alpha = \frac{1}{2}$, $\gamma = \frac{1}{2}$, and $\Delta t = 10^{-5}$. Assume zero initial conditions.
- 13.63–13.66** Analyze Problems 13.50–13.53 for transient response. Use $\alpha = \frac{1}{2}$, $\gamma = \frac{1}{2}$, and $\Delta t \approx \Delta t_{\text{cri}}$.

Plate Bending (Chapter 12)

- 13.67** Analyze the plate problem in Fig. P12.2 using (a) 2×4 and (b) 4×8 meshes of CPT(N) elements in the half-plate, and compare the maximum deflections and stresses. Use $E = 10^7 \text{ psi}$, $\nu = 0.25$, $h = 0.25 \text{ in.}$, and $q_0 = 10 \text{ lb/in.}^2$.
- 13.68** Repeat Problem 13.67 with a CPT(C) element.
- 13.69** Repeat Problem 13.67 with an 4×8 mesh of linear plate elements and a 2×4 mesh of nine-node quadratic plate elements based on the first-order plate theory.
- 13.70–13.72** Analyze the plate bending problems shown in Figs. P12.3, P12.4 and P12.8 with the CPT (C) elements. Use the meshes shown in the figures, and take $E = 10^7 \text{ psi}$, $\nu = 0.25$, $h = 0.25 \text{ in.}$, and $q_0 = 10 \text{ lb/in.}^2$.

- 13.73–13.75** Repeat Problems 13.70–13.72 using SDT and meshes shown in Figs. P12.3, P12.4, and P12.8.
- 13.76** Analyze the annular plate in Fig. P12.5 using a four element mesh of CPT(C) elements. Use $E = 10^7$ psi, $\nu = 0.25$, $a = 10$ in., $b = 5$ in., $h = 0.25$ in., and $Q_0 = 1$ lb/in.
- 13.77** Repeat Problem 13.76 with four-node SDT elements.
- 13.78** Analyze the plate problem in Fig. P12.2 for its transient response. Use a mesh of 2×4 CPT(N) elements and $E = 10^7$ psi, $\nu = 0.25$, $\rho = 1$ lb/in.³, $h = 0.25$ in., $q_0 = 10$ lb/in., $\Delta t = 0.05$, and $\alpha = \gamma = 0.5$.
- 13.79** Repeat Problem 13.78 using 2×4 mesh of four-node SDT elements.
- 13.80** Determine the transient response of the annular plate in Fig. P12.5 using four SDT elements, $\Delta t = 0.05$, $\rho = 1.0$, and $\alpha = \gamma = 0.5$. Plot the deflection at node 1 as a function of time for at least two periods.

REFERENCES FOR ADDITIONAL READING

Fluid Mechanics

1. Bird, R. B., Stewart, W. E., and Lightfoot, E. N., *Transport Phenomena*, John Wiley, New York, 1960.
2. Gresho, P. M. and Sani, R. L., *Incompressible Flow and the Finite Element Method*, John Wiley, West Sussex, UK, 2000.
3. Schlichting, H., *Boundary-Layer Theory* (translated by Kestin, J.), 7th ed., McGraw-Hill, New York, 1979.
4. Verruijt, A., *Theory of Groundwater Flow*, Gordon and Breach, New York, 1970.
5. White, F. M., *Fluid Mechanics*, 4th ed., McGraw-Hill, New York, 1999.

Heat Transfer

6. Carslaw, H. S. and Jaeger, J. C., *Conduction of Heat in Solids*, Oxford University Press, Oxford, 1959.
7. Holloman, J. P., *Heat Transfer*, 7th ed., McGraw-Hill, New York, 1990.
8. Kreith, F. and Bohn, M. S., *Principles of Heat Transfer*, 5th ed., West Publishing Co., St. Paul, MN 1993.
9. Myers, G. E., *Analytical Methods in Conduction Heat Transfer*, McGraw-Hill, New York, 1972.
10. Özisik, M. N., *Heat Conduction*, 2nd ed., John Wiley, New York, 1993.

Elasticity

11. Budynas, R. G., *Advanced Strength and Applied Stress Analysis*, 2nd ed., McGraw-Hill, New York, 1999.
12. Harris, C. M. and Crede, C. E., *Shock and Vibration Handbook*, vol. 1, McGraw-Hill, New York, 1961.
13. Slaughter, W. S., *The Linearized Theory of Elasticity*, Birkhäuser, Boston, MA, 2002.
14. Ugrual, A. C. and Fenster, S. K., *Advanced Strength and Applied Elasticity*, Prentice-Hall, Upper Saddle River, NJ, 1995.
15. Volterra, E. and Gaines, J. H., *Advanced Strength of Materials*, Prentice-Hall, Englewood Cliffs, NJ, 1971.

Plates

16. Reddy, J. N., *Theory and Analysis of Elastic Plates*, Taylor and Francis, Philadelphia, PA, 1999.
17. Reddy, J. N., *Energy Principles and Variational Methods in Applied Mechanics*, 2nd ed., John Wiley, New York, 2002.

710 AN INTRODUCTION TO THE FINITE ELEMENT METHOD

18. Reddy, J. N., *Mechanics of Laminates Composite Plates and Shells: Theory and Analysis*, 2nd ed., CRC Press, Boca Raton, FL, 2004.
19. Szilard, R., *Theories and Applications of Plate Analysis*, John Wiley, New York, 2004.
20. Timoshenko, S. and Woinowsky-Krieger, S., *Theory of Plates and Shells*, 2nd ed., McGraw-Hill, New York, 1959.

Computer Implementation

21. Akay, H. U., Willhite, P. G., and Didandeh, H., "UCODE2, Version 87.1," Computational Fluid Dynamics Laboratory, Department of Mechanical Engineering, Indiana University-Purdue University at Indianapolis (IUPUI), Indianapolis, 1987.
22. Bathe, K. J., *Finite Element Procedures*, Prentice Hall, Englewood Cliffs, NJ, 1996.
23. Burnett, D. S., *Finite Element Analysis*, Addison-Wesley, Reading, MA, 1987.
24. Chandrupatla, T. R. and Belegundu, A. D., *Introduction to Finite Elements in Engineering*, 3rd ed., Prentice Hall, Upper Saddle River, NJ, 2002.
25. Zienkiewicz, O. C. and Taylor, R. L., *The Finite Element Method*, 4th ed., vol. 1 *Basic Formulation and Linear Problems*, McGraw-Hill, London, UK, 1989.

Chapter 14

PRELUDE TO ADVANCED TOPICS

14.1 INTRODUCTION

The introduction to the finite element method presented in the preceding chapters is sufficient to provide the essential background for the development of finite element models and the associated computer programs for most linear boundary, initial, and eigenvalue problems in one and two dimensions. The background should also help one to intelligently use commercially available finite element software. However, there are many additional ideas that deserve some attention. In this chapter, we discuss some immediate extensions of the material presented in Chapters 8 through 12. These include alternative finite element models, finite element models of three-dimensional problems, finite element analysis of nonlinear problems, and errors in finite element analysis. The discussions presented here are brief and they are only meant to give some idea of the applicability of the finite element method to these advanced topics. The reader interested in a detailed treatment of any of these topics should consult the books listed at the end of the chapter.

14.2 ALTERNATIVE FINITE ELEMENT MODELS

14.2.1 Introductory Comments

The finite element models presented in Chapters 3 through 12 were based on *weak formulations* of governing differential equations. These models can be termed the *Ritz finite element models* or *weak-form finite element models*. The phrase “Galerkin finite element models” is used in the literature often to mean the weak-form (Ritz) models. A truly Galerkin finite element model is based on weighted integral statements and not on weak forms. This distinction is made here to differentiate between Galerkin’s method and the Ritz method. In most cases, especially when the governing differential equations contain derivatives of even order, weak forms (which always include the natural boundary conditions) can be developed using the three-step procedure. In some cases, the governing equations may be recast in an alternative form that facilitates the use of lower-order (C^0) interpolations. In this section, we discuss a couple of such formulations and demonstrate the use of the weighted residual methods of Section 2.5.5 to develop alternative finite element models. More specifically, we shall study the following formulations:

1. Weighted residual formulations
2. Mixed formulations

While specific sets of equations are chosen to illustrate the basic ideas behind the two formulations, the ideas are applicable to other field equations and to two- and three-dimensional problems.

14.2.2 Weighted Residual Finite Element Models

In a weak formulation, integration by parts is used to introduce the secondary variables (i.e., natural boundary conditions) into the integral form. On the other hand, weighted residual methods are based on a weighted integral statement of a given differential equation and no integration by parts is employed. They are the natural and only choice for first-order equations, which do not admit a weak formulation. For second- and higher-order equations, we have a choice between the weak formulation and the weighted residual formulation to construct finite element models that will be different from each other. We begin with the description of weighted residual finite element models of a first-order differential equation in one dimension.

First-Order Equation in One Dimension

Consider the first-order equation

$$a \frac{du}{dx} + cu = f \quad \text{for } 0 < x < L \quad (14.2.1)$$

where a , c , and f are given functions of x . An example of a situation in which the above equation arises is given by Newton's law of cooling of a body with temperature u in an environment at temperature u_0 :

$$\frac{du}{dx} + k(u - u_0) = 0$$

which is the same as (14.2.1) with $c = k$, $a = 1$, and $f = ku_0$.

When u is approximated by an n -parameter approximation

$$u(x) \approx u_h^e(x) = \sum_{j=1}^n u_j^e \psi_j^e(x) \quad (14.2.2)$$

we need n algebraic equations to solve for the parameters u_j^e . The n equations are provided by n different (i.e., linearly independent) choices of the weight function w in the weighted residual statement

$$0 = \int_{x_a}^{x_b} w R_e \, dx, \quad R_e = \left(a \frac{du_h^e}{dx} + c u_h^e - f \right) \quad (14.2.3)$$

where R_e is the error, called the *residual*, in the approximation of the differential equation. Different choices of w dictate different methods.

Since the equation under consideration is first-order, there is no advantage in transferring the derivative to the weight function w . Note that there are no "flux" terms in (14.2.3). An examination of the weighted integral statement (14.2.3) shows that the minimum differentiability on the approximation functions ψ_j is the same as in the original differential

equation. In the present case, ψ_j should be once-differentiable with respect to x . Consequently, the Lagrange family of interpolation functions (i.e., C^0 approximations) are admissible.

The only requirements on the weight function w are that it (a) be integrable in the sense that (14.2.3) can be evaluated and (b) belong to a linearly independent set $\{w_i\}_{i=1}^n$ so that the resulting algebraic equations are solvable. The i th algebraic equation is obtained by replacing w in (14.2.3) with w_i . Different choices for the set $\{w_i\}$ have been suggested, and the resulting models bear the names of the original scientists who suggested them. The best-known choices for w_i are given below.

1. Petrov–Galerkin method: $w_i = \phi_i$ and $\phi_i \neq \psi_i$
 2. Bubnov–Galerkin method: $w_i = \psi_i$
 3. Collocation method: $w_i = \delta(x - x_i)$, the Dirac delta function
 4. Subdomain method: $w_i = \delta_{ij}$ (i.e., $w_i = 1$ in the i th subdomain)
 5. Least-squares method: $w_i = A(\psi_i)$, where A is the operator in the differential equation $Au = f$
- (14.2.4)

Although the least-squares method is listed as a member of weighted residual methods, it is based on the idea of minimizing the error (R_e) introduced in the approximation of an equation. The finite element models of (14.2.1), based on various methods, are discussed next.

The Petrov–Galerkin Model. Substitute (14.2.3) for u and $w = \phi_i$ into (14.2.2) to obtain

$$0 = \sum_{j=1}^n K_{ij} u_j - f_i \quad \text{or} \quad [K^e] \{u^e\} = \{f^e\} \quad (14.2.5a)$$

where

$$K_{ij}^e = \int_{x_a}^{x_b} \left(a \phi_i^e \frac{d\psi_j^e}{dx} + c \phi_i^e \psi_j^e \right) dx, \quad f_i^e = \int_{x_a}^{x_b} \phi_i^e f dx \quad (14.2.5b)$$

The Bubnov–Galerkin Model. Here we substitute $w = \psi_i^e$ into (14.2.3) to obtain the finite element model

$$[K^e] \{u^e\} = \{f^e\} \quad (14.2.6a)$$

where

$$K_{ij}^e = \int_{x_a}^{x_b} \left(a \psi_i^e \frac{d\psi_j^e}{dx} + c \psi_i^e \psi_j^e \right) dx, \quad f_i^e = \int_{x_a}^{x_b} \psi_i^e f dx \quad (14.2.6b)$$

Collocation Model. In this case, we take $w = \delta(x - x_i)$, the Dirac delta function. The collocation points x_i can be chosen arbitrarily, usually as the quadrature points in $\Omega_e = [x_a, x_b]$. We have

$$K_{ij}^e = a(x_i) \frac{d\psi_j^e}{dx}(x_i) + c(x_i) \psi_j^e(x_i), \quad f_i^e = f(x_i) \quad (14.2.7)$$

Subdomain Model. In this model the element domain Ω_e is subdivided further into n subdomains. The weight function for the i th subdomain Ω_i^e is unity over the subdomain

and zero outside it

$$w(x) = \begin{cases} 1 & \text{for } x \in \Omega_i^e \\ 0 & \text{for } x \notin \Omega_i^e \end{cases} \quad (14.2.8)$$

We obtain

$$K_{ij}^e = \int_{\Omega_i^e} \left(a \frac{d\psi_j^e}{dx} + c\psi_j^e \right) dx, \quad f_i^e = \int_{\Omega_i^e} f dx \quad (14.2.9)$$

Least-Squares Model. The weight function in this case is $w \equiv A(\psi_i) = a(d\psi_i^e/dx) + c\psi_i^e$. Consequently, we have

$$K_{ij}^e = \int_{x_a}^{x_b} \left(a \frac{d\psi_i^e}{dx} + c\psi_i^e \right) \left(a \frac{d\psi_j^e}{dx} + c\psi_j^e \right) dx \quad (14.2.10a)$$

$$f_i^e = \int_{x_a}^{x_b} \left(a \frac{d\psi_i^e}{dx} + c\psi_i^e \right) f dx \quad (14.2.10b)$$

Note that only the least-squares method gives a symmetric coefficient matrix. This is a strong point (in addition to the fact that it actually minimizes the error R_e) of the least-squares method over other methods.

Example 14.2.1

Here, we solve Eq. (14.2.1) with the boundary condition $u(0) = 1$ and data $a = 1$, $c = 2$, $f = 1$, and $L = 1$. We shall use two linear elements in the domain.

For the Bubnov-Galerkin model, we have

$$[K^e] = \frac{1}{2} \begin{bmatrix} -1 & 1 \\ -1 & 1 \end{bmatrix} + \frac{h_e}{3} \begin{bmatrix} 2 & 1 \\ 1 & 2 \end{bmatrix}, \quad \{f^e\} = \frac{h_e}{2} \begin{Bmatrix} 1 \\ 1 \end{Bmatrix} \quad (14.2.11)$$

The assembled equations (here, assembly is required only to reduce the number of equations to the number of unknowns) are given by

$$\left(\frac{1}{2} \begin{bmatrix} -1 & 1 & 0 \\ -1 & 0 & 1 \\ 0 & -1 & 1 \end{bmatrix} + \frac{1}{6} \begin{bmatrix} 2 & 1 & 0 \\ 1 & 4 & 1 \\ 0 & 1 & 2 \end{bmatrix} \right) \begin{Bmatrix} U_1 \\ U_2 \\ U_3 \end{Bmatrix} = \frac{1}{4} \begin{Bmatrix} 1 \\ 2 \\ 1 \end{Bmatrix} \quad (14.2.12)$$

Using the boundary condition, $U_1 = 1$, we obtain the following condensed equations:

$$\frac{1}{6} \begin{bmatrix} 4 & 4 \\ -2 & 5 \end{bmatrix} \begin{Bmatrix} U_2 \\ U_3 \end{Bmatrix} = \frac{1}{6} \begin{Bmatrix} 5 \\ 1.5 \end{Bmatrix} \quad (14.2.13)$$

The solution is $U_2 = 0.6786$ and $U_3 = 0.5714$. The exact solution of the problem is

$$u(x) = u(0)e^{-(c/a)x} - \frac{f}{c}(1 - e^{-(c/a)x}) = e^{-2x} - \frac{1}{2}(1 - e^{-2x}) \quad (14.2.14)$$

The exact values of u at $x = \frac{1}{3}$ and 1 are 0.6389 and 0.5677, respectively.

For the collocation model, we choose $x_1 = \frac{1}{3}h_e$ and $x_2 = \frac{2}{3}h_e$, and obtain

$$[K^e] = \frac{1}{h_e} \begin{bmatrix} -1 & 1 \\ -1 & 1 \end{bmatrix} + \frac{2}{3} \begin{bmatrix} 2 & 1 \\ 1 & 2 \end{bmatrix}, \quad \{f^e\} = \begin{Bmatrix} 1 \\ 1 \end{Bmatrix} \quad (14.2.15)$$

Table 14.2.1 Comparison of the numerical solution of (14.2.1) with the exact solution (Example 14.2.1).

Nodal values	Bubnov–Galerkin	Collocation	Subdomain	Least-squares	Exact
$u(0.5)$	0.6786	0.6786	0.6053	0.6793	0.6839
$u(1.0)$	0.5714	0.5714	0.4737	0.5094	0.5677

Clearly, the element equations obtained using the collocation points $x_1 = \frac{1}{3}h_e$ and $x_2 = \frac{2}{3}h_e$ are the same as those obtained in the Bubnov–Galerkin method (actually a multiple of $\frac{1}{2}h_e$). Hence, we obtain the same solution as in the Bubnov–Galerkin method.

In the case of the subdomain model, we use $\Omega_1^e = (0, \frac{1}{2}h_e)$ and $\Omega_2^e = (\frac{1}{2}h_e, h_e)$. For this choice, we obtain

$$[K^e] = \frac{1}{2} \begin{bmatrix} -1 & 1 \\ -1 & 1 \end{bmatrix} + \frac{h_e}{4} \begin{bmatrix} 3 & 1 \\ 1 & 3 \end{bmatrix}, \quad \{f^e\} = \frac{3h_e}{8} \begin{Bmatrix} 1 \\ 1 \end{Bmatrix} \quad (14.2.16)$$

The assembled equations become

$$\frac{1}{8} \begin{bmatrix} -1 & 5 & 0 \\ -3 & 6 & 5 \\ 0 & -3 & 7 \end{bmatrix} \begin{Bmatrix} U_1 \\ U_2 \\ U_3 \end{Bmatrix} = \frac{3}{16} \begin{Bmatrix} 1 \\ 2 \\ 1 \end{Bmatrix} \quad (14.2.17)$$

The solution, from the last two equations, is $U_2 = 0.6053$ and $U_3 = 0.4737$.

Last, we consider the least-squares model. We have

$$[K^e] = \frac{1}{h_e} \begin{bmatrix} 1 & -1 \\ -1 & 1 \end{bmatrix} + \frac{4h_e}{6} \begin{bmatrix} 2 & 1 \\ 1 & 2 \end{bmatrix} + \begin{bmatrix} -2 & 0 \\ 0 & 2 \end{bmatrix} \quad (14.2.18a)$$

$$\{f^e\} = \begin{Bmatrix} -1 \\ 1 \end{Bmatrix} + h_e \begin{Bmatrix} 1 \\ 1 \end{Bmatrix} \quad (14.2.18b)$$

The assembled equations are

$$\frac{1}{3} \begin{bmatrix} -2.5 & -0.5 & 0.0 \\ -0.5 & 7.0 & -0.5 \\ 0.0 & -0.5 & 9.5 \end{bmatrix} \begin{Bmatrix} U_1 \\ U_2 \\ U_3 \end{Bmatrix} = \begin{Bmatrix} -0.5 \\ 1.0 \\ 1.5 \end{Bmatrix} \quad (14.2.19)$$

The solution of these equations is

$$U_2 = 0.6793, \quad U_3 = 0.5094$$

Table 14.2.1 gives a summary of the solutions obtained using various models. Since the exact solution is exponential or hyperbolic, it is obvious that the meshes and degree of interpolation used are very crude. The accuracy of the finite element solutions can be improved by higher degree polynomials.

Second-Order Equations in One Dimension

Use of weighted residual finite element models in the solution of second- and higher-order equations is more involved. There are two possible ways to construct the weighted residual forms of higher-order equations: (1) Use the higher-order equations but use C^k -continuous functions, where $k \geq m$, m being the order of the highest derivative in the differential

equation; and (2) rewrite the higher-order equations as a set of first-order equations and use C^0 -continuous functions. The latter requires a consistent set of approximations for the new variables introduced in rewriting the higher-order equations as a first-order set. Here we consider the first method and leave the second as an exercise to the reader (see Problem 14.1).

Consider the model second-order equation

$$-\frac{d}{dx} \left(a \frac{du}{dx} \right) = f \quad (14.2.20)$$

For the weak formulation of this equation, the approximation functions ψ_i^e must be such that u is continuous across interelement boundaries. The weak form includes the natural boundary conditions associated with the equation, and therefore interpolation of only u (but not its derivatives) is required.

In the weighted residual formulation of Eq. (14.2.20), we use the weighted integral form of the differential equation without weakening the differentiability on u . Therefore, the continuity conditions on the interpolation functions used in the weighted residual methods are dictated by the order of the differential equation. For example, the second-order differential equation (14.2.20) requires the approximation functions to be twice-differentiable with respect to x . In addition, the approximate solution must satisfy the end conditions on the primary and secondary variables (identified with the help of the weak formulation) of the problem. This amounts to, for second-order equations, using approximation functions that make the primary and secondary variables continuous between elements (i.e., interelement nodes). For the second-order equations under consideration, the natural boundary condition involves specifying the secondary variable $a(du/dx)$ at the element boundaries. Therefore, the interpolation functions must be selected such that u and $a(du/dx)$ are continuous across an interface between elements. This in turn, implies that, if a is continuous, du/dx is continuous throughout the domain $\Omega = (0, L)$. Hence, a C^1 approximation (i.e., Hermite interpolation) of u is required.

Because u and du/dx are required to be continuous across an interface between elements, and a typical element (in one dimension) has two such interfaces, the polynomial approximation of u must involve four parameters, i.e., it must be a cubic polynomial. Thus, the finite element is a line element with two nodes and two degrees of freedom, u and du/dx , at each node. The element is different from the Lagrange cubic element, which has four nodes with one degree of freedom per node. The Lagrange interpolation functions (of any order) do not satisfy the continuity of du/dx across element interfaces and therefore do not belong to $C^1(0, L)$. The two-node element with continuous u and du/dx at element interfaces is the Hermite cubic element developed in Section 5.2 for the Euler–Bernoulli beam element. We have

$$u_h^e(x) = \sum_{j=1}^4 u_j^e \phi_j^e(x) \quad (14.2.21)$$

where u_1^e and u_3^e are the nodal values of u_h^e , u_2^e and u_4^e are the nodal values of du_h^e/dx at the two nodes, and ϕ_j^e are the Hermite cubic interpolation functions in (5.2.12). We consider various weighted residual finite element models of (14.2.20).

The weighted residual form of (14.2.20) over an element $\Omega_e = (x_a, x_b)$ is

$$0 = \int_{x_a}^{x_b} w R_e dx, \quad R_e = \left[-\frac{d}{dx} \left(a \frac{du_h^e}{dx} \right) - f \right] \quad (14.2.22)$$

Substituting ψ_i^e for the weight function w and (14.2.21) for u , we obtain

$$0 = \sum_{j=1}^4 K_{ij}^e u_j^e - f_i^e, \quad \text{or} \quad [K^e] \{u^e\} = \{f^e\} \quad (14.2.23a)$$

where

$$K_{ij}^e = \int_{x_a}^{x_b} \left[-\psi_i^e \frac{d}{dx} \left(a \frac{d\phi_j^e}{dx} \right) \right] dx, \quad f_i^e = \int_{x_a}^{x_b} \psi_i^e f dx \quad (14.2.23b)$$

Equation (14.2.23a) is the Petrov–Galerkin model of (14.2.20) when $\phi_i^e \neq \psi_i^e$.

For different choices of ψ_i^e in (14.2.23b), we obtain different finite element models. These are presented below.

The Bubnov–Galerkin Model. For $\psi_i^e = \phi_i^e$, (14.2.23b) becomes

$$K_{ij}^e = \int_{x_a}^{x_b} \left[-\phi_i^e \frac{d}{dx} \left(a \frac{d\phi_j^e}{dx} \right) \right] dx, \quad f_i^e = \int_{x_a}^{x_b} \phi_i^e f dx \quad (14.2.24)$$

Least-Squares Model. For $\psi_i^e = A(\phi_i^e) \equiv -(d/dx)(ad\phi_i^e/dx)$, we have

$$K_{ij}^e = \int_{x_a}^{x_b} \frac{d}{dx} \left(a \frac{d\phi_i^e}{dx} \right) \frac{d}{dx} \left(a \frac{d\phi_j^e}{dx} \right) dx, \quad f_i^e = - \int_{x_a}^{x_b} \frac{d}{dx} \left(a \frac{d\phi_i^e}{dx} \right) f dx \quad (14.2.25)$$

Collocation Model. For $\psi_i^e = \delta(x - x_i)$, (14.2.23b) takes the form

$$K_{ij}^e = - \left\{ \frac{d}{dx} \left[a(x) \frac{d\phi_j^e}{dx}(x) \right] \right\}_{x=x_i}, \quad f_i^e = f(x_i) \quad (14.2.26)$$

where x_i are the collocation points.

While the Bubnov–Galerkin and least-squares models have the same form as the Ritz model, i.e., they are defined by integral expressions, the collocation model does not. In the latter, we simply evaluate the coefficient matrices and column vector at the collocation points, instead of evaluating the integral expressions. The number of collocation points should be equal to the number of unknowns after imposition of the boundary conditions of the problem. For second-order equations, we have two boundary conditions and $2(N+1)$ nodal degrees of freedom for an N -element model. Hence, a total of $2N$ collocation points, two per element, are needed. Also, note that the coefficient matrix in (14.2.26) is of order 2×4 ($i = 1, 2$), and there is no overlap of element matrices because there is no summation of equations over the number of elements. However, the continuity conditions on nodal variables are imposed in all the other models.

Example 14.2.2

Consider the boundary value problem

$$-\frac{d}{dx} \left[(1+x) \frac{du}{dx} \right] = 0 \quad \text{for } 0 < x < 1 \quad (14.2.27a)$$

$$u(0) = 0, \quad \left[(1+x) \frac{du}{dx} \right]_{x=1} = 1 \quad (14.2.27b)$$

The exact solution of this problem is

$$u = \ln(1 + x) \quad (14.2.28)$$

We wish to solve the problem using various weighted residual finite element models.

Consider a two-element discretization of the problem. There are three nodes and six degrees of freedom. The known degrees of freedom for the weighted residual models are

$$U_1 = 0, \quad U_6 = 0.5 \quad (14.2.29)$$

whereas, in the four-element Ritz model (i.e., the weak-form finite element model) with linear elements, they are

$$U_1 = 0, \quad Q_5 = 1.0 \quad (14.2.30)$$

For the collocation model, the two-point Gauss-Legendre quadrature points are used as the collocation points. The two- and four-element finite element solutions obtained from three weighted residual finite element models, all using the Hermite cubic polynomials, are compared with the exact solution and the solution of the weak-form finite element model in Table 14.2.2. All the models give accurate results.

Table 14.2.2 Comparison of weighted residual finite element solutions[†] with the exact solution of the problem in (14.2.27a) and (14.2.27b).

x	Exact	Collocation	Bubnov-Galerkin	Least-squares	Ritz
0.00	u	0.00000	0.00000	0.00000	0.00000
	u'	1.00000	0.99390	0.99604	0.99902
	u''	1.00000	0.99967	0.99930	0.99993
0.25	u	0.22314	—	—	—
	u'	0.22314	0.22326	0.22313	0.22315
	u''	0.80000	—	—	—
0.50	u	0.40547	0.40487	0.40537	0.40554
	u'	0.40547	0.40562	0.40546	0.40547
	u''	0.66667	0.66299	0.66707	0.66645
0.75	u	0.55962	—	—	—
	u'	0.55962	0.55975	0.55961	0.55962
	u''	0.57143	—	—	—
1.00	u	0.69315	0.69202	0.69309	0.69324
	u'	0.69315	0.69325	0.69314	0.69315
	u''	0.50000	0.50000	0.50000	0.50102

[†]The first and third rows for each value of x corresponds to two elements and the second and fourth rows to four elements.

Second-Order Equations in Two Dimensions

Here we describe the Bubnov–Galerkin, least-squares, and collocation finite element models of a second-order equation in two dimensions. We consider the Poisson equation ($Au = f$)

$$-\frac{\partial}{\partial x} \left(a_{11} \frac{\partial u}{\partial x} \right) - \frac{\partial}{\partial y} \left(a_{22} \frac{\partial u}{\partial y} \right) = f \quad \text{in } \Omega \quad (14.2.31)$$

In the weighted residual finite element model, we seek an approximate solution u_h^e of u in Ω_e in the form

$$u_h^e(x, y) = \sum_{j=1}^{16} u_j^e \phi_j^e(x, y) \quad (14.2.32)$$

where $\phi_j^e(x, y)$ are the conforming Hermite interpolation functions of the four-node rectangular element (see Table 9.2.1); u_1^e, u_5^e, u_9^e , and u_{13}^e are the nodal values of u_h^e at the four nodes of the element; u_2^e, u_6^e, u_{10}^e , and u_{14}^e are the nodal values of $\partial u_h^e / \partial x$ at the four nodes; and so on.

The weighted residual statement of (14.2.31) over an element is given by

$$0 = \int_{\Omega_e} w \left[-\frac{\partial}{\partial x} \left(a_{11} \frac{\partial u}{\partial x} \right) - \frac{\partial}{\partial y} \left(a_{22} \frac{\partial u}{\partial y} \right) - f \right] dx dy \quad (14.2.33)$$

Substituting $w = \psi_i^e$ and replacing u by (14.2.32), we obtain the usual form of the element equations

$$[K^e]\{u^e\} = \{f^e\} \quad (14.2.34)$$

The specific forms of $[K^e]$ and $\{f^e\}$ are defined below for various models.

The Bubnov–Galerkin Model. For $w = \psi_i^e$, the coefficient matrix $[K^e]$ and column vector $\{f^e\}$ are defined by

$$K_{ij}^e = - \int_{\Omega_e} \psi_i^e \left[\frac{\partial}{\partial x} \left(a_{11} \frac{\partial \psi_j^e}{\partial x} \right) + \frac{\partial}{\partial y} \left(a_{22} \frac{\partial \psi_j^e}{\partial y} \right) \right] dx dy \quad (14.2.35a)$$

$$f_i^e = \int_{\Omega_e} \psi_i^e f dx dy \quad (14.2.35b)$$

The Least-Squares Model. For $w = A(\psi_i^e)$, where A is the differential operator in (14.2.31), the coefficients of $[K^e]$ and $\{f^e\}$ are defined by

$$\begin{aligned} K_{ij}^e &= \int_{\Omega_e} \left[\frac{\partial}{\partial x} \left(a_{11} \frac{\partial \psi_i^e}{\partial x} \right) + \frac{\partial}{\partial y} \left(a_{22} \frac{\partial \psi_i^e}{\partial y} \right) \right] \\ &\quad \times \left[\frac{\partial}{\partial x} \left(a_{11} \frac{\partial \psi_j^e}{\partial x} \right) + \frac{\partial}{\partial y} \left(a_{22} \frac{\partial \psi_j^e}{\partial y} \right) \right] dx dy \end{aligned} \quad (14.2.36a)$$

$$f_i^e = - \int_{\Omega_e} \left[\frac{\partial}{\partial x} \left(a_{11} \frac{\partial \psi_i^e}{\partial x} \right) + \frac{\partial}{\partial y} \left(a_{22} \frac{\partial \psi_i^e}{\partial y} \right) \right] f dx dy \quad (14.2.36b)$$

The Collocation Model. In this model, we select four collocation points per element and satisfy (14.2.31) exactly at those four points of each element. For the best results, the

Gauss-Legendre quadrature points are selected. We have

$$K_{ij}^e = \left[-\frac{\partial}{\partial x} \left(a_{11} \frac{\partial \psi_i^e}{\partial x} \right) - \frac{\partial}{\partial y} \left(a_{22} \frac{\partial \psi_j^e}{\partial y} \right) \right] \Big|_{(x,y)=(x_i, y_i)} \quad (14.2.37a)$$

$$f_i^e = f(x_i, y_i) \quad (14.2.37b)$$

for $i = 1, 2, 3, 4$ and $j = 1, 2, \dots, 16$. Note that the coefficient matrix is rectangular (4×16) and that each coefficient of the global matrix and column vector has a contribution from no more than one element. After imposing the boundary conditions of the problem, the number of linearly independent equations (which is equal to four times the number of elements in the finite element mesh) will be equal to the number of unknown nodal degrees of freedom.

Example 14.2.3

Consider the Dirichlet problem for the Poisson equation

$$\begin{aligned} -\nabla^2 u &= 2 && \text{in } \Omega \\ u &= 0 && \text{on } \Gamma \end{aligned} \quad (14.2.38)$$

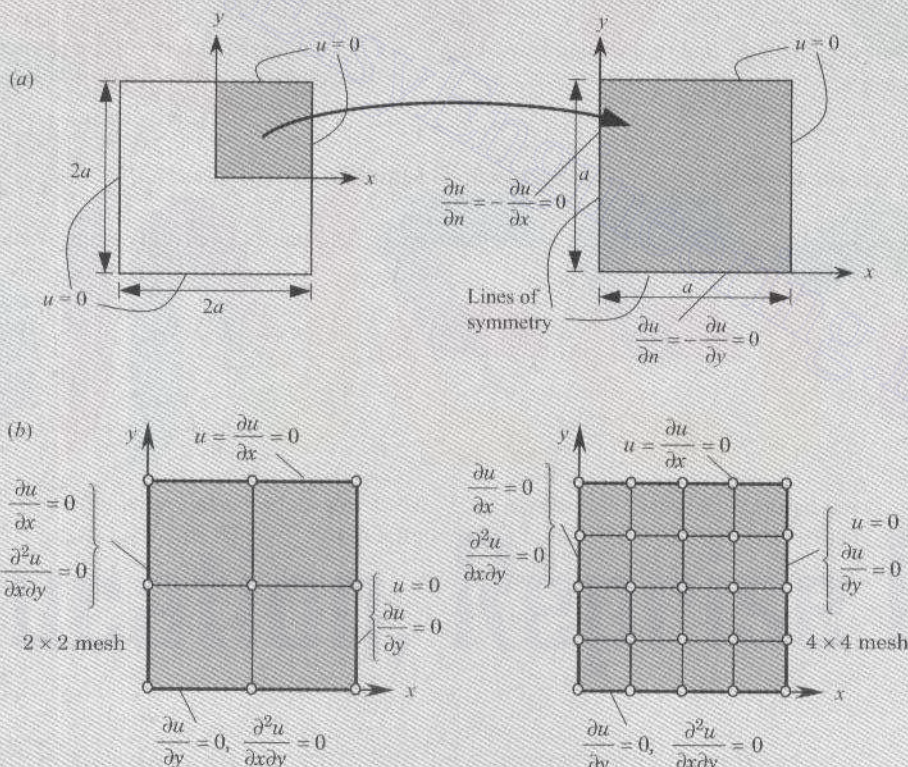


Figure 14.2.1 (a) Domain, boundary conditions and (b) finite element meshes of the problem in Example 14.2.3.

where Ω is a square region [see Fig. 14.2.1(a)]. The exact solution of this problem is given by (8.5.62a). Exploiting the biaxial symmetry, we model only a quadrant, say the region bounded by the positive axes.

Two different uniform meshes, shown in Fig. 14.2.1(b), of Hermite rectangular elements are used to solve the problem, employing various finite element models. Since the element has u , $\partial u / \partial x$, $\partial u / \partial y$, and $\partial^2 u / \partial x \partial y$ as nodal degrees of freedom, we must impose all known boundary values of these quantities. For the problem at hand, we impose the following boundary conditions: $u = 0$ on the lines $x = 1$ and $y = 1$, $\partial u / \partial x = 0$ on the line $x = 0$, and $\partial u / \partial y = 0$ on the line $y = 0$. The boundary conditions for the weighted residual models are indicated in Fig. 14.2.1(b). For the 2×2 mesh, the number of known boundary conditions is 20, whereas the number of total nodal variables is 36. Thus, for the collocation model, we have 16 unknowns and 16 equations, 4 from each element. Similarly, for the 4×4 mesh, we have 36 boundary conditions, among 100 nodal variables, requiring 64 collocation equations, which are provided by the 16 elements.

The finite element solutions obtained from the three finite element models for the two meshes are compared with the exact solution (8.5.62a) in Table 14.2.3. The collocation finite element solution is relatively more accurate than the other two solutions. The numerical convergence of all three models is apparent from the results.

Table 14.2.3 Comparison of the various finite element solutions[†] with the exact solution of the Dirichlet problem for the Poisson equation (14.2.38) (Example 14.2.3).

x	y	$u(x, y)$				$\partial u / \partial x$			
		Exact	Bubnov-Galerkin	Least-squares	Col-location	Exact	Bubnov-Galerkin	Least-squares	Col-location
0.0	0.0	0.5894	0.5890	0.5890	0.5893	0.0000	0.0000	0.0000	0.0000
			0.5894	0.5894	0.5894				
0.25	0.0	0.5378	0.5577	0.5577	0.5578	0.2554	0.2557	0.2557	0.2557
0.50	0.0	0.4587	0.4584	0.4585	0.4586	0.5455	0.5444	0.5454	0.5455
			0.4587	0.4589	0.4587				
0.75	0.0	0.2795	0.2794	0.2795	0.2795	0.9027	0.9018	0.9018	0.9019
1.00	0.00	0.0000	0.0000	0.0000	0.0000	1.3349	1.3463	1.3491	1.3507
							1.3504	1.3506	1.3506
0.25	0.25	0.5283	0.5283	0.5283	0.5283	0.2383	0.2368	0.2386	0.2386
0.50	0.25	0.4356	0.4356	0.4356	0.4356	0.5117	0.5116	0.5116	0.5117
0.75	0.25	0.2667	0.2666	0.2667	0.2667	0.8551	0.8542	0.8543	0.8544
1.00	0.25	0.0000	0.0000	0.0000	0.0000	1.2819	1.2971	1.2974	1.2975
0.50	0.50	0.3623	0.3619	0.3620	0.3623	0.4079	0.4074	0.4069	0.4072
			0.3623	0.3623	0.3623				
0.75	0.50	0.2255	0.2254	0.2255	0.2255	0.7042	0.7032	0.7031	0.7034
1.00	0.50	0.0000	0.0000	0.0000	0.0000	1.1102	1.1158	1.1182	1.1227
							1.12448	1.1252	1.12552
0.75	0.75	0.1456	0.1456	0.1456	0.1456	0.4242	0.4236	0.4231	0.4232

[†]The first line in each case corresponds to the solution obtained using a 2×2 mesh and the second to a 4×4 mesh. The Ritz finite element solution coincides with the Galerkin solution for the same choice of the Hermite interpolation.

14.2.3 Mixed Formulations

Higher-order differential equations place higher-order continuity on the approximation functions, as witnessed in the case of Euler–Bernoulli beam theory (Chapter 5) and the classical plate theory in Chapter 12. When the governing differential equations are second- or higher-order, it is possible to rewrite them as a set of lower-order differential equations and then develop their finite element models by using either their weak forms or weighted residual statements. Such alternative formulations are often considered primarily in the interest of using C^0 finite element approximations. Rewriting of higher-order differential equations as a set of lower-order equations requires introduction of additional variables, which are often physical quantities. The variables appearing in the original differential equations and the additional variables introduced in rewriting as a set of lower-order equations have quite different meaning. In fact, they are like primary and secondary variables of the original higher-order equation. Formulations that independently approximate both primary and secondary variables (of the traditional formulation) are termed *mixed* or *hybrid formulations*. The mixed formulations in turn can be based on weak forms or weighted residual methods. We shall illustrate these ideas with the help of the equations governing the Euler–Bernoulli beam theory.

Model Equation

The equation governing the bending of beams according to the Euler–Bernoulli beam theory is given by [Eq. (5.2.1) with $c_f = 0$]

$$\frac{d^2}{dx^2} \left(EI \frac{d^2w}{dx^2} \right) - q = 0 \quad (14.2.39)$$

where w is the transverse deflection, q the distributed transverse load, and EI the bending stiffness. As we have seen in Chapter 5, the weak-form finite element model of this fourth-order equation requires Hermite cubic interpolation of w that includes w and dw/dx as the nodal variables (i.e., a C^1 element). On the other hand, a weighted integral finite element model of (14.2.39) requires an approximation of w that includes w , dw/dx , $EI d^2w/dx^2$, and $(d/dx)(EI d^2w/dx^2)$ as the nodal degrees of freedom (i.e., seventh-degree Hermite polynomial and C^3 element). To reduce the differentiability requirements on w in the weak form and include the bending moment (or stress) as a nodal degree of freedom, Eq. (14.2.39) can be decomposed into a pair of lower-order equations:

$$-\frac{d^2M}{dx^2} - q = 0, \quad -\frac{d^2w}{dx^2} - \frac{M}{EI} = 0 \quad (EI > 0) \quad (14.2.40)$$

The assumption $EI \neq 0$ always holds in practice because neither the modulus of elasticity nor the moment of inertia is zero. We can develop either a weak-form finite element model or a weighted integral finite element model of the pair of equations in (14.2.40). These two models are discussed next. It is also possible to further reduce the order of the equations, say, to four first-order equations and then use the weighted residual method. Such a mixed formulation would include the deflection, rotation, bending moment, and shear force and will result in C^0 approximation of all unknowns. We will not discuss the details here.

Weak-Form Mixed Finite Element Model

The weak forms of the two equations in (14.2.40) are

$$0 = \int_{x_a}^{x_b} \left(\frac{dv_1}{dx} \frac{dM}{dx} - v_1 q \right) dx - v_1(x_a) \bar{Q}_1 - v_1(x_b) \bar{Q}_2, \quad (14.2.41a)$$

$$0 = \int_{x_a}^{x_b} \left(\frac{dv_2}{dx} \frac{dw}{dx} - v_2 \frac{M}{EI} \right) dx - v_2(x_a) \Theta_1 + v_2(x_b) \Theta_2, \quad (14.2.41b)$$

where (v_1, v_2) are the weight functions that have the interpretation of virtual deflection δw and virtual moment δM , respectively, and

$$\begin{aligned} \bar{Q}_1 &= -\left(\frac{dM}{dx}\right)_{x=x_a}, \quad \bar{Q}_2 = \left(\frac{dM}{dx}\right)_{x=x_b}, \\ \Theta_1 &= \left(-\frac{dw}{dx}\right)_{x=x_a}, \quad \Theta_2 = \left(-\frac{dw}{dx}\right)_{x=x_b}. \end{aligned} \quad (14.2.42)$$

The weak forms (14.2.41a) and (14.2.41b) suggest that both w and M may be approximated using the Lagrange interpolation. Suppose that w and M are approximated as (see Fig. 14.2.2)

$$w(x) \approx \sum_{i=1}^m w_i \phi_i(x), \quad M(x) \approx \sum_{i=1}^n M_i \psi_i(x) \quad (14.2.43)$$

where (ϕ_i, ψ_i) are the Lagrange interpolation functions of different degree used for w and M , respectively. Substituting Eq. (14.2.43) for w and M , and $v_1 = \phi_i$ and $v_2 = \psi_i$ into Eqs. (14.2.41a) and (14.2.41b), we obtain

$$\begin{bmatrix} \mathbf{0} & \mathbf{K}^e \\ (\mathbf{K}^e)^T & -\mathbf{G}^e \end{bmatrix} \begin{Bmatrix} \mathbf{w}^e \\ \mathbf{M}^e \end{Bmatrix} = \begin{Bmatrix} \mathbf{F}^e + \bar{\mathbf{Q}}^e \\ \bar{\Theta}^e \end{Bmatrix} \quad (14.2.44)$$

where

$$\begin{aligned} K_{ij}^e &= \int_{x_a}^{x_b} \frac{d\phi_i}{dx} \frac{d\psi_j}{dx} dx, \quad G_{ij} = \frac{1}{EI} \int_{x_a}^{x_b} \psi_i \psi_j dx \\ F_i^e &= \int_{x_a}^{x_b} q \phi_i dx, \quad \bar{\Theta}_i^e = (-1)^{i+1} \Theta_i \end{aligned} \quad (14.2.45)$$

This completes the development of the weak-form mixed model.

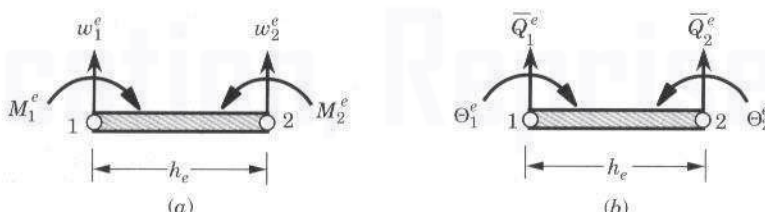


Figure 14.2.2 (a) Generalized displacements and (b) generalized forces for the mixed finite element formulation of the fourth-order equation (14.2.39) [or the weak-form model of (14.2.40)].

The pair of matrix equations (14.2.44) in terms of the nodal values of the displacements and moments can be reduced to a single matrix equation in terms of the generalized displacements \mathbf{w}^e and Θ^e (i.e., converting a mixed model to a displacement model). In the interest of brevity, we omit the element label “ e ” in the quantities. Solving the second equation in (14.2.44) for \mathbf{M} , we obtain

$$\mathbf{M} = \mathbf{G}^{-1} [\mathbf{K}^T \mathbf{w} - \bar{\Theta}] \quad (14.2.46a)$$

Substituting the result into the first equation in (14.2.44), we obtain

$$\mathbf{K}\mathbf{G}^{-1}\mathbf{K}^T\mathbf{w} - \mathbf{K}\mathbf{G}^{-1}\bar{\Theta} = \mathbf{F} + \bar{\mathbf{Q}} \quad (14.2.46b)$$

Now we can write Eqs. (14.2.46a) and (14.2.46b) in a single matrix equation as

$$\begin{bmatrix} \mathbf{K}_w & -\mathbf{K}_\theta \\ -\mathbf{K}_\theta^T & \mathbf{G}^{-1} \end{bmatrix} \begin{Bmatrix} \mathbf{w} \\ \Theta \end{Bmatrix} = \begin{Bmatrix} \mathbf{F} + \bar{\mathbf{Q}} \\ -\mathbf{M} \end{Bmatrix} \quad (14.2.47a)$$

where

$$\mathbf{K}_w = \mathbf{K}\mathbf{G}^{-1}\mathbf{K}^T, \quad \mathbf{K}_\theta = \mathbf{K}\mathbf{G}^{-1} \quad (14.2.47b)$$

It is interesting to note that for the choice of linear interpolation of both w and M , the element stiffness matrix in (14.2.47a) can be shown to be the same as that in Eq. (5.2.18) (see Problem 14.5).

Weighted Residual Mixed Finite Element Model

The weighted residual mixed finite element model of the pair in Eq. (14.2.40) requires higher-order approximations of both w and M because they must satisfy both essential and natural boundary conditions. This leads to a complicated set of finite element equations. Here we present the main ideas behind the development of the model.

The weighted residual statements of the pair of equations is

$$0 = \int_{x_a}^{x_b} v_1 \left(-\frac{d^2 w_0}{dx^2} - \frac{M}{EI} \right) dx \quad (14.2.48a)$$

$$0 = \int_{x_a}^{x_b} v_2 \left(-\frac{d^2 M}{dx^2} - q \right) dx \quad (14.2.48b)$$

where (v_1, v_2) are the weight functions. A close examination of the above statements indicate that $v_1 \sim M$ and $v_2 \sim w$. Suppose that w and M are approximated as

$$w(x) \approx \sum_{i=1}^4 \Delta_i \varphi_i^{(1)}(x), \quad M(x) \approx \sum_{i=1}^4 \Lambda_i \varphi_i^{(2)}(x) \quad (14.2.49)$$

For the Galerkin finite element model, we take $v_1 \sim \varphi_i^{(2)}$ and $v_2 \sim \varphi_i^{(1)}$ and obtain the finite element model

$$\begin{bmatrix} \mathbf{0} & \mathbf{K}^{12} \\ \mathbf{K}^{21} & \mathbf{K}^{22} \end{bmatrix} \begin{Bmatrix} \Delta^e \\ \Lambda^e \end{Bmatrix} = \begin{Bmatrix} \mathbf{F}^e \\ \mathbf{0} \end{Bmatrix} \quad (14.2.50a)$$

where

$$\begin{aligned} K_{ij}^{12} &= \int_{x_a}^{x_b} \varphi_i^{(1)} \frac{d^2 \varphi_j^{(2)}}{dx^2} dx, \quad F_i^e = - \int_{x_a}^{x_b} q \varphi_i^{(1)} dx, \\ K_{ij}^{21} &= \int_{x_a}^{x_b} \varphi_i^{(2)} \frac{d^2 \varphi_j^{(1)}}{dx^2} dx, \quad K_{ij}^{22} = \int_{x_a}^{x_b} \varphi_i^{(2)} \frac{d^2 \varphi_j^{(2)}}{dx^2} dx \end{aligned} \quad (14.2.50b)$$

The coefficient matrix in Eq. (14.2.50a) is *not* symmetric.

The least-squares finite element model is based on the variational statement

$$\begin{aligned} 0 &= \delta \int_{x_a}^{x_b} \left[\left(\frac{d^2 w}{dx^2} + \frac{M}{EI} \right)^2 + \left(\frac{d^2 M}{dx^2} + q \right)^2 \right] dx \\ &= 2 \int_{x_a}^{x_b} \left[\left(\frac{d^2 w}{dx^2} + \frac{M}{EI} \right) \left(\frac{d^2 \delta w}{dx^2} + \frac{\delta M}{EI} \right) + \left(\frac{d^2 M}{dx^2} + q \right) \frac{d^2 \delta M}{dx^2} \right] dx \end{aligned}$$

or

$$0 = \int_{x_a}^{x_b} \frac{d^2 \delta w}{dx^2} \left(\frac{d^2 w}{dx^2} + \frac{M}{EI} \right) dx \quad (14.2.51a)$$

$$0 = \int_{x_a}^{x_b} \left[\delta M \left(\frac{d^2 w}{dx^2} + \frac{M}{EI} \right) + EI \frac{d^2 \delta M}{dx^2} \left(\frac{d^2 M}{dx^2} + q \right) \right] dx \quad (14.2.51b)$$

Substituting the approximations in (14.2.49) into Eqs. (14.1.51a) and (14.2.51b), we obtain

$$\begin{bmatrix} \mathbf{A}^e & \mathbf{B}^e \\ (\mathbf{B}^e)^T & \mathbf{D}^e \end{bmatrix} \begin{Bmatrix} \mathbf{\Lambda}^e \\ \mathbf{\Delta}^e \end{Bmatrix} = \begin{Bmatrix} \mathbf{F}^e \\ \mathbf{0} \end{Bmatrix} \quad (14.2.52a)$$

where

$$\begin{aligned} A_{ij}^e &= \int_{x_a}^{x_b} \left(EI \frac{d^2 \varphi_i^{(2)}}{dx^2} \frac{d^2 \varphi_j^{(2)}}{dx^2} + \varphi_i^{(2)} \varphi_j^{(2)} \right) dx, \quad F_i^e = - \int_{x_a}^{x_b} \frac{d^2 \varphi_i^{(2)}}{dx^2} q dx \\ B_{ij}^e &= \int_{x_a}^{x_b} \varphi_i^{(2)} \frac{d^2 \varphi_j^{(1)}}{dx^2} dx, \quad D_{ij}^e = \int_{x_a}^{x_b} \frac{d^2 \varphi_i^{(1)}}{dx^2} \frac{d^2 \varphi_j^{(1)}}{dx^2} dx \end{aligned} \quad (14.2.52b)$$

14.3 THREE-DIMENSIONAL PROBLEMS

Most of the basic ideas covered in Chapter 8 for two-dimensional problems can be extended to three-dimensional problems. For the sake of completeness, here we discuss finite element formulations of (1) the Poisson equation governing three-dimensional heat transfer, (2) three-dimensional elasticity equations, and (3) equations governing three-dimensional flows of viscous incompressible fluids. In addition, some of the commonly used three-dimensional finite elements will be presented. To keep the size as well as the scope of the book to reasonable limits, only essential steps are presented and only one numerical example is included.

14.3.1 Heat Transfer

Consider the Poisson equation

$$-\frac{\partial}{\partial x} \left(k_x \frac{\partial T}{\partial x} \right) - \frac{\partial}{\partial y} \left(k_y \frac{\partial T}{\partial y} \right) - \frac{\partial}{\partial z} \left(k_z \frac{\partial T}{\partial z} \right) = g \quad \text{in } \Omega \quad (14.3.1)$$

subjected to boundary conditions of the form

$$T = \hat{T} \quad \text{on } \Gamma_1, \quad k_x \frac{\partial T}{\partial x} n_x + k_y \frac{\partial T}{\partial y} n_y + k_z \frac{\partial T}{\partial z} n_z + \beta(T - T_\infty) = \hat{q} \quad \text{on } \Gamma_2 \quad (14.3.2)$$

where k_x , k_y , and k_z are conductivities of an orthotropic solid in the three coordinate directions, g is the internal heat generation per unit volume in a three-dimensional domain Ω , and \hat{T} and \hat{q} are specified functions of position on the portions Γ_1 and Γ_2 , respectively, of the surface Γ of the domain (see Fig. 14.3.1); β is the convection coefficient and T_∞ is the ambient temperature.

The weak form of (14.3.1) over an element Ω_e is given by

$$\begin{aligned} 0 &= \int_{\Omega_e} w \left[-\frac{\partial}{\partial x} \left(k_x \frac{\partial T}{\partial x} \right) - \frac{\partial}{\partial y} \left(k_y \frac{\partial T}{\partial y} \right) - \frac{\partial}{\partial z} \left(k_z \frac{\partial T}{\partial z} \right) - g \right] d\mathbf{x} \\ &= \int_{\Omega_e} \left[k_x \frac{\partial w}{\partial x} \frac{\partial T}{\partial x} + k_y \frac{\partial w}{\partial y} \frac{\partial T}{\partial y} + k_z \frac{\partial w}{\partial z} \frac{\partial T}{\partial z} - wg \right] d\mathbf{x} \\ &\quad + \oint_{\Gamma_e} \beta w T ds - \oint_{\Gamma_e} w (q_n + \beta T_\infty) ds \end{aligned} \quad (14.3.3)$$

where w is the weight function.

Assume a finite element interpolation of the form

$$T = \sum_{j=1}^n T_j^e \psi_j^e(x, y, z) \quad (14.3.4)$$

over the element Ω_e (see Fig. 14.3.1). Substituting $w = \psi_i^e$ and (14.3.4) into (14.3.3), we obtain the finite element model

$$\mathbf{K}^e \mathbf{T}^e = \mathbf{f}^e + \mathbf{Q}^e \quad (14.3.5a)$$

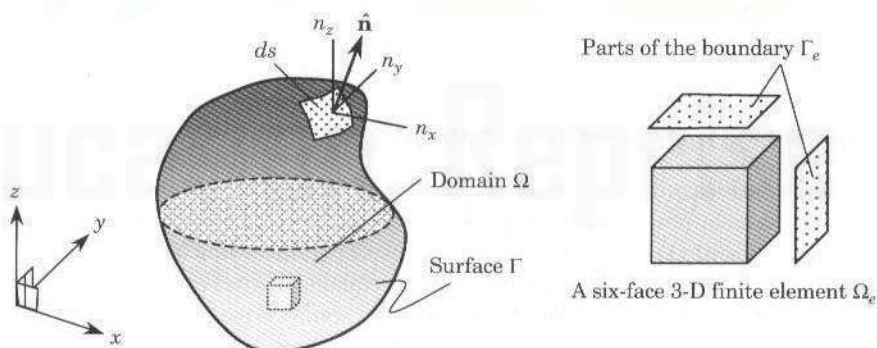


Figure 14.3.1 A three-dimensional domain Ω , its boundary Γ with unit normal $\hat{\mathbf{n}}$, and a typical three-dimensional finite element.

where

$$\begin{aligned} K_{ij}^e &= \int_{\Omega_e} \left(k_x \frac{\partial \psi_i^e}{\partial x} \frac{\partial \psi_j^e}{\partial x} + k_y \frac{\partial \psi_i^e}{\partial y} \frac{\partial \psi_j^e}{\partial y} + k_z \frac{\partial \psi_i^e}{\partial z} \frac{\partial \psi_j^e}{\partial z} \right) d\mathbf{x} + \oint_{\Gamma_e} \beta \psi_i^e \psi_j^e ds \\ f_i^e &= \int_{\Omega_e} g \psi_i^e d\mathbf{x}, \quad Q_i^e = \oint_{\Gamma_e} (q_n + \beta T_\infty) \psi_i^e ds \end{aligned} \quad (14.3.5b)$$

Note that the boundary Γ_e of a three-dimensional element is a collection of two-dimensional elements. The numerical integration of volume and surface integrals is carried out in the same way as described in Chapter 9.

14.3.2 Flows of Viscous Incompressible Fluids

Here we develop the penalty finite element model of the Stokes equations governing three-dimensional flows of incompressible fluids. The governing equations consist of three momentum equations and a continuity equation

$$\begin{aligned} 2\mu \frac{\partial^2 v_x}{\partial x^2} + \mu \frac{\partial}{\partial y} \left(\frac{\partial v_x}{\partial y} + \frac{\partial v_y}{\partial x} \right) + \mu \frac{\partial}{\partial z} \left(\frac{\partial v_x}{\partial z} + \frac{\partial v_z}{\partial x} \right) - \frac{\partial P}{\partial x} + f_x &= 0 \\ 2\mu \frac{\partial^2 v_y}{\partial y^2} + \mu \frac{\partial}{\partial x} \left(\frac{\partial v_x}{\partial y} + \frac{\partial v_y}{\partial x} \right) + \mu \frac{\partial}{\partial z} \left(\frac{\partial v_y}{\partial z} + \frac{\partial v_z}{\partial y} \right) - \frac{\partial P}{\partial y} + f_y &= 0 \\ 2\mu \frac{\partial^2 v_z}{\partial z^2} + \mu \frac{\partial}{\partial x} \left(\frac{\partial v_x}{\partial z} + \frac{\partial v_z}{\partial x} \right) + \mu \frac{\partial}{\partial y} \left(\frac{\partial v_y}{\partial z} + \frac{\partial v_z}{\partial y} \right) - \frac{\partial P}{\partial z} + f_z &= 0 \\ \frac{\partial v_x}{\partial x} + \frac{\partial v_y}{\partial y} + \frac{\partial v_z}{\partial z} &= 0 \end{aligned} \quad (14.3.6)$$

In developing the penalty finite element model, we replace the pressure P in the momentum equations with

$$P = -\gamma \left(\frac{\partial v_x}{\partial x} + \frac{\partial v_y}{\partial y} + \frac{\partial v_z}{\partial z} \right) = 0 \quad (14.3.7)$$

and omit the continuity equation. The variational problem of the resulting equations can be cast in vector form as [see Eqs. (10.4.18) and (10.4.19)]

$$B_p(\mathbf{w}, \mathbf{v}) = l(\mathbf{w}) \quad (14.3.8)$$

where the bilinear forms $B_p(\mathbf{w}, \mathbf{v})$ and $\bar{B}_p(\mathbf{w}, P)$ and the linear form $l(\mathbf{w})$ are defined as in Eqs. (10.3.10a) and (10.4.19)

$$\mathbf{w} = \begin{Bmatrix} w_1 \\ w_2 \\ w_3 \end{Bmatrix}, \quad \mathbf{v} = \begin{Bmatrix} v_x \\ v_y \\ v_z \end{Bmatrix}, \quad \mathbf{f} = \begin{Bmatrix} f_x \\ f_y \\ f_z \end{Bmatrix}, \quad \mathbf{t} = \begin{Bmatrix} t_x \\ t_y \\ t_z \end{Bmatrix} \quad (14.3.9)$$

$$\begin{aligned} B_p(\mathbf{w}, \mathbf{v}) &= \int_{\Omega_e} (\mathbf{D}\mathbf{w})^T \mathbf{C} (\mathbf{D}\mathbf{v}) d\mathbf{x} + \int_{\Omega_e} \gamma_e (\mathbf{D}_1^T \mathbf{w})^T \mathbf{D}_1^T \mathbf{v} d\mathbf{x} \\ l(\mathbf{w}) &= \int_{\Omega_e} \mathbf{w}^T \mathbf{f} dx dy + \oint_{\Gamma_e} \mathbf{w}^T \mathbf{t} ds \end{aligned} \quad (14.3.10)$$

$$\mathbf{D} = \begin{bmatrix} \frac{\partial}{\partial x} & 0 & 0 \\ 0 & \frac{\partial}{\partial y} & 0 \\ 0 & 0 & \frac{\partial}{\partial z} \\ \frac{\partial}{\partial y} & \frac{\partial}{\partial x} & 0 \\ \frac{\partial}{\partial z} & 0 & \frac{\partial}{\partial x} \\ 0 & \frac{\partial}{\partial z} & \frac{\partial}{\partial y} \end{bmatrix}, \quad \mathbf{D}_1 = \begin{Bmatrix} \frac{\partial}{\partial x} \\ \frac{\partial}{\partial y} \\ \frac{\partial}{\partial z} \end{Bmatrix}, \quad \mathbf{C} = \mu \begin{bmatrix} 2 & 0 & 0 & 0 & 0 & 0 \\ 0 & 2 & 0 & 0 & 0 & 0 \\ 0 & 0 & 2 & 0 & 0 & 0 \\ 0 & 0 & 0 & 1 & 0 & 0 \\ 0 & 0 & 0 & 0 & 1 & 0 \\ 0 & 0 & 0 & 0 & 0 & 1 \end{bmatrix} \quad (14.3.11)$$

We assume finite element approximation of the form

$$\mathbf{v} = \begin{Bmatrix} v_x \\ v_y \\ v_z \end{Bmatrix} = \Psi \Delta, \quad \mathbf{w} = \begin{Bmatrix} w_1 \\ w_2 \\ w_3 \end{Bmatrix} = \Psi \delta \Delta \quad (14.3.12)$$

where

$$\Psi = \begin{bmatrix} \psi_1 & 0 & 0 & \psi_2 & 0 & 0 & \dots & \psi_n & 0 & 0 \\ 0 & \psi_1 & 0 & 0 & \psi_2 & 0 & 0 & \dots & \psi_n & 0 \\ 0 & 0 & \psi_1 & 0 & 0 & \psi_2 & 0 & 0 & \dots & \psi_n \end{bmatrix} \quad (3 \times 3n) \quad (14.3.13)$$

$$\Delta = \{v_x^1 \ v_y^1 \ v_z^1 \ v_x^2 \ v_y^2 \ v_z^2 \ \dots \ v_x^n \ v_y^n \ v_z^n\}^T \quad (3n \times 1)$$

Substituting (14.3.12) into the variational statement (14.3.8), we obtain the following finite element equation:

$$(\mathbf{K}_v + \mathbf{K}_p)\Delta = \mathbf{F} \quad (14.3.14)$$

where \mathbf{K}_v is the contribution of the viscous terms (i.e., terms containing the viscosity μ), \mathbf{K}_p is the contribution of the penalty terms (i.e., terms containing the penalty parameter γ), and \mathbf{K}_v and \mathbf{K}_p are of the order $3n \times 3n$; and \mathbf{F} is the contribution of the body forces (f_x, f_y, f_z) as well as the boundary stresses (t_x, t_y, t_z), and \mathbf{F} is of the order $3n \times 1$

$$\begin{aligned} \mathbf{K}_v &= \int_{\Omega_e} \mathbf{B}_v^T \mathbf{C} \mathbf{B}_v \, dx, \quad \mathbf{K}_p = \int_{\Omega_e} \gamma_e \mathbf{B}_p^T \mathbf{B}_p \, dx \\ \mathbf{F} &= \int_{\Omega_e} \Psi^T \mathbf{f} \, dx + \oint_{\Gamma_e} \Psi^T \mathbf{t} \, ds \\ \mathbf{B}_v &= \mathbf{D}\Psi, \quad \mathbf{B}_p = \mathbf{D}_1^T \Psi \end{aligned} \quad (14.3.15)$$

This completes the finite element model development.

14.3.3 Elasticity

Here, we develop the finite element models of three-dimensional elasticity problems [see Eqs. (2.3.48)–(2.3.53)]. First, we write the governing equations (2.3.51)–(2.3.53) in vector form.

Strain-Displacement Relations

$$\begin{aligned}\varepsilon_{xx} &= \frac{\partial u_x}{\partial x}, \quad \varepsilon_{yy} = \frac{\partial u_y}{\partial y}, \quad \varepsilon_{zz} = \frac{\partial u_z}{\partial z} \\ 2\varepsilon_{xy} &= \frac{\partial u_x}{\partial y} + \frac{\partial u_y}{\partial x}, \quad 2\varepsilon_{xz} = \frac{\partial u_x}{\partial z} + \frac{\partial u_z}{\partial x}, \quad 2\varepsilon_{yz} = \frac{\partial u_y}{\partial z} + \frac{\partial u_z}{\partial y} \quad (14.3.16a)\end{aligned}$$

or

$$\boldsymbol{\varepsilon} = \mathbf{D}\mathbf{u}, \quad \boldsymbol{\varepsilon} = \begin{bmatrix} \varepsilon_{xx} \\ \varepsilon_{yy} \\ \varepsilon_{zz} \\ 2\varepsilon_{xz} \\ 2\varepsilon_{yz} \\ 2\varepsilon_{xy} \end{bmatrix}, \quad \mathbf{D}^T = \begin{bmatrix} \partial/\partial x & 0 & 0 & \partial/\partial z & 0 & \partial/\partial y \\ 0 & \partial/\partial y & 0 & 0 & \partial/\partial z & \partial/\partial x \\ 0 & 0 & \partial/\partial z & \partial/\partial x & \partial/\partial y & 0 \end{bmatrix} \quad (14.3.16b)$$

Equations of Motion

$$\begin{aligned}\frac{\partial \sigma_{xx}}{\partial x} + \frac{\partial \sigma_{xy}}{\partial y} + \frac{\partial \sigma_{xz}}{\partial z} + f_x &= \rho \frac{\partial u_x}{\partial t^2} \\ \frac{\partial \sigma_{xy}}{\partial x} + \frac{\partial \sigma_{yy}}{\partial y} + \frac{\partial \sigma_{yz}}{\partial z} + f_y &= \rho \frac{\partial u_y}{\partial t^2} \\ \frac{\partial \sigma_{xz}}{\partial x} + \frac{\partial \sigma_{yz}}{\partial y} + \frac{\partial \sigma_{zz}}{\partial z} + f_z &= \rho \frac{\partial u_z}{\partial t^2} \quad (14.3.17a)\end{aligned}$$

or

$$\mathbf{D}^T \boldsymbol{\sigma} + \mathbf{f} = \rho \ddot{\mathbf{u}} \quad (14.3.17b)$$

where f_x , f_y , and f_z denote the components of the body force vector (measured per unit volume) along the x , y , and z directions, respectively, ρ is the density of the material, and

$$\boldsymbol{\sigma} = \begin{bmatrix} \sigma_{xx} \\ \sigma_{yy} \\ \sigma_{zz} \\ \sigma_{xy} \\ \sigma_{xz} \\ \sigma_{yz} \end{bmatrix}, \quad \mathbf{f} = \begin{bmatrix} f_x \\ f_y \\ f_z \end{bmatrix}, \quad \mathbf{u} = \begin{bmatrix} u_x \\ u_y \\ u_z \end{bmatrix} \quad (14.3.17c)$$

Stress-Strain (or Constitutive) Relations

$$\begin{bmatrix} \sigma_{xx} \\ \sigma_{yy} \\ \sigma_{zz} \\ \sigma_{xz} \\ \sigma_{yz} \\ \sigma_{xy} \end{bmatrix} = \begin{bmatrix} c_{11} & c_{12} & c_{13} & 0 & 0 & 0 \\ c_{12} & c_{22} & c_{23} & 0 & 0 & 0 \\ c_{13} & c_{23} & c_{33} & 0 & 0 & 0 \\ 0 & 0 & 0 & c_{44} & 0 & 0 \\ 0 & 0 & 0 & 0 & c_{55} & 0 \\ 0 & 0 & 0 & 0 & 0 & c_{66} \end{bmatrix} \begin{bmatrix} \varepsilon_{xx} \\ \varepsilon_{yy} \\ \varepsilon_{zz} \\ 2\varepsilon_{xz} \\ 2\varepsilon_{yz} \\ 2\varepsilon_{xy} \end{bmatrix} \quad \text{or } \boldsymbol{\sigma} = \mathbf{C}\boldsymbol{\varepsilon} \quad (14.3.18)$$

where c_{ij} ($c_{ji} = c_{ij}$) are the elasticity (material) constants for an orthotropic medium with the material principal directions (x_1, x_2, x_3) coinciding with the coordinate axes (x, y, z) used to describe the problem. The c_{ij} can be expressed in terms of the engineering constants ($E_1, E_2, E_3, \nu_{12}, \nu_{13}, \nu_{23}, G_{12}, G_{13}, G_{23}$) for an orthotropic material by Eqs. (2.3.48b).

Boundary Conditions

$$\left. \begin{array}{l} t_x \equiv \sigma_{xx}n_x + \sigma_{xy}n_y + \sigma_{xz}n_z = \hat{t}_x \\ t_y \equiv \sigma_{xy}n_x + \sigma_{yy}n_y + \sigma_{yz}n_z = \hat{t}_y \\ t_z \equiv \sigma_{xz}n_x + \sigma_{yz}n_y + \sigma_{zz}n_z = \hat{t}_z \end{array} \right\} \text{on } \Gamma_\sigma \quad (14.3.19)$$

$$\text{Essential } \mathbf{u} = \hat{\mathbf{u}} \text{ on } \Gamma_u \quad (14.3.20)$$

The principle of virtual displacements for the three-dimensional elasticity problem can be expressed in vector form as in (11.3.4)

$$0 = \int_{\Omega_e} [(\mathbf{D}\delta\mathbf{u})^T \mathbf{C} (\mathbf{D}\mathbf{u}) + \rho \mathbf{u}^T \ddot{\mathbf{u}}] d\mathbf{x} - \int_{\Omega_e} (\delta\mathbf{u})^T \mathbf{f} d\mathbf{x} - \oint_{\Gamma_e} (\delta\mathbf{u})^T \mathbf{t} ds \quad (14.3.21)$$

The finite element approximation is assumed to be in the form

$$\mathbf{u} = \begin{Bmatrix} u_x \\ u_y \\ u_z \end{Bmatrix} = \Psi \Delta, \quad \mathbf{w} = \delta\mathbf{u} = \begin{Bmatrix} w_1 = \delta u_x \\ w_2 = \delta u_y \\ w_3 = \delta u_z \end{Bmatrix} = \Psi \delta \Delta \quad (14.3.22)$$

where

$$\Psi = \begin{bmatrix} \psi_1 & 0 & 0 & \psi_2 & 0 & 0 & \dots & \psi_n & 0 & 0 \\ 0 & \psi_1 & 0 & 0 & \psi_2 & 0 & 0 & \dots & \psi_n & 0 \\ 0 & 0 & \psi_1 & 0 & 0 & \psi_2 & 0 & \dots & 0 & \psi_n \end{bmatrix} \quad (14.3.23)$$

$$\Delta = \{u_x^1 \ u_y^1 \ u_z^1 \ u_x^2 \ u_y^2 \ u_z^2 \ \dots \ u_x^n \ u_y^n \ u_z^n\}^T$$

Substituting Eq. (14.3.22) into the statement of the principle of virtual work (14.3.21), we arrive at the finite element model of a three-dimensional elastic body

$$\mathbf{M}^e \ddot{\Delta}^e + \mathbf{K}^e \Delta^e = \mathbf{F}^e + \mathbf{Q}^e \quad (14.3.24)$$

where

$$\begin{aligned} \mathbf{K}^e &= \int_{\Omega_e} \mathbf{B}^T \mathbf{C} \mathbf{B} d\mathbf{x}, \quad \mathbf{M}^e = \int_{\Omega_e} \rho \Psi^T \Psi^e d\mathbf{x} \\ \mathbf{F}^e &= \int_{\Omega_e} \Psi^T \mathbf{f} d\mathbf{x}, \quad \mathbf{Q}^e = \oint_{\Gamma_e} \Psi^T \mathbf{t} ds \end{aligned} \quad (14.3.25)$$

The element mass matrix \mathbf{M}^e and stiffness matrix \mathbf{K}^e are of order $3n \times 3n$ and the element load vector \mathbf{F}^e and the vector of internal forces \mathbf{Q}^e is of order $3n \times 1$, where n is the number of nodes in a finite element.

Computer implementation of three classes of problems described in this section is straightforward, and we can modify the computer program **FEM2D** to implement the finite

element models in (14.3.5a), (14.3.14), and (14.3.24). The main change is in the subroutine **SHAPE3D** in which the interpolation functions and their global derivatives are evaluated. In the next section, interpolation functions for a number of commonly used three-dimensional finite elements are presented. We note that in going from two dimensions to three dimensions, we increase the number of geometries (i.e., shapes) that can be used to define finite element interpolation functions.

14.3.4 Three-Dimensional Finite Elements

The element matrices in (14.3.5b), (14.3.15), and (14.3.25) require the use of C^0 (i.e., the Lagrange) family of interpolation functions. The interpolation functions can be derived as described in Chapters 8 and 9 for two-dimensional elements, and they have the same interpolation properties as those of two-dimensional elements

$$\sum_{i=1}^n \psi_i^e(x, y, z) = 1, \quad \psi_i^e(x_j, y_j, z_j) = \delta_{ij} \quad (14.3.26)$$

For example, consider the linear elements shown in the first column of Fig. 14.3.2. The polynomials used to develop the interpolation functions for these elements are of the form

$$\begin{aligned} u(x, y, z) &= a_0 + a_1x + a_2y + a_3z && \text{(four-node tetrahedral element)} \\ u(x, y, z) &= a_0 + a_1x + a_2y + a_3z + a_4xz + a_5yz && \text{(six-node prism element)} \\ u(x, y, z) &= a_0 + a_1x + a_2y + a_3z + a_4yz + a_5xz \\ &\quad + a_6xy + a_7xyz && \text{(eight-node brick or hexahedral element)} \end{aligned} \quad (14.3.27)$$

In evaluating the element matrices numerically, the geometry of the elements can be described by the transformation equations

$$x = \sum_{i=1}^m x_i \hat{\psi}_i(\xi, \eta, \zeta), \quad y = \sum_{i=1}^m y_i \hat{\psi}_i(\xi, \eta, \zeta), \quad z = \sum_{i=1}^m z_i \hat{\psi}_i(\xi, \eta, \zeta) \quad (14.3.28)$$

Under these transformations, the master tetrahedral and prism elements transform to the arbitrary tetrahedral, prism, and hexahedral elements shown in Fig. 14.3.2. The definition of the Jacobian matrix and the numerical quadrature rules described in Chapter 9 can easily be extended to the three-dimensional case. For example, Eqs. (9.3.8) and (9.3.9) take the form

$$[J] = \begin{bmatrix} \frac{\partial x}{\partial \xi} & \frac{\partial y}{\partial \xi} & \frac{\partial z}{\partial \xi} \\ \frac{\partial x}{\partial \eta} & \frac{\partial y}{\partial \eta} & \frac{\partial z}{\partial \eta} \\ \frac{\partial x}{\partial \zeta} & \frac{\partial y}{\partial \zeta} & \frac{\partial z}{\partial \zeta} \end{bmatrix} = \begin{bmatrix} \frac{\partial \hat{\psi}_1}{\partial \xi} & \frac{\partial \hat{\psi}_2}{\partial \xi} & \dots & \frac{\partial \hat{\psi}_m}{\partial \xi} \\ \frac{\partial \hat{\psi}_1}{\partial \eta} & \frac{\partial \hat{\psi}_2}{\partial \eta} & \dots & \frac{\partial \hat{\psi}_m}{\partial \eta} \\ \frac{\partial \hat{\psi}_1}{\partial \zeta} & \frac{\partial \hat{\psi}_2}{\partial \zeta} & \dots & \frac{\partial \hat{\psi}_m}{\partial \zeta} \end{bmatrix} \begin{bmatrix} x_1 & y_1 & z_1 \\ x_2 & y_2 & z_2 \\ \vdots & \vdots & \vdots \\ x_m & y_m & z_m \end{bmatrix} \quad (14.3.29)$$

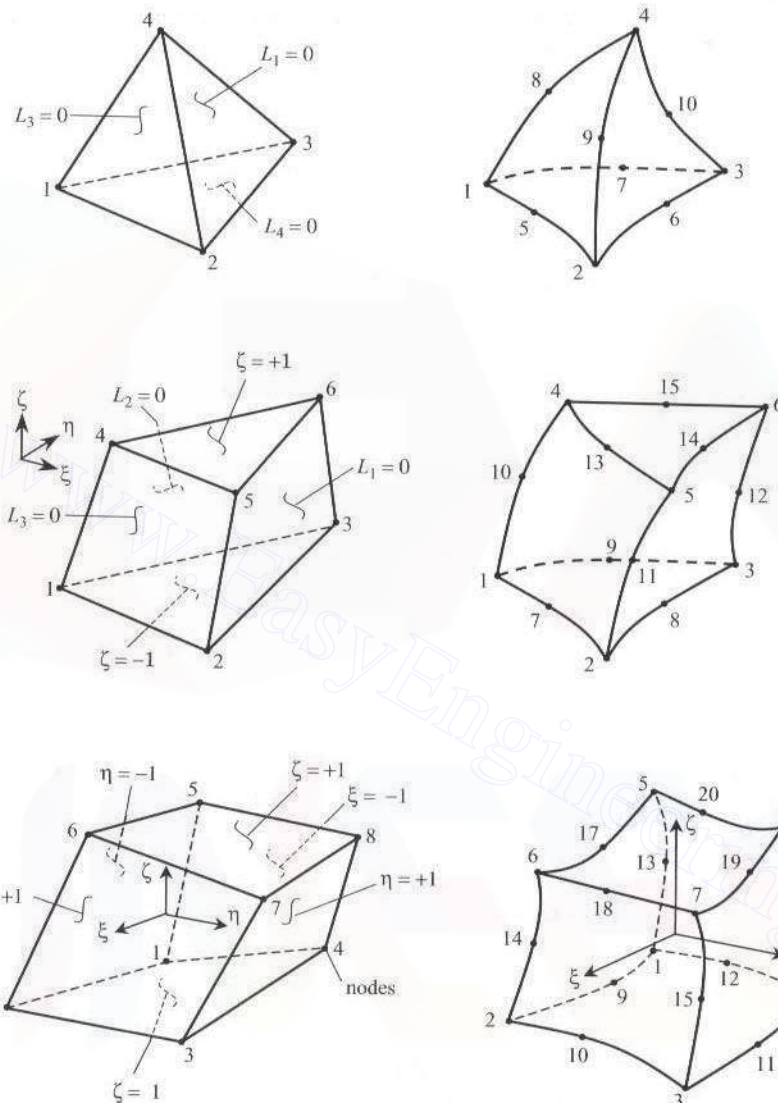


Figure 14.3.2 Linear and quadratic tetrahedral, prism, and brick elements (whose surfaces are two-dimensional triangular or quadrilateral elements).

$$\begin{Bmatrix} \frac{\partial \psi_i^e}{\partial x} \\ \frac{\partial \psi_i^e}{\partial y} \\ \frac{\partial \psi_i^e}{\partial z} \end{Bmatrix} = [J]^{-1} \begin{Bmatrix} \frac{\partial \psi_i^e}{\partial \xi} \\ \frac{\partial \psi_i^e}{\partial \eta} \\ \frac{\partial \psi_i^e}{\partial \zeta} \end{Bmatrix} \quad (14.3.30)$$

Interpolation functions for some standard elements are recorded in Eqs. (14.3.31)–(14.3.35) [see Reddy and Gartling (2001)].

Linear and Quadratic Hexhedral (Brick) Elements

$$\{\Psi^e\} = \frac{1}{8} \begin{Bmatrix} (1-\xi)(1-\eta)(1-\zeta) \\ (1+\xi)(1-\eta)(1-\zeta) \\ (1+\xi)(1+\eta)(1-\zeta) \\ (1-\xi)(1+\eta)(1-\zeta) \\ (1-\xi)(1-\eta)(1+\zeta) \\ (1+\xi)(1-\eta)(1+\zeta) \\ (1+\xi)(1+\eta)(1+\zeta) \\ (1-\xi)(1+\eta)(1+\zeta) \end{Bmatrix} \quad (14.3.31)$$

$$\{\Psi^e\} = \frac{1}{8} \begin{Bmatrix} (1-\xi)(1-\eta)(1-\zeta)(-\xi-\eta-\zeta-2) \\ (1+\xi)(1-\eta)(1-\zeta)(\xi-\eta-\zeta-2) \\ (1+\xi)(1+\eta)(1-\zeta)(\xi+\eta-\zeta-2) \\ (1-\xi)(1+\eta)(1-\zeta)(-\xi+\eta-\zeta-2) \\ (1-\xi)(1-\eta)(1+\zeta)(-\xi-\eta+\zeta-2) \\ (1+\xi)(1-\eta)(1+\zeta)(\xi-\eta+\zeta-2) \\ (1+\xi)(1+\eta)(1+\zeta)(\xi+\eta+\zeta-2) \\ (1-\xi)(1+\eta)(1+\zeta)(-\xi+\eta+\zeta-2) \\ 2(1-\xi^2)(1-\eta)(1-\zeta) \\ 2(1+\xi)(1-\eta^2)(1-\zeta) \\ 2(1-\xi^2)(1+\eta)(1-\zeta) \\ 2(1-\xi)(1-\eta^2)(1-\zeta^2) \\ 2(1-\xi)(1-\eta)(1-\zeta^2) \\ 2(1+\xi)(1-\eta)(1-\zeta^2) \\ 2(1+\xi)(1+\eta)(1-\zeta^2) \\ 2(1-\xi)(1+\eta)(1-\zeta^2) \\ 2(1-\xi^2)(1-\eta)(1+\zeta) \\ 2(1+\xi)(1-\eta^2)(1+\zeta) \\ 2(1-\xi^2)(1+\eta)(1+\zeta) \\ 2(1-\xi)(1-\eta^2)(1+\zeta) \end{Bmatrix} \quad (14.3.32)$$

Linear and Quadratic Prism Elements

$$\{\Psi^e\} = \frac{1}{2} \begin{Bmatrix} L_1(1 - \zeta) \\ L_2(1 - \zeta) \\ L_3(1 - \zeta) \\ L_1(1 + \zeta) \\ L_2(1 + \zeta) \\ L_3(1 + \zeta) \end{Bmatrix} \quad (14.3.33)$$

$$\{\Psi^e\} = \frac{1}{2} \begin{Bmatrix} L_1[(2L_1 - 1)(1 - \zeta) - (1 - \zeta^2)] \\ L_2[(2L_2 - 1)(1 - \zeta) - (1 - \zeta^2)] \\ L_3[(2L_3 - 1)(1 - \zeta) - (1 - \zeta^2)] \\ L_1[(2L_1 - 1)(1 + \zeta) - (1 - \zeta^2)] \\ L_2[(2L_2 - 1)(1 + \zeta) - (1 - \zeta^2)] \\ L_3[(2L_3 - 1)(1 + \zeta) - (1 - \zeta^2)] \\ 4L_1L_2(1 - \zeta) \\ 4L_2L_3(1 - \zeta) \\ 4L_3L_1(1 - \zeta) \\ 2L_1(1 - \zeta^2) \\ 2L_2(1 - \zeta^2) \\ 2L_3(1 - \zeta^2) \\ 4L_1L_2(1 + \zeta) \\ 4L_2L_3(1 + \zeta) \\ 4L_3L_1(1 + \zeta) \end{Bmatrix} \quad (14.3.34)$$

Linear and Quadratic Tetrahedral Elements

$$\{\Psi^e\} = \begin{Bmatrix} L_1 \\ L_2 \\ L_3 \\ L_4 \end{Bmatrix}, \quad \{\Psi^e\} = \begin{Bmatrix} L_1(2L_1 - 1) \\ L_2(2L_2 - 1) \\ L_3(2L_3 - 1) \\ L_4(2L_4 - 1) \\ 4L_1L_2 \\ 4L_2L_3 \\ 4L_3L_1 \\ 4L_1L_4 \\ 4L_2L_4 \\ 4L_3L_4 \end{Bmatrix} \quad (14.3.35)$$

The volume coordinates, L_i , are used to describe the interpolation functions for linear and quadratic elements, where $L_1 + L_2 + L_3 + L_4 = 1$.

14.3.5 A Numerical Example

Here, we consider an example of heat conduction in a three-dimensional solid. The problem is analyzed using program **FEM3D**, which is an extension of **FEM2D**. The program **FEM3D** is not discussed here.

Example 14.3.1

Consider an isotropic slab of dimensions $1 \times 1 \times 10$ m. The left face is maintained at a temperature of 100°C while the bottom, top and the right faces are maintained at 0°C , as shown in Fig. 14.3.3(a). The front and back faces are assumed to be insulated. There is no internal heat generation. Since only temperature boundary conditions are involved, the solution will be independent of the conductivity of the medium. Using the symmetry, a quadrant of the domain is modeled using a $4 \times 2 \times 2$ mesh of eight-node brick elements [see Fig. 14.3.3(b)].

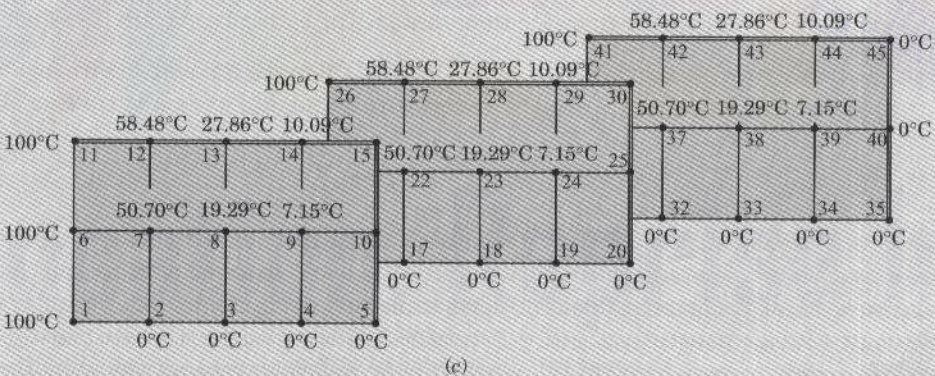
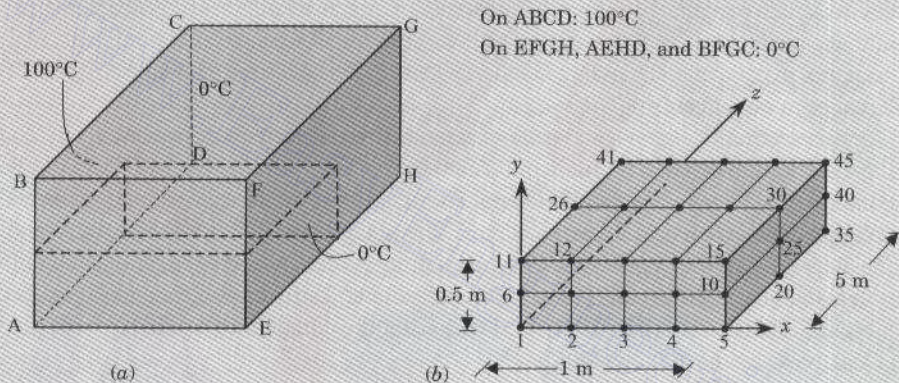


Figure 14.3.3 Heat conduction in an isotropic slab. (a) Geometry and boundary conditions. (b) Computational domain. (c) Predicted temperature field.

The resulting temperature field is depicted in Fig. 14.3.3(c). As we might expect, the three-dimensional solution is the same as the two-dimensional (in the xy plane) solution because the two-dimensional problem is equivalent to assuming that the slab is infinitely long in the z direction. Thus, all planes parallel to the plane $z = 0$ have the same temperature distribution. The three-dimensional solution would have been different from the two-dimensional one if we had specified, for example, the temperature on the front and back faces (AEFB and DHGC).

14.4 NONLINEAR PROBLEMS

14.4.1 General Comments

Many engineering problems are described by nonlinear differential equations. Under certain simplifying assumptions, these problems can be described by linear differential equations. While a small percentage (about 10 percent) of practical engineering problems require nonlinear analysis, it is not a trivial task to determine when to use nonlinear analysis. It requires a good understanding of the system being analyzed and the allowed design tolerances in manufacturing the system.

In this section, we give some taste of nonlinear finite element formulations by considering the one-dimensional problem of beam bending and two-dimensional flows of viscous incompressible fluids. The finite element formulation of nonlinear problems proceeds in much the same way as for linear problems. The main difference lies in the solution of the finite element algebraic equations. For more complete details and applications to nonlinear problems in heat transfer, fluid dynamics, and solid and structural mechanics (e.g., beams, plates, and shells), the reader is advised to consult the companion nonlinear finite element analysis book by the author (2004).

14.4.2 Bending of Euler–Bernoulli Beams

The equations governing the large-deflection bending of elastic beams are [see Reddy (2004)]

$$-\frac{d}{dx} \left\{ EA \left[\frac{du}{dx} + \frac{1}{2} \left(\frac{dw}{dx} \right)^2 \right] \right\} - f = 0 \quad (14.4.1)$$

$$\frac{d^2}{dx^2} \left(EI \frac{d^2 w}{dx^2} \right) - \frac{d}{dx} \left\{ EA \frac{dw}{dx} \left[\frac{du}{dx} + \frac{1}{2} \left(\frac{dw}{dx} \right)^2 \right] \right\} - q = 0 \quad (14.4.2)$$

where u is the longitudinal displacement, w is the transverse deflection, E is the modulus of elasticity, A is the cross-sectional area, f is the axial distributed load, and q is the transverse loading. Under the assumption that the slope dw/dx is small compared with unity [i.e., $(dw/dx)(du/dx) \approx 0$, $(dw/dx)^2 \approx 0$], Eqs. (14.4.1) and (14.4.2) become uncoupled and reduce to the bar equation (3.2.1) and beam equation (14.2.39), respectively. However, when the slope dw/dx is not too small, we must solve the coupled set of nonlinear equations (14.4.1) and (14.4.2).

These weak forms of (14.4.1) and (14.4.2) over an element (x_a, x_b) are

$$0 = \int_{x_a}^{x_b} \left\{ EA \frac{dv_1}{dx} \left[\frac{du}{dx} + \frac{1}{2} \left(\frac{dw}{dx} \right)^2 \right] - v_1 f \right\} dx - Q_1^e v_1(x_a) - Q_4^e v_1(x_b) \quad (14.4.3a)$$

where v_1 is the weight function ($v_1 \sim \delta u$) and

$$Q_1^e = - \left\{ EA \left[\frac{du}{dx} + \frac{1}{2} \left(\frac{dw}{dx} \right)^2 \right] \right\} \Big|_{x_a}, \quad Q_4^e = \left\{ EA \left[\frac{du}{dx} + \frac{1}{2} \left(\frac{dw}{dx} \right)^2 \right] \right\} \Big|_{x_b} \quad (14.4.3b)$$

Similarly,

$$\begin{aligned} 0 = & \int_{x_a}^{x_b} \left\{ EI \frac{d^2 v_2}{dx^2} \frac{d^2 w}{dx^2} + EA \frac{dv_2}{dx} \frac{dw}{dx} \left[\frac{du}{dx} + \frac{1}{2} \left(\frac{dw}{dx} \right)^2 \right] - v_2 q \right\} dx \\ & - Q_2^e v_2(x_a) - Q_3^e \left(-\frac{dv_2}{dx} \right) \Big|_{x_a} - Q_5^e v_2(x_b) - Q_6^e \left(-\frac{dv_2}{dx} \right) \Big|_{x_b} \end{aligned} \quad (14.4.4a)$$

where v_2 is the weight function ($v_2 \sim \delta w$), and

$$\begin{aligned} Q_2^e &= \left\{ \frac{d}{dx} \left(EI \frac{d^2 w}{dx^2} \right) - EA \frac{dw}{dx} \left[\frac{du}{dx} + \frac{1}{2} \left(\frac{dw}{dx} \right)^2 \right] \right\} \Big|_{x_a} \\ Q_5^e &= - \left\{ \frac{d}{dx} \left(EI \frac{d^2 w}{dx^2} \right) - EA \frac{dw}{dx} \left[\frac{du}{dx} + \frac{1}{2} \left(\frac{dw}{dx} \right)^2 \right] \right\} \Big|_{x_b} \\ Q_3^e &= \left(EI \frac{d^2 w}{dx^2} \right) \Big|_{x_a}, \quad Q_6^e = - \left(EI \frac{d^2 w}{dx^2} \right) \Big|_{x_b} \end{aligned} \quad (14.4.4b)$$

The primary variables of the formulation (as in the frame element formulation of the Euler–Bernoulli beam theory) are

$$u, \quad w, \quad \theta \equiv -\frac{dw}{dx}$$

From the discussions presented in Chapters 3 and 5, it is clear that we must use a Lagrange interpolation of u and a Hermite interpolation of w :

$$u = \sum_{j=1}^n u_j \psi_j(x), \quad w = \sum_{j=1}^4 \Delta_j \phi_j(x) \quad (14.4.5)$$

where ψ_j are the Lagrange interpolation functions of degree $n - 1$ and ϕ_j are the Hermite cubic interpolation functions. For $n = 2$ (i.e., linear approximation of u), the elements used for u and w contain the same number of nodes, which is convenient in the computer implementation of the model (see Fig. 14.4.1).

Substituting the approximations (14.4.5) for u and w , and $v_1 = \psi_i$ and $v_2 = \phi_i$, into (14.4.3a) and (14.4.4a), we obtain the finite element model

$$\begin{bmatrix} \mathbf{K}^{11} & \mathbf{K}^{12} \\ \mathbf{K}^{21} & \mathbf{K}^{22} \end{bmatrix} \begin{Bmatrix} \mathbf{u} \\ \Delta \end{Bmatrix} = \begin{Bmatrix} \mathbf{F}^1 \\ \mathbf{F}^2 \end{Bmatrix} \quad (14.4.6a)$$

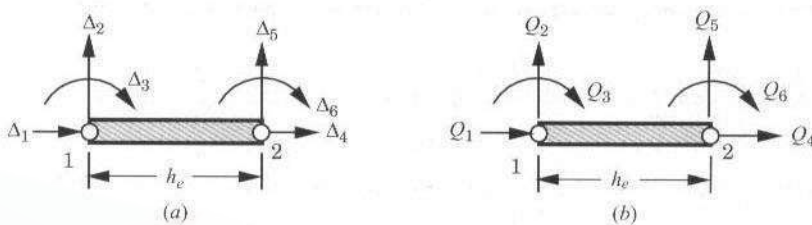


Figure 14.4.1 Nonlinear Euler–Bernoulli beam element based on linear interpolation of the axial displacement u and Hermite cubic interpolation of the transverse deflection w .

where

$$\begin{aligned}
 K_{ij}^{11} &= \int_{x_a}^{x_b} EA \frac{d\psi_i}{dx} \frac{d\psi_j}{dx} dx, \quad K_{ij}^{12} = \int_{x_a}^{x_b} \frac{1}{2} EA \frac{dw}{dx} \frac{d\psi_i}{dx} \frac{d\phi_j}{dx} dx \\
 K_{ij}^{22} &= \int_{x_a}^{x_b} EI \frac{d^2\phi_i}{dx^2} \frac{d^2\phi_j}{dx^2} dx + \int_{x_a}^{x_b} \frac{1}{2} EA \left(\frac{dw}{dx} \right)^2 \frac{d\phi_i}{dx} \frac{d\phi_j}{dx} dx \\
 K_{ji}^{21} &= \int_{x_a}^{x_b} EA \frac{dw}{dx} \frac{d\phi_j}{dx} \frac{d\psi_i}{dx} dx, \quad F_i^1 = \int_{x_a}^{x_b} \psi_i f dx + Q_{3i-2} \\
 F_i^2 &= \int_{x_a}^{x_b} \phi_i q dx + Q_{i+1} \quad \begin{cases} I = 1 & \text{if } i = 1 \text{ or } 2 \\ I = 2 & \text{if } i = 3 \text{ or } 4 \end{cases}
 \end{aligned} \tag{14.4.6b}$$

This completes the finite element model of the nonlinear bending of beams.

14.4.3 The Navier–Stokes Equations in Two Dimensions

When the inertial effects are larger than the viscous effects, Eqs. (10.2.9) and (10.2.10) must be modified to include the convective terms, i.e., the following Navier–Stokes equations must be solved:

$$\begin{aligned} \rho \left(v_x \frac{\partial v_x}{\partial x} + v_y \frac{\partial v_x}{\partial y} \right) - \mu \left[2 \frac{\partial^2 v_x}{\partial x^2} + \frac{\partial}{\partial y} \left(\frac{\partial v_x}{\partial y} + \frac{\partial v_y}{\partial x} \right) \right] + \frac{\partial P}{\partial x} &= f_x \\ \rho \left(v_x \frac{\partial v_y}{\partial x} + v_y \frac{\partial v_y}{\partial y} \right) - \mu \left[\frac{\partial}{\partial x} \left(\frac{\partial v_x}{\partial y} + \frac{\partial v_y}{\partial x} \right) + 2 \frac{\partial^2 v_y}{\partial y^2} \right] + \frac{\partial P}{\partial y} &= f_y \\ \frac{\partial v_x}{\partial x} + \frac{\partial v_y}{\partial y} &= 0 \end{aligned} \quad (14.4.7)$$

where ρ is the density of the fluid and all the other symbols have the same meaning as in Chapter 10.

Here, we present the penalty finite element model of the Navier–Stokes equations (14.4.7) over an element, i.e., replace the pressure P by

$$P = -\gamma \left(\frac{\partial v_x}{\partial x} + \frac{\partial v_y}{\partial y} \right) \quad (14.4.8)$$

and omit the continuity equation. The weak form is given by (see Section 10.3 for details)

$$\begin{aligned} \int_{\Omega_e} \left\{ w_1 \rho \left(v_x \frac{\partial v_x}{\partial x} + v_y \frac{\partial v_x}{\partial y} \right) + [\dots] \right\} d\mathbf{x} - \int_{\Omega_e} w_1 f_x d\mathbf{x} - \oint_{\Gamma_e} w_1 t_x ds &= 0 \\ \int_{\Omega_e} \left\{ w_2 \rho \left(v_x \frac{\partial v_y}{\partial x} + v_y \frac{\partial v_y}{\partial y} \right) + [\dots] \right\} d\mathbf{x} - \int_{\Omega_e} w_2 f_y d\mathbf{x} - \oint_{\Gamma_e} w_2 t_y ds &= 0 \end{aligned} \quad (14.4.9)$$

where [...] denotes the expressions (omitting the time-derivative terms) in the square brackets of Eqs. (10.4.21) and (10.4.22) (also, note that $w_1 = \delta v_x$ and $w_2 = \delta v_y$). The finite element model of these equations is given by

$$(\mathbf{K}_c + \mathbf{K}_v + \mathbf{K}_p)\Delta = \mathbf{F} \quad (14.4.10a)$$

where \mathbf{K}_v , \mathbf{K}_p , and \mathbf{F} are defined in Eq. (10.4.28) [also, see Eq. (10.3.10b)] and \mathbf{K}_c is the contribution of the nonlinear (convective) terms to the coefficient matrix

$$\mathbf{K}_c = \int_{\Omega_e} \rho (\Psi \bar{\mathbf{v}}^T \mathbf{D}_1)^T \Psi d\mathbf{x}, \quad \bar{\mathbf{v}} = \Psi \bar{\Delta} \quad (14.4.10b)$$

and $\bar{\Delta}$ is the solution vector known from the previous iteration.

14.4.4 Solution Methods for Nonlinear Algebraic Equations

Note that the element coefficient matrices in Eqs. (14.4.6a) and (14.4.10a) are nonlinear and unsymmetric. In the case of beams, the element stiffness matrix is a function of the unknown transverse deflection, whereas in the case of fluid flow, the coefficient matrix is a function of unknown velocity components. The assembled nonlinear equations must be solved, after imposing boundary conditions, by a suitable method. Here, we describe two iterative methods in which we seek an approximate solution to the nonlinear algebraic equations by linearization. The iterative methods are outlined using a nonlinear matrix equation of the form

$$\mathbf{K}(\Delta)\Delta = \mathbf{F} \quad (14.4.11)$$

where Δ is the vector of unknown nodal values; the dependence of \mathbf{K} on Δ is clearly indicated.

The *direct iteration method*, also known as the *Picard method*, is based on the scheme

$$\mathbf{K}(\Delta^r)\Delta^{r+1} = \mathbf{F} \quad (14.4.12)$$

where Δ^r denotes the solution at the r th iteration. Thus, in the direct iteration method, the coefficients K_{ij} (and hence $K_{ij}^{\alpha\beta}$) are evaluated using the solution Δ^r from the previous iteration, and the solution at the $(r+1)$ th iteration is obtained by solving (14.4.12):

$$\Delta^{r+1} = (\mathbf{K}(\Delta^r))^{-1} \mathbf{F} \quad (14.4.13)$$

At the beginning of the iteration (i.e., $r=0$), we assume a solution Δ^0 based on our qualitative understanding of the solution behavior. For example, $\Delta^0 = \mathbf{0}$ for large-deflection bending would reduce the nonlinear stiffness matrix to a linear one, and (14.4.13) would

yield the linear solution of the problem at the end of the first iteration, Δ^1 . The iteration is continued [i.e., (14.4.13) is solved in each iteration] until the difference between Δ^r and Δ^{r+1} reduces to a preselected error tolerance. The *error criterion* is of the form (other criteria may also be used)

$$\frac{|\Delta^{r+1} - \Delta^r|}{|\Delta^{r+1}|} < \epsilon \quad (\text{say}, 10^{-3}) \quad (14.4.14)$$

where $|\cdot|$ denotes the Euclidean norm (root-mean-square value) of N nodal values, where N is the total number of primary unknowns (i.e., generalized displacements) in the finite element mesh.

The other iterative method is the *Newton–Raphson method*, which is based on the Taylor series expansion of the algebraic equations (14.4.11) about the known solution Δ^r . To describe the method, we rewrite (14.4.11) in the form

$$\mathbf{R} \equiv \mathbf{K}\Delta - \mathbf{F} = \mathbf{0} \quad (14.4.15)$$

where \mathbf{R} denotes the residual due to the linearization of \mathbf{K} . Expanding \mathbf{R} about Δ^r , we obtain

$$\mathbf{0} = \mathbf{R} = \mathbf{R}^r + \left(\frac{\partial \mathbf{R}}{\partial \Delta} \right)_r (\Delta^{r+1} - \Delta^r) + \frac{1}{2!} \left(\frac{\partial^2 \mathbf{R}}{\partial \Delta^2} \right)_r (\Delta^{r+1} - \Delta^r)^2 + \dots \quad (14.4.16a)$$

or

$$\mathbf{0} \approx \mathbf{R}^r + \mathbf{K}_T^r \delta\Delta + O(\delta\Delta)^2 \quad (14.4.16b)$$

where $\delta\Delta$ denotes the increment in Δ and \mathbf{K}_T is the *tangent (stiffness) matrix*

$$\begin{aligned} \mathbf{K}_T^r &\equiv \frac{\partial \mathbf{R}}{\partial \Delta} \quad \text{evaluated at } \Delta = \Delta^r \\ \delta\Delta &= \Delta^{r+1} - \Delta^r \quad (\text{incremental solution}) \end{aligned} \quad (14.4.17)$$

For structural problems with variational principles, it can be shown that \mathbf{K}_T is symmetric even if \mathbf{K} is not. From (14.4.16b), we have

$$\delta\Delta = -(\mathbf{K}_T)^{-1} \mathbf{R}^r = (\mathbf{K}_T(\Delta^r))^{-1} (\mathbf{F} - \mathbf{K}(\Delta^r)\Delta^r) \quad (14.4.18a)$$

and the total solution at the $(r + 1)$ th iteration is given by

$$\Delta^{r+1} = \Delta^r + \delta\Delta \quad (14.4.18b)$$

The iteration in (14.4.18a) is continued until the convergence criteria in (14.4.14) is satisfied or the residual \mathbf{R} [measured in the same way as the solution error in (14.4.14)] is less than a certain preselected value. For additional details on iterative methods, consult the references at the end of the chapter [e.g., Reddy (2004) and Reddy and Gartling (2001)].

14.4.5 Numerical Examples

In this section we present some representative numerical examples of nonlinear bending of beams and fluid flow. A more complete discussion of the nonlinear formulations presented in Sections 14.4.2 and 14.4.3 as well as examples presented here can be found in Reddy (2004).

Example 14.4.1

Consider a straight beam made of steel ($E = 30 \times 10^6$ psi), of length $L = 100$ in., width B , and height H , and subjected to uniformly distributed load of intensity q_0 lb/in. The beam is assumed to be fixed at both ends. Noting the symmetry of the solution about $x = L/2$, one-half of the domain is used as the computational domain. The geometric boundary conditions for the computational domain of the problem are

$$u(0) = w(0) = \frac{dw}{dx} \Big|_{x=0} = u\left(\frac{L}{2}\right) = \frac{dw}{dx} \Big|_{x=\frac{L}{2}} = 0 \quad (14.4.19)$$

The load increments of $\Delta q_0 = 1.0$ lb/in., a tolerance of $\epsilon = 10^{-3}$, and maximum allowable iterations of 25 (per load step) are used in the analysis. The initial solution vector is chosen to be the zero vector. The exact solution to the linear problem is

$$u(x) = 0, \quad w(x) = \frac{q_0 L^4}{24D} \left(\frac{x}{L} - 2\frac{x^3}{L^3} + \frac{x^4}{L^4} \right) \quad (14.4.20)$$

and the maximum deflections occurs at $L/2$. For $q_0 = 1$ lb/in., $L = 100$ in., $B \times H = 1$ in. \times 1 in., and $E = 30 \times 10^6$ psi, they are given by ($D = EH^3/12$, $H = 1$)

$$w\left(\frac{L}{2}\right) = \frac{q_0 L^4}{384D} = 0.1042 \text{ in.} \quad (14.4.21)$$

Table 14.4.1 contains the results of the nonlinear analysis of the clamped-clamped beam; the results were obtained with both the direct and Newton-Raphson iteration methods. The two-point Gauss rule for the linear terms and one-point Gauss rule for nonlinear terms is used to eliminate the so-called membrane locking (Reddy, 2004). Figure 14.4.2 shows the load-deflection curve for the beam.

Table 14.4.1 Finite element results for the deflections of a clamped-clamped beam under uniform load.

Load q_0	Direct iteration		Newton-Raphson iteration	
	4 elements	8 elements	4 elements	8 elements
1.0	0.1033 (3)*	0.1034 (3)	0.1034 (3)	0.1034 (3)
2.0	0.2022 (4)	0.2023 (4)	0.2022 (3)	0.2023 (3)
3.0	0.2938 (4)	0.2939 (4)	0.2939 (3)	0.2939 (3)
4.0	0.3773 (5)	0.3774 (5)	0.3773 (3)	0.3774 (3)
5.0	0.4529 (5)	0.4531 (5)	0.4528 (3)	0.4530 (3)
6.0	0.5213 (6)	0.5215 (6)	0.5214 (3)	0.5216 (3)
7.0	0.5840 (7)	0.5842 (7)	0.5839 (3)	0.5841 (3)
8.0	0.6412 (8)	0.6412 (8)	0.6413 (3)	0.6414 (3)
9.0	0.6945 (9)	0.6944 (9)	0.6943 (3)	0.6943 (3)
10.0	0.7433 (10)	0.7431 (10)	0.7435 (3)	0.7433 (3)

* Number of iterations taken to converge.

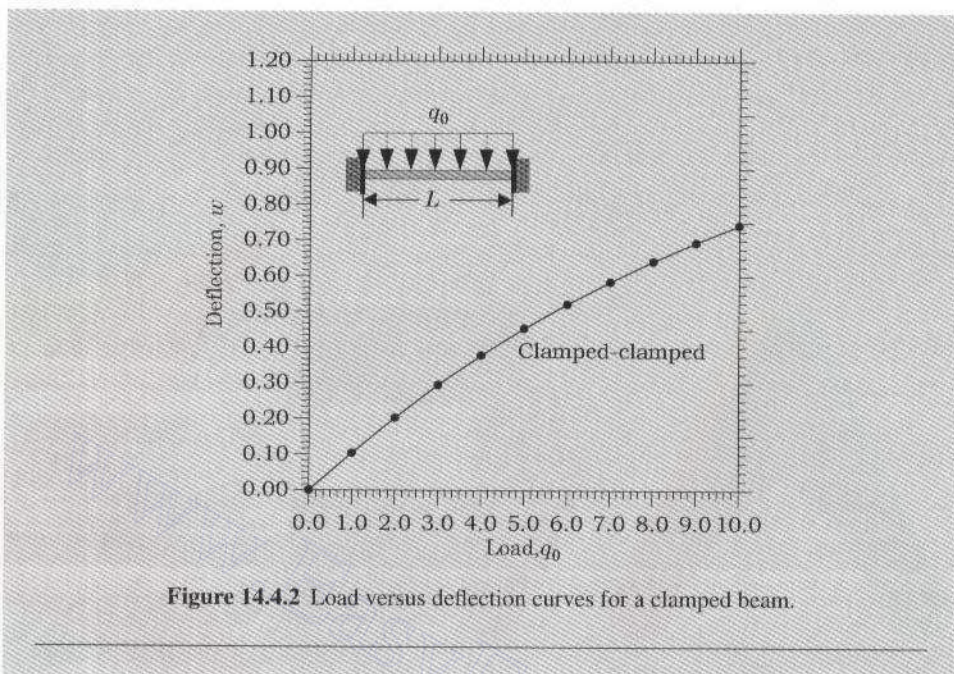


Figure 14.4.2 Load versus deflection curves for a clamped beam.

Example 14.4.2

Here, we consider the lid-driven cavity problem of Example 10.6.3 for nonlinear analysis (i.e., solve Navier–Stokes equations). For the problem at hand, the Reynolds number, $Re = \rho v_0 d / \mu$, can be varied by varying the density while keeping the viscosity constant. Thus, we take ($v_0 = 1$ and $a = 1$) $\mu = 1$ so that $Re = \rho$. The problem is solved using uniform 8×8 mesh of linear elements as well as 4×4 mesh of nine-node quadratic elements, and the results are presented in Table 14.4.2 for $Re = 100$, 500 , and 700 ($\gamma = 10^8$ and $\epsilon = 10^{-2}$). The converged nonlinear solution of the preceding Reynolds number, is used as the initial guess in the first iteration of the next Reynolds number. In general, for very high Reynolds numbers, underrelaxation must be used to accelerate the convergence by using the weighted average of velocities from two

Table 14.4.2 Velocity $v_x(0.5, y)$ obtained with linear and quadratic elements and for various values of the Reynolds number.

y	8 × 8L			4 × 4Q9		
	$Re \rightarrow$	100(5)	500(8)	700(9)	100(5)	500(8)
0.125	-0.0498	-0.0242	-0.0140	-0.0554	-0.0141	-0.0106
0.250	-0.0870	-0.0503	-0.0345	-0.0968	-0.0540	-0.0089
0.375	-0.1164	-0.0733	-0.0564	-0.1313	-0.1143	-0.0672
0.500	-0.1231	-0.0700	-0.0586	-0.1414	-0.1252	-0.1181
0.625	-0.0635	0.0027	0.0039	-0.0814	-0.0455	-0.0831
0.750	0.0649	0.0389	0.0354	0.0486	0.1045	0.0808
0.875	0.3750	0.1761	0.1241	0.3629	0.2113	0.1628

* Number in parentheses denotes the number of iterations taken for convergence.

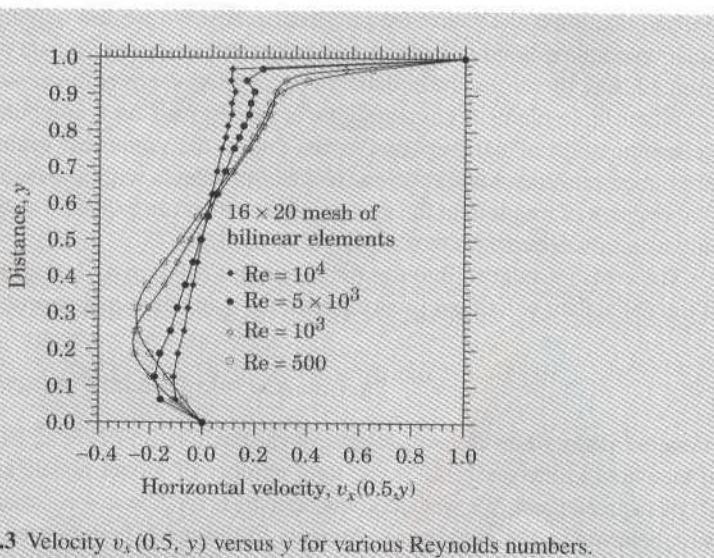


Figure 14.4.3 Velocity $v_x(0.5, y)$ versus y for various Reynolds numbers.

consecutive iterations

$$\bar{\mathbf{v}}^r = \beta \mathbf{v}^{(r)} + (1 - \beta) \mathbf{v}^{(r-1)} \quad (14.4.22)$$

to compute the coefficient matrix. Here β is known as the acceleration parameter. Figure 14.4.3 contains plots of the horizontal velocity obtained with 16×20 mesh for $Re = 500, 10^3, 5 \times 10^3, 10^4$ (the increment of Re is taken to be 500 and $\beta = 0.5$).

14.5 ERRORS IN FINITE ELEMENT ANALYSIS

14.5.1 Types of Errors

The errors introduced into the finite element solution of a given differential equation can be attributed to three basic sources:

1. *Domain approximation error*, which is due to the approximation of the domain.
2. *Quadrature and finite arithmetic errors*, which are due to the numerical evaluation of integrals and the numerical computation on a computer.
3. *Approximation error*, which is due to the approximation of the solution:

$$u \approx u_h \equiv \sum_{I=1}^N U_I \Phi_I \quad (14.5.1)$$

where U_I denotes the value of u at global node I and Φ_I denotes the global interpolation function associated with global node I (see Fig. 3.2.9).

In the one-dimensional problems, the domains considered have been straight lines. Therefore, no approximation of the domain has been necessary. In two-dimensional problems involving nonrectangular domains, domain (or boundary) approximation errors are introduced into the finite element solutions. In general, these can be interpreted as errors in

the specification of the data of the problem because we are now solving the given differential equation on a modified domain. As we refine the mesh, the domain is more accurately represented, and, therefore, the boundary approximation errors are expected to approach zero.

When finite element computations are performed on a computer, round-off errors in the computation of numbers and errors due to the numerical evaluation of integrals are introduced into the solution. In most linear problems with a reasonably small number of total degrees of freedom in the system, these errors are expected to be small (or zero when only a certain decimal point accuracy is desired).

The error introduced into the finite element solution u_h^e because of the approximation of the dependent variable u in an element Ω_e is inherent to any problem

$$u \approx u_h = \sum_{e=1}^N \sum_{i=1}^n u_i^e \psi_i^e = \sum_{I=1}^M U_I \Phi_I \quad (14.5.2)$$

where u_h is the finite element solution over the domain ($u_h = u_h^e$ in Ω_e), N is the number of elements in the mesh, M is the total number of global nodes, and n is the number of nodes in an element. We wish to know how the error $E = u - u_h$, measured in a meaningful way, behaves as the number of elements in the mesh is increased. It can be shown that the approximation error is zero for the single second-order and fourth-order equations with elementwise-constant coefficients.

14.5.2 Measures of Errors

There are several ways in which we can measure the “difference” (or distance) between any two functions u and u_h . The *pointwise error* is the difference of u and u_h at each point of the domain. We can also define the difference of u and u_h to be the maximum of all absolute values of the differences of u and u_h in the domain $\Omega = (a, b)$:

$$\|u - u_h\|_\infty \equiv \max_{a \leq x \leq b} |u(x) - u_h(x)| \quad (14.5.3)$$

This measure of difference is called the *supmetric*. Note that the supmetric is a real number, whereas the pointwise error is a function and does not qualify as a distance or *norm* in a strict mathematical sense. The norm of a function is a nonnegative real number.

More generally used measures (or norms) of the difference of two functions are the *energy norm* and the *L_2 norm* (pronounced “L-two norm”). For any square-integrable functions u and u_h defined on the domain $\Omega = (a, b)$, the two norms are defined by

$$\text{energy norm} \quad \|u - u_h\|_m = \left(\int_a^b \sum_{i=0}^m \left| \frac{d^i u}{dx^i} - \frac{d^i u_h}{dx^i} \right|^2 dx \right)^{1/2} \quad (14.5.4)$$

$$L_2 \text{ norm} \quad \|u - u_h\|_0 = \left(\int_a^b |u - u_h|^2 dx \right)^{1/2} \quad (14.5.5)$$

where $2m$ is the order of the differential equation being solved. The term “energy norm” is used to indicate that this norm contains the same-order derivatives as the quadratic functional (which, for most solid mechanics problems, denotes the energy) associated with the equation. Various measures of the distance between two functions are illustrated in Fig. 14.5.1. These definitions can easily be modified for two-dimensional domains.

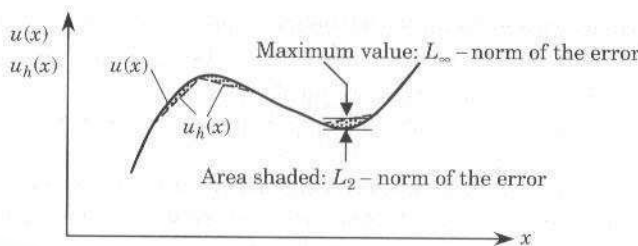


Figure 14.5.1 Different measures of the error $E = u - u_h$ between the exact solution u and the finite element solution u_h . The maximum norm and the L_2 norms are illustrated.

14.5.3 Convergence and Accuracy of Solutions

The finite element solution u_h in (14.5.1) is said to *converge in the energy norm* to the true solution u if

$$\|u - u_h\|_m \leq ch^p \quad \text{for } p > 0 \quad (14.5.6)$$

where c is a constant independent of u and u_h , and h is the characteristic length of an element. The constant p is called the *rate of convergence*. Note that the convergence depends on h as well as on p ; p depends on the order of the derivative of u in the weak form and the degree of the polynomials used to approximate u [see (14.5.15) below]. Therefore, the error in the approximation can be reduced either by reducing the size of the elements or increasing the degree of approximation. Convergence of the finite element solutions with mesh refinements (i.e., more of the same kind of elements are used) is termed *h-convergence*. Convergence with increasing degree of polynomials is called *p-convergence*.

Returning to the question of estimating the approximation error, we consider a $2m$ th-order differential equation in one dimension ($m = 1$, second-order equations; $m = 2$, fourth-order equations):

$$\sum_{i=1}^m (-1)^i \frac{d^i}{dx^i} \left(a_i \frac{d^i u}{dx^i} \right) = f \quad \text{for } 0 < x < L \quad (14.5.7)$$

where the coefficients $a_i(x)$ are assumed to be positive. Suppose that the essential boundary conditions of the problem are

$$u(0) = u(L) = 0 \quad (m = 1, 2) \quad (14.5.8)$$

$$\left(\frac{du}{dx} \right) \Big|_{x=0} = \left(\frac{du}{dx} \right) \Big|_{x=L} = 0 \quad (m = 2) \quad (14.5.9)$$

The variational formulation of (14.5.7) and (14.5.9) is given by

$$0 = \int_0^L \left(\sum_{i=1}^m a_i \frac{d^i v}{dx^i} \frac{d^i u}{dx^i} - vf \right) dx \quad (14.5.10)$$

The quadratic functional corresponding to the variational form is

$$I(u) = \int_0^L \frac{1}{2} \left[\sum_{i=1}^m a_i \left(\frac{d^i u}{dx^i} \right)^2 \right] dx - \int_0^L uf dx \quad (14.5.11)$$

Now consider a finite element discretization of the domain by N elements of equal length h . If u_h denotes the finite element solution in (14.5.1), we have, from (14.5.11),

$$I(u_h) = \int_0^L \frac{1}{2} \left[\sum_{i=1}^m a_i \left(\frac{d^i u_h}{dx^i} \right)^2 \right] dx - \int_0^L u_h f dx \quad (14.5.12)$$

In the following paragraphs, we show that the energy I associated with the finite element solution approaches the true energy from above, and we then give an error estimate. We confine our discussion, for the sake of simplicity, to the second-order equation ($m = 1$).

From (14.5.11) and (14.5.12), and

$$f = -\frac{d}{dx} \left(a_1 \frac{du}{dx} \right)$$

we have

$$\begin{aligned} I(u_h) - I(u) &= \int_0^L \frac{1}{2} \left[a_1 \left(\frac{du_h}{dx} \right)^2 - a_1 \left(\frac{du}{dx} \right)^2 + 2f(u - u_h) \right] dx \\ &= \int_0^L \left[\frac{a_1}{2} \left(\frac{du_h}{dx} \right)^2 - \frac{a_1}{2} \left(\frac{du}{dx} \right)^2 - \frac{d}{dx} \left(a_1 \frac{du}{dx} \right) (u - u_h) \right] dx \\ &= \int_0^L \left\{ \frac{a_1}{2} \left[\left(\frac{du_h}{dx} \right)^2 - \left(\frac{du}{dx} \right)^2 \right] + a_1 \frac{du}{dx} \frac{d}{dx} (u - u_h) \right\} dx \\ &= \int_0^L \frac{a_1}{2} \left[\left(\frac{du_h}{dx} \right)^2 + \left(\frac{du}{dx} \right)^2 - 2 \frac{du}{dx} \frac{du_h}{dx} \right] dx \\ &= \int_0^L \frac{a_1}{2} \left(\frac{du_h}{dx} - \frac{du}{dx} \right)^2 dx \geq 0 \end{aligned} \quad (14.5.13)$$

Thus,

$$I(u_h) \geq I(u) \quad (14.5.14)$$

The equality holds only for $u = u_h$. Equation (14.5.14) implies that the convergence of the energy of the finite element solution to the true energy is from above. Since the relation in (14.5.14) holds for any u_h , the inequality also indicates that the true solution u minimizes the energy. A similar relation can be established for the fourth-order equation ($m = 2$).

Now suppose that the finite element interpolation functions Φ_I ($I = 1, 2, \dots, M$) are complete polynomials of degree k . Then the error in the energy norm can be shown to satisfy the inequality [see Reddy (1991), p. 401]

$$\|e\|_m \equiv \|u - u_h\|_m \leq ch^p, \quad p = k + 1 - m > 0 \quad (14.5.15)$$

where c is a constant. This estimate implies that the error goes to zero as the p th power of h as h is decreased (or the number of elements is increased). In other words, the logarithm of the error in the energy norm versus the logarithm of h is a straight line whose slope is $k + 1 - m$. The greater the degree of the interpolation functions, the more rapid the rate of convergence. Note also that the error in the energy goes to zero at the rate of $k + 1 - m$;

the error in the L_2 norm will decrease even more rapidly, namely, at the rate of $k + 1$, i.e., derivatives converge more slowly than the solution itself.

Error estimates of the type in (14.5.15) are very useful because they give an idea of the accuracy of the approximate solution, whether or not we know the true solution. While the estimate gives an idea of how rapidly the finite element solution converges to the true solution, it does not tell us when to stop refining the mesh. This decision rests with the analysts, because only they know what a reasonable tolerance is for the problems they are solving.

As an example of estimating the error in the approximation, i.e., (14.5.15), consider the linear (two-node) element for a second-order equation ($m = 1$). We have for an element

$$u_h = u_1(1 - s) + u_2s \quad (14.5.16)$$

where $s = \bar{x}/h$ and \bar{x} is the local coordinate. Since u_2 can be viewed as a function of u_1 via (14.5.16), we can expand u_2 in a Taylor series around node 1 to obtain

$$u_2 = u_1 + u'_1 + \frac{1}{2}u''_1 + \dots \quad (14.5.17)$$

where $u' \equiv du/ds$. Substituting this into (14.5.16), we obtain

$$u_h = u_1 + u'_1s + \frac{1}{2}u''_1s^2 + \dots \quad (14.5.18)$$

Expanding the true solution in a Taylor series about node 1, we obtain

$$u = u_1 + u'_1s + \frac{1}{2}u''_1s^2 + \dots \quad (14.5.19)$$

Therefore, we have, from (14.5.18) and (14.5.19),

$$|u_h - u| \leq \frac{1}{2}(s - s^2) \max_{0 \leq s \leq 1} \left| \frac{d^2u_1}{ds^2} \right| = \frac{1}{2}(s - s^2)h^2 \max_{0 \leq \bar{x} \leq h} \left| \frac{d^2u}{d\bar{x}^2} \right| \quad (14.5.20)$$

$$\left| \frac{d}{\bar{x}}(u_h - u) \right| \leq \frac{1}{2}h \max_{0 \leq \bar{x} \leq h} \left| \frac{d^2u_1}{d\bar{x}^2} \right| \quad (14.5.21)$$

These lead to

$$\|u - u_h\|_0 \leq c_1 h^2, \quad \|u - u_h\|_1 \leq c_2 h \quad (14.5.22)$$

where the constants c_1 and c_2 depend only on the length L of the domain. The reader may wish to perform a similar error analysis for the fourth-order equation (14.2.39).

Example 14.5.1

Here we consider a computational example to verify the error estimates in (14.5.22). Consider the differential equation

$$-\frac{d^2u}{dx^2} = 2 \quad \text{for } 0 < x < 1 \quad (14.5.23)$$

with

$$u(0) = u(1) = 0$$

The exact solution is

$$u(x) = x(1-x) \quad (14.5.24)$$

while the finite element solutions are, for $N=2$,

$$u_h = \begin{cases} h^2(x/h) & \text{for } 0 \leq x \leq h \\ h^2(2 - x/h) & \text{for } h \leq x \leq 2h \end{cases}$$

for $N=3$,

$$u_h = \begin{cases} 2h^2(x/h) & \text{for } 0 \leq x \leq h \\ 2h^2(2 - x/h) + 2h^2(x/h - 1) & \text{for } h \leq x \leq 2h \\ 2h^2(3 - x/h) & \text{for } 2h \leq x \leq 3h \end{cases} \quad (14.5.25)$$

and, for $N=4$,

$$u_h = \begin{cases} 3h^2(x/h) & \text{for } 0 \leq x \leq h \\ 3h^2(2 - x/h) + 4h^2(x/h - 1) & \text{for } h \leq x \leq 2h \\ 4h^2(3 - x/h) + 3h^2(x/h - 2) & \text{for } 2h \leq x \leq 3h \\ 3h^2(4 - x/h) & \text{for } 3h \leq x \leq 4h \end{cases}$$

For the two-element case ($h=0.5$), the errors are given by

$$\begin{aligned} \|u - u_h\|_0^2 &= \int_0^h (x - x^2 - hx)^2 dx + \int_h^{2h} (x - x^2 - 2h^2 + xh)^2 dx \\ &= 0.002083 \end{aligned} \quad (14.5.26)$$

$$\begin{aligned} \left\| \frac{du}{dx} - \frac{du_h}{dx} \right\|_0^2 &= \int_0^h (1 - 2x - h)^2 dx + \int_h^{2h} (1 - 2x + h)^2 dx \\ &= 0.08333 \end{aligned}$$

Similar calculations can be performed for $N=3$ and $N=4$. Table 14.5.1 gives the errors for $N=2, 3$, and 4 .

Plots of $\log \|e\|_0$ and $\log \|e\|_1$ versus $\log h$ show that (see Fig. 14.5.2)

$$\log \|e\|_0 = 2 \log h + \log c_1, \quad \log \|e\|_1 = \log h + \log c_2 \quad (14.5.27)$$

In other words, the rate of convergence of the finite element solution is 2 in the L_2 norm and 1 in the energy norm, verifying the estimates in (14.5.22).

Table 14.5.1 The L_2 error and error in the energy norm of the solution to (14.5.23) (Example 14.5.1).

h	$\log_{10} h$	$\ e\ _0$	$\log_{10} \ e\ _0$	$\ e\ _1$	$\log_{10} \ e\ _1$
$\frac{1}{2}$	-0.301	0.04564	-1.341	0.2887	-0.5396
$\frac{1}{3}$	-0.477	0.02028	-1.693	0.1925	-0.7157
$\frac{1}{4}$	-0.601	0.01141	-1.943	0.1443	-0.8406

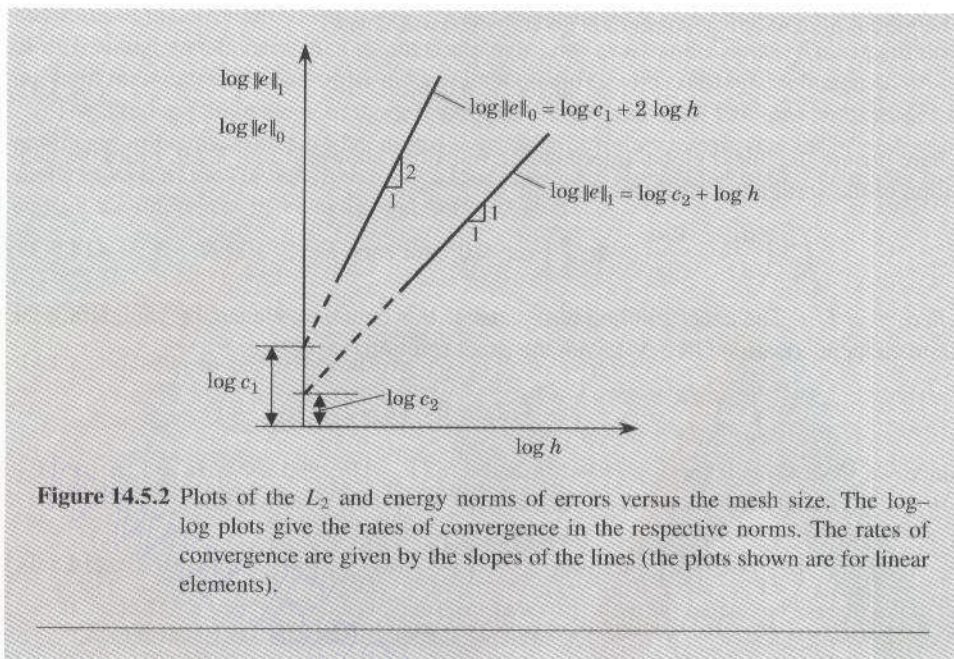


Figure 14.5.2 Plots of the L_2 and energy norms of errors versus the mesh size. The log-log plots give the rates of convergence in the respective norms. The rates of convergence are given by the slopes of the lines (the plots shown are for linear elements).

Much of the discussion presented in this section can be carried over to curved elements and two-dimensional elements. When the former, i.e., elements with nonstraight sides, are involved, the error estimate also depends on the Jacobian of the transformation. Because of the introductory nature of the present study, these topics are not discussed here. Interested readers can consult Wait and Mitchell (1985), Oden and Reddy (1982), Strang and Fix (1973), and Reddy (1991).

As noted earlier, in the case of both second- and fourth-order equations in a single unknown and with constant coefficients a and b , the finite element solutions of the equations

$$-\frac{d}{dx} \left(a \frac{du}{dx} \right) = f(x) \quad (14.5.28)$$

$$-\frac{d^2}{dx^2} \left(b \frac{d^2u}{dx^2} \right) = f(x) \quad (14.5.29)$$

coincide with the exact solutions at the nodes. The proof is presented below for the second-order equation.

Consider the equation

$$-a \frac{d^2u}{dx^2} = f \quad \text{for } 0 < x < L \quad (14.5.30)$$

with

$$u(0) = 0, \quad u(L) = 0 \quad (14.5.31)$$

The global finite element solution is given by ($U_1 = U_N = 0$)

$$u_h = \sum_{I=2}^{N-1} U_I \Phi_I \quad (14.5.32)$$

where Φ_I are the linear global interpolation functions shown in Fig. 3.2.9. From the definition of the variational problem, we have

$$\int_0^L \left(\frac{du}{dx} - \frac{du_h}{dx} - \Phi_I \hat{f} \right) dx = 0 \quad \text{for each } I = 2, \dots, N-1 \quad (14.5.33)$$

where $\hat{f} = f/a$. The exact solution also satisfies this equation. Hence, by subtracting the finite element equation (14.5.33) from the exact solution, we obtain

$$\int_0^L \left(\frac{du}{dx} - \frac{du_h}{dx} \right) \frac{d\Phi_I}{dx} dx = 0 \quad (I = 2, \dots, N-1)$$

Since we have $\Phi_I = 0$ for $x \leq (I-1)h$ and $x \geq Ih$, and $d\Phi_I/dx = 1/h$ for $(I-1)h \leq x \leq Ih$ and $d\Phi_I/dx = -1/h$ for $Ih \leq x \leq (I+1)h$, it follows that

$$\int_{(I-1)h}^{Ih} \left(\frac{du}{dx} - \frac{du_h}{dx} \right) \frac{1}{h} dx + \int_{Ih}^{(I+1)h} \left(\frac{du}{dx} - \frac{du_h}{dx} \right) \left(-\frac{1}{h} \right) dx = 0 \quad (14.5.34)$$

for $I = 2, 3, \dots, N-1$. Denoting $\epsilon(x) = u(x) - u_h(x)$, we have

$$\frac{1}{h} (\epsilon_I - \epsilon_{I-1}) + \left(-\frac{1}{h} \right) (\epsilon_{I+1} - \epsilon_I) = 0$$

or

$$\frac{1}{h} (-\epsilon_{I-1} + 2\epsilon_I - \epsilon_{I+1}) = 0 \quad (I = 2, 3, \dots, N-1) \quad (14.5.35)$$

where $\epsilon_I = \epsilon(Ih)$ (i.e., the value of ϵ at $x = Ih$). Since $\epsilon_0 = \epsilon_N = 0$ (because both u and u_h satisfy the essential boundary conditions), it follows from the above homogeneous equations that the solution is trivial: $\epsilon_1 = \epsilon_2 = \dots = \epsilon_{N-1} = 0$. This implies that the finite element solution coincides with the exact solution at the nodes.

14.6 SUMMARY

Three advanced topics have been discussed in this chapter: (1) weighted residual and mixed finite element formulations of differential equations; (2) finite element models of three-dimensional problems; and (3) finite element models of nonlinear equations. The weighted residual models discussed include the Petrov–Galerkin model, Bubnov–Galerkin model, collocation model, subdomain model, and least-squares model. First- and second-order differential equations have been considered. Three-dimensional finite element models of heat transfer, flows of viscous incompressible fluids, and elasticity have been also presented. A library of interpolation functions of some commonly used three-dimensional finite elements have been presented. Nonlinear finite element models of the Euler–Bernoulli beam theory and the Navier–Stokes equations governing two-dimensional viscous incompressible flows have been developed. Two iterative schemes, Picard and Newton–Raphson, for solving nonlinear algebraic equations have been discussed. Finally, various types of errors in the finite element approximation of differential equations have been discussed and different

measures of the error have been defined. It has been shown that the finite element solutions of differential equations with constant coefficients are exact at the nodes. This result does not hold for coupled second-order differential equations with constant coefficients.

The alternate finite element models presented in Section 14.2 can also be extended to nonlinear problems. For example, mixed least-squares finite element models of plates and shells as well as the Navier–Stokes equations have been already reported. The reader may consult the references listed at the end of the chapter.

PROBLEMS

- 14.1** Consider the second-order equation

$$-\frac{d}{dx} \left(a \frac{du}{dx} \right) = f \quad (1)$$

and rewrite it as a pair of first-order equations,

$$-\frac{du}{dx} + \frac{P}{a} = 0, \quad -\frac{dP}{dx} - f = 0 \quad (2)$$

Construct the weighted residual finite element model of the equations, and specialize it to the Galerkin model. Assume interpolation in the form

$$u = \sum_{j=1}^m u_j \psi_j(x), \quad P = \sum_{j=1}^n P_j \phi_j(x) \quad (3)$$

and use the equations in (2) in the right order that yields symmetric element equations:

$$\begin{bmatrix} [K^{11}] & [K^{12}] \\ [K^{12}]^T & [K^{22}] \end{bmatrix} \begin{Bmatrix} \{u\} \\ \{P\} \end{Bmatrix} = \begin{Bmatrix} \{F^1\} \\ \{F^2\} \end{Bmatrix} \quad (4)$$

The model can also be called a mixed model because (u, P) are of different kinds.

- 14.2** Evaluate the coefficient matrices $[K^{\alpha\beta}]$ in Problem 14.1 for $a = \text{constant}$ and column vectors $\{F^\alpha\}$ for $f = \text{constant}$. Assume that $\psi_i = \phi_i$ are the linear interpolation functions. Eliminate $\{P\}$ from the two sets of equations (4) to obtain an equation of the form

$$[K]\{u\} = \{F\}$$

Compare the coefficient matrix $[K]$ and vector $\{F\}$ with those obtained with the weak form finite element model of (1). What conclusions can you draw?

- 14.3** Develop the least-squares finite element model of (2) in Problem 14.1, and compute element coefficient matrices and vectors when $\psi_i = \phi_i$ are the linear interpolation functions.
- 14.4** Solve the problem in Example 14.3.1 using three elements of the least-squares model developed in Problem 14.3. Compare the results with the exact solution and those of the weak form finite element model.
- 14.5** Show that the mixed finite element model of the Euler–Bernoulli beam theory, Eq. (14.2.47a), is the same as that used in Eq. (5.2.18) for the linear interpolation of w and M .
- 14.6** Consider the pair of equations

$$\nabla u - \mathbf{q}/k = 0, \quad \nabla \cdot \mathbf{q} + f = 0 \quad \text{in } \Omega$$

where u and \mathbf{q} are the dependent variables, and k and f are given functions of position (x, y) in a two-dimensional domain Ω . Derive the finite element formulation of the equations in the form

$$\begin{bmatrix} [K^{11}] & [K^{12}] & [K^{13}] \\ & [K^{22}] & [K^{23}] \\ \text{symm.} & & [K^{33}] \end{bmatrix} \begin{Bmatrix} \{u\} \\ \{q^1\} \\ \{q^2\} \end{Bmatrix} = \begin{Bmatrix} \{F^1\} \\ \{F^2\} \\ \{F^3\} \end{Bmatrix}$$

Caution: Do not eliminate the variable u from the given equations.

- 14.7** Compute the element coefficient matrices $[K^{\alpha\beta}]$ and vectors $\{F^\alpha\}$ of Problem 14.6 using linear triangular elements for all variables. Assume that k is a constant.

- 14.8** Repeat Problem 14.7 with linear rectangular elements.

- 14.9** Consider the following form of the governing equations of the classical plate theory:

$$-\left(\frac{\partial^2 M_{xx}}{\partial x^2} - 4D_{66} \frac{\partial^4 w}{\partial x^2 \partial y^2} + \frac{\partial^2 M_{yy}}{\partial y^2} \right) = q \quad (a)$$

$$\frac{\partial^2 w}{\partial x^2} = -(\bar{D}_{22} M_{xx} + \bar{D}_{12} M_{yy}),$$

$$\frac{\partial^2 w}{\partial y^2} = -(\bar{D}_{12} M_{xx} + \bar{D}_{11} M_{yy}) \quad (b)$$

where M_{xx} and M_{yy} are the bending moments, w is the transverse deflection, q is the distributed load, ν is the Poisson ratio, and

$$\bar{D}_{ij} = \frac{D_{ij}}{D_0}, \quad D_0 = D_{11} D_{22} - D_{12}^2$$

- (a) Give the weak form of the equations, and (b) assume approximation of the form

$$w = \sum_{i=1}^4 w_i \psi_i^1, \quad M_{xx} = \sum_{i=1}^2 M_{xi} \psi_i^2, \quad M_{yy} = \sum_{i=1}^2 M_{yi} \psi_j^3$$

to develop the (mixed) finite element model in the form

$$\begin{bmatrix} [K^{11}] & [K^{12}] & [K^{13}] \\ & [K^{22}] & [K^{23}] \\ \text{symm.} & & [K^{33}] \end{bmatrix} \begin{Bmatrix} \{w\} \\ \{M_x\} \\ \{M_y\} \end{Bmatrix} = \begin{Bmatrix} \{F^1\} \\ \{F^2\} \\ \{F^3\} \end{Bmatrix}$$

Comment on the choice of the functions ψ_i^α for $\alpha = 1, 2, 3$.

- 14.10** Use the interpolation

$$w = \sum_{i=1}^4 w_i \psi_i^1, \quad M_{xx} = \sum_{i=1}^2 M_{xi} \psi_i^2, \quad M_{yy} = \sum_{i=1}^2 M_{yi} \psi_j^3$$

with

$$\psi_1^1 = \left(1 - \frac{x}{a}\right) \left(1 - \frac{y}{b}\right), \quad \psi_2^1 = \frac{x}{a} \left(1 - \frac{y}{b}\right), \quad \psi_3^1 = \frac{x}{a} \frac{y}{b}, \quad \psi_4^1 = \left(1 - \frac{x}{a}\right) \frac{y}{b}$$

$$\psi_1^2 = 1 - \frac{x}{a}, \quad \psi_2^2 = \frac{x}{a}, \quad \psi_1^3 = 1 - \frac{y}{b}, \quad \psi_2^3 = \frac{y}{b}$$

for a rectangular element with sides a and b to evaluate the matrices $[K^{\alpha\beta}]$ ($\alpha, \beta = 1, 2, 3$) in Problem 14.9.

- 14.11 Repeat Problem 14.10 for the case in which $\phi_i^1 = \phi_i^2 = \psi_i$.
- 14.12 Evaluate the element matrices in (14.4.6b) by assuming that the nonlinear parts in the element coefficients are elementwise constant.
- 14.13 Give the finite element formulation of the following nonlinear equation over an element (x_a, x_b) :

$$-\frac{d}{dx} \left(u \frac{du}{dx} \right) + 1 = 0 \quad \text{for } 0 < x < 1$$

$$\left. \left(\frac{du}{dx} \right) \right|_{x=0} = 0, \quad u(1) = \sqrt{2}$$

- 14.14 Compute the tangent coefficient matrix for the nonlinear problems in Problem 14.13. What restriction(s) should be placed on the initial guess vector?
- 14.15 Compute the tangent stiffness matrix \mathbf{K}_T in (14.4.17) for the Euler–Bernoulli beam element in (14.4.6a).
- 14.16 Develop the nonlinear finite element model of the Timoshenko beam theory. Equations (14.4.1) and (14.4.2) are valid for this case, with the following changes. In place of $(d^2/dx^2)(EI d^2w/dx^2)$ use $-(d/dx)(EI d\Psi/dx) + GAk(dw/dx + \Psi)$ and add the following additional equation for w :

$$-\frac{d}{dx} \left[GAk \left(\frac{dw}{dx} + \Psi \right) \right] = q$$

See Section 5.3 for additional details.

- 14.17 Compute the tangent stiffness matrix for the Timoshenko beam element in Problem 14.16.
- 14.18 (Natural convection flow between heated vertical plates) Consider the flow of a viscous incompressible fluid in the presence of a temperature gradient between two stationary long vertical plates. Assuming zero pressure gradient between the plates, we can write $v_x = v_x(y)$, $v_y = 0$, $T = T(y)$, and

$$0 = \rho\beta g(T - T_m) + \mu \frac{d^2 v_x}{dy^2}, \quad 0 = k \frac{d^2 T}{dy^2} + \mu \left(\frac{dv_x}{dy} \right)^2$$

where $T_m = \frac{1}{2}(T_0 + T_1)$ is the mean temperature of the two plates, g the gravitational acceleration, ρ the density, β the coefficient of thermal expansion, μ the viscosity, and k the thermal conductivity of the fluid. Give a finite element formulation of the equations and discuss the solution strategy for the computational scheme.

- 14.19 Derive the interpolation functions ψ_1 , ψ_5 , and ψ_8 for the eight-node prism element using the alternative procedure described in Section 8.2 for rectangular elements.
- 14.20 Evaluate the source vector components f_i^e and coefficients K_{ij}^e over a master prism element when f is a constant, f_0 , and $k_x = k_y = k_z = k$, a constant in (14.3.5b).

REFERENCES FOR ADDITIONAL READING

1. Bathe, K. J., *Finite Element Procedures*, Prentice-Hall, Englewood Cliffs, NJ, 1996.
2. Bell, B. C. and Surana, K. S., “A Space-Time Coupled p -Version Least-Squares Finite Element Formulation for Unsteady Fluid Dynamics Problems,” *International Journal for Numerical Methods in Engineering*, **37**, 3545–3569, 1994.

3. Belytschko, T., Liu, W. K., and Moran, B., *Nonlinear Finite Elements for Continua and Structures*, John Wiley, Chichester, UK, 2000.
4. Bochev, P. B. and Gunzburger, M. D., "Finite Element Methods of Least-Squares Type," *SIAM Review*, **40**, 789–837, 1998.
5. Brezzi, F. and Fortin, M., *Mixed and Hybrid Finite Element Methods*, Springer-Verlag, Berlin (1991).
6. Crisfield, M. A., *Non-Linear Finite Element Analysis of Solids and Structures, Vol. 1: Essentials*, John Wiley, Chichester, UK, 1991.
7. Crisfield, M. A., *Non-Linear Finite Element Analysis of Solids and Structures, Vol. 2: Advanced Topics*, John Wiley, Chichester, UK, 1997.
8. Gresho, P. M. and Sani, R. L., *Incompressible Flow and the Finite Element Method*, John Wiley, West Sussex, UK, 2000.
9. Hinton, E. (ed.) *NAFEMS Introduction to Nonlinear Finite Element Analysis*, NAFEMS, Glasgow, UK, 1992.
10. Irons, B. and Ahmad, S., "Quadrature Rules for Brick-Based Finite Elements," *International Journal for Numerical Methods in Engineering*, **3**, 293–294, 1971.
11. Jiang, B. N., "The Least-Squares Finite Element Method for Elasticity. Part II: Bending of Thin Plates," *International Journal for Numerical Methods in Engineering*, **54**, 1459–1475, 2002.
12. Oden, J. T., *Finite Elements of Nonlinear Continua*, McGraw-Hill, New York, 1972.
13. Oden, J. T. and Reddy, J. N., *An Introduction to the Mathematical Theory of Finite Elements*, Wiley-Interscience, New York, 1982.
14. Owen, D. R. J. and Hinton, E., *Finite Elements in Plasticity: Theory and Practice*, Pineridge Press, Swansea, UK, 1991.
15. Pontaza, J. P. and Reddy, J. N., "Spectral/ hp Least-Squares Finite Element Formulation for the Navier–Stokes Equations," *Journal of Computational Physics*, **190**(2), 523–549, 2003.
16. Pontaza, J. P. and Reddy, J. N., "Mixed Plate Bending Elements Based on Least-Squares Formulation," *International Journal for Numerical Methods in Engineering*, **60**, 891–922, 2004.
17. Pontaza, J. P. and Reddy, J. N., "Hierarchical Least-Squares Shear Deformable Shell Elements," *Computer Methods in Applied Mechanics and Engineering*, to appear.
18. Pontaza, J. P. and Reddy, J. N., "Space-Time Coupled Spectral/ hp Least-Squares Finite Element Formulation for the Incompressible Navier–Stokes Equations," *Journal of Computational Physics*, **197**(2), 418–459, 2004.
19. Putcha, N. S. and Reddy, J. N., "A Mixed Shear Flexible Finite Element for the Analysis of Laminated Plates," *Computer Methods in Applied Mechanics and Engineering*, **44**, 213–227, 1984.
20. Reddy, J. N., *Applied Functional Analysis and Variational Methods in Engineering*, McGraw-Hill, New York, 1986; Krieger, Melbourne, FL, 1991.
21. Reddy, J. N., *Energy Principles and Variational Methods in Applied Mechanics*, 2nd ed., John Wiley, New York, 2002.
22. Reddy, J. N., *An Introduction to Nonlinear Finite Element Analysis*, Oxford University Press, Oxford, UK, 2004.
23. Reddy, J. N., "Penalty-Finite-Element Analysis of 3-D Navier–Stokes Equations," *Computer Methods in Applied Mechanics and Engineering*, **35**, 87–106, 1982.
24. Reddy, J. N. and Gartling, D. K., *The Finite Element Method in Heat Transfer and Fluid Dynamics*, 2nd ed., CRC Press, Boca Raton, FL, 2001.
25. Reddy, J. N. and Sandidge, D., "Mixed Finite Element Models for Laminated Composite Plates," *Journal of Engineering for Industry*, **109**, 39–45, 1987.
26. Reddy, J. N. and Tsay, C. S., "Mixed Rectangular Finite Elements for Plate Bending," *Proceedings of the Oklahoma Academy of Science*, **47**, 144–148, 1977.
27. Reddy, J. N. and Tsay, C. S., "Stability and Vibration of Thin Rectangular Plates by Simplified Mixed Finite Elements," *Journal of Sound & Vibration*, **55**(2), 289–302, 1977.
28. Reddy, M. P. and Reddy, J. N., "Finite-Element Analysis of Flows of Non-Newtonian Fluids in Three-Dimensional Enclosures," *International Journal of Non-Linear Mechanics*, **27**, 9–26, 1992.

29. Pian, T. H. H. and Tong, P., "Basis of Finite Element Methods for Solid Continua," *International Journal of Numerical Methods in Engineering*, **1**, 3–28, 1969.
30. Strang, G. and Fix, G. J., *An Analysis of the Finite Element Method*, Prentice-Hall, Englewood Cliffs, NJ, 1973.
31. Tong, P., "New Displacement Hybrid Finite Element Methods for Solid Continua," *International Journal of Numerical Methods in Engineering*, **2**, 73–85, 1970.
32. Wait, R. and Mitchell, A. R., *Finite Element Analysis and Applications*, John Wiley, New York, 1985.
33. Wang, C. M., Reddy, J. N., and Lee, K. H., *Shear Deformable Beams and Plates. Relationships with Classical Solutions*, Elsevier, Oxford, UK, 2000.
34. Winterscheidt, D. and Surana, K. S., " p -Version Least-Squares Finite Element Formulation for Two-Dimensional Incompressible Fluid Flow," *International Journal for Numerical Methods in Fluids*, **18**, 43–69, 1994.
35. Zienkiewicz, O. C. and Taylor, R. L., *The Finite Element Method*, 4th ed., Vol. 1: *Basic Formulation and Linear Problems*, McGraw-Hill, London, UK, 1989.
36. Zienkiewicz, O. C. and Taylor, R. L., *The Finite Element Method*, 4th ed., Vol. 2: *Solid and Fluid Mechanics, Dynamics and Non-linearity*, McGraw-Hill, London, UK, 1989.

FOR MORE EXCLUSIVE
(Civil, Mechanical, EEE, ECE)
ENGINEERING & GENERAL STUDIES
(Competitive Exams)

TEXT BOOKS, IES GATE PSU's TANCET & GOVT EXAMS
NOTES & ANNA UNIVERSITY STUDY MATERIALS

VISIT

www.EasyEngineering.net

AN EXCLUSIVE WEBSITE FOR ENGINEERING STUDENTS &
GRADUATES



****Note:** Other Websites/Blogs Owners Please do not Copy (or) Republish this Materials, Students & Graduates if You Find the Same Materials with EasyEngineering.net Watermarks or Logo, Kindly report us to easyengineeringnet@gmail.com